nature

SCIENCE IN GERMANY
The fruits of reform

NIH II
A good system gets better

GENOME-WIDE ANALYSIS
Genetics of seven common diseases

A NEW TAKE ON CLONING

The reprogramming potential of fertilized zygotes

NATURE.COM
Stem cell research

nature

www.nature.com/nature

Vol 447 | Issue no. 7145 | 7 June 2007

Half way to real reform

Universities in Germany have undertaken overdue reform, but more change is needed to fully tap their potential.

Germany is the world's fourth largest investor in research and development, and its overall scientific impact suggests that much of the money is well spent. But a great deal of that impact comes from the 80 institutes of the Max Planck Society. The university sector is underperforming (see page 630).

The reasons for this can be traced back to the country's turbulent twentieth-century history and the ideologies that invaded the universities before and after the Second World War, on both sides of the Iron Curtain. By the 1990s, universities were overpopulated with students that they had not themselves selected, underfunded, and hide-bound by rules preventing them from competing with each other.

These problems have been recognized for a while, and other European countries may learn from Germany's response. Reforms implemented during the past few years have given the universities much more control over their own destinies, sending shockwaves through the academic landscape. For example, universities may now offer competitive salaries and conditions to selected researchers by transferring support from less productive colleagues.

To encourage institutions that are reluctant to make the most of their new freedoms, research organizations have launched competitions that highlight which universities are doing well and which badly. Perhaps the most influential has been the federal research ministry's Excellence Initiative, which selects a handful of élite universities.

All of this makes for a good start on university reform, but there is a long way to go. Visitors to German universities are unlikely to see, for example, the diversity of gender, age and nationality that they would encounter in a typical US research university. The number of female professors remains dismally small. New initiatives to increase the number of young professors have so far made only a small dent in academic demographics.

And Germany remains less attractive to young foreign scientists than it ought to be. The latest figures from the European Commission's Marie Curie programme, which funds young European Union (EU) researchers to work in a second EU country, show that only 11.5% choose to go to Germany — hardly changed from five years ago and still well below France (16%) and the United Kingdom (32%).

One reason for Britain's popularity is language — English is already widely spoken and a few years in an institution where it is the working language helps a scientific career. But the fact remains that German universities could do more to create a receptive environment for foreign students and staff.

It will be some time before the positive impact of the reforms undertaken so far shows up in statistics. In the meantime Germany needs to address a few extra problems that have been either caused or highlighted by the reforms themselves.

As efforts concentrate on building up a young faculty, the traditional position of the low-level academic, the *Mittelbau*, whose nearest equivalent is perhaps the assistant professor, is disappearing. The heavy teaching load that these people used to bear now falls on young professors who ought to be devoting themselves to research. This is a hard conflict to resolve, as the teaching is equally important — but recruitment must be broadened to address it.

"German universities could do more to create a receptive environment for foreign staff."

Additionally, many universities are still loath to appoint tenured professors from among their own junior staff. This principle was intended to avoid parochial appointments, but it has become less necessary in the current era of constant evaluation, where there is a natural pressure to appoint the best candidate. The rule often serves as an obstacle to young researchers seeking a route to tenure.

The universities will also benefit indirectly from the deal cut two years ago between federal and state governments, Germany's non-university research institutes, and the DFG, the main grant-funding agency. In return for guaranteed 3% annual budget increases until 2010, these institutes are expected, among other things, to encourage greater collaboration with both industry and research universities.

This is a positive development for all concerned, giving institutes such as the Max Planck stable budgets and the universities better access to their resources. It is no coincidence that two of three universities selected by the Excellence Initiative had already developed unusually tight links with local Max Planck institutes. ■

Bad execution

China won't achieve a tenable drug regulation policy by hanging public officials.

The sentencing to death of Zheng Xiaoyu, the former head of China's State Food and Drug Administration (SFDA), is a throwback to the nation's ugly past that will do little to further its professed goal of building a fair drug-regulation regime.

Zheng was sentenced to death in a Beijing court on 29 May on charges of accepting bribes, two years after he he was sacked from the drug regulator. Given the secrecy of China's judicial process, it is difficult to assess his guilt or innocence. But accusations involving the bribery of hundreds of officials have shadowed the agency for years. It is good that the Chinese government is facing up to the problem and taking public steps to clean up its drug-regulation process.

But hanging a man and vilifying him in state-controlled newspapers does not inspire confidence that China is building an effective drug-regulatory process. If the sentence is carried out, it is more likely

to confirm the pharmaceutical industry's worst fears that there is little chance of doing business fairly in a country where the rule of law remains patchy and subject to political influence.

Drug regulation is vitally important to China as it seeks to develop an internationally competitive drug industry of its own, while attracting investment from and collaboration with the rest of the world. The country rightly sees the establishment of such an industry as critical to both public health and the nurturing of innovation in the life sciences. In common with most other governments — but with rather better prospects of success — China regards the successful combination of research in biology and genetics, and innovation in biotechnology and pharmaceuticals, as an important element of its plans for scientific and economic development.

From the global industry's point of view, the establishment of a sound regulatory regime in China is just as important. The world's leading drug companies see the country, with its burgeoning middle class, as a market of great potential. Yet participation in that market remains something of an enigma. All of the major drug companies have stepped tentatively into direct participation in research activities in China. They view the risks of investment in China as considerable, but the benefits will only reveal themselves if and when a reliable regulatory regime is established.

So everyone in the industry, at home and abroad, supports the professed aims of Beijing's drive to eliminate widespread corruption from drug regulation. But they are entitled to be suspicious of its implementation. Corruption has been widespread and no one believes that Zheng — supposing that the charges against him are proven — was the only, or even the worst, culprit.

"Regulation is vitally important to China as it seeks to develop a competitive drug industry of its own."

Articles appearing in *China Daily* and elsewhere in condemnation of the official and his family have the smell of old-fashioned, stalinist scapegoating, more likely to sweep the problem under the carpet than resolve it. Genuinely fair regulation of drugs is a complex matter that depends on transparency and on sophisticated checks and balances — such as scientific staff who are paid by the government but can be seen to be independent — not on fear and arbitrary justice.

Hanging a man may create the public impression that the problem is being zealously tackled. Real movement towards fair regulation would involve steps a great deal less melodramatic that yet seem beyond China's grasp — steps towards a transparent drug-review process, functioning under open, public scrutiny. ■

Community service

Introducing three free-access websites for research networking and outreach.

The mission statement that appeared in the second issue of *Nature* in 1869 and is reproduced every week on our printed table of contents may use archaically high-flown language, but it still applies. In essence, we exist to help scientists communicate with each other and to communicate science to wider audiences.

Precisely that duality applies to two websites to be launched this week: *Nature Reports Climate Change* and *Nature Reports Stem Cells*. Aimed at researchers and at anyone else who is interested, both give an editorial perspective of their fields through a combination of original journalism and commissioned comment, alongside archived material from other Nature publications. Both sites also facilitate community interactions through blogs.

For example, the climate-change site focuses on post-Kyoto agendas, both journalistically and with an analysis of the obstacles by development expert Jeffrey Sachs (see www.nature.com/climate). The stem-cells site contains a similar blend of news about the latest research and comments, as well as a featured editor — this month, cloning researcher Ian Wilmut. It also goes behind the research papers with an editorial commentary and extracts from referees' comments (with their permission) of the paper in this issue of *Nature* on developmental reprogramming by Egli *et al.* (see page 679 and www.nature.com/stemcells).

These sites will develop further by way of community interactions and applications in the coming months. The original content of both is freely accessible.

Also free is a very different website to be launched next week: *Nature Precedings*. As its title implies, this site will enable researchers to share, discuss and cite their early findings. It provides a lightly moderated and relatively informal channel for scientists to disseminate information, especially recent experimental results and emerging conclusions. In this sense, it is designed to complement traditional peer-reviewed journals, allowing researchers to make informal communications such as conference papers or presentations more widely available and enabling them to be formally cited. This, in turn, allows them to solicit community feedback and establish priority over their results or ideas.

Intended to cover biomedicine, chemistry and the Earth sciences, the site (http://precedings.nature.com) will host a wide range of research documents, including preprints, unpublished manuscripts, white papers, technical papers, supplementary findings, posters and presentations. All submissions will be reviewed by staff curators and accepted only if they are considered to be legitimate scientific contributions of likely interest to others in that field. No judgement is to be made about the quality or uniqueness of the work, and submissions are not subjected to peer review before they are released. Because of this, accepted submissions will usually be published within one working day, and no charge is made to either authors or readers.

Nature Precedings will make full use of participative features such as tagging, voting and commenting to facilitate the discovery of especially interesting and relevant content. We anticipate that the content will be mirrored by academic partner organizations, several of whom have been involved with us in developing this service. As well as allowing it to become incorporated into the substantial information hubs already provided by these organizations, this federated approach will also help to ensure the long-term availability of the content — and act as a practical guarantee of the Nature Publishing Group's pledge not to charge readers for access. ■

RESEARCH HIGHLIGHTS

Mouse model for malaria

PLoS Pathog. **3,** e72 (2007)

A global collaboration has come up with the first non-primate animal model for human malaria — and on the way explained how a key antibody protects infected people.

Richard Pleass of the University of Nottingham, UK, and his colleagues engineered an antibody that matches those found in Gambian adults who are immune to malaria. The antibody binds a *Plasmodium falciparum* protein known as $MSP1_{19}$, an important vaccine target. The picture shows infected red blood cells.

To test the antibody in mice, the researchers engineered the mouse malarial parasite *Plasmodium berghei* to express $MSP1_{19}$. They also made transgenic mice carrying a gene that encodes the human immune-cell receptor FcγR1, suspected to play a role in the antibodies' protective effect. The antibodies protected only the transgenic mice from infection, confirming the importance of FcγR1.

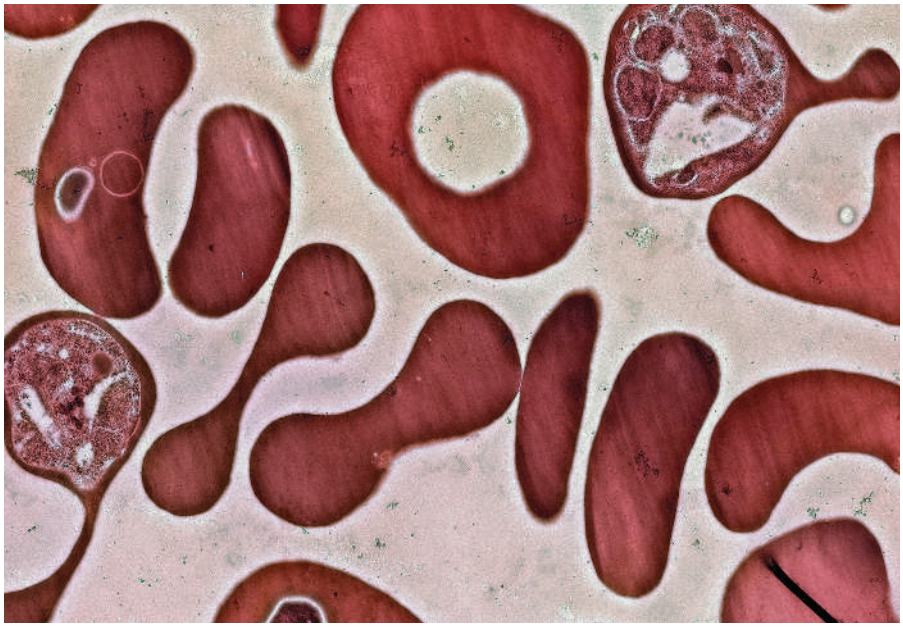

G. GAUGLER/SPL

CLIMATE SCIENCE

Uncertain forecast

Science doi:10.1126/science.1140746 (2007)

Global warming could boost rainfall by more than double the amount predicted by current climate models, a new study suggests.

Frank Wentz and his colleagues at Remote Sensing Systems in Santa Rosa, California, analysed weather-satellite data from 1987 to 2006. Climate models project that worldwide rainfall will increase by between 1 and 3% per degree of warming, but the satellite data suggest rainfall will go up in line with the atmosphere's water vapour content — at a rate of around 7% per degree. The models forecast less rain because they predict that weakening surface winds will reduce water evaporation. But the data show that surface winds actually increased with warming.

It is, for now, unclear whether the discrepancy is due to flaws in the models or problems with the data. It is also unclear where the extra rain, if it arrives, might fall — whether it will make wet places wetter, or bring relief to drought-stricken regions.

NANOTECHNOLOGY

Spot the ball

J. Am. Chem. Soc. **129,** 6666–6667 (2007)

The highly symmetrical atomic structure of the football-shaped C_{60} molecule has been seen for the first time using electron microscopy.

Kazu Suenaga and his co-workers at the National Institute of Advanced Industrial Science and Technology in Tsukuba, Japan, imaged individual C_{60} molecules tethered to the surface of carbon nanotubes. Comparisons between these images (example pictured below left) and image simulations (right) based on the molecules' 20-sided cage structure (middle) allow the observed two-dimensional shapes to be assigned to various projections of the carbon shells. These are made from pentagonal and hexagonal rings.

The researchers also see several distorted, non-spherical shells that they assign to C_{58} molecules, formed when C_2 units are kicked out of the shells by the electron beam.

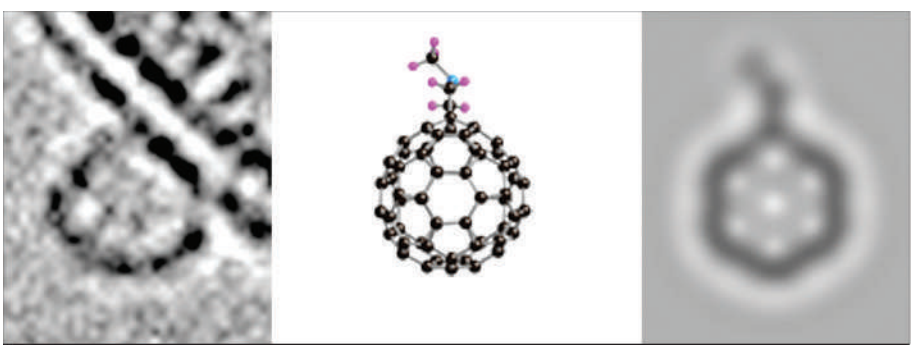

ACS

COSMOLOGY

When the Universe began

Astrophys. J. **170** (Suppl.), 263–287; 288–334; 335–376 and 377–408 (2007)

Four papers describing data from one of cosmology's greatest experiments have been published, a year after the results were made public.

The Wilkinson Microwave Anisotropy Probe was launched in 2001 to study the radiation left over from the inferno of the Universe's birth. By mapping temperature fluctuations in this cosmic microwave background and measuring the polarization of the radiation, the probe has provided evidence that the Universe is made up mostly of dark matter and dark energy. It has also shed light on aspects of the Universe's history, such as when the first stars were born. The four papers report observations collected over three years.

NEUROSCIENCE

Cellular angst

Nature Neurosci. doi:10.1038/nn1919 (2007)

Anxious people tend to expect the worst in uncertain situations — a trait that researchers have now linked in mice to particular cells within the brain's hippocampus.

Cornelius Gross of the European Molecular Biology Laboratory in Monterotondo, Italy, and his team studied

mice genetically engineered for increased anxiety. These mice froze in fear for the same length of time when exposed to a cue — such as a flash of light — that was always followed by an electric shock as they did when exposed to a different cue that was only sometimes associated with a shock. Normal mice responded less strongly to the ambiguous than to the certain cue.

The researchers showed that inhibiting the granule cells in the anxious mice's hippocampal dentate gyrus restored normal behaviour.

GEOLOGY

Ancient lava fossils dated

Geology **35,** 487–490 (2007)

Radiometric dating has confirmed that microscopic tubular structures in ancient lavas date back billions of years. These structures are thought to show that life thrived in volcanic rocks deep within the early Earth.

Neil Banerjee of the University of Western Ontario in London, Canada, and his colleagues found the microfossils in pillow lavas in the Pilbara Craton of western Australia. The tubes contain traces of organic carbon, and appear identical to those left in basaltic rocks by modern microbes.

The tubular structures at this site also contained the mineral titanite, which allowed them to be dated by measuring trace amounts of lead and uranium. This revealed the structures to be 3 billion years old.

CANCER BIOLOGY

The price of silence

Cell **129,** 879–890 (2007)

Researchers have identified a possible genetic culprit behind one of the most common forms of adult leukaemia.

Albert de la Chapelle and Christoph Plass of Ohio State University in Columbus and their colleagues found that reduced activity of a gene called death-associated protein kinase 1 (*DAPK1*) is linked to both inherited and spontaneous forms of chronic lymphocytic leukaemia. *DAPK1* regulates programmed cell death in blood cells called lymphoid cells, and loss of that function could aid the leukaemia.

In most cases of the disease, the gene had been silenced by the addition of methyl groups to the DNA region controlling *DAPK1* expression. But the team also discovered, in affected members of a family with a history of the leukaemia, a mutation that reduces *DAPK1* expression.

BIOCHEMISTRY

Single handedly

J. Am. Chem. Soc. doi:10.1021/ja0708870 (2007)

Why are all amino acids in living organisms left-handed? Donna Blackmond and her co-workers at Imperial College London, UK, suggest a new way in which crystallization could have played a part.

The reactions expected to have produced amino acids on the early Earth generally create both left- and right-handed forms of the molecules. For some amino acids, such as serine, a tiny excess of one form can lead to that form's preferential removal by precipitation of crystals, leaving the solution enriched in the other.

Blackmond and her colleagues have now shown that this enrichment can be engineered for amino acids that don't display it by themselves. Small molecules such as dicarboxylic acids added to the mixture become incorporated into the crystals and promote the extraction of one form of the amino acid.

MATERIALS SCIENCE

Reflect on this

Nature Mater. doi:10.1038/nmat1930 (2007)

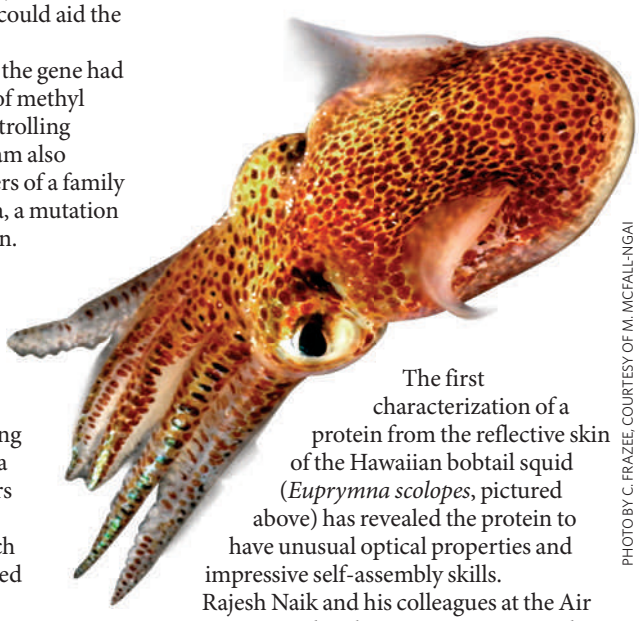

PHOTO BY C. FRAZEE, COURTESY OF M. MCFALL-NGAI

The first characterization of a protein from the reflective skin of the Hawaiian bobtail squid (*Euprymna scolopes*, pictured above) has revealed the protein to have unusual optical properties and impressive self-assembly skills.

Rajesh Naik and his colleagues at the Air Force Research Laboratory in Dayton, Ohio, engineered bacteria to produce the squid protein reflectin. They found that it has the highest refractive index — a measure of how slowly light travels through a material — reported for any naturally occurring protein.

When deposited from a particular type of solvent, the reflectin proteins self-organized into a film of regularly spaced stripes, the separation of which could be tuned. This functioned as a diffraction grating, which splits light into its different wavelength components.

JOURNAL CLUB

Gautam R. Desiraju
University of Hyderabad, India

A chemist applauds an algorithm able to predict crystal structures from chemical composition alone.

I work in crystal engineering, a field that involves designing and constructing crystals with desired physical, chemical or pharmaceutical properties from small organic molecules. It is an experimental science based on pattern recognition and retrosynthetic strategies, in which the structure is considered as the sum of smaller, simpler parts.

Improvements to computational crystal-structure prediction could make design protocols more reliable. But this is such a difficult problem that only a handful of groups in the field work on it. In this context, I found a recent paper presenting a seemingly reliable method to be thought-provoking (A. R. Oganov and C. W. Glass *J. Chem. Phys.* **124,** 244704; 2006).

Typically, crystal-structure prediction involves computer generation of putative crystal structures using a force field, which represents the interactions between atoms in neighbouring molecules. The correct structure is presumed to be that which minimizes the crystal's energy.

The procedure is problematic because the force fields may not be well tailored to the molecules being studied, and because the experimental structure may not be the lowest-energy arrangement. It is also impossible to explore all conceivable structures, which are mind-boggling in number.

Oganov and Glass use an evolutionary algorithm to localize the search to the most promising structures. Their approach is attractive in that it requires no system-specific knowledge — the input is just the molecule's chemical composition, not even its structure — and their ability to predict the unusual tetragonal structure of urea is impressive.

Is this the long-awaited breakthrough in crystal engineering? Perhaps not, but surely it's an important step forward.

Discuss this paper at **http/blogs.nature.com/nature/journalclub**

NEWS

Simple switch turns cells embryonic

Research reported this week by three different groups shows that normal skin cells can be reprogrammed to an embryonic state in mice[1–3]. The race is now on to apply the surprisingly straightforward procedure to human cells.

If researchers succeed, it will make it relatively easy to produce cells that seem indistinguishable from embryonic stem cells, and that are genetically matched to individual patients. There are limits to how useful and safe these would be for therapeutic use in the near term, but they should quickly prove a boon in the lab.

"It would change the way we see things quite dramatically," says Alan Trounson of Monash University in Victoria, Australia. Trounson wasn't involved in the new work but says he plans to start using the technique "tomorrow". "I can think of a dozen experiments right now — and they're all good ones," he says.

"It's unbelievable, just amazing. It's like Dolly. It's that type of accomplishment."

In theory, embryonic stem cells can propagate themselves indefinitely and are able to become any type of cell in the body. But so far, the only way to obtain embryonic stem cells involves destroying an embryo, and to get a genetic match for a patient would mean, in effect, cloning that person — all of which raise difficult ethical questions.

As well as having potential ethical difficulties, the 'cloning' procedure is technically difficult. It involves obtaining unfertilized eggs, replacing their genetic material with that from an adult cell and then forcing the cell to divide to create an early-stage embryo, from which the stem cells can be harvested. Those barriers may have now been broken down.

"Neither eggs nor embryos are necessary. I've never worked with either," says Shinya Yamanaka of Kyoto University, who has pioneered the new technique.

Last year, Yamanaka introduced a system that uses mouse fibroblasts, a common cell type that can easily be harvested from skin, instead of eggs[4]. Four genes, which code for four specific proteins known as transcription factors, are transferred into the cells using retroviruses. The proteins trigger the expression of other genes that lead the cells to become pluripotent, meaning that they could potentially become any of the body's cells. Yamanaka calls them induced pluripotent stem cells (iPS cells). "It's easy. There's no trick, no magic," says Yamanaka.

The results were met with amazement, along with a good dose of scepticism. Four factors seemed too simple. And although the cells had some characteristics of embryonic cells — they formed colonies, could propagate continuously and could form cancerous growths called teratomas — they lacked others. Introduction of iPS cells into a developing embryo, for example, did not produce a 'chimaera' — a mouse carrying a mix of DNA from both the original embryo and the iPS cells throughout its body. "I was not comfortable with the term 'pluripotent' last year," says Hans Schöler, a stem-cell specialist at the Max Planck Institute for Molecular Biomedicine in Münster who is not involved with any of the three articles.

This week, Yamanaka presents a second generation of iPS cells[1], which pass all these tests. In addition, a group led by Rudolf Jaenisch[2] at the Whitehead Institute for Biomedical Research in Cambridge, Massachusetts, and a collaborative effort[3] between Konrad Hochedlinger of the Harvard Stem Cell Institute and Kathrin Plath of the University of California, Los Angeles, used the same four factors and got strikingly similar results.

"It's a relief as some people questioned our results, especially after the Hwang scandal," says Yamanaka, referring to the irreproducible cloning work of Woo Suk Hwang, which turned out to be fraudulent. Schöler agrees: "Now we can be confident that this is something worth building on."

The improvement over last year's results was simple. The four transcription factors used by Yamanaka reprogramme cells inconsistently and inefficiently, so that less than 0.1% of the million cells in a simple skin biopsy will be fully reprogrammed. The difficulty is isolating those in which reprogramming has been successful. Researchers do this by inserting a gene for antibiotic resistance that is activated only when proteins characteristic of stem cells are expressed. The cells can then be doused with

Bush's climate plan 'nothing new'

President George W. Bush's 31 May announcement of a "new framework" for international efforts to confront climate change sounded, at first, like a sharp turnaround by the White House. But as analysts dissected his statements, many concluded that he had said little new.

In a speech in Washington DC to the Global Leadership Campaign, a group that lobbies for greater spending on international affairs, Bush called for the top-emitting countries to meet by the end of 2008 to set a long-term global goal for greenhouse-gas emissions. The notion of Bush proposing a global target to tackle climate change caused a flurry of excitement.

But in a briefing afterwards, James Connaughton, the president's environmental adviser, said that Bush was referring only to "a long-term aspirational goal" rather than a binding commitment. "It is the implementing mechanisms that become binding," he said.

"It remains to be seen whether this initiative means anything," says Bert Metz, a climatologist at the Netherlands Environmental Assessment Agency in Bilthoven. Stabilizing atmospheric levels of greenhouse gases, he says, requires "ambitious and urgent international

J. SCOTT APPLEWHITE/AP

Leadership talk: George Bush hints at setting global targets.

NASA/JOHNS HOPKINS UNIV./SOUTHWEST RES. INST.

LIGHT FOUNDATIONS
Jupiter-sized planets in unexpected places spur debate.
www.nature.com/news

S. OGDEN

The birth of this chimaeric mouse suggests that the cells used to generate it behave like embryonic stem cells.

antibiotics, killing off the failures.

The protein Yamanaka used as a marker for stem cells last year was not terribly good at identifying reprogrammed cells. This time, all three groups used two other protein markers — Nanog and Oct4 — to great effect. All three groups were able to produce chimaeric mice using iPS cells isolated in this way; and the mice passed iPS DNA on to their offspring.

Jaenisch also used a special embryo to produce fetuses whose cells were derived entirely from iPS cells. "Only the best embryonic stem cells can do this," he says.

"It's unbelievable, just amazing," says Schöler, who heard Jaenisch present his results at a meeting on 31 May in Bavaria. "For me it's like Dolly [the first cloned mammal]. It's that type of accomplishment."

The method is inviting. Whereas cloning with humans was limited by the number of available eggs and by a tricky technique that takes some six months to master, Yamanaka's method can use the most basic cells and can be accomplished with simple lab techniques.

But applying the method to human cells has yet to be successful. "We are working very hard — day and night," says Yamanaka. It will probably require more transcription factors, he adds.

If it works, researchers could produce iPS cells from patients with conditions such as Parkinson's disease or diabetes and observe the molecular changes in the cells as they develop. This 'disease in a dish' would offer the chance to see how different environmental factors contribute to the condition, and to test the ability of drugs to check disease progression.

But the iPS cells aren't perfect, and could not be used safely to make genetically matched cells for transplant in, for example, spinal-cord injuries. Yamanaka found that one of the factors seems to contribute to cancer in 20% of his chimaeric mice. He thinks this can be fixed, but the retroviruses used may themselves also cause mutations and cancer. "This is really dangerous. We would never transplant these into a patient," says Jaenisch. In his view, research into embryonic stem cells made by cloning remains "absolutely essential".

If the past year is anything to judge by, change will come quickly. "I'm not sure if it will be us, or Jaenisch, or someone else, but I expect some big success with humans in the next year," says Yamanaka. ■

David Cyranoski
Additional reporting by Heidi Ledford

1. Okita, K., Ichisaka, T. & Yamanaka, S. *Nature* doi:10.1038/nature05934 (2007).
2. Wernig, M. *et al. Nature* doi:10.1038/nature05944 (2007).
3. Maherali, N. *et al. Cell Stem Cell* doi:10.1016/j.stem.2007.05.014 (2007).
4. Takahashi, K. & Yamanaka, S. *Cell* **126,** 663–676 (2006).

For more on alternative stem-cell work, see page 649; and see www.nature.com/stemcells

collaboration. Only starting the discussions on this next year sounds rather strange."

Arriving before the annual G8 meeting of the richest nations' leaders in Germany this week, many have interpreted Bush's proposal as a tactical manoeuvre to lighten the pressure on him to agree to do anything firm about climate change at that meeting. Alden Meyer, a climate specialist at the Union of Concerned Scientists in Cambridge, Massachusetts, adds that it "could serve as a huge diversion" at the planned United Nations (UN) negotiations about climate change in Bali in December.

Others argue that Bush's proposed framework may help rather than hinder progress. "I think that there is a good chance that whatever comes out of this process will merge into the UN process," says Jeff Holmstead, a former environment official with the Bush administration, now at the law firm Bracewell and Giuliani in Washington DC.

Stephen Schneider, a climatologist at Stanford University in California, thinks that a side deal, separate from but not replacing the UN process, could in theory be helpful. But he says that the last such side deal initiated by Bush — the Asia-Pacific partnership of July 2005, which heavily emphasized technology developments to address climate change — is widely regarded as a flop. "It lets greenhouse gases continue to rise at the same rate and under-funds research by a factor of 100. People who are cynical and view [the new proposal] as disingenuous have a long historical trail to base this on," he adds.

"It remains to be seen whether this initiative means anything."

Japan and Australia, participants in the Asia-Pacific deal, have welcomed Bush's plan. Shinzo Abe, Japan's prime minister, has said he thinks the United States is "finally getting serious in dealing with global warming". Last week, Abe launched Japan's plan for a non-binding arrangement to halve global greenhouse-gas emissions by 2050.

China, another Asia-Pacific partner and the world's second largest emitter of carbon dioxide after the United States, also announced its plan to tackle climate change this week. It intends to focus on improving environmental management and agricultural and energy efficiencies and, like the United States, boost research and development for alternative energy, but without compromising economic development. China notes that its per-capita emissions are lower than the world average, and much lower than those of the United States. The United States, it says, should take the lead in reducing emissions. ■

Emma Marris and Colin Macilwain
Additional reporting by Quirin Schiermeier and David Cyranoski

NASA explores scope for far-flung fix

HONOLULU, HAWAII

Researchers credit servicing missions involving astronauts with rescuing the Hubble Space Telescope and keeping it alive for the past 17 years. But an idea to create a similar, if simpler, capability for Hubble's successor is raising eyebrows among project scientists, who fear it will be impractical and expensive.

The James Webb Space Telescope (JWST), currently scheduled for launch in 2013, will make infrared observations from a position in space 1.5 million kilometres from Earth. That puts it farther away than Hubble, which sits in low-Earth orbit just 600 kilometres away, within easy reach of the shuttle. So the JWST was designed assuming that it would fly without any servicing — by astronaut or robot — for its five-to-ten-year career.

"Wouldn't it make sense to ensure that astronauts could go to the telescope if they could fix it?"

But Edward Weiler, head of NASA's Goddard Space Flight Center in Greenbelt, Maryland, which manages the JWST, has indicated that there may be scope for a manned mission to service or make simple repairs to the telescope.

"It might be valuable if astronauts could fly to the JWST to do something that was a critical, but easy fix," says Weiler, "like opening a stuck antenna." Weiler, who used to be NASA's science chief, floated the idea of attaching a docking port to the telescope to allow a future mission to hook up.

But the concept got a chilly reception last week at the American Astronomical Society's biannual meeting in Honolulu, Hawaii. When the JWST was being developed, it seemed impossible that it would ever receive guests — it will be well beyond the reach of the shuttle. Only the decision to develop the Orion crew exploration vehicle, due to replace the shuttle

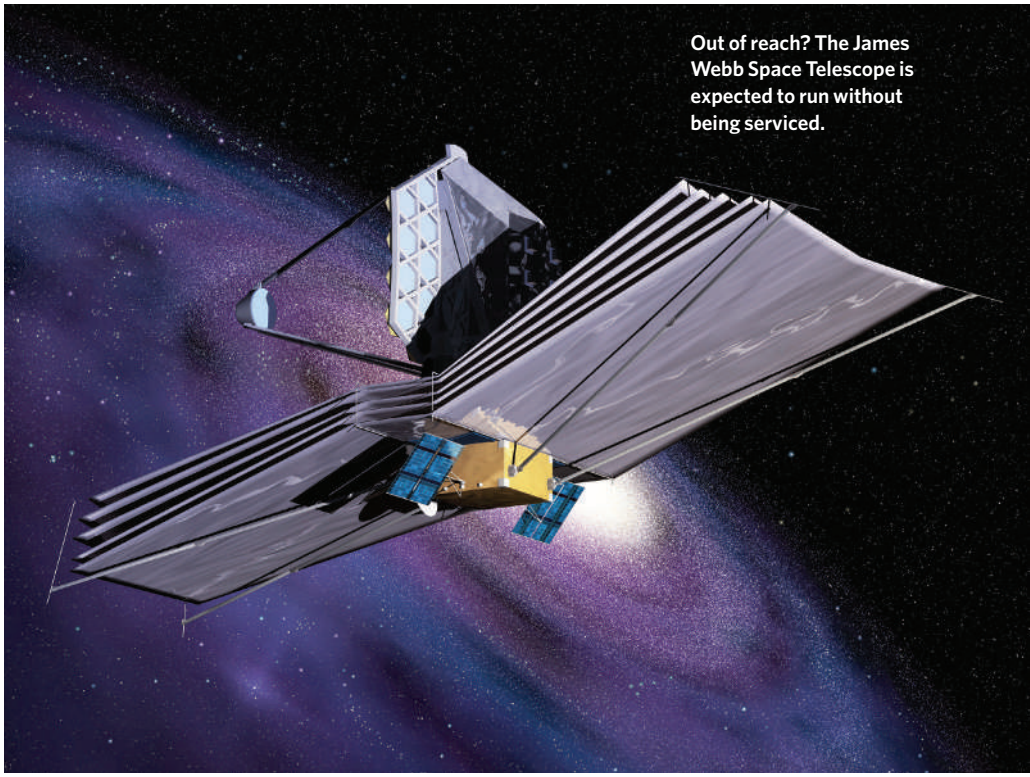

Out of reach? The James Webb Space Telescope is expected to run without being serviced.

ESA

DNA reveals how the chicken crossed the sea

The discovery of chicken bones with Polynesian DNA at an archaeological site in Chile has added hard, physical evidence to the controversial theory that ancient seafarers from the south Pacific visited the New World long before Columbus.

When the Spanish conquistador Francisco Pizarro first visited Peru in 1532, he noted the importance of chickens in the daily lives and religious rituals of the Incas. But how the birds got there was a mystery. Chickens were first domesticated in Asia, and their absence from archaeological sites in the Americas indicates that they were not carried by migrating peoples over a land bridge from Asia to Alaska.

One alternative theory — that Polynesians visited the Americas, bringing livestock with them and perhaps influencing cultural and technological development in the region — has long been disparaged by mainstream archaeologists, as it has largely been supported by supposition rather than evidence.

"It's essentially unequivocal evidence."

So Alice Storey of the University of Auckland, New Zealand, was not particularly enthusiastic when a colleague in Chile asked her to sequence DNA from a trove of ancient chicken bones he had excavated at El Arenal, a site occupied between 700 and 1390 AD, to see if their origins could be traced to the Pacific islands. "I thought, 'Well, we'll give it a go'," she says.

Storey and her team reconstructed a 400-base-pair fragment of mitochondrial DNA from both the Chilean bones and chicken bones excavated on five archipelagos in Polynesia. Mitochondrial DNA doesn't mutate much and so is useful for tracing evolutionary lines. The Chilean sequences were identical to those from prehistoric sites in Tonga and Samoa (A. A. Storey *et al. Proc. Natl Acad. Sci. USA* doi:10.1073/pnas.0703993104; 2007). Radiocarbon analysis dated the bones to between 1304 and 1424 AD, firmly before Europeans arrived on the east coast of South America in the 1500s. The same sequences are also present in the modern-day Araucana chicken, an odd Chilean breed that has tufted 'ears', lays blue eggs and lacks a tail.

The study has left the research community cautiously optimistic that hard evidence for migration of Polynesians has been found. Jaime Gongora, a molecular geneticist at the University of Sydney, Australia, says the paper is a significant

R. D. FLAVIN

FATHERS OF THE ZODIAC TRACKED DOWN
Astronomer shows when and where his ancient counterparts worked.
www.nature.com/news

after its retirement in 2010 and take astronauts back to the Moon, puts the telescope within reach. "If Orion is available, and we have a really simple, but significant problem on the JWST, wouldn't it make sense to ensure that astronauts could go to the JWST if they could fix it?" asks Weiler.

But the harsh radiation environment in deep space would probably make it far too dangerous for astronauts, says John Mather, the JWST's chief project scientist at Goddard. And a robot mission could probably do very little. It might be able to give the satellite a good shake to loosen a stuck solar panel, says Mather, but would be unlikely to cope with more complex tasks. And in its repair efforts, it might dirty the telescope's outer mirrors.

Mather says the JWST's team is now conducting a feasibility study to find out whether a docking port could be added. But given that it is unlikely that a problem so simple it could be fixed by a robot will surface during the mission, Mather says he is not keen to add something to the already grossly over-budget telescope. "If it costs more than a few thousand dollars," he says, "I'm not interested."

Repair missions to spacecraft closer to Earth than the JWST have so far been rare, but not unheard of. An orbiting mission to study the Sun was rescued by a service mission carried out by astronauts on the space shuttle *Challenger* in 1984. The first servicing mission to Hubble in 1993 fixed a critical error, installing a corrective optics system to fix the telescope's blurry vision. It has since been serviced a further three times. ■

Geoff Brumfiel

Disgraced official was paid work bonus

Further troubling reports have surfaced in the case of a disgraced US official accused of political interference in the workings of the Endangered Species Act. It has been disclosed that Julie MacDonald, former deputy assistant secretary for fish, wildlife and parks at the Department of the Interior (DOI), received a performance award of nearly $10,000 in 2005. Yet the report of an investigation into her conduct, released on 27 March this year, reveals that MacDonald violated federal regulations while in that position. She resigned on 1 May.

The report, by the DOI's office of inspector general, paints a portrait of a woman determined to minimize the Endangered Species Act's effect on the economy. It includes evidence from colleagues that she heavily edited science reports from the field despite having no formal scientific training, and bullied and intimidated field scientists into producing documents along the lines she wanted.

Observers say the case highlights how appointees of President George W. Bush can and have pushed political agendas within federal agencies. "She was a little bit more overt and transparent and shameless about her political antics and dealings, but she was not a lone ranger," says Jamie Rappaport Clark, executive vice-president of the environmental group Defenders of Wildlife in Washington DC and former director of the US Fish and Wildlife Service.

MacDonald was also chastised for sharing "nonpublic information with private sector sources", including a nonprofit lobby group called the California Farm Bureau Federation; the Pacific Legal Foundation, a law firm that represents development interests; and a friend from an online game. The report outlines how she sent internal departmental documents to a friend in the game *World of Warcraft* "to have another set of eyes give an unfiltered opinion of them". MacDonald could not be reached for comment by *Nature*.

The latest chapter comes from Steve Davies, editor of the newsletter *Endangered Species & Wetlands Report*. Davies learned through a Freedom of Information Act request that MacDonald received a Special Thanks for Achieving Results award of $9,628 in March 2005, during the period covered by the investigation. The DOI will not detail the reasons for the award; it says the justification is included in her performance evaluation, which is private.

Meanwhile, Democrats in Congress are investigating MacDonald for her role in removing the Sacramento splittail fish from the endangered species list. MacDonald owns a farm in a floodplain that is a habitat for the fish, according to an investigation by the *Contra Costa Times*, a newspaper in California. ■

Emma Marris

DEREK SASAKI/WWW.MYPETCHICKEN.COM

It's all relative: Chile's Araucana chicken shares its DNA with ancient birds from Polynesia.

contribution to the field, but warns that the small fragments obtained from ancient DNA may tell only part of the story. The final verdict will require more extensive DNA data to make a full family tree of both modern and ancient breeds, he says.

Archaeologist Terry Jones at California Polytechnic State University in San Luis Obispo, who has studied prehistoric Polynesian contact in the New World, is less circumspect. "It's essentially unequivocal evidence," he says.

Evidence of contact between the communities has been put forward in the past. In 1947, Thor Heyerdahl famously filmed his journey by raft from Peru across the Pacific to try to prove that South Americans could have settled the Pacific islands; although the theory was at odds with much of the evidence.

More recently, Jones, along with Kathryn Klar at the University of California, Berkeley, has argued that the Polynesians introduced complex fish hooks and sewn plank canoes to the Chumash and Gabrielino Indians in southern California and the Mapuche Indians in Chile (K. A. Klar and T. L. Jones *Am. Antiquity* 70, 457–484; 2005). Others argue that Polynesians must have visited the tropical coast of South America in order to bring back the sweet potato and the bottle gourd. The voyage to South America is no more daunting than other trips Polynesians are known to have made.

Even so, one of the co-authors on the chicken study, Atholl Anderson at the Australian National University, Canberra, is wary of overestimating the extent of this cultural diffusion without further study. Although the chickens provide hard evidence of transoceanic contact, the evidence that large-scale cultural exchange occurred remains largely circumstantial, he says. ■

Brendan Borrell

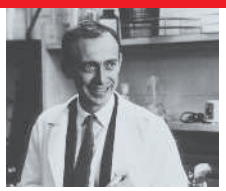

NATIONAL LIBRARY OF MEDICINE

JAMES WATSON'S DNA SEQUENCED
Discoverer of the double helix blazes trail for personal genomics.
www.nature.com/news

Genome miners rush to stake claims

This February, Laura Scott, a genetic epidemiologist at the University of Michigan, Ann Arbor, spent her holiday sitting in a ski lodge in front of her computer, "very occasionally trying to go out and ski". She was working on one of three papers that appeared online in *Science* in April, the same day that a competing group announced similar findings in *Nature Genetics*[1–4]. All four papers identify genes implicated in adult-onset diabetes, one of western society's commonest ailments. And all four are part of a new genetics gold rush that uses such 'genome-wide association studies' to flag disease-related genes. Hence Scott's indoor skiing trip: "The feeling was: 'It's gotta get out there'," she says.

As in any gold rush, prospectors are pursuing the spoils as quickly as their tools, skills and finances will allow. This week, *Nature* publishes the biggest pot of gold yet: a report tagging more than 20 genetic markers associated with seven common diseases, from bipolar disorder to hypertension, teased out from the DNA of 17,000 people (see page 661).

Science is always competitive. But human genetics is going through a particularly intense burst of activity. The race is to identify single-letter DNA variations that are more frequent in patients with common, complex diseases and thus serve as markers for susceptibility.

Technological advances that have come fully on-line only in the past 18 months are allowing geneticists to examine common diseases such as diabetes, which are caused by both environmental influences and by an unknown number of genes that contribute to different degrees. To find these small genetic influences, scientists must screen a thousand or more patients with each disease for hundreds of thousands of single-letter markers, and compare the results against similar screens of people without the disease.

Such studies are still expensive — costing, at minimum, nearly a million dollars — and there are only a limited number of strong genetic associations to be found for the most common diseases. So the race is on to be first to pick and publish this low-hanging fruit, which many expect to be collected within a year or two.

"If you've invested a large amount of money and a lot of time in doing one of these studies, you don't want to publish your paper a month after someone else has found the same things," says statistician Peter Donnelly of the University of Oxford, who is chairman of the Wellcome Trust Case Control Consortium and a lead author on today's study.

CMSP/SCIENCE FACTION

Trail of blood: many genes influence the development of common diseases such as diabetes.

Many scientists, including Donnelly, welcome the competition. A host of suspect genes published in the early days of the rush have turned out to be false positives. The way that results today are being confirmed through multiple, overlapping findings published near-simultaneously by competing groups "is fantastic for the field", says Donnelly.

"The way that results are being confirmed by multiple findings published near-simultaneously is fantastic for the field."

In some cases, the prospectors are working together in the hope of improving their claims. The authors of the three papers on diabetes that appeared in *Science*, for instance, agreed months before publication to pool their initial data to improve their chances of identifying truly significant genetic variants.

A working group at the US National Institutes of Health (NIH) that today publishes a set of proposed standards for genome-wide association studies (see page 655) stresses the desirability of simultaneously publishing independent replication of results. It notes, however, that some work may be so important as to justify its publication before it has been replicated.

The results published by Donnelly and colleagues today do not include independent replication. "The referees were unanimous that this advance was powerful enough as a landmark not to necessitate the conditions recommended by the NIH," says Philip Campbell, *Nature*'s editor-in-chief. Indeed, the pace of the field means that several other groups have already confirmed and published some genetic links highlighted in this paper.

Many of these findings will lead to genetic tests to identify those at greater risk of common disease. But tests may be of limited use without an obvious intervention, such as statin drugs for those at increased risk of heart disease. Patients must now wait for cell biologists to discover how the suspect genes do their damage — and for drug companies to exploit those findings. ■

Meredith Wadman

1. Diabetes Genetics Initiative of Broad Institute of Harvard and MIT, Lund University, and Novartis Institutes of BioMedical Research *Science* **316,** 1331–1336 (2007).
2. Zeggini, E. *et al. Science* **316,** 1336–1341 (2007).
3. Scott, L. *et al. Science* **316,** 1341–1345 (2007).
4. Steinthorsdottir, V. *et al. Nature Genet.* **39,** 770–775 (2007).

SIDELINES

ON THE RECORD

"I am not sure that it is fair to say that it is a problem we must wrestle with."

NASA administrator Michael Griffin discusses climate change on US radio.

"Global temperature is nearing the level of dangerous climate effects."

NASA scientist Jim Hansen and his colleagues express a rather different view in a recent publication.

SCORECARD

Meditation
Mitch Altman's Brain Machine (pictured) claims to induce a state of deep calm by synching users' brain activity to flashing LEDs and beeps.

Concentration
Researchers at University College London have developed a psychometric test to measure proneness to distraction. The test could help employers such as airlines that need staff able to... oh look, a chicken!

ZOO NEWS

Cock up
Britain's Royal Society for the Protection of Birds was ridiculed last week when its software automatically removed the word 'cock' from a forum posting about male blackbirds, replacing it with asterisks. Great tits (*Parus major*) are apparently still acceptable.

NUMBER CRUNCH

15 cm is the average length of an erect human penis, as determined by 11,531 measurements.

12% of men in a survey of 50,000 believed that they had small penises.

0% of men complaining of small penises in a similar study actually had a 'micropenis', defined as a flaccid length of less than 7 cm.

Sources: NPR, Atmos. Chem. Phys., makezine.com, Psychol. Sci., Daily Telegraph, BJU Intl

Diplomatic talks spur hope in Libya HIV case

Diplomats are cautiously optimistic that a deal may be within reach, perhaps by the end of June, to save the lives of five Bulgarian nurses and a Palestinian doctor condemned to death in Libya for allegedly deliberately injecting over 400 children with HIV in 1998.

Private negotiations have recently intensified between Libya and the European Union — which Bulgaria joined on 1 January — to try to find a way out of the politically charged case. Any deal would have to balance provision of humanitarian aid for long-term treatment of the infected children, and support for their families, against compromising the medical workers' defence with implied guilt. Islamic law allows for blood money to substitute for punishment.

"The talks are going in the right direction. Let's say I'm less pessimistic than a few months ago."

The medics were condemned to death on 19 December 2006. Arrested in 1999, they were first found guilty and sentenced to death in May 2004, but the Libyan Supreme Court overturned the verdict and ordered a retrial. When that retrial also found them guilty, it sparked a worldwide political and public outcry. Scientists argue that medical evidence exonerates the six, and that contaminated medical supplies and equipment caused the outbreak. This evidence was denied a hearing in court. The six have lodged an ultimate appeal to the Supreme Court, but no date has been set for this.

The case has seen many false starts, but diplomats are now cautiously optimistic that progress is being made. On 27 May, the medics were acquitted of a separate but related case of slander, for accusing police of torturing them to extract confessions.

Other political moves have been afoot. Tony Blair, Britain's outgoing prime minister, met with Libyan leader Muammar Gaddafi on a farewell trip to Africa last week. Blair's office said their discussion would include the medics' case. In public, Blair announced strengthened cooperation between the two countries — perhaps significant, as the HIV case has become an obstacle to Libya's ongoing integration into the international community.

After meeting with Blair, a representative for the infected childrens' families indicated his openness to reaching a solution. At the same time, Libya's foreign ministry issued a statement that the ongoing talks were intended "to find a solution favourable for all sides".

Nicolas Sarkozy, the new French president, made resolution of the case a foreign-policy priority in his victory speech last month. And George W. Bush, in an interview on Bulgarian

Terror terms for arsonists

Ten radical environmental activists have been sentenced over the past few weeks for a string of arsons committed in the late 1990s and early 2000s. The group, extremists claiming to be members of the Earth Liberation Front and Animal Liberation Front, targeted scientists and sites involved in activities such as logging and the culling of wild horses. As *Nature* went to press, most of the sentences had been handed out, and they ranged from 3 to 13 years.

Lauren Regan, a lawyer working with the convicted arsonists, says the sentences are "not surprising and within the realm of reasonable", but that 'terrorism enhancements' added to many sentences will make their treatment in jail much more harsh and will label them for the rest of their lives.

Remains of the day: arsonists destroyed many years' work.

J. DEARING/BUREAU OF LAND MANAGEMENT/AP

The judge in the case, Ann Aiken, ruled that crimes carried out with "intent or desire to influence, affect, or retaliate against government conduct" were eligible for these enhancements. She made it clear, though, that she was ruling only on the narrow legal question of whether the crimes fit the legal criteria for the enhancement, and not on the broader, more controversial question of whether the people involved

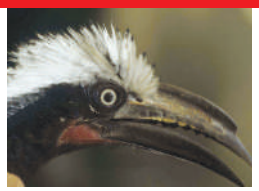

W. JETZ, UC SAN DIEGO

BYE-BYE, BIRDIE
Climate change and human intrusion converge to imperil birds.
www.nature.com/news

P. MACDIARMID/GETTY

Tony Blair's meeting with Muammar Gaddafi in Libya last week may speed progress to a resolution.

Television last week, reiterated the United States's desire for the case to "be solved quickly and in a way that is satisfactory to the Bulgarian people."

Diplomats hope that the activity might result in a resolution before a summit of European Union heads of state in Vienna on 21 June, just before Germany's presidency of the European Union ends.

"We are greatly appreciative of the very strong European diplomatic activity," says Emmanuel Altit, a member of the medic's defence team. "The talks are going in the right direction. Let's say I'm less pessimistic than a few months ago." ■

Declan Butler

should be labelled as terrorists.

One of the biggest fires, and perhaps the most memorable to the scientific community, was the torching of a building in the Center for Urban Horticulture at the University of Washington in Seattle on 21 May 2001. The fire targeted the work of Toby Bradshaw, whom the group thought was genetically engineering poplar trees. "I am delighted that the perpetrators have been caught," says Bradshaw, "and satisfied that the criminal-justice system is capable of determining an appropriate punishment."

Group members were also found responsible for torching a lab of the US Department of Agriculture's Animal and Plant Health Inspection Service (APHIS) in Olympia, Washington, on 21 June 1998. Lab worker Dale Nolte, who now works on avian flu for the service, says that he hasn't followed the trial and has no opinion on the sentencings. "My focus from the beginning was to recover our facilities, to keep up the morale of our scientists and keep the work going," he says. One of this group was sentenced to more than 12 years in prison, which included a terrorism enhancement.

The sentencing memo depicts a group of ideological activists who were not always successful at crime. Their cars broke down, accomplices dropped out at the last minute, members of the group were busted for shoplifting and time and again their incendiary devices failed to go off. Yet, according to federal prosecutors, they racked up more than US$40 million in damages between 1995 and 2001. No one was harmed during the group's actions, although many contend that this was more through luck than careful planning. ■

Emma Marris

Sibling rivalry hits Swiss institutes

Tempers erupted last week at the Swiss Federal Institute of Technology Zürich (ETHZ), with faculty members claiming that its board had sneakily siphoned its budget off to Switzerland's other federal institute, the EPFL in Lausanne.

Interim president of ETHZ Konrad Osterwalder has complained formally to the Swiss government, saying that the ETH Board — a politically independent body responsible for both universities and for four federal research institutes — "made serious errors in both the form and content of [its] decision on the allocation of the 2008 budget". Department heads at ETHZ have also asked Pascal Couchepin, the government minister responsible for research and higher education, for his support in solving the crisis.

As part of Switzerland's push to bolster its research and higher education sector, the ETH Board's budget for 2008 will be nearly 4% higher than that for this year. The board decided to give a disproportionate sum to EPFL, even though there has been no political decision about how Switzerland might afford a second top-level university, say staff from ETHZ. The staff say that the board used different starting budgets to calculate the percentage increase for each institute, and that it did not release the information within the required time before the meeting.

ETHZ also hit the headlines last November when faculty members forced its president, Ernst Hafen, to resign. Hafen had tried to implement organizational changes at the university that had been desired by the board but that the faculty members thought were detrimental to the institute.

"The source of all the problems is the ETH Board," says Kathy Rifkin, spokeswoman for the Swiss parliamentary committee on science and research. She says that parliament is discussing the abolition of the board, to bring more decision-making back into the government — most particularly decisions about apportioning the budget.

Alexander Zehnder, president of the ETH Board, says that he is surprised by the reaction. "The extra money given to Lausanne was not core money, but strategic funds used to integrate cancer research into that university plus some extra to reward the improvement in its research quality," he says. He adds that the board's procedures for budget allocation were transparent. The government has declined to comment on the dispute. ■

Alison Abbott

Bush requests $30 billion to fight AIDS worldwide

President George W. Bush is seeking to double US funding for fighting HIV and AIDS globally, requesting $30 billion to be spent over five years from October 2008. The money, which would be focused on prevention and treatment, should also benefit research projects in many of the 15 countries targeted in the developing world.

The three-year-old President's Emergency Plan for AIDS Relief, funded by the Department of State, doesn't support research directly. But the fact that it treats so many people — 1.1 million so far — "broadens the research questions that we can ask", says Anthony Fauci, director of the US National Institute of Allergy and Infectious Diseases. For instance, scientists can examine the effect of antiretroviral treatment on the progress of other diseases, such as tuberculosis.

Bush's request, announced on 30 May, is expected to be approved by Congress.

University union calls for academic boycott of Israel

Representatives of Britain's University and College Union (UCU) voted last week to call on its more than 120,000 members to consider a boycott of Israeli universities. The resolution, passed by 158 votes to 99, asks that union members "consider the moral implications of existing and proposed links with Israeli academic institutions".

The union was formed in 2006 in a merger of two of Britain's leading associations of higher-education teachers. Both these associations had previously voted to boycott Israeli universities, and then rescinded or downgraded their resolutions. The latest vote drew prompt criticism, not only from outside but also from within the union. "I do not believe a boycott is supported by the majority of UCU members," says Sally Hunt, the union's general secretary.

Plane passengers asked to check in over TB risk

The US Centers for Disease Control and Prevention (CDC) in Atlanta, Georgia, is to look at how one of its employees was involved in a case of extensively drug-resistant, or XDR, tuberculosis (TB) that triggered a health advisory to be issued last week.

The CDC announced on 29 May that a man, who has XDR tuberculosis, had taken two transatlantic flights, and that it was seeking passengers who had travelled with him. Andrew Speaker had flown to Europe for his wedding and honeymoon after being diagnosed with TB, but before learning that it was the XDR strain. He is now in hospital.

On 2 June, the CDC said that it would review the role in the matter of the man's new father-in-law — a CDC microbiologist who works in the Division of Tuberculosis Elimination. In a statement, the father-in-law, Robert Cooksey, said: "My son-in-law's TB did not originate from myself or the CDC's labs, which operate under the highest levels of biosecurity".

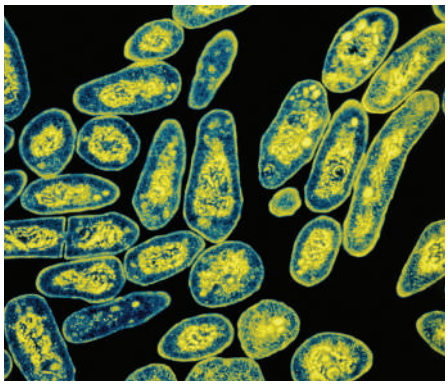

KWANGSHIN KIM/SPL

Tuberculosis bacteria that are resistant to nearly all drugs have sparked a health alert.

Foundation reasserts claims in stem-cell patents

A return shot has been fired over three key stem-cell patents that the US Patent and Trademark Office made moves to revoke in April.

Critics of the patents, which cover primate embryonic stem cells and methods for making them, have claimed that the patents are overreaching and undeserved.

On 31 May, the organization that administers the patents, the Wisconsin Alumni Research Foundation (WARF), filed its official response to the agency's decision. In this, WARF says previous research was done in mice, which was difficult to translate into human cells, and that the patented work was therefore not "obvious" — a crucial yardstick for determining whether a research advance deserves a patent.

Those who contested the patents now have a month to respond to WARF's filing, and a long appeals process could follow.

Japan's health ministry calls for tests on Tamiflu

Japan's health ministry has said that it will ask the Japanese distributor of Tamiflu to conduct tests on possible side effects of the anti-influenza drug.

Reports of strange and sometimes suicidal behaviour in people taking Tamiflu have already prompted investigations in Japan (see *Nature* 446, 358–359; 2007). The country accounts for roughly 75%

Hidden papers revealed on neutron's 75th anniversary

ROYAL SOC.

The letter shown on the right was released by London's Royal Society on 1 June, along with five packets of scientific papers that had been hidden away during the Second World War. The papers describe experiments on nuclear fission and provide details that could be used to build a nuclear reactor.

"The outbreak of war marked the end of nuclear science being a collective investigation," notes Keith Moore, the society's head of library and archives.

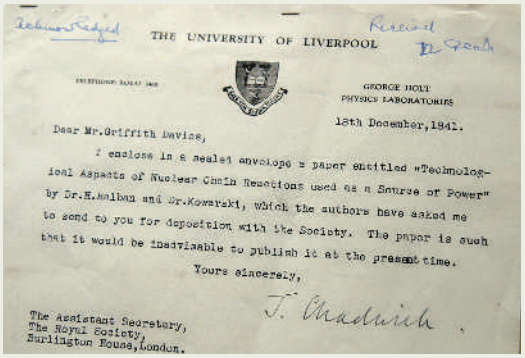

THE UNIVERSITY OF LIVERPOOL

GEORGE HOLT PHYSICS LABORATORIES

18th December, 1941.

Dear Mr. Griffith Davies,

I enclose in a sealed envelope a paper entitled "Technological Aspects of Nuclear Chain Reactions used as a Source of Power" by Dr. H. Halban and Dr. Kowarski, which the authors have asked me to send to you for deposition with the Society. The paper is such that it would be inadvisable to publish it at the present time.

Yours sincerely,

J. Chadwick

The Assistant Secretary,
The Royal Society,
Burlington House, London.

This letter accompanied one of the packets and is signed by the English physicist James Chadwick, who discovered the neutron in 1932. The papers were released to coincide with the 75th anniversary of his discovery.

of worldwide prescriptions of the drug, produced by Swiss firm Roche.

The ministry will ask Chugai Pharmaceuticals, Roche's Japanese partner, to carry out five types of *in vitro* and animal test to examine how the drug is metabolized and transported in the brain. Chugai was waiting for an official order from the ministry as *Nature* went to press; a representative said the company plans to comply with its demands.

Xtreme team takes the high road for blood tests

A team of researchers and climbers, engaged in a study of how the body responds to low-oxygen conditions, has pushed to the summit of Mount Everest.

The group didn't quite manage its goal of taking blood samples on the peak. "We decided that taking an arterial blood sample on the summit itself was too dangerous," team member Dan Martin wrote in his online diary for *Nature* on 30 May (see http://tinyurl.com/2g3mxn). Instead, members of the Caudwell Xtreme Everest expedition descended a few hundred metres to a spot where gloves could be removed more safely. This is still, they say, the highest altitude at which blood gas content has ever been examined. The team also collected data on oxygen use from subjects on an exercise bike at 8,000 metres.

They hope the data will help inform the treatment of patients back at sea level who have difficulty shunting oxygen around the body.

R. I'ANSON/LONELY PLANET IMAGES/GETTY

Everest has played host to an experiment assessing how the body copes with low oxygen.

Indo-US nuclear talks stall for a fourth time

Indian and US negotiators have once again failed to agree on a nuclear deal mooted in July 2005 (see *Nature* 436, 446–447; 2005).

The deal promises India nuclear fuel and technology from the United States, in return for India opening its civilian reactors to inspection. But, like three earlier rounds of talks, the latest discussions ended in New Delhi on 2 June without a final agreement.

Despite both sides claiming they have made some progress, sources in India's Department of Atomic Energy told *Nature* that the talks have reached a stalemate that will only be resolved at the highest political level. India wants the right to reprocess spent fuel to recover plutonium and to retain the option of carrying out nuclear tests.

Over a pork barrel

The US Congress is well-known for tucking special provisions for favoured projects into budget bills. **David Goldston** explains why 'earmarks' for research and development have risen so dramatically in recent years.

Summer is appropriations season in Washington DC. Congress is beginning to write the spending bills for fiscal year 2008, with the hope of having the House of Representatives and the Senate each vote on their versions before the August recess. The process is likely to be even more politically charged than usual: the new Democratic leadership in Congress will be trying to show that the president stints on domestic priorities, while the president will aim to paint Congress as profligate.

No doubt the age-old battle over congressional 'earmarks' will figure prominently in the effort to shape public perceptions of the budget. Indeed, this January the president called on Congress to halve the number of these earmarks, which provide money for a specific project or entity to help a constituent or friend.

Interestingly, Congress itself has been feeling a little queasy about earmarks of late. Although generally it sees earmarks as a fundamental prerogative, an egregious example occasionally makes headlines and cools the ardour for 'pork-barrel spending'. (The name alone points to the nineteenth-century origins of the practice.) The most recent case was the $200-million 'bridge to nowhere' — a project, pushed through by then-chairman of the House Transportation and Infrastructure Committee Don Young (Republican, Alaska), to link a small city and an airport in Alaska that are now connected by ferry. Congress eventually rescinded the money — but not before the span gained mythical status as a symbol of wasteful spending.

Along with other scandals, that incident led the new Congress to change the rules for earmarking as one of its first orders of business. Every earmark must now be publicly listed, along with the name of the legislator who sought it.

But 'transparency' is an odd way to limit earmarking. The whole point of earmarks is to get public credit for them — at least back home. The new rules might act as a brake on the total spending on earmarks, or on particularly embarrassing projects, but they haven't reduced the demand for pork. Members of the House have requested more than 31,000 earmarks for fiscal 2008, probably a record number.

It is safe to assume that the number of earmarks requested in research and development (R&D) programmes has grown apace. The American Association for the Advancement of Science estimates that R&D earmarks grew from about $1.5 billion in fiscal 2002 to about $2.4 billion in fiscal 2006. (Most of the earmarks were for colleges and universities.) That's not a huge number in an R&D budget of more than $140 billion, but it can put a noticeable dent in funding for specific agencies, such as the National Oceanic and Atmospheric Administration, and programmes, such as the Department of Energy's hydrogen effort. Moreover, the rate of growth is a legitimate cause for concern.

PARTY OF ONE

Why has 'academic pork' grown so rapidly? The most obvious reason is also the most often overlooked: more colleges and universities want it. Earmark requests almost always originate with the beneficiary, not with the representatives. As schools and faculty members have become more entrepreneurial, and as federal funding has come to be seen as a test of prestige, more schools have sought money — often to do the kinds of projects the government isn't otherwise funding or for programmes that aren't strong enough to win awards in traditional grant competitions. And once one school wins some federal cash from Congress, more want to play.

And there are ever more people in Washington DC who want to help them win. Lobbying is a growth industry, generally offering high salaries. It seems that no retiring congressman goes back home anymore; they all stay in Washington and lobby — looking for clients, including research institutions, and encouraging them to seek federal funds. This structural change — a burgeoning 'private sector' that needs ever more lobbying clients to thrive — makes it hard to foresee any significant reversal in earmarking trends.

Finally, Congress has bought into the notion that R&D is the key to economic competitiveness. So helping colleges and universities get some federal money is more enticing than it was when institutions of higher education seemed to have little relevance to larger political concerns. And economic development has always been a justification for pork-barrel projects.

With all the factors pushing towards growth in academic pork, the real surprise is that there isn't even more of it. Fortunately, academic pork is still viewed as somewhat suspect, especially among the congressmen who most closely follow science issues. Pork is seen as a way to salve the injustices and inadequacies in the standard grant-making process, not as a sign that the overall system is in need of surgery. Notably, what are arguably the two most prestigious R&D agencies, the National Science Foundation (NSF) and the National Institutes of Health, have never been earmarked — perhaps both an effect and cause of their prestige. (Congress does sometimes push specific large construction projects at the NSF, but those are first proposed by the agency, not Congress, and Congress does not choose where to locate them.)

That doesn't mean that there hasn't been pressure to earmark the two agencies, especially from those who see peer review as a clubby system that benefits only the 'haves'. In a happy coincidence, some of the 'have nots', often schools from the south and Rocky Mountain west, are represented by conservatives who see any form of earmarking as a kind of budgetary incontinence.

Also, Congress has tried to divert some of the earmarking pressure by setting aside competitive funds for institutions in states that do not get a large share of federal R&D funds. The programme began at the NSF decades ago, and Congress has gradually replicated it in other agencies.

So for now, academic earmarks will probably continue to grow, but not without limit. Congress is likely to remain nervous through this political cycle that too much pork will smear it with a reputation for fiscal irresponsibility. And when it comes to academic grant making, Congress still tends to believe, to paraphrase Winston Churchill, that peer review is the worst system except for all the others. ■

David Goldston is a visiting lecturer at Princeton University's Woodrow Wilson School of Public and International Affairs.

BUSINESS

Meeting in the middle

Support for copycat versions of biotechnology drugs is growing quickly in the US Congress. **Meredith Wadman** reports.

D. GRUBBS/AP

Cancer drug Avastin can help patients such as Richard Lewis — but at a cost of up to $100,000 a year.

In an immaculate, glass-fronted complex in a suburb of Seattle, Washington, more than a hundred scientists at the biotechnology company Amgen are busy cranking out a new generation of anticancer drugs, and honing manufacturing processes they hope will eventually deliver treatments to millions of patients.

And 3,000 miles away on Capitol Hill, congressman Jay Inslee (Democrat, Washington) — whose district is home to the Amgen facility — is busy with a project of his own: pushing a draft law that, he says, will enable the Amgens of the future to survive and prosper.

In April, Inslee introduced legislation that would insulate inventors of biologics — complicated, large-molecule drugs — from generic competition for 14 years. The bill is intended to fend off stricter legislation that, Inslee says, could cripple the whole industry. "We can create a pathway to lower-cost copies of biotech drugs without eliminating incentives to create breakthrough medicines," he says.

Other lawmakers see it differently. Bills introduced by Henry Waxman (Democrat, California) in the House and Hillary Clinton (Democrat, New York) in the Senate in February would allow biogenerics that are similar to brand-name biotech drugs — but not similar enough to infringe patents — to appear from the moment the original drugs hit the market. "This will lead to healthy competition and long-term savings for patients," says Waxman.

> "Leading voices are talking more about how we do this than whether we should do it."
> — Michael Werner

The bills reflect a growing momentum to get generic versions of biologics to market in a Congress controlled by Democrats since January. With the first generation of patents on biologics now expiring, and increasing public disquiet about drug prices, lawmakers say they are determined to make generic biologics a reality by writing a law giving the US Food and Drug Administration (FDA) the explicit authority to approve them for market.

In Congress, "the leading voices are talking more about how do we do this than whether we should do it," says Michael Werner, a former chief of policy at the Biotechnology Industry Organization (BIO) who now runs a consulting firm in Washington DC.

It is not only Democrats who are pushing for the change. A bipartisan group of senators, including Ted Kennedy (Democrat, Massachusetts), Orrin Hatch (Republican, Utah) and Mike Enzi (Republican, Wyoming) will next week unveil compromise biogenerics legislation that they hope to bring to a Senate vote by July. Biogenerics are "an issue whose time has come", says Craig Orfield, a spokesman for Enzi.

Finding a bill that can pass into law will involve balancing the interests of the still-risky biotech industry with those of employers, insurance companies and patients complaining about paying tens of thousands of dollars annually for biologics.

"Without generic competition, the cost of biologics is unsustainable," claims Missy Jenkins, a spokeswoman for the Coalition for a Competitive Pharmaceutical Market, an organization of employers and health insurers lobbying for action on biogenerics.

The coalition, which backs Waxman's bill, points to the price of drugs such as Avastin (bevacizumab), Genentech's cancer drug, which costs up to US$100,000 for a year's treatment.

Those who would like to produce the copycat drugs, meanwhile, point out that the makers of standard, small-molecule pharmaceuticals have prospered, despite the Hatch-Waxman Act that opened the door to generic versions of their products in 1984. "For more than 20 years, generic medicines have been improving lives," says Kathleen Jaeger, the president of the Generic Pharmaceutical Association in Arlington, Virginia.

The biotechnology industry, however, disputes claims that generic biologics could save billions of dollars in healthcare costs, arguing that the drugs they imitate operate in a limited, niche market. It also argues that biogenerics wouldn't offer new cures or treatments.

Biotech firms are at pains to point out that their very business model will be put at risk — and patients will suffer — if Congress acts without considering the costs to innovator companies. "Wall Street will evaluate [the legislation's] impact on the profitability of investing in biologics companies," says Jim Greenwood, president of BIO. "If that's likely to decline, it will reduce the amount of investment in these companies and we will have a commensurate reduction in new and spectacular products."

Among Greenwood's chief complaints is that the strictest bills would provide innovator companies no guarantee of any period of market dominance. BIO is calling for 14 generic-free years for innovator biologics — the same period written into Inslee's bill. Last year, the European Union settled on ten years as a suitable period for biologics to be insulated from generic competition (see *Nature Rev. Drug Disc.* **5,** 445; 2006).

And it looks as though Congress will pass a law that involves a similar compromise. "If Waxman's bill is the stake in the ground for the generic companies, Inslee's bill is the stake in the ground for the innovator companies," says Werner. "I think the final product will be somewhere in the middle." ■

P. KNEFFEL/DPA

A beacon of reform

Long a symbol of East German pride, the Charité medical school is flourishing in the twenty-first-century shake-up of German universities. **Alison Abbott** reports.

The concrete high-rise of the historic Charité hospital was the pride of communist East Germany's medical sciences. Built in 1982, its 21 stories were a riposte to the Verlagshochhaus — a 19-storey tower that the Springer publishing group built close to the wall in west Berlin, and that was seen as a way to taunt people in east Berlin with visions of western freedom, progress and wealth. The monolithic response from the other side of the wall was a showcase building for a top research institute — one of the few institutes in the former republic that gave some scientists the freedom to travel abroad and provided a certain independence from the all-pervading communist ideology. The 'Charité' sign on the top of the building could be read kilometres away — a proclamation that one of the city's proudest and oldest scientific institutions stood tall in the east.

Today, the Charité still holds its head up high. Last year it was ranked top university medical school in Germany by an independent research assessment, creeping ahead of schools in Heidelberg and Munich. Much of its success is due to its having grabbed, with an alacrity not shown by most other universities, the opportunities offered by recent government reforms.

Founded in 1710 as a plague house outside the city gates, the Charité was later converted into a hospital, and developed close links with the University of Berlin (now Humboldt University). It was the intellectual home of, for example, Rudolf Virchow, the father of modern pathology, and Emil von Behring, the bacteriologist who discovered the diphtheria toxin. The Charité officially became Berlin's university hospital in 1927.

This was a time when Germany was the world leader in science and medicine; when it was unthinkable, for example, that anyone planning a research career would not learn German. But only a few years after the Charité won its university hospital status, the Nazis came to power, and by the end of the Second World War the picture had changed entirely. Physical and moral destruction had left the country's scientific landscape in ruins. The Charité's historic buildings had to be rebuilt brick by brick from the rubble. Reading German would never again be compulsory for scientists from Chicago to Shanghai.

On both sides of the wall, German science eventually recovered from the war and from the subsequent shock of reunification. Today the country's scientific impact is among the world's top five, thanks in large part to the network of Max Planck Institutes that serves as home to the majority of Germany's most-cited scientists. But the country's politicians think that things would be even better if the university sector, too, were to house similar excellence. They are aware that Germany boasts no heavyweights to rival the giants of Cambridge in Massachusetts — or, closer to home, of London or Paris. Although Germany spends more on research than either France or the United Kingdom, Heidelberg, Munich and Berlin do not shine in the world rankings. German universities rarely feature in lists of the top 50 worldwide.

The shackles holding back the universities, critics say, were forged from a mixture of traditional stodginess and utopian zeal. In the post-war years, the strong hierarchy within German universities meant, among other things, that young scientists were rarely able to run their own research. Herr Professor — or the very

occasional Frau Professorin — made all the decisions, applied for all the research grants and received guaranteed levels of research money from the university, no matter how productive he, or she, happened to be.

The spirit of '68 and the political awakening it brought to Europe's students dovetailed with the postwar generation's concern that many of those in charge of the universities had served the Nazi regime. The result was a drive to democratize academia. For example, student, administrative and technical representatives were included on all university committees, including the selection boards for faculty appointments. Decisions became painfully slow. The university president had very few powers, and it was never clear who was responsible for anything. "It is really time to say goodbye to this collective irresponsibility," says physicist Jürgen Mlynek, former president of Humboldt University, where the professors have a majority of just one in the highest academic committee, the senate.

M. SCHREIBER/AP

Former research minister Edelgard Bulmahn helped remove barriers to innovation and reform.

All things being equal

In the 1970s, a series of developments enshrined the concept of the 'equality of universities' in law. A degree from one university was supposed to be as good as one from any other university and the law prevented universities from selecting their own students and from charging for tuition. The roughly equal funding of the roughly equal universities provided adequate education for all but it didn't promote competition or innovation.

And some of the biological sciences suffered other political constraints. The idea of genetic engineering was mostly rejected — an understandable reaction to the appalling abuses of Josef Mengele and his cohorts — and that held back the development of molecular biology. The first German factory for producing genetically engineered human insulin was supposed to open in the early 1980s, but was famously delayed for nearly a decade. Although the regulations for genetic engineering are now in line with those elsewhere, research on embryonic stem cells remains among the most restricted of European countries.

Meanwhile in eastern Germany, research had been more or less stamped out of most universities. The freedom of thought it required was not seen as sitting comfortably with the teaching of young minds. Most research took place in the Soviet-style institutes of the German Academy of Sciences. The Charité was one of the few institutions spared.

In the 1990s, reunification, with its bankrupting costs, forced the restructuring of East German institutes. The upheaval also provided an opportunity to take a closer look at the stagnating system in the west, and in particular at the perceived loss of the best young researchers to the United States.The result was a series of schemes to enliven the universities, for example by cutting the time it took students to graduate and by increasing competition between institutions. But the effect of federal initiatives is limited by the 16 state governments that hold sway over Germany's 100 or so research universities.

In 2001, the research minister at the time, Edelgard Bulmahn, pushed through legislation aimed at removing the obstacles to innovation and reform that had been put in place by some of the state governments. Among its provisions was a new salary system for professors that allowed performance-related pay. Another important reform was the creation of fixed-term 'junior professorships' also paid for by the federal purse. These independent positions have allowed 1,145 young academics to set up their own research groups at a university. At the same time the *Habilitation* qualification required for university teachers stopped being mandatory, removing years from potential qualifying times.

Competitive streak

Since 2001, the federal government has succeeded in forcing research organizations over which it has more direct control, such as the Helmholtz Association (see 'Uncoiling the dead hand', page 633) to become more competitive. But despite the relaxation of rules on salaries, *Habilitation* and hiring of young academics, the universities were not obliged to change their ways, and at first most didn't — even when some state governments, such as those of Bavaria, Baden Württemberg and North Rhine-Westphalia, joined the reform bandwagon and passed local laws that encouraged their universities to modernize and to use their budgets flexibly.

The Charité, by contrast, has been one of the few universities to take up all opportunities for reform without hesitation. Unlike many of its counterparts in western Germany, the medical school was never burdened by inertia. Quite the opposite — it had been turned upside down and inside out by reunification. Alongside major restructuring, the Charité staff had their political backgrounds examined: those found to have collaborated with the Stasi to the detriment of

A. PALIEGE & E. SCHOTT

Flexibility at the Charité

With her PhD and medical qualifications, Seija Lehnhardt (pictured) could have carried on working at Harvard Medical School. There she would have found a way to divide her week sensibly between the clinic and research. Most institutes in Germany don't have such flexibility. Clinicians work under rigid employment conditions that mean that lab work has to be relegated to evenings and days off — a system that some say explains why so much of the clinical research in the country is poor.

But Lehnhardt wanted to return to her family and friends in Germany, while

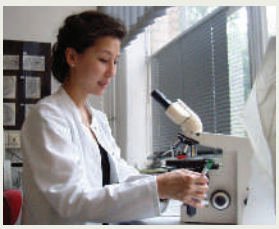

continuing her research and qualifying as a neurologist. The answer was to be found at the Charité University Hospital in Berlin (see main text), where a flexible attitude to financing and the support of her clinical chief allows her to work part time on an unorthodox contract.

The Charité has set aside funds to promote the careers of female scientists. A Rehel-Hirsch fellowship pays Lehnhardt a full-time salary as a researcher and provides support for her small research group, which works on the brain's immune system. That allows her to work 'unpaid' in the Charité's neurology clinics for three days a week — work that will allow her to qualify in her speciality.

She sees herself as a fortunate exception in a system that makes it hard for clinician-researchers to do either job well. "In Boston I knew a lot of happy people doing clinics and research — I don't see a lot of happy people in this situation here." **A.A.**

their colleagues were dismissed. Many others were dismissed simply because of massive overstaffing, particularly among the technical-support staff.

Joining forces

Staff morale might have been low, but funding prospects were better at the Charité than at the two medical schools of the Free University in west Berlin, which lost their lavish federal subsidies in the cutbacks after reunification. In 2003, the cash-strapped Berlin state government decided to merge the city's medical schools under the umbrella of the Charité, making it a university in its own right, but demanding an additional 33% budget cut to be phased in by 2010.

The fresh if traumatic start forced on the Charité made it easier to make the necessary changes. Commercial activities, such as clinical-trial services, add 10% to the €200 million (US$270 million) budget it gets from Berlin's state government. And it is pulling in enough grant money to make up for the reduction in state funds. "The early years after reunification were psychologically difficult on both sides," recalls Detlev Ganten, head of the merged medical schools. "But I'm optimistic now — we are really starting to identify with the scientific spirit in Berlin before the Nazi period."

To weaken the rigid academic hierarchy, whenever any academic staff left the Charité, Ganten pooled their institutional money and support staff and used the shared resources competitively, for example to offer good starting packages for young academic staff, to improve career opportunities for women and to support top performing staff (see 'Flexibility at the Charité', page 631). Already a third of faculty resources are shared out in these ways, and the beneficiaries have to reapply every year for their share. The pool will grow further at the end of this year when all packages agreed over the decades will be cancelled and renegotiated.

Today, the Charité hosts 25 junior professorships, the highest number of any medical school. Unlike some other institutions, it has appointed to those positions people whom it truly intends to see tenured at the end of the process. Elsewhere, the reforms have been less impressive. By 2004, only two-thirds of the junior professors had gone on to get tenured positions, fewer than had been anticipated. Most universities didn't want to offer the few open faculty positions they had to junior professors (see 'The Emmy awards').

Detlev Ganten is head of the expanded Charité medical school.

HAFFNER|CHARITÉ UNIV.MED. BERLIN

Attractive incentives

In 2005, the federal government adopted new tactics and decided it could best persuade universities to adopt reforms by dangling carrots — in the form of competitions that could be won only by universities able to attract the best students and faculty and to network effectively with their neighbours. The most influential of these competitions is the massive three-part Excellence Initiative — €1.9-billion over 5 years. For comparison, the country's science-funding agency, the DFG, has an annual budget of €1.3 billion.

The initiative is now halfway through. Eighteen graduate schools and seventeen 'clusters of excellence' have been rewarded in the first funding round. The initiative can name up to five 'élite universities' from among the winners of the other categories. In the first round, three universities — two in Munich and one in Karlsruhe — earned the élite label. This should mark the end of the pervasive myth that all German universities are equal. "The competition has challenged the dogma of equality, making the difference between universities apparent," says Peter Strohschneider, chair of the German Science Council in Cologne. "A new paradigm in Germany science policy has been established and it has far-reaching effects for the whole university system."

"The competition's really put new momentum into all the universities," says DFG president Matthias Kleiner, whose agency is helping to administer the initiative. "For one thing it got people interacting — faculties had previously behaved like little kingdoms but they had to cooperate for the Excellence Initiative."

The Charité is already reaping the benefits of the more competitive structure it has created. It won an Excellence Initiative award for its graduate school in neuroscience — the Berlin School of Mind and Brain — worth €1million a year for five years, and has been short-listed in the second round, to be decided this autumn, for a neuroscience research cluster worth around €6.5 million per year for five years. This success adds to a prestigious award

The Emmy awards

The Emmy Noether awards are run by Germany's main funding agency, the DFG. They aim to encourage young German scientists working abroad to come home.

This spring, *Nature* surveyed this year's 77 award recipients about their attitudes to Germany as a place to do research. Of the 55 that responded, more than half described Germany as being either as attractive or more attractive to young scientists as the countries they had left. "I find conditions surprisingly good," says biomathematican Korbinian Strimmer, who spent two years as a postdoc in Oxford, UK, and now works at the University of Leipzig in Germany. "Right now the intellectual climate is better in the United Kingdom, but Leipzig is getting very interesting, and the critical mass is now arriving."

However, more than half the recipients judged university hierarchies to be more intrusive in Germany than in the country they had left, and more than a third said that they thought the *Habilitation* qualification was still important for their career in Germany. Many complained that the effect of performance-related pay has been to lower salaries, because the basic rate has been reduced and the universities are tight-fisted with bonuses.

"In practice, this reform has served only to cut costs — it is a battle for scientists to get the same salary they had before," says 38-year-old Joachim Hermisson, who leads an Emmy Noether group in population genetics at the Ludwig Maximilians University of Munich. **A.A. & S.S.**

it won from the federal research ministry last year to create the Berlin-Brandenburg Center for Regenerative Therapies, which comprises 23 research groups and is funded with €45 million over four years. Also last year it was ranked top German medical school in impact and grant money by the independent Bertelsmann Foundation in Gütersloh.

Slowly but surely

Some of the older Charité professors were not happy with the rapid pace of change, says Ganten. But the young faculty members are. "I'd be a liar if I said the atmosphere here was quite the same as San Francisco and Berkeley but there is already a huge difference compared with when I studied here in the mid-1990s," says Charité neuroscientist Dietmar Schmitz. "It's getting there slowly."

Schmitz returned to Germany in 2002 with both a junior professorship and an Emmy Noethar award, designed to attract back emigré scientists, and now has tenure and coordinates the Charité neuroscience cluster. Two main things attracted him back from the United States. "The Charité offer was tenure track with a good package," he says. And he was aware of a growing neuroscience buzz around the city and its academic community. The city had chosen neuroscience as a focus and built up appropriate infrastructure. Top neuroscientists had already started to arrive there from elsewhere.

R. LURZ

Cosmopolitan Berlin: Charité researcher Christian Spahn discusses his work with Venezuelan colleague Francisco Triana-Alonso.

"German universities are getting more professional," observes Christian Spahn, a structural biologist with tenure who also joined Charité as a junior professor in 2002 — despite the offer of a faculty position in the United States. He is now being courted by other German universities and knows he will get the facilities he needs to match his research ambitions. But Spahn doesn't think that the changes in Germany go far enough in trying to improve competition. "What we really need now is for funding agencies to introduce [payment to cover] overheads," he says, "so universities know that if they employ a good scientist he or she will bring in regular money — more regular than the occasional competition like the Excellence Initiative."

As things gradually improve for German universities, the Charité is planning to upgrade its concrete high-rise to celebrate its rise in status. An €86-million restoration project has been launched to give it a new façade and seven additional floors. The reasons are practical — the medical school needs more space. But the extension and expansion are not without their own propaganda purpose. The newly heightened building will go by the name of the Leuchtturm der Lebenswissenschaften Berlin — the Beacon of Life Sciences. ■

Alison Abbott is *Nature*'s senior European correspondent. Additional reporting by Sophie Stiegler.

See Editorial, page 613.

Uncoiling the dead hand

Germany's Helmholtz Association runs 15 large national research centres addressing a range of government priorities. The association has acquired a reputation for stodginess and civil-servant mentality, and with federal money providing 90% of its income, it was a prime target for Germany's reforms. A bill introduced in 2001 (see main story) aimed to make the research centres more competitive and responsive to changing government strategies, and the association's drive to implement these changes has been ruthless.

Then-president Jürgen Mlynek changed the system from a guaranteed budget for every centre to one in which the entire €1.6-billion (US$2.2 billion) annual budget is pooled into strategic areas from which scientists must apply for support. The strategic value and quality of the research proposals are evaluated by panels of experts, half of whom are foreign. Less than 5% of the allocations have shifted since the practice was introduced in 2001, but some research areas have received a big boost. Financing of energy efficiency, for instance, has increased by 15% and the budget for photovoltaics has doubled.

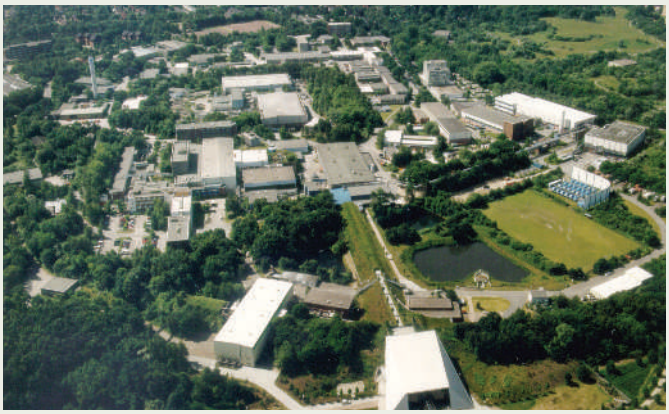

DESY

Mlynek has partitioned off an annual €25 million, rising to €60 million next year, for a president's initiative fund, which allows him to indulge in some social engineering he thinks is much needed. For example, centres that appoint women to top positions get a million-euro top-up, and the fund also finances up to 100 tenure-track junior research groups.

The president's fund also supports, with €10 million over 5 years, a suite of 'Helmholtz alliances' between centres and universities. The 'Physics on the Terascale' alliance includes the particle-physics centre DESY in Hamburg, the Research Centre Karlsruhe and 17 German universities. Its strategic aim is to keep the German particle-physics community, about to lose the country's main particle accelerator HERA at the DESY lab (pictured), in good enough shape to exploit the Large Hadron Collider at CERN in Geneva when it starts pumping out the particles in 2008. **A.A.**


J. ERIKSSON

Peaceful primates, violent acts

Brought up in the Congo basin, Jonas Eriksson has worked through a war and battled poachers to help reveal the secrets of bonobo societies. **Carl Gierstorfer** reports.

In 1998 in Lomako, a study site in the northwestern Équateur province of the Democratic Republic of Congo, a peace-loving primate closely related to the chimpanzee showed its darker side. A group of bonobos (*Pan paniscus*) was feeding when a male started to act aggressively towards a female with an infant — an unwelcome act in the typically female-dominated primates. Suddenly, all hell broke loose. The females banded together to attack the male, and beat him viciously for more than a half hour. The other males fled, and the wounded aggressor disappeared, never to be seen again.

The event epitomizes a paradox in bonobo societies. DNA studies[1] done at the site have shown that the females aren't related, so cooperation would not benefit their kin directly. So why would females cooperate to exclude aggressive males? That is one thing that Gottfried Hohmann and Barbara Fruth from the Max Planck Institute (MPI) for Evolutionary Anthropology in Leipzig, Germany, had been studying at the Lomako site for eight years before the thrashing. But soon after the incident, violent raids from a different primate — human rebels from nearby Rwanda — evolved into a full-blown war that eventually reached Lomako and forced the researchers to leave.

A year before the event, Jonas Eriksson (pictured above), a former graduate student at the University of Uppsala in Sweden had joined the research team. The son of Swedish Baptist missionaries, Eriksson had spent his childhood in the pristine forests of the Salonga National Park in the central Congo basin and had gained a detailed knowledge of the region. While working on his degree, he learned about primate behaviour and field studies. The softly spoken 38-year-old says that he thought of his childhood hunting trips with bow and poison arrow and knew he could contribute something to the field. He was to prove instrumental in keeping the research going during the crisis.

> **"Many researchers overestimate genetic relatedness when they see cooperation."**
> — Brenda Bradley

In 2000, Hohmann and Eriksson set out on a trip worthy of Henry Morton Stanley's epic exploration of the Congo basin in the 1870s. They combed the better part of the bonobo's range — around 200,000 square kilometres — by foot and bicycle, hunting for bonobo faeces, scooping them from the forest floor, sealing them in plastic bags and sending them to Leipzig to sequence their DNA. Although a dirty job, this way of collecting DNA samples puts as little stress on the bonobos as possible. Their analysis of 34 males from four distinct sites[2] showed that males from the same site had more similar Y chromosomes than did those from different sites, indicating that related males stay together, as they do in chimp societies. But mitochondrial DNA from these males, which is inherited down the female line, did not show such clustering, indicating that females tend to leave the group. Combined with their observation that females will work together to maintain their dominant status within their society, these findings further challenged the idea that genetic relatedness plays any part in female cooperation.

Brenda Bradley, an evolutionary geneticist at the University of Cambridge, UK, says that many researchers realized that they were "overestimating genetic relatedness when they see cooperation." Eriksson and colleagues' work helped to clarify that issue by providing data on long-range gene flow in the apes, she says.

Chimpanzees (*Pan troglodytes*) have a similar kinship pattern but behave differently. Like the bonobos, female chimps in a group are

generally unrelated. But unlike the bonobos, chimp societies tend to be dominated by the males. Whereas violent encounters are the norm in the chimp society, conflicts such as that observed at Lomako are rare in bonobos. Perturbations to bonobos' social order are generally defused through sexual acts, often in homoerotic encounters between females.

Secret for success

Eriksson and Hohmann had been hunting for more than just bonobo droppings on their trek. They had also been looking for a new study site and settled on the southern reaches of Salonga National Park. Eriksson's mastery of the Congolese language and culture were integral to securing permission from villagers to use the site. "He has a strong emotional attachment to Congo and the Congolese people," Hohmann says.

Fruth says that she admires Eriksson's ability to penetrate the Congolese culture. But his intimate link also has its downsides: Fruth says that Eriksson's 'Congolese' way of approaching things means that he refuses the pace of the western world and prefers a more laid-back lifestyle. "He has to be pushed to bring things to an end," he says. Nevertheless, the team managed to secure the study site in 2000, and work could resume. For Hohmann, Fruth and Eriksson, a new opportunity to explore the bonobo paradox began to take shape.

The researchers think that the cooperation between unrelated females to keep aggressive males in check was to protect against infanticide, which is common in male chimps — bonobos closest relatives. Moreover, the females may pool their efforts to collect high-value resources such as meat. Hohmann and Fruth have found that at Salonga, meat consumption is much more pronounced than previously thought in the normally fruit-eating apes. The prey is caught by females, possibly even in groups, and males rarely share in their spoils — a striking contrast to chimpanzees. "They are just sitting there, begging for meat, or even guarding the kids only to score well with the females," Fruth says.

The lack of male aggression could be down to the plentiful supply of good-quality resources. Meat might be a delicacy enjoyed only by the females, but fruit is abundant and sex is readily available, reducing the need for competition.

F. LANTING/FRANS LANTING PHOTOGRAPHY

Bonobos cooperate more than genetics predicts.

But while Eriksson was in Leipzig sequencing the bonobo droppings, a new problem erupted. The bitter war that shook the country and cost an estimated four million human lives had ended, but leftover weapons were being put to use in the bush-meat trade.

"Suddenly, in 2005, I got these reports from my friends in Congo that the poachers were coming closer and closer to that area that's really fond to me," says Eriksson. For more than two years poachers had been moving steadily into the Salonga National Park, mainly targeting the abundant and easy to kill red colobus monkey. "They pick them off like fruit," Eriksson says. As colobus numbers dwindle, the bonobos are more likely to be targeted.

Trading places

So, with support from his mentors, Eriksson abandoned his research to protect the site. He convinced local park rangers and villagers to help him chase out the poachers, armed with automatic weapons. "I think the combination of being foreign, white-skinned, but speaking to them in a way that penetrates their culture and language is the key," Eriksson says. His approach has been effective in keeping the poachers out of the study site, at least for now.

Having put down his pipette for an AK-47, Eriksson says that he's determined to return to science, but not necessarily in the same role. "I probably won't spend too much more time in a lab; it's a waste of time. There are other people who are much more skilled than me." Hohmann chides that Eriksson's "academic ambitions are easily outrun by his liking for adventures". Nevertheless, Salonga is still in danger and the conflict is bound to escalate as the poachers take greater risks. Eriksson says that he has already received death threats.

Having seen their Lomako site collapse, the team is determined to hold on to the one in Salonga. Too many questions remain about how bonobos manage to avoid violent conflicts. Ironically, saving the peaceful bonobos from the poachers may require more aggressive displays. Eriksson says: "I did not spend years studying to run around in the forest with a Kalashnikov and my finger on the trigger. But emotionally, it is very easy to convince myself that these steps are necessary. I have to try to do something." ■

J. ERIKSSON

The bush-meat trade is starting to threaten the bonobo study site.

Carl Gierstorfer is a freelance writer in Berlin.

To see a video of Jonas Eriksson discussing his work, see http://tinyurl.com/ywnv47.

1. Gerloff, U., Hartung, B., Fruth, B., Hohmann, G. & Tautz, D. *Proc. R. Soc. Lond. B* **266,** 1189–1195 (1999).
2. Eriksson, J. *et al. Mol. Ecol.* **15,** 939–949 (2006).

Those who are crossing boundaries need less talk, more help and flexibility

SIR — Interdisciplinary, cross-disciplinary, multidisciplinary and transdisciplinary research are increasingly perceived to be at the frontier of science. But as Adina Payton and Mary Lou Zoback point out in Recruiters ('Crossing boundaries, hitting barriers' *Nature* **445,** 950; 2007), it is not clear how the scientific community can gain from their evolution.

Despite a shift towards an interdisciplinary research culture, we are yet to grapple with how to support a growing number of interdisciplinary researchers. As interdisciplinary postgraduate research students, we face this reality head-on.

We have found it difficult to synthesize the separate perspectives of two or more disciplines into a meaningful middle ground. Unless the scientific community identifies strategies for supporting interdisciplinary researchers to negotiate this middle ground, little progress can be made. Here we suggest two useful approaches.

First, interdisciplinary researchers are expected to develop a different skill set from that of their single-discipline colleagues. In this 'interlocker' role, they engage in a shared conversation between disciplines and work through the tensions this creates. This is more than simply negotiating the different languages and ways of working — it is about appreciating a breadth of knowledge in theory, approach and discourse.

Unfortunately, few systems accommodate this type of researcher — as is sadly demonstrated by emerging frameworks designed to assess research quality in New Zealand, the United Kingdom and Australia. Interdisciplinary committees are needed to assess research proposals, to review grant applications and to examine theses. This would be more effective than the current practice of putting interdisciplinary researchers in assessment 'silos' where they are unrealistically measured against, and by, people in a single discipline.

A second challenge is the disjunct between, on one hand, rhetoric encouraging interdisciplinary research and, on the other, the lack of institutional structure and support for it. Although we are encouraged to work in interdisciplinary environments and to join interdisciplinary research clusters, we face numerous administrative hurdles. Cross-enrolment of interdisciplinary students is seldom acknowledged, and adequate resources and structures — such as guidance on writing for interdisciplinary audiences, or longer candidatures for postgraduate students — are rarely provided to support the interdisciplinary researcher.

It would be simple for institutional leaders to ask current interdisciplinary researchers about the challenges they face and to document these issues. These leaders could then address the issues by formalizing the interdisciplinary researcher role and reducing demands to satisfy the needs of multiple disciplines. Supportive environments must be created if we are committed to achieving interdisciplinary research goals.

James A. Smith*†, Gemma E. Carey*‡
*Discipline of Public Health, School of Population Health and Clinical Practice, University of Adelaide
†Discipline of Medicine, School of Medicine, University of Adelaide
‡Discipline of Anthropology, School of Social Sciences, University of Adelaide, South Australia 5005, Australia

Readers are welcome to comment at http://blogs.nature.com/nautilus/2007/06/creating_an_interdisciplinary.html

Limitations of molecular genetics in conservation

SIR — Your News Feature 'The species and the specious' (*Nature* **446,** 250–253; 2007) provided an interesting assessment of recent research on genetics, species taxonomy and conservation.

Although mitochondrial DNA (mtDNA) and other molecular genetic data are informative, they must be viewed in the context of natural history and population biology. A strictly phylogenetic approach using genetic data may not consider the limitations of gene phylogenies or the relevance of organism-level data. The sciences of systematics, population genetics, phylogenetics and taxonomy require assessment of different types of data. As you note, boundaries between groups within species are not always clear, which has led to extensive assessment of the appropriate units for fish and wildlife management and conservation. I suggest that management should focus on a species' occurrence in geographical areas rather than seemingly endless debate over vague terms such as genetic discreteness or evolutionary legacy, and proliferation of new intraspecific terminology for what are essentially populations.

One example of this debate is provided in your News Feature, in which you note that there is similar mtDNA in polar bears and brown bears that brings their status as species into question. However, morphology, behaviour and habitats show these to be different species regardless of their mtDNA relationship; therefore management of polar bears and brown bears as separate species is appropriate.

The limitations of genetic data are apparent from the contrasting patterns of similar mtDNA in different species (polar bears and brown bears) and divergent mtDNA within populations of one species, black bears (M. A. Cronin *et al. Can. J. Zool.* **69,** 2985–2992; 1991).

Matthew A. Cronin
University of Alaska Fairbanks, School of Natural Resources and Agricultural Sciences, Palmer Research Center, 533 East Fireweed Avenue, Palmer, Alaska 99645, USA

Information from patent office could aid replication

SIR — Your News Feature 'The hard copy' (*Nature* **446,** 485–486; 2007) accurately highlights the limited availability of information on stem-cell research methodologies — owing to competition among labs, the commercial value of such information and space restrictions in high-quality journals — which contributes to other labs' inability to replicate and verify the results.

It might sometimes repay scientists to look beyond conventional journals for information, in this or other disciplines, particularly to patents or patent applications. Thanks to the strict enablement requirements of patent law and patent offices in relation to inventions, one can often find more detailed methodology in patent documents than in journals with severe page limits.

A very good example of comprehensive detail in certain non-embryonic stem-cell methodologies is a PCT application WO/2006/028723 (Non-Embryonic Totipotent Blastomer-Like Stem Cells and Methods Therefor), which includes surgical procedures in organ removal, isolation of cells, and composition and preparation of culture media. In this instance, the level of detail and volume of text relating to methodology far exceeds that which many peer-reviewed journals can accommodate.

Some journals publish methodology and protocols online as Supplementary Information to the main paper or in separate publications (an example is *Nature Protocols*, which encourages user comments). Often, though, journals are only starting points in complex paper trails related to methods. In these circumstances, patent documents could contain the most methodology related to an invention in a single document.

Harry Thangaraj
Centre for the Management of Intellectual Property in Health Research and Development (MIHR), Oxford Centre for Innovation, Mill Street, Oxford OX2 0JX, UK

Science publishing issues of interest to authors are regularly featured at Nautilus (http://blogs.nature.com/nautilus), where we welcome comments and debate.

BOOKS & ARTS

Scot on the rocks

Hugh Miller — Stonemason, Geologist, Writer
Michael A Taylor
National Museums of Scotland Publishing: 2007. 144 pp. £12.99

Philippe Janvier

The Cromarty Firth in Scotland currently harbours huge oil-drilling platforms. At night, the town of Cromarty offers a spectacular ballet of illuminated Eiffel Towers swaying silently on the sea, opposite the shore where, around 1830, Hugh Miller (1802–1856) took his first steps in geology by collecting fossils. The oil from the North Sea and the platforms are symbols of utilitarian geology, but few people today know of Miller's role in defending and popularizing the notion of long geological time and the use of fossils for dating rocks, thereby making Victorian economists realize that "geology... has also its cash value".

Michael Taylor's *Hugh Miller* is a remarkable account of the life of this extraordinary Scotsman, known by scientists for his role in the early history of palaeontology and geology, and by Scotsmen for his writings about Scottish folklore, history and nature, as well as for his role in the disruption that led to the birth of the Free Church of Scotland (the 'Kirk') in 1843. Much has been written about the various aspects of Miller's life, but often in an unbalanced way, focusing on nature, society or religion. Taylor's biography provides an outstanding synthesis of all the facets of Miller's activities, from his childhood in Cromarty, his manual labour as a stonemason and his discoveries as a self-taught palaeontologist, to his career as editor of the newspaper *The Witness* and his suicide in 1856. Moreover, this book draws heavily on Hugh Miller's writings and letters.

Taylor reconstructs the character: how Miller, draped in plaid, rambled in search for fossils or inspiration, and how he behaved in family life or when socializing and debating "Kirk" questions. This gives colour to the austere text and engravings of his books *Old Red Sandstone* (1841), *Footprints of the Creator* (1849) and *Testimony of the Rocks* (1857), which are classics in Britain and among the Scottish diaspora worldwide, and are masterpieces of Victorian popular science.

Miller's previous biographies seeded some myths that Taylor refutes. For example, Miller did not become interested in fossils because he was a stonemason in his youth, since the stones he carved were generally barren. Also, he did not commit suicide because he could not reconcile the long geological time with Genesis,

G. THOMSON/FREE CHURCH OF SCOTLAND

Hugh Miller, reporting for *The Witness* newspaper on the launch of the Free Church of Scotland in 1843.

Taylor argues, nor because he was depressed by the disastrous causes of the Highland Clearances. He was simply overworked and suffered from a brain disorder that caused him unbearable headaches and dreadful nightmares.

Miller's interest in geology was triggered by his findings on the shore of the Cromarty Firth, notably of the strange 390-million-year-old armoured fishes in red sandstone from the Devonian period, whose anatomy was then mysterious. John Malcolmson, a learned amateur naturalist, introduced Miller to the great names of geology and palaeontology, such as Roderick Murchison and Louis Agassiz, who confirmed that his findings were the earliest fishes known at that time.

Miller was fascinated by these fishes from "a different creation", now known as antiarchs (*Pterichthyodes*) and arthrodires (*Coccosteus*) and, as he was a talented artist and a remarkable observer, he provided the first reconstructions of their bony armour, which Agassiz praised. Encouraged by this international recognition, Miller developed a tremendous interest in the relative age of rock layers and the fossils they contain. This field of geology, now called biostratigraphy, had just begun to be formalized and the succession of entirely different fossil animals and plants through time was generally interpreted as a series of catastrophes and new creations, an explanation that at first seemed to fit with Miller's religious faith.

However, he quickly realized that a literal explanation of this succession of creations in the light of Genesis was untenable. Rejecting the pre-darwinian, transformist ideas of his time, such as Jean-Baptiste Lamarck's or Robert Chambers', he took Agassiz' views of the 'three-fold parallelism' as evidence for a divine plan. He believed in the classification of living beings based on the hierarchy of the characteristics — the more general the characteristics, the earlier they appear in time and the earlier they occur in the embryo. By this reasoning, the earliest fossil organisms, being closer to Creation, were, like early embryos, more 'perfect', whereas their living representatives, like adults, were 'degraded'. This idea of the 'progress of degradation' was widespread among naturalists of that time and at odds with

the darwinian view of evolution as a progress toward adaptation and fitness.

Miller died three years before Darwin's *Origin of Species* was published. He is, as Taylor puts it, "regarded as a loser in the crucial evolutionary debate... That is simply because it never really began in Miller's lifetime." But Miller, along with other contemporary palaeontologists, paved the way to evolutionary concepts. All that was missing was a process that did not need divine intervention, and Darwin provided it.

Hugh Miller is superbly written, clear and readily accessible to those who have no background in geology, palaeontology or Scottish history. It is to be strongly recommended to historians of science, lay naturalists and any reader interested in Scottish life and history. ■

Philippe Janvier is at the CNRS, Département Histoire de la Terre, Muséum National d'Histoire Naturelle, 75005 Paris, France.

Brain botch

The Accidental Mind: How Brain Evolution Has Given Us Love, Memory, Dreams, and God
By David Linden
Harvard University Press: 2007. 288 pp. $25.95, £16.95

Georg Striedter

The human brain, and hence the human mind, is not an optimal, designed-from-scratch apparatus. Rather, it is an imperfect amalgam of shoddy components. That is the central thesis of David Linden's new book *The Accidental Mind*. Neurons are slow, leaky, and unreliable — hardly ideal computing elements. The whole brain, too, is not designed to the plan of some omnipotent engineer. Instead, evolution has endowed it with plenty of 'anachronistic junk'. Which is why, according to Linden, our minds often distort reality and can lead us to act foolishly. For example, when you reach out to touch something, your brain filters out what it expects. This selective neglect of expected input allows us to focus on unexpected stimuli, but it can be counterproductive. It may explain, for instance, why pushing and shoving confrontations tend to escalate. When someone pushes you, you feel it more than when you push the other with the same force, because the sensation caused by your own push is largely, though unconsciously, expected by your brain.

Linden tells his story well, in an engaging style, with plenty of erudition and a refreshing honesty about how much remains unknown. The book should easily hold the attention of readers with little background in biology and no prior knowledge of brains. It would make an excellent present for curious non-scientists and a good book for undergraduates who are just entering into the brain's magic menagerie. Even readers trained in neuroscience are likely to enjoy the many tidbits of rarely taught information — on love, sex, gender, sleep and dreams — that spice up Linden's main argument. *The Accidental Mind* stands out for being highly readable and clearly educational. No doubt, the human brain evolved along a constrained path and is, in some respects, designed imperfectly. Linden will send that message home.

Regrettably, Linden neglects to cover some material that could have boosted his thesis.

G. GAY/ALAMY

Brain evolution: new scoops on an old cone?

Particularly interesting would have been a discussion of the various "fast and frugal heuristics" that humans use to understand the world (for example, if you recognize one object but not another, then the former is probably bigger, better or more valuable). Even though such heuristics may sometimes yield inaccurate results, they evolved because they are generally 'good enough' and faster to execute than 'optimal' cognitive strategies. This, incidentally, is why such heuristics are used by engineers to build autonomous robots. Old-style robots that try to analyse their world veridically by computing all costs and benefits of possible actions, were slow, fragile and cumbersome. The newer robots act foolishly in some contexts, but they are fast and effective in their normal terrain. In many ways, they imitate our brains.

Another area Linden oddly neglects is evolutionary neuroscience. This field has made impressive strides in the past 20 years, but instead of discussing these, Linden reiterates the now outdated theory that mammal brains evolved by adding a neocortex to a "reptilian brain core". This theory is probably false, as most experts agree that the mammalian neocortex evolved out of a structure that exists in all reptiles, though the reptilian cortex does not have the complexity or size of its mammalian counterpart. Amending Linden's analogy, one might say that human brains evolved not by the addition of new scoops to an old ice cream cone, but by the modification of pre-existing scoops. This insight would actually have bolstered Linden's thesis that brains are subject to historical constraints. More difficult to show is that the use of pre-existing parts imposes functional constraints or 'bad design'.

Linden does write about some functional constraints on human brains, such as neuronal noise. This is an interesting idea, but noisy neurons may be flawed mainly in comparison to standard computer components. A shift in perspective suggests that noisy neurons, assembled en masse, excel at overcoming component failure (that is, brain lesions). Indeed, in the rough and tumble world of real organisms, fault-tolerance may well be more vital than ultra-fast, exhaustive computing. In other words, in order to distinguish neuronal design features from bugs, we need to know the brain's performance specifications, which still remain debatable. One could reasonably argue, for example, that pushing your opponent harder than they pushed you is adaptive, or good design in evolutionary terms, because it demonstrates your physical combat strength efficiently.

Linden is right to stress that brains evolved, but hasty to conclude that they are flawed in their design. We still know too little about the brain's inner workings to judge how well it does its job. What we do know, and what *The Accidental Mind* helps us to realize, is that the human brain is not designed as many have imagined. Our brains are not hydraulic devices (as Descartes had claimed), phone switchboards or desktop computers. All those analogies are weak. Indeed, our predilection for solving problems by analogy often misleads. Still, analogical thinking probably worked well enough in our past to be selected for. Whether we view it as a boon or a bug depends on our perspective. ■

Georg Striedter is an associate professor at the Department of Neurobiology and Behaviour, Univ. of California, Irvine, California 92697, USA.

Rare insights

Madagascar's biodiversity is unique and imperilled. Separated from the mainland of Africa for 160 million years, the island is home to thousands of species found nowhere else, as detailed in *The Natural History of Madagascar*, a paperback edition of which was published in March (University of Chicago Press, $50). This hefty desk reference features expert contributions covering the history of scientific exploration in Madagascar, its geology, climate, ecology and conservation, as well as its plants, invertebrates, fishes, amphibians, reptiles, birds and mammals. The book also includes over four hundred illustrations and photos — including this one of a lowland streaked tenrec (*Hemicentetes semispinosus*), found in the forest of Andrambovato in the south east of the island. These small, insect-eating mammals live together in burrows and make subsonic calls by rustling their spines; like many Malagasy species they are losing habitat to deforestation.

H. SCHÜTZ

Cancer case histories

The Cancer Treatment Revolution
David G Nathan
Wiley: 2007. 272 pp. $24.95, £16.99

Karol Sikora

Using the histories of three of his patients, David Nathan tells the remarkable, sometimes frustrating, story of the development of modern cancer drugs. *The Cancer Treatment Revolution* is extremely well written by this retired, leading figure in the US cancer scene, who has contributed greatly to the scientific and clinical research.

Its detailed account of the history of chemotherapy is fascinating, even if it does suggest that everything was done in Boston. It is so difficult to imagine how the early human experiments could ever have been carried out in today's ethical climate. Pumping little children full of horrible drugs to obtain just a few weeks survival benefit is no fun for any doctor. But without those pioneers and the suffering children, we would not have the drugs for cancer we routinely use today.

The book gives a very readable account of the discovery and clinical development of molecularly targeted therapies over the past ten years. This has been a major triumph for the rational application of molecular biology to one of the greatest unmet medical needs of our time. We now seem to be at the beginning of a revolution — moving on from cancer treatment that blasts away malignant cells using toxic chemicals to cause widespread havoc to the patient's physiology, towards a more specific and gentler, patient-tailored approach. Converting cancer into a chronic, controllable illness now seems to be a distinct possibility. But we're not quite there yet.

The tensions between the medical community, the research funders and institutes, the US Food and Drug Administration, the pharmaceutical industry and the taxpayers have dramatically increased and are well outlined by Nathan. He clearly doesn't like the politics — stating "science policy in the Bush administration can only be described as absurd and dangerous". Wonderful stuff — in some countries he could find himself without a job, in others in jail for treason and in a few just disappear. But I'm sure most readers would like some elaboration. Nonetheless, there is no doubt that the United States has committed huge amounts of money to the war on cancer. Whether it has been a worthwhile quest remains to be seen but, as Nathan points out, it has heavily subsidized the entire biomedical research endeavour.

The biggest difficulty with this book is working out exactly who it is written for. Most patients and their carers would find it scientifically too demanding. Even with its glossary, the vocabulary is more for a *Nature* subscriber than a newspaper reader. Most of it would be simply irrelevant to any individual with cancer — of the three detailed case histories covered, two are about extremely rare conditions (gastrointestinal stromal tumour and mixed-lineage leukaemia). The emotional content all seems a little hollow — almost as though it's been added as an afterthought. Doctors on the whole shudder when they see a chapter headed "Ken's story". We tend to try to box off the human side of disease so we can get on with the business in hand: doing the best we can to cure or prolong life. When we read about the science of cancer we want it unbundled from the fear, concern and hope. There are plenty of excellent psychosocial texts around. And patients prefer a much more user-friendly and less technical communication style tailored to their precise clinical problem. There are some excellent examples of this genre from various cancer charities on both sides of the Atlantic as well as Adam Wishart's *One in Three* (Profile Books, 2006) or Rosy Daniel's "Cancer Lifeline Kit" (www.healthcreation.co.uk/kit.htm).

Maybe senior academic physicians should stick to writing about the science of cancer treatment and get others to do the popularization. Currently, the alternative medicine movement dominates the bookstore shelves on cancer. Wacky diets, bizarre relaxation exercises, crank healers and of course herbal remedies all promise a cure without any side effects. These texts are inspirational, conclusive and positive. In an era of patient choice, that seems to be what the customers really want. So while I enjoyed and learned a lot from this great account of the wonderful achievements of science and medicine, I feel it is unlikely to be a bestseller at the airport. ■

Karol Sikora is the Medical Director of CancerPartnersUK, 21 Barrett Street, London W1U 1BD.

DETERMINISM

Chaos tamed

Even though our view of the physical world has shifted from that of determinism to randomness, randomness itself can now be exploited to retrieve a system's deterministic response.

Kees Wapenaar and Roel Snieder

J. GREUNE/GETTY

In the nineteenth century, the world of physics was one of order. Pierre-Simon Laplace was a key proponent of the deterministic Universe. In this model, the future is completely predictable if one knows the forces between all particles as well as their positions and velocities at any one moment. Take, for instance, a ball kicked into a forest. The ball bounces repeatedly off the tree trunks, but if you know the original position of the ball, its velocity and the trees' locations, you can determine the future motion of the ball from the player's initial kick.

In the twentieth century, Heisenberg's uncertainty principle shattered the deterministic dream. In the quantum world, only the probabilities for events are constrained by the laws of quantum mechanics. So for an atom-sized soccer ball kicked into the forest, the trajectory is not determined, but the probability for every imaginable trajectory is.

Even for macroscopic systems, determinism did not survive into the twentieth century. At that point Henri Poincaré, in a visionary anticipation of chaos theory, showed that even tiny uncertainties in initial conditions can grow exponentially with time to make motion at a later time indeterminable, for all practical purposes. So, when the soccer ball is kicked a number of times in slightly different directions, it hits the same trees during the first few bounces at slightly different positions; but over time the trajectories diverge, and after a few bounces the ball may move in completely different ways between the trees.

So much for particles: waves behave completely differently. If a referee blows her whistle in the same forest repeatedly at slightly different positions, the sound waves scattering between the trees change much less than the motion of the ball. One reason is that waves have an intrinsic length scale, the wavelength, and any perturbations affecting the waves over this length scale are effectively smoothed out.

Recent research has shown that acoustic noise can be used to synthesize deterministic waves generated by a point source — like the whistle-blowing referee. Imagine it's raining in the forest. Every raindrop excites acoustic waves that bounce among the trees in an apparently random fashion. Nevertheless, the trees leave an imprint on the wave field that is characteristic for the forest. The unravelling of this imprint turns out to be surprisingly simple. Let's say that, instead of a whistle-blowing referee, there are two microphones in the forest. With a standard computer operation — cross-correlation — we can reconstruct the sound of the referee's whistle from the recorded noise of falling raindrops.

Take one raindrop that falls in line with the two microphones. The sound wave it generates travels forward, reaching the nearest microphone first and then continuing to the farther one. The difference in the time it takes for the wave to reach each microphone equals the time it takes for the wave to travel between the two microphones. The cross-correlation of the sound waves recorded by the microphones produces a signal at precisely this travel time. So it is as if the first microphone acts as a source, transmitting a weak sound wave to the second. This is enhanced by other raindrops falling in line with the microphones; the rest of the raindrops do not produce a coherent signal. Taking all the coherent waves together, the first microphone acts as if it is transmitting the sound of the whistle to the second. The reproduced sound can be used for imaging — say, to determine the position of nearby trees. This principle presents the opportunity to do wave experiments without using active sources.

It has been known since Albert Einstein's seminal 1905 paper on brownian motion that the diffusion of a particle is related to the way it slows down when it is disturbed in some way. This principle was later generalized to the fluctuation-dissipation theorem, which states that for systems in thermal equilibrium, the deterministic response of the system is related to thermal fluctuations. This principle can be extended to systems so large that thermal fluctuations are irrelevant, such as the sound waves generated by raindrops falling in the forest. It has recently been shown theoretically that the principle holds for a wide class of linear systems, including electromagnetism, flowing media and quantum mechanics.

Extracting the deterministic response of a system from noise is amazing enough, but there is more. According to theory, noise sources must be distributed homogeneously throughout space, and be uncorrelated. That is, the raindrops must fall everywhere in the forest, and fall at statistically independent times and locations. Astonishingly, in many applications the extraction of the system response from noise is fairly robust when noise sources are limited and irregularly distributed, probably because of the stability of wave propagation.

Our view of the Universe may have shifted from the deterministic to the random, but since the turn of the last century physics itself has provided a less simplistic view. Fields generated by random sources can be used for imaging and for monitoring of systems such as Earth's subsurface, or of mechanical structures such as bridges. Randomness is no longer at odds with determinism, it has instead become a new window on the deterministic response of the physical world. ■

Kees Wapenaar is in the Department of Geotechnology, Delft University of Technology, PO Box 5048, 2600 GA Delft, the Netherlands.
Roel Snieder is at the Center for Wave Phenomena, Colorado School of Mines, Golden, Colorado 80401-1887, USA.

FURTHER READING
Berry, M. V. *Proc. R. Soc. Lond. A* **413,** 183–198 (1987).
Snieder, R. K. & Scales, J. A. *Phys. Rev. E* **58,** 5668–5675 (1998).
Snieder, R., Wapenaar, K. & Wegler, U. *Phys. Rev. E* **75,** 036103 (2007).
Weaver, R. L. *Science* **307,** 1568 (2005).

CONCEPTS

NEWS & VIEWS

GENOMICS

Guilt by association

Anne M. Bowcock

In a tour-de-force demonstration of feasibility, a consortium of 50 research teams uses 500,000 genetic markers from each of 17,000 individuals to identify 24 genetic risk factors for 7 common human diseases.

Mr Woodhouse, the comical hypochondriac of Jane Austen's *Emma*, takes great comfort in blaming his various ailments on the rain, the cold and an unfortunate piece of wedding cake. He would, no doubt, have been greatly surprised to learn that even his most rudimentary ailments resulted, at least in part, from genetic factors. Reporting on page 661 of this issue[1], a consortium of more than 50 British groups, known collectively as the Wellcome Trust Case Control Consortium (WTCCC), asserts just that. In the largest study of its type so far, the WTCCC has examined the genetic underpinnings of seven common human diseases: rheumatoid arthritis, hypertension, Crohn's disease (the most common form of inflammatory bowel disease), coronary artery disease, bipolar disorder — also known as manic depression — and type 1 and type 2 diabetes.

The WTCCC study is groundbreaking in various respects. It not only confirms the involvement of some genes for which disease association has previously been reported, but it also identifies several novel genes that affect susceptibility to common diseases. Moreover, it models a successful and instructive approach to large-scale genomic scans of this type, showing that a set of common controls can be used for a variety of diseases with relatively little loss of analytical power. Its success also provides strong grounds for performing such studies on an even larger scale.

The WTCCC investigators examined genetic variation at 500,000 different positions within the genomes of 17,000 individuals living in Britain using a genome-wide association scan (Fig. 1). This statistical approach compares the frequencies of genetic variation in disease cases and in healthy controls from the same population. Using the signal from each position as an indicator for the DNA sequence that surrounds it, genome-wide association scans examine the relationship between each DNA position and a particular trait (such as diabetes). Strong 'association' between a DNA position and a trait marks the general locale of the offending alteration, even if it is not itself the cause.

The concept of drawing an association between biological traits and disease is hardly new[2], but the scope and scale that the WTCCC attained in their application of this concept is unprecedented. Crucial to both the success of this study and keeping its cost reasonable were DNA from large numbers of unrelated patients; the availability of the complete DNA sequence of the human genome; the subsequent cataloguing of a large component of variation in the genome in the form of single nucleotide polymorphisms (SNPs)[3]; the completion of the HapMap project[4], which provided information on the statistical relatedness of SNPs; and the availability of high-throughput technologies that allowed for parallel typing of 500,000 markers representing most of the common variation in the genome.

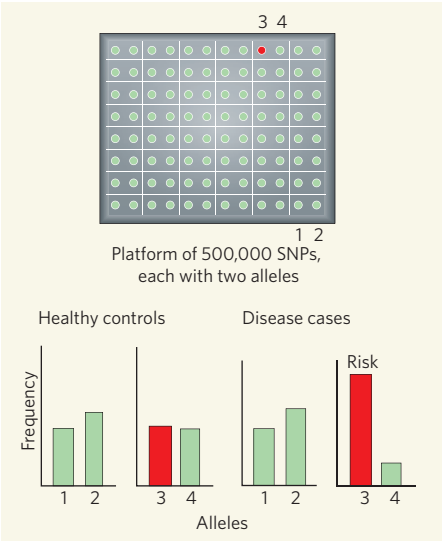

Figure 1 | Genome-wide association scan. To identify genetic risk factors for common diseases, the WTCCC researchers[1] scanned DNA from patients (2,000 per disease) and controls (3,000 shared for all seven diseases studied) for the frequency with which they contained each of the 500,000 genetic markers, or single nucleotide polymorphisms (SNPs), from the human genome. After statistical evaluation of the data, they found that most markers showed very little difference in the frequency of their two constituent forms — or alleles — between controls and cases. However, some SNPs occurred at a greater frequency in patients. Such alleles (one is shown in red) can be considered a genetic risk factor for a particular disease.

For the seven diseases studied by the WTCCC, strong statistical evidence for association was obtained for 12 previously identified genomic regions and a similar number of new regions. Although this WTCCC report is based on initial studies, independent groups[5–9] have confirmed the involvement of all but one of these most significant regions through replication studies. Some of the other identified regions with less statistically significant disease association are also likely to be true indicators of genetic risk; so these will need to be further evaluated in additional large sets of patients and controls. Indeed, because the WTCCC data will be publicly available, they will be a useful resource to other groups and consortia embarking on similar efforts to investigate genetic-association markers in these and other diseases. These researchers include members of the Genetic Association Information Network[10] (GAIN), the Framingham Genetic Research Study and the Women's Health Study.

With many of the genomic regions identified by the WTCCC, the next step will be to study the exact nature of the disease-causing variants, rather than the marker SNP with which each is associated. From this and previous studies, it seems that variations leading to common disease are diverse; some alter the coding sequences of genes, others lie within their non-coding sequences, and some are even located within gene deserts — regions of a chromosome that contain no genes. So understanding the biological function of disease-risk-associated genomic regions will be challenging.

Two replication studies relating to the WTCCC findings are also published today[5,6], revealing connections between the genomic regions associated with the risk of type 1 diabetes and Crohn's disease and their underlying biology. Some of the known and newly identified genetic risk factors for type 1 diabetes alter the development or function of immune cells, leading to aberrant recognition of pancreatic islet cells as foreign particles. But additional susceptibility genes identified recently[5] do not fit easily into this simple model.

For Crohn's disease, one of the newly identified[6] susceptibility genes is of particular interest because it is proposed to control the spread

of intracellular pathogens by autophagy — the process of cellular self-digestion. This is the second gene to be implicated in Crohn's disease through involvement in autophagy; the first was identified earlier this year[11,12]. Moreover, an increasing body of evidence, including the latest replication study[6], points to defects in the early immune response and the handling of intracellular gut bacteria in the pathogenesis of Crohn's disease.

The overall increase in risk (1.2–1.5 times) conferred by the genetic factors identified in the WTCCC study[1] is in agreement with those reported by others. However, these factors are unlikely to explain completely the clustering of any of these diseases in families, and there are other genes (possibly many of very small effect) — or rare variants of genes — that are still to be identified for these and other diseases.

One unexpected result of the WTCCC study was the identification of 13 regions with pronounced geographical variation within Britain. Among these regions is a large cluster of genes that encodes the major histocompatibility complex, which is well known for its function in the immune response and autoimmune disease[13], and a gene that is involved in lactase persistence, or the ability to digest milk[14,15]. Some of the other regions are thought to function in preventing diseases such as pellagra, tuberculosis and leprosy. Although the infectious agents responsible for tuberculosis and leprosy are now rare in Britain, they have left behind genetic footprints in the existing population that probably led to some degree of protection in the past. Several of these are also candidate genes for autoimmune disease[5].

Despite the magnitude and wealth of information that this study[1] provides, other questions about the genetic basis of common disease remain. The answers will become increasingly important as we enter an era of personalized medicine, in which therapy is tailored to an individual's genetic constitution. It will become crucial to discover which genes predispose individuals to these diseases; how genes interact with each other to increase the risk of a particular disease; and what proportion of disease is due to rare variants that would be hard to detect with current approaches.

We will also want to know whether different patients can be stratified into subpopulations on the basis of genetic risk factors, and what role the environment has in triggering disease. The Genes, Environment and Health Initiative (GEI) of the US National Institutes of Health already aims to develop tools to assess environmental contribution and to answer some of the other questions. Ultimately, comprehensive answers that would allow the translation of genetic susceptibility into scientifically sound medical practice will require much larger patient populations, well-annotated clinical databases and sophisticated environmental assessment. One wonders what Mr Woodhouse would have to say to that. ■

Anne M. Bowcock is in the Departments of Genetics, Pediatrics and Medicine, Division of Human Genetics, Washington University School of Medicine, 4559 Scott Avenue, Saint Louis, Missouri 63110, USA.
e-mail:bowcock@genetics.wustl.edu

1. Wellcome Trust Case Control Consortium *Nature* **447,** 661–678 (2007).
2. Buckwalter, J. A., Wohlwend, C. B., Colter, D. C., Tidrick, R. T. & Knowler, L. A. *Surg. Gynecol. Obstet.* **104,** 176–179 (1957).
3. Carlson, C. S. *et al. Am. J. Hum. Genet.* **74,** 106–120 (2004).
4. International HapMap Consortium *Nature* **437,** 1299–1320 (2005).
5. Todd, J. A. *et al. Nature Genet.* doi:10.1038/ng2068 (2007).
6. Parkes, M. *et al. Nature Genet.* doi:10.1038/ng2061 (2007).
7. Zeggini, E. *et al. Science* doi:10.1126/science.1142364 (2007).
8. Saxena, R. *et al. Science* doi:10.1126/science.1142358 (2007).
9. Frayling, T. M. *et al. Science* doi:10.1126/science.1141634 (2007).
10. www.fnih.org/GAIN2/home_new.shtml
11. Hampe, J. *et al. Nature Genet.* **39,** 207–211 (2007).
12. Rioux, J. D. *et al. Nature Genet.* **39,** 596–604 (2007).
13. Tomlinson, I. P. & Bodmer, W. F. *Trends Genet.* **11,** 493–498 (1995).
14. Cavalli-Sforza, L. *Am. J. Hum. Genet.* **25,** 82–104 (1973).
15. Enattah, N. S. *et al. Nature Genet.* **30,** 233–237 (2002).

SPECTROSCOPY

The magic of solenoids

Arthur S. Edison and Joanna R. Long

A technique known as magic-angle spinning has helped make nuclear magnetic resonance spectroscopy as sensitive for solids as it is for solutions. Inductive thinking leads to even better signal detection.

The great strength of nuclear magnetic resonance (NMR) spectroscopy is that it can determine, non-invasively and at atomic resolution, the chemistry, structure, dynamics and overall architecture of samples in solid, liquid or even gaseous forms. The liquid version of the technique, solution NMR, is used routinely to identify small molecules, study protein structures and dynamics, and probe intermolecular interactions. Solid-state NMR teases out the structure and properties of materials, surfaces and biological solids such as human tissue. But compared with many other analytical techniques, NMR has extremely poor sensitivity. A great deal of research has sought to improve this situation: on page 694 of this issue[1], Sakellariou *et al.* describe a potential leap forward for solid-state NMR.

When atomic nuclei with non-zero spin are placed in an external magnetic field, they become polarized, precessing rather as a gyroscope does in Earth's gravitational field. When electromagnetic radiation of a frequency (energy) that corresponds exactly to that of the energy gap between two states of different polarization is applied to the sample, the nuclei resonate, jumping between those states. The accompanying gyroscopic precession of the spins induces a current in a conducting coil placed around the sample. This basic principle is both NMR's blessing and its bane as a spectroscopic technique: the small energies make the approach non-destructive, but they also make it difficult to distinguish the characteristic polarization (or signal) from thermal noise.

The signal-to-noise ratio in NMR measurements can be improved by either one of two general routes. The first of these is enhancing

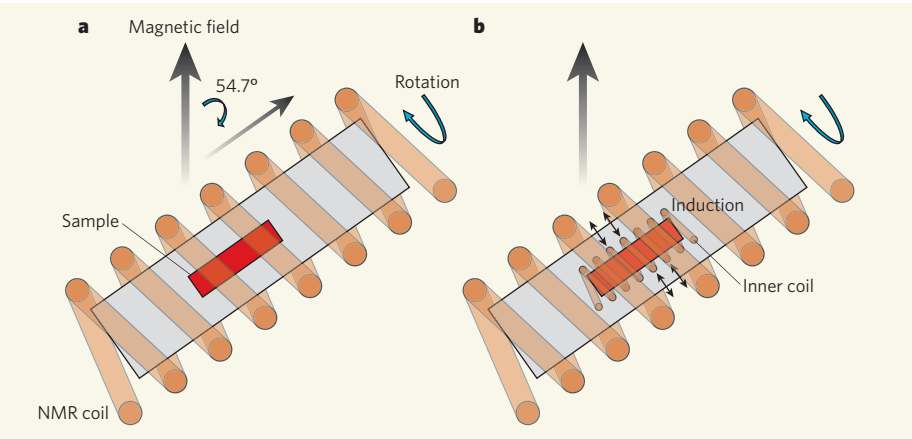

Figure 1 | Inductive logic. a, In the traditional 'magic-angle spinning' approach to solid-state NMR, a spectrum of better resolution is achieved by rapidly rotating the sample, at an angle of 54.7° relative to the main magnetic field, within a static coil assembly. **b**, Sakellariou and colleagues' alternative approach[1] uses the inductive coupling of a smaller coil rotating with the sample to the larger static coil to produce a similar effect. The result is a higher sensitivity and the capability to investigate smaller samples.

the starting polarization. NMR resonant energies are proportional to the strength of the magnetic field. Therefore, stronger magnetic fields improve the initial polarization and lead to more signal. But generating strong, uniform magnetic fields throughout a sample is expensive and requires considerable infrastructure, posing serious practical limitations. Dynamic nuclear polarization[2,3], in which the relatively large polarization of electrons compared with nuclei is transferred to nuclei, is rapidly gaining popularity and applicability, but requires specialized equipment and substantial manipulation of the sample. Furthermore, it might not work for all samples and experiments.

The second general route to more sensitive NMR is to design detection schemes that make better use of the polarization signal. Several research groups are developing procedures that rely on mechanical coupling of the polarization to very sensitive cantilevers[4], or optical rotation of a probe beam running through the sample[5], to improve sensitivity. But these technologies, too, have limited practical application.

Sakellariou and colleagues[1] build on what has proved to be one of the most general and cost-effective ways to improve the sensitivity of solution NMR: detecting the voltages induced in a coil that is optimized for and is closer to the sample. Such a coil is by its nature more efficient, because the signal-to-noise per unit mass of sample scales inversely with the diameter of the coil[6]. Furthermore, the 'filling factor' — the volume within the coil that is taken up by the sample — is an important variable. In solution NMR, solenoidal microcoils have been used to analyse liquid sample volumes of a few nanolitres[7] and to perform magnetic resonance microscopy of individual neurons[8]. Systems for analysing volumes of 1–10 microlitres are available commercially, and the ability to reduce the sample size has also allowed for the collection of many NMR spectra simultaneously[9]. As well as being highly sensitive, solenoidal coils are quite easy to construct on a very small scale.

Until now, however, solid-state NMR had not enjoyed as much benefit from microcoils as had solution NMR. Unlike molecules in solutions, those in solid samples do not tumble rapidly or isotropically on the NMR timescale. The anisotropic interactions provide important structural information, but they also lead to broad, nondescript NMR spectra that are intractable to analysis. This problem can be countered, and solid-state spectra can achieve a resolution similar to that of their solution NMR counterparts[10] by a trick known as magic-angle spinning (MAS), in which the sample is rotated at a speed of several kilohertz and at an angle of 54.7° relative to the magnetic field. In traditional MAS NMR, the sample is spun in a rotor within a static assembly containing a fixed coil that is some distance from the sample and therefore has a poor filling factor.

Sakellariou and colleagues' simple advance[1] is to wind a solenoid microcoil directly around the sample — greatly improving the filling factor — and to spin the sample and coil together (Fig. 1). The spinning microcoil couples inductively to a coil that, just as in the conventional approach, remains static in the surrounding assembly. This 'magic-angle coil spinning' (MACS) technique uses existing commercial MAS solid-state NMR probe technology, while offering the advantages of small coil size and excellent filling factor that have been the province of solution NMR for over a decade[7].

The authors' set-up can improve the signal-to-noise ratio by about an order of magnitude, and so allows smaller samples to be studied. The microcoil can also significantly increase the radio-frequency fields for a given current within the static coil, allowing more efficient manipulation of the spin polarization with radio-frequency pulses. The MACS technique has many conceivable applications, including structural measurements of very small protein samples, 'metabolomics' studies of the biochemistry of microscopic tissue extracts, and NMR measurements of radioactive materials that must be contained by specialized barriers[1].

As with any technology, not all samples will be ideal candidates for the approach. This is especially true of samples in which the signal of interest is present in limited concentrations, such as those for trace amounts of metabolites in tissue, or membrane proteins that aggregate at higher concentrations. At low concentrations, the amount of material will still need to be increased. But for many applications in chemistry, biology and materials science, Sakellariou and colleagues' advance opens up new opportunities simply by reducing the amount of material required for solid-state NMR studies, without needing to invest substantially in new technologies. ■

Arthur S. Edison and Joanna R. Long are in the Department of Biochemistry and Molecular Biology, McKnight Brain Institute, and National High Magnetic Field Laboratory, University of Florida, Box 100245, Gainesville, Florida 32610-0245, USA.
e-mails: art@mbi.ufl.edu; jrlong@mbi.ufl.edu

1. Sakellariou, D., Le Goff, G. & Jacquinot, J.-F. *Nature* **447,** 694–697 (2007).
2. Hall, D. A. *et al. Science* **276,** 930–932 (1997).
3. Navon, G. *et al. Science* **271,** 1848–1851 (1996).
4. Rugar, D., Yannoni, C. S. & Sidles, J. A. *Nature* **360,** 563–566 (1992).
5. Savukov, I. M., Lee, S.-K. & Romalis, M. V. *Nature* **442,** 1021–1024 (2006).
6. Hoult, D. I. & Richards, R. E. *J. Magn. Reson.* **24,** 71–85 (1976).
7. Olson, D. L., Peck, T. L., Webb, A. G., Magin, R. L. & Sweedler, J. V. *Science* **270,** 1967–1970 (1995).
8. Grant, S. C. *et al. Magn. Res. Med.* **44,** 19–22 (2000).
9. Li, Y., Wolters, A. M., Malawey, P. V., Sweedler, J. V. & Webb, A. G. *Anal. Chem.* **71,** 4815–4820 (1999).
10. Andrew, E. R. *Phil. Trans. R. Soc. Lond. A* **299,** 505–520 (1981).

CLIMATOLOGY

Tempests in time

James B. Elsner

The frequency of severe hurricanes in the North Atlantic has increased during the past decade. Scrutiny of the prehistoric record left by such storms helps to assess the factors contributing to hurricane activity.

A hurricane is a product of its environment: a warm ocean provides sustenance; calm atmospheric conditions nurture an infant storm; and a high-pressure cell in the subtropical atmosphere drives it in a given direction. Increases in oceanic heat from global warming will raise a hurricane's potential intensity, all else being equal. Yet increases in wind shear — in which winds at different altitudes blowing in different directions may tear apart the developing storm — could counter this tendency by dispersing the storm's heat.

In the long run, which effect will win out? Limited instrumental records of hurricanes and climate change make it difficult to answer this question. So researchers have turned to prehistoric 'proxy' data to uncover clues about what to expect in a warmer world. Two new papers, one published on 24 May[1] and one on page 698 of this issue[2], illustrate how the approach has been applied to hurricanes in the North Atlantic.

Palaeotempestology is the study of prehistoric storms from geological and biological evidence. Coastal wetlands and lakes are subject to 'overwash' during hurricanes, when barrier sand dunes are surmounted by storm surge. The assumption is that the waves and wind-driven storm surge reach high enough over the barrier to deposit a fan of sand in the lake[3]. A sediment core from the bottom of the lake shows that fan as a sand layer distinct from the fine organic mud that accumulates slowly under normal conditions.

Donnelly and Woodruff[1] analysed sediment cores they extracted from a lagoon on the Puerto Rican island of Vieques. The lagoon is separated from the ocean by a stable barrier of sand. In the core, they found coarse-grained sand layers embedded in several metres of organic-rich silt. The layers are clearly the result of barrier and nearshore sediments that have been washed into the lagoon by strong hurricanes, the recent layers being correlated

in time with known hurricane strikes. The authors calibrated the sensitivity of the site to storm surge by noting the intensity of known strikes that did not leave sand in the core.

Donnelly and Woodruff find more sand layers during the latter half of the Little Ice Age. This occurred between 300 and 150 years ago, and towards the end of this interval sea temperatures near Puerto Rico were 2 °C cooler than they are now. The authors say this is evidence that today's warmth is not needed for increased storminess. Not surprisingly, they find that intervals in which more hurricanes occurred correspond with periods of fewer El Niño events. El Niño events suppress hurricane activity in the North Atlantic by increasing the amount of wind shear and sinking air.

Nyberg *et al.*[2] describe a different approach that has led them to the same conclusion — that, in the long run, shear is more important than ocean temperature in modulating hurricane activity. They use proxy records of shearing winds and ocean temperature to reconstruct a two-and-a-half century record of major hurricanes and wind shear. The proxies are based on luminescence banding in coral cores retrieved from sites in the northeastern Caribbean, and on a marine sediment core from further south.

However, studies relying on a spatially limited set of coring and proxy locations are not able to resolve changes in hurricane tracks. The northeastern Caribbean is in the direct path of hurricanes today, but has it always been? More hurricanes occurring locally could mean a shift in their direction rather than their abundance. Donnelly and Woodruff[1] find that changes in hurricane frequency over the northeastern Caribbean seem to mirror the changes in frequency inferred from cores collected in New York, but the degree of correlation is not quantified. Proxy data from the Gulf coast show a pattern of frequent hurricanes between 3,800 and 1,000 years ago, followed by relatively few hurricanes during the most recent millennium, which has been explained in terms of the shifting position of the subtropical high-pressure zone[4]. Unravelling the causes of changes in local hurricane activity requires an understanding of the factors that influence what track they will take[5]. So further work is needed.

In addition, the assumption that hurricanes are simply passive responders to climate change should be challenged. Hurricane activity influences the observations and proxies used to compute mean quantities such as wind-shear and precipitation conditions, so the arguments can easily become circular. Reduced rainfall and greater mean shear are possible consequences of fewer hurricanes, not necessarily the causes. More importantly, a hurricane removes heat and water from the ocean and transports them upward and poleward, thereby modifying the environment that supports it. A strong hurricane cools the ocean surface beneath it as a result of evaporation and mixing of water layers. This makes the area less favourable for the next storm, but at depth adds heat to the ocean that can, in the long run, influence the climate system[6].

GOES 12 SATELLITE/NASA/NOAA

Figure 1 | One for the modern record. Hurricane Katrina made its infamous assaults on the Bahamas, Cuba, south Florida and the Gulf coast in late August 2005.

Palaeotempestology is a valuable tool for answering questions on hurricane climatology. But more records are needed before localized prehistoric activity can be used to make sense of large-scale patterns of storminess. As Liu[3] has pointed out, each record serves as a 'palaeoweather station', sensitive only to nearby hurricanes. At present, fewer than a dozen sequences that have been dated and validated are available in hurricane-prone regions of the United States and Caribbean. However, the new analyses[1] and those of others[4,7] are a start.

When more palaeoweather stations have been established, a network can be constructed with links connecting sites that share similar periods of storminess. That network can then be compared to a network of storminess from modern records (Fig. 1) to better understand the evolving mechanisms responsible for changing hurricane risk. ■

James B. Elsner is in the Department of Geography, Florida State University, Tallahassee, Florida 32306-2190, USA.
e-mail: jelsner@fsu.edu

1. Donnelly, J. P. & Woodruff, J. D. *Nature* **447,** 465–468 (2007).
2. Nyberg, J. *et al. Nature* **447,** 698–701 (2007).
3. Liu, K.-b. *Am. Sci.* **95,** 126–133 (2007).
4. Liu, K.-b. & Fearn, M. L. *Geology* **21,** 793–796 (1993).
5. Elsner, J. B. *Bull. Am. Meteorol. Soc.* **84,** 353–356 (2003).
6. Sriver, R. L. & Huber, M. *Nature* **447,** 577–580 (2007).
7. Nott, J. F. & Hayne, M. *Nature* **413,** 508–512 (2001).

STEM CELLS

Recycling the abnormal

Alan Colman and Justine Burley

Using human eggs in the quest to make donor-specific embryonic stem cells is controversial. A method developed in mice, if applicable to humans, could eliminate the need to obtain eggs for this purpose.

On page 679 of this issue, Egli *et al.*[1] describe a promising method for generating embryonic stem-cell (ESC) lineages using the technique of somatic-cell nuclear transfer (SCNT). Conventional SCNT involves replacement of the nuclear genetic material of an unfertilized egg (oocyte), with that of a somatic (non-germ) cell. After 'fertilization', which is induced by chemical or electrical triggers, the embryo undergoes several rounds of cell division and, after implantation into a foster mother, may develop to term. So far, this technique has been used successfully to clone 12 species. It also has been used in mice to generate ESCs from a 3.5-day-old mouse embryo[2] — a blastocyst.

Since Dolly the Sheep was cloned by SCNT more than ten years ago[3], it has been hoped that this technique would serve to create patient-matched ESCs for therapy, and human-disease-specific ESC lines for use in basic research and drug development. However, in contrast to SCNT in mice, the use of this technique in humans has been thwarted by technical difficulties, as well as logistical and ethical concerns about obtaining oocytes. Now, Egli and colleagues[1] describe a different approach to produce donor/disease-specific ESC lines that may well revolutionize the field of human stem-cell research, and that removes one of the main ethical objections to such work. The

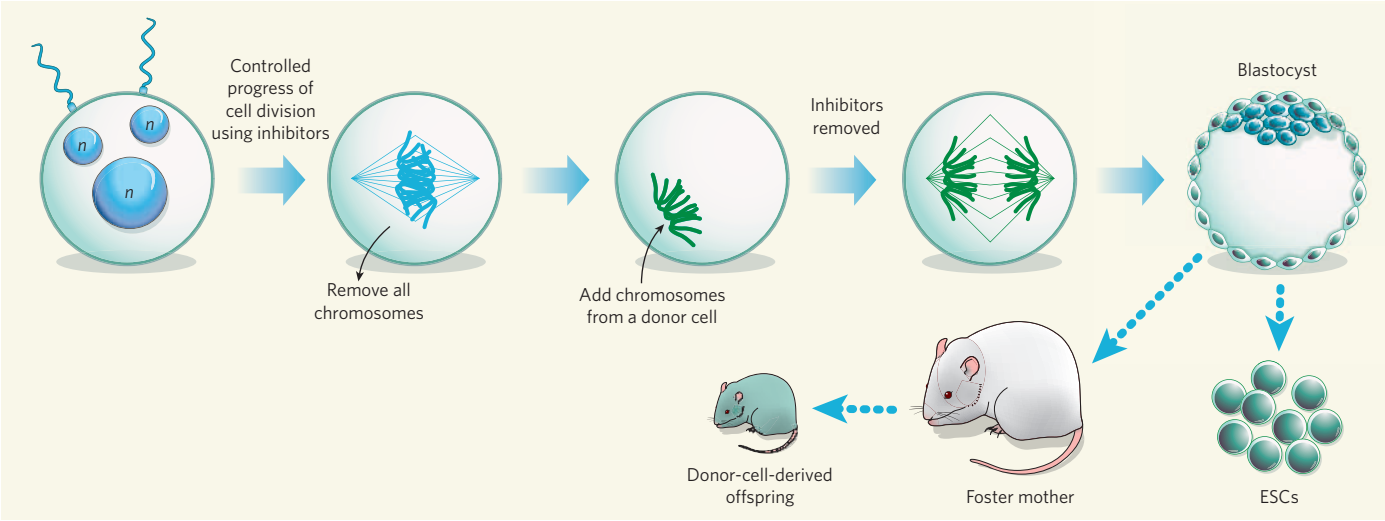

Figure 1 | Somatic-cell nuclear transfer using abnormal embryos. Egli *et al.*[1] generated abnormal mouse zygotes, in which the egg was fertilized with two sperm cells (*n* indicate pronuclei). Such zygotes are often useless by-products of human *in vitro* fertilization procedures. However, using inhibitors, the authors allowed the abnormal mouse zygote to progress through the cell cycle up to the point during mitosis at which its chromosomes aligned on the mitotic spindle. They then mechanically removed the spindle and replaced it with the condensed chromosomal content of a donor embryonic stem cell (ESC), also arrested at mitosis. Removal of the inhibitors allowed development to resume, and a blastocyst formed. This is a promising technical feat, as the authors also found that blastocysts formed in this way but using ESCs or adult tail-tip cells as donors and normal zygotes as recipients led to live offspring or, alternatively, new ESCs.

crux of their contribution is the use of fertilized eggs, instead of oocytes, as SCNT recipients.

Historically, fertilized mouse eggs at the one-cell stage — the zygote — have been successfully used as recipients of nuclear genetic material[4], but only when the donor cells were also zygotes and not from later developmental stages[5]. Possible reasons for this limitation include loss of essential non-DNA factors with the removed genetic material[6], and inadequate time for the reprogramming of the donor's genetic material in its new environment[5].

Egli *et al.* reasoned that the loss of the crucial factors could be minimized or eliminated if nuclear transfer is conducted when both the recipient zygote and the donor cell are temporarily arrested at the mitotic cell division. To test this, they used the drug nocodazole to arrest mitosis in mouse zygotes at the stage when chromosomes condense. Replacing nocodazole with another inhibitor allowed chromosome alignment along the mitotic spindle, but prevented further cell-cycle progression. The spindle could then be seen using optical devices, and removed mechanically.

Donor zygotes and two- and eight-celled embryos were also arrested with nocodazole. The condensed chromosomes were then identified, removed from individual cells, and injected into the cytoplasm of treated recipient zygotes. Removal of the inhibitors allowed development to resume, and the resulting blastocysts were returned to foster mothers. Donors from all three stages of development led to some live births.

Next, the authors used mouse ESCs as donors. The resultant blastocysts were either returned to foster mothers — leading to nine live births — or were used to make new ESC lines. By injecting these SCNT-derived ESCs into normal host blastocysts they showed that these cells had the full range of developmental potencies expected from bona fide mouse ESCs.

Finally, adult tail-tip cells were used as recipients to make donor-specific SCNT-derived ESCs. Previously, mitotic, embryonic[7] and somatic cells[8] have all been used as donors in nuclear transfer experiments. But Egli *et al.* are the first to use a mitotic cytoplasm as a recipient. Using cells at this stage of the cell cycle as recipients may expedite reprogramming of donor chromosomes, because at other stages reprogramming factors are probably sequestered within cells' nuclei[9].

In terms of efficiency, the method reported by Egli *et al.*[1] is not better than previous ones. So why all the excitement? After all, the new method seems to be ethically inferior, as in generating SCNT-derived ESCs, two, rather than one, developing embryos are disrupted — the original zygote and the SCNT-derived embryo. The answer can be found in the results of their last experiment.

The researchers generated an embryo containing three sets of chromosomes — in which two sperm cells fertilized a single oocyte. Such embryos never develop normally. Nevertheless, replacement of these three sets of chromosomes with one set from an ESC led to a normally developing embryo, which could potentially be used to generate a new ESC line (Fig. 1). This finding could have a profound effect on developing a viable and tractable method of SCNT in humans.

The failure of SCNT in humans and monkeys has been attributed by some[10] to fundamental differences between primate and non-primate unfertilized eggs in the way their spindles form during cell division. However, even if this difficulty could be surmounted, obtaining freshly ovulated human oocytes would remain of logistical and ethical concern; unfortunately, in contrast to recent success in mice[11], aged, unfertilized oocytes — a by-product of normal *in vitro* fertilization (IVF) procedures — have been inadequate for SCNT in humans[12]. However, if the technique developed by Egli and colleagues could be used successfully in humans, all of these problems would be circumvented.

It is estimated that 3–5% of fertilized human zygotes contain supernumerary sets of chromosomes[13]. Such zygotes are always excluded from clinical use in IVF centres because they cannot develop, and are therefore disposed of. The possibility of recycling non-viable zygotes to produce ESC lines obviates the need for oocyte donation. So those who have been troubled by this ethical aspect of human SCNT stem-cell research will be very encouraged by the results of Egli and his colleagues[1]. ■

Alan Colman is at ES Cell International and the A*STAR Institute of Medical Biology, 11 Biopolis Way, 05-06 Helios, Singapore 138667. Justine Burley is in the Graduate School for Integrative Sciences and Engineering, National University of Singapore, CeLS 05-01, 28 Medical Drive, Singapore 117456.
e-mail: acolman@escellinternational.com

1. Egli, D., Rosains, J., Birkhoff, G. & Eggan, K. *Nature* **447,** 679–685 (2007).
2. Munsie, M. *et al. Curr. Biol.* **10,** 989–992 (2000).
3. Wilmut, I., Schnieke, A. E., McWhir, J., Kind, A. J. & Campbell, K. H. *Nature* **385,** 810–813 (1997).
4. McGrath, J. & Solter, D. *Science* **220,** 1300–1302 (1983).
5. McGrath, J. & Solter, D. *Science* **226,** 1317–1319 (1994).
6. Polejaeva, I. A. *et al. Nature* **407,** 86–90 (2000).
7. Kwon, O. Y. & Kono, T. *Proc. Natl Acad. Sci. USA* **93,** 13010–13013 (1996).
8. Ono, Y., Shimozawa, N., Ito, M. & Kono, T. *Biol. Reprod.* **64,** 44–50 (2001).
9. Do, J. T. & Scholer, H. R. *Stem Cells* **22,** 941–949 (2004).
10. Simerly, C. *et al. Science* **300,** 297 (2003).
11. Wakayama, S. *et al. Curr. Biol.* **17,** R120–R121 (2007).
12. Hall, V. J. *et al. Hum. Reprod.* **22,** 52–62 (2007).
13. Aoki, V. W. *et al. J. Exp. Clin. Assist. Reprod.* **2,** 3 (2005).

ASTROPHYSICS

Gravitational waves constrained

Michele Maggiore

Cosmic gravitational waves could provide unprecedented information on the early Universe. The effects that are of interest are small, but experiments are gradually achieving a sensitivity that will test cosmological models.

Gravitational waves are tiny disturbances in space-time. They can be triggered during cataclysmic events involving stars or black holes, and they could even have been generated in the very early Universe, well before any star formed, merely as a consequence of the dynamics and expansion of the Universe. In the latter case, these waves should provide a 'background' signal of gravitational waves coming from all directions in space — if indeed they can be spotted. One particularly sensitive experiment recruited to the search for gravitational waves is LIGO, the Laser Interferometer Gravitational-Wave Observatory. It has just published the results from its fourth bout (S4) of data-taking in *The Astrophysical Journal*[1].

Gravitational waves are not the only known source of cosmic 'noise'. Most famously, the Universe is filled with a background of electromagnetic radiation left behind by the hot Big Bang; it has now cooled to its present temperature of about 2.7 kelvin by the subsequent expansion of the Universe. The discovery of this 'cosmic microwave background' by Arno Penzias and Robert Wilson in 1964 is a milestone in the history of modern cosmology, and its detailed study provides some of our best information on the early Universe. In 1992, NASA's Cosmic Background Explorer (COBE) satellite reported its measurement of the spectrum of the microwave background and found it to have a perfect 'black-body' form with a characteristic temperature that has tiny variations across the sky — the 'seeds' for galaxy formation[2]. Subsequent experiments, in particular NASA's follow-up WMAP (Wilkinson Microwave Anisotropy Probe) mission, have provided a more detailed picture, and ushered in an epoch of precision cosmology, in which the agreement between experimental data and theoretical models can be at the level of a few per cent.

The discovery of a cosmological background of gravitational radiation would arguably be even more fundamental. Any background of relic particles provides us with a snapshot of the Universe at a very definite time: the time at which these particles decoupled from the primordial plasma. For the photons of the cosmic microwave background, this happened when the Universe was just 270,000 years old. The photons we see today in the cosmic microwave background are a true photograph of the Universe at that age.

LIGO LABORATORY

Figure 1 | Long arms for gravitational waves. The LIGO site at Hanford, Washington.

50 YEARS AGO

An investigation during 1954–56, into hygiene in restaurants and public houses, was then described... In the first survey covering fifty representative kitchens only twenty-seven out of 260 washed utensils examined attained the United States Public Health Standard. Only two from forty-two drying cloths showed less than 500 organisms per square inch. Only seven from forty-two wash and rinse waters yielded less than 500 organisms per ml. 74 per cent of kitchens yielded fæcal *Bacterium coli* from one or more items but no recognized types of food-poisoning pathogens were isolated apart from *Staphylococcus aureus*... Arrangements in many kitchens were poor, the paramount need being for improved ventilation and more hot water at 180° F.

From *Nature* 8 June 1957

100 YEARS AGO

The Origin of Radium by E. Rutherford — In a previous letter to *Nature* (January 17) I gave an account of some experiments which I had made upon the growth of radium in preparations of actinium. ...I think we may [now] safely conclude that, in the ordinary commercial preparations of actinium, there exists a new substance which is slowly transformed into radium. This intermediate parent of radium is chemically quite distinct from actinium and radium and their known products, and is capable of separation from them.

It is not possible at present to decide definitely whether this parent substance is a final product of the transformation of actinium or not. It is not improbable that it may prove to be the long-looked-for intermediate product of slow transformation between uranium X and radium, but with no direct radio-active connection with actinium. If this be the case, the position of actinium in the radio-active series still remains unsettled.

From *Nature* 7 June 1907

50 & 100 YEARS AGO

The more weakly a particle interacts, the earlier it detaches itself from the primordial plasma. Weakly interacting neutrinos, for instance, decoupled when the Universe was only about a second old. Because the gravitational force is so very small in the realm of elementary particles, the interaction of gravitational waves with the primordial plasma is negligible — they have been propagating freely ever since they were generated. In particular, gravitational waves produced during the Big Bang would carry a genuine picture of the Big Bang itself, providing information that no other messenger can carry.

LIGO, together with its European counterpart VIRGO near Pisa, Italy, is the most ambitious project to date to search for gravitational waves. It consists of three detectors, two on a site in Washington (Fig. 1) and one, 3,000 kilometres away, on a site in Louisiana. The passage of a gravitational wave would cause a tiny delay in the passage of laser beams reflected up and down LIGO's 4-kilometre-long detector arms. Although LIGO has not made a positive detection of gravitational waves, the upper bound on the intensity of a random background is an interesting result in its own right.

The strength of the gravitational-wave background is quantified by its energy density, ρ_{gw}. In cosmology, there is a natural unit for energy density, the critical density for 'closing' the Universe, ρ_c. If the Universe's density is greater than ρ_c, the force of its own gravity will at some point cause it to begin contracting, ending in a reverse of the Big Bang, the Big Crunch; if, however, it is smaller than this critical density, the Universe's expansion will continue unchecked for ever. It is thus convenient to use the 'normalized' energy density, $\Omega_{gw} = \rho_{gw}/\rho_c$. LIGO's latest upper bound[1] for the stochastic gravitational-wave background is $\Omega_{gw} < 6.5 \times 10^{-5}$.

This experimental limit is interesting because it represents a sensitivity at which current models of cosmology tell us the detection of gravitational waves is not excluded. Upper bounds on Ω_{gw} can be deduced from various astrophysical and cosmological observations[3]. In the frequency range accessible to LIGO, the most important limit comes from the production of light elements other than hydrogen in the first few minutes of the Universe, known as Big-Bang nucleosynthesis. The abundance of these light elements is fixed by the balance between the rate of the nuclear reactions that produce them and the expansion rate of the Universe, which dilutes them.

The latter rate is determined, through the equations of general relativity, by the total energy density of the Universe. This consists of the energy density carried by the known elementary particles, plus the energy density carried by any other more exotic form of matter — or indeed by gravitational waves. When only the known elementary particles are included in the computation, theory and observation agree beautifully. The energy density of any other extra particle, and of gravitational waves, at the epoch of nucleosynthesis, is then constrained in order not to spoil this agreement. This puts an upper bound on Ω_{gw} at the level of a few times 10^{-5}, which is comparable to LIGO's new upper bound[1].

Certain cosmological models predict values of Ω_{gw} that could be almost as large as is allowed by the nucleosynthesis bound. In particular, a pre-Big-Bang model that includes the low-energy effects of string theory[4] predicts a stochastic background of gravitational waves that, for some values of its input parameters, approaches this bound[5]. Such cosmological models are thus now seeing experimental constraints.

The data from LIGO's S4 run that have now been published[1] were taken over a period of one month, between February and March 2005. The duration of the data-taking is a major factor because of the way the stochastic background is extracted by correlating the data of two detectors. This procedure allows the gravitational-wave signal to be extracted from the much greater effect of noise local to the detectors — laser fluctuations, seismic rumblings and so on. This signal-to-noise ratio scales as the square-root of the total observation time.

LIGO is now engaged in its fifth period of data-taking (S5), which will collect one year of coincident data between its detectors, with an improved sensitivity over the S4 data[1]. The combination of better sensitivity and the longer run is expected to improve the sensitivity to Ω_{gw} by a factor of a further 10–100. In a few years, an upgrade of the experiment, known as Advanced LIGO, should eventually reach sensitivities between 10^{-8} and 10^{-9}. That should allow us to penetrate deep into a totally unknown region, where the answers to fundamental questions could well be waiting. ■

Michele Maggiore is in the Department of Theoretical Physics, University of Geneva, 1211 Geneva 4, Switzerland.
e-mail: michele.maggiore@physics.unige.ch

1. Abbott, B. *et al.* (The LIGO Scientific Collaboration) *Astrophys. J.* **659,** 918–930 (2007).
2. http://nobelprize.org/nobel_prizes/physics/laureates/2006
3. Maggiore, M. *Phys. Rep.* **331,** 283–367 (2000).
4. Gasperini, M. & Veneziano, G. *Phys. Rep.* **373,** 1–212 (2003).
5. Brustein, R., Gasperini, M. & Veneziano, G. *Phys. Rev. D* **55,** 3882–3885 (1997).

DISEASE ECOLOGY

The silence of the robins

Carsten Rahbek

A continent-wide analysis suggests that West Nile virus has severely affected bird populations associated with human habitats in North America. The declines parallel patterns of human disease caused by the virus.

Scenes reminiscent of those described in Rachel Carlson's *Silent Spring*[1] have been occurring in suburban America. This time, it is not pesticides that are to blame for a decline in bird populations, but outbreaks of West Nile virus[2]. A study by LaDeau and colleagues[3] on page 710 of this issue shows that reductions in bird populations correlate with the prevalence of the virus, that these patterns are upheld across years and throughout the continent, and that the patterns are geographically correlated with epidemics of human infection by West Nile virus*.

West Nile virus emerged in New York City from the Old World in 1999, and then spread rapidly across the entire continent. The primary hosts of the virus are birds, in which virus numbers are also amplified before the virus is transmitted by mosquitoes to the next victim. Besides birds, the virus can infect other vertebrates, including humans, and has caused the death of as many as 1,000 people[4] in the United States alone, as well as uncounted casualties in birds and other vertebrates[2,4] (Box 1).

*This article and the paper concerned[3] were published online on 16 May 2007.

LaDeau and colleagues have dealt with several analytical challenges to demonstrate that West Nile virus is indeed the main factor behind the observed large-scale declines in bird populations. Continent-wide fluctuations of this kind have been documented previously[5,6], but they have been explained by changes in the local environment related to habitat, land use and climate. LaDeau and colleagues had to disentangle virus-induced mortality from these confounding effects.

To do so, they designed species-specific predictive models based on knowledge of the prevalence of the virus, exposure to mosquitoes and overall mortality for 20 different bird species, each species representing a specific combination of urban (human) association and susceptibility to the virus. The model was applied to 26 years of population data for six geographical regions to construct probability distributions for the expected abundance of each bird species in a given region before and after the arrival of the virus.

The results are revealing: significant population changes in seven of the 20 species were in agreement with specific expectations

NEWS & VIEWS

DISEASE ECOLOGY

The silence of the robins

Carsten Rahbek

A continent-wide analysis suggests that West Nile virus has severely affected bird populations associated with human habitats in North America. The declines parallel patterns of human disease caused by the virus.

Scenes reminiscent of those described in Rachel Carlson's *Silent Spring*[1] have been occurring in suburban America. This time, it is not pesticides that are to blame for a decline in bird populations, but outbreaks of West Nile virus[2]. A study by LaDeau and colleagues[3], published on *Nature*'s website today, shows that reductions in bird populations correlate with the prevalence of the virus, that these patterns are upheld across years and throughout the continent, and that the patterns are geographically correlated with epidemics of human infection by West Nile virus.

West Nile virus emerged in New York City from the Old World in 1999, and then spread rapidly across the entire continent. The primary hosts of the virus are birds, in which virus numbers are also amplified before the virus is transmitted by mosquitoes to the next victim. Besides birds, the virus can infect other vertebrates, including humans, and has caused the death of as many as 1,000 people[4] in the United States alone, as well as uncounted casualties in birds and other vertebrates[2,4] (Box 1).

LaDeau and colleagues have dealt with several analytical challenges to demonstrate that West Nile virus is indeed the main factor behind the observed large-scale declines in bird populations. Continent-wide fluctuations of this kind have been documented previously[5,6], but they have been explained by changes in the local environment related to habitat, land use and climate. LaDeau and colleagues had to disentangle virus-induced mortality from these confounding effects.

To do so, they designed species-specific predictive models based on knowledge of the prevalence of the virus, exposure to mosquitoes and overall mortality for 20 different bird species, each species representing a specific combination of urban (human) association and susceptibility to the virus. The model was applied to 26 years of population data for six geographical regions to construct probability distributions for the expected abundance of each bird species in a given region before and after the arrival of the virus.

R. NUSSBAUMER/NATUREPL.COM

Figure 1 | Viral victim: the American robin. Populations of this bird and of the American crow are among the seven species most clearly identified by LaDeau *et al.*[3] as suffering from mortality caused by West Nile virus. The other five species for which there is a robust correlation between population declines and virus infection are the blue jay (*Cyanocitta cristata*), tufted titmouse (*Baeolophus bicolor*), house wren (*Troglodytes aedon*), chickadee (*Poecile* spp.) and Eastern bluebird (*Sialia sialis*).

The results are revealing: significant population changes in seven of the 20 species were in agreement with specific expectations based on the direct adverse impact of virus infections. Although this may seem a modest effect, LaDeau and colleagues' analyses deliberately included tolerant bird species that were unlikely to be greatly affected for various ecological reasons. For the species thought to be susceptible to West Nile virus, there was a disturbingly consistent general relationship between the predicted effects of the virus and the observed declines in population abundance. The correlation was far from perfect. But it suggests that West Nile virus could potentially change the composition of bird communities across the entire continent.

Strikingly, the seven bird species that are most clearly affected by the virus are all 'peridomestic' — that is, they are associated with human populations, in this case those in town and city suburbs. Among the disappearing species is an icon of North American garden birds, the American robin (*Turdus migratorius*; Fig. 1). It is also thought-provoking that no fewer than 13 of the 20 species experienced a 10-year population low following the human epidemics of West Nile virus in 2002–03 in the United States[3]. This is a notable observation in light of the debate about the spread of the highly pathogenic avian influenza virus (H5N1 strain), and the potential role of migratory, peridomestic and domestic birds as reservoirs and dispersers of this disease.

LaDeau *et al.*[3] caution against over-simplified interpretations of their results. The spatial patterns of disease that they detected may still reflect regional differences in the intensity of viral transmission, and these may be linked to spatial patterns in habitat, land use and climate — all of which are traditionally used to explain large-scale patterns of changes in bird populations.

The authors partly incorporated the potential influence of the El Niño/Southern Oscillation in their models as a crude measurement of climate variability, but their analysis does not include environmental or climatic parameters at the appropriate spatial scale. This may explain why, with the exception of the American crow (*Corvus brachyrhynchos*), the results are qualitatively rather inconsistent for individual species. But the results for the crow are compelling, not least given the

NATURE|AOP|doi:10.1038/nature05889|Published online 16 May 2007

Box 1 | West Nile virus in the Old and New Worlds

West Nile virus was first isolated in 1937 in the West Nile province of Uganda[10], an area known for other mosquito-transmitted diseases such as malaria, schistosomiasis, dengue and yellow fever. It has apparently only recently caused serious illness among humans[11], and largely outside the tropics.

The first documented human epidemic occurred in Israel in 1951–54, with another in 1957. Major outbreaks occurred in South Africa (1974) and Israel (2000), with minor incidences in France (1962), Algeria (1994), Romania (1996) and Russia (1999), but only one in central Africa (1998).

Following its detection in the New World in 1999, West Nile virus spread quickly[9] during the dry summer of 2002, and now occurs throughout North and Central America, and in the Caribbean[4]. It has killed individuals of almost 200 bird species in North America, as well as other wild and domestic animals[2,4]. By contrast, it seems that infected Old World birds rarely show adverse symptoms[12].

The Old World human epidemics have generally been local and short-lived. But, as is the case with birds, the human effects of the virus in the New World are much more severe. Between 1999 and 2006, 23,974 cases were reported in the United States: 14,125 were of the mild West Nile fever, and 9,849 of the severe West Nile meningitis or encephalitis (inflammation of the spinal cord and brain), including 962 deaths[4]. There is currently no vaccine for humans.

The different effects of West Nile virus in the Old and New Worlds could be an example of host–parasite coevolution, in which the virus has coevolved with birds and humans in tropical Africa in particular, and so has a less lethal effect on its hosts[12]. If so, evolutionary adaptation might occur among New World species, which will minimize the virus's future impact. **C.R.**

geographical correlation with human infection shown in Figure 2 of the paper[3].

More detailed analyses and studies on further species will be needed to fully understand the impact of West Nile virus on large-scale changes in North American bird populations. But even as it stands, this research reminds us once more of the threat of infectious diseases to both biodiversity and human health. The migratory passenger pigeon (*Ectopistes migratorius*) of North America, once the most abundant bird of its time with an estimated population of between 3 billion and 5 billion, was driven to extinction within a century by human agency and, possibly, diseases[7]. The disappearance of such an abundant species must have had a considerable effect on the communities in which it occurred. Indeed, it has been suggested that the rise in incidence of Lyme disease in humans is a delayed consequence of the removal of the passenger pigeon from the ecosystems of North America[7,8].

We are witnessing the emergence of novel diseases at an unprecedented rate[9]. Epstein and colleagues[9] have argued that human-induced changes in ecological systems and climate are now triggering "a barrage of emerging diseases that afflict humans, livestock, wildlife, marine organisms, and the very habitat we depend upon". LaDeau and colleagues' study is a timely example of the effect that such diseases can have on communities of wild species and humans alike, even at a continental scale. ■

Carsten Rahbek is at the Center for Macroecology, Institute of Biology, University of Copenhagen, Universitetsparken 15, DK-2100 Copenhagen, Denmark.
e-mail: crahbek@.bi.ku.dk

1. Carson, R. *Silent Spring* (Mariner/Houghton Mifflin, Boston, 1962).
2. Marra, P. P. *et al. BioScience* **54,** 393–402 (2004).
3. LaDeau, S. L., Kilpatrick, A. M. & Marra, P. P. *Nature* doi:10.1038/nature05829 (2007).
4. www.cdc.gov/ncidod/dvbid/westnile/index.htm
5. Sauer J. R., Hines, J. E. & Fallon. J. *The North American Breeding Bird Survey: Results and Analysis 1966–2002* Version 2003.1 (USGS Patuxent Wildlife Research Center, Laurel, MD, 2003).
6. Wilcove, D. S. & Terborgh, J. W. *Am. Birds* **38,** 10–13 (1984).
7. Blockstein, D. E. in *The Birds of North America* (eds Poole, A. & Gill, F.) No. 611 (Birds of North America, Philadelphia, PA, 2002).
8. Chapin, F. S. *et al. Nature* **405,** 234–242 (2000).
9. Epstein, P. R., Chivian, E. & Frith K. *Environ. Health Perspect.* **111,** A506–A507 (2003).
10. Smithburn, K. C., Hughes, T. P., Burke, A. W. & Paul, J. A. *Am. J. Trop. Med.* **20,** 471–492 (1940).
11. Galli, M., Bernini, F. & Zehender, G. A. *Emerging Infect. Dis. J.* **10,** 1332–1333 (2004).
12. Peterson, A. T. *et al. Bird Conserv. Int.* **14,** 215–232 (2004).

OBITUARY

Theodore H. Maiman (1927–2007)

Maker of the first laser.

BETTMANN/CORBIS

The physicist Theodore (Ted) Maiman died on 5 May in Vancouver, British Columbia, at the age of 79. As creator of the first operating laser, he has left an enduring mark on science and technology.

Maiman was born in Los Angeles, California, and showed an early aptitude for electrical engineering which took him first to the University of Colorado and then to Stanford University, where he was awarded a PhD in 1955. Subsequently, as a young scientist at Hughes Aircraft Company in Malibu, California, he worked on the amplification of microwaves by masers, and was eager to produce similar amplification at light wavelengths. His superiors at Hughes were wary of such work, wanting Maiman to do "something useful". But on his insistence, they let him proceed.

His breakthrough involved the use of a ruby crystal, which others interested in lasers thought would probably not work. However, Maiman introduced a technique that had not been considered, the excitation of ruby with an intense flash lamp. And it worked! A powerful red light beam was produced, lasting only the short time of the exciting flash, but nevertheless providing remarkably high intensity — many orders of magnitude more intense than any previous light source. And it formed a coherent, highly directed beam. Because the laser pulses produced lasted only a short time, others were eager to produce continuously operating lasers, which they soon did. But the very short pulses that lasers produce are themselves now exciting tools used in science and for wireless communication systems.

Maiman initially sent a description of his device to *Physical Review Letters*. But it was rejected because so many manuscripts on masers had been submitted to the journal that its editors made the unusual decision to accept no more papers in the field. So Maiman sent it to *Nature*, where his now famous paper, "Stimulated optical radiation in ruby", appeared on 6 August 1960 (T. H. Maiman *Nature* **187,** 493–494; 1960). It was very brief, and I have previously commented that this article was probably more important per word than any of the papers published by *Nature* over the past century. The device was quickly replicated by many other scientists, still other types were invented, and soon the word laser — for 'light amplification by stimulated emission of radiation' — was common currency.

Few applications for lasers were initially envisaged by most scientists; it was sometimes referred to as "a solution looking for a problem". But the ensuing development of the principle produced many forms of laser — ranging in size from the minuscule to the enormous — and they have now permeated almost all fields of science and technology. Lasers are widespread in industry and are tools for much new science: their use underlies the award of several Nobel prizes. They are now exploited in cutting and welding; in communications; for high-precision measurements and convenient directional control; in nanotechnology; in innovative forms of microscopy and for manipulating microorganisms; in computing; and in medicine.

Precise measurement of the distance between Earth and the Moon has been provided by lasers, and some scientists are looking for possible laser signals from planets around distant stars, guessing that intelligent extraterrestrial beings would use them to signal to us. Maiman himself was particularly pleased with the medical applications of lasers, such as reattachment of detached retinas. He did not like, and played down, their use as weapons. This was a popular idea for a while after the tremendous potential power of the technology was recognized.

Infrared lasers (wavelength 30–1,000 μm) have found application in detecting explosives and in chemical-warfare agents. If the word 'erasers' were not already in use, perhaps infrared amplification by stimulated emission would be produced by 'irasers'. But the term laser actually refers to such systems with wavelengths up to 1 mm (above which the name maser takes over), and also to much shorter wavelengths: X-ray and γ-ray lasers are now with us, and their likely further development may prompt yet further scientific progress.

Stimulated emission of radiation, the critical process behind the laser, was first recognized by Albert Einstein as early as 1918. But it was only in 1951 that its use for practical amplification of electromagnetic waves was recognized, and in 1954 the first such device, the maser (for 'microwave amplification by stimulated emission'), operating at centimetre wavelengths, was constructed. Art Schawlow and I pointed out in 1958 how the same process could be made to work for light waves, which then set off a flurry of work in many places to actually build such a device.

All the earliest types of laser were invented in industry by recently hired young physicists who came from university work in radio or microwave spectroscopy. This appropriately brought together engineering and spectroscopy. Maiman's background was just such a case: at Stanford he had been a student of Willis Lamb, a Nobel laureate for his research on the spectrum of hydrogen. The next type of laser, similar to Maiman's but using a different type of crystal, was made by Peter Sorokin and Mirek Stevenson at IBM in Yorktown Heights, New York. The next was a continuously operating laser produced by an electrical discharge, created by Ali Javan, William Bennett and Don Herriott at the Bell Telephone Labs in Murray Hill, New Jersey.

After his invention, Maiman did early research in nonlinear optics, a field made possible by intense laser beams. He also formed several companies devoted to laser development and applications, including, in 1962, the Korad Corporation. His own account of his discovery was published in his book *The Laser Odyssey*, which was published in 2000.

Theodore Maiman's contribution, the first operating laser on Earth (they have now been found to occur naturally in astronomical objects) was truly historic, and has been widely recognized. He was chosen to be a member of the National Inventors Hall of Fame and of the US National Academies, and received many awards, including the Wolf Prize in Physics, the Oliver Buckley Prize and the Japan Prize.

Charles H. Townes
Charles H. Townes is in the Department of Physics, University of California, Berkeley, California 94720, USA. Together with Nicolay Basov and Aleksandr Prokhorov, he was awarded the 1964 Nobel Prize in Physics for his work on the maser–laser principle.
e-mail: cht@ssl.berkeley.edu

nature

FEATURE

Replicating genotype–phenotype associations

What constitutes replication of a genotype–phenotype association, and how best can it be achieved?

NCI-NHGRI Working Group on Replication in Association Studies

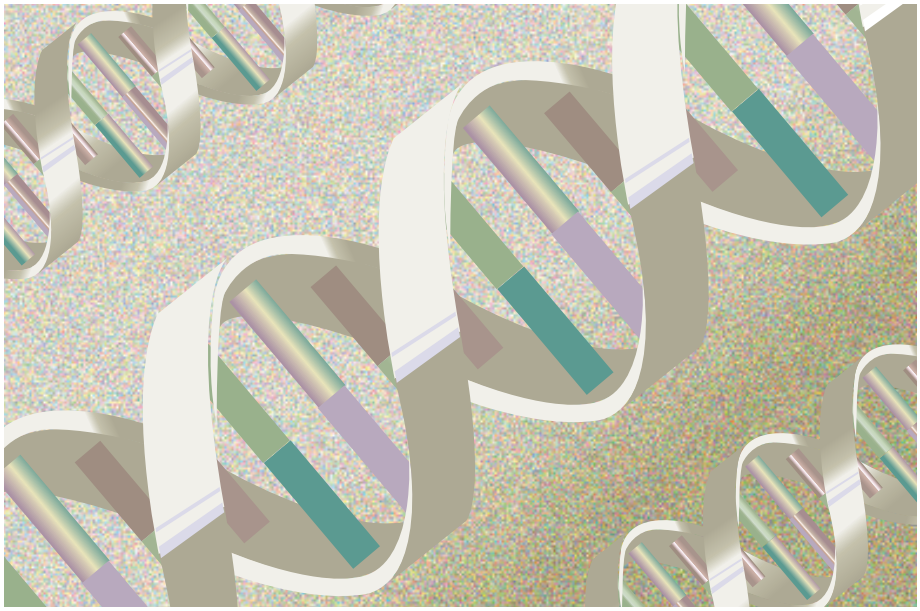

The study of human genetics has recently undergone a dramatic transition with the completion of both the sequencing of the human genome and the mapping of human haplotypes of the most common form of genetic variation, the single nucleotide polymorphism (SNP)[1–3]. In concert with this rapid expansion of detailed genomic information, cost-effective genotyping technologies have been developed that can assay hundreds of thousands of SNPs simultaneously. Together, these advances have allowed a systematic, even 'agnostic', approach to genome-wide interrogation, thereby relaxing the requirement for strong prior hypotheses.

So far, comprehensive reviews of the published literature, most of which reports work based on the candidate-gene approach, have demonstrated a plethora of questionable genotype–phenotype associations, replication of which has often failed in independent studies[4–7]. As the transition to genome-wide association studies occurs, the challenge will be to separate true associations from the blizzard of false positives attained through attempts to replicate positive findings in subsequent studies. The purpose of a replication study is to evaluate a positive finding from a previous study, to provide credibility that the initial finding is valid. Replication is essential for establishing the credibility of a genotype–phenotype association, whether derived from candidate-gene or genome-wide association studies. However, there is a lack of agreement about what constitutes a finding deserving of replication, what constitutes an adequate replication study and what constitutes a replication or refutation.

Investigators and journal editors have offered guidelines for how to address this problem[8–12], but these initial efforts have been hampered by limited experience and conflicting empirical data. However, as evidence has accumulated, several instructive examples have emerged of genotype–phenotype associations being reproduced reliably in follow-up studies. These include peroxisome proliferator-activated receptor-γ (*PPARG*)[13] and the transcription factor *TCF7L2* (refs 14–19), related to diabetes; nucleotide-binding oligomerization domain containing 2 (*NOD2*) and Crohn's disease[20–22]; complement factor H (*CFH*) and age-related macular degeneration[23–26]; and chromosome region 8q24 and prostate cancer risk[27–31].

Many instances have arisen in which initial findings have not been reproduced in follow-up studies because of issues in either the initial study or the attempted replication[4–6,32,33]. Small sample size is a frequent problem and can result in insufficient power to detect minor contributions of one or more alleles. Similarly, small sample sizes can provide imprecise or incorrect estimates of the magnitude of the observed effects. Poor study design — particularly a lack of comparability between cases and controls — can increase the risk of biases because there can be heterogeneity in exposure to environmental challenges and population stratification. The latter arises when investigators fail to account for case–control differences in the genetic structure of the underlying population. Heterogeneity in classification of outcomes across studies can undermine the opportunity to compare among them. Similarly, data 'dredging' can be a major problem, especially when criteria for defining phenotypes are altered to achieve statistical significance worthy of publication.

Another challenge arises when follow-up studies analyse different variants. An example is the reported association between *DTNBP1* and schizophrenia, initially identified in Irish pedigrees[34] and 'confirmed' in independent European studies[35]. Unfortunately, different risk alleles and haplotypes were reported in each study, making comparison difficult[36–39]. Although it is plausible that more than one variant could contribute to schizophrenia risk at the *DTNBP1* locus, it is difficult to draw this conclusion from the literature because follow-up studies have not consistently analysed the same markers or those in perfect linkage disequilibrium ($r^2 = 1.0$). Other recent examples for which initial reports of association have been inconsistently replicated include insulin-induced gene 2 (*INSIG2*) and obesity[40–44], and cyclic-AMP-specific phosphodiesterase (*PDE4D*) and stroke[45,46]. These have been accompanied by controversies about what actually constitutes replication.

This paper presents the conclusions of a working group on the replication of genotype–phenotype associations — whether identified in genome-wide or candidate-gene studies — convened by the National Cancer Institute and the National Human Genome Research Institute. The group was composed of experts from diverse disciplines, including biostatistics, clinical medicine, epidemiology, genetics and scientific publishing. The purpose was to review the current state of the field and propose best practices for the design, conduct and publication of replication studies that aim to follow up notable findings, particularly in genome-wide association studies. The group addressed three topics. First, assessment of the validity and limitations of any single genetic association study. Second, criteria for establishing replication in genetic association studies. Third, points to consider for publication of high-quality genotype–phenotype association reports (Box 1).

Box 1 | Points to consider in genotype–phenotype association reports

This checklist is intended to serve as a guide for authors, journal editors and referees to allow clear and unambiguous interpretation of the data and results of genome-wide and other genotype–phenotype association studies.

Study information
- A detailed description of the study design and its implementation
- The source of cases and controls (or cohort members, if based on cohort design), including time period and location(s) of subject recruitment
- Methods for ascertaining and validating affected or unaffected status and reproducibility of classification
- Participation rates for cases, controls or cohort members
- Presentation of case and control selection in a flow chart, including exclusion points for missing and erroneous data (possibly as supplementary tables)
- Initial table comparing relevant characteristics (such as demographics, risk factors and exposures) of cases and controls
- Success rate for DNA acquisition, including comparisons of those with and without collection, extraction failures and exclusions due to inconsistent data

Data issues
- Statement on availability of results and data so that, as far as possible, others can analyse them independently
- Links to supplemental online resources and database accession numbers

Genotyping and quality control procedures
- Sample tracking methods, such as bar-coding, to ensure accuracy of analysis
- Description of genotyping assays and protocols, particularly when new or applied in a non-standard method
- Description of genotyping calling algorithm
- Genotype quality control design for samples, including numbers, plating locations, selection criteria for:
  - External control samples from standard accepted sets (such as HapMap)
  - Internal control samples (duplicate samples; it should be specified whether these are from the same or different DNA collection, extraction or aliquot)
- Assay and DNA quality metrics by locus, sample, plate or 'batch'
- Assay call rates
- Average error rates estimated by internal duplicates or external samples
- Assay reproducibility: concordance for performance of extraction, aliquoting (internal control samples) and assay reproducibility
- Concordance with published or previously generated genotypes
- Mendelian consistency checks if related individuals are present
- Detection of inconsistent or cryptic relatedness in study subjects
- Evaluation of deviations from Hardy–Weinberg proportions to detect failed assays or large-scale stratification (for example, testing Hardy–Weinberg equilibrium 'violations') separately in cases and controls
- Assessment of population heterogeneity, including
  - Average or median value of chi-square and full distribution
  - Q–Q plots of chi-square analysis and *P*-values (with specific description of type of test used to generate the values)
- Validation of most critical results on an independent genotyping platform

Results
- Analysis methods in sufficient detail to reconstruct the analytical approach and reproduce all reported results
- Description of any pre-analysis weighting scheme for selecting variants for replication
- Simple single-locus and multi-marker (haplotype) association analyses
- Genetic models tested (unconstrained genotype effects — dominant, additive, multiplicative or trend)
- Graphical display of genotype clustering for assays of high interest
- Verification of results at highly correlated loci
- Discussion of choice of threshold for significance and the statistical basis for any adjustment for multiple testing and the relationship to overall study power
- Significance of any known 'positive controls' (that is, loci established in previous genetic associations)
- Consistency of results before and after application of quality control filters

Replication studies
- Description of replication samples, including source, ascertainment and comparability to initial sample
- Discussion of choice of threshold for significance and the statistical basis for any adjustment for multiple testing and the relationship to overall study power
- Summary of replication and analysis attempts by authors
- Summary of all known replication attempts by others, including non-replications

Genotyping data and specifications for deposition in standard databases
- Availability of 'raw' genotype data in the technology and vendor format, consistent with the requirements or restrictions imposed by funding agencies or informed consent
- Data extraction and processing protocols
- Normalization, transformation and data selection procedures and parameters

Points for reviewers and authors to consider regarding priority for publication
- Strength of observation
- Suitably large sample size
- Sufficiently stringent criteria for significance (small *P*-values)
- High quality of study design, including selection of study population, reliability of phenotypes, measurement and adjustment for potential confounders
- Discussion and conclusions commensurate with sample size, power, *P*-value and epidemiological quality of study design
- Quality control standards used, including assessment of genotype quality and completeness
- Usefulness of observations to others for subsequent research
- Value of initial hypothesis described
- Brief presentation of implications, especially as they relate to further follow-up both of genetic markers and for corroborative studies to investigate plausibility
- Explanations of notable findings
- Appropriate alternative explanations proposed and briefly discussed
- Biological or functional explanations based firmly on available data

Initial association studies

The initial study of any association represents an important discovery tool. In the near future, it is unlikely that a single study will unequivocally establish a valid genotype–phenotype association and not require replication. A number of points relating to the study design and reporting should be considered in determining whether a finding in an initial genome-wide or candidate-gene study merits follow-up replication studies (Box 2). Attempts to replicate a reported association are often complicated by lack of methodological detail in the initial report or lack of methodological rigour in the original study.

Because of the enormous number of genotype–phenotype associations tested in each genome-wide study, spurious associations will substantially outnumber true ones unless rigorous statistical thresholds are applied. Although no universal threshold can be specified for statistical significance in all circumstances, smaller *P*-values generally provide greater support for a true association. Extremely small *P*-values should be interpreted carefully, however, until completion of replication studies, because many can be due to inappropriate reliance on asymptotic distributions of test statistics, or to technical artefact or genotype errors that are distributed differently between cases and controls. Cluster plots for highly significant markers should be examined carefully. It may be desirable to include confirmatory data from a second genotyping technology in the initial report to verify genotype accuracy. Cases and controls should be drawn from populations that are generally comparable both in terms of genetic background and environmental exposures[47], and should be analysed for

confounding population stratification. This may require genotyping of ancestry informative markers (AIMs), which should be strongly encouraged as genotype costs fall and AIMs become increasingly well-characterized within marker sets. Family-based studies are affected by population stratification, so researchers should opt for methods robust to this, such as transmission disequilibrium methods[48]. They may be particularly valuable in the initial study if there is evidence for ethnic differences in the genetic effect of a trait, although at the cost of increased genotyping. Cautious interpretation is required either if significance is observed only for unusual or highly specific phenotypes (especially if they represent a small proportion of the study sample) or if significance depends on a particular analytical method that is not publicly available for confirmation.

Approaches for dealing with multiple comparisons are beyond the scope of this report, but more robust methods are clearly needed[49]. Permutation testing is an effective strategy to address the problem of multiple comparisons, especially if a large number of phenotypes are being analysed. Many methods for addressing the problem of multiple comparisons invoke a conservative approach, namely a standard Bonferroni correction, which assumes the independence of all tests performed. In many association studies, markers are not independent because they are in linkage disequilibrium, and so a standard Bonferroni correction is overly conservative. Lowering the threshold for calling a finding of particular variants — such as non-synonymous coding SNPs — positive in the analysis scheme (weighting) has merit but must be declared before initiation of the analysis and not once the analysis has begun[49,50]. The number of variants for which there is either credible laboratory evidence or a validated *in silico* prediction *a priori* is quite small. However, the temptation to create a credible biological hypothesis *post hoc* can be quite strong.

At present, many studies are barely powered to identify, much less to establish, associations of common alleles of weak effect in complex diseases[51,52]. Recently, appreciation of this crucial issue has led to larger, more definitive studies, such as the Cancer Genetic Markers of Susceptibility (CGEMS) project and the Wellcome Trust Case Control Consortium, (WTCCC). An estimated large effect (that is, with an odds ratio greater than 2) in a well-powered study can lend credence to an association, because unknown confounding factors are less likely to produce large effects[53]. Unfortunately, many risk variants contribute less than this. Small studies are prone to large variation in risk estimates, of which only selected strong positives are initially detected and reported. Furthermore, the estimate of the effect declines as replication studies are pursued, a phenomenon known as 'winner's curse'[54,55].

Consortial studies comprised of multiple independent studies combined into a pooled analysis can be viewed as a practical approach that overcomes many of the disadvantages of a disconnected set of underpowered studies. In addition, consortia may meet the need for rapid replication by achieving sufficiently large sample size[40,56]. Collaborations among multiple independent studies can offer important advantages over a single large study, particularly regarding the generalizability of findings observed in multiple studies that typically have greater diversity of populations and/or exposures.

As far as possible, similarly rigorous criteria should be considered for evaluation of genotype–phenotype association studies with limited or no availability of subjects for replication, such as studies of rare diseases or severe toxicity due to therapy or environmental exposures. In these circumstances, additional information gathered from laboratory techniques, bioinformatic tools and *a priori* biological insight should be used to provide plausibility for interpreting genetic association findings. The expectation for demonstrated replication might be relaxed if it is unethical to attempt replication — such as in studies that link genetic variation with adverse effects of therapy or environmental exposure (for example, benzene or cigarette smoke). Similarly, the public health impact of a finding may lessen the stringency of expectation for replication before initial publication — for example, in an urgent situation in which effective intervention is available and can be readily implemented.

Genotype–phenotype associations that have been replicated widely have often used clearly defined phenotypes classified by standard and widely-accepted criteria, such as diabetes and age-related macular degeneration[57,58]. Use of accepted criteria should reduce misclassification rates[59]. Some association studies have reported intermediate phenotypes (known as endophenotypes) but have provided little detail on the actual measure or its reliability[60]. In the absence of standard criteria, sufficient detail should be provided for both the definition of the phenotypes investigated and assessment of their validity and comparability across studies.

Replication of initial studies

To establish a positive replication of a genotype–phenotype association, many of the same considerations important for genome-wide association or candidate-gene studies should be fulfilled (Box 3). In replication studies, every effort should be made to analyse phenotypes comparable to those reported in the initial study. In the first attempt to replicate a finding, comparable populations should be analysed not only for the main effect but also to guard against confounding population stratification, either in the initial or replication studies[61,62]. Because many initial studies and replication studies have been reported in populations of European descent, the challenge remains to extend the studies to other populations. It has already been shown that many variants that have a significant association with disease in several studies in one population may not necessarily have the same association in another (such as *TCF7L2* in West Africa and

Box 2 | Suggested criteria for establishing the soundness of an initial association report

These criteria are intended for studies of genotype–phenotype associations assessed by genome-wide or candidate-gene approaches.

- Statistical analyses demonstrating the level of statistical significance of a finding should be published or at least available so that others can attempt to reproduce the reported results
- Explicit information should be provided about the study's power to detect a range of effects
- The study should be epidemiologically sound, with careful accounting for potential biases in selection of subjects, characterization of phenotypes, comparability of environmental exposures (when possible) and underlying population structure in cases and controls
- Phenotypes should be assessed according to standard definitions provided in the report
- Associations should be consistent (within the range of expected statistical fluctuation) and reported for the same phenotypes across study subgroups or across similar phenotypes in the entire study group
- Significance should not depend on altering the quality control methods beyond standard approaches that could change inclusion or exclusion of large numbers of samples or loci
- Measures to assess the quality of genotype data should include results of known study sample duplicates or publicly available samples
- The results for concordance between duplicate samples (if applicable) as well as completion and call rates per SNP and per subject should be disclosed, along with rates of missing data
- A subset of notable SNPs should be evaluated with a second technology that verifies the same result with excellent concordance, because no technology is error-free
- Associations with nearby SNPs in strong linkage disequilibrium with the putatively associated SNP should be reported (and should be similar)
- The results of replication studies of previous findings should be reported even if the results are not significant
- Testing for differences in underlying population structure in case and control groups should be performed and reported
- Appropriate correction for multiple comparisons across all statistical tests examined should be reported. Comparison to genome-wide thresholds should be described. Similarly, for bayesian approaches, the choice of prior probabilities should be described

Box 3 | Suggested criteria for establishing positive replication

These criteria are intended for follow-up studies of initial reports of genotype–phenotype associations assessed by genome-wide or candidate-gene approaches.

- Replication studies should be of sufficient sample size to convincingly distinguish the proposed effect from no effect
- Replication studies should preferably be conducted in independent data sets, to avoid the tendency to split one well-powered study into two less conclusive ones
- The same or a very similar phenotype should be analysed
- A similar population should be studied, and notable differences between the populations studied in the initial and attempted replication studies should be described
- Similar magnitude of effect and significance should be demonstrated, in the same direction, with the same SNP or a SNP in perfect or very high linkage disequilibrium with the prior SNP (r^2 close to 1.0)
- Statistical significance should first be obtained using the genetic model reported in the initial study
- When possible, a joint or combined analysis should lead to a smaller *P*-value than that seen in the initial report[75]
- A strong rationale should be provided for selecting SNPs to be replicated from the initial study, including linkage-disequilibrium structure, putative functional data or published literature
- Replication reports should include the same level of detail for study design and analysis plan as reported for the initial study (Box 1)

East Asia[18,63,64]; in this case, it has provided an opportunity to refine the signal to a restricted region). In some circumstances, it might be impossible to conduct follow-up studies because of the uniqueness of a study population or the lack of availability of additional subjects for replication. If replication is not an option, interpretation of association findings could be supplemented by biological insights derived from the laboratory.

Evaluation of an association in populations of different ancestry from that of the initial report would generally be expected, because genomic variation is greater when compared across populations, and should increase confidence in the finding. By contrast, failure to replicate in a population different from that of the initial report does not necessarily invalidate the original finding. In some cases, the differences in linkage disequilibrium relationships across populations can be used to narrow the region of interest for later genetic and possible functional analysis. Owing to their robustness to population stratification, as noted above, family-based studies can also serve as valuable replication studies for notable findings[48].

Reports of attempts at replication should distinguish between tests of the same SNP as in the original study, SNPs in strong linkage disequilibrium with the reported SNP, and other SNPs that were genotyped to search for additional variants associated with disease in the region (Fig. 1). In some circumstances, the initial study might have identified a marker that is not in strong linkage disequilibrium with the causal variant, which could lead to a false refutation in a different population, whereas testing additional SNPs in the region might reveal another association worthy of follow-up. For clarity, if new, previously untested SNPs are included, they should be clearly identified and the rationale for their inclusion explicitly stated. If differences in linkage disequilibrium patterns across populations are used to invoke an association at a new marker but not at the originally tested marker, the different linkage disequilibrium patterns should be empirically demonstrated in the appropriate populations and shown to be a plausible and consistent explanation for both the new and original results. Otherwise, the new association cannot be considered a replication.

Publication of associations

The evaluation of a publication addressing one or more genotype–phenotype associations is a daunting task in the age of large, dense datasets. To this end, published genome-wide association reports should include detailed descriptions of design, genotyping and statistical methods, and results, even if available only through online supplements, or perhaps in a separate journal. A checklist of key possible issues is provided in Box 1 — this could be used as a guide for authors, editors, reviewers and the general readership.

It is a challenge to make the case for the importance of the replication finding(s) without exaggerating the significance of the observation. Remarks about possible follow-up of genetic markers and corroborative studies to investigate plausibility should be brief and well referenced. Authors should practise sound judgement and temper enthusiasm based on prior publications (especially from the same investigative group), particularly if the replication study results differ from those of the initial study. Disclosure of known previous attempts to replicate the reported findings, whether positive or negative, by the authors or others is important for interpreting the replication study.

Although it is desirable for the initial report of a genotype–phenotype association to include adequately powered replication studies, requiring replication with every initial study may not be necessary, as long as the preliminary nature of a study without replication is emphasized. Such studies can still provide valuable information if the entire set of results is made available, and releasing such results before replication would be of value to the field. However, there is substantial added value in presenting robust findings based on an initial scan together with follow-up replication, and an appropriate balance is needed that facilitates rapid publication of valid findings and encourages collaboration[19,65]. If replication studies are included, each should be described or referenced in the same detail as the initial study and should include the results for all SNPs tested at each stage. As noted above, replication studies should preferably investigate the same or a very similar phenotype.

In many cases, the follow-up study will fail to replicate the initial results. Such findings are valuable for distinguishing false-positives from the true-positive signals that should be pursued for putative causal variants. The preference for publishing positive findings, even if derived from suboptimal studies, presents a formidable barrier to the dissemination of well-conducted negative studies. Failure to disseminate results from well-conducted negative studies withholds essential pieces of evidence for investigators who may be deciding whether to launch a follow-up study to replicate or to extend the original study. Thus, high-quality instances of 'meaningful negativity' are useful and should be reported succinctly in the literature. Criteria for a meaningful negative

Figure 1 | Linkage disequilbrium across the region containing SNPs associated with breast cancer in *FGFR2*. Black diamonds represent four single nucleotide polymorphisms (SNPs; rs11200014, rs2981579, rs1219648 and rs2420946) for which associations with breast cancer were replicated in multiple studies[73,74]. Estimates of the square of the correlation coefficient (r^2) were calculated for each pairwise comparison of SNPs in the initial genome-wide association study across the *FGFR2* region[73]. The log(10) r^2 values are colour-coded.

replication study are the same as those for a positive study (Box 3), with the added requirements that the same trait should be studied in a population of comparable underlying structure with sufficient power to measure the appropriate effect size and yield a negative result.

Negative studies are difficult to publish but they are crucial for separating true-positive from false-positive findings. Journals are strongly encouraged to publish high-quality negative studies refuting earlier positive reports of genotype–phenotype associations. The journal in which the initial scan is published is encouraged to solicit and publish well-conducted follow-up studies within a specified time frame, perhaps between 3 and 9 months of the initial report. A case in point is the recent collection of reports published by *The American Journal of Human Genetics*[66–71] that failed to replicate the initial findings of a genome-wide association study on Parkinson's disease. A handful of journals — such as *Cancer Epidemiology, Biomarkers and Prevention* and the new *PLoS* series[72] — currently feature well-conducted negative reports, and such efforts are to be lauded. The value of a well-executed negative study cannot be overemphasized; more venues are needed to capture these valuable results.

Although there are challenges to making data on individual research participants available to other investigators, every effort should be made to provide researchers with an opportunity to reproduce the reported results and to investigate new hypotheses and methods. To facilitate this research in genome-wide association studies, a public data archive known as the Database of Genotypes and Phenotypes, or dbGaP (http://view.ncbi.nlm.nih.gov/dbgap) has been established at the National Library of Medicine's National Center for Biotechnology Information and will be used by many National Institutes of Health (NIH)-supported studies. dbGaP will provide study documentation and aggregated genotype and phenotype data through its website with no account or authorization required. Access to individual, de-identified genotype and phenotype data will require an authorization and approval process that is currently under development. Whether through dbGaP or other venues, genotype summaries of computed analyses should be published online unless there are strong reasons not to do so, such as data derived from special populations (that is, isolated populations or minority communities) or other groups that will not permit such sharing. There are substantial informatic challenges for data presentation and data archiving, especially on public and journal websites. Best practices for retrieval and analysis of such data continue to evolve.

Conclusion

The history of genotype–phenotype association studies has focused on initial discoveries as opposed to careful replication. Earlier attention to the appropriate design of subsequent replication studies might have helped limit the plethora of false-positive results. Determination of valid genotype–phenotype associations presents a series of challenges that will require a logical strategy for conducting well-designed studies, based on excellent quality control practices interwoven with sound analytical methods and judicious interpretation. Other than the obvious differences in the drawbacks involved in multiple comparisons, standards for assessing the validity of the initial findings of a genotype–phenotype association should not differ substantially between the candidate-gene approach and genome-wide association studies. As experience accumulates, we can look forward to methodological advances that will facilitate our interpretation of studies, such as continued improvement of proposed methods for lowering the threshold for positive findings, adjustments for population structure, and exploitation of linkage disequilibrium structure in a candidate region.

The best practices suggested here for reporting initial and replication studies are based on sufficient disclosure of study methods to permit independent confirmation of study findings. Often a sequence of studies will be required to establish a valid genotype–phenotype association, perhaps involving several rounds of replication studies. And, of course, the conclusive demonstration of a replicated association represents only the beginning of the process towards finding the causal genetic variant(s). Labour-intensive and costly investigation will subsequently be required to sequence the candidate interval in depth, genotype all the common and perhaps uncommon variants that are markers for the outcomes of interest in multiple population samples, understand their functional consequences, examine their potential interactions with other genes or environmental factors, and devise strategies for preventative or therapeutic interventions. None of these steps should proceed far, however, without conclusive replication of findings from an initial genotype–phenotype association study. ■

Note added in proof: Recently, a series of papers have also shown replication across as well as within genome-wide association studies in common complex diseases such as breast cancer, type 2 diabetes, and coronary disease[73,74,76–81].

1. International Human Genome Sequencing Consortium. Finishing the euchromatic sequence of the human genome. *Nature* **431,** 931–945 (2004).
2. The International HapMap Consortium. A haplotype map of the human genome. *Nature* **437,** 1299–1320 (2005).
3. Hinds, D. A. *et al.* Whole-genome patterns of common DNA variation in three human populations. *Science* **307,** 1072–1079 (2005).
4. Hirschhorn, J. N., Lohmueller, K., Byrne, E. & Hirschhorn, K. A comprehensive review of genetic association studies. *Genet. Med.* **4,** 45–61 (2002).
5. Ioannidis, J. P., Ntzani, E. E., Trikalinos, T. A. & Contopoulos-Ioannidis, D. G. Replication validity of genetic association studies. *Nature Genet.* **29,** 306–309 (2001).
6. Lohmueller, K. E., Pearce, C. L., Pike, M., Lander, E. S. & Hirschhorn, J. N. Meta-analysis of genetic association studies supports a contribution of common variants to susceptibility to common disease. *Nature Genet.* **33,** 177–182 (2003).
7. Ioannidis, J. P. Common genetic variants for breast cancer: 32 largely refuted candidates and larger prospects. *J. Natl Cancer Inst.* **98,** 1350–1353 (2006).
8. Freely associating. *Nature Genet.* **22,** 1–2 (1999).
9. Todd, J. A. Statistical false positive or true disease pathway? *Nature Genet.* **38,** 731–733 (2006).
10. Neale, B. M. & Sham, P. C. The future of association studies: gene-based analysis and replication. *Am. J. Hum. Genet.* **75,** 353–362 (2004).
11. Clark, A. G., Boerwinkle, E., Hixson, J. & Sing, C. F. Determinants of the success of whole-genome association testing. *Genome Res.* **15,** 1463–1467 (2005).
12. Freimer, N. B. & Sabatti, C. Human genetics: variants in common diseases. *Nature* **445,** 828–830 (2007).
13. Altshuler, D. *et al.* The common PPARγ Pro12Ala polymorphism is associated with decreased risk of type 2 diabetes. *Nature Genet.* **26,** 76–80 (2000).
14. Field, S. F. *et al.* Analysis of the type 2 diabetes gene, *TCF7L2*, in 13,795 type 1 diabetes cases and control subjects. *Diabetologia* **50,** 212–213 (2007).
15. Grant, S. F. *et al.* Variant of transcription factor 7-like 2 (*TCF7L2*) gene confers risk of type 2 diabetes. *Nature Genet.* **38,** 320–323 (2006).
16. Groves, C. J. *et al.* Association analysis of 6,736 U.K. subjects provides replication and confirms *TCF7L2* as a type 2 diabetes susceptibility gene with a substantial effect on individual risk. *Diabetes* **55,** 2640–2644 (2006).
17. Saxena, R. *et al.* Common single nucleotide polymorphisms in *TCF7L2* are reproducibly associated with type 2 diabetes and reduce the insulin response to glucose in nondiabetic individuals. *Diabetes* **55,** 2890–2895 (2006).
18. Helgason, A. *et al.* Refining the impact of *TCF7L2* gene variants on type 2 diabetes and adaptive evolution. *Nature Genet.* **39,** 218–225 (2007).
19. Sladek, R. *et al.* A genome-wide association study identifies novel risk loci for type 2 diabetes. *Nature* **445,** 881–885 (2007).
20. Hugot, J. P. *et al.* Association of NOD2 leucine-rich repeat variants with susceptibility to Crohn's disease. *Nature* **411,** 599–603 (2001).
21. Ogura, Y. *et al.* A frameshift mutation in NOD2 associated with susceptibility to Crohn's disease. *Nature* **411,** 603–606 (2001).
22. Economou, M., Trikalinos, T. A., Loizou, K. T., Tsianos, E. V. & Ioannidis, J. P. Differential effects of NOD2 variants on Crohn's disease risk and phenotype in diverse populations: a metaanalysis. *Am. J. Gastroenterol.* **99,** 2393–2404 (2004).
23. Edwards, A. O. *et al.* Complement factor H polymorphism and age-related macular degeneration. *Science* **308,** 421–424 (2005).
24. Hageman, G. S. *et al.* A common haplotype in the complement regulatory gene factor H (HF1/CFH) predisposes individuals to age-related macular degeneration. *Proc. Natl Acad. Sci. USA* **102,** 7227–7232 (2005).
25. Klein, R. J. *et al.* Complement factor H polymorphism in age-related macular degeneration. *Science* **308,** 385–389 (2005).
26. Haines, J. L. *et al.* Complement factor H variant increases the risk of age-related macular degeneration. *Science* **308,** 419–421 (2005).
27. Freedman, M. L. *et al.* Admixture mapping identifies 8q24 as a prostate cancer risk locus in African-American men. *Proc. Natl Acad. Sci. USA* **103,** 14068–14073 (2006).
28. Amundadottir, L. T. *et al.* A common variant associated with prostate cancer in European and African populations. *Nature Genet.* **38,** 652–658 (2006).
29. Gudmundsson, J. *et al.* Genome-wide association study identifies a second prostate cancer susceptibility variant at 8q24. *Nature Genet.* **39,** 631–637 (2007).
30. Haiman, C. A. *et al.* Multiple regions within 8q24 independently affect risk for prostate cancer. *Nature Genet.* **39,** 638–644 (2007).
31. Yeager, M. *et al.* Genome-wide association study of prostate cancer identifies a second risk locus at 8q24. *Nature Genet.* **39,** 645–649 (2007).
32. Colhoun, H. M., McKeigue, P. M. & Davey, S. G. Problems of reporting genetic associations with complex outcomes. *Lancet* **361,** 865–872 (2003).
33. Ioannidis, J. P., Trikalinos, T. A. & Khoury, M. J. Implications of small effect sizes of individual genetic variants on the design and interpretation of genetic association studies of complex diseases. *Am. J. Epidemiol.* **164,** 609–614 (2006).

34. Straub, R. E. *et al.* Genetic variation in the 6p22.3 gene *DTNBP1*, the human ortholog of the mouse dysbindin gene, is associated with schizophrenia. *Am. J. Hum. Genet.* **71,** 337–348 (2002).
35. Van Den, B. A. *et al.* The *DTNBP1* (dysbindin) gene contributes to schizophrenia, depending on family history of the disease. *Am. J. Hum. Genet.* **73,** 1438–1443 (2003).
36. Bray, N. J. *et al.* Haplotypes at the dystrobrevin binding protein 1 (*DTNBP1*) gene locus mediate risk for schizophrenia through reduced *DTNBP1* expression. *Hum. Mol. Genet.* **14,** 1947–1954 (2005).
37. Funke, B. *et al.* Association of the *DTNBP1* locus with schizophrenia in a U.S. population. *Am. J. Hum. Genet.* **75,** 891–898 (2004).
38. Kirov, G. *et al.* Strong evidence for association between the dystrobrevin binding protein 1 gene (*DTNBP1*) and schizophrenia in 488 parent-offspring trios from Bulgaria. *Biol. Psychiatry* **55,** 971–975 (2004).
39. Mutsuddi, M. *et al.* Analysis of high-resolution HapMap of *DTNBP1* (Dysbindin) suggests no consistency between reported common variant associations and schizophrenia. *Am. J. Hum. Genet.* **79,** 903–909 (2006).
40. Herbert, A. *et al.* A common genetic variant is associated with adult and childhood obesity. *Science* **312,** 279–283 (2006).
41. Hall, D. H., Rahman, T., Avery, P. J. & Keavney, B. INSIG-2 promoter polymorphism and obesity related phenotypes: association study in 1428 members of 248 families. *BMC Med. Genet.* **7,** 83 (2006).
42. Rosskopf, D. *et al.* Comment on 'A common genetic variant is associated with adult and childhood obesity'. *Science* **315,** 187 (2007).
43. Dina, C. *et al.* Comment on 'A common genetic variant is associated with adult and childhood obesity'. *Science* **315,** 187 (2007).
44. Loos, R. J., Barroso, I., O'rahilly, S. & Wareham, N. J. Comment on 'A common genetic variant is associated with adult and childhood obesity'. *Science* **315,** 187 (2007).
45. Gretarsdottir, S., Gulcher, J., Thorleifsson, G., Kong, A. & Stefansson, K. Comment on the phosphodiesterase 4D replication study by Bevan *et al. Stroke* **36,** 1824 (2005).
46. Rosand, J., Bayley, N., Rost, N. & de Bakker, P. I. Many hypotheses but no replication for the association between *PDE4D* and stroke. *Nature Genet.* **38,** 1091–1092 (2006).
47. Manolio, T. A., Bailey-Wilson, J. E. & Collins, F. S. Genes, environment and the value of prospective cohort studies. *Nature Rev. Genet.* **7,** 812–820 (2006).
48. Spielman, R. S. & Ewens, W. J. The TDT and other family-based tests for linkage disequilibrium and association. *Am. J. Hum. Genet.* **59,** 983–989 (1996).
49. Roeder, K., Bacanu, S. A., Wasserman, L. & Devlin, B. Using linkage genome scans to improve power of association in genome scans. *Am. J. Hum. Genet.* **78,** 243–252 (2006).
50. Wacholder, S., Chanock, S., Garcia-Closas, M., El Ghormli, L. & Rothman, N. Assessing the probability that a positive report is false: an approach for molecular epidemiology studies. *J. Natl Cancer Inst.* **96,** 434–442 (2004).
51. Risch, N. & Merikangas, K. The future of genetic studies of complex human diseases. *Science* **273,** 1516–1517 (1996).
52. Risch, N. J. Searching for genetic determinants in the new millennium. *Nature* **405,** 847–856 (2000).
53. Angell, M. The interpretation of epidemiologic studies. *N. Engl. J. Med.* **323,** 823–825 (1990).
54. Clarke, R. *et al.* Lymphotoxin-α gene and risk of myocardial infarction in 6,928 cases and 2,712 controls in the ISIS case-control study. *PLoS Genet.* **2,** e107 (2006).
55. Zollner, S. & Pritchard, J. Overcoming the winner's curse: estimating penetrance parameters from case-control. *Am. J. Hum. Genet.* **80,** 605–615 (2007).
56. Rothman, N. *et al.* Genetic variation in *TNF* and *IL10* and risk of non-Hodgkin lymphoma: a report from the InterLymph Consortium. *Lancet Oncol.* **7,** 27–38 (2006).
57. Report of the Expert Committee on the Diagnosis and Classification of Diabetes Mellitus. *Diabetes Care* **20,** 1183–1197 (1997).
58. A randomized, placebo-controlled, clinical trial of high-dose supplementation with vitamins C and E and beta carotene for age-related cataract and vision loss. AREDS report no. 9. *Arch. Ophthalmol.* **119,** 1439–1452 (2001).
59. Freimer, N. & Sabatti, C. The human phenome project. *Nature Genet.* **34,** 15–21 (2003).
60. Flint, J. & Munafo, M. R. The endophenotype concept in psychiatric genetics. *Psychol. Med.* **37,** 163–180 (2007).
61. Wacholder, S., Rothman, N. & Caporaso, N. Population stratification in epidemiologic studies of common genetic variants and cancer: quantification of bias. *J. Natl Cancer Inst.* **92,** 1151–1158 (2000).
62. Price, A. L. *et al.* Principal components analysis corrects for stratification in genome-wide association studies. *Nature Genet.* **38,** 904–909 (2006).
63. Chandak, G. R. *et al.* Common variants in the *TCF7L2* gene are strongly associated with type 2 diabetes mellitus in the Indian population. *Diabetologia* **50,** 63–67 (2007).
64. Horikoshi, M. *et al.* A genetic variant of the transcription factor 7-like 2 gene is associated with risk of type 2 diabetes in the Japanese population. *Diabetologica* **50,** 747–751 (2007).
65. Duerr, R. H. *et al.* A genome-wide association study identifies *IL23R* as an inflammatory bowel disease gene. *Science* **314,** 1461–1463 (2006).
66. Maraganore, D. M. *et al.* High-resolution whole-genome association study of Parkinson disease. *Am. J. Hum. Genet.* **77,** 685–693 (2005).
67. Myers, D. R. Considerations for genomewide association studies in Parkinson disease. *Am. J. Hum. Genet.* **78,** 1081–1082 (2006).
68. Clarimon, J. *et al.* Conflicting results regarding the semaphorin gene (*SEMA5A*) and the risk for Parkinson disease. *Am. J. Hum. Genet.* **78,** 1082–1084 (2006).
69. Farrer, M. J. *et al.* Genomewide association, Parkinson disease, and *PARK10*. *Am. J. Hum. Genet.* **78,** 1084–1088 (2006).
70. Goris, A. *et al.* No evidence for association with Parkinson disease for 13 single-nucleotide polymorphisms identified by whole-genome association screening. *Am. J. Hum. Genet.* **78,** 1088–1090 (2006).
71. Li, Y. *et al.* A case-control association study of the 12 single-nucleotide polymorphisms implicated in Parkinson disease by a recent genome scan. *Am. J. Hum. Genet.* **78,** 1090–1092 (2006).
72. Patterson, M. & Cardon, L. Replication publication. *PLoS. Biol.* **3,** e327 (2005).
73. Hunter, D. J. *et al.* A genome-wide association study identifies alleles in *FGFR2* associated with risk of sporadic postmenopausal breast cancer. *Nature Genet.* Advance online publication, 27 May 2007 (doi:10.1038/ng2075).
74. Easton, D. F. *et al.* Genome-wide association study identifies novel breast cancer susceptibility loci. *Nature* Advance online publication, 27 May 2007 (doi:10.1038/nature05887).
75. Skol, A. D., Scott, L. J., Abecasis, G. R. & Boehnke, M. Joint analysis is more efficient than replication-based analysis for two-stage genome-wide association studies. *Nature Genet.* **38,** 209–213 (2006).
76. Stacey, S. N. *et al.* Common variants on chromosomes 2q35 and 16q12 confer susceptibility to estrogen receptor-positive breast cancer. *Nature Genet.* Advance online publication, 27 May 2007 (doi:10.1038/ng2064)
77. Saxena, R. *et al.* Genome-wide association analysis identifies loci for type 2 diabetes and triglyceride levels. *Science* **316,** 1331–1336 (2007).
78. Scott, L. J. *et al.* A genome-wide association study of type 2 diabetes in Finns detects multiple susceptibility variants. *Science* **316,** 1341–1345 (2007).
79. Zeggini, E. Replication of genome-wide association signals in UK samples reveals risk loci for type 2 diabetes. *Science* **316,** 1336–1341 (2007).
80. Helgadottir, A. *et al.* A common variant on chromosome 9p21 affects the risk of myocardial infarction. *Science* Advance online publication, 3 May 2007 (doi:10.1126/science.1142842).
81. McPherson, R. *et al.* A common allele on chromosome 9 associated with coronary heart disease. *Science* Advance online publication, 3 May 2007 (doi:10.1126/science.1142447).

Author Contributions S.J.C. and T.M. contributed equally to this manuscript.

Author Information Reprints and permissions information is available at www.nature.com/reprints. The authors declare no competing financial interests. Correspondence and requests for materials should be addressed to S.J.C. or T.M. (e-mails: chanocks@mail.nih.gov; manoliot@nhgri.nih.gov).

Authorship of National Cancer Institute–National Human Genome Research Institute (NCI-NHGRI) Working Group on Replication in Association Studies

Stephen J. Chanock[1,2], Teri Manolio[3], Michael Boehnke[4], Eric Boerwinkle[5], David J. Hunter[6], Gilles Thomas[1], Joel N. Hirschhorn[7], Goncalo Abecasis[4], David Altshuler[8], Joan E. Bailey-Wilson[3], Lisa D. Brooks[3], Lon R. Cardon[9], Mark Daly[8], Peter Donnelly[10], Joseph F. Fraumeni Jr[1], Nelson B. Freimer[11], Daniela S. Gerhard[12], Chris Gunter[13], Alan E. Guttmacher[3], Mark S. Guyer[3], Emily L. Harris[3], Josephine Hoh[14], Robert Hoover[1], C. Augustine Kong[15], Kathleen R. Merikangas[16], Cynthia C. Morton[17], Lyle J. Palmer[18], Elizabeth G. Phimister[19], John P. Rice[20], Jerry Roberts[3], Charles Rotimi[21], Margaret A. Tucker[1], Kyle J. Vogan[22], Sholom Wacholder[1], Ellen M. Wijsman[23], Deborah M. Winn[24], Francis S. Collins[3]

[1]Division of Cancer Epidemiology and Genetics, and [2]Center for Cancer Research, National Cancer Institute, Bethesda, Maryland 20892-4605, USA. [3]National Human Genome Research Institute, National Institutes of Health, 31 Center Drive, Bethesda, Maryland 20892-2154, USA. [4]Department of Biostatistics, University of Michigan, 1420 Washington Heights, Ann Arbor, Michigan 48109-2029, USA. [5]Human Genetics Center, University of Texas Health Science Center, 1200 Herman Pressler, Houston, Texas 77030, USA. [6]Program in Molecular and Genetic Epidemiology, Harvard School of Public Health, Channing Laboratory, 181 Longwood Avenue, Boston, Massachusetts 02115, USA. [7]Children's Hospital Boston, Harvard Medical School, Broad Institute of MIT and Harvard, Seven Cambridge Center, Cambridge, Massachusetts 02114, USA. [8]Massachusetts General Hospital, Broad Institute of MIT and Harvard, 185 Cambridge Street, Cambridge, Massachusetts 02114, USA. [9]Human Biology Division, Fred Hutchinson Cancer Research Center, 1100 Fairview Avenue North, P.O. Box 19024, Seattle, Washington 98109-1024, USA. [10]University of Oxford, 1 South Parks Road, Oxford OX1 3TG, UK. [11]Center for Neurobehavioral Genetics, University of California, Los Angeles, 695 Charles E Young Drive South, Box 708822, Los Angeles, California 90095-7088, USA. [12] Office of Cancer Genomics, National Cancer Institute, National Institutes of Health, 31 Center Drive, Bethesda, Maryland 20892-2580, USA. [13]*Nature*, Ninth Floor, 75 Varick Street, New York, New York 10013, USA. [14]Epidemiology and Public Health, Yale University School of Medicine, 60 College Street, P.O. Box 208034, New Haven, Connecticut 06510, USA. [15]DeCode Genetics, 8 IS-101 Sturlugata, Reykjavik, Iceland. [16]National Institutes of Mental Health, National Institutes of Health, 35 Convent Drive, Bethesda, Maryland 20892-3720, USA. [17]Brigham and Women's Hospital, Harvard Medical School, 77 Avenue Louis Pasteur, Boston, Massachusetts 02115, USA. [18]Western Australian Institute for Medical Research and University of Western Australia, Queen Elizabeth II Medical Centre, Hospital Avenue, Nedlands WA6009, Australia. [19]*New England Journal of Medicine*, 10 Shattuck Street, Boston, Massachusetts 02115-6094, USA. [20]Washington University School of Medicine, Box 8134, 660 South Euclid Avenue, St Louis, Missouri 63110, USA. [21]Genetic Epidemiology Unit, Howard University, National Human Genome Center, 2041 Georgia Avenue, NW Washington, DC 20060, USA. [22]*Nature Genetics*, Suite 104, 25 First Street, Cambridge, Massachusetts 02141, USA. [23]Division of Medical Genetics and Department of Biostatistics, University of Washington, Box 357720, Seattle, Washington 98195-7720, USA. [24]Epidemiology and Genetics Research Program, National Cancer Institute, National Institutes of Health, 6130 Executive Boulevard, Bethesda, Maryland 20892-7393, USA.

ARTICLES

Genome-wide association study of 14,000 cases of seven common diseases and 3,000 shared controls

The Wellcome Trust Case Control Consortium*

There is increasing evidence that genome-wide association (GWA) studies represent a powerful approach to the identification of genes involved in common human diseases. We describe a joint GWA study (using the Affymetrix GeneChip 500K Mapping Array Set) undertaken in the British population, which has examined ~2,000 individuals for each of 7 major diseases and a shared set of ~3,000 controls. Case-control comparisons identified 24 independent association signals at $P < 5 \times 10^{-7}$: 1 in bipolar disorder, 1 in coronary artery disease, 9 in Crohn's disease, 3 in rheumatoid arthritis, 7 in type 1 diabetes and 3 in type 2 diabetes. On the basis of prior findings and replication studies thus-far completed, almost all of these signals reflect genuine susceptibility effects. We observed association at many previously identified loci, and found compelling evidence that some loci confer risk for more than one of the diseases studied. Across all diseases, we identified a large number of further signals (including 58 loci with single-point *P* values between 10^{-5} and 5×10^{-7}) likely to yield additional susceptibility loci. The importance of appropriately large samples was confirmed by the modest effect sizes observed at most loci identified. This study thus represents a thorough validation of the GWA approach. It has also demonstrated that careful use of a shared control group represents a safe and effective approach to GWA analyses of multiple disease phenotypes; has generated a genome-wide genotype database for future studies of common diseases in the British population; and shown that, provided individuals with non-European ancestry are excluded, the extent of population stratification in the British population is generally modest. Our findings offer new avenues for exploring the pathophysiology of these important disorders. We anticipate that our data, results and software, which will be widely available to other investigators, will provide a powerful resource for human genetics research.

Despite extensive research efforts for more than a decade, the genetic basis of common human diseases remains largely unknown. Although there have been some notable successes[1], linkage and candidate gene association studies have often failed to deliver definitive results. Yet the identification of the variants, genes and pathways involved in particular diseases offers a potential route to new therapies, improved diagnosis and better disease prevention. For some time it has been hoped that the advent of genome-wide association (GWA) studies would provide a successful new tool for unlocking the genetic basis of many of these common causes of human morbidity and mortality[1].

Three recent advances mean that GWA studies that are powered to detect plausible effect sizes are now possible[2]. First, the International HapMap resource[3], which documents patterns of genome-wide variation and linkage disequilibrium in four population samples, greatly facilitates both the design and analysis of association studies. Second, the availability of dense genotyping chips, containing sets of hundreds of thousands of single nucleotide polymorphisms (SNPs) that provide good coverage of much of the human genome, means that for the first time GWA studies for thousands of cases and controls are technically and financially feasible. Third, appropriately large and well-characterized clinical samples have been assembled for many common diseases.

The Wellcome Trust Case Control Consortium (WTCCC) was formed with a view to exploring the utility, design and analyses of GWA studies. It brought together over 50 research groups from the UK that are active in researching the genetics of common human diseases, with expertise ranging from clinical, through genotyping, to informatics and statistical analysis. Here we describe the main experiment of the consortium: GWA studies of 2,000 cases and 3,000 shared controls for 7 complex human diseases of major public health importance—bipolar disorder (BD), coronary artery disease (CAD), Crohn's disease (CD), hypertension (HT), rheumatoid arthritis (RA), type 1 diabetes (T1D), and type 2 diabetes (T2D). Two further experiments undertaken by the consortium will be reported elsewhere: a GWA study for tuberculosis in 1,500 cases and 1,500 controls, sampled from The Gambia; and an association study of 1,500 common controls with 1,000 cases for each of breast cancer, multiple sclerosis, ankylosing spondylitis and autoimmune thyroid disease, all typed at around 15,000 mainly non-synonymous SNPs. By simultaneously studying seven diseases with differing aetiologies, we hoped to develop insights, not only into the specific genetic contributions to each of the diseases, but also into differences in allelic architecture across the diseases. A further major aim was to address important methodological issues of relevance to all GWA studies, such as quality control, design and analysis. In addition to our main association results, we address several of these issues below, including the choice of controls for genetic studies, the extent of population structure within Great Britain, sample sizes necessary to detect genetic effects of varying sizes, and improvements in genotype-calling algorithms and analytical methods.

Samples and experimental analyses

Individuals included in the study were living within England, Scotland and Wales ('Great Britain') and the vast majority had

*Lists of participants and affiliations appear at the end of the paper.

self-identified themselves as white Europeans (153 individuals with non-Caucasian ancestry were excluded from final analysis—see below). The seven conditions selected for study are all common familial diseases of major public health importance both in the UK and globally[4], and for which suitable nationally representative sample sets were available. The control individuals came from two sources: 1,500 individuals from the 1958 British Birth Cohort (58C) and 1,500 individuals selected from blood donors recruited as part of this project (UK Blood Services (UKBS) controls). See Methods and Supplementary Table 1 for sample recruitment, phenotypes and summary details for each collection.

We adopted an experimental design with 2,000 cases for each disease and 3,000 combined controls. All 17,000 samples were genotyped with the GeneChip 500K Mapping Array Set (Affymetrix chip), which comprises 500,568 SNPs, as described in Methods. The power of this study (estimated from simulations that mimic linkage disequilibrium patterns in the HapMap Caucasian sample (CEU), see Methods) averaged across SNPs with minor allele frequencies (MAFs) above 5% is estimated to be 43% for alleles with a relative risk of 1.3, increasing to 80% for a relative risk of 1.5, for a *P*-value threshold of 5×10^{-7} (Supplementary Table 2).

We developed a new algorithm, CHIAMO, which we applied to simultaneously call the genotypes from all individuals (see Methods and Supplementary Information). Cross-platform comparison showed CHIAMO to outperform BRLMM (the standard Affymetrix algorithm) by having an error rate under 0.2% (Supplementary Table 3), and comparison of 10^8 duplicate genotypes in our study gave a discordance rate of 0.12%.

We excluded 809 samples after checks for contamination, false identity, non-Caucasian ancestry and relatedness (see Methods and Supplementary Table 4); 16,179 individuals remained in the study.

Genome-wide, 469,557 SNPs (93.8%) passed our quality control filters (described in Methods) giving an average call rate of 99.63%. Of those, 392,575 have study-wide MAFs $>1\%$ (45,106 have MAFs $<$ 0.1%; see also Supplementary Figs 1 and 2). Initial analyses of the polymorphic SNPs suggest that patterns of linkage disequilibrium in our samples are very similar to those in HapMap (Supplementary Fig. 3). Therefore, we expect genome coverage with the Affymetrix 500K set in this study to be similar to that estimated for the HapMap CEU panel[2].

All SNPs passing quality control filters were used in the association analyses, although power is very low for SNPs with low MAFs (unless they have unusually large effects). On visual inspection of the cluster plots of SNPs showing apparently strong association, we removed a further 638 SNPs with poor clustering.

Control groups

Our main purpose in using two control groups was to assess possible bias in ascertaining control samples. In addition, noting that DNA sample processing differed between these groups, comparison of control groups also provides a check for effects of differential genotyping errors as a result of differences in DNA collection and preparation. Figure 1a shows the results of 1-d.f. Mantel-extension tests[5] for differences in allele frequencies of SNPs between subjects from the 58BC and UKBS collections, stratified by 12 broad regions of Great Britain (see Supplementary Table 5 and Supplementary Fig. 4 for region definitions). The associated quantile-quantile plot (see Methods for background) in Fig. 1b shows good agreement with the null distribution (similar results are obtained for tests that do not stratify by geography, data not shown). The fact that we see few significant differences between these two control groups despite the fact that they differ in population groups sampled, DNA processing, and age, indicates that there would be little bias due to use of either sample as a control group for any of the case series, and justifies our combining of the two control groups to form a single group of 3,000 subjects for our main analyses.

One consequence of using a shared control group (for which detailed phenotyping for all traits of interest is not available) relates to the potential for misclassification bias: a proportion of the controls is likely to have the disease of interest (and therefore might meet the criteria for inclusion as a case) and some others will develop it in the future. However, the effect this has on power is modest unless the extent of misclassification bias is substantial; for example, if 5% of controls would meet the definition of cases at the same age, the loss of power is approximately the same as that due to a reduction of the sample size by 10%[6]. Even for the higher prevalence conditions examined by the WTCCC (such as HT, CAD and T2D), the precise ascertainment schemes used here (which enriched for more extreme phenotypes and/or strong family history) will have limited the proportions of controls meeting case criteria to low levels (for example, to $<5\%$). Although a study design which used 'hypercontrols' (that is, selection of control individuals from the lower extremity of the relevant trait distribution) would generally be the most powerful approach in a study focusing on one disease, the merits of such an approach need to be weighed against the additional costs associated with the need to phenotype and genotype each control sample.

Geographical variation and population structure

An additional cause of false positive findings is hidden population structure. Case and control samples may differ in the distribution of their ancestry, either owing to control sampling effects, as discussed above, or to confounding when different ancestries carry higher disease risk and are, as a result, over-represented in cases. Even after exclusion of individuals with evidence of recent non-European ancestry, the British population is heterogeneous, having been shaped by several waves of immigration from southern and northern Europe. Whether the differences between these incoming populations are sufficiently large to distort the findings of population-based case-control studies is an open question.

We first examined our samples for non-European ancestry, using multidimensional scaling after 'seeding' our data with those from the three HapMap analysis panels (see Supplementary Fig. 5 and

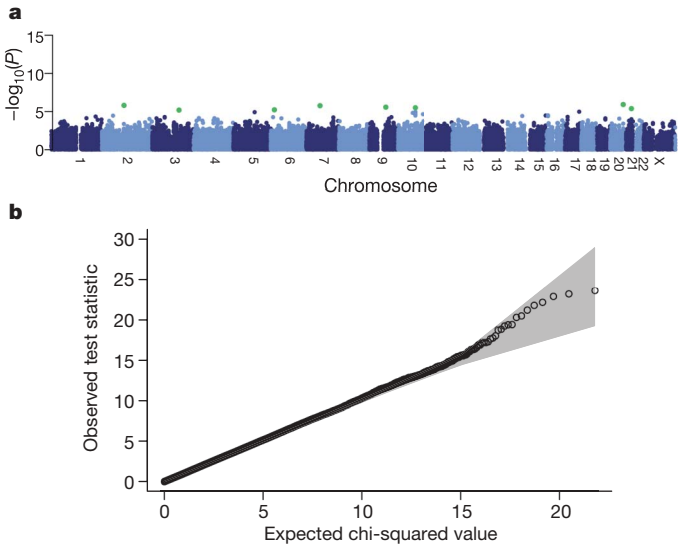

Figure 1 | Genome-wide scan for allele frequency differences between controls. **a**, *P* values from the trend test for differences between SNP allele frequencies in the two control groups, stratified by geographical region. SNPs have been excluded on the basis of failure in a test for Hardy–Weinberg equilibrium in either control group considered separately, a low call rate, or if minor allele frequency is less than 1%, but not on the basis of a difference between control groups. Green dots indicate SNPs with a *P* value $<1 \times 10^{-5}$. **b**, Quantile-quantile plots of these test statistics. In this and subsequent quantile-quantile plots, the shaded region is the 95% concentration band (see Methods).

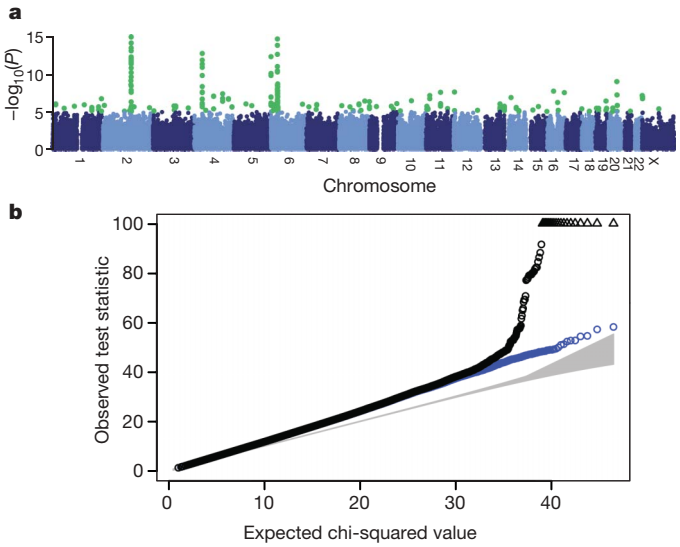

Figure 2 | Genome-wide picture of geographic variation. a, *P* values for the 11-d.f. test for difference in SNP allele frequencies between geographical regions, within the 9 collections. SNPs have been excluded using the project quality control filters described in Methods. Green dots indicate SNPs with a *P* value $<1 \times 10^{-5}$. **b**, Quantile-quantile plots of these test statistics. SNPs at which the test statistic exceeds 100 are represented by triangles at the top of the plot, and the shaded region is the 95% concentration band (see Methods). Also shown in blue is the quantile-quantile plot resulting from removal of all SNPs in the 13 most differentiated regions (Table 1).

Methods), and excluded 153 individuals on this basis. We next looked for evidence of population heterogeneity by studying allele frequency differences between the 12 broad geographical regions (defined in Supplementary Fig. 4). The results for these 11-d.f. tests and associated quantile-quantile plots are shown in Fig. 2. Widespread small differences in allele frequencies are evident as an increased slope of the line (Fig. 2b); in addition, a few loci show much larger differences (Fig. 2a and Supplementary Fig. 6).

Thirteen genomic regions showing strong geographical variation are listed in Table 1, and Supplementary Fig. 7 shows the way in which their allele frequencies vary geographically. The predominant pattern is variation along a NW/SE axis. The most likely cause for these marked geographical differences is natural selection, most plausibly in populations ancestral to those now in the UK. Variation due to selection has previously been implicated at *LCT* (lactase) and major histocompatibility complex (MHC)[7–9], and within-UK differentiation at 4p14 has been found independently[10], but others seem to be new findings. All but three of the regions contain known genes. Aside from evolutionary interest, genes showing evidence of natural selection are particularly interesting for the biology of traits such as infectious diseases; possible targets for selection include *NADSYN1* (NAD synthetase 1) at 11q13, which could have a role in prevention of pellagra, as well as *TLR1* (toll-like receptor 1) at 4p14, for which a role in the biology of tuberculosis and leprosy has been suggested[10].

There may be important population structure that is not well captured by current geographical region of residence. Present implementations of strongly model-based approaches such as STRUCTURE[11,12] are impracticable for data sets of this size, and we reverted to the classical method of principal components[13,14], using a subset of 197,175 SNPs chosen to reduce inter-locus linkage disequilibrium. Nevertheless, four of the first six principal components clearly picked up effects attributable to local linkage disequilibrium rather than genome-wide structure. The remaining two components show the same predominant geographical trend from NW to SE but, perhaps unsurprisingly, London is set somewhat apart (Supplementary Fig. 8).

The overall effect of population structure on our association results seems to be small, once recent migrants from outside Europe are excluded. Estimates of over-dispersion of the association trend test statistics (usually denoted λ; ref. 15) ranged from 1.03 and 1.05 for RA and T1D, respectively, to 1.08–1.11 for the remaining diseases. Some of this over-dispersion could be due to factors other than structure, and this possibility is supported by the fact that inclusion of the two ancestry informative principal components as covariates in the association tests reduced the over-dispersion estimates only slightly (Supplementary Table 6), as did stratification by geographical region. This impression is confirmed on noting that *P* values with and without correction for structure are similar (Supplementary Fig. 9). We conclude that, for most of the genome, population structure has at most a small confounding effect in our study, and as a consequence the analyses reported below do not correct for structure. In principle, apparent associations in the few genomic regions identified in Table 1 as showing strong geographical differentiation should be interpreted with caution, but none arose in our analyses.

Disease association results

We assessed evidence for association in several ways (see Methods for details), drawing on both classical and bayesian statistical approaches. For polymorphic SNPs on the Affymetrix chip, we performed trend tests (1 degree of freedom[16]) and general genotype tests (2 degrees of freedom[16], referred to as genotypic) between each case collection and the pooled controls, and calculated analogous Bayes factors. There are examples from animal models where genetic effects act differently in males and females[17], and to assess this in our data we applied a

Table 1 | Highly differentiated SNPs

Chromosome	Genes	Region (Mb)	SNP	Position	*P* value
2q21	*LCT*	135.16–136.82	rs1042712	136,379,576	5.54×10^{-13}
4p14	*TLR1, TLR6, TLR10*	38.51–38.74	rs7696175	386,43,552	1.51×10^{-12}
4q28		137.97–138.01	rs1460133	137,999,953	4.43×10^{-08}
6p25	*IRF4*	0.32–0.42	rs9378805	362,727	5.39×10^{-13}
6p21	*HLA*	31.10–31.55	rs3873375	31,359,339	1.07×10^{-11}
9p24	*DMRT1*	0.86–0.88	rs11790408	866,418	4.96×10^{-07}
11p15	*NAV2*	19.55–19.70	rs12295525	19,661,808	7.44×10^{-08}
11q13	*NADSYN1, DHCR7*	70.78–70.93	rs12797951	70,820,914	3.01×10^{-08}
12p13	*DYRK4,AKAP3,NDUFA9, RAD51AP1,GALNT8*	4.37–4.82	rs10774241	45,537,27	2.73×10^{-08}
14q12	*HECTD1,AP4S1,STRN3*	30.41–31.03	rs17449560	30,598,823	1.46×10^{-07}
19q13	*GIPR,SNRPD2,QPCTL, SIX5,DMPK,DMWD, RSHL1,SYMPK,FOXA3*	50.84–51.09	rs3760843	50,980,546	4.19×10^{-07}
20q12		38.30–38.77	rs2143877	38,526,309	1.12×10^{-09}
Xp22		2.06–2.08	rs6644913	2,061,160	1.23×10^{-07}

Properties of SNPs that show large allele frequency differences between samples of individuals from 12 regions across Great Britain. Regions showing differentiated SNPs are given with details of the SNP with the smallest *P* value in each region for differentiation on the 11-d.f. test of differences in SNP allele frequencies between geographical regions, within the 9 collections. Cluster plots for these SNPs have been examined visually. Signal plots appear in Supplementary Information. Positions are in NCBI build-35 coordinates.

Box 1 | Significance levels in genome-wide studies

There has been much debate concerning interpretation of significance levels in genome-wide association studies and whether, and how, these should be corrected for multiple testing. Classical multiple testing theory in statistics is concerned with the problem of 'multiple tests' of a single 'global' null hypothesis. This, we would argue, is a problem far removed from that which faces us in genome-wide association studies, where we face the problem of testing 'multiple hypotheses' (for a particular disease, one hypothesis for each SNP, or region of correlated SNPs, in the genome) and we thus do not subscribe to the view that one should correct significance levels for the number of tests performed to obtain 'genome-wide significance levels'. Nonetheless, our aim is to keep the false positive rate within acceptable bounds and this still leads to the view that very low *P* values are needed for strong evidence of association. But the factor determining the threshold is not the number of tests performed, but the a priori probability that there is likely to be a true association at any specified location in the genome. Of course, we cannot know this prior probability from objective evidence, but we can perhaps estimate an order of magnitude.

There are two linked questions. The first concerns the choice of an appropriate 'threshold' for reporting possible associations as likely to be genuine. Here the mathematics is quite straightforward if we make the simplifying assumption that we have the same power to detect all true associations. Then we have[18]

Posterior odds for true association = Prior odds × Power/Significance threshold

That is, for a given significance threshold, the probability of a true association depends on the prior odds and, crucially, the power. A plausible estimate for the prior odds of true association at any specified locus might be of the order of 100,000:1 against, for example, on the basis of 1,000,000 'independent' regions of the genome and an expectation of 10 detectable genes involved in the condition. (Other plausible estimates might vary from this by an order of magnitude or so in either direction.) Then, assuming a power of 0.5 and a significance threshold of 5×10^{-7}, the posterior odds in favour of a 'hit' being a true association would be 10:1. However, if we relax this significance threshold by a factor of ten, or alternatively if the power were lower by a factor of 10, the posterior odds that a 'hit' is a true association would also be reduced by a factor of ten. This simple mathematical analysis is little affected by allowing for the fact that true associations come in various sizes with varying power to detect them; the above formula is simply modified by interpreting 'power' as the mean power.

The above discussion concerns 'average' properties of 'hits' achieving given significance levels. After the association data are available, a related but different question is whether a particular positive finding is likely to be a true one. For that calculation, the prior odds must be multiplied by the Bayes factor, the ratio of the probability of the observed data under the assumption that there is a true association to its probability under the null hypothesis. As in power calculations, the calculation of Bayes factors requires assumptions about effect sizes (see Methods for details).

A key point from both perspectives is that interpreting the strength of evidence in an association study depends on the likely number of true associations, and the power to detect them which, in turn, depends on effect sizes and sample size. In a less-well-powered study it would be necessary to adopt more stringent thresholds to control the false-positive rate. Thus, when comparing two studies for a particular disease, with a hit with the same MAF and *P* value for association, the likelihood that this is a true positive will in general be greater for the study that is better powered, typically the larger study. In practice, smaller studies often employ less stringent *P*-value thresholds, which is precisely the opposite of what should occur.

sex-differentiated test which is sensitive to associations of a different magnitude and/or direction in the two sexes.

Our study also allows us to look for loci which may have an effect in more than one disease. To assess this, we compared our common controls with all cases in each of three natural groupings of diseases: CAD+HT+T2D (metabolic and cardiovascular phenotypes with potential aetiological overlap, for example, involving defects in insulin action); RA+T1D (already known to share common loci); and CD+RA+T1D (all autoimmune diseases).

To help to capture putative disease loci not on the Affymetrix chip we used a new multilocus method in which a population genetics model is applied to our genotype data and the HapMap reference samples to simulate, or impute, genotype data at 2,193,483 HapMap SNPs not on the Affymetrix chip. These imputed, or *in silico*, genotypes are then tested for association in the same ways as SNPs genotyped in the project.

Before detailing the principal results for each disease, we first summarize our main observations. Table 2 details the findings from the WTCCC scan for the 15 variants for which there was strong prior evidence of association with one or more of the diseases studied, based on extensive replication studies. All but two of these show associations in our study, with the magnitude of the evidence generally consistent with their effect sizes as estimated from prior studies. One of the signals for which we failed to obtain evidence of replication (*APOE* in CAD) is poorly tagged by the Affymetrix 500K chip. The other (*INS* in T1D) is represented by a single SNP that marginally failed our study-wide quality control filters (overall missingness 5.2%) but which was nonetheless strongly associated with T1D when examined. Quantile-quantile plots for the trend test for each of the seven diseases show only very minor deviations from the null distribution, except in the extreme tails which correspond to associations reported below (Fig. 3). The quantile-quantile plots and the results at positive controls (Table 2) give confidence in the quality of our data and the robustness of our analyses.

Our genome-wide results for the trend test are illustrated in Fig. 4. The single-disease trend and genotypic tests for SNPs on the chip identified 21 signals across the 7 diseases that exceeded a threshold of 5×10^{-7} (Table 3). For each of these SNPs (except those within the MHC), cluster plots are shown in Supplementary Fig. 10 and 'signal plots' in Fig. 5. These signal plots estimate the likely demarcation of the hit region and show the signal at genotyped and imputed SNPs together with local genomic context. Four further strong (with $P < 5 \times 10^{-7}$) associations were revealed by the other primary analyses described (Table 3). One locus (in RA) was revealed by the sex-differentiated analysis, two through multilocus approaches (both for T1D) and one through an analysis which combined cases from more than one autoimmune disease (signal plots in Supplementary Figs 11, 12 and 13, respectively).

All of these signals were subjected to visual inspection of cluster plots, and in all cases (with one exception noted below) nearby correlated SNPs also showed a strong signal (see signal plots). Thus, genotyping artefacts are unlikely to be responsible for these associations. Indeed, at the time of writing, 12 of these 25 strong signals represent replications of previously reported findings (only those with extensive prior replication are reported in Table 2). Of the remainder, follow-up studies (reported elsewhere) have confirmed all but one of the loci (ten in total) for which replication has been attempted[10,19–24]. The other replication study gave equivocal results. Of the 18 loci implicated in autoimmune diseases, 5 show associations ($P < 0.001$) to more than 1 condition, leading to a number of further potential new associations, at least one of which has also been replicated[10].

It is likely that further susceptibility genes will be identified through follow-up of other signals for which the evidence from our scan is less conclusive (see below for some specific examples). For example, there are 58 further signals with single-point *P* values between 10^{-5} and 5×10^{-7} for which inspection of cluster plots verifies CHIAMO calls (Table 4). As described below, analyses which make use of selected case samples to expand the reference group should also provide a useful route to the prioritization of such putative signals for further analysis. For convenience, the strongest association results are presented separately for each disease in Supplementary Table 7.

Several general points are relevant to interpretation of these disease-association data. First, replication studies are required to confirm associations from GWAs. For the reasons given in the box, we regard very low *P* values (say $P < 5 \times 10^{-7}$) in our comparatively large sample size as strong evidence for association, and indeed all

Table 2 | Evidence for signal of association at previously robustly replicated loci

Collection	Gene	Chromosome	Reported SNP	WTCCC SNP	HapMap r^2	Trend *P* value	Genotypic *P* value
CAD	*APOE*	19q13	*	rs4420638	-	1.7×10^{-01}	1.7×10^{-01}
CD	*NOD2*	16q12	rs2066844	rs17221417	0.23	9.4×10^{-12}	4.0×10^{-11}
CD	*IL23R*	1p31	rs11209026	rs11805303	0.01	6.5×10^{-13}	5.9×10^{-12}
RA	*HLA-DRB1*	6p21	*	rs615672	-	2.6×10^{-27}	7.5×10^{-27}
RA	*PTPN22*	1p13	rs2476601	rs6679677	0.75	4.9×10^{-26}	5.6×10^{-25}
T1D	*HLA-DRB1*	6p21	*	rs9270986	-	4.0×10^{-116}	2.3×10^{-122}
T1D	*INS*	11p15	rs689	†	-	-	-
T1D	*CTLA4*	2q33	rs3087243	rs3087243	1	2.5×10^{-05}	1.8×10^{-05}
T1D	*PTPN22*	1p13	rs2476601	rs6679677	0.75	1.2×10^{-26}	5.4×10^{-26}
T1D	*IL2RA*	10p15	rs706778	rs2104286	0.25	8.0×10^{-06}	4.3×10^{-05}
T1D	*IFIH1*	2q24	rs1990760	rs3788964	0.26	1.9×10^{-03}	7.6×10^{-03}
T2D	*PPARG*	3p25	rs1801282	rs1801282	1	1.3×10^{-03}	5.4×10^{-03}
T2D	*KCNJ11*	11p15	rs5219	rs5215	0.9	1.3×10^{-03}	5.6×10^{-03}
T2D	*TCF7L2*	10q25	rs7903146	rs4506565	0.92	5.7×10^{-13}	5.1×10^{-12}

Where information on the strength of association at a particular SNP had been previously published and replicated we tabulated the *P* value of both the trend and genotype test at the same SNP (if in our study), or the best tag SNP (defined to be the SNP with highest r^2 with the reported SNP, calculated in the CEU sample of the HapMap project). Positions are in NCBI build-35 coordinates. *Previous reports relate to haplotypes rather than single SNPs. †Not well tagged by SNPs that pass the quality control, see main text.

or most of the loci we find at this level are either already known or have now been confirmed by subsequent replication. Such replication studies are also the substrate for efforts to determine the range of associated phenotypes and to identify and characterize pathologically relevant variation.

Second, failure to detect a prominent association signal in the present study cannot provide conclusive exclusion of any given gene. This is the consequence of several factors including: less-than-complete coverage of common variation genome-wide on the Affymetrix chip; poor coverage (by design) of rare variants, including many structural variants (thereby reducing power to detect rare, penetrant, alleles)[25]; difficulties with defining the full genomic extent of the gene of interest; and, despite the sample size, relatively low power to detect, at levels of significance appropriate for genome-wide analysis, variants with modest effect sizes (odds ratio (OR) < 1.2).

Third, whereas the association signals detected can help to define regions of interest, they cannot provide unambiguous identification of the causal genes. Nevertheless, assessments on the basis of positional candidacy carry considerable weight, and, as we show, these already allow us, for selected diseases, to highlight pathways and mechanisms of particular interest. Naturally, extensive resequencing and fine-mapping work, followed by functional studies will be required before such inferences can be translated into robust statements about the molecular and physiological mechanisms involved.

We turn now to a discussion of the main findings for each disease, focusing here only on the most significant and interesting results

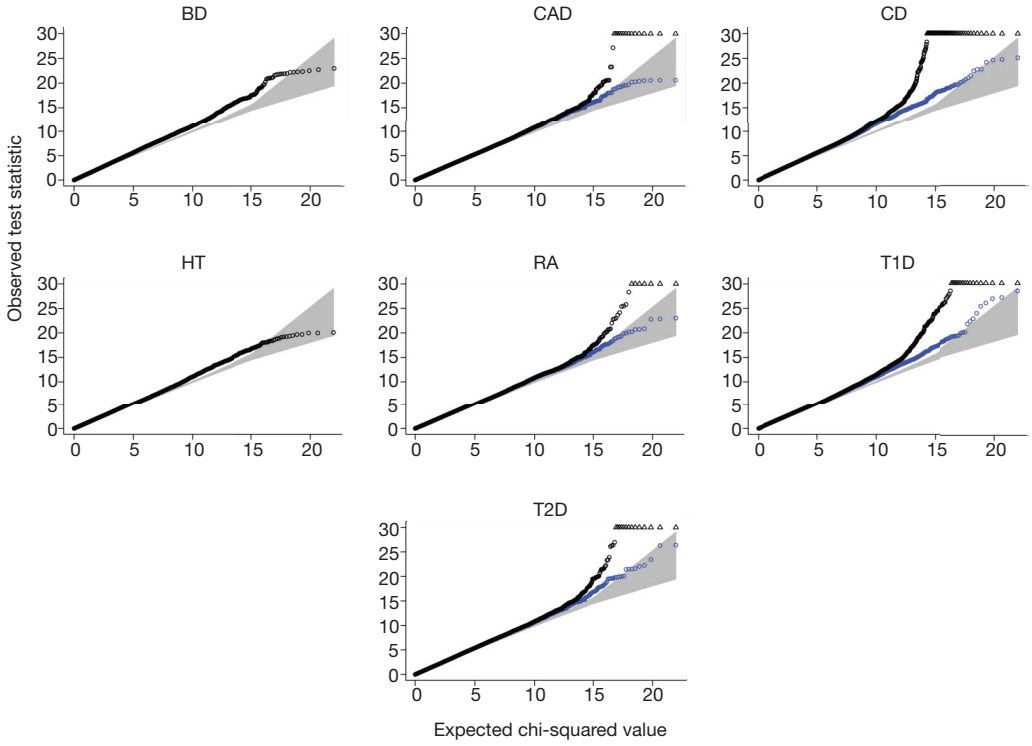

Figure 3 | Quantile-quantile plots for seven genome-wide scans. For each of the seven disease collections, a quantile-quantile plot of the results of the trend test is shown in black for all SNPs that pass the standard project filters, have a minor allele frequency >1% and missing data rate <1%. SNPs that were visually inspected and revealed genotype calling problems were excluded. These filters were chosen to minimize the influence of genotype-calling artefacts. Each quantile-quantile plot shown in black involves around 360,000 SNPs. SNPs at which the test statistic exceeds 30 are represented by triangles. Additional quantile-quantile plots, which also exclude all SNPs located in the regions of association listed in Table 3, are superimposed in blue (for BD, the exclusion of these SNPs has no visible effect on the plot, and for HT there are no such SNPs). The blue quantile-quantile plots show that departures in the extreme tail of the distribution of test statistics are due to regions with a strong signal for association.

from the analyses described above, and consideration of an expanded reference group, described below.

Bipolar disorder (BD). Bipolar disorder (BD; manic depressive illness[26]) refers to an episodic recurrent pathological disturbance in mood (affect) ranging from extreme elation or mania to severe depression and usually accompanied by disturbances in thinking and behaviour: psychotic features (delusions and hallucinations) often occur. Pathogenesis is poorly understood but there is robust evidence for a substantial genetic contribution to risk[27,28]. The estimated sibling recurrence risk (λ_s) is 7–10 and heritability 80–90%[27,28]. The definition of BD phenotype is based solely on clinical features because, as yet, psychiatry lacks validating diagnostic tests such as those available for many physical illnesses. Indeed, a major goal of molecular genetics approaches to psychiatric illness is an improvement in diagnostic classification that will follow identification of the biological systems that underpin the clinical syndromes. The phenotype definition that we have used includes individuals that have suffered one or more episodes of pathologically elevated mood (see Methods), a criterion that captures the clinical spectrum of bipolar mood variation that shows familial aggregation[29].

Several genomic regions have been implicated in linkage studies[30] and, recently, replicated evidence implicating specific genes has been reported. Increasing evidence suggests an overlap in genetic susceptibility with schizophrenia, a psychotic disorder with many similarities to BD. In particular association findings have been reported with both disorders at *DAOA* (D-amino acid oxidase activator), *DISC1* (disrupted in schizophrenia 1), *NRG1* (neuregulin1) and *DTNBP1* (dystrobrevin binding protein 1)[31].

The strongest signal in BD was with rs420259 at chromosome 16p12 (genotypic test $P = 6.3 \times 10^{-8}$; Table 3) and the best-fitting genetic model was recessive (Supplementary Table 8). Although recognizing that this signal was not additionally supported by the expanded reference group analysis (see below and Supplementary Table 9) and that independent replication is essential, we note that several genes at this locus could have pathological relevance to BD, (Fig. 5). These include *PALB2* (partner and localizer of *BRCA2*), which is involved in stability of key nuclear structures including chromatin and the nuclear matrix; *NDUFAB1* (NADH dehydrogenase (ubiquinone) 1, alpha/beta subcomplex, 1), which encodes a subunit of complex I of the mitochondrial respiratory chain; and *DCTN5* (dynactin 5), which encodes a protein involved in intracellular transport that is known to interact with the gene 'disrupted in schizophrenia 1' (*DISC1*)[32], the latter having been implicated in susceptibility to bipolar disorder as well as schizophrenia[33].

Of the four regions showing association at $P < 5 \times 10^{-7}$ in the expanded reference group analysis (Supplementary Table 9), it is of interest that the closest gene to the signal at rs1526805 ($P = 2.2 \times 10^{-7}$) is *KCNC2* which encodes the Shaw-related voltage-gated potassium channel. Ion channelopathies are well-recognized as causes of episodic central nervous system disease, including seizures, ataxias

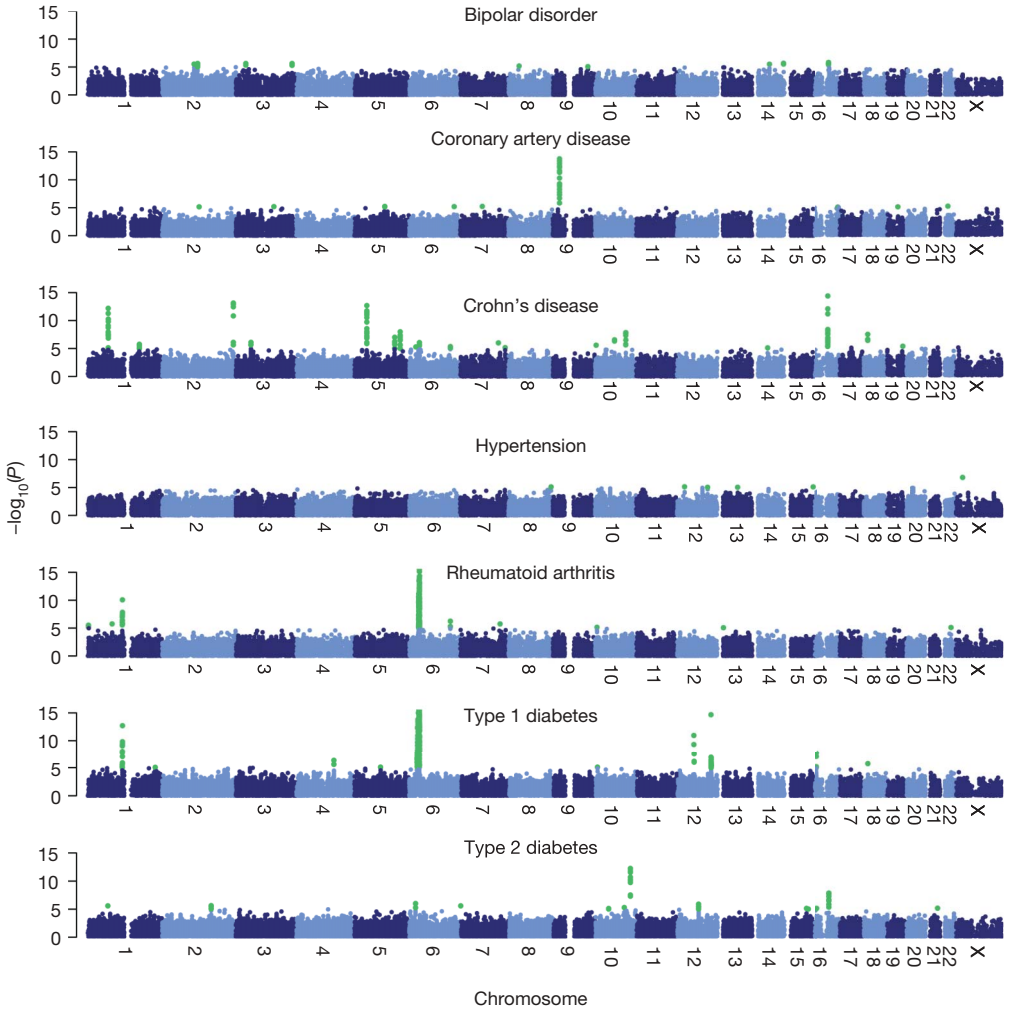

Figure 4 | Genome-wide scan for seven diseases. For each of seven diseases $-\log_{10}$ of the trend test *P* value for quality-control-positive SNPs, excluding those in each disease that were excluded for having poor clustering after visual inspection, are plotted against position on each chromosome. Chromosomes are shown in alternating colours for clarity, with *P* values $< 1 \times 10^{-5}$ highlighted in green. All panels are truncated at $-\log_{10}(P \text{ value}) = 15$, although some markers (for example, in the MHC in T1D and RA) exceed this significance threshold.

Table 3 | Regions of the genome showing the strongest association signals

Collection	Chromosome	Region (Mb)	SNP	Trend *P* value	Genotypic *P* value	$\log_{10}$(BF), additive	$\log_{10}$(BF), general	Risk allele	Minor allele	Heterozygote odds ratio	Homozygote odds ratio	Control MAF	Case MAF
Standard analysis													
BD	16p12	23.3–23.62	rs420259	2.19×10^{-04}	6.29×10^{-08}	1.96	4.79	A	G	2.08 (1.60–2.71)	2.07 (1.6–2.69)	0.282	0.248
CAD	9p21	21.93–22.12	rs1333049	1.79×10^{-14}	1.16×10^{-13}	11.66	11.19	C	C	1.47 (1.27–1.70)	1.9 (1.61–2.24)	0.474	0.554
CD	1p31	67.3–67.48	rs11805303	6.45×10^{-13}	5.85×10^{-12}	10.07	9.41	T	T	1.39 (1.22–1.58)	1.86 (1.54–2.24)	0.317	0.391
CD	2q37	233.92–234	rs10210302	7.10×10^{-14}	5.26×10^{-14}	11.11	11.28	T	C	1.19 (1.01–1.41)	1.85 (1.56–2.21)	0.481	0.402
CD	3p21	49.3–49.87	rs9858542	7.71×10^{-07}	3.58×10^{-08}	4.24	5.22	A	A	1.09 (0.96–1.24)	1.84 (1.49–2.26)	0.282	0.331
CD	5p13	40.32–40.66	rs17234657	2.13×10^{-13}	1.99×10^{-12}	10.41	9.89	G	G	1.54 (1.34–1.76)	2.32 (1.59–3.39)	0.125	0.181
CD	5q33	150.15–150.31	rs1000113	5.10×10^{-08}	3.15×10^{-07}	5.36	5.01	T	T	1.54 (1.31–1.82)	1.92 (0.92–4.00)	0.067	0.098
CD	10q21	64.06–64.31	rs10761659	2.68×10^{-07}	1.75×10^{-06}	4.69	4.13	G	A	1.23 (1.05–1.45)	1.55 (1.3–1.84)	0.461	0.406
CD	10q24	101.26–101.32	rs10883365	1.41×10^{-08}	5.82×10^{-08}	5.91	5.48	G	G	1.2 (1.03–1.39)	1.62 (1.37–1.92)	0.477	0.537
CD	16q12	49.02–49.4	rs17221417	9.36×10^{-12}	3.98×10^{-11}	8.93	8.47	G	G	1.29 (1.13–1.46)	1.92 (1.58–2.34)	0.287	0.356
CD	18p11	12.76–12.91	rs2542151	4.56×10^{-08}	2.03×10^{-07}	5.42	5.00	G	G	1.3 (1.14–1.48)	2.01 (1.46–2.76)	0.163	0.208
RA	1p13	113.54–114.16	rs6679677	4.90×10^{-26}	5.55×10^{-25}	22.36	21.99	A	A	1.98 (1.72–2.27)	3.32 (1.93–5.69)	0.096	0.168
RA	6	MHC	rs6457617*	3.44×10^{-76}	5.18×10^{-75}	74.84	73.18	T	T	2.36 (1.97–2.84)	5.21 (4.31–6.30)	0.489	0.685
T1D	1p13	113.54–114.16	rs6679677	1.17×10^{-26}	5.43×10^{-26}	23.07	22.83	A	A	1.82 (1.59–2.09)	5.19 (3.15–8.55)	0.096	0.169
T1D	6	MHC	rs9272346*	2.42×10^{-134}	5.47×10^{-134}	141.9	142.2	A	G	5.49 (4.83–6.24)	18.52 (27.03–12.69)	0.387	0.150
T1D	12q13	54.64–55.09	rs11171739	1.14×10^{-11}	9.71×10^{-11}	8.89	8.24	C	C	1.34 (1.17–1.54)	1.75 (1.48–2.06)	0.423	0.493
T1D	12q24	109.82–111.49	rs17696736	2.17×10^{-15}	1.51×10^{-14}	12.53	11.88	G	G	1.34 (1.16–1.53)	1.94 (1.65–2.29)	0.424	0.506
T1D	16p13	10.93–11.37	rs12708716	9.24×10^{-08}	4.92×10^{-07}	5.15	4.70	A	G	1.19 (0.97–1.45)	1.55 (1.27–1.89)	0.350	0.297
T2D	6p22	20.63–20.84	rs9465871	1.02×10^{-06}	3.34×10^{-07}	4.15	3.98	C	C	1.18 (1.04–1.34)	2.17 (1.6–2.95)	0.178	0.218
T2D	10q25	114.71–114.81	rs4506565	5.68×10^{-13}	5.05×10^{-12}	10.14	9.43	T	T	1.36 (1.2–1.54)	1.88 (1.56–2.27)	0.324	0.395
T2D	16q12	52.36–52.41	rs9939609	5.24×10^{-08}	1.91×10^{-07}	5.35	5.05	A	A	1.34 (1.17–1.52)	1.55 (1.3–1.84)	0.398	0.453
Multi-locus analysis													
T1D	4q27	123.26–123.92	rs6534347	4.48×10^{-07}	1.83×10^{-06}	5.15	4.69	A	A	1.30 (1.10–1.55)	1.49 (1.25–1.78)	0.351	0.402
T1D	12p13	9.71–9.86	rs3764021	7.19×10^{-05}	5.08×10^{-08}	2.12	4.55	C	T	1.57 (1.38–1.79)	1.48 (1.25–1.75)	0.467	0.426
Sex differentiated analysis													
RA	7q32	130.80–130.84	rs11761231	3.91×10^{-07}	1.37×10^{-06}	-	-	G	A	1.44 (1.19–1.75)	1.64 (1.35–1.99)	0.375	0.327
Combined cases													
RA+T1D	10p15	6.07–6.17	rs2104286	5.92×10^{-08}	2.52×10^{-07}	5.26	4.45	T	C	1.35 (1.11–1.65)	1.62 (1.34–1.97)	0.286	0.245

Regions with at least one SNP with a *P* value of less than 5×10^{-7} for our primary analyses. The $\log_{10}$ value of the Bayes factor (BF) for the bayesian analysis corresponding to the trend and genotypic tests is also given. Region marks the boundaries of signal defined by recombination and return of test statistics to background levels. The minor allele is defined in the controls and its frequency in that group as well as the case sample is reported. MAF, minor allele frequency. Cluster plots for each SNP have been inspected visually, and are shown in Supplementary Fig. 10. Positions are in NCBI build-35 coordinates *Multiple SNPs in the MHC region are significant, we report the most extreme.

and paralyses[34]. It is possible that this may extend to episodic disturbances of mood and behaviour.

Amongst the other higher ranked signals in the BD data set (Supplementary Table 7), there is support for the previously suggested importance of GABA neurotransmission (rs7680321 ($P = 6.2 \times 10^{-5}$) in *GABRB1* encoding a ligand-gated ion channel (GABA A receptor, beta 1))[35], glutamate neurotransmission (rs1485171 ($P = 9.7 \times 10^{-5}$) in *GRM7* (glutamate receptor, metabotropic 7))[35] and synaptic function (rs11089599 ($P = 7.2 \times 10^{-5}$) in *SYN3* (synapsin III)[36]).

We note that a broad range of genetic and non-genetic data point to the importance of analyses that use alternative approaches to phenotype definition, including symptom dimensions[31]. Although beyond the scope of the current paper, such analyses will be required to maximize the potential of the current BD data set.

Coronary artery disease (CAD). Coronary artery disease (coronary atherosclerosis) is a chronic degenerative condition in which lipid and fibrous matrix is deposited in the walls of the coronary arteries to form atheromatous plaques[37]. It may be clinically silent or present with angina pectoris or acute myocardial infarction. Pathogenesis is complex, with endothelial dysfunction, oxidative stress and inflammation contributing to development and instability of the atherosclerotic plaque[37].

In addition to lifestyle and environmental factors, genes are important in the aetiology of CAD[38]. For early myocardial infarction, estimates of λ_s range from ~2 to ~7 (ref. 39). Genetic variation is thought likely to influence risk of CAD both directly and through effects on known CAD risk factors including hypertension, diabetes and hypercholesterolaemia. Genome-wide linkage studies have mapped several loci that may affect susceptibility to CAD/myocardial infarction[40] although for only two of these has the likely gene been identified (*ALOX5AP* (arachidonate 5-lipoxygenase-activating protein) and *LTA4H* (leukotriene A4 hydrolase))[41,42]. Association studies have identified several plausible genetic variants affecting lipids, thrombosis, inflammation or vascular biology but for most the evidence is not yet conclusive[40]. We did not find evidence for strong association at any of these genes within our study (Table 2 and Supplementary Table 10).

The most notable new finding for CAD is the powerful association on chromosome 9p21.3 (Table 3; Fig. 5). Although the strongest signal is seen at rs1333049 ($P = 1.8 \times 10^{-14}$), associations are seen for SNPs across > 100 kilobases. This region has not been highlighted in previous studies of CAD or myocardial infarction[40,43]. The region of interest contains the coding sequences of genes for two cyclin dependent kinase inhibitors, *CDKN2A* (encoding $p16^{INK4a}$) and *CDKN2B* ($p15^{INK4b}$), although the most closely associated SNP is some distance removed. Both genes have multiple isoforms, have an important role in the regulation of the cell cycle and are widely expressed[44], with *CDKN2B* known to be expressed in the macrophages but not the smooth muscle cells of fibrofatty lesions[45,46]. It is of interest that expression of *CDKN2B* is induced by transforming growth factor beta (TGF-β) and that the TGF-β signalling system is implicated in the pathogenesis of human atherosclerosis[45,46]. Besides *CDKN2A* and *CDKN2B*, the only other known gene nearby is *MTAP* which encodes methylthioadenosine phosphorylase, an enzyme that contributes to polyamine metabolism and is important for the salvage of both adenine and methionine. *MTAP* is ubiquitously expressed, including in the cardiovascular system[47]. Further work is required to determine whether the CAD association at this locus is mediated through *CDKN2A/B, MTAP* or some other mechanism. The same region also shows replicated evidence of association to T2D in the WTCCC and other data sets[19,21,22], though different SNPs seem to be involved.

None of the loci showing more modest associations with CAD (Table 4) includes genes hitherto strongly implicated in the pathogenesis of CAD. A potentially interesting association is at rs6922269 ($P = 6.3 \times 10^{-6}$), an intronic SNP in *MTHFD1L*, which encodes

methylenetetrahydrofolate dehydrogenase ($NADP^+$-dependent) 1-like, the mitochondrial isozyme of C1-tetrahydrofolate (THF) synthase[48,49]. C_1-THF synthases interconvert the one carbon units carried by the biologically active form of folic acid, C1-tetrahydrofolate. These are used in a variety of cellular processes including purine and methionine synthesis[48]. Another enzyme in the same pathway, methylene THF reductase (encoded by *MTHFR*) is subject to a common mutation which influences plasma homocysteine level[50] and has been associated with increased risk of coronary and other atherosclerotic disease[51]. The possibility of a link between variants in *MTHFD1L* and CAD risk is supported by evidence that *MTHFD1L* activity also contributes to plasma homocysteine[52] and that defects in the *MTHFD1L* pathway may increase plasma homocysteine level[48,53].

An intronic SNP in *ADAMTS17* (a disintegrin and metalloproteinase with thrombospondin motifs 17), which showed modest association (rs1994016; $P = 1.1 \times 10^{-4}$) in our primary analysis, showed a much stronger association in the expanded reference group analysis (see below and Supplementary Table 9). Although the specific function of *ADAMTS17* has not been determined, other members of the ADAMTS family have been implicated in vascular extracellular matrix degradation, vascular remodelling and atherosclerosis[54,55].

Crohn's disease (CD). Crohn's disease is a common form of chronic inflammatory bowel disease[56]. The pathogenic mechanisms are poorly understood, but probably involve a dysregulated immune response to commensal intestinal bacteria and possibly defects in mucosal barrier function or bacterial clearance[57]. Genetic predisposition to

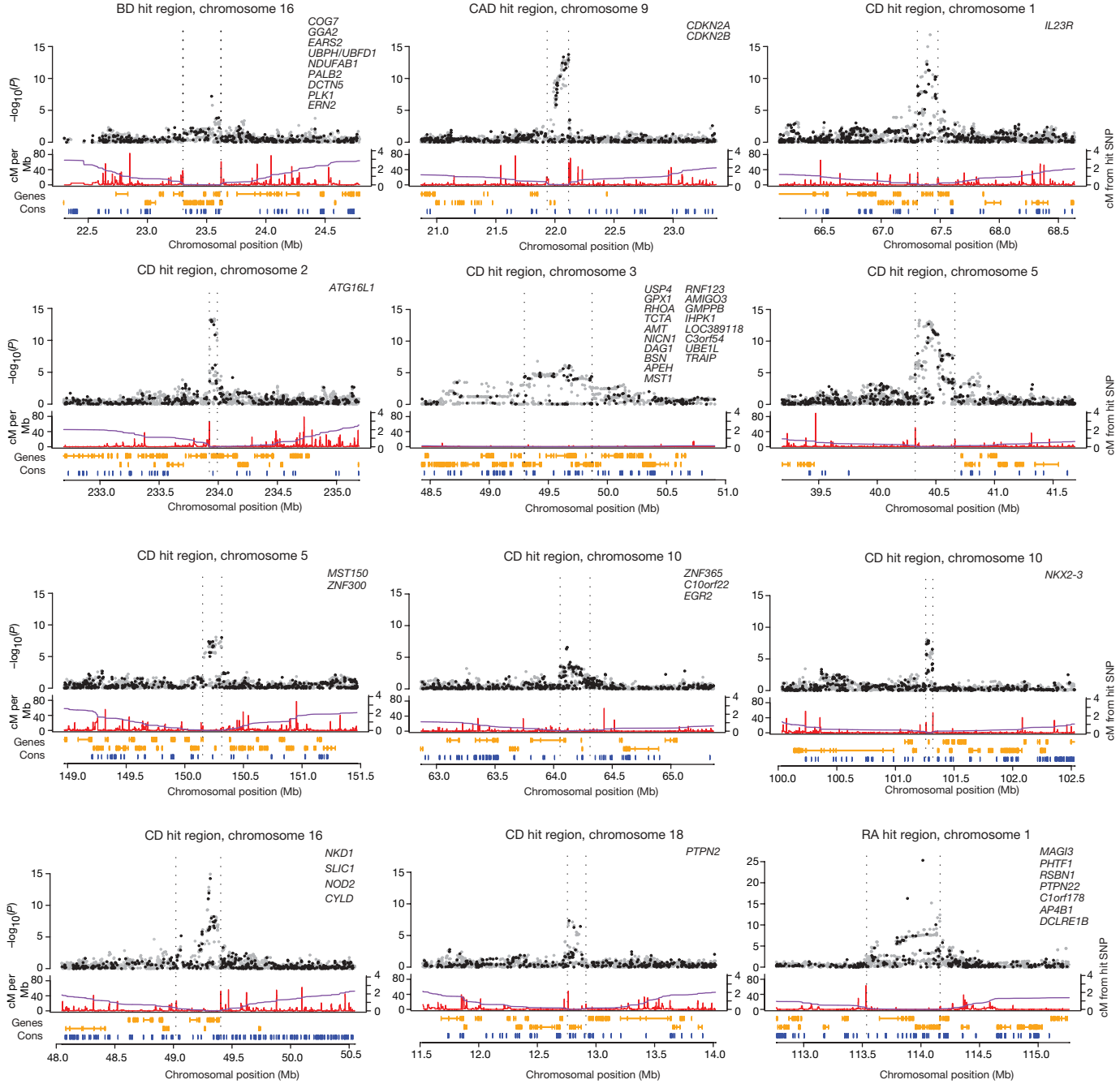

Figure 5 | Regions of the genome showing strong evidence of association. Characteristics of genomic regions 1.25 Mb to either side of 'hit SNPs'—SNPs with lowest *P* values. Region boundaries (vertical dotted lines) were chosen to coincide with locations where test statistics returned to background levels and, where possible, recombination hotspots. Upper panel, $-\log_{10}(P$ values) for the test (trend or genotypic) with the smallest *P* value at the hit SNP. Black points represent SNPs typed in the study, and grey points represent SNPs whose genotypes were imputed. SNPs imputed with higher confidence are shown in darker grey. Middle panel, fine-scale recombination rate (centimorgans per Mb) estimated from Phase II HapMap. The purple line shows the cumulative genetic distance (in cM)

CD is suggested by a λ_s of 17–35 and by twin studies that contrast monozygotic concordance rates of 50% with only 10% in dizygotic pairs[58,59].

A number of CD-susceptibility loci have previously been defined, and all of these generate strong signals in our data (Table 2). In 2001, positional cloning identified *CARD15* (caspase recruitment domain family, member 15; *NOD2*) as the first confirmed CD-susceptibility gene[60,61]. In the present study, this locus is represented by rs17221417 ($P = 9.4 \times 10^{-12}$). A second association, on chromosome 5q31 (ref. 62) has been widely replicated, although the identity of the causative gene is disputed owing to extensive regional linkage disequilibrium[63]. Here, the previously described risk haplotype is tagged by rs6596075 ($P = 5.4 \times 10^{-7}$).

More recent studies have identified four further CD-susceptibility loci, all of which are strongly replicated in the present study. The association between CD and SNPs within *IL23R* (interleukin 23 receptor)[63] is here represented by a cluster of associated SNPs, including rs11805303 ($P = 6.5 \times 10^{-13}$). The strongest signal for CD in the present scan (at rs10210302; $P = 7.1 \times 10^{-14}$) maps to the *ATG16L1* (ATG16 autophagy related 16-like 1) gene and is in strong linkage disequilibrium ($r^2 = 0.97$) with a non-synonymous SNP (T300A, rs2241880) associated with CD in a German non-synonymous SNP scan[64]. The third is a locus at chromosome 10q21 around rs10761659 ($P = 2.7 \times 10^{-7}$) and represents a non-coding intergenic SNP mapping 14-kb telomeric to gene *ZNF365* and 55-kb centromeric to the pseudogene antiquitin-like 4—a

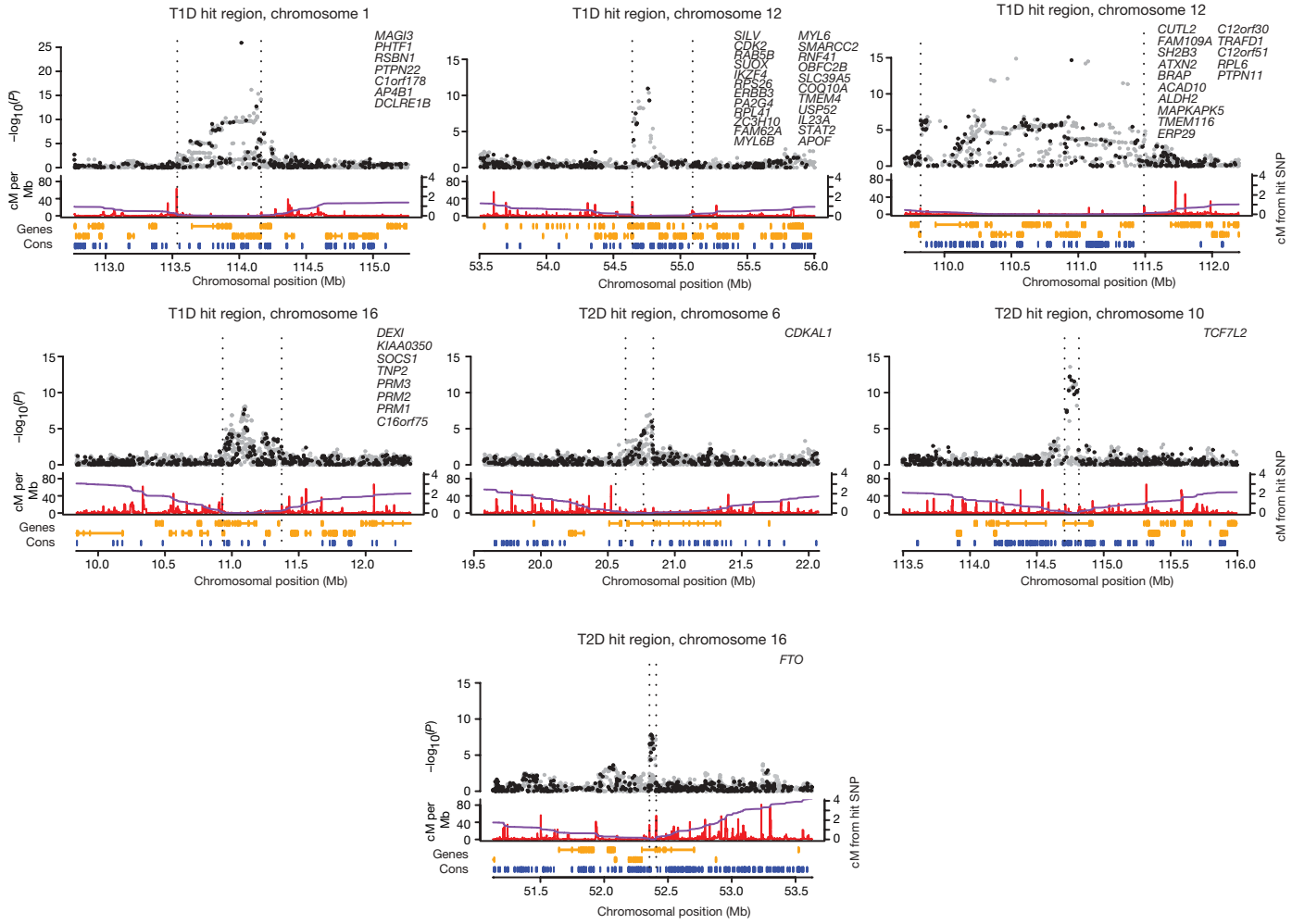

from the hit SNP. Lower panel, known genes, and sequence conservation in 17 vertebrates. Known genes (orange) in the hit region are listed in the upper right part of each plot in chromosomal order, starting at the left edge of the region. The top track shows plus-strand genes and the middle track shows minus-strand genes. Sequence conservation (bottom track) scores are based on the phylogenetic hidden Markov model phastCons. Highly conserved regions (phastCons score ≥600) are shown in blue. Information in middle and lower panels is taken from the UCSC Genome Browser. Positions are in NCBI build-35 coordinates. See Supplementary Information on 'signal plots'.

Table 4 | Regions of the genome showing moderate evidence of association

Collection	Chromosome	Region (Mb)	SNP	Trend *P* value	Genotypic *P* value	$\log_{10}$(BF), additive	$\log_{10}$(BF), general	Risk allele	Minor allele	Heterozygote odds ratio	Homozygote odds ratio	Control MAF	Case MAF
BD	2p25	11.94–12.00	rs4027132	1.31×10^{-05}	9.68×10^{-06}	3.07	2.84	A	G	1.39 (1.19–1.64)	1.51 (1.27–1.79)	0.459	0.414
BD	2q12	104.41–104.58	rs7570682	3.11×10^{-06}	1.64×10^{-05}	3.68	3.23	A	A	1.23 (1.09–1.40)	1.64 (1.28–2.12)	0.214	0.255
BD	2q14	115.63–116.11	rs1375144	2.43×10^{-06}	1.31×10^{-05}	3.80	2.92	A	G	1.32 (1.07–1.63)	1.59 (1.29–1.96)	0.337	0.291
BD	2q37	241.23–241.28	rs2953145	1.11×10^{-05}	6.57×10^{-06}	3.22	3.50	C	G	1.84 (1.31–2.58)	2.14 (1.53–2.98)	0.226	0.189
BD	3p23	32.26–32.33	rs4276227	4.57×10^{-06}	2.62×10^{-05}	3.52	3.04	C	T	1.20 (0.99–1.46)	1.49 (1.23–1.81)	0.371	0.326
BD	3q27	184.29–184.40	rs683395	2.30×10^{-06}	5.11×10^{-06}	3.87	3.73	G	G	1.47 (1.26–1.71)	1.30 (0.69–2.46)	0.080	0.109
BD	6p21	42.82–42.86	rs6458307	3.43×10^{-01}	4.35×10^{-06}	−0.80	2.84	T	T	0.84 (0.75–0.96)	1.39 (1.13–1.69)	0.312	0.321
BD	8p12	34.22–34.61	rs2609653	6.86×10^{-06}	-	3.44	3.21	C	C	1.43 (1.19–1.71)	3.62 (1.26–10.44)	0.052	0.074
BD	9q32	114.31–114.39	rs10982256	8.80×10^{-06}	4.41×10^{-05}	3.23	2.37	T	C	1.26 (1.08–1.47)	1.47 (1.24–1.74)	0.471	0.425
BD	14q22	57.17–57.24	rs10134944	3.21×10^{-06}	6.89×10^{-06}	3.73	3.59	T	T	1.45 (1.24–1.68)	1.32 (0.74–2.33)	0.086	0.115
BD	14q32	103.43–103.62	rs11622475	2.10×10^{-06}	8.14×10^{-06}	3.87	3.24	C	T	1.13 (0.89–1.44)	1.47 (1.17–1.86)	0.300	0.256
BD	16q12	51.36–51.50	rs1344484	1.64×10^{-06}	1.03×10^{-05}	3.94	3.41	T	C	1.24 (1.03–1.48)	1.52 (1.27–1.82)	0.402	0.353
BD	20p13	3.70–3.73	rs3761218	4.43×10^{-05}	6.71×10^{-06}	2.58	3.18	T	C	0.97 (0.81–1.15)	1.31 (1.09–1.57)	0.397	0.356
CAD	1q43	236.77–236.85	rs17672135	1.04×10^{-04}	2.35×10^{-06}	2.36	3.88	T	C	0.70 (0.61–0.81)	1.32 (0.79–2.22)	0.134	0.108
CAD	5q21	99.98–100.11	rs383830	5.72×10^{-06}	1.34×10^{-05}	3.49	3.26	T	A	1.60 (1.16–2.21)	1.92 (1.40–2.63)	0.220	0.182
CAD	6q25	151.34–151.42	rs6922269	6.33×10^{-06}	1.50×10^{-05}	3.38	3.14	A	A	1.17 (1.04–1.32)	1.65 (1.32–2.06)	0.253	0.294
CAD	16q23	81.72–81.79	rs8055236	9.73×10^{-06}	5.60×10^{-06}	3.28	3.59	G	T	1.91 (1.33–2.74)	2.23 (1.56–3.17)	0.198	0.162
CAD	19q12	34.74–34.78	rs7250581	9.12×10^{-06}	2.50×10^{-05}	3.30	2.87	G	A	1.06 (0.79–1.43)	1.40 (1.05–1.86)	0.220	0.182
CAD	22q12	25.01–25.06	rs688034	6.90×10^{-06}	3.75×10^{-06}	3.33	3.15	T	T	1.11 (0.98–1.25)	1.62 (1.34–1.95)	0.310	0.355
CD	1q24	169.53–169.67	rs12037606	1.79×10^{-06}	1.09×10^{-05}	3.89	3.35	A	A	1.22 (1.07–1.40)	1.52 (1.28–1.82)	0.388	0.438
CD	5q23	131.40–131.90	rs6596075	5.40×10^{-07}	3.19×10^{-06}	4.54	4.01	C	G	1.55 (1.00–2.39)	2.06 (1.35–3.14)	0.166	0.127
CD	6p22	20.83–20.85	rs6908425	5.13×10^{-06}	1.10×10^{-05}	3.55	3.38	C	T	1.63 (1.18–2.25)	1.95 (1.43–2.67)	0.230	0.190
CD	6p21	32.79–32.91	rs9469220	8.65×10^{-07}	2.28×10^{-06}	4.19	3.92	A	A	1.14 (0.98–1.32)	1.52 (1.28–1.79)	0.481	0.534
CD	6q23	138.06–138.17	rs7753394	4.42×10^{-06}	2.59×10^{-05}	3.52	2.99	C	C	1.21 (1.04–1.40)	1.48 (1.25–1.76)	0.482	0.531
CD	7q36	147.62–147.70	rs7807268	6.89×10^{-06}	4.42×10^{-06}	3.33	3.58	G	G	1.38 (1.20–1.60)	1.47 (1.24–1.74)	0.462	0.509
CD	10p15	38.52–38.57	rs6601764	2.56×10^{-06}	8.95×10^{-06}	3.74	3.01	C	C	1.16 (1.01–1.33)	1.52 (1.28–1.80)	0.408	0.458
CD	19q13	50.89–51.07	rs8111071	6.14×10^{-06}	1.75×10^{-05}	3.48	3.29	G	G	1.47 (1.25–1.73)	1.28 (0.56–2.88)	0.070	0.096
HT	1q43	235.67–235.79	rs2820037	5.76×10^{-05}	7.66×10^{-07}	2.54	3.99	T	T	1.54 (1.03–2.31)	1.09 (0.74–1.62)	0.141	0.171
HT	8q24	140.17–140.35	rs6997709	7.88×10^{-06}	4.36×10^{-05}	3.32	2.60	G	T	1.20 (0.94–1.52)	1.49 (1.18–1.89)	0.285	0.244
HT	12p12	24.86–24.95	rs7961152	7.39×10^{-06}	3.03×10^{-05}	3.29	2.51	A	A	1.16 (1.01–1.32)	1.47 (1.25–1.74)	0.415	0.461
HT	12q23	100.52–100.58	rs11110912	9.18×10^{-06}	1.94×10^{-05}	3.27	3.11	G	G	1.33 (1.18–1.51)	1.34 (0.96–1.86)	0.165	0.200
HT	13q21	66.90–67.04	rs1937506	9.23×10^{-06}	4.53×10^{-05}	3.25	2.85	G	A	1.33 (1.04–1.69)	1.60 (1.26–2.02)	0.289	0.248
HT	15q26	94.60–94.67	rs2398162	7.85×10^{-06}	5.67×10^{-06}	3.33	3.40	A	G	0.97 (0.76–1.25)	1.31 (1.03–1.67)	0.258	0.218
RA	1p36	2.44–2.77	rs6684865	5.37×10^{-06}	3.14×10^{-05}	3.47	2.97	G	A	1.27 (1.02–1.56)	1.54 (1.25–1.90)	0.338	0.294
RA	1p31	80.16–80.36	rs11162922	1.80×10^{-06}	-	4.11	3.80	A	G	1.27 (0.41–4.01)	2.00 (0.64–6.20)	0.072	0.048
RA	4p15	24.99–25.13	rs3816587	7.65×10^{-03}	9.25×10^{-06}	0.50	2.64	C	C	0.91 (0.80–1.04)	1.35 (1.14–1.59)	0.406	0.434
RA	6q23	138.00–138.06	rs6920220	4.99×10^{-06}	1.58×10^{-05}	3.49	3.17	A	A	1.20 (1.06–1.36)	1.72 (1.33–2.22)	0.223	0.263
RA	7q32	130.80–130.84	rs11761231	1.74×10^{-06}	2.65×10^{-06}	3.92	3.42	C	T	1.44 (1.19–1.75)	1.64 (1.35–1.99)	0.375	0.327
RA	10p15	6.07–6.16	rs2104286	7.02×10^{-06}	2.52×10^{-05}	3.37	2.57	T	C	1.41 (1.10–1.81)	1.68 (1.31–2.14)	0.286	0.244
RA	13q12	19.845–19.855	rs9550642	8.44×10^{-06}	3.90×10^{-05}	3.35	3.02	A	A	1.34 (1.15–1.56)	2.23 (1.21–4.13)	0.084	0.112
RA	21q22	41.430–41.465	rs2837960	3.45×10^{-02}	1.68×10^{-06}	0.05	2.70	G	G	0.95 (0.83–1.08)	2.30 (1.64–3.23)	0.171	0.188
RA	22q13	35.870–35.885	rs743777	7.92×10^{-06}	1.15×10^{-06}	3.29	3.52	G	G	1.09 (0.97–1.24)	1.72 (1.40–2.11)	0.292	0.336
T1D	1q42	221.92–222.17	rs2639703	8.46×10^{-06}	1.74×10^{-05}	3.25	3.06	C	C	1.15 (1.02–1.30)	1.61 (1.31–1.99)	0.276	0.318
T1D	4q27	123.02–123.92	rs17388568	5.01×10^{-07}	3.27×10^{-06}	4.42	3.89	A	A	1.26 (1.11–1.42)	1.58 (1.27–1.95)	0.260	0.307
T1D	5q14	86.20–86.50	rs2544677	8.23×10^{-06}	4.43×10^{-05}	3.32	2.70	C	G	1.34 (1.00–1.79)	1.65 (1.24–2.18)	0.242	0.204
T1D	5q31	132.64–132.67	rs17166496	6.06×10^{-01}	5.20×10^{-06}	−0.97	3.25	C	G	0.77 (0.68–0.87)	1.09 (0.92–1.29)	0.391	0.386
T1D	10p15	6.07–6.18	rs2104286	7.96×10^{-06}	4.32×10^{-05}	3.31	2.88	T	C	1.30 (1.02–1.65)	1.57 (1.25–1.99)	0.286	0.245
T1D	12p13	9.71–9.80	rs11052552	1.02×10^{-04}	7.24×10^{-07}	2.22	3.80	G	T	1.49 (1.28–1.73)	1.43 (1.21–1.69)	0.486	0.446
T1D	18p11	12.76–12.91	rs2542151	1.89×10^{-06}	1.16×10^{-05}	3.91	3.52	G	G	1.30 (1.15–1.47)	1.62 (1.17–2.24)	0.163	0.201
T2D	1p31	66.04–66.36	rs4655595	2.68×10^{-06}	1.33×10^{-05}	3.81	3.47	G	G	1.37 (1.17–1.59)	2.33 (1.23–4.42)	0.080	0.108
T2D	2q24	160.90–161.17	rs6718526	2.40×10^{-06}	1.16×10^{-05}	3.86	3.35	C	T	1.49 (1.05–2.11)	1.86 (1.32–2.63)	0.209	0.171
T2D	3p14	55.24–55.32	rs358806	4.77×10^{-01}	3.05×10^{-06}	−0.83	2.72	A	A	0.86 (0.75–0.97)	1.78 (1.34–2.36)	0.198	0.204
T2D	4q27	122.92–123.02	rs7659604	2.1×10^{-02}	9.42×10^{-06}	0.13	2.74	T	T	1.35 (1.19–1.54)	1.09 (0.91–1.30)	0.380	0.403
T2D	10q11	43.43–43.63	rs9326506	7.78×10^{-06}	2.99×10^{-05}	3.27	2.92	C	C	1.28 (1.11–1.48)	1.46 (1.24–1.72)	0.492	0.538
T2D	12q13	49.50–49.87	rs12304921	5.37×10^{-02}	7.07×10^{-06}	−0.09	2.68	G	G	2.50 (1.53–4.09)	1.94 (1.20–3.15)	0.145	0.159
T2D	12q15	69.58–69.96	rs1495377	1.31×10^{-06}	6.52×10^{-06}	4.01	3.15	G	G	1.28 (1.11–1.49)	1.51 (1.28–1.78)	0.497	0.547
T2D	15q24	72.24–72.50	rs2930291	7.72×10^{-06}	4.40×10^{-05}	3.30	2.42	G	A	1.25 (1.04–1.51)	1.50 (1.24–1.82)	0.377	0.332
T2D	15q25	78.12–78.36	rs2903265	9.57×10^{-06}	4.98×10^{-05}	3.24	2.53	G	A	1.18 (0.93–1.49)	1.47 (1.17–1.86)	0.284	0.243

Regions with at least one SNP with a *P* value of greater than 5×10^{-7} and less than 1×10^{-5} for either the trend or the genotypic test. Columns as for Table 3. Cluster plots for each SNP have been inspected visually. Positions are in NCBI build-35 coordinates. Genotypic *P* values were not calculated for SNPs with the lowest MAFs owing to low numbers of rare-allele homozygotes and sensitivity to genotype calling errors.

recently detected signal[65]. Finally, strong association with a cluster of SNPs around rs17234657 ($P = 2.1\times10^{-13}$) within a 1.2 Mb gene desert on chromosome 5p13.1, recapitulates the finding of a recent GWA study[66].

The current study identifies four further new strong association signals in CD, located on chromosomes 3p21, 5q33, 10q24 and 18p11 (Table 3; Fig. 5). Successful replication for all four loci is reported elsewhere[23].

The first of these includes several SNPs around *IRGM* (immunity-related guanosine triphosphatase; the human homologue of the mouse *Irgm/Lrg47*), the strongest signal being at rs1000113 ($P = 5.1\times10^{-8}$). *IRGM* encodes a GTP-binding protein which induces autophagy and is involved in elimination of intracellular bacteria, including *Mycobacterium tuberculosis*[67]. Reduced function and/or activity of this gene would be expected to lead to persistence of intracellular bacteria, consistent with existing models of CD pathogenesis[57] and the recent *ATG16L1* association[64] (see above).

The second novel CD association is seen at rs9858542 ($P = 7.7\times10^{-7}$), a synonymous coding SNP within the *BSN* (bassoon) gene on chromosome 3p21. *BSN* is thought to encode a scaffold protein expressed in brain and involved in neurotransmitter release; a more plausible regional candidate is *MST1* (macrophage

stimulating 1), which encodes a protein influencing motile activity and phagocytosis by resident peritoneal macrophages[68].

The third novel association involves a cluster of SNPs around rs10883365 ($P = 1.4 \times 10^{-8}$) on chromosome 10q24.2. The most credible candidate here is the *NKX2-3* (NK2 transcription factor related, locus 3) gene, a member of the NKX family of homeodomain-containing transcription factors. Targeted disruption of the murine homologue of *NKX2-3* results in defective development of the intestine and secondary lymphoid organs[69]. Abnormal expression of *NKX2-3* may alter gut migration of antigen-responsive lymphocytes and influence the intestinal inflammatory response.

The final novel association, at rs2542151 ($P = 4.6 \times 10^{-8}$) maps 5.5-kb upstream of *PTPN2* (protein tyrosine phosphatase, non-receptor type 2) on chromosome 18p11. *PTPN2* encodes the T cell protein tyrosine phosphatase TCPTP, a key negative regulator of inflammatory responses. The same locus also shows strong association with T1D susceptibility (trend test $P = 1.9 \times 10^{-6}$) and a consistent, though weaker, association with RA ($P = 1.9 \times 10^{-2}$), supporting the existence of overlapping pathways in the pathogenesis of very distinct inflammatory phenotypes (combined trend test *P* value for all three diseases $= 9 \times 10^{-8}$) (Table 3; ref. 10).

Several further loci generating less strong evidence for association are of interest on the basis of their biological candidacy (Table 4). For example, rs9469220 ($P = 8.7 \times 10^{-7}$) mapping to the human leukocyte antigen (HLA) system class II region was detected in the 'second tier' of associations (Table 4). This suggests a significant contribution of HLA to CD-susceptibility, though less marked than seen in classical autoimmune conditions such as RA and T1D. Another interesting candidate flagged in Table 4 is *TNFAIP3* (TNFα induced protein 3), the closest gene to rs7753394 on chromosome 6q23. The protein product inhibits TNFα-induced NFκB-dependent gene expression by interfering with RIP- or TRAF-2-mediated transactivation signals—hence interacting with the same pathway as *CARD15* (*NOD2*). Markers with lower levels of significance include rs6478108 ($P = 9.0 \times 10^{-5}$) within *TNFSF15* (tumour necrosis factor super family, member 15), previously reported associated with CD[70]; and rs3816769 ($P = 3.1 \times 10^{-5}$) which maps within *STAT3* (signal transducers and activator of transcription, member 3). On the X chromosome rs2807261 ($P = 1.3 \times 10^{-7}$) maps 50-kb from the gene *CD40LG* (CD40 ligand—previously known as TNF superfamily, member 5), implicated in the regulation of B-cell proliferation, adhesion and immunoglobulin class switching[71]. As described in the section on T1D, a modest association between CD and SNPs in the vicinity of the *PTPN11* gene on chromosome 12q24 ($P = 1.5 \times 10^{-3}$) probably reflects a locus influencing general autoimmune predisposition.

An emerging theme from molecular genetic studies of CD is the importance of defects in autophagy and the processing of phagocytosed bacteria. A number of other specific components within innate and adaptive immune pathways are also highlighted.

Hypertension (HT). Hypertension refers to a clinically significant increase in blood pressure and constitutes an important risk factor for cardiovascular disease (http://www.who.int/whr/2002/en/; ref. 72). Lifestyle exposures that elevate blood pressure, including sodium intake, alcohol and excess weight[73] are well-described risk factors. Genetic factors are also important[74,75]. Estimates of λ_s are approximately 2.5–3.5.

Experimental models have highlighted a number of quantitative trait loci but these have yet to translate into insights into human hypertension[76]. Linkage studies are consistent with susceptibility genes of modest effect size[77] and well-replicated findings have yet to emerge from association approaches.

None of the variants previously associated with HT showed evidence for association in our study although we note that some, such as promoter of the *WNK1* (WNK lysine deficient protein kinase 1) gene[78,79], are not well tagged by the Affymetrix chip.

For HT there were no SNPs with significance below 5×10^{-7} (Table 3) but the number and distribution of association signals in the range 10^{-4} to 10^{-7} was similar to that of the other diseases studied (Table 4 and Supplementary Table 7). There are several possible explanations. First, HT may have fewer common risk alleles of larger effect sizes than some of the other complex phenotypes. If so, then identification of susceptibility variants for HT is likely to be reliant on the synthesis of findings from multiple large-scale studies. Second, the present study may have failed to detect genuine common susceptibility variants of large effect size because they happened to be poorly tagged by the set of SNPs genotyped in the current study. If so, further rounds of genotyping using resources that offer increased density (or complementary SNP sets), and/or improved analytical methods (for example, imputation-based) should facilitate their discovery. Third, study of HT may be more susceptible than other phenotypes to the diluting effects of misclassification bias due to the presence of hypertensive individuals within the control samples. If so, power can be improved in future studies by use of controls specifically screened to exclude individuals with elevated blood pressure.

The most strongly associated SNPs (Table 4) do not identify genes from physiological systems previously implicated by clinical or genetic studies in hypertension. The strongest signal overall is with rs2820037 on 1q43 (genotypic test, $P = 7.7 \times 10^{-7}$). The closest genes are *RYR2* (encoding the ryanodine receptor 2), mutations in which are associated with stress-induced polymorphic ventricular tachycardia and arrhythmogenic right ventricular dysplasia[80,81]; *CHRM3*, encoding the cholinergic receptor muscarinic 3, a member of the G protein-coupled receptor family[32]; and *ZP4,* the product of which is zona pellucida glycoprotein 4[81]. The strong association signals on the X chromosome using an expanded reference group (see below and Supplementary Table 9) are of substantial interest but they do not identify known genes of obvious relevance to HT.

Rheumatoid arthritis (RA). Rheumatoid arthritis is a chronic inflammatory disease characterized by destruction of the synovial joints resulting in severe disability, particularly in patients who remain refractory to available therapies[82]. Susceptibility to, and severity of, RA are determined by both genetic and environmental factors, with λ_s estimates ranging from 5–10 (ref. 83).

An association between RA and alleles of the *HLA-DRB1* locus has long been established[84]. Despite extensive linkage[85–87] and association studies, only one other RA susceptibility locus has been convincingly identified in Caucasians. In common with several autoimmune diseases including T1D, carriage of the T allele of the rs2476601 SNP in the *PTPN22* (protein tyrosine phosphatase, non-receptor type 22) gene has been reproducibly associated with RA, conferring a genetic relative risk of approximately 1.8 (refs 88, 89). These known associations with *HLA-DRB1* and *PTPN22* explain around 50% of the familial aggregation of RA.

Both these previous associations emerge strongly here (Table 2). The most associated marker within *PTPN22* (rs6679677: chromosome 1p13) is perfectly correlated (HapMap CEU data $r^2 = 1$) with the functionally relevant SNP (rs2476601) described previously, and the effect size is consistent with previous estimates[89]. Amongst other putative RA susceptibility genes, two SNPs mapping to *CTLA-4* (cytotoxic T-lymphocyte associated 4) rs3087243 and rs11571300 were only nominally significant ($P = 0.085$ and $P = 0.034$, respectively) (Supplementary Table 10).

RA was the sole disease for which the sex-differentiated analysis generated a strong signal due to different genetic effects in males and females. The SNP rs11761231 (chromosome 7) generates a *P* value of 3.9×10^{-7} for the 2-degrees of freedom (d.f.) sex-differentiated test which combines trend tests in males and females (Table 3). (The trend test ignoring the sex of the individuals has a *P* value of 1.7×10^{-6}.) This genotype has no effect on disease status in males, but a strong apparently additive effect in females (*P* value in a logistic regression model with additive log-odds is 0.68 in males and 6.8×10^{-8} in females, additive OR for females 1.32), and may represent one of the first sex-differentiated effects in human diseases. Cluster plots for this SNP seem good, but it is surrounded by

recombination hotspots and has no other SNPs on the Affymetrix chip with $r^2 > 0.1$ (Supplementary Fig. 11). Some caution is therefore required, but this represents a potentially interesting finding which warrants further investigation, particularly given the sex-related prevalence difference characteristic of this condition.

None of the 9 SNPs with nominal *P* values in the range 10^{-5} to 5×10^{-7} (Table 4) map to loci previously associated with RA. Of particular interest is the association of SNPs mapping close to both the alpha and beta chains of the IL2 receptor (rs2104286 in the case of *IL2RA;* rs743777 and *IL2RB*). The IL2 receptor mediates IL2 stimulation of T lymphocytes and is thereby thought to have an important role in preventing autoimmunity. A rare 4-base-pair deletion of *IL2RA* has been associated with development of severe autoimmune disease[90], and there is evidence (from previous data[91], and from this study and its follow-up) that SNPs within the *IL2RA* gene region are associated with T1D (see also T1D section).

Several of the SNPs with nominal significance in the range 10^{-4} to 10^{-5} (Supplementary Table 7) map to genes with plausible biological relevance. Examples include SNPs within genes implicated in the TNF pathway (for example, rs2771369 in *TNFAIP2* (tumour necrosis factor, alpha-induced protein 2)) or in the regulation of T-cell function (rs854350 in *GZMB* (granzyme B) and rs4750316 in *PRKCQ* (protein kinase C, theta)). The association with rs10786617 in *KAZALD1* (Kazal-type serine protease inhibitor domain-containing protein 1 precursor), a gene whose product is known to have a role in bone regeneration after injury, may be relevant to the development of bone erosions in RA.

RA and T1D were already known to have two disease susceptibility genes in common: at the MHC, and at *PTPN22*. As detailed elsewhere, our study provides data indicating that this list can be extended to include variants around *IL2RA* (chromosome 10p15), *PTPN2* (chromosome 18p11) and the chromosome 12q24 region (Supplementary Table 11), all apparently novel in RA.

Type 1 diabetes (T1D). Type 1 diabetes is a chronic autoimmune disorder with onset usually in childhood[92]. The λ_s for T1D is ~15 and twin data suggest that over 85% of the phenotypic variance is due to genetic factors[93]. There are six genes/regions for which there is strong pre-existing statistical support for a role in T1D-susceptibility: these are the major histocompatibility complex (MHC), the genes encoding insulin, CTLA-4 (cytotoxic T-lymphocyte associated 4) and PTPN22 (protein tyrosine phosphatase, non-receptor type 22), and the regions around the interleukin 2 receptor alpha (*IL2RA/CD25*) and interferon-induced helicase 1 genes (*IFIH1*/MDA5)[94]. However, these signals can explain only part of the familial aggregation of T1D. Five of these previously identified associations were detected in this scan ($P \leq 0.001$) (Table 2 and Supplementary Table 10), the exception being the *INS* gene discussed above.

In this study, single-point analyses revealed three novel regions (on chromosomes 12q13, 12q24 and 16p13) showing strong evidence of association ($P < 5 \times 10^{-7}$; Table 3). Four further regions attained similar levels of significance either through multilocus analyses (chromosomes 4q27 and 12p13: Table 3, Supplementary Fig. 12), or through the combined analysis of autoimmune cases (chromosomes 18p11 and the 10p15 CD25 region: Table 3, Supplementary Fig. 13). The associations with T1D for chromosomes 12q13, 12q24, 16p13 and 18p11 have been confirmed in independent and multiple populations[10].

The two signals on chromosome 12 (at 12q13 and 12q24) map to regions of extensive linkage disequilibrium covering more than ten genes (Fig. 5). Several of these represent functional candidates because of their presumed roles in immune signalling, considered to be a major feature of T1D-susceptibility. These include *ERBB3* (receptor tyrosine-protein kinase erbB-3 precursor) at 12q13 and *SH2B3/LNK* (SH2B adaptor protein 3), *TRAFD1* (TRAF-type zinc finger domain containing 1) and *PTPN11* (protein tyrosine phosphatase, non-receptor type 11) at 12q24. For these signal regions in particular, extensive resequencing, further genotyping and targeted functional studies will be essential steps in identifying which gene, or genes, are causal[95]. Of those listed, *PTPN11* is a particularly attractive candidate given a major role in insulin and immune signalling[96]. It is also a member of the same family of regulatory phosphatases as *PTPN22*, already established as an important susceptibility gene for T1D and other autoimmune diseases[94,97]. Indeed, the 12q24 variant most associated with T1D also features in both the CD and RA scans, generating a combined signal for all autoimmune cases of 9.3×10^{-10} (Supplementary Table 11).

In contrast, available annotations suggest that the 16p13 region contains only two genes of unknown function, *KIAA0350* and dexamethasone-induced transcript (Fig. 5). Also, the region of association identified on 18p11 (Supplementary Fig. 14), which seems to confer susceptibility to all three autoimmune conditions studied (combined trend test $P = 9 \times 10^{-8}$, $P = 4.6 \times 10^{-8}$ for CD, 1.9×10^{-2} for RA, and 1.9×10^{-6} for T1D: Supplementary Table 11), maps to a single gene, *PTPN2* (protein tyrosine phosphatase, non-receptor type 2), a member of the same family as *PTPN22* and *PTPN11* and involved in immune regulation[96].

Our scan found associations with SNPs within the chromosome 10p15 region containing CD25, encoding the high-affinity receptor for IL-2. This is consistent with a previous report of associations of this region with T1D[91]. The *CD25* region has previously been shown to be associated with Graves' disease[98] and the present study also provides evidence of association with RA (combined trend test $P = 5 \times 10^{-8}$, $P = \sim 7 \times 10^{-6}$ for RA and T1D separately, Supplementary Table 11). This finding has clear biological connections to the evidence of association between T1D and a region of 4q27 revealed by the multilocus analysis (Supplementary Table 12, Supplementary Fig. 12). This region contains the genes encoding both IL-2 and IL-21. Together with studies in the NOD (nonobese diabetic) mouse model of T1D, which have shown that a major non-MHC locus (*Idd3*) reflects regulatory variation of the *Il2* gene[99], our results point to the primary importance of the IL-2 pathway in T1D and other autoimmune diseases.

One further region deserves comment. In the multilocus analysis, there was increased support for a region on chromosome 12p13 containing several candidate genes, including *CD69* (CD69 antigen (p60, early T-cell activation antigen)) and multiple *CLEC* (C-type lectin domain family) genes. In contrast to the chromosome 4 region where the effect of imputation is to tip an already-strong signal (5.01×10^{-7} for typed rs17388568, trend test) over the arbitrary threshold of 5×10^{-7}, the 12p13 locus involves a more marked change between imputed and actual (7.2×10^{-7} for rs11052552, general test). Replication studies of this imputed SNP to date have produced equivocal results (for details see ref. 10).

Type 2 diabetes (T2D). Type 2 diabetes is a chronic metabolic disorder typically first diagnosed in the middle to late adult years[100]. Strongly associated with obesity, the condition features defects in both the secretion and peripheral actions of insulin[101]. The appreciable familial aggregation of T2D (an estimated λs of ~3.0 in European individuals)[73] reflects both shared family environment and genetic predisposition. Heritability values vary widely with most estimates between 30 and 70%[101].

To date, robust, widely replicated associations in non-isolate populations are limited to variants in three genes: *PPARG* (encoding the peroxisomal proliferative activated receptor gamma; P12A[102]), *KCNJ11* (the inwardly-rectifying Kir6.2 component of the pancreatic beta-cell KATP channel; E23K[103]) and *TCF7L2* (transcription factor 7-like 2; rs7903146 (refs 104, 105)).

All three of these signals are detected here with effect-sizes consistent with previous reports (Table 2). A cluster of SNPs on chromosome 10q, within *TCF7L2,* represented by rs4506565 (trend test, OR 1.36, $P = 5.7 \times 10^{-13}$) generates the strongest association signal for T2D (Table 3, Fig. 5). Rs4506565 is in tight linkage disequilibrium (r^2 of 0.92 in the CEU component of HapMap) with rs7903146, the variant with the strongest aetiological claims[104,106]. In fact, our

imputation analysis confirms that rs7903146, though unrepresented on the chip, is responsible for the strongest association effect in this region (Fig. 5). TCF7L2 acts within the WNT-signalling pathway, and effects on diabetes risk seem to be mediated predominantly through beta-cell dysfunction[107].

As expected, given existing effect-size estimates, the signals associated with variants within the other established T2D-susceptibility genes, *KCNJ11* (rs5215, r^2 of 0.9 with rs5219, E23K) and *PPARG* (rs17036328, r^2 of 1 with rs1801282, P12A) are less dramatic (trend test, OR 1.15 and 1.23 respectively, both $P = \sim 0.001$). These examples illustrate how genuine disease-susceptibility variants can generate association signals which would not attract immediate attention for follow-up in the genomewide context.

Apart from *TCF7L2,* the scan reveals two signals for T2D with *P* values less than 5×10^{-7} (Table 3, Fig. 5). The first of these maps within the *FTO* (fat-mass and obesity-associated) gene on chromosome 16q. Several adjacent SNPs (including rs9939609, rs7193144 and rs8050136) generate signals characterized by a per-allele OR for T2D of ~1.25 and a risk-allele frequency of ~40% in controls. As recently described in follow-up studies prompted by this finding, the effect of these variants on T2D-risk has been replicated and is mediated entirely by their marked effect on adiposity[24].

The third association signal (chromosome 6p22) features a cluster of highly associated SNPs (including rs9465871) with risk-allele frequencies between 18 and 35%, mapping to intron 5 of the *CDKAL1* (CDK5 regulatory subunit associated protein 1-like 1) gene. Although the function of CDKAL1 is not known, it shares homology at the protein domain level with CDK5 regulatory subunit associated protein 1 (CDK5RAP1). CDK5RAP1 is known to inhibit the activation of CDK5, a cyclin-dependent kinase which has been implicated in the maintenance of normal beta-cell function[108]. Our own follow-up studies, and scans by other groups have shown strong replication of this finding[19–22]. The effect of this variant on T2D-risk shows significant departures from additivity (Supplementary Table 8).

One notable inclusion amongst the variants with more modest association signals is a cluster of SNPs on chromosome 10 including rs10748582 and rs7923866, which generate trend test *P* values between 10^{-4} and 10^{-5}. This cluster maps in the vicinity of the *HHEX* (homeobox, hematopoietically expressed) and *IDE* (insulin-degrading enzyme) genes, in a region recently highlighted in a GWA scan for T2D performed in 1363 subjects of French origin[109]. The SNPs showing association in our data are proxies for those reported in the French study and generate similar effect-size estimates for T2D.

Of the three other regions highlighted by the French scan[109], none can be confirmed by our data. The SNP in *SLC30A8* associated with T2D in the French report (rs13266634) is poorly correlated with SNPs on the Affymetrix chip ($r^2 < 0.01$), and extensive recombination events in the region limit the value of data-imputation methods. Coverage of the *LOC387761* and *EXT2* signals is considerably better, but, for these, neither genotyped nor imputed SNPs show evidence for association with T2D.

WTCCC data contributed to identification of two additional robustly replicating T2D signals, mapping to the *IGF2BP2* gene and *CDKN2A/CDKN2B* regions[19,21,22], although neither generated impressive *P* values on the primary scan analysis (neither single-point *P* was $<10^{-4}$). The latter signal maps to the same region as the CAD signal on chromosome 9 though different SNPs are involved. The other SNPs in Table 4 do not map to genes or regions previously implicated in T2D pathogenesis, and replication efforts to date have not identified any confirmed signals[19].

Expanded reference group analyses. For a fixed number of cases, power of a case-control study can be increased by enlarging the reference group. Our main analyses used a control:case ratio of 1.5:1 for each disease. The availability of the other 6 disease data sets gave us the opportunity to expand the reference group up to a ratio of ~7.5:1, with potential reciprocal benefits for the analysis of each disease. For BD and T2D the expanded reference group comprised the 58C and UKBS controls supplemented by the other 6 disease sets; for CAD and HT this expanded reference group was reduced to exclude HT and CAD respectively; for CD, RA and T1D, the reference group was augmented only by the cases from the non-autoimmune diseases.

The utility of the expanded reference group approach was demonstrated by increased evidence for association at most of the loci that received strongest support from our primary analysis, including many of the signals at loci known to show robust association in T1D, T2D and CD (Supplementary Table 9). Additionally, this analysis elevated several loci with modest levels of statistical significance in the primary analysis, to the top tier of statistical significance ($P < 5 \times 10^{-7}$).

Our data indicate that this approach may be a useful adjunct to conventional analysis and that loci identified as highly significant should be considered for follow up. There are two important caveats. First, susceptibility genes that influence both the test disease and one or more of the diseases included in the reference group will cause loss of power. Second, a 'mirror-image' effect could occur whereby a strong association within the expanded reference sample (for example, HLA in autoimmune diseases) causes spurious association with the opposite allele in the test disease. Thus, a positive association using an expanded reference group must be interpreted within the context of association findings in the diseases included within the reference group.

Disease models. It is of interest to consider which statistical models best describe the data at and between loci that are strongly associated with disease status. Biological interpretation of these statistical models is not straightforward but they can help in choosing more powerful statistical tools for detecting associations.

First, consider separately each of the 19 non-MHC SNPs showing strong evidence for association on either the trend or genotypic test in Table 3. For four of these 19, the *P* value on the 2-d.f. genotypic test was smaller than that on the 1-d.f. trend test (Table 3). When comparing disease models, these were also the four SNPs with evidence for departure from a simple model in which odds of disease increase multiplicatively with the number of copies of the risk allele (Supplementary Table 8). This supports our view that the genotypic test should be carried out in addition to the trend test, although should perhaps be viewed more cautiously for two reasons: it is more susceptible to genotyping errors; and (on the basis of our findings) experience does not favour strong dominance effects.

A separate question relates to the best models for the way in which different loci combine to affect susceptibility to a disease, and as a consequence on the extent to which methods explicitly allowing interactions between loci should be employed to detect associations[110]. None of the analyses reported here includes such interactions, so we are not well placed to address the general question. Nonetheless, within each collection with multiple associated regions (CD, T1D and T2D) we considered all pairs of non-MHC SNPs in Table 3 and looked for a departure from the model in which the two loci combine to increase log-odds in an additive fashion. We found suggestive evidence of a departure from multilocus additivity between rs1000113 and rs10761659 in CD (unadjusted *P* value = 0.002) and between rs9465871 and rs4506565 in T2D (unadjusted *P* value = 0.004). Further investigation of this question, preferably on unbiased sets of disease loci found through the application of single locus and interaction-based approaches, would seem warranted.

Discussion

We have studied seven common familial diseases by genome-wide association analysis in 16,179 individuals. Our findings inform understanding of the genetic basis of the diseases concerned and provide methodological insights relevant to the pursuit of GWA studies in general.

A simple but important observation is that GWA analysis provides a highly effective approach for exploring the genetic underpinnings of common familial diseases. Our yield of novel, highly significant

association findings is comparable to, or exceeds, the number of those hitherto-generated by candidate gene or positional cloning efforts. For many of the compelling signals, replication has already been obtained, including regions on chromosomes 3p21, 5q33, 10q24 and 18p11 for CD[23], 12q13, 12q24, 16p13 and 18p11 in T1D[10] and 6p22 and 16q12 in T2D[19–22,24]. For others, replication is required to establish a definitive relationship with disease. Additional findings of particular interest include the identification of several loci that seem to influence susceptibility to multiple autoimmune diseases, and the suggestion of a novel locus for RA which shows sex-specific effects.

Our study enables us to make several general recommendations relevant to GWA studies. The first relates to the importance of careful quality control. In such large data sets, small systematic differences can readily produce effects capable of obscuring the true associations being sought[111,112]. We implemented extensive quality control checks to minimize differences in sample DNA concentration, quality and handling procedures and combined a new genotype-calling algorithm (CHIAMO) with a set of filtering heuristics to select SNPs for further analysis. Given that infallible detection of incorrect genotype calls is not yet possible, the criteria used for SNP exclusion need to strike a compromise between stringency (which may discard true signals or generate spurious positives through differential missingness) and leniency (with the danger that true signals are swamped by spurious findings due to poor genotype calling). As such, systematic visual inspection of cluster plots for SNPs of interest remains an integral part of the quality control process.

The potential for population structure to undermine inferences in case-control association studies has long been debated[113] but limited empirical data have been available to assess the issue. Our study highlighted several loci, some known and some new, which demonstrate substantial geographical variation in allele frequencies across Britain (Table 1), most probably due to natural selection in ancestral populations. Outside these loci, the effects of population structure are relatively minor, and do not represent a major source of confounding, provided that individuals with appreciable non-European ancestry are excluded. Although these conclusions may not generalize to studies in other locations, this finding reinforces the logistical and economic benefits of the case-control design over alternatives (such as family-based association studies).

Our study allowed us to address another important methodological issue: the adequacy, or otherwise, of using a common set of controls, rather than a sample recruited explicitly for use with a defined disease sample. It is often assumed that failure to match cases and controls for socio-demographic variables will lead to substantial inflation of the type I error rate. Our study demonstrates that, within the context of large-scale genetic association studies, for British populations at least, this concern has been overstated. A related argument against use of population controls relates to the perceived impact of misclassification bias when a proportion of controls meet the criteria used to define cases. However, the consequent loss of power is modest unless the trait of interest is very common[6]. Given the above, the present study provides a compelling case for both the suitability and efficiency of the common control design in Britain and warrants its serious consideration elsewhere. Further benefits can be expected from use of this common control genotype data set in future GWA studies in Britain. Finally, in failing to detect significant differences in performance between the epidemiological sample (58C) and that derived from blood donors (UKBS), we validate the use of the latter samples for cost-effective, large-scale control DNA provision.

In terms of general biological insights, the most profound relate to inferences about the allelic architecture of common traits. The novel variants we have uncovered are characterized by modest effect size (that is, per-allele ORs between 1.2 and 1.5) and even these estimates are likely to be inflated[114]. We identified no additional common variants of very large effect (akin to HLA in T1D: Supplementary Fig. 15). The observed distribution of effect sizes is consistent with models based on theoretical considerations and empirical data from animal models[87,115,116] that suggest that, for any given trait, there will be few (if any) large effects, a handful of modest effects and a substantial number of genes generating small or very small increases in disease risk.

There are several important corollaries. Notwithstanding the incomplete coverage afforded by the genotyping reagents employed, most of the susceptibility effects yet to be uncovered for these diseases (at least those attributable to, or tagged by, common SNPs) are likely to have effects of similar or smaller magnitude to those we have highlighted. Beyond the signals with the strongest evidence for association, most of which are likely to be real (and many of which have already been confirmed), there will be many additional susceptibility variants for which the WTCCC provides some evidence, but for which extensive replication will be required to establish validity. *PPARG* and *KCNJ11* provide examples of proven susceptibility genes (for T2D) that generated only modest evidence for association within the WTCCC, and which would only have been revealed by such replication efforts. Given the likely preponderance of susceptibility variants of small effect, the potential for identifying further loci is limited only by the clinical resources available for replication (assuming suitable study design, accurate genotyping and appropriate analysis and inference). Provided the attribution of a causal relationship with the trait of interest is robust, even variants of very small effect can offer fundamental biological insights.

The patterns of allelic architecture uncovered mean that replication efforts will need to feature comparably large sample sizes: even if one accepts more relaxed significance thresholds given the prior evidence, one has to consider the inflation in effect-size estimates in the primary study. Caution is required in reaching negative conclusions on the basis of a single failed attempt at replication, or any set of replication attempts that are inadequately powered.

One of our major design considerations was sample size. We set out to include samples larger than those previously examined for genome-wide association, and our results suggest that such large sample sizes were necessary. Even with 2,000 cases and 3,000 controls,

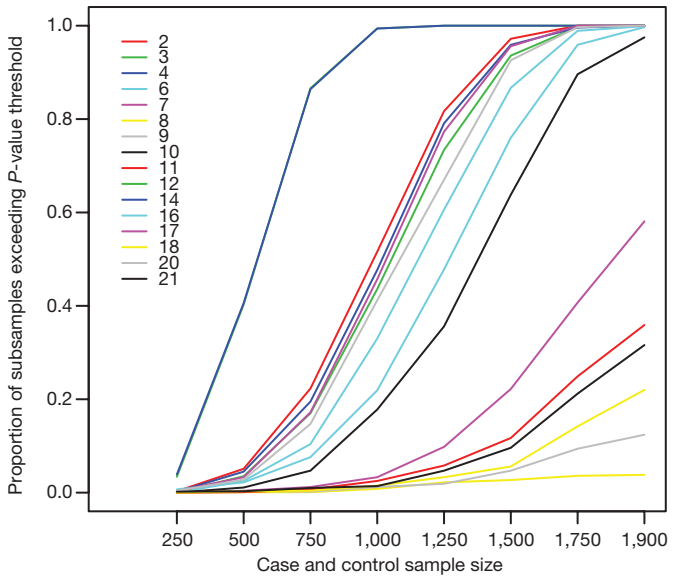

Figure 6 | Strong associations in subsamples of our data. For the 16 SNPs in Table 3 (outside the MHC) with *P* values for the trend test below 5×10^{-7}, we randomly generated 1,000 subsets of our full data set corresponding to case-control studies with different numbers of cases, and the same number of controls (*x* axis). The *y* axis gives the proportion of subsamples of a given size in which that SNP achieved a *P* value for the trend test below 5×10^{-7}. SNPs are numbered according to the row in which they occur in Table 3 (so that, for example, the CAD hit is numbered 2, and the *TCF7L2* hit on chromosome 10 for T2D is numbered 20).

adequate power is restricted to common variants of relatively large effect (see Supplementary Table 2). We carried out an experiment to see which SNPs showing strong evidence of association in the full data (that is, signals outside MHC with trend test $P < 5 \times 10^{-7}$), would have been detected at that same threshold in only a subset of our data (Fig. 6). Because it focuses on a particular but arbitrary *P*-value threshold, some care is needed in interpreting the figure. Nonetheless, for subsamples of 1,000 cases and 1,000 controls, of the 16 loci detected in the full study, we would have been certain of seeing only 2, with an expectation of about 6; for subsamples of 1,500 cases and 1,500 controls, we could expect to have seen about 9. These figures provide stark evidence that the larger the study sample, the more loci can be expected to reach threshold significance values. Indeed, given the likely distribution of effect sizes for most complex traits (see above), there are strong grounds for the prosecution of GWA studies on an even larger scale than ours, and, wherever possible, combining the results from existing GWA scans performed for the same trait. To assist such efforts, individual level data from this study will be widely available through the Consortium's Data Access Committee (follow links from http://www.wtccc.org.uk).

In our study, T1D and CD, the conditions showing strongest familial aggregation (as quantified by their sibling relative risks, λ_s), generated the largest number of highly significant associations. This relationship was not sustained in comparisons between the other five diseases. It is important to recognize that the association signals so far identified account for only a small proportion of overall familiality. There is a disparity in scale between the modest locus-specific λ_s effects attributable to the identified associations (for instance, the prominent *TCF7L2* signal for T2D translates into a λ_s of only 1.03) and the estimates of overall familiality that reflects the combined effects of all genes and shared family environment. These estimates demonstrate the limited potential of the variants thus far identified (singly or in combination) to provide clinically useful prediction of disease[117,118].

The identification and characterization of the aetiological variants that underlie replicated associations will necessitate extensive fine-mapping and functional validation. We view the WTCCC study and data set as an important first step towards harnessing the powerful molecular genomic tools now available to dissect the biological basis of common disease and translating those findings into improvements in human health.

METHODS SUMMARY

A detailed description of materials and methods is given in Methods. The workflow and organization of the project are given in Supplementary Fig. 16. Case series came from previously established collections with nationally representative recruitment: 2,000 samples were genotyped for each. The control samples came from two sources: half from the 1958 Birth Cohort and the remainder from a new UK Blood Service sample. The latter collection was established specifically for this study and is a UK national repository of anonymized DNA samples from 3,622 consenting blood donors. The vast majority of subjects were self-reported as of European Caucasian ancestry. All DNA samples were requantified and tested for degradation and PCR amplification. Genotyping was performed using GeneChip 500K arrays at the Affymetrix Services Lab (California): arrays not passing the 93% call rate threshold at $P = 0.33$ with the Dynamic Model algorithm were repeated. CEL (cell intensity) files were transferred to WTCCC for quantile normalization, and genotypes called using a new genotyping algorithm, CHIAMO, developed for this project. QC/QA measures included sample call rate, overall heterozygosity and evidence of non-European ancestry (809 samples excluded; 16,179 retained for analysis). SNPs were excluded from analysis because of missing data rates, departures from Hardy–Weinberg equilibrium and other metrics (31,011 excluded; 469,557 retained). Standard 1-d.f. and 2-d.f. tests of case-control association were supplemented with bayesian approaches, multilocus methods (data imputation) and analyses with combined data sets, either as additional cases (to detect variants influencing multiple phenotypes) or as an expanded reference group (to increase power). Results for each SNP for all analyses reported will be available from http://www.wtccc.org.uk, as will details allowing other researchers to apply for access to WTCCC genotype data. Software packages developed within the WTCCC are available on request (see Methods for details).

Full Methods and any associated references are available in the online version of the paper at www.nature.com/nature.

Received 26 March; accepted 11 May 2007.

1. Hirschhorn, J. N. & Daly, M. J. Genome-wide association studies for common diseases and complex traits. *Nature Rev. Genet.* **6,** 95–108 (2005).
2. Barrett, J. C. & Cardon, L. R. Evaluating coverage of genome-wide association studies. *Nature Genet.* **38,** 659–662 (2006).
3. The International HapMap consortium. A haplotype map of the human genome. *Nature* **437,** 1299–1320 (2005).
4. Murray, C. J. & Lopez, A. D. Evidence-based health policy—lessons from the Global Burden of Disease Study. *Science* **274,** 740–743 (1996).
5. Mantel, N. Chi-square tests with one degree of freedom: Extension of the Mantel–Haenszel procedure. *J. Am. Stat. Ass.* **58,** 690–700 (1963).
6. Colhoun, H. M., McKeigue, P. M. & Davey Smith, G. Problems of reporting genetic associations with complex outcomes. *Lancet* **361,** 865–872 (2003).
7. Bersaglieri, T. *et al.* Genetic signatures of strong recent positive selection at the lactase gene. *Am. J. Hum. Genet.* **74,** 1111–1120 (2004).
8. Coelho, M. *et al.* Microsatellite variation and evolution of human lactase persistence. *Hum. Genet.* **117,** 329–339 (2005).
9. Sabeti, P. C. *et al.* Positive natural selection in the human lineage. *Science* **312,** 1614–1620 (2006).
10. Todd, J. A. *et al.* Robust associations of four new chromosome regions from genome-wide analyses of type 1 diabetes. *Nature Genet.* advance online publication, doi:10.1038/ng2068 (6 June 2007).
11. Falush, D., Stephens, M. & Pritchard, J. K. Inference of population structure using multilocus genotype data: linked loci and correlated allele frequencies. *Genetics* **164,** 1567–1587 (2003).
12. Pritchard, J. K., Stephens, M. & Donnelly, P. Inference of population structure using multilocus genotype data. *Genetics* **155,** 945–959 (2000).
13. Menozzi, P., Piazza, A. & Cavalli-Sforza, L. Synthetic maps of human gene frequencies in Europeans. *Science* **201,** 786–792 (1978).
14. Price, A. L. *et al.* Principal components analysis corrects for stratification in genome-wide association studies. *Nature Genet.* **38,** 904–909 (2006).
15. Devlin, B. & Roeder, K. Genomic control for association studies. *Biometrics* **55,** 997–1004 (1999).
16. Clayton, D. in *Handbook of Statistical Genetics* (eds Balding, D. J., Bishop, M. & Cannings, C.) 939–960 (Wiley, New York, 2003).
17. Mackay, T. F. & Anholt, R. R. Of flies and man: *Drosophila* as a model for human complex traits. *Annu. Rev. Genomics Hum. Genet.* **7,** 339–367 (2006).
18. Wacholder, S., Chanock, S., Garcia-Closas, M., El Ghormli, L. & Rothman, N. Assessing the probability that a positive report is false: an approach for molecular epidemiology studies. *J. Natl. Cancer Inst.* **96,** 434–442 (2004).
19. Zeggini, E. *et al.* Replication of genome-wide association signals in U.K. samples reveals risk loci for type 2 diabetes. *Science* online publication, doi:10.1126/science.1142364 (26 April 2007).
20. Steinthorsdottir, V. *et al.* A variant in CDKAL1 influences insulin response and risk of type 2 diabetes. *Nature Genet.* advance online publication, doi:10.1038/ng2043 (26 April 2007).
21. Scott, L. J. *et al.* A genome-wide association study of type 2 diabetes in Finns detects multiple susceptibility variants. *Science* online publication, doi:10.1126/science.1142382 (26 April 2007).
22. Diabetes Genetics Institute. Genome-wide association analysis identifies loci for type 2 diabetes and triglyceride levels. *Science* online publication, doi:10.1126/science.1142358 (26 April 2007).
23. Parkes, M. *et al.* Sequence variants in the autophagy gene *IRGM* and multiple other replicating loci contribute to Crohn's disease susceptibility. *Nature Genet.* advance online publication, doi:10.1038/ng2061 (6 June 2007).
24. Frayling, T. M. *et al.* A common variant in the *FTO* gene is associated with body mass index and predisposes to childhood and adult obesity. *Science* **316,** 889–894 (2007).
25. Cohen, J. C. *et al.* Multiple rare alleles contribute to low plasma levels of HDL cholesterol. *Science* **305,** 869–872 (2004).
26. Muller-Oerlinghausen, B., Berghofer, A. & Bauer, M. Bipolar disorder. *Lancet* **359,** 241–247 (2002).
27. Craddock, N., O'Donovan, M. C. & Owen, M. J. The genetics of schizophrenia and bipolar disorder: dissecting psychosis. *J. Med. Genet.* **42,** 193–204 (2005).
28. McGuffin, P. *et al.* The heritability of bipolar affective disorder and the genetic relationship to unipolar depression. *Arch. Gen. Psychiatry* **60,** 497–502 (2003).
29. Rice, J. *et al.* The familial transmission of bipolar illness. *Arch. Gen. Psychiatry* **44,** 441–447 (1987).
30. McQueen, M. B. *et al.* Combined analysis from eleven linkage studies of bipolar disorder provides strong evidence of susceptibility loci on chromosomes 6q and 8q. *Am. J. Hum. Genet.* **77,** 582–595 (2005).
31. Craddock, N. & Owen, M. J. The beginning of the end for the Kraepelinian dichotomy. *Br. J. Psychiatry* **186,** 364–366 (2005).
32. Ozeki, Y. *et al.* Disrupted-in-Schizophrenia-1 (*DISC-1*): mutant truncation prevents binding to NudE-like (*NUDEL*) and inhibits neurite outgrowth. *Proc. Natl Acad. Sci. USA* **100,** 289–294 (2003).

33. Blackwood, D. H. *et al.* Schizophrenia and affective disorders—cosegregation with a translocation at chromosome 1q42 that directly disrupts brain-expressed genes: clinical and P300 findings in a family. *Am. J. Hum. Genet.* **69,** 428–433 (2001).
34. Graves, T. D. & Hanna, M. G. Neurological channelopathies. *Postgrad. Med. J.* **81,** 20–32 (2005).
35. Krystal, J. H. *et al.* Glutamate and GABA systems as targets for novel antidepressant and mood-stabilizing treatments. *Mol. Psychiatry* **7** (Suppl. 1), S71–S80 (2002).
36. Vawter, M. P. *et al.* Reduction of synapsin in the hippocampus of patients with bipolar disorder and schizophrenia. *Mol. Psychiatry* **7,** 571–578 (2002).
37. Libby, P. & Theroux, P. Pathophysiology of coronary artery disease. *Circulation* **111,** 3481–3488 (2005).
38. Yusuf, S. *et al.* Effect of potentially modifiable risk factors associated with myocardial infarction in 52 countries (the INTERHEART study): case-control study. *Lancet* **364,** 937–952 (2004).
39. Lusis, A. J., Mar, R. & Pajukanta, P. Genetics of atherosclerosis. *Annu. Rev. Genomics Hum. Genet.* **5,** 189–218 (2004).
40. Watkins, H. & Farrall, M. Genetic susceptibility to coronary artery disease: from promise to progress. *Nature Rev. Genet.* **7,** 163–173 (2006).
41. Helgadottir, A. *et al.* The gene encoding 5-lipoxygenase activating protein confers risk of myocardial infarction and stroke. *Nature Genet.* **36,** 233–239 (2004).
42. Helgadottir, A. *et al.* A variant of the gene encoding leukotriene A4 hydrolase confers ethnicity-specific risk of myocardial infarction. *Nature Genet.* **38,** 68–74 (2006).
43. Topol, E. J., Smith, J., Plow, E. F. & Wang, Q. K. Genetic susceptibility to myocardial infarction and coronary artery disease. *Hum. Mol. Genet.* **15** (Spec. No. 2), R117–R123 (2006).
44. Lowe, S. W. & Sherr, C. J. Tumor suppression by *Ink4a–Arf*: progress and puzzles. *Curr. Opin. Genet. Dev.* **13,** 77–83 (2003).
45. Hannon, G. J. & Beach, D. $p15^{INK4B}$ is a potential effector of TGF-β-induced cell cycle arrest. *Nature* **371,** 257–261 (1994).
46. Kalinina, N. *et al.* Smad expression in human atherosclerotic lesions: evidence for impaired TGF-β/Smad signaling in smooth muscle cells of fibrofatty lesions. *Arterioscler. Thromb. Vasc. Biol.* **24,** 1391–1396 (2004).
47. Schmid, M. *et al.* A methylthioadenosine phosphorylase (MTAP) fusion transcript identifies a new gene on chromosome 9p21 that is frequently deleted in cancer. *Oncogene* **19,** 5747–5754 (2000).
48. Prasannan, P., Pike, S., Peng, K., Shane, B. & Appling, D. R. Human mitochondrial C_1-tetrahydrofolate synthase: gene structure, tissue distribution of the mRNA, and immunolocalization in Chinese hamster ovary calls. *J. Biol. Chem.* **278,** 43178–43187 (2003).
49. Walkup, A. S. & Appling, D. R. Enzymatic characterization of human mitochondrial C_1-tetrahydrofolate synthase. *Arch. Biochem. Biophys.* **442,** 196–205 (2005).
50. Frosst, P. *et al.* A candidate genetic risk factor for vascular disease: a common mutation in methylenetetrahydrofolate reductase. *Nature Genet.* **10,** 111–113 (1995).
51. Klerk, M. *et al.* MTHFR 677C→T polymorphism and risk of coronary heart disease: a meta-analysis. *J. Am. Med. Assoc.* **288,** 2023–2031 (2002).
52. Gregory, J. F. III *et al.* Primed, constant infusion with [$^2H_3$]serine allows *in vivo* kinetic measurement of serine turnover, homocysteine remethylation, and transsulfuration processes in human one-carbon metabolism. *Am. J. Clin. Nutr.* **72,** 1535–1541 (2000).
53. Randak, C. *et al.* Three siblings with nonketotic hyperglycinaemia, mildly elevated plasma homocysteine concentrations and moderate methylmalonic aciduria. *J. Inherit. Metab. Dis.* **23,** 520–522 (2000).
54. Wight, T. N. The ADAMTS proteases, extracellular matrix, and vascular disease — Waking the sleeping giant(s)! *Arterioscler. Thromb. Vasc. Biol.* **25,** 12–14 (2005).
55. Jonsson-Rylander, A. *et al.* The role of ADAMTS-1 in atherosclerosis: Remodeling of carotid artery, immunohistochemistry, and proteolysis of versican. *Arter. Thromb. Vas. Bio.* **25,** 180–185 (2004).
56. Travis, S. P. *et al.* European evidence based consensus on the diagnosis and management of Crohn's disease: current management. *Gut* **55** (Suppl. 1), i16–i35 (2006).
57. Sartor, R. B. Mechanisms of disease: pathogenesis of Crohn's disease and ulcerative colitis. *Nature Clin. Pract. Gastroenterol. Hepatol.* **3,** 390–407 (2006).
58. Tysk, C., Lindberg, E., Jarnerot, G. & Floderusmyrhed, B. Ulcerative-colitis and Crohns-disease in an unselected population of monozygotic and dizygotic twins — a study of heritability and the influence of smoking. *Gut* **29,** 990–996 (1988).
59. Gaya, D. R., Russell, R. K., Nimmo, E. R. & Satsangi, J. New genes in inflammatory bowel disease: lessons for complex diseases? *Lancet* **367,** 1271–1284 (2006).
60. Hugot, J. P. *et al.* Association of NOD2 leucine-rich repeat variants with susceptibility to Crohn's disease. *Nature* **411,** 599–603 (2001).
61. Ogura, Y. *et al.* A frameshift mutation in NOD2 associated with susceptibility to Crohn's disease. *Nature* **411,** 603–606 (2001).
62. Rioux, J. D. *et al.* Genetic variation in the 5q31 cytokine gene cluster confers susceptibility to Crohn disease. *Nature Genet.* **29,** 223–228 (2001).
63. Duerr, R. H. *et al.* A genome-wide association study identifies IL23R as an inflammatory bowel disease gene. *Science* **314,** 1461–1463 (2006).
64. Hampe, J. *et al.* A genome-wide association scan of nonsynonymous SNPs identifies a susceptibility variant for Crohn disease in *ATG16L1*. *Nature Genet.* **39,** 207–211 (2007).
65. Rioux, J. D. *et al.* Genome-wide association study identifies new susceptibility loci for Crohn disease and implicates autophagy in disease pathogenesis. *Nature Genet.* **39,** 596–604 (2007).
66. Libioulle, C. *et al.* Novel crohn disease locus identified by genome-wide association maps to a gene desert on 5p13.1 and modulates expression of *PTGER4*. *PLoS Genet.* **3,** e58 (2007).
67. Singh, S. B., Davis, A. S., Taylor, G. A. & Deretic, V. Human IRGM induces autophagy to eliminate intracellular mycobacteria. *Science* **313,** 1438–1441 (2006).
68. Leonard, E. J. Biological aspects of macrophage-stimulating protein (MSP) and its receptor. *Ciba Found Symp.* **212,** 183–191; discussion 192–197 (1997).
69. Pabst, O., Forster, R., Lipp, M., Engel, H. & Arnold, H. H. NKX2.3 is required for MAdCAM-1 expression and homing of lymphocytes in spleen and mucosa-associated lymphoid tissue. *EMBO J.* **19,** 2015–2023 (2000).
70. Yamazaki, K. *et al.* Single nucleotide polymorphisms in *TNFSF15* confer susceptibility to Crohn's disease. *Hum. Mol. Genet.* **14,** 3499–3506 (2005).
71. Pietravalle, F. *et al.* Human native soluble CD40L is a biologically active trimer, processed inside microsomes. *J. Biol. Chem.* **271,** 5965–5967 (1996).
72. Battegay, E. J., Lip, G. Y. H. & Badris, G. L. (eds) *Hypertension; Principles and Practice* (Taylor Francis Group, 2005).
73. Kobberling, J. & Tattersall, R. (eds) *The Genetics of Diabetes Mellitus* (Academic Press, London, 1982).
74. Dominiczak, A. F. *et al.* Genetics of hypertension: Lessons learnt from Mendelian and polygenic syndromes. *Clin. Exp. Hypertens.* **26,** 611–620 (2004).
75. Mein, C. A., Caulfield, M. J., Dobson, R. J. & Munroe, P. B. Genetics of essential hypertension. *Hum. Mol. Genet.* **13,** R169–R175 (2004).
76. Hubner, N. *et al.* Integrated transcriptional profiling and linkage analysis for identification of genes underlying disease. *Nature Genet.* **37,** 243–253 (2005).
77. Caulfield, M. *et al.* Genome-wide mapping of human loci for essential hypertension. *Lancet* **361,** 2118–2123 (2003).
78. Newhouse, S. J. *et al.* Haplotypes of the *WNK1* gene associate with blood pressure variation in a severely hypertensive population from the British Genetics of Hypertension study. *Hum. Mol. Genet.* **14,** 1805–1814 (2005).
79. Tobin, M. D. *et al.* Association of *WNK1* gene polymorphisms and haplotypes with ambulatory blood pressure in the general population. *Circulation* **112,** 3423–3429 (2005).
80. Otsu, K. *et al.* Molecular cloning of cDNA encoding the Ca^{2+} release channel (ryanodine receptor) of rabbit cardiac muscle sarcoplasmic reticulum. *J. Biol. Chem.* **265,** 13472–13483 (1990).
81. Benkusky, N. A., Farrell, E. F. & Valdivia, H. H. Ryanodine receptor channelopathies. *Biochem. Biophys. Res. Commun.* **322,** 1280–1285 (2004).
82. Worthington, J., Barton, A. & John, S. L. The epidemiology of rheumatoid arthritis and the use of linkage and association studies to identify disease genes (Birkhauser, Basel, 2005).
83. Wordsworth, P. & Bell, J. Polygenic susceptibility in rheumatoid arthritis. *Ann. Rheum. Dis.* **50,** 343–346 (1991).
84. Gregersen, P. K., Silver, J. & Winchester, R. J. The shared epitope hypothesis. An approach to understanding the molecular genetics of susceptibility to rheumatoid arthritis. *Arthritis Rheum.* **30,** 1205–1213 (1987).
85. Jawaheer, D. *et al.* A genomewide screen in multiplex rheumatoid arthritis families suggests genetic overlap with other autoimmune diseases. *Am. J. Hum. Genet.* **68,** 927–936 (2001).
86. John, S. *et al.* Whole-genome scan, in a complex disease, using 11,245 single-nucleotide polymorphisms: comparison with microsatellites. *Am. J. Hum. Genet.* **75,** 54–64 (2004).
87. MacKay, K. *et al.* Whole-genome linkage analysis of rheumatoid arthritis susceptibility loci in 252 affected sibling pairs in the United Kingdom. *Arthritis Rheum.* **46,** 632–639 (2002).
88. Begovich, A. B. *et al.* A missense single-nucleotide polymorphism in a gene encoding a protein tyrosine phosphatase (*PTPN22*) is associated with rheumatoid arthritis. *Am. J. Hum. Genet.* **75,** 330–337 (2004).
89. Hinks, A., Eyre, S., Barton, A., Thomson, W. & Worthington, J. Investigation of genetic variation across PTPN22 in UK rheumatoid arthritis (RA) patients. *Ann. Rheum. Dis.* **66,** 683–686 (2006).
90. Sharfe, N., Dadi, H. K., Shahar, M. & Roifman, C. M. Human immune disorder arising from mutation of the α chain of the interleukin-2 receptor. *Proc. Natl Acad. Sci. USA* **94,** 3168–3171 (1997).
91. Vella, A. *et al.* Localization of a type 1 diabetes locus in the *IL2RA/CD25* region by use of tag single-nucleotide polymorphisms. *Am. J. Hum. Genet.* **76,** 773–779 (2005).
92. Devendra, D., Liu, E. & Eisenbarth, G. S. Type 1 diabetes: recent developments. *Br. Med. J.* **328,** 750–754 (2004).
93. Hyttinen, V., Kaprio, J., Kinnunen, L., Koskenvuo, M. & Tuomilehto, J. Genetic liability of type 1 diabetes and the onset age among 22,650 young Finnish twin pairs: a nationwide follow-up study. *Diabetes* **52,** 1052–1055 (2003).
94. Smyth, D. J. *et al.* A genome-wide association study of nonsynonymous SNPs identifies a type 1 diabetes locus in the interferon-induced helicase (*IFIH1*) region. *Nature Genet.* **38,** 617–619 (2006).
95. Todd, J. A. Statistical false positive or true disease pathway? *Nature Genet.* **38,** 731–733 (2006).
96. Mustelin, T., Vang, T. & Bottini, N. Protein tyrosine phosphatases and the immune response. *Nature Rev. Immunol.* **5,** 43–57 (2005).

97. Bottini, N. *et al.* A functional variant of lymphoid tyrosine phosphatase is associated with type I diabetes. *Nature Genet.* **36,** 337–338 (2004).
98. Brand, O. J. Association of the interleukin-2 receptor alpha (*IL-2Rα*)/*CD25* gene region with Graves' disease using a multilocus test and tag SNPs. *Clin. Endocrinol.* **66,** 508–512 (2007).
99. Yamanouchi, J. *et al.* Interleukin-2 gene variation impairs regulatory T cell function and causes autoimmunity. *Nature Genet.* **39,** 329–337 (2007).
100. Zimmet, P., Alberti, K. G. & Shaw, J. Global and societal implications of the diabetes epidemic. *Nature* **414,** 782–787 (2001).
101. Stumvoll, M., Goldstein, B. J. & van Haeften, T. W. Type 2 diabetes: principles of pathogenesis and therapy. *Lancet* **365,** 1333–1346 (2005).
102. Altshuler, D. *et al.* The common PPARγ Pro12Ala polymorphism is associated with decreased risk of type 2 diabetes. *Nature Genet.* **26,** 76–80 (2000).
103. Gloyn, A. L. *et al.* Large-scale association studies of variants in genes encoding the pancreatic β-cell KATP channel subunits Kir6.2 (*KCNJ11*) and SUR1 (*ABCC8*) confirm that the KCNJ11 E23K variant is associated with type 2 diabetes. *Diabetes* **52,** 568–572 (2003).
104. Grant, S. F. *et al.* Variant of transcription factor 7-like 2 (*TCF7L2*) gene confers risk of type 2 diabetes. *Nature Genet.* **38,** 320–323 (2006).
105. Zeggini, E. & McCarthy, M. I. *TCF7L2*: the biggest story in diabetes genetics since HLA? *Diabetologia* **50,** 1–4 (2007).
106. Helgason, A. *et al.* Refining the impact of *TCF7L2* gene variants on type 2 diabetes and adaptive evolution. *Nature Genet.* **39,** 218–225 (2007).
107. Saxena, R. *et al.* Common single nucleotide polymorphisms in *TCF7L2* are reproducibly associated with type 2 diabetes and reduce the insulin response to glucose in nondiabetic individuals. *Diabetes* **55,** 2890–2895 (2006).
108. Ubeda, M., Rukstalis, J. M. & Habener, J. F. Inhibition of cyclin-dependent kinase 5 activity protects pancreatic β cells from glucotoxicity. *J. Biol. Chem.* **281,** 28858–28864 (2006).
109. Sladek, R. *et al.* A genome-wide association study identifies novel risk loci for type 2 diabetes. *Nature* **445,** 881–885 (2007).
110. Marchini, J., Donnelly, P. & Cardon, L. R. Genome-wide strategies for detecting multiple loci that influence complex diseases. *Nature Genet.* **37,** 413–417 (2005).
111. Clayton, D. G. *et al.* Population structure, differential bias and genomic control in a large-scale, case-control association study. *Nature Genet.* **37,** 1243–1246 (2005).
112. Zondervan, K. T. & Cardon, L. R. The complex interplay among factors that influence allelic association. *Nature Rev. Genet.* **5,** 89–100 (2004).
113. Hutchison, K. E., Stallings, M., McGeary, J. & Bryan, A. Population stratification in the candidate gene study: fatal threat or red herring? *Psychol. Bull.* **130,** 66–79 (2004).
114. Lohmueller, K. E., Pearce, C. L., Pike, M., Lander, E. S. & Hirschhorn, J. N. Meta-analysis of genetic association studies supports a contribution of common variants to susceptibility to common disease. *Nature Genet.* **33,** 177–182 (2003).
115. Hayes, B. & Goddard, M. E. The distribution of the effects of genes affecting quantitative traits in livestock. *Genet. Sel. Evol.* **33,** 209–229 (2001).
116. Valdar, W. *et al.* Genome-wide genetic association of complex traits in heterogeneous stock mice. *Nature Genet.* **38,** 879–887 (2006).
117. Yang, Q., Khoury, M. J., Friedman, J., Little, J. & Flanders, W. D. How many genes underlie the occurrence of common complex diseases in the population? *Int. J. Epidemiol.* **34,** 1129–1137 (2005).
118. Janssens, A. C. *et al.* Predictive testing for complex diseases using multiple genes: fact or fiction? *Genet. Med.* **8,** 395–400 (2006).

Supplementary Information is linked to the online version of the paper at www.nature.com/nature.

Acknowledgements The principal funder of this project was the Wellcome Trust. Case collections were funded by: Arthritis Research Campaign, BDA Research, British Heart Foundation, British Hypertension Society, Diabetes UK, Glaxo-Smith Kline Research and Development, Juvenile Diabetes Research Foundation, National Association for Colitis and Crohn's disease, SHERT (The Scottish Hospitals Endowment Research Trust), St Bartholomew's and The Royal London Charitable Foundation, UK Medical Research Council, UK NHS R&D and the Wellcome Trust. Statistical analyses were funded by a Commonwealth Scholarship, EU, EPSRC, Fundação para a Ciência e a Tecnologia (Portugal), National Institutes of Health, National Science Foundation and the Wellcome Trust. We acknowledge the many physicians, research fellows and research nurses who contributed to the various case collections, and the collection teams and senior management of the UK Blood Services responsible for the UK Blood Services Collection. For the 1958 Birth Cohort, venous blood collection was funded by the UK Medical Research Council and cell-line production, DNA extraction and processing by the Juvenile Diabetes Research Foundation and the Wellcome Trust. We recognize the contributions of: P. Shepherd (1958 Birth Cohort); those at Affymetrix responsible for genotype assay optimization, data production and data delivery (particularly S. Cawley, R. Mei, H. Fakhrai-Rad, H. Francis-Land, R. Pillai); L. Forty, G. Fraser, J. Heron, S. Hyde, A. Massey; F. Oyebode, E. Russell, M. Sinclair, A. Stern, N. Walker and S. Zammitt (recruitment and phenotypic assessment of BD cases); M. Yuille, B. Ollier and the UK DNA Banking Network and members of the BHF Family Heart Study Research Group (CAD case recruitment and DNA provision); S. Goldthorpe, D. Soars and J. Whittaker for CD collections; J. Pembroke, M. Bruce, S. Colville-Stewart, K. Edwards, L. Gatherer, C. Gemmell, K. Gilmour, S. Hampson, S. Hood, J. Hunt, J. Hussein, J. Jamieson, J. Kent, D. Lloyd, K. MacFarlane, S. Mellow, A. Nixon, J. Pheby, D. Picton, F. Porteus, P. Whitworth, K. Witte, A. Zawadzka, C. Mein and the Barts and The London Genome Centre (HT sample collection); H. Withers, the research nurses and the membership of the British Society for Paediatric Endocrinology and Diabetes (T1D case recruitment); and M. Sampson, S. O'Rahilly, S. Howell, M. Murphy and A. Wilson (T2D case recruitment). Essential informatics support was provided by the administration, systems, bioinformatics, data services and DNA teams of the JDRF/WT DIL; the Web System teams at the Sanger Institute (particularly R. Pettitt); D. Holland and R. Vincent. T. Dibling, C. Hind, D. Simpkin, P. Ewels and D. Moore provided genotyping assistance. Personal support was provided by: Arthritis Research Campaign (A.B., H.Do., S.E., P.G., S.H., A.H., S.J., C.P., A.S., D.S., W.T., J.Wo.); British Heart Foundation (S.G.B., N.J.S., A.Do., C.W.); Cancer Research UK (D.Ea.); Diabetes UK (R.M.F.); Cure Crohn's and Colitis Fund (F.R.C.); CORE (C.M.O.); SIM (G.B.); Leverhulme Trust (A.P.M.); Throne-Holst Foundation (C.M.L.); UK Medical Research Council (D.P.K., M.D.T., J.R.P.); Vandervell Foundation (M.N.W.); and Wellcome Trust (D.G.C., L.R.C., C.M., J.Sat., M.T., A.T.H., E.Z., C.B., S.J.B., A.C., K.D., J.Gh., R.G., S.E.H., A.K., E.K., R.McG., S.P., R.R., P.Wh., D.W., P.De.).

Author Information Affymetrix GeneChip Mapping 500K Set Arrays 250K_Nsp_SNP and 250K_Sty2_SNP are deposited in NCBI GEO under accession numbers GPL3718 and GPL3720, respectively. Reprints and permissions information is available at www.nature.com/reprints. The authors declare no competing financial interests. Correspondence and requests for materials should be addressed to P.D. (donnelly@stats.ox.ac.uk).

The Wellcome Trust Case Control Consortium

Management Committee Paul R. Burton[1], David G. Clayton[2], Lon R. Cardon[3], Nick Craddock[4], Panos Deloukas[5], Audrey Duncanson[6], Dominic P. Kwiatkowski[3,5], Mark I. McCarthy[3,7], Willem H. Ouwehand[8,9], Nilesh J. Samani[10], John A. Todd[2] & Peter Donnelly (Chair)[11]

Data and Analysis Committee Jeffrey C. Barrett[3], Paul R. Burton[1], Dan Davison[11], Peter Donnelly[11], Doug Easton[12], David Evans[3], Hin-Tak Leung[2], Jonathan L. Marchini[11], Andrew P. Morris[3], Chris C. A. Spencer[11], Martin D. Tobin[1], Lon R. Cardon (Co-chair)[3] & David G. Clayton (Co-chair)[2]

UK Blood Services and University of Cambridge Controls Antony P. Attwood[5,8], James P. Boorman[8,9], Barbara Cant[8], Ursula Everson[13], Judith M. Hussey[14], Jennifer D. Jolley[8], Alexandra S. Knight[8], Kerstin Koch[8], Elizabeth Meech[15], Sarah Nutland[2], Christopher V. Prowse[16], Helen E. Stevens[2], Niall C. Taylor[8], Graham R. Walters[17], Neil M. Walker[2], Nicholas A. Watkins[8,9], Thilo Winzer[8], John A. Todd[2] & Willem H. Ouwehand[8,9]

1958 Birth Cohort Controls Richard W. Jones[18], Wendy L. McArdle[18], Susan M. Ring[18], David P. Strachan[19] & Marcus Pembrey[18,20]

Bipolar Disorder Gerome Breen[21], David St Clair[21] (Aberdeen); Sian Caesar[22], Katherine Gordon-Smith[22,23], Lisa Jones[22] (Birmingham); Christine Fraser[23], Elaine K. Green[23], Detelina Grozeva[23], Marian L. Hamshere[23], Peter A. Holmans[23], Ian R. Jones[23], George Kirov[23], Valentina Moskvina[23], Ivan Nikolov[23], Michael C. O'Donovan[23], Michael J. Owen[23], Nick Craddock[23] (Cardiff); David A. Collier[24], Amanda Elkin[24], Anne Farmer[24], Richard Williamson[24], Peter McGuffin[24] (London); Allan H. Young[25] & I. Nicol Ferrier[25] (Newcastle)

Coronary Artery Disease Stephen G. Ball[26], Anthony J. Balmforth[26], Jennifer H. Barrett[26], D. Timothy Bishop[26], Mark M. Iles[26], Azhar Maqbool[26], Nadira Yuldasheva[26], Alistair S. Hall[26] (Leeds); Peter S. Braund[10], Paul R. Burton[1], Richard J. Dixon[10], Massimo Mangino[10], Suzanne Stevens[10], Martin D. Tobin[1], John R. Thompson[1] & Nilesh J. Samani[10] (Leicester)

Crohn's Disease Francesca Bredin[27], Mark Tremelling[27], Miles Parkes[27] (Cambridge); Hazel Drummond[28], Charles W. Lees[28], Elaine R. Nimmo[28], Jack Satsangi[28] (Edinburgh); Sheila A. Fisher[29], Alastair Forbes[30], Cathryn M. Lewis[29], Clive M. Onnie[29], Natalie J. Prescott[29], Jeremy Sanderson[31], Christopher G. Mathew[29] (London); Jamie Barbour[32], M. Khalid Mohiuddin[32], Catherine E. Todhunter[32], John C. Mansfield[32] (Newcastle); Tariq Ahmad[33], Fraser R. Cummings[33] & Derek P. Jewell[33] (Oxford)

Hypertension John Webster[34] (Aberdeen); Morris J. Brown[35], David G. Clayton[2] (Cambridge); G. Mark Lathrop[36] (Evry); John Connell[37], Anna Dominiczak[37] (Glasgow); Nilesh J. Samani[10] (Leicester); Carolina A. Braga Marcano[38], Beverley Burke[38], Richard Dobson[38], Johannie Gungadoo[38], Kate L. Lee[38], Patricia B. Munroe[38], Stephen J. Newhouse[38], Abiodun Onipinla[38], Chris Wallace[38], Mingzhan Xue[38], Mark Caulfield[38] (London); Martin Farrall[39] (Oxford)

Rheumatoid Arthritis Anne Barton[40], The Biologics in RA Genetics and Genomics Study Syndicate (BRAGGS) Steering Committee*, Ian N. Bruce[40], Hannah Donovan[40], Steve Eyre[40], Paul D. Gilbert[40], Samantha L. Hider[40], Anne M. Hinks[40], Sally L. John[40],

Catherine Potter[40], Alan J. Silman[40], Deborah P. M. Symmons[40], Wendy Thomson[40] & Jane Worthington[40]

Type 1 Diabetes David G. Clayton[2], David B. Dunger[2,41], Sarah Nutland[2], Helen E. Stevens[2], Neil M. Walker[2], Barry Widmer[2,41] & John A. Todd[2]

Type 2 Diabetes Timothy M. Frayling[42,43], Rachel M. Freathy[42,43], Hana Lango[42,43], John R. B. Perry[42,43], Beverley M. Shields[43], Michael N. Weedon[42,43], Andrew T. Hattersley[42,43] (Exeter); Graham A. Hitman[44] (London); Mark Walker[45] (Newcastle); Kate S. Elliott[3,7], Christopher J. Groves[7], Cecilia M. Lindgren[3,7], Nigel W. Rayner[3,7], Nicholas J. Timpson[3,46], Eleftheria Zeggini[3,7] & Mark I. McCarthy[3,7] (Oxford)

Tuberculosis Melanie Newport[47], Giorgio Sirugo[47] (Gambia); Emily Lyons[3], Fredrik Vannberg[3] & Adrian V. S. Hill[3] (Oxford)

Ankylosing Spondylitis Linda A. Bradbury[48], Claire Farrar[49], Jennifer J. Pointon[48], Paul Wordsworth[49] & Matthew A. Brown[48,49]

Autoimmune Thyroid Disease Jayne A. Franklyn[50], Joanne M. Heward[50], Matthew J. Simmonds[50] & Stephen C. L. Gough[50]

Breast Cancer Sheila Seal[51], Breast Cancer Susceptibility Collaboration (UK)*, Michael R. Stratton[51,52] & Nazneen Rahman[51]

Multiple Sclerosis Maria Ban[53], An Goris[53], Stephen J. Sawcer[53] & Alastair Compston[53]

Gambian Controls David Conway[47], Muminatou Jallow[47], Melanie Newport[47], Giorgio Sirugo[47] (Gambia); Kirk A. Rockett[3] & Dominic P. Kwiatkowski[3,5] (Oxford)

DNA, Genotyping, Data QC and Informatics Suzannah J. Bumpstead[5], Amy Chaney[5], Kate Downes[2,5], Mohammed J. R. Ghori[5], Rhian Gwilliam[5], Sarah E. Hunt[5], Michael Inouye[5], Andrew Keniry[5], Emma King[5], Ralph McGinnis[5], Simon Potter[5], Rathi Ravindrarajah[5], Pamela Whittaker[5], Claire Widden[5], David Withers[5], Panos Deloukas[5] (Wellcome Trust Sanger Institute, Hinxton); Hin-Tak Leung[2], Sarah Nutland[2], Helen E. Stevens[2], Neil M. Walker[2] & John A. Todd[2] (Cambridge)

Statistics Doug Easton[12], David G. Clayton[2] (Cambridge); Paul R. Burton[1], Martin D. Tobin[1] (Leicester); Jeffrey C. Barrett[3], David Evans[3], Andrew P. Morris[3], Lon R. Cardon[3] (Oxford) Niall J. Cardin[11], Dan Davison[11], Teresa Ferreira[11], Joanne Pereira-Gale[11], Ingileif B. Hallgrimsdóttir[11], Bryan N. Howie[11], Jonathan L. Marchini[11], Chris C. A. Spencer[11], Zhan Su[11], Yik Ying Teo[3,11], Damjan Vukcevic[11] & Peter Donnelly[11] (Oxford)

Primary Investigators David Bentley[5]†, Matthew A. Brown[48,49], Lon R. Cardon[3], Mark Caulfield[38], David G. Clayton[2], Alistair Compston[53], Nick Craddock[23], Panos Deloukas[5], Peter Donnelly[11], Martin Farrall[39], Stephen C. L. Gough[50], Alistair S. Hall[26], Andrew T. Hattersley[42,43], Adrian V. S. Hill[3], Dominic P. Kwiatkowski[3,5], Christopher G. Mathew[29], Mark I. McCarthy[3,7], Willem H. Ouwehand[8,9], Miles Parkes[27], Marcus Pembrey[18,20], Nazneen Rahman[51], Nilesh J. Samani[10], Michael R. Stratton[51,52], John A. Todd[2] & Jane Worthington[40]

*See Supplementary Information for details.

Affiliations for participants: [1]Genetic Epidemiology Group, Department of Health Sciences, University of Leicester, Adrian Building, University Road, Leicester LE1 7RH, UK. [2]Juvenile Diabetes Research Foundation/Wellcome Trust Diabetes and Inflammation Laboratory, Department of Medical Genetics, Cambridge Institute for Medical Research, University of Cambridge, Wellcome Trust/MRC Building, Cambridge CB2 0XY, UK. [3]Wellcome Trust Centre for Human Genetics, University of Oxford, Roosevelt Drive, Oxford OX3 7BN, UK. [4]Department of Psychological Medicine, Henry Wellcome Building, School of Medicine, Cardiff University, Heath Park, Cardiff CF14 4XN, UK. [5]The Wellcome Trust Sanger Institute, Wellcome Trust Genome Campus, Hinxton, Cambridge CB10 1SA, UK. [6]The Wellcome Trust, Gibbs Building, 215 Euston Road, London NW1 2BE, UK. [7]Oxford Centre for Diabetes, Endocrinology and Medicine, University of Oxford, Churchill Hospital, Oxford OX3 7LJ, UK. [8]Department of Haematology, University of Cambridge, Long Road, Cambridge CB2 2PT, UK. [9]National Health Service Blood and Transplant, Cambridge Centre, Long Road, Cambridge CB2 2PT, UK. [10]Department of Cardiovascular Sciences, University of Leicester, Glenfield Hospital, Groby Road, Leicester LE3 9QP, UK. [11]Department of Statistics, University of Oxford, 1 South Parks Road, Oxford OX1 3TG, UK. [12]Cancer Research UK Genetic Epidemiology Unit, Strangeways Research Laboratory, Worts Causeway, Cambridge CB1 8RN, UK. [13]National Health Service Blood and Transplant, Sheffield Centre, Longley Lane, Sheffield S5 7JN, UK. [14]National Health Service Blood and Transplant, Brentwood Centre, Crescent Drive, Brentwood CM15 8DP, UK. [15]The Welsh Blood Service, Ely Valley Road, Talbot Green, Pontyclun CF72 9WB, UK. [16]The Scottish National Blood Transfusion Service, Ellen's Glen Road, Edinburgh EH17 7QT, UK. [17]National Health Service Blood and Transplant, Southampton Centre, Coxford Road, Southampton SO16 5AF, UK. [18]Avon Longitudinal Study of Parents and Children, University of Bristol, 24 Tyndall Avenue, Bristol BS8 1TQ, UK. [19]Division of Community Health Services, St George's University of London, Cranmer Terrace, London SW17 0RE, UK. [20]Institute of Child Health, University College London, 30 Guilford Street, London WC1N 1EH, UK. [21]University of Aberdeen, Institute of Medical Sciences, Foresterhill, Aberdeen AB25 2ZD, UK. [22]Department of Psychiatry, Division of Neuroscience, Birmingham University, Birmingham B15 2QZ, UK. [23]Department of Psychological Medicine, Henry Wellcome Building, School of Medicine, Cardiff University, Heath Park, Cardiff CF14 4XN, UK. [24]SGDP, The Institute of Psychiatry, King's College London, De Crespigny Park, Denmark Hill, London SE5 8AF, UK. [25]School of Neurology, Neurobiology and Psychiatry, Royal Victoria Infirmary, Queen Victoria Road, Newcastle upon Tyne, NE1 4LP, UK. [26]LIGHT and LIMM Research Institutes, Faculty of Medicine and Health, University of Leeds, Leeds LS1 3EX, UK. [27]IBD Research Group, Addenbrooke's Hospital, University of Cambridge, Cambridge CB2 2QQ, UK. [28]Gastrointestinal Unit, School of Molecular and Clinical Medicine, University of Edinburgh, Western General Hospital, Edinburgh EH4 2XU, UK. [29]Department of Medical & Molecular Genetics, King's College London School of Medicine, 8th Floor Guy's Tower, Guy's Hospital, London SE1 9RT, UK. [30]Institute for Digestive Diseases, University College London Hospitals Trust, London, NW1 2BU, UK. [31]Department of Gastroenterology, Guy's and St Thomas' NHS Foundation Trust, London SE1 7EH, UK. [32]Department of Gastroenterology & Hepatology, University of Newcastle upon Tyne, Royal Victoria Infirmary, Newcastle upon Tyne NE1 4LP, UK. [33]Gastroenterology Unit, Radcliffe Infirmary, University of Oxford, Oxford OX2 6HE, UK. [34]Medicine and Therapeutics, Aberdeen Royal Infirmary, Foresterhill, Aberdeen, Grampian AB9 2ZB, UK. [35]Clinical Pharmacology Unit and the Diabetes and Inflammation Laboratory, University of Cambridge, Addenbrookes Hospital, Hills Road, Cambridge CB2 2QQ, UK. [36]Centre National de Genotypage, 2, Rue Gaston Cremieux, Evry, Paris 91057, France. [37]BHF Glasgow Cardiovascular Research Centre, University of Glasgow, 126 University Place, Glasgow G12 8TA, UK. [38]Clinical Pharmacology and Barts and The London Genome Centre, William Harvey Research Institute, Barts and The London, Queen Mary's School of Medicine, Charterhouse Square, London EC1M 6BQ, UK. [39]Cardiovascular Medicine, University of Oxford, Wellcome Trust Centre for Human Genetics, Roosevelt Drive, Oxford OX3 7BN, UK. [40]arc Epidemiology Research Unit, University of Manchester, Stopford Building, Oxford Rd, Manchester M13 9PT, UK. [41]Department of Paediatrics, University of Cambridge, Addenbrooke's Hospital, Cambridge CB2 2QQ, UK. [42]Genetics of Complex Traits, Institute of Biomedical and Clinical Science, Peninsula Medical School, Magdalen Road, Exeter EX1 2LU, UK. [43]Diabetes Genetics, Institute of Biomedical and Clinical Science, Peninsula Medical School, Barrack Road, Exeter EX2 5DU, UK. [44]Centre for Diabetes and Metabolic Medicine, Barts and The London, Royal London Hospital, Whitechapel, London E1 1BB, UK. [45]Diabetes Research Group, School of Clinical Medical Sciences, Newcastle University, Framlington Place, Newcastle upon Tyne NE2 4HH, UK. [46]The MRC Centre for Causal Analyses in Translational Epidemiology, Bristol University, Canynge Hall, Whiteladies Rd, Bristol BS2 8PR, UK. [47]MRC Laboratories, Fajara, The Gambia. [48]Diamantina Institute for Cancer, Immunology and Metabolic Medicine, Princess Alexandra Hospital, University of Queensland, Woolloongabba, Qld 4102, Australia. [49]Botnar Research Centre, University of Oxford, Headington, Oxford OX3 7BN, UK. [50]Department of Medicine, Division of Medical Sciences, Institute of Biomedical Research, University of Birmingham, Edgbaston, Birmingham B15 2TT, UK. [51]Section of Cancer Genetics, Institute of Cancer Research, 15 Cotswold Road, Sutton SM2 5NG, UK. [52]Cancer Genome Project, The Wellcome Trust Sanger Institute, Wellcome Trust Genome Campus, Hinxton, Cambridge CB10 1SA, UK. [53]Department of Clinical Neurosciences, University of Cambridge, Addenbrooke's Hospital, Hills Road, Cambridge CB2 2QQ, UK. †Present address: Illumina Cambridge, Chesterford Research Park, Little Chesterford, Nr Saffron Walden, Essex CB10 1XL, UK.

METHODS

BD phenotype description. BD cases were all over the age of 16 yr, living in mainland UK and of European descent. Recruitment was undertaken throughout the UK by teams based in Aberdeen (8% of cases), Birmingham (35% cases), Cardiff (33% cases), London (15% cases) and Newcastle (9% cases). Individuals who had been in contact with mental health services were recruited if they suffered with a major mood disorder in which clinically significant episodes of elevated mood had occurred. This was defined as a lifetime diagnosis of a bipolar mood disorder according to Research Diagnostic Criteria[119] and included the bipolar subtypes that have been shown in family studies to co-aggregate for example[29]: bipolar I disorder (71% cases), schizoaffective disorder bipolar type (15% cases), bipolar II disorder (9% cases) and manic disorder (5% cases). After providing written informed consent, all subjects were interviewed by a trained psychologist or psychiatrist using a semi-structured lifetime diagnostic psychiatric interview (in most cases the Schedules for Clinical Assessment in Neuropsychiatry[120] and available psychiatric medical records were reviewed). Using all available data, best-estimate ratings were made for a set of key phenotypic measures on the basis of the OPCRIT checklist (which covers both psychopathology and course of illness)[121,122] and lifetime psychiatric diagnoses were assigned according to the Research Diagnostic Criteria[119]. The reliability of these methods has been shown to be high[119,123,124]. Further details of clinical methodology can be found in Green, 2005 (ref. 123) and Green, 2006 (ref. 124).

CAD phenotype description. CAD cases had a validated history of either myocardial infarction or coronary revascularization (coronary artery bypass surgery or percutaneous coronary angioplasty) before their 66th birthday. Verification of the history of CAD was required either from hospital records or the primary care physician. Recruitment was carried out on a national basis in the UK through a direct approach to the public via (1) the media and (2) mailing all general practices (family physicians) with information about the study, as previously described[125]. In an initial pilot phase, potential participants were also identified and approached through local CAD databases in the two lead centres (Leeds and Leicester). Although the majority of subjects had at least one further sib also affected with premature CAD, only one subject from each family was included in the present study.

CD phenotype description. CD cases were attendees at inflammatory bowel disease clinics in and around the five centres which contributed samples to the WTCCC (Cambridge, Oxford, London, Newcastle, Edinburgh). Ascertainment was based on a confirmed diagnosis of Crohn's disease (CD) using conventional endoscopic, radiological and histopathological criteria[126]. We included all subtypes of CD as classified by disease extent and behaviour and the collection was not specifically enriched for family history or early age of onset. The median age of diagnosis was 26.1 yr and 62% of the collection had undergone CD-related abdominal surgery. A small proportion had previously been recruited as members of multiply affected families but only one affected individual was included per family.

HT phenotype description. HT cases comprised severely hypertensive probands ascertained from families with multiplex affected sibships or as parent–offspring trios. They were of white British ancestry (up to level of grand-parents) and were recruited from the Medical Research Council General Practice Framework and other primary care practices in the UK[77]. Each case had a history of hypertension diagnosed before 60 yr of age, with confirmed blood pressure recordings corresponding to seated levels $>150/100$ mm Hg (if based on one reading), or the mean of 3 readings greater than 145/95 mm Hg. These criteria correspond to the threshold for the uppermost 5% of blood pressure distribution in a contemporaneous health screening survey of 5,000 British men and women in 1995 (N. Wald and M. Law, personal communication). We excluded hypertensive individuals who self-reportedly consumed >21 units of alcohol per week and those with diabetes, intrinsic renal disease, a history of secondary hypertension or co-existing illness. Cases did not undergo systematic genetic screening to exclude the (rare) known monogenic causes of HT. We focused on the recruitment of hypertensive individuals with body mass indices $<30\,kg\,m^{-2}$. The probands were extensively phenotyped by trained nurses (see http://www.brightstudy.ac.uk for standard operating procedures, additional phenotypes and study questionnaires). Sample selection for WTCCC was based on DNA availability and quality.

RA phenotype description. RA cases were recruited to studies coordinated by the ARC (Arthritis Research Campaign) Epidemiology Unit. All subjects were Caucasian over the age of 18 yr and satisfied the 1987 American College of Rheumatology Criteria for RA[127] modified for genetic studies[128]. Of the cases, 404 were recruited as part of the arc National Repository of Family Material[129]: of these, 301 were probands from affected sibling pair families and 103 were cases from trio families, having both parents or one parent and one unaffected sibling available for study. A further 109 cases were recruited from the Norfolk Arthritis Register, a primary care-based inception collection[130]. All other cases ($n = 1348$) were recruited from NHS Rheumatology Clinics throughout the UK. Samples for WTCCC were selected from the various studies on the basis of the quality and availability of DNA.

T1D phenotype description. T1D cases were recruited from paediatric and adult diabetes clinics at 150 National Health Service hospitals across mainland UK. The total T1D case data set ($n=\sim$8,000) from which the WTCCC cases were selected, represents close to half the T1D cases seen in such clinics. Nationwide coverage was achieved through the voluntary efforts of members of the British Society for Paediatric Endocrinology and Diabetes, who recruited about half of cases, the rest coming from peripatetic nurses employed by the JDRF/WT GRID project (http://www-gene.cimr.cam.ac.uk/todd/)[131]. To establish a positive diagnosis of T1D (and, in particular, to distinguish it from the more common, but later onset T2D), we required all cases to have an age of diagnosis below 17 yr and insulin dependence since diagnosis (with a minimum period of at least 6 months). However, a very few subjects were subsequently discovered to be suffering from rare monogenic disorders, such as maturity onset diabetes of the young (MODY), and latterly permanent neonatal diabetes (PNDM): these were excluded.

T2D phenotype description. The T2D cases were selected from UK Caucasian subjects who form part of the Diabetes UK Warren 2 repository. In each case, the diagnosis of diabetes was based on either current prescribed treatment with sulphonylureas, biguanides, other oral agents and/or insulin or, in the case of individuals treated with diet alone, historical or contemporary laboratory evidence of hyperglycaemia (as defined by the World Health Organization). Other forms of diabetes (for example, maturity-onset diabetes of the young, mitochondrial diabetes, and type 1 diabetes) were excluded by standard clinical criteria based on personal and family history. Criteria for excluding autoimmune diabetes included absence of first-degree relatives with T1D, an interval of $\geq$1 yr between diagnosis and institution of regular insulin therapy and negative testing for antibodies to glutamic acid decarboxylase (anti-GAD). Cases were limited to those who reported that all four grandparents had exclusively British and/or Irish origin, by both self-reported ethnicity and place of birth. All were diagnosed between age 25 and 75. Approximately 30% were explicitly recruited as part of multiplex sibships[132] and $\sim$25% were offspring in parent–offspring 'trios' or 'duos' (that is, families comprising only one parent complemented by additional sibs)[133]. The remainder were recruited as isolated cases but these cases were (compared to population-based cases) of relatively early onset and had a high proportion of T2D parents and/or siblings[134]. Cases were ascertained across the UK but were centred around the main collection centres (Exeter, London, Newcastle, Norwich, Oxford). Selection of the samples typed in WTCCC from the larger collections was based primarily on DNA availability and success in passing Diabetes and Inflammation Laboratory (DIL)/Wellcome Trust Sanger Institute (WTSI) DNA quality control.

1958 Birth Cohort Controls (58BC). The 1958 Birth Cohort (also known as the National Child Development Study) includes all births in England, Wales and Scotland, during one week in 1958. From an original sample of over 17,000 births, survivors were followed up at ages 7, 11, 16, 23, 33 and 42 yr (http://www.cls.ioe.ac.uk/studies.asp?section=000100020003)[135]. In a biomedical examination at 44-45 yr[136] (http://www.b58cgene.sgul.ac.uk/followup.php), 9,377 cohort members were visited at home providing 7,692 blood samples with consent for future Epstein–Barr virus (EBV)-transformed cell lines. DNA samples extracted from 1,500 cell lines of self-reported white ethnicity and representative of gender and each geographical region were selected for use as controls.

UK Blood Services Controls (UKBS). The second set of common controls was made up of 1,500 individuals selected from a sample of blood donors recruited as part of the current project. WTCCC in collaboration with the UK Blood Services (NHSBT in England, SNBTS in Scotland and WBS in Wales) set up a UK national repository of anonymized samples of DNA and viable mononuclear cells from 3,622 consenting blood donors, age range 18–69 yr (ethical approval 05/Q0106/74). A set of 1,564 samples was selected from the 3622 samples recruited based on sex and geographical region (to reproduce the distribution of the samples of the 1958 Birth Cohort) for use as common controls in the WTCCC study. DNA was extracted as described below with a yield of $3054 \pm 1207\,\mu g$ (mean $\pm$ 1 s.d.).

Protocol for DNA extraction. White blood cells were isolated from the filters by first pushing 10 ml air through the filter in contra direction to the initial blood flow through the filter, followed by 40 ml PBS, collecting into a 50 ml centrifuge tube, and centrifugation (2.000 r.p.m., 10 min, 20 °C).Cells were lysed by adding 40 ml Lysis buffer (320 mM Sucrose, 1% Triton-X-100, 4.9 mM $MgCl_2$, 1 mM TRIS-HCl pH 7.4) and pelleted by centrifugation (2,500 r.p.m., 15 min, 4 °C). Pellets were frozen before extraction. Pellets were digested overnight at 37 °C with 5.25 M GuHCl, 490 mM NH_4Ac, 1.25% Na Sarcosyl and $0.125\,mg\,ml^{-1}$ Proteinase K and then mixed with 2 ml chloroform to form a white emulsion. The aqueous layer was separated by centrifugation (2,500 r.p.m., 3 min) and

DNA was precipitated in ethanol overnight at −20 °C. DNA was further precipitated by rotation (40 r.p.m., 5 min) and then pelleted by centrifugation (3,000 r.p.m., 15 min). Pellets were washed twice by rinsing with 2 ml 70% ethanol, followed by centrifugation (3,000 r.p.m., 5 min). DNA pellets were air-dried before re-suspension in TE buffer (10 mM Tris, 0.1 mM EDTA).

Sample handling. Each participating sample collection was issued unique WTCCC barcode labels and a spreadsheet with unique sample identifiers for logging information on case/control status, DNA concentration (requested at 100 ng μl^{-1}), DNA extraction method, sex, broad geographical region and age at requirement. Each collection supplied 10 μg aliquots of anonymized samples in bar-coded, deep 96-well plates. On receipt, samples had their DNA concentration measured by Picogreen (triplicate measurements), were checked for DNA degradation on a 0.75% agarose gel, and genotyped with up to 38 SNPs arranged in two multiplex reactions using the MassExtend (hME) and/or iPLEX[37] assay. The above SNPs served for obtaining a molecular fingerprint (25 of the 38 SNPs were present on the GeneChip 500K) and experimentally confirming the sex of each sample.

Samples with concentrations ≥50 ng μl^{-1}, showing limited or no degradation, having a minimum of 7/10 (hME reaction) and/or 14/23 (iPLEX reaction) SNPs typed, and having the sex markers in agreement or not violating the supplied information were deemed fit for whole genome genotyping. Note that the hME set was replaced with a second iPLEX reaction in the course of the project to increase marker density. We selected 2,000 and 1,500 samples from each disease and control collection respectively. Selected samples were normalized to 50 ng μl^{-1} and re-arrayed robotically into 96-well plates so that each plate was composed of 94 samples representing at least two different collections at a ratio of 1:1. For each collection, the selected samples were balanced first for sex and then geographical region (see above).

Genotyping. SNP genotyping was performed with the commercial release of the GeneChip 500K arrays at Affymetrix Services Lab. A modified version of the genotyping assay developed for the 100K Mapping Array[137] was used. In brief, two aliquots of 250 ng of DNA each are digested with *Nsp*I and *Sty*I, respectively, an adaptor is ligated and molecules are then fragmented and labelled. At this stage each enzyme preparation is hybridized to the corresponding SNP array (262,000 and 238,000 on the *Nsp*I and *Sty*I array respectively). Samples were processed in 96-well plate format, each plate carried a positive and a negative control, up to the hybridization step. Individual arrays not passing the 93% call rate threshold at $P = 0.33$ with the Dynamic Model algorithm[138] were repeated (fresh aliquot of initial end-labelled reaction). Samples failing twice at the hybridization stage were reprocessed using a fresh DNA aliquot. Affymetrix delivered successful samples as those having a Dynamic Model call rate of 93% at $P = 0.33$ for each array, over 90% concordance for the 50 SNPs that are common to the two arrays, both arrays agreed on gender, and showed over 70% identity to the Sequenom genotypes supplied by WTCCC.

CEL files provided the intensities of the various probes on each chip. Initially, genotypes were called with the Dynamic Model[138] algorithm. Affymetrix subsequently developed an improved algorithm, BRLMM (Bayesian Robust Linear Model with Mahalanobis distance classifier[139,140]). This processes batches of samples and uses clustering techniques to call genotypes (the 'mismatch' probe intensities are not used). In Affymetrix's standard protocol it is applied in batches of 96 samples (plates). This is, of course, a very small sample size and, for some SNPs, some clusters will contain few, if any, observations. This might be countered by combining information about cluster location over a large number of SNPs.

Throughout, physical coordinates refer to NCBI build-35 of the human genome. Alleles are expressed in the forward (+) strand of the reference human genome (NCBI build-35).

Power calculations. We assessed power of the Affymetrix 500K chip using the following simulation experiment. Separately for each SNP with MAF >5% in the 10 HapMap ENCODE regions, we assumed the SNP was causative and simulated genotype data at all SNPs in the same region as the putative disease SNP in case-control panels of 2,000 cases and 3,000 controls with linkage disequilibrium patterns that match those in HapMap. For controls, these simulations were based on the imputation algorithm described below (with all genotype data initially set to missing in the 3,000 control individuals). For cases, the assumed effect size was first used to calculate genotype frequencies in cases (via Bayes' theorem), and genotypes in cases at the putative SNP were then simulated independently from theses calculated frequencies. Genotypes at all other SNPs in the region in cases were then simulated using the imputation algorithm described below (with all data other than the genotypes at the causative SNP initially set to missing in the cases). For each such simulated case-control panel, trend tests were performed at each of the SNPs in the region that are actually on the Affymetrix chip, and if any of these reached the stated *P*-value threshold the putative disease SNP was deemed to be detected, and otherwise to be undetected. Power estimates are then calculated as the proportion of putative disease SNPs with MAFs >5% across the HapMap ENCODE regions that are detected at the given *P*-value threshold. There are various approximations here. Actual numbers of cases and controls for each disease are slightly smaller than the 3,000:2,000 values used in the simulations, but in the other direction, our simulations ignore the possibility that a disease SNP might be detected by a genotyped SNP outside its ENCODE region. The accuracy reported below of the imputation algorithm in imputing genotypes leads us to believe these simulations should be a reasonable proxy for real data. Some such simulation is needed if power calculations are to take account of the fact that any given putative disease SNP could typically be detected by several SNPs on the chip. Exploitation of this simulation approach to assess power across different platforms and SNP chips and for different experimental designs will be reported elsewhere.

CHIAMO. We developed a new genotype calling algorithm, CHIAMO, which is applied after quantile normalization of the data from each sample. A complete description is given in Supplementary Information. We briefly summarize some features here. Normalized intensities for each genotype were mapped to a two-dimensional intensity vector and then we applied CHIAMO, which uses a bayesian hierarchical 4-class mixture model to call genotypes for the whole project. We used optimization based on 12 random starts to find the set of parameters ($\hat{\theta}$) that maximize the posterior distribution of the model. This parameter set was used to calculate the maximum a posteriori estimates of the probabilities of each genotype call, $\Pr\left(Z_{ij} \middle| Data, \hat{\theta}\right)$, where $Z_{ij} \in \{0, 1, 2, 3\} \equiv \{AA, AB, BB, null\}$ is the genotype call for individual *j* in collection *i*. All CHIAMO genotype calls analysed in this paper were based on an a posteriori probability threshold of 0.9 for making a call, following our analysis of the relationship between concordance and missing data rates (data not shown). CHIAMO differs from BRLMM in several respects: (1) it uses a different transformation of the CEL files to give the two-dimensional summary for each individual at an SNP leading to better defined clusters; (2) it makes use of mis-match probe signals; (3) it uses a different method for fitting the clusters; and (4) it allows the data for all samples to be called simultaneously, thus allowing better estimation of cluster location and shape parameters, while making allowance for possible differences in these parameter values between case/control groups that could arise as a result of differences in DNA quality. This is achieved using a hierarchical statistical model that specifies the joint distribution of the three cluster centres, their spread, and likely allele frequencies (using HapMap) and genotype frequencies (centred on Hardy–Weinberg proportions but allowing some variation).

CHIAMO improved both call rate and accuracy in comparison to BRLMM, the current standard Affymetrix calling algorithm (Supplementary Table 3)—it roughly halved missing data rates and discordance rates with another platform. See Supplementary Information for full details, discussion of some challenges for genotype calling, and example cluster plots (Supplementary Figs 10 and 17).

Quantile-quantile plots. Quantile-quantile (Q-Q) plots are constructed by ranking a set of values of a statistic from smallest to largest (the 'order statistics') and plotting them against their expected values, given the assumption that the values have been sampled from a distribution of known theoretical form (in our case, the chi-squared distribution, usually on one degree of freedom—for example, the distribution of our trend tests under the null hypothesis). Deviations from the line of equality indicate either that the theoretical distribution is incorrect, or that the sample is contaminated with values generated in some other manner (for example, by a true association). To aid interpretation of such plots we have also calculated 95% 'concentration bands' (shaded grey in all Q-Q plots). These are formed by calculating, for each order statistic, the 2.5th and 97.5th centiles of the distribution of the order statistic under random sampling and the null hypothesis (for details see ref. 141). We should add two notes of caution. First, concentration bands are calculated point by point and, although there are very strong correlations between nearby order statistics, the probability that a real quantile-quantile plot will stray outside the concentration band at some point is some bit larger than 5%. Second, the theoretical chi-squared distribution is an approximation, valid for large samples; it is not clear whether this approximation continues to hold into the extreme right hand tail of the distribution explored in a GWA study (although the indications are that it is probably not far wrong for a study as large as ours).

Data quality control. Of samples for which Affymetrix returned CEL files, a total of 809 were excluded from the analysis. A complete breakdown by collection is given in Supplementary Table 4. Missing data rate per sample acts as an indicator of low DNA quality. Most samples had very low rates of missing data (study-wide average 0.00925, standard deviation 0.0187) and we chose to exclude 250 samples with >3% missing data across all SNPs (Supplementary Fig. 18, and Supplementary Tables 4 and 13). We also set empirical thresholds on genome-wide heterozygosity (excess heterozygosity in particular may indicate contamination). Six samples with >30% heterozygosity and a further three with <23% heterozygosity were excluded (see Supplementary Fig. 18). We excluded 16 samples

with discrepancies between WTCCC information and external identifying information (such as genotypes from another experiment, blood type or incorrect disease status). We sought to detect individuals with non-Caucasian ancestry using multi-dimensional scaling to provide a two-dimensional projection of the data whose axes represent geographic genetic variation. In the interest of computational efficiency and to avoid confounding of the multi-dimensional scaling by extended linkage disequilibrium we thinned the data to a set of 71,458 SNPs, within which no pair were correlated with $r^2 > 0.2$. For this set of nearly independent SNPs we computed genome-wide average identity by state (sum of the number of identical-by-state alleles at each locus divided by twice the number of loci) between each pair of individuals in each sample collection along with the 270 HapMap samples. We converted these identity by-state-relationships to distances by subtracting them from 1, and the matrix of pairwise identity by state values was used as input to multi-dimensional scaling. The projection onto the two multi-dimensional scaling axes is shown in Supplementary Fig. 5. We excluded 153 samples that were clearly separate from the main cluster of WTCCC individuals. Exclusion of these individuals resulted in a substantial reduction in estimates of over-dispersion in test statistic distributions (data not shown). We also excluded 295 duplicated (>99% identity) and 86 related (86–98% identity) samples from the analysis.

Filtering out suboptimal markers depends on both the platform and the genotype calling algorithm. We experimented with various quality metrics for CHIAMO calls, for example, based on the location and/or separation of the clusters, but found that the best indicator of a SNP being difficult to call was the amount of missing data in its calls: CHIAMO consistently marked many individuals missing for SNPs with poorly defined or overlapping clusters, whereas it successfully called genotypes for nearly all individuals on high-quality SNPs (data not shown). We excluded 26,567 SNPs with a study-wide missing data rate >5% (Supplementary Fig. 19), or >1% for SNPs with a study-wide MAF < 5%. We additionally excluded 4,351 SNPs with Hardy–Weinberg exact P value $< 5.7 \times 10^{-7}$ in the combined set of 2,938 controls, and 93 SNPs with P value $< 5.7 \times 10^{-7}$ for either a one- or two-degree of freedom test of association between the two control groups (corresponding to a 1 d.f. chi-squared statistic of about 25). See Supplementary Fig. 20 and Fig. 1 respectively for the empirical distributions of these statistics used to motivate the thresholds above.

Overall, we found that the 809 excluded individuals (which represent 4.8% of the study samples) accounted for 35.6% of the missing data at non-excluded SNPs. In total, 469,557 SNPs passed the quality control filters.

Supplementary Fig. 20 shows the effect of quality control filters, and visual inspection of the cluster plots of SNPs showing apparently strong association, on quantile-quantile plots for one disease (T2D, others are similar), and the success of these filters in excluding poorly performing SNPs. The figure (panel d) also shows the marked effect on the tails of the distribution of test statistics of regions of genuine association (for this disease the three regions removed because of strong evidence of association have all been independently replicated, see main text). The aim in filtering is to exclude poor SNPs but without removing genuine associations. No single criterion will do this. In order not to exclude possible genuine associations, we chose to apply relatively light quality control filters but then to subject all apparently associated SNPs to visual inspection of cluster plots (see Supplementary Information). Around 100 cluster plots were assessed per disease.

We used X-chromosome SNPs to check for sex discrepancies with the sample files (Supplementary Fig. 21). These were fed back to disease groups for amendment and verification. The ~80 samples where it was not possible to discern the source of the discrepancy were left in the study for analysis, on the grounds that mishandling was considered unlikely to have introduced samples with altogether different phenotypes.

DNA quality between cases and controls could result in false-positive associations through differential effects on genotype calling[111]. DNAs in our study came from various sources between, and in some cases within, case and control series, but with the combination of centralized sample quality control, simultaneous genotype calling with CHIAMO (which explicitly allows for differences between collections), and inspection of cluster plots for SNPs with very small P values, our study did not experience such difficulties.

Comparing linkage disequilibrium. Two questions which have been raised about the HapMap data are how well it describes linkage disequilibrium in populations other than the ones that were sampled, and whether the sample sizes in HapMap (60 Caucasian individuals, for example) are adequate to describe patterns of linkage disequilibrium. With data on 2,938 controls and 16,179 individuals in total at around 400,000 polymorphic SNPs, we are well placed to address this for the British population. Initial analyses suggest that patterns of linkage disequilibrium in our samples are very similar to those in HapMap. As an example, Supplementary Fig. 3 compares patterns of linkage disequilibrium in HapMap CEU individuals and our 58C sample at SNPs on the Affymetrix chip across 22× 1 Mb regions of the genome and they seem almost identical. We calculated r^2 values directly from the phased haplotypes available in HapMap, but using unphased genotype data from our study. Note that visual representations of linkage disequilibrium in this form can be very sensitive to SNP density so comparisons across regions is difficult without correction for SNP density, and direct comparison of linkage disequilibrium patterns at all HapMap SNPs with those at the subset of SNPs on the Affymetrix 500K chip is not straightforward.

Geographical variation and population structure. Principal component analysis was performed as a two-stage process: we formed a matrix of estimated correlations (formally, the inner product measure of similarity) between all pairs of individuals, and then computed the eigenvectors and eigenvalues of that matrix. We estimated the correlation between two individuals as described by[14]. We identified components that reflected genome-wide structure in two ways. First, we created two subsets of the data containing SNPs from the odd- and even-numbered chromosomes, repeated the PCA on each of these, and inspected scatter plots of pairs of components between the two subsets of the data. A component which is due to a region of linkage disequilibrium on a chromosome (as opposed to genome-wide structure) will appear only when analysing the data set containing SNPs from that chromosome. Second, we computed the score of every SNP on the components. For a component that is due to a region of linkage disequilibrium, there will be a spike of high SNP scores only in that region. To minimize the contribution from regions of extensive strong linkage disequilibrium, the correlation estimates were based on a subset of 197,175 SNPs that were spaced at least 0.001 cM apart (HapMap estimates) and specifically excluded the MHC region.

To assess the level of over-dispersion in each collection we first created a very clean set of data to ameliorate the effects of over-dispersion due to calling problems and missing data. In addition to the main filters described above, we filtered out all SNPs that had a clear genotype-calling problem revealed by visual inspection, SNPs with a study-wide missing data rate >1% and SNPs with study-wide minor allele frequency <1%. Around 360,000 SNPs passed these filters. Estimates of λ were calculated using an estimator based on the median test statistic[15]. Estimates of λ were also calculated from tests that conditioned on the scores for each individual along the two estimated principal components described above. The tests (1 d.f. and 2 d.f.) were carried out by including the scores as additional covariates in a logistic regression model fit.

Bayes factors. The box in the main text makes the point that understanding the strength of evidence conveyed by a particular P value also requires knowledge of power. In contrast, the Bayes factor (BF) provides a single measure of the strength of the evidence for an association, and we report these in addition to P values (Supplementary Table 14). As for power, calculation of Bayes factors requires assumptions about effect sizes. The assumptions underlying our calculations are given below and in Supplementary Information.

There is broad agreement between the way in which P values and our Bayes factors rank SNPs, except for SNPs with low MAFs (Supplementary Fig. 22). This is intuitive: unless one believed, a priori, that rare causative SNPs have substantially larger effect sizes, there will be reduced power for these SNPs and hence weaker evidence for association than for common SNPs with the same P value.

One perspective on GWAs is that in practice they will be used to prioritize SNPs for further study or additional typing. In addition to BFs providing a single quantity that can be directly compared between SNPs, it is also straightforward for investigators to give different a priori weights to different classes of SNPs, such as non-synonymous (ns)SNPs, genic SNPs, SNPs in highly conserved regions, or SNPs in linkage disequilibrium with many (or few) other SNPs.

We now describe calculation of the Bayes factors. We use M_0 to denote a model of no association, M_1 for a model with an additive effect on the log-odds scale and M_2 for a general 3 parameter model of association. At each SNP we calculate two Bayes factors: one for the additive model versus the null model, BF_1, and one for the general model versus the null model, BF_2. That is,

$$BF_1 = \frac{\Pr(Data|M_1)}{\Pr(Data|M_0)},\ BF_2 = \frac{\Pr(Data|M_2)}{\Pr(Data|M_0)},$$

where $\Pr(Data|M_i) = \int \Pr(Data|\theta_i, M_i)\Pr(\theta_i|M_i)d\theta$, where θ denotes the parameters for the model. For all 3 models we use a logistic regression model for the likelihood $\Pr(Data|\theta_i, M_i)$ where the log-odds for individual i is equal to μ for model M_0, $\mu+\gamma Z_i$ for model M_1 and $\mu+\gamma I(Z_i=1)+\phi(2\gamma I(Z_i=2))$ for model M_2. Z_i is the genotype (coded 0, 1 and 2) for individual i and $I(Z_i=m)$ is the indicator function that individual i has the genotype coded as m. For each model we choose the priors on the parameters, $\Pr(\theta_i|M_i)$, to reflect our belief about the likely effect sizes underlying complex trait loci.

The parameter γ in models M_1 and M_2 is the increase in log-odds of disease for every copy of the allele coded as 1, and e^{γ} is the additive model odds ratio. For both models we use a $N(0, 0.2)$ prior on γ. This prior puts probability 0.31 on

odds ratios above 1.2 or below 0.8, and probability 0.02 on odds ratios above 1.5 or below 0.5. The parameter μ in all three models represents the baseline odds of disease. In a case-control design the numbers of cases in the sample have been elevated artificially, which will have a large effect on likely values of μ. Our prior beliefs about the baseline risk of disease must take this into account. For all three models we have used a $N(0, 1)$ for μ and have found that the resulting Bayes factors are relatively insensitive to choice of priors for this parameter as long as the same prior is used for the two models being compared. The parameter ϕ in model M_2 represents a recessive effect over and above an additive effect. We use a $N(1, 1)$ prior for ϕ. Combined with the prior on γ, this results in a prior probability of 0.25 on the odds ratios above 1.5 and below 0.5 for the genotype coded as 2. In addition, we note that the evaluation of the Bayes factors will depend on the way the alleles at the SNP have been coded 0 and 1. To account for this we average over the two possible codings of each SNP with equal weight. A fuller description of the priors used can be found in Supplementary Information.

Sex-differentiated tests. We examined the possibility of differential genetic effects in males and females by reapplying the two single-locus analyses (trend test and genotypic test) separately in males and females and combining the results (simply adding the chi-squared statistics for the male and female analyses, and comparing with the 2 d.f. or 4 d.f. null hypothesis; results are shown in Supplementary Table 15). We refer to this as a sex-differentiated test. This test is sensitive to association that is of a different magnitude and/or direction in the two sexes, although it is less powerful than the simple test when the effect size does not vary with sex.

X Chromosome analysis. For several reasons the X chromosome needs to be treated differently from the autosomes (note that the Affymetrix chip used does not assay the Y chromosome). First, samples sizes and hence power are different from the autosomes (only one copy of X in males). Also, because the effective population size on the X chromosome is smaller than the autosomes, linkage disequilibrium extends further. And unlike the autosomes, there are choices in how to implement even single locus analyses: these relate to the relative weight to be given to males and females in comparisons between cases and controls.

For autosomal SNPs, the 1 d.f. trend test statistic is calculated by dividing the square of the difference between means of the SNP genotypes (scored 0, 1, 2) between cases and controls by an estimate of its variance. The variance estimate used is an empirical estimate that does not assume Hardy–Weinberg equilibrium. The numerator can also be represented as the squared difference in allele frequencies between cases and controls, as in the allele counting test. At first sight, a natural generalization of this test to deal with SNPs on the X chromosome would involve comparing allele frequencies, by allele counting, but using a variance estimate which does not assume Hardy–Weinberg equilibrium in females. However, we took the view that, because most loci on the X chromosome are subject to X chromosome inactivation, it is more logical to treat males as if they were homozygous females. Thus we score female genotypes 0, 1 or 2 and male genotypes 0 or 2, comparing mean scores of cases and controls as before. The variance estimate allows for the different variance of male and female contributions and does not assume Hardy–Weinberg equilibrium in females.

A stratified version of the test is constructed using the same principles by which the trend test is extended to the Mantel extension test; a score that contrasts cases and controls is computed for each stratum together with its variance; these are then summed over strata. The final test is the squared total score divided by the total variance. To extend these tests to a 2 d.f. test, we add a score that compares heterozygosity between cases and controls. Clearly, only females contribute to this component. Results of these analyses of X chromosome SNPs are shown in Supplementary Table 16.

Multilocus analysis. We use (1) the genotype data of this study, (2) the HapMap data, and (3) a population genetics model, to simulate genotypes at the HapMap SNPs that are not on the Affymetrix 500K chip. Informally, we determine which haplotypes are present in each individual in a region, and then use HapMap to 'fill in' these haplotypes at untyped SNPs (see below for details). These 'in silico' genotypes are then tested for association with the disease as before. This powerful multilocus tool for association studies[143] has the advantage of using information from all markers in linkage disequilibrium with an untyped SNP, but in a way that decreases with genetic distance. Our imputation method was applied to individuals passing project filters, and used markers which passed the project filters and in addition had MAF $>$ 1%. As a validation we compared our imputed genotypes for 58C individuals with genotypes obtained on an Illumina platform for 10,180 SNPs that are polymorphic in CEU HapMap samples. At these SNPs, for imputed genotypes with posterior call probabilities above 0.95, there was 98.4% agreement with the Illumina genotypes.

In our association analyses we imputed genotypes at 2,139,483 HapMap SNPs, and tested these for association with each disease using the trend test or the genotypic test. We included the results from imputed SNPs in the signal plots (Fig. 5) because they are useful in (1) assessing signal strength within a region; (2) providing a wider range of SNPs for follow up; and (3) indicating possible locations for the causal variant. For example in the case of *TCF7L2* in T2D, there is a substantially stronger signal from rs7903146 than for any of the typed SNPs (see also Supplementary Fig. 12).

To be conservative, stringent quality control filters were applied to genomic regions where imputed SNPs (but not genotyped SNPs) were responsible for a strong signal for association. These were as follows: (1) any such region was required to contain more than one imputed SNP showing the required level of association with a MAF $>$ 2% and posterior probability for imputed genotypes averaged across the SNP $>$0.95 (empirical studies showed imputation at low MAF SNPs more prone to error); (2) all cluster plots for genotyped SNPs within 0.3 cM (from HapMap Phase II estimated recombination rates) were checked and where there was evidence of any mis-calling the region was rejected (the major problem with imputation arises around SNPs with genotype calling errors); and (3) if there was no genotyped SNP with a P value $< 10^{-4}$ for association on either trend or genotypic test, the region was rejected. Note that accuracy of imputation with these filters applied will be larger than the figure of 98.4% reported above.

We use $H=\{H_1,\ldots, H_N\}$ to denote a set of N known haplotypes where $H_i=\{H_{i1},\ldots, H_{iL}\}$ is an individual haplotype and L is the number of SNP loci. In practice, we set H to be the 120 CEU haplotypes estimated as part of the HapMap project owing to the expected similarity in haplotype structure between the CEU and UK populations. We let $G=\{G_1,\ldots, G_k\}$ denote the genotype data on the K individuals in the study where $G_i=\{G_{i1},\ldots, G_{iL}\}$ and $G_{ij}\in\{0, 1, 2, \text{missing}\}$. In this setting, the majority of SNPs will have entirely missing genotypes, because the Affymetrix 500K chip has approximately 1/6th of the number of SNPs in the Phase II HapMap. The missing genotypes are imputed by modelling the distribution of each individual's genotype vector G_i conditional on the known set of haplotypes H, $\Pr(G_i|H)$. Our model for each individual's genotype vector is a Hidden Markov Model in which the hidden states are a sequence of pairs of the N known haplotypes in the set H. That is,

$$\Pr(G_i|H)=\sum_{Z_i^{(1)},\,Z_i^{(2)}}\Pr\left(G_i\middle|Z_i^{(1)},\,Z_i^{(2)},\,H\right)\Pr\left(Z_i^{(1)},\,Z_i^{(2)}\right),$$

where $Z_i^{(1)}=\left\{Z_{i1}^{(1)},\ldots,Z_{iL}^{(1)}\right\}$ and $Z_i^{(2)}=\left\{Z_{i1}^{(2)},\ldots,Z_{iL}^{(2)}\right\}$ are the two sequences of copying states at the L sites and $Z_{il}^{(j)}\in\{1,\ldots,N\}$. Here, $\Pr\left(Z_i^{(1)},\,Z_i^{(2)}\right)$ defines our prior probability on how the sequences of copying states change along the sequence and $\Pr\left(G_i\middle|Z_i^{(1)},\,Z_i^{(2)},\,H\right)$ models how the observed genotypes will be close to but not exactly the same as the haplotypes being copied. The precise form of these terms (described in ref. 142) are based on an approximate population genetics model that makes direct use of the recently estimated fine-scale recombination map across the genome[142,143]. At each of the missing genotypes in the study, we use this model to calculate probabilities for the three possible genotypes. At each imputed SNP, we used these probabilities to calculate the 2×3 table of expected genotype counts for cases and controls and used these counts to carry out a standard test of association.

Disease models. To test for deviations from additivity (in log-odds) at a locus we fit a logistic regression model using the function glm in the statistical software R (http://www.r-project.org/). For each region we considered the most significant SNP and compared an additive model to a general 2-d.f. model by fitting a model with an additive sub-model nested in a general model. The additive effect was modelled by a variable encoded 0, 1, or 2 for the effect at the three genotypes and a second term for a general model was included by a variable encoded 1 for heterozygotes and 0 otherwise. We rejected an additive model if the second term was significant and then compared a dominant or recessive model to a general model. For the pairwise interaction analysis, we fixed the marginal model at each locus on the basis of the single locus analysis. We compared the two locus model with these marginals and no interaction terms with a larger model including interactions. This larger interaction model has 1, 2, or 4 additional parameters depending on whether both marginal models are additive, one is additive and one general, or both general.

Software. Several software packages were developed within the WTCCC for data analysis, data management and simulation studies. We found it necessary to normalize the Affymetrix probe intensity data to minimize chip-to-chip variability. A C++ program was written to carry out this normalization efficiently. To obtain a copy of the software please email Hin-Tak Leung at hin-tak.leung@cimr.cam.ac.uk.

We developed a new genotype calling algorithm, CHIAMO, implemented in C++. CHIAMO uses a hierarchical statistical model, which allows it to simultaneously call genotypes at all data samples. To obtain a copy of the software please email J. L. Marchini at marchini@stats.ox.ac.uk.

To perform genome-wide association analysis we developed two software packages: snpMatrix and SNPTEST. snpMatrix is an R package and is freely available from http://www-gene.cimr.cam.ac.uk/clayton/software/. Both quantitative and qualitative phenotypes can by analysed using snpMatrix and flexible association testing functions are provided that control for potential confounding by quantitative and qualitative covariates. SNPTEST is a standalone C++ program that implements both frequentist tests and bayesian analysis of association and allows the user to include quantitative or qualitative covariates. This program works directly with the output of CHIAMO and IMPUTE (see below). To obtain a copy of the software please email J. L. Marchini at marchini@stats.ox.ac.uk.

Genotypes at SNPs that are in HapMap but not on the Affymetrix 500K chip were imputed using the C++ program IMPUTE, which makes use of genotype information at neighbouring SNPs. To obtain a copy of the software please email J. L. Marchini at marchini@stats.ox.ac.uk.

119. Spitzer, R. L., Endicott, J. & Robins, E. Research diagnostic criteria: rationale and reliability. *Arch. Gen. Psychiatry* **35,** 773–782 (1978).
120. Wing, J. K. B. T. *et al.* SCAN. Schedules for Clinical Assessment in Neuropsychiatry. *Arch. Gen. Psychiatry* **47,** 589–593 (1990).
121. Craddock, M. *et al.* Concurrent validity of the OPCRIT diagnostic system. Comparison of OPCRIT diagnoses with consensus best-estimate lifetime diagnoses. *Br. J. Psychiatry* **169,** 58–63 (1996).
122. McGuffin, P., Farmer, A. & Harvey, I. A polydiagnostic application of operational criteria in studies of psychotic illness. Development and reliability of the OPCRIT system. *Arch. Gen. Psychiatry* **48,** 764–770 (1991).
123. Green, E. K. *et al.* Operation of the schizophrenia susceptibility gene, neuregulin 1, across traditional diagnostic boundaries to increase risk for bipolar disorder. *Arch. Gen. Psychiatry* **62,** 642–648 (2005).
124. Green, E. K. *et al.* Genetic variation of brain-derived neurotrophic factor (BDNF) in bipolar disorder: case-control study of over 3000 individuals from the UK. *Br. J. Psychiatry* **188,** 21–25 (2006).
125. Samani, N. J. *et al.* A genomewide linkage study of 1,933 families affected by premature coronary artery disease: The British Heart Foundation (BHF) Family Heart Study. *Am. J. Hum. Genet.* **77,** 1011–1020 (2005).
126. Lennard-Jones, J. E. Classification of inflammatory bowel disease. *Scand. J. Gastroenterol.* (Suppl.) **170**, 2–6; discussion 6–9 (1989).
127. Arnett, F. C. *et al.* The American Rheumatism Association 1987 revised criteria for the classification of rheumatoid arthritis. *Arthritis Rheum.* **31,** 315–324 (1988).
128. MacGregor, A. J., Bamber, S. & Silman, A. J. A comparison of the performance of different methods of disease classification for rheumatoid arthritis. Results of an analysis from a nationwide twin study. *J. Rheumatol.* **21,** 1420–1426 (1994).
129. Worthington, J. *et al.* The Arthritis and Rheumatism Council's National Repository of Family Material: pedigrees from the first 100 rheumatoid arthritis families containing affected sibling pairs. *Br. J. Rheumatol.* **33,** 970–976 (1994).
130. Symmons, D. P., Barrett, E. M., Bankhead, C. R., Scott, D. G. & Silman, A. J. The incidence of rheumatoid arthritis in the United Kingdom: results from the Norfolk Arthritis Register. *Br. J. Rheumatol.* **33,** 735–739 (1994).
131. Smyth, D. *et al.* Replication of an association between the lymphoid tyrosine phosphatase locus (*LYP/PTPN22*) with type 1 diabetes, and evidence for its role as a general autoimmunity locus. *Diabetes* **53,** 3020–3023 (2004).
132. Wiltshire, S. *et al.* A genomewide scan for loci predisposing to type 2 diabetes in a U.K. population (the Diabetes UK Warren 2 Repository): analysis of 573 pedigrees provides independent replication of a susceptibility locus on chromosome 1q. *Am. J. Hum. Genet.* **69,** 553–569 (2001).
133. Frayling, T. M. *et al.* Parent–offspring trios: a resource to facilitate the identification of type 2 diabetes genes. *Diabetes* **48,** 2475–2479 (1999).
134. Groves, C. J. *et al.* Association analysis of 6,736 U.K. subjects provides replication and confirms *TCF7L2* as a type 2 diabetes susceptibility gene with a substantial effect on individual risk. *Diabetes* **55,** 2640–2644 (2006).
135. Power, C. & Elliott, J. Cohort profile: 1958 British birth cohort (National Child Development Study). *Int. J. Epidemiol.* **35,** 34–41 (2006).
136. Strachan, D. P. *et al.* Lifecourse influences on health among British adults: Effects of region of residence in childhood and adulthood. *Int. J. Epidemiol.* Advance online publication, doi:10.1093/ije/dyl309 (25 January 2007).
137. Matsuzaki, H. *et al.* Genotyping over 100,000 SNPs on a pair of oligonucleotide arrays. 1, 104–105. *Nat Methods* **1,** 104–105 (2004).
138. Di, X. *et al.* Dynamic model based algorithms for screening and genotyping over 100 K SNPs on oligonucleotide microarrays. *Bioinformatics* **21,** 1958–1963 (2005).
139. Rabbee, N. & Speed, T. A genotype calling algorithm for affymetrix SNP arrays. *Bioinformatics* **22,** 7–12 (2006).
140. Affymetrix. in Technical Report (2006).
141. Stirling, W. D. Enhancements to Aid Interpretation of Probability Plots. *Statistician* **31,** 211–220 (1982).
142. Li, N. & Stephens, M. Modeling linkage disequilibrium and identifying recombination hotspots using single-nucleotide polymorphism data. *Genetics* **165,** 2213–2233 (2003).
143. Marchini, J., Howie, B., Myers, S., McVean, G. & Donnelly, P. A new multipoint method for genome-wide association studies via imputation of genotypes. *Nature Genet.* doi:10.1038/ng2088 (in the press).

ARTICLES

Developmental reprogramming after chromosome transfer into mitotic mouse zygotes

Dieter Egli[1], Jacqueline Rosains[1], Garrett Birkhoff[1] & Kevin Eggan[1]

Until now, animal cloning and the production of embryonic stem cell lines by somatic cell nuclear transfer have relied on introducing nuclei into meiotic oocytes. In contrast, attempts at somatic cell nuclear transfer into fertilized interphase zygotes have failed. As a result, it has generally been assumed that unfertilized human oocytes will be required for the generation of tailored human embryonic stem cell lines from patients by somatic cell nuclear transfer. Here we report, however, that, unlike interphase zygotes, mouse zygotes temporarily arrested in mitosis can support somatic cell reprogramming, the production of embryonic stem cell lines and the full-term development of cloned animals. Thus, human zygotes and perhaps human embryonic blastomeres may be useful supplements to human oocytes for the creation of patient-derived human embryonic stem cells.

In the first successful mouse nuclear transfer experiments, McGrath and Solter[1] exchanged the pronuclei of two fertilized zygotes. The resulting embryos developed *in vitro* into blastocysts and *in vivo* into mice. However, when the authors transferred nuclei from cells at later developmental stages into zygotes, the embryos failed to develop[2,3]. On the basis of their initial technical success but ultimate failure to reprogramme more differentiated nuclei, they concluded that mammalian cloning would be impossible[2].

The mammalian cloning field was reinvigorated when it was demonstrated that, unlike the zygote, the cytoplasm of the unfertilized oocyte could support reprogramming after nuclear transfer. This realization allowed the generation of sheep[4], rabbits[5], pigs[6] and mice[7] from embryonic blastomeres, the production of sheep from cultured embryonic fibroblasts[8], and ultimately the cloning of Dolly[9]. Numerous mammalian species have now been cloned from adult cells by somatic cell nuclear transfer into unfertilized oocytes[10–14].

More recently, the ability of mouse and bovine zygotes to support nuclear reprogramming has been reinvestigated[15,16]. In these experiments, developmental potential after nuclear transfer was highest when unfertilized oocytes were used and decreased rapidly after either fertilization or artificial activation. Together, these studies in oocytes and zygotes[2,9,10,15,16] suggest that activities crucial for nuclear transfer and/or reprogramming are lost to the oocyte cytoplasm after fertilization.

Conclusions drawn from animal experiments have also informed thinking about efforts to produce human embryonic stem cell lines by somatic cell nuclear transfer, and it is therefore generally accepted that unfertilized human oocytes will be needed for this procedure. Unfortunately, human oocytes are difficult to obtain and their procurement raises medical, logistical and ethical questions, primarily surrounding the participation of women as oocyte donors[17,18].

We have revisited nuclear transfer into zygotes and considered the possibility that factors required for either reprogramming or embryonic development[19–21], present in the cytoplasm of unfertilized meiotic oocytes, become sequestered in the pronuclei of zygotes (Fig. 1a). Such partitioning could explain the failure of enucleated interphase zygotes to support development after nuclear transfer[2,15], because removal of the pronuclei during enucleation would deplete these factors and prevent development. In contrast, removal of the condensed chromosomes from a metaphase II, meiotic egg would not do so. If this model is correct, breakdown of the pronuclear envelope at entry into the first embryonic mitosis might liberate the critical factor or factors into the cytoplasm, once again allowing chromosome removal without factor depletion (Fig. 1a).

To test whether the cytoplasm of a mitotic zygote could indeed support nuclear reprogramming, we reversibly arrested mouse zygotes in mitosis, removed their chromosomes and replaced them with the chromosomes from either embryonic or somatic donor cells. We found that these reconstructed zygotes could be used to generate cloned animals and embryonic stem (ES) cell lines.

Reversible mitotic arrest of mouse zygotes

To synchronize zygotes in mitosis, we transferred interphase zygotes, containing two distinct pronuclei (Fig. 1c), into the microtubule-depolymerizing drug nocodazole. The spindle assembly checkpoint detects defects in spindle structure and delays chromosome segregation until they are corrected[22]. Therefore, spindle disruption with nocodazole results in mitotic arrest[23]. At entry into mitosis, we observed breakdown of the pronuclear envelope and condensation of both maternal and paternal genomes (Fig. 1d). In the presence of nocodazole, condensed chromosomes were not assembled onto a spindle and zygotes did not proceed through mitosis. Although nocodazole stably and reversibly arrested zygotes (Supplementary Tables 1 and 2, Supplementary Movie 1), chromosome position could not be observed (Fig. 1d, top panel) without the DNA dye Hoechst 33342 and illumination with ultraviolet light, which compromised later development. We therefore could not routinely remove the chromosomes, a key step in nuclear transplantation.

To allow spindle polymerization and the determination of chromosome position while preventing progression out of mitosis, we transferred the mitotic zygotes into the proteasome inhibitor MG-132. The metaphase-to-anaphase transition requires degradation of the cyclin B subunit of the maturation promoting factor by

[1]The Stowers Medical Institute, Harvard Stem Cell Institute and Department of Molecular and Cellular Biology, Harvard University, Cambridge, Massachusetts 02138, USA.

the proteasome[24]. In the presence of MG-132, the metaphase-to-anaphase transition and exit from mitosis are blocked[25]. We found that short-term treatment of zygotes with MG-132 led to a reversible arrest in metaphase (Supplementary Tables 1 and 2) and spindle polymerization, allowing the observation of chromosome location by light microscopy or optical birefringence (Fig. 1e).

To determine whether the chromosomes of these arrested zygotes could be reliably removed, we incubated them with Hoechst 33342 and observed DNA content after spindle removal (Fig. 2a–d). When the spindle was removed by micromanipulation, we found that in all cases the chromosomes were also removed ($n = 120/120$; Fig. 2c, d).

Zygotes in mitosis support nuclear reprogramming

To determine whether zygotes 'enucleated' by removal of the spindle in mitosis had a greater capacity to support reprogramming than zygotes enucleated in interphase, we compared the results of genome transfer from embryonic donor cells into these two recipients.

When pronuclei from interphase zygotes were replaced by microinjection with pronuclei from another zygote, the resulting embryos developed to the blastocyst stage and into mice (Table 1, and Supplementary Fig. 1a). Nuclei from two-cell-stage embryos were also able to direct development to the blastocyst stage after transfer into interphase zygotes, but at a lower efficiency (Table 1). However, when interphase nuclei from eight-cell-stage blastomeres were used, development of the embryos was arrested in the first two cleavage divisions (Table 1, and Supplementary Fig. 1c). These observations agree with historical results[2,26] and suggest that the cytoplasm of zygotes enucleated in interphase cannot routinely reprogramme the nuclei of cells that have advanced to the eight-cell stage.

To test whether mitotic zygotes had an enhanced ability to reprogramme more differentiated cells, we removed their chromosomes, microinjected mitotic chromosomes from nocodazole-arrested donor zygote, two-cell-stage or eight-cell-stage embryos and monitored development after removal of the drug. In contrast to nuclear transfer

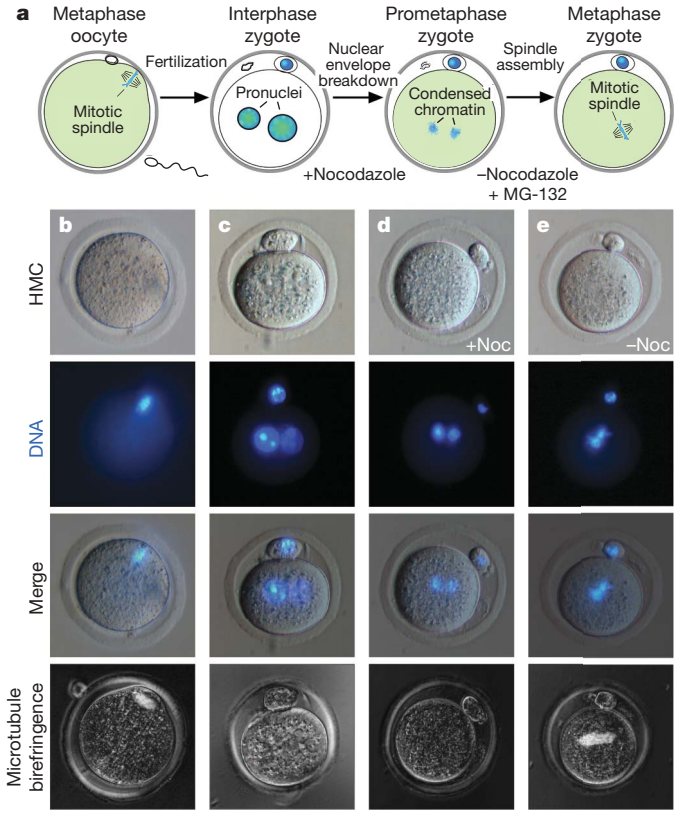

Figure 1 | The first embryonic cell cycle. **a**, Diagram of the first cell cycle. In the metaphase oocyte, condensed chromosomes (blue) are aligned on a metaphase plate, whereas nuclear factors that might be required for reprogramming or development (green) are dispersed throughout the cytoplasm. After fertilization, the parental genomes and required nuclear factors are sequestered in the pronuclei. After entry into mitosis and nuclear envelope break down (NEBD), the factors should be released into the cytoplasm. **b**, Oocyte arrested in metaphase of meiosis II, 15 h after injection with hCG. **c**, Zygote in interphase with two pronuclei, 28 h after injection with hCG. **d**, Zygote arrested in prometaphase of mitosis by nocodazole (noc), 30 h after injection with hCG. Noc, nocodazole. **e**, Zygote entering metaphase in the presence of MG-132, 30.5 h after injection with hCG. As in the unfertilized oocyte, a prominent microtubule spindle could be seen under either Hoffman modulation contrast (HMC) or optical birefringence, enabling chromosome removal.

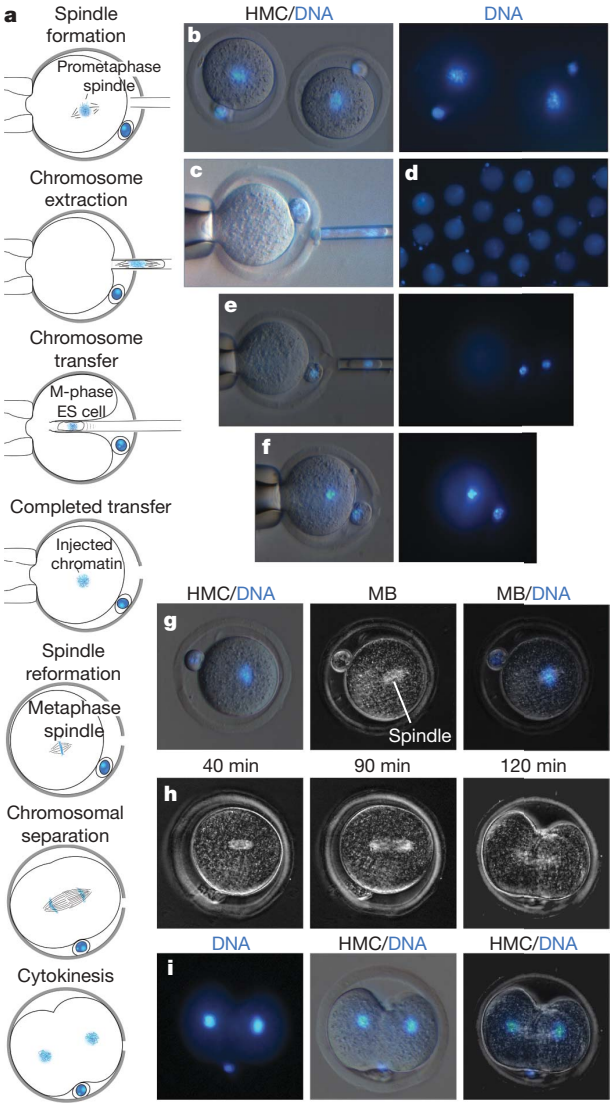

Figure 2 | Chromosome transfer into zygotes arrested in mitosis. **a**, Diagram outlining the method of chromosome transfer into zygotes arrested in mitosis. **b**, Arrested zygotes before spindle and chromosome removal, 10 min after the shift from nocodazole to MG-132. HMC, Hoffman modulation contrast. **c**, Removal of the zygote spindle and chromosomes by micromanipulation. **d**, A large group of zygotes after spindle removal, all lacking chromosomes. **e**, Piezo-actuated injection of a nocodazole-arrested ES cell into a mitotic zygote. **f**, ES cell chromosomes in the zygote immediately after the transfer. **g**, At 80 min after transfer, a new spindle has formed and the chromosomes have aligned in a new metaphase plate. MB, microtubule birefringence. **h, i**, Progression through the first mitosis after ES cell chromosome transfer. **h**, From left to right: prometaphase/metaphase, anaphase, and telophase/cytokinesis, shown under microtubule birefringence. Times after transfer are shown. **i**, Equal chromosome segregation into the two daughter blastomeres at 120 min after transfer.

Table 1 | Developmental potency of zygotes reconstructed with genomes of different developmental and cell cycle stages

Recipient (cell cycle stage)	Donor (cell cycle stage)	Method	No. manipulated	No. cleaved (% of manipulated)	Morulae, day 3.5	Blastocysts, day 3.5	Morulae and blastocysts (% of cleaved)	No. of embryos transferred (recipients)	No. of pregnant recipients	Pups
Zyg. (M)*	Zyg. (M)	Inj.	46	21 (46)	0	17†	81			
Zyg. (M)‡	Zyg.(M)	Inj.	93	66 (71)	36	17	80	48 (4)	4	16
Zyg. (I)‡	Zyg. (I)	Elec.	20	17 (85)	2	12	82	5 (1)	1	1
Zyg. (M)	2-cell (M)	Inj.	90	70 (78)	19	51	100	65 (5)	4	12
Zyg. (I)	2-cell (I)	Inj.	42	30 (70)	10	3	43	8 (1)	0	0
Zyg. (I)	2-cell (I)	Elec.	13	12 (92)	3†	3†	50			
Zyg. (M)	8-cell (M)	Inj.	30	13 (43)	2	7	69	9 (2)	2	2
Zyg. (I)	8-cell (I)	Inj.	30	16 (53)	0	0	0			
Zyg. (M)	ESC (M)	Inj.	1,093	323 (30)	92	109	62	174 (11)	4	9
Zyg. (I)	ESC (I)	Inj.	47	16 (34)	0	0	0			
Zyg. (I)	ESC (M)	Inj.	55	35 (64)	0	0	0			
Ooc. (MII)[27]	ESC (I)	Inj.	275	212§			34	73 (9)		9
Zyg. (M)	Fib. (M)	Inj.	775	231 (30)	72†	26†	42			
♂♀♀ Zyg. (M)	ESC (M)	Inj.	23	15 (65)	6	8	93			
♀♂♂ Zyg. (M)	ESC (M)	Inj.	75	27 (37)	7	11	66			

Zyg., zygote; ♀♂♂, dispermic; ♂♀♀, digynic; ESC, embryonic stem cell; ooc., oocyte; Fib, somatic cell fibroblast; M, mitosis; MII, metaphase of meiosis II; I, interphase; elec., electrofusion; inj., direct injection.
* The genome was transferred back into the same zygote.
† The numbers of morulae and blastocysts were scored on day 4. The table includes results from all, even initial, experiments.
‡ The genome was exchanged between different zygotes.
§ The number of embryos with interphase nuclei was taken as 100% for the calculation of the percentage that reached the morula and blastocyst stages.

in interphase, chromosome transfer in mitosis resulted in efficient development to the blastocyst stage *in vitro* and to adulthood after embryo transfer for all three of the donor cell types, including cells from the eight-cell embryo (Table 1, and Supplementary Fig. 1e–g).

Cloned mice generated by zygote chromosome transfer

To understand chromosome dynamics after chromosome transfer and to try producing cloned mice from cultured cell lines, we performed experiments using ES cells as chromosome donors. To distinguish between zygote and donor cell chromosomes, we used donor ES cells that expressed a doxycycline (dox)-inducible histone H2B-cherry, a red fluorescent fusion protein (Fig. 3b, and Supplementary Fig. 2).

Donor cells were arrested in mitosis with nocodazole (Fig. 2e, f) until microinjection, and consequently their chromosomes were transferred into the mitotic zygotes without a spindle (Fig. 3a).

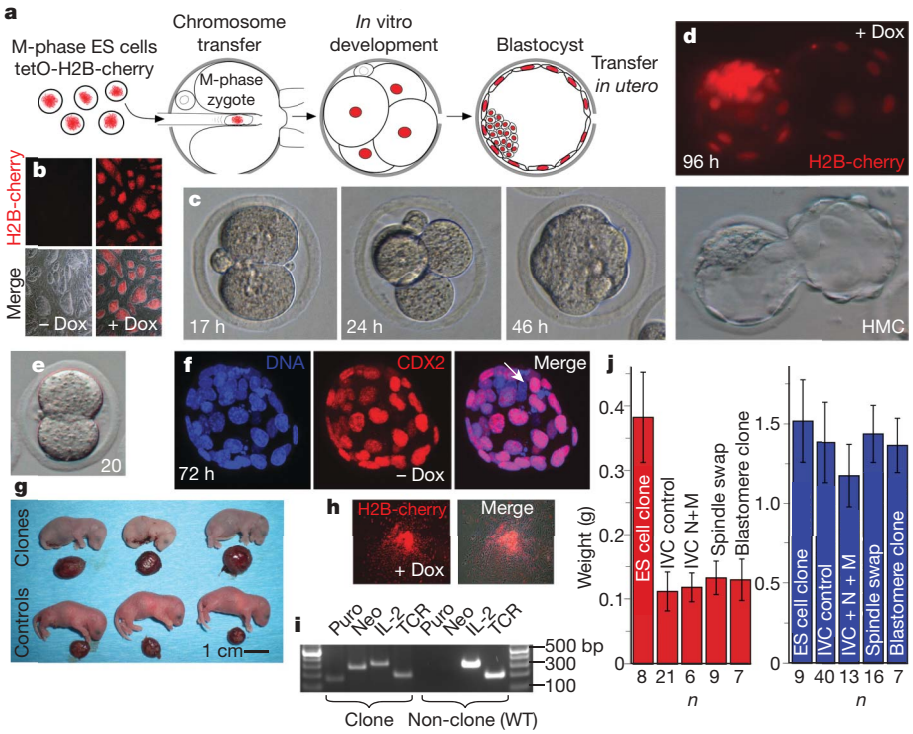

Figure 3 | Developmental potential *in vitro* and *in vivo* after chromosome transfer from ES cells into mitotic zygotes. **a**, Experimental outline. **b**, H2B-cherry donor ES cells with and without induction of the transgene by doxycycline (dox). **c**, **d**, Development of preimplantation embryos after zygote chromosome transfer, from the two-cell stage (**c**, left) to the blastocyst stage (**d**). Times after chromosome transfer are shown. **e**, Developmental arrest at the two-cell stage after the transfer of an ES cell genome into an enucleated interphase zygote. **f**, Cdx2 expression in trophectoderm cells but not in inner cell mass cells (arrow) of a blastocyst-stage embryo after chromosome transfer. **g**, Cloned pups produced by chromosome transfer, and control pups after caesarian section. Their placentas are also shown. Note the large placentas of clones but not the controls, and the dark bluish skin colour of clones as a result of respiratory failure. **h**, Primary culture of skin cells from a cloned pup. **i**, Genotyping by PCR of a cloned pup derived from the transgenic donor cells. Size markers are shown at left and right. Puro, puromycin; neo, neomycin; IL-2, interleukin-2; WT, wild type. **j**, Bar diagram showing weights (means ± s.d.) of pups (right) and their placentas (left) produced by chromosome transfer from ES cells, mitotic spindles of either another zygote or of a two-cell-stage blastomere, and of controls. Numbers below the bars are numbers of individuals. N, nocodazole treatment 28–36 h after injection with hCG; M, treatment with 1 μM MG-132 36.0–36.5 h after injection with hCG. IVC, *in vitro* cultured.

After release from MG-132, a new spindle rapidly nucleated around the ES cell chromosomes. Chromosome segregation and cytokinesis were often observed within 90–150 min (Fig. 2g–i). Manipulated embryos cleaved at a frequency of 30%, and 60% of those that cleaved developed to the morula and blastocyst stages (Table 1 and Fig. 3c, d). This efficiency was comparable to that previously observed in nuclear transfer experiments using interphase ES cell donor nuclei and unfertilized oocytes[27]. In contrast, when zygotes enucleated during interphase were used as recipients for either interphase ES cell donor nuclei or mitotic ES cell chromosomes, the resulting embryos arrested at the one-cell or two-cell stage (Table 1, Fig. 3e, and Supplementary Fig. 1d).

Blastocysts derived by ES cell chromosome transfer into mitotic zygotes expressed H2B-cherry, demonstrating their donor cell origin (Fig. 3d). These blastocysts also recapitulated the normal expression pattern of the Cdx2 protein, which is expressed in the trophectoderm but not in ES cells[28,29], confirming that reprogramming of gene expression had accompanied preimplantation development (Fig. 3f).

We assessed the developmental potential of these ES-cell-derived blastocysts *in vivo* by embryo transfer to pseudopregnant recipients (Table 1 and Fig. 3). From a total of 174 transferred morulae and blastocysts, 9 living pups were recovered after caesarean section at embryonic day 19.5 (Fig. 3g). Seven of the nine pups failed to respire normally and died. Two pups established regular respiration, but one was humanely killed because of a midline closure defect and the other was rejected by its foster mother. We cultured skin cells from these animals and either assessed red fluorescence after induction with doxycycline or genotyped the cells by means of the polymerase chain reaction (PCR). All nine pups were transgenic (Fig. 3h, i), demonstrating that they were cloned animals.

In a manner reminiscent of the overgrowth phenotype observed in other cloned animals[30], these cloned newborns had placentas that were markedly larger than those of controls (Fig. 3j). In contrast, mice derived by chromosome transfer from zygote, two-cell-stage and eight-cell-stage embryo donor cells had placental weights within the normal range. These blastomere-derived animals also regularly established normal respiration and survived to adulthood (Fig. 3j, and Supplementary Fig. 1).

Zygotes can reprogramme adult somatic chromosomes

The experiments described so far have demonstrated that chromosomes can be successfully transferred into zygotes arrested in mitosis, allowing the derivation of cloned mice. However, if zygotes are to be useful recipient cytoplasts for producing genetically tailored human ES cell lines, they must be capable of reprogramming the genome of an adult somatic cell. We therefore performed chromosome transfer with mitotically arrested, adult tail-tip cells that carried a green fluorescent protein (GFP) transgene under the control of the *Oct3/4* promoter (*Oct4::GFP*)[31]. *Oct3/4* is expressed in early pluripotent cells but not in somatic tissues[32] and therefore the reactivation of *Oct3/4* is a measure of successful reprogramming[33]. Embryos into which chromosomes from somatic cells had been transferred cleaved at an efficiency (30%) similar to that observed with ES cell chromosome donors but developed to the morula and blastocyst stages at a lower efficiency (42% of cleaved embryos; Table 1). Consistent with successful nuclear reprogramming, we observed that *Oct4::GFP* expression became visible in late-cleavage-stage embryos and was strongly expressed at the blastocyst stage (Supplementary Fig. 3).

ES cells derived by chromosome transfer into zygotes

We next sought to determine whether fertilized zygotes could be used in chromosome transfer experiments to produce ES cell lines from both embryonic (see Supplementary Fig. 4 for embryonic donor cell results) and somatic (Fig. 4) donor cells. As somatic donor cells we chose nocodazole-arrested skin fibroblasts derived from mice carrying the inducible H2B-cherry transgene (Fig. 4a, b).

After transfer of skin fibroblast chromosomes into mitotic zygotes, embryos were allowed to develop to the blastocyst stage and were then used for ES cell derivation (Table 1) (Fig. 4c). We transferred 21 blastocysts into culture for ES cell derivation; 14 of these attached to the mouse embryonic fibroblast feeder layer and 8 developed outgrowths of the inner cell mass (Fig. 4d). Six of the outgrowths gave rise to cell lines that grew in phase-bright colonies that fluoresced red when exposed to doxycycline (Fig. 4e).

These cell lines were immunoreactive to antibodies specific for the Oct3/4 protein and the stage-specific embryonic antigen-1, which are expressed in ES cells but not in skin fibroblasts (Fig. 4f, g). Karyotyping revealed the presence of a normal 40XY mouse karyotype for five of the cell lines (Fig. 4h). We injected cells from one of these cell lines into non-agouti blastocysts and transferred the blastocysts to recipient mice whose water was supplemented with doxycycline. At embryonic day 11.5 we recovered ten embryos and found that five of them possessed a high degree of chimaerism as judged by red fluorescence (Fig. 4i). When allowed to develop to term, postnatal chimaeric mice also displayed a high degree of agouti coat-colour chimaerism, suggesting that they were largely derived from the injected cells (Fig. 4j, and Supplementary Table 4). To test for germline chimaerism, we crossed a high-contribution chimaeric male to a non-agouti female

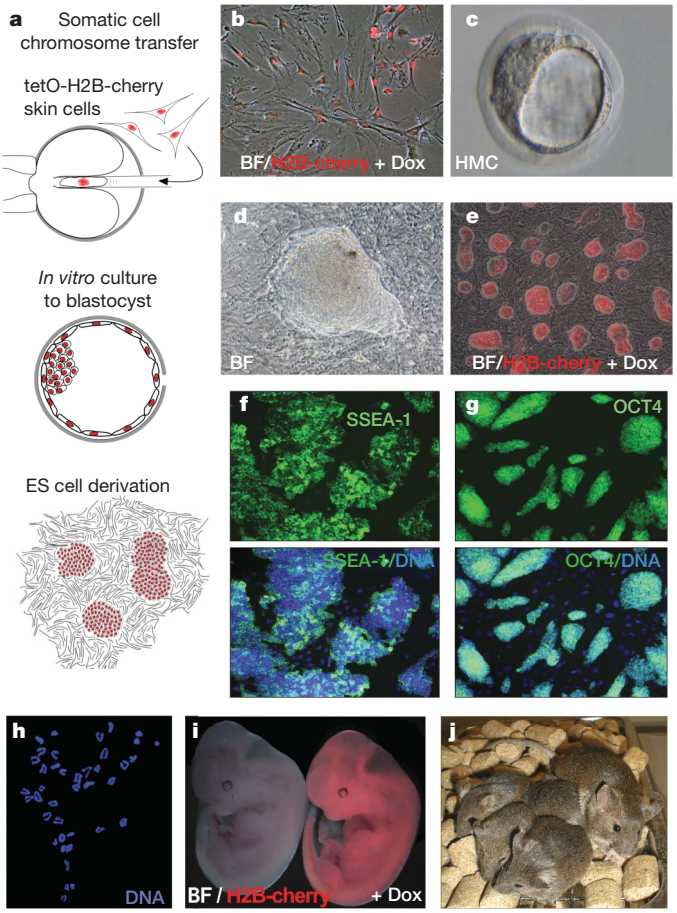

Figure 4 | Derivation of ES cell lines from somatic-cell chromosome transfer blastocysts. **a**, Diagram of zygote somatic-cell chromosome transfer (SCCT) and derivation of SCCT ES cells. **b**, Somatic donor cell line with fibroblast morphology. BF, bright field. **c**, Zygote SCCT blastocyst, 72 h after transfer. **d**, Outgrowth of zygote SCCT inner cell mass 16 days after plating. **e**, Zygote SCCT ES cell culture. **f**, **g**, Expression of the pluripotency marker gene *Oct4* (**g**) and the embryonic antigen SSEA-1 (**f**) in zygote SCCT ES cells, detected by immunostaining. **h**, Mitotic chromosomal spread of a zygote SCCT ES cell line with a normal set of 40 mouse chromosomes. **i**, Chimaera analysis after injection of zygote SCCT ES cells into blastocysts. An embryonic chimaera (right) and a non-transgenic sibling (left). **j**, A male chimaera (right) and its germline offspring (left).

and observed that 5 of 11 pups displayed agouti coat colour, demonstrating that these cells had contributed to the germ line and were genuine ES cells (Fig. 4j).

Discussion and relevance

Our observation that meiotic oocytes and mitotic zygotes can reprogramme somatic genomes, whereas zygotes enucleated in interphase cannot, suggests that the ability of the embryonic cytoplasm to support reprogramming fluctuates with the cell cycle. It is possible that some reprogramming factors are destroyed and renewed with each cell cycle, but it seems more likely that one or more factors critical for embryonic development or reprogramming localize to the pronuclei during interphase (Fig. 1a). Thus, removal of the pronuclei during enucleation removes the relevant factor or factors. In contrast, during meiosis and mitosis, many nuclear factors become dispersed throughout the cytoplasm, and the condensed chromosomes can be removed from the oocyte or zygote without depleting the factors' activity. Consistent with our model is the recent demonstration that if the interphase pronuclei of the zygote are punctured before removal of the chromatin, reprogramming activity in the interphase zygote can be stimulated[34]. In addition, when the germinal vesicles of immature oocytes are removed before nuclear envelope breakdown and meiotic metaphase arrest, the oocytes become unsuitable as recipients for nuclear transfer[21]. Reprogramming factors in ES cells[35–37] may also reside in the nucleus, because enucleated cytoplasts generated from ES cells have so far failed to reprogramme somatic cells[19].

The cloning of animals has relied almost exclusively on unfertilized oocytes and therefore has required artificial activation procedures that poorly mimic fertilization. As a result it has been difficult to determine whether non-physiological oocyte activation contributes to some abnormalities observed in cloned animals. Experiments transferring nuclei into fertilized cow oocytes at telophase of meiosis suggest that artificial activation may indeed contribute to poor clone development[16]. In addition, when the pronuclei of one-cell-stage embryos generated by oocyte nuclear transfer and artificial activation are serially transferred into an enucleated fertilized zygote, development is improved[12,38], again suggesting that normal fertilization improves the ability of the zygote cytoplasm to support the development of NT embryos.

Chromosome transfer into mitotic zygotes bypasses the need for artificial activation, because the sperm has already initiated development. We found that mice cloned from ES cells by chromosome transfer into zygotes displayed at least two phenotypes commonly observed in other cloned animals: neonatal respiratory failure and placental overgrowth[30]. These phenotypes, common to many cloned animals, therefore do not result solely from artificial activation of oocytes. In addition, neonatal mice derived by transferring chromosomes from blastomeres into zygotes did not display these phenotypes, suggesting that they do not arise solely from this mechanical procedure but probably result from failures in nuclear reprogramming.

Our experiments show that reprogramming activities are not permanently lost from the egg cytoplasm after fertilization, which is relevant to the continuing efforts to produce human ES cell lines by nuclear transfer from somatic cells. The most readily available human oocytes are aged ones that failed to be fertilized during *in vitro* fertilization reactions. Mouse oocytes aged in this way have decreased developmental competence and their human counterparts have so far been unsuitable recipients for nuclear transfer[39–41]. Although fresh unfertilized human oocytes would be preferable, there are substantial logistical, medical and societal difficulties in obtaining sufficient numbers. In contrast to fresh unfertilized oocytes, which generally do not exist in excess of clinical need, normal fertilized zygotes are frozen with some regularity. In many cases these frozen zygotes are discarded by couples who have completed their assisted reproduction treatment[42,43] and they could instead be donated for stem cell research.

More significantly, 3–5% of all human zygotes are found to contain an abnormal number of pronuclei after *in vitro* fertilization[44–46]. We estimate that these aneuploid zygotes number in the tens of thousands each year in the United States[47]. These zygotes are

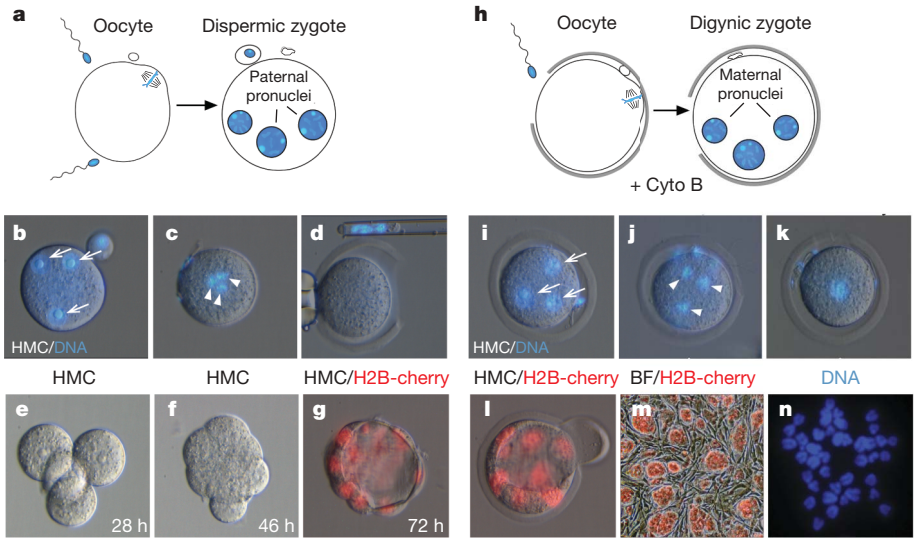

Figure 5 | Aneuploid zygotes with more than two pronuclei can be used as recipients for chromosome transfer. **a**, Diagram of an *in vitro* fertilization (IVF) reaction without a zona pellucida. The increased access to sperm results in a high frequency of polyspermic zygotes. **b**, Dispermic zygote in interphase, with two paternal pronuclei and a single maternal pronucleus (arrows); 6 h after IVF. **c**, Dispermic zygote at prometaphase, after pronuclear envelope breakdown and chromosome condensation with three groups of haploid genomes (arrowheads); 20 h after IVF. **d**, Removal of the triploid mitotic genome, 10 min after treatment with nocodazole. **e**–**g**, Clones at the four-cell (**e**), morula (**f**) and blastocyst (**g**) stages derived after chromosome transfer of an ES cell genome into a polyspermic zygote. Times after transfer are shown. **h**, Diagram of fertilization with a failure to extrude the second polar body. Cyto B, cytochalasin B. **i**, Digynic zygote in interphase, with three pronuclei (arrows); 10 h after IVF. **j**, Nocodazole-arrested digynic zygote at prometaphase, with three haploid genomes (arrowheads); 20 h after IVF. **k**, Mitotic chromosomes of a digynic zygote assembling in a single spindle, 10 min after treatment with nocodazole. **l**, Clone at the blastocyst stage derived by chromosome transfer of an H2B-cherry transgenic ES cell genome into a digynic zygote; 76 h after transfer. **m**, H2B-cherry transgenic ES cell line derived after chromosome transfer into a triploid digynic zygote. **n**, A mitotic chromosomal spread of the same cell line, showing a diploid karyotype.

excluded from clinical use at the one-cell stage because their abnormal ploidy is incompatible with normal postimplantation development; they, too, could be donated for research without interfering with that couple's reproductive efforts. Human polyspermic zygotes routinely undergo cleavage division[46,48] and might therefore be arrested in mitosis and the zygotic chromosomes removed by using the methods we have described. After introducing the correct number of human somatic chromosomes from a mitotic donor cell, our results suggest that reconstructed zygotes might support development to the blastocyst stage and human ES cell derivation.

We have tested whether aneuploid mouse zygotes resulting from polyspermy and failed polar body extrusion can support nuclear reprogramming by inducing these conditions *in vitro* and using the resulting zygotes as recipients for mitotic chromosome transfer (Fig. 5). We found in both cases that, on entry into mitosis, the pronuclei broke down and the supernumerary chromosome sets congregated on a single spindle in the centre of the zygote. When this spindle was removed, the chromosomes were also removed (Fig. 5d). After transfer of ES cell chromosomes from mitotic donor cells into these cytoplasts they developed to the blastocyst stage (Table 1) and could be used to derive ES cell lines with a normal karyotype (Fig. 5n).

Thus, our results provide several previously unexplored and technically feasible avenues towards the production of 'genetically tailored' human ES cell lines that are not constrained by the limitations of oocyte donation for research.

The finding that oocytes, zygotes and ES cells each harbour reprogramming activities suggests that a continuum of activity may extend from the unfertilized egg through cells of the preimplantation embryo to the ES cells derived from them. Cells from one-cell, two-cell, four-cell or eight-cell embryos might therefore all be useful recipients for the chromosome transfer methods we have described. Similarly, it may be possible to generate cytoplasts from ES cells that have been arrested in mitosis and test whether they can support nuclear reprogramming. If cells from discarded cleavage-stage human preimplantation embryos could be used as recipients for chromosome transfer, or if ES cells arrested in mitosis could be used to generate cytoplasts with reprogramming activity, it would substantially advance efforts to produce human ES cell lines for disease modelling and transplantation medicine.

METHODS SUMMARY

Chromosome transfer into mouse zygotes in mitosis. Zygotes were retrieved from mated females 20–24 h after injection with human chorionic gonadotropin (hCG) and placed into KSOM embryo culture medium with 0.1 μg ml^{-1} nocodazole 25–29 h after injection with hCG. Small groups of zygotes arrested in mitosis were washed and transferred into KSOM with 2 μM MG-132 for about 10 min. Manipulations (Supplementary Movie 2) were conducted on a heated stage in the presence of 5 μg ml^{-1} cytochalasin B, within 10–20 min while zygotes were still in prometaphase of mitosis. Mitotic donor cells were obtained by mitotic shake-off from a cell culture grown for 6 h in the presence of 0.1 μg ml^{-1} nocodazole. Cells were treated with trypsin and then mixed with 1% polyvinylpyrrolidone containing 0.1 μg ml^{-1} nocodazole. A detailed description of materials and methods is provided in Supplementary Information.

Full Methods and any associated references are available in the online version of the paper at www.nature.com/nature.

Received 12 January; accepted 25 April 2007.

1. McGrath, J. & Solter, D. Nuclear transplantation in the mouse embryo by microsurgery and cell fusion. *Science* **220,** 1300–1302 (1983).
2. McGrath, J. & Solter, D. Inability of mouse blastomere nuclei transferred to enucleated zygotes to support development *in vitro*. *Science* **226,** 1317–1319 (1984).
3. Robl, J. M. *et al.* Nuclear transplantation in bovine embryos. *J. Anim. Sci.* **64,** 642–647 (1987).
4. Willadsen, S. M. Nuclear transplantation in sheep embryos. *Nature* **320,** 63–65 (1986).
5. Stice, S. L. & Robl, J. M. Nuclear reprogramming in nuclear transplant rabbit embryos. *Biol. Reprod.* **39,** 657–664 (1988).
6. Prather, R. S., Sims, M. M. & First, N. L. Nuclear transplantation in early pig embryos. *Biol. Reprod.* **41,** 414–418 (1989).
7. Cheong, H. T., Takahashi, Y. & Kanagawa, H. Development of mouse embryonic nuclei transferred to enucleated oocytes and zygotes. *Jpn. J. Vet. Res.* **40,** 149–159 (1992).
8. Campbell, K. H., McWhir, J., Ritchie, W. A. & Wilmut, I. Sheep cloned by nuclear transfer from a cultured cell line. *Nature* **380,** 64–66 (1996).
9. Wilmut, I., Schnieke, A. E., McWhir, J., Kind, A. J. & Campbell, K. H. Viable offspring derived from fetal and adult mammalian cells. *Nature* **385,** 810–813 (1997).
10. Wakayama, T., Perry, A. C., Zuccotti, M., Johnson, K. R. & Yanagimachi, R. Full-term development of mice from enucleated oocytes injected with cumulus cell nuclei. *Nature* **394,** 369–374 (1998).
11. Chesne, P. *et al.* Cloned rabbits produced by nuclear transfer from adult somatic cells. *Nature Biotechnol.* **20,** 366–369 (2002).
12. Polejaeva, I. A. *et al.* Cloned pigs produced by nuclear transfer from adult somatic cells. *Nature* **407,** 86–90 (2000).
13. Kato, Y. *et al.* Eight calves cloned from somatic cells of a single adult. *Science* **282,** 2095–2098 (1998).
14. Zhou, Q. *et al.* Generation of fertile cloned rats by regulating oocyte activation. *Science* **302,** 1179 (2003).
15. Wakayama, T., Tateno, H., Mombaerts, P. & Yanagimachi, R. Nuclear transfer into mouse zygotes. *Nature Genet.* **24,** 108–109 (2000).
16. Schurmann, A., Wells, D. N. & Oback, B. Early zygotes are suitable recipients for bovine somatic nuclear transfer and result in cloned offspring. *Reproduction* **132,** 839–848 (2006).
17. Steinbrook, R. Egg donation and human embryonic stem-cell research. *N. Engl. J. Med.* **354,** 324–326 (2006).
18. Norsigian, J. in *Boston Globe* 25 February A13 (2005).
19. Do, J. T. & Scholer, H. R. Nuclei of embryonic stem cells reprogram somatic cells. *Stem Cells* **22,** 941–949 (2004).
20. Takahashi, K. & Yamanaka, S. Induction of pluripotent stem cells from mouse embryonic and adult fibroblast cultures by defined factors. *Cell* **126,** 663–676 (2006).
21. Gao, S. *et al.* Germinal vesicle material is essential for nucleus remodeling after nuclear transfer. *Biol. Reprod.* **67,** 928–934 (2002).
22. Rudner, A. D. & Murray, A. W. The spindle assembly checkpoint. *Curr. Opin. Cell Biol.* **8,** 773–780 (1996).
23. Hamilton, B. T. & Snyder, J. A. Rapid completion of mitosis and cytokinesis in PtK cells following release from nocodazole arrest. *Eur. J. Cell Biol.* **28,** 190–194 (1982).
24. Glotzer, M., Murray, A. W. & Kirschner, M. W. Cyclin is degraded by the ubiquitin pathway. *Nature* **349,** 132–138 (1991).
25. Ehrhardt, A. G. & Sluder, G. Spindle pole fragmentation due to proteasome inhibition. *J. Cell. Physiol.* **204,** 808–818 (2005).
26. Cheong, H. T. & Kanagawa, H. Assessment of cytoplasmic effects on the development of mouse embryonic nuclei transferred to enucleated zygotes. *Theriogenology* **39,** 451–461 (1993).
27. Wakayama, T., Rodriguez, I., Perry, A. C., Yanagimachi, R. & Mombaerts, P. Mice cloned from embryonic stem cells. *Proc. Natl Acad. Sci. USA* **96,** 14984–14989 (1999).
28. Beck, F., Erler, T., Russell, A. & James, R. Expression of Cdx-2 in the mouse embryo and placenta: possible role in patterning of the extra-embryonic membranes. *Dev. Dyn.* **204,** 219–227 (1995).
29. Niwa, H. *et al.* Interaction between Oct3/4 and Cdx2 determines trophectoderm differentiation. *Cell* **123,** 917–929 (2005).
30. Eggan, K. *et al.* Hybrid vigor, fetal overgrowth, and viability of mice derived by nuclear cloning and tetraploid embryo complementation. *Proc. Natl Acad. Sci. USA* **98,** 6209–6214 (2001).
31. Yoshimizu, T. *et al.* Germline-specific expression of the Oct-4/green fluorescent protein (GFP) transgene in mice. *Dev. Growth Differ.* **41,** 675–684 (1999).
32. Scholer, H. R., Dressler, G. R., Balling, R., Rohdewohld, H. & Gruss, P. Oct-4: a germline-specific transcription factor mapping to the mouse t-complex. *EMBO J.* **9,** 2185–2195 (1990).
33. Boiani, M., Eckardt, S., Scholer, H. R. & McLaughlin, K. J. Oct4 distribution and level in mouse clones: consequences for pluripotency. *Genes Dev.* **16,** 1209–1219 (2002).
34. Greda, P., Karasiewicz, J. & Modlinski, J. A. Mouse zygotes as recipients in embryo cloning. *Reproduction* **132,** 741–748 (2006).
35. Tada, M., Tada, T., Lefebvre, L., Barton, S. C. & Surani, M. A. Embryonic germ cells induce epigenetic reprogramming of somatic nucleus in hybrid cells. *EMBO J.* **16,** 6510–6520 (1997).
36. Tada, M., Takahama, Y., Abe, K., Nakatsuji, N. & Tada, T. Nuclear reprogramming of somatic cells by *in vitro* hybridization with ES cells. *Curr. Biol.* **11,** 1553–1558 (2001).
37. Cowan, C. A., Atienza, J., Melton, D. A. & Eggan, K. Nuclear reprogramming of somatic cells after fusion with human embryonic stem cells. *Science* **309,** 1369–1373 (2005).
38. Ono, Y., Shimozawa, N., Ito, M. & Kono, T. Cloned mice from fetal fibroblast cells arrested at metaphase by a serial nuclear transfer. *Biol. Reprod.* **64,** 44–50 (2001).
39. Hall, V. J. *et al.* Developmental competence of human *in vitro* aged oocytes as host cells for nuclear transfer. *Hum. Reprod.* **22,** 52–62 (2007).

40. Wakayama, S. *et al.* Establishment of mouse embryonic stem cell lines from somatic cell nuclei by nuclear transfer into aged, fertilization-failure mouse oocytes. *Curr. Biol.* **17,** R120–R121 (2007).
41. Wakayama, S. *et al.* Production of offspring from one-day-old oocytes stored at room temperature. *J. Reprod. Dev.* **50,** 627–637 (2004).
42. Nikolettos, N. & Al-Hasani, S. Frozen pronuclear oocytes: advantages for the patient. *Mol. Cell. Endocrinol.* **169,** 55–62 (2000).
43. Damario, M. A., Hammitt, D. G., Galanits, T. M., Session, D. R. & Dumesic, D. A. Pronuclear stage cryopreservation after intracytoplasmic sperm injection and conventional IVF: implications for timing of the freeze. *Fertil. Steril.* **72,** 1049–1054 (1999).
44. Van der Ven, H. H. *et al.* Polyspermy in *in vitro* fertilization of human oocytes: frequency and possible causes. *Ann. NY Acad. Sci.* **442,** 88–95 (1985).
45. Munne, S. & Cohen, J. Chromosome abnormalities in human embryos. *Hum. Reprod. Update* **4,** 842–855 (1998).
46. Kola, I., Trounson, A., Dawson, G. & Rogers, P. Tripronuclear human oocytes: altered cleavage patterns and subsequent karyotypic analysis of embryos. *Biol. Reprod.* **37,** 395–401 (1987).
47. Anon. Assisted reproductive technology in the United States: 2000 results generated from the American Society for Reproductive Medicine/Society for Assisted Reproductive Technology Registry. *Fertil. Steril.* **81,** 1207–1220 (2004).
48. Sathananthan, A. H. *et al.* Centrioles in the beginning of human development. *Proc. Natl Acad. Sci. USA* **88,** 4806–4810 (1991).

Supplementary Information is linked to the online version of the paper at www.nature.com/nature.

Acknowledgements We thank A. Murray for insight into the regulation of the cell cycle; K. Hochedlinger and C. Beard for KH2 ES cells and plasmids; A. Greenwood for H2B and cherry plasmids; C. Cowan, K. Niakan, J. Dimos, I. Tabansky, W. Strausack, A. Schier, A. McMahon, R. Jaenisch and D. Melton for advice and discussions; and D. Melton, A. Schier, D. Lopez, R. Jaenisch, A. Meissner, A. McMahon, A. Murray and A. Chen for critical reading of the manuscript. This work was supported by funds from the Stowers Medical Institute, The Harvard Stem Cell Institute and the National Institutes of Health to K.E. and by a fellowship from the Swiss National Science Foundation to D.E. K.E. is a fellow of the John D. and Catherine T. MacArthur Foundation.

Author Contributions K.E. and D.E. designed the experiments. D.E. constructed the H2B-cherry mouse ES cell line and mouse. D.E., J.R. and K.E. performed chromosome transfer experiments and stem cell derivation. G.B. assisted D.E. with blastocyst injections and embryo transfer and prepared the figures. K.E. and D.E. wrote the paper. All authors discussed the results and commented on the manuscript.

Author Information Reprints and permissions information is available at www.nature.com/reprints. The authors declare no competing financial interests. Correspondence and requests for materials should be addressed to K.E. (eggan@mcb.harvard.edu).

METHODS

Mice and cell lines. BDF1 mice used as zygote donors were obtained from Charles River Laboratories, and B6jcBA-Tg(Pou5fl-EGFP)2Mnn/J mice originating from the lab of Hans Schoeler[31] were obtained from Jackson Laboratories. KH2 cells as well as plasmids pBS31tetOpgkATGfrt and pCAGGS-Flpe-pur for the construction of KH2-H2B-cherry ES cells (approx. passage 40) were obtained from Konrad Hochedlinger[49]. The H2B-cherry fusion protein was constructed by recombinogenic PCR with the primers 5′-ACA CCA GCG CTA AGG ATC CAC CGG TCG CCA TGG TGA GCA AGG GCG AG-3′ and 5′-AGC CTT TAA GCC TGC CCA GAA GAC-3′, and 5′-GCG ACC GGT GGA TCC TTA GCG CTG GTG TAC TTG GTG ACG GCC TTA GTA CC-3′ and 5′-CAC CGT CGA CGG TAC CGC CAC CA-3′; it was then cloned into the *Eco*RI site of pBS31tetOpgkATGfrt. Somatic donor cells from skin and tail were cultured as described previously[50]. To induce the tetO-H2B-cherry transgene, doxycycline (catalogue no. D9891; Sigma) was added to the drinking water of mice at a concentration of 1 mg ml^{-1} and to cell cultures at 1 μg ml^{-1}.

Chromosome transfer into zygotes arrested in mitosis. BDF1 females 6–8 weeks old were superovulated as described previously[51] and mated to BDF1 males. Zygotes were retrieved from the oviducts of plugged females 20–24 h after injection with hCG, and placed into KSOM medium. Embryos were transferred into KSOM containing 0.1 μg ml^{-1} nocodazole (catalogue no. M1404; Sigma) 25–29 h after injection with hCG. Zygotes arrested in mitosis were washed through one to three drops of KSOM to remove residual nocodazole and then transferred into KSOM (Chemicon) with 1–2 μM MG-132 for 5–20 min and then, for manipulations, transferred on the stage into oil-covered droplets of HCZB supplemented with 5 μg ml^{-1} cytochalasin B (catalogue no. C6762; Sigma) and 1–2 μM MG-132 (catalogue no. 474790; Calbiochem). In some cases, MG-132 was completely omitted and replaced with 0.0025–0.03 μg ml^{-1} nocodazole during the manipulations to delay mitotic progression of the zygote while not dissociating the spindle (Supplementary Fig. 5). This modification resulted in a smaller spindle volume and a more regular cleaveage of clones. Mitotic donor cells were obtained after culturing cells with 0.1 μg ml^{-1} nocodazole for 6–12 h. Cells were obtained by mitotic shake-off from the culture dish, treated with trypsin and then mixed with 1–7% polyvinylpyrrolidone containing 0.1 μg ml^{-1} nocodazole. Mitotic cells were selected under the microscope and then transferred with a 10-μm needle for mitotic ES cells and with a 12–14 μm needle (Humagen) for mitotic somatic cells. Removal of the spindle chromosome complex and transfer of broken cells were done in one step, taking care that the cell was deposited approximately in the middle of the zygote (Supplementary Movie 2). The average survival rate that we obtained was 85%.

All manipulations were done on a heated stage (37 °C) of a Nikon microscope equipped with Hoffman modulation contrast optics; they were completed within a 5–45-min window after the release from nocodazole. The microscope was equipped with a Xyclone laser (Hamilton Thorne Biosciences) for zona drilling and a piezo unit (PrimeTech) for breaking the zygotic plasma membrane. After manipulations had been completed, chromosome transfer embryos and control embryos were cultured in droplets of KSOM covered with mineral oil.

Mitotic spindles of zygotes and blastomeres were transferred with needles 13 or 14 μm in diameter with the method as described for ES cells. Manipulation of interphase zygotes was performed 24–26 h after injection with hCG with the methods described above, with the addition of 0.1–0.3 μg ml^{-1} nocodazole to the manipulation medium and the use of a 14-μm needle for enucleation and transfer. Nuclei of two-cell-stage embryos were transferred by direct injection or by electrofusion with an LF101 electrofusion apparatus with two direct-current pulses of 1.8 kV cm^{-1} in medium containing 0.26 mM mannitol, 0.1 mM $MgSO_4$, 0.5 mM HEPES and 0.05% bovine serum albumin. Images of optical birefringence were taken with the Oosight system (Cambridge Research and Instrumentation).

In vitro fertilization (IVF) was performed as described[51]. In brief, oocytes were collected from hormone-stimulated females 14 h after injection with hCG. Sperm was obtained from the cauda epididymis of a non-transgenic male and incubated at 37 °C for 30–60 min in HTF medium (IVF Online) supplemented with 5% fetal bovine serum before the addition of the oocytes. The presence of pronuclei was scored 10 h after the initiation of the IVF reaction, and zygotes with more than two pronuclei were selected for chromosome transfer. Unlike in humans, in whom only the zona pellucida acts as a barrier to polyspermy, in the mouse both the oolemma and the plasma membrane inhibit polyspermy[52]. *In vitro*, the mouse zona pellucida acts as an efficient barrier to sperm even without any fertilization. To induce high levels of fertilization, we removed the zona pellucida either partly with a laser pulse or completely with acidic Tyrode's solution. Dispermic and digynic zygotes normally entered the first mitosis in the presence of nocodazole, and the removal of nocodazole (10 min) resulted in the assembly of all chromosomes in a single spindle that could be removed as in a normally fertilized zygote (Fig. 5d, k). Also in humans, chromosomes of dispermic embryos assemble in a single spindle in the centre of the egg[46]. To induce digynic zygotes experimentally in the mouse, cytochalasin B was added to the IVF reaction at a concentration of 3 μg ml^{-1} for 5 h. In humans, a failure to extrude the second polar body occurs at a frequency of about 4% after fertilization by intracytoplasmic sperm injection[45].

ES cell derivation, embryo transfer and genotyping. For the derivation of mouse ES (mES) cells, cloned blastocysts were plated on irradiated mouse embryonic fibroblast feeder layers in mES medium containing the mitogen-activated protein kinase inhibitor PD98059 (Cell Signalling) and LIF (Chemicon). Mitotic spreads of ES cells were made by incubating ES cells for 12 h in 0.1 μg ml^{-1} nocodazole to arrest them in mitosis; they were then treated with trypsin and incubated in 0.56% w/v KCl, stained with Hoechst and then fixed with a 1:3 mixture of glacial acetic acid and methanol. Chimeric mice were made by injection of ES cells into non-agouti BDF2 blastocysts and embryo transfer into day 2.5 pseudopregnant albino ICR females. Cloned and control blastocysts were transferred to the uterus of day 2.5 pseudopregnant ICR females. Caesarian section was performed on embryonic day 19.5. Surviving pups were fostered to an ICR foster mother that had given birth either on the same day or 1–4 days earlier. Primers for genotyping of puromycin, neomycin, interleukin-2 and T-cell antigen receptor genes are as described by the Jackson Laboratory (http://www.jax.org/). Experiments with animals were performed in accordance with the guidelines established by the Harvard University/Faculty of Arts and Sciences IACUC for the humane care and use of animals in research.

Immunostaining. Preimplantation stage embryos were stained with a Cdx2 antibody (Biogenex) as described[53]. The secondary antibody was coupled to rhodamine-X.

ES cells (Fig. 5) and somatic donor cells were stained with antibodies specific for OCT4 (sc5279; Santa Cruz) and SSEA-1 (sc21702; Santa Cruz).

49. Beard, C., Hochedlinger, K., Plath, K., Wutz, A. & Jaenisch, R. Efficient method to generate single-copy transgenic mice by site-specific integration in embryonic stem cells. *Genesis* **44**, 23–28 (2006).
50. Wakayama, T. & Yanagimachi, R. Cloning of male mice from adult tail-tip cells. *Nature Genet.* **22**, 127–128 (1999).
51. Nagy, A., Gertsenstein, M., Vintersten, K. & Behringer, R. *Manipulating the Mouse Embryo: A Laboratory Manual* 3rd edn (Cold Spring Harbor Laboratory Press, New York, 2003).
52. Wolf, J. P. *et al.* Absence of block to polyspermy at the human oolemma. *Fertil. Steril.* **67**, 1095–1102 (1997).
53. Strumpf, D. *et al.* Cdx2 is required for correct cell fate specification and differentiation of trophectoderm in the mouse blastocyst. *Development* **132**, 2093–2102 (2005).

ARTICLES

DNA repair is limiting for haematopoietic stem cells during ageing

Anastasia Nijnik[1], Lisa Woodbine[2], Caterina Marchetti[2,3], Sara Dawson[4], Teresa Lambe[1], Cong Liu[2], Neil P. Rodrigues[5], Tanya L. Crockford[1], Erik Cabuy[6], Alessandro Vindigni[3], Tariq Enver[5], John I. Bell[1], Predrag Slijepcevic[6], Christopher C. Goodnow[4]*, Penelope A. Jeggo[2]* & Richard J. Cornall[1]*

Accumulation of DNA damage leading to adult stem cell exhaustion has been proposed to be a principal mechanism of ageing. Here we address this question by taking advantage of the highly specific role of DNA ligase IV in the repair of DNA double-strand breaks by non-homologous end-joining, and by the discovery of a unique mouse strain with a hypomorphic *Lig4*^{Y288C} mutation. The *Lig4*^{Y288C} mouse, identified by means of a mutagenesis screening programme, is a mouse model for human LIG4 syndrome, showing immunodeficiency and growth retardation. Diminished DNA double-strand break repair in the *Lig4*^{Y288C} strain causes a progressive loss of haematopoietic stem cells and bone marrow cellularity during ageing, and severely impairs stem cell function in tissue culture and transplantation. The sensitivity of haematopoietic stem cells to non-homologous end-joining deficiency is therefore a key determinant of their ability to maintain themselves against physiological stress over time and to withstand culture and transplantation.

Long-lived multicellular organisms depend on tissue replenishment from small pools of slowly dividing stem cells that must be self-renewed and maintained with a minimum of mutations throughout life[1]. This principle is best characterized for the haematopoietic system, which is maintained from small numbers of stem cells within the bone marrow. Haematopoietic failure follows the loss of haematopoietic stem cells in humans and animals exposed to a threshold level of genotoxic agents such as ionizing radiation or cytotoxic drugs[2,3], and one of the most pathogenic forms of DNA damage in these situations is a double-strand break[4]. Endogenous double-strand breaks arise predominantly from oxidative DNA damage caused by reactive oxygen species (ROS)[5] and are repaired by non-homologous end-joining (NHEJ)[6,7] and homologous recombination[4]. Selective induction of senescence in haematopoietic stem cells by ionizing radiation[3] and by elevated levels of ROS observed in ataxia-telangiectasia mutated-deficient ($ATM^{-/-}$) mice[8] indicates that double-strand break damage may limit haematopoietic stem cell function, and unrepaired double-strand breaks have been shown to accumulate in human and mouse tissues during ageing[9]. Furthermore, p53 and Rad50, which are involved in responses to genotoxic stress and repair, both affect the numbers and function of stem cells during ageing[10,11]. However, the effects of physiological levels of double-strand break damage and the direct contribution of DNA repair pathways to haematopoietic stem cell maintenance in ageing are not known.

Six components of NHEJ have been identified: Ku70, Ku80, DNA-PK_{cs}, XRCC4, DNA ligase IV (LigIV)[6,7] and XRCC4-like factor (XLF)[12,13]. The viable Ku and DNA-PK_{cs} knockout mice are the currently established models of NHEJ deficiency[7]. However, some end-joining can occur in the absence of Ku and DNA-PK_{cs}[14], and these proteins have NHEJ-independent functions, including telomere maintenance[15,16]. In contrast, LigIV is essential and has no known functions outside DNA repair by NHEJ; however, because of lethality of the *Lig4*-null mice[17,18] there are no viable animal models of LigIV deficiency. Instead, hypomorphic mutations in *LIG4* result in the human LigIV syndrome, characterized by growth defects, immunodeficiency and hitherto unexplained pancytopenia[19–24]. The same pattern of human disease is also induced by mutations in XLF[12,13,25].

Mouse model of human LigIV syndrome

One of the principal advantages of mutagenesis induced by ethylnitrosourea (ENU) is its ability to reproduce under controlled conditions the most common type of natural human variation, by generating one round of single-nucleotide substitutions in a known genome sequence at a rate of about 1 per 10^6 bases[26,27]. We therefore screened a library of C57BL/6 (B6) mice segregating ENU-induced substitutions for immunodeficiency phenotypes similar to LigIV syndrome by using flow cytometry, and identified a new strain, *tiny*, with reduced lymphocytes in peripheral blood (Fig. 1a) and growth retardation (Fig. 1b, c) inherited together as a recessive trait. The *tiny* mutation resulted in partial embryonic lethality on the inbred B6 background, but homozygotes were born at about 40% of the expected frequency and grew to adulthood, although with small size. In a 550-animal F_2 intercross, the mutation mapped to a 2.30-megabase (Mb) region between 8.54 and 10.84 Mb on chromosome 8 (Fig. 1d, and Supplementary Table 1). Complementary DNAs of the three known genes in the interval (*Tnfsf13b*, *Lig4* and *Efnb2*) were sequenced and a single 1067A→G substitution in *Lig4* was identified and confirmed in genomic DNA (Fig. 1e). The mutation encodes a Y288C substitution in the catalytic domain (Fig. 1f). This *Lig4*^{Y288C} mutant is the first viable model of LigIV deficiency.

Lig4^{Y288C} encodes a hypomorphic mutation

Examination of double-strand break repair in *Lig4*^{Y288C} mouse embryonic fibroblasts (MEFs) by γ-H2AX foci analysis revealed a

[1]Henry Wellcome Building for Molecular Physiology, Oxford University, Oxford OX3 9DU, UK. [2]Genome Damage and Stability Centre, University of Sussex, Brighton BN1 9RQ, UK. [3]International Centre for Genetic Engineering and Biotechnology, 34012 Trieste, Italy. [4]Australian Cancer Research Foundation Genetics Laboratory, John Curtin School of Medical Research, Australian National University, Australia & Australian Phenomics Facility, Canberra, ACT 2601, Australia. [5]Weatherall Institute of Molecular Medicine, Oxford University, Oxford OX3 9DS, UK. [6]Brunel Institute of Cancer Genetics and Pharmacogenomics, Brunel University, Uxbridge UB8 3PH, UK.
*These authors contributed equally to this work.

similar repair defect to that in *Lig4*-null cells after 3-Gy γ-irradiation (Fig. 2a, left panel). However, after 1-Gy γ-irradiation, residual repair capacity was observed in *Lig4*^{Y288C} but not in *Lig4*-null MEFs, suggesting that Y288C creates a hypomorphic mutation that markedly impairs LigIV function (Fig. 2a, right panel). The repair defect was fully corrected by wild-type *Lig4* cDNA (Fig. 2b). Western blotting and immunofluorescence showed that LigIV expression was reduced about fivefold in *Lig4*^{Y288C} MEFs (Fig. 2c, and Supplementary Fig. 1a). Low LigIV expression was not due to reduced expression of XRCC4, with which all LigIV is stably complexed[28] (Supplementary Fig. 1b). After immunoprecipitation with anti-XRCC4 antibodies, we observed a fivefold reduction in LigIV levels, but adenylation activity was undetectable, showing *in vivo* activity reduced at least tenfold (Fig. 2d–f). Recombinant human LigIV^{Y288C} interacted efficiently with XRCC4, but adenylation and double-strand break ligation activities of LigIV^{Y288C}–XRCC4 complexes were decreased about twofold (Fig. 2g, h, and Supplementary Fig. 1d–f). Co-expression of LigIV^{Y288C} and XRCC4 in rabbit reticulocyte lysates also showed efficient LigIV^{Y288C}–XRCC4 interaction (Supplementary Fig. 1c). Thus, the mutation affects the expression and catalytic function of LigIV, reducing *in vivo* activity at least tenfold, which is similar to human LigIV syndrome mutations[19,29].

Diminished NHEJ limits cellular proliferation

The mutation severely impaired the proliferation of *Lig4*^{Y288C} MEFs at both 20% O_2 and 3% O_2 (Fig. 3a). To investigate the basis of impaired proliferation, we examined the cells for γ-H2AX and p1981-ATM foci. We observed higher numbers of foci in *Lig4*^{Y288C} MEFs; the foci increased with population doublings (Fig. 3b) and were more frequent and occurred at earlier passages at 20% O_2 than at 3% O_2, suggesting that they arise from oxidative damage. This was not due to differences in ROS levels in the MEFs (Supplementary Fig. 2a). Reduced proliferation was also not attributable to telomere attrition, because the rate of telomere shortening with passage number was similar in wild-type and *Lig4*^{Y288C} MEFs (Fig. 3c), and the γ-H2AX foci in *Lig4*^{Y288C} MEFs were not located at telomeres (Supplementary Fig. 2b). We conclude that the reduced proliferation capacity in *Lig4*^{Y288C} MEFs is due to the specific failure to repair double-strand breaks, probably arising from oxidative DNA damage. To assess whether such damage can arise in non-dividing cells, we maintained passage 1 MEFs in the plateau phase for 4 weeks. Once again, *Lig4*^{Y288C} MEFs accumulated increased γ-H2AX foci, and this time with little protection afforded by lower O_2 tension (Fig. 3d). These findings show that NHEJ is important in repairing double-strand breaks that occur at physiological O_2 tension in both resting and proliferating cells.

NHEJ maintains stem cells during ageing

To examine the role of NHEJ in the maintenance of adult stem cells we focused on haematopoietic stem cells in bone marrow and enumerated the well-defined population of multipotent KLS (c-Kit$^+$, Sca1$^+$, lineage$^-$) cells[30] in *Lig4*^{Y288C} bone marrow. The percentage

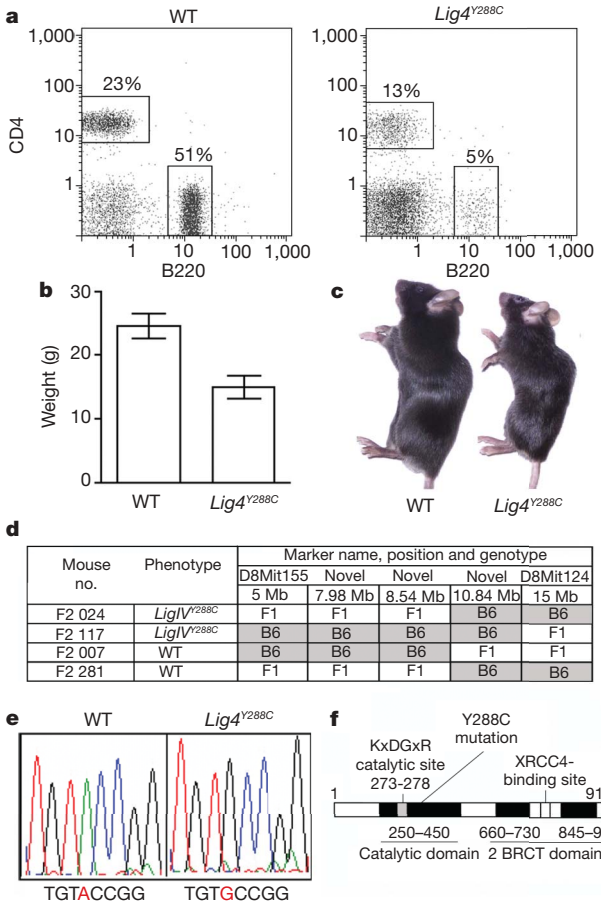

Figure 1 | Identification of an ENU-induced missense substitution in *LigIV* in the *tiny* mouse strain. **a**, Flow cytometry of blood, stained for B220 and CD4, from B6 wild-type (WT) and *Lig4*^{Y288C} homozygous mice. **b**, **c**, Weight (**b**) and size (**c**) of 8-week-old sex-matched *Lig4*^{Y288C} homozygous and wild-type B6 littermates (means and 95% confidence intervals are shown in **b**). **d**, Mapping the phenotype to chromosome 8. **e**, A1067G substitution in *Lig4* cDNA. **f**, Location of the mutation in the domain structure of LigIV.

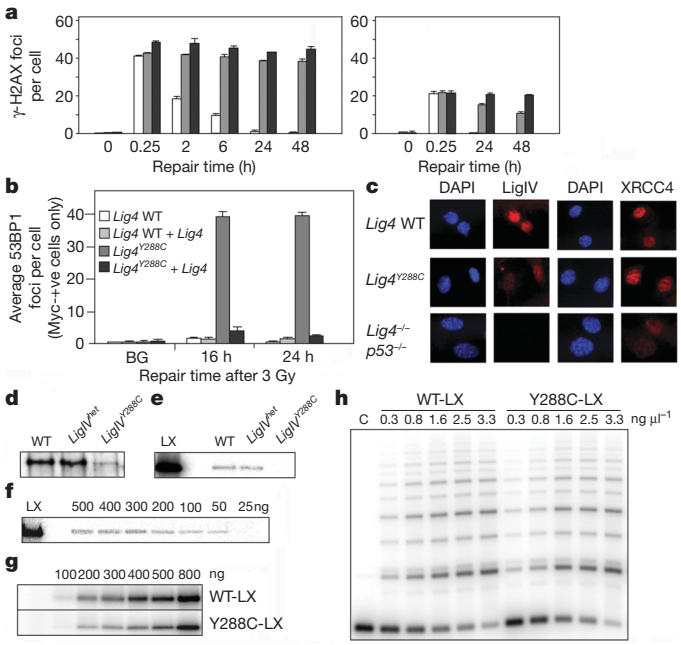

Figure 2 | Impact of the Y288C mutation. **a**, γ-H2AX foci analysis in plateau-phase wild-type (WT; white bars), *Lig4*^{Y288C} (grey bars) or *Lig4*$^{-/-}$*p53*$^{-/-}$ (black bars) MEFs after γ-irradiation at 3 Gy (left) or 1 Gy (right). **b**, Complementation of the double-strand break repair defect in transformed *Lig4*^{Y288C} MEFs after transfection with Myc-tagged WT human *Lig4* cDNA; results are means and s.d. for three experiments. **c**, Immunofluorescence of WT, *Lig4*^{Y288C} and *Lig4*$^{-/-}$*p53*$^{-/-}$ MEFs showing reduced LigIV in *Lig4*^{Y288C} but normal levels of XRCC4. **d**, *Lig4* western blot after co-immunoprecipitation with anti-XRCC4 antibodies from 500 ng of whole cell extract of WT, *Lig4*^{Y288C} heterozygote (*LigIV*^{het}) and homozygote (*LigIV*^{Y288C}) MEFs. **e**, Adenylation activity of the same samples as in **d**, with 300 ng of recombinant LigIV–XRCC4 complex (LX) as control. **f**, Serial dilution of extracts from WT MEFs shows the limit of detectable adenylation activity to be 50 ng of extract. **g**, **h**, Adenylation of insect-cell-expressed human WT and Y288C-LX complexes pretreated with PP_i (**g**), and double-strand break ligation of a 442-base-pair substrate by insect-cell-expressed human WT and Y288C-LX complexes (**h**) (see also Supplementary Fig. 1f).

of KLS cells was within normal range at 5–12 weeks, but was decreased by 20–26 weeks compared with age-matched $Lig4^{+/+}$ ($P < 0.001$) and 5–12-week $Lig4^{Y288C}$ ($P < 0.01$; Fig. 4a, c) mice. This contrasts with the expansion of the KLS population with age in wild-type B6 mice[31]. The loss of the KLS cells correlated with a decline in bone marrow cellularity ($P < 0.01$) and erythrocyte precursors ($P < 0.05$) in the $Lig4^{Y288C}$ mice between 5–12 weeks of age and 20–26 weeks, whereas the marrow cell count was unchanged between 5 and 30 weeks of life in wild-type controls (Fig. 4c).

The KLS population includes $CD34^-Flt3^-$ long-term haematopoietic stem cells, which give rise to $CD34^+Flt3^-$ short-term stem cells and then $CD34^+Flt3^+$ multipotent progenitors (Fig. 4a). At 20–26 weeks, the absolute number of cells was reduced in all KLS subcompartments in $Lig4^{Y288C}$ bone marrow, but $CD34^-Flt3^-$ long-term haematopoietic stem cells were preserved as a percentage of the KLS compartment, and cell loss was most marked in the more rapidly dividing $CD34^+Flt3^+$ multipotent progenitors (Fig. 4b). The relative preservation of long-term haematopoietic stem cells and diminution of multipotent progenitors was also seen in young (7–12-week) $Lig4^{Y288C}$ mice (Supplementary Fig. 3a) and resembles the changes in the KLS subpopulations observed during normal ageing[32].

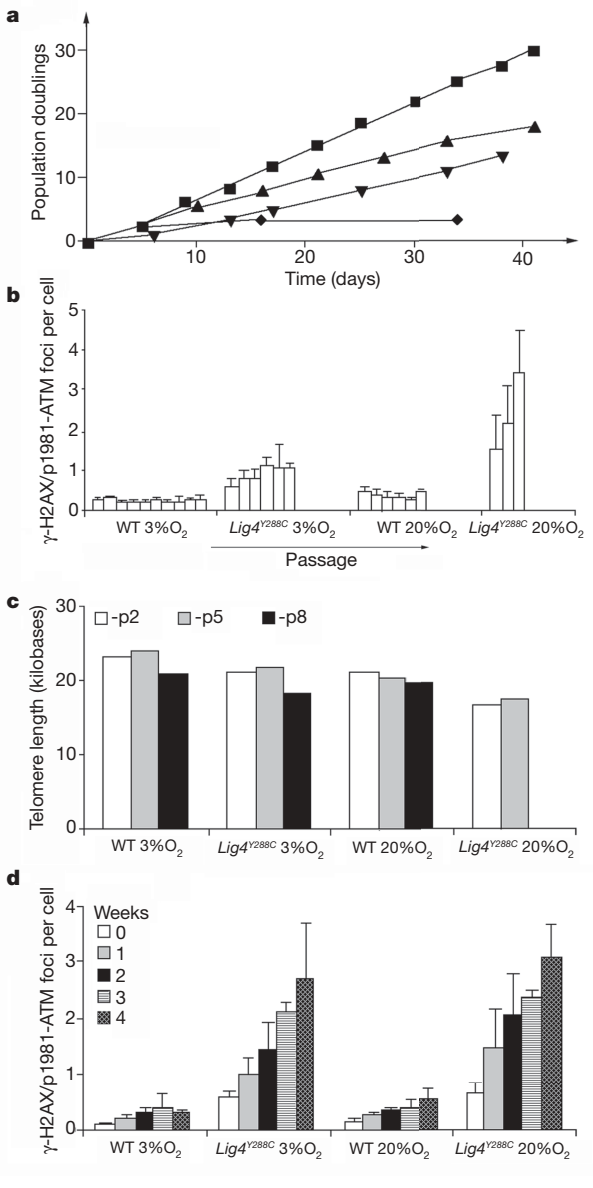

Figure 3 | Double-strand breaks accumulate in $Lig4^{Y288C}$ embryonic fibroblasts independently of replication and confer impaired proliferation. **a**, Cumulative population doublings in wild-type (WT; squares and inverted triangles) and $Lig4^{Y288C}$ homozygous (upright triangles and diamonds) MEFs growing at 20% O_2 (inverted triangles and diamonds) or 3% O_2 (squares and upright triangles). **b**, γ-H2AX and p1981-ATM foci in the same systems as **a**; results are means and s.d. for three experiments. **c**, Telomere length estimated by Flow-FISH in WT and $Lig4^{Y288C}$ MEFs at passages 2 (white bars), 5 (grey bars) and 8 (black bars) at the indicated oxygen tensions. **d**, γ-H2AX and p1981-ATM foci in non-dividing WT and $Lig4^{Y288C}$ MEFs at 20% or 3% O_2 (mean and s.d. of three experiments).

Mechanism of stem cell failure

We next analysed the basis for the failure to maintain haematopoietic stem cell numbers with age in $Lig4^{Y288C}$ mice, by using a range of functional assays. Co-transplantation experiments into irradiated recipients with CD45 allotype-marked bone marrow excluded the possibility that the haematopoietic stem cell defects in $Lig4^{Y288C}$ mice were secondary to abnormalities in bone marrow stroma or macrophages, instead showing that $Lig4^{Y288C}$ marrow had a cell-autonomous deficiency in long-term haematopoietic stem cell function (Fig. 5a). The intrinsic defect in $Lig4^{Y288C}$ bone marrow was not due simply to poor relative expansion of lineage-restricted progeny, because it affected the long-term reconstitution of KLS cells themselves and that of downstream pro-B and granulocyte populations measured at 16 weeks in mice that had been injected with equal numbers of wild-type and $Lig4^{Y288C}$ donor KLS cells (Fig. 5b). In tissue culture, 18–26-week $Lig4^{Y288C}$ bone marrow stem cells also showed greatly impaired performance in the cobblestone-area-forming cell (CAFC) assay (Fig. 5c).

To gauge the competitiveness of $Lig4^{Y288C}$ stem cells *in situ* without removal from their physiological niche or exposure to high O_2 tension in tissue culture, we transferred 5×10^6 CD45.1-marked wild-type B6 bone marrow cells into non-irradiated 10–14-week B6 wild-type and $Lig4^{Y288C}$ recipients. We also transferred CD45.2 wild-type bone marrow into $(CD45.1 \times CD45.2)F_1$ B6 mice to control for immunological rejection against CD45 (ref. 33). Remarkably, transplanted wild-type bone marrow stem cells made a long-term multi-lineage contribution to haematopoiesis in $Lig4^{Y288C}$ recipients such that, by 14–17 weeks after transplantation, $81 \pm 17\%$ of KLS cells in the bone marrow and $92 \pm 2\%$ (mean $\pm$ s.d.) of granulocytes in the blood were donor derived (Fig. 5d). By contrast, little if any measurable stem cell engraftment occurred in wild-type recipients in which the stem cell niche was populated with normal self-renewing haematopoietic stem cells as expected. The competitive replacement of most host $Lig4^{Y288C}$ haematopoietic stem cells by a small number of donor wild-type haematopoietic stem cells indicates that there is a much greater defect in stem cell function than is reflected in steady-state long-term haematopoietic stem cell numbers, the latter possibly being compensated for by increased proliferation. Examination of the rate of turnover of the haematopoietic stem cell populations *in vivo* by the incorporation of bromodeoxyuridine (BrdU) revealed that twice as many KLS and long-term haematopoietic stem cells proliferated during a 40-h period in $Lig4^{Y288C}$ compared with the wild type (Fig. 5e). Taken together with the diminished KLS population with age and the pancytopenia noted in human LigIV syndrome[19], these results show that reduced NHEJ impairs the self-renewal function of long-term adult haematopoietic stem cells.

The decline in number and marked functional impairment of haematopoietic stem cells in $Lig4^{Y288C}$ suggests that, as in the $Lig4^{Y288C}$ embryonic fibroblasts, double-strand breaks arise in haematopoietic stem cells under normal O_2 tensions. We observed increased double-strand breaks in bone marrow from $rag1^{-/-}Lig4^{Y288C}$ mice, showing the impact of the repair defect *in vivo* (see Methods). We observed a similar increase in double-strand breaks in flow-sorted KLS cells from 18-week-old mice (9 out of 572 (1.57%) in $Lig4^{Y288C}$ versus 2 out of 1,917 (0.10%) in wild-type; $\chi^2 = 21.61$, $P < 0.0001$). The low

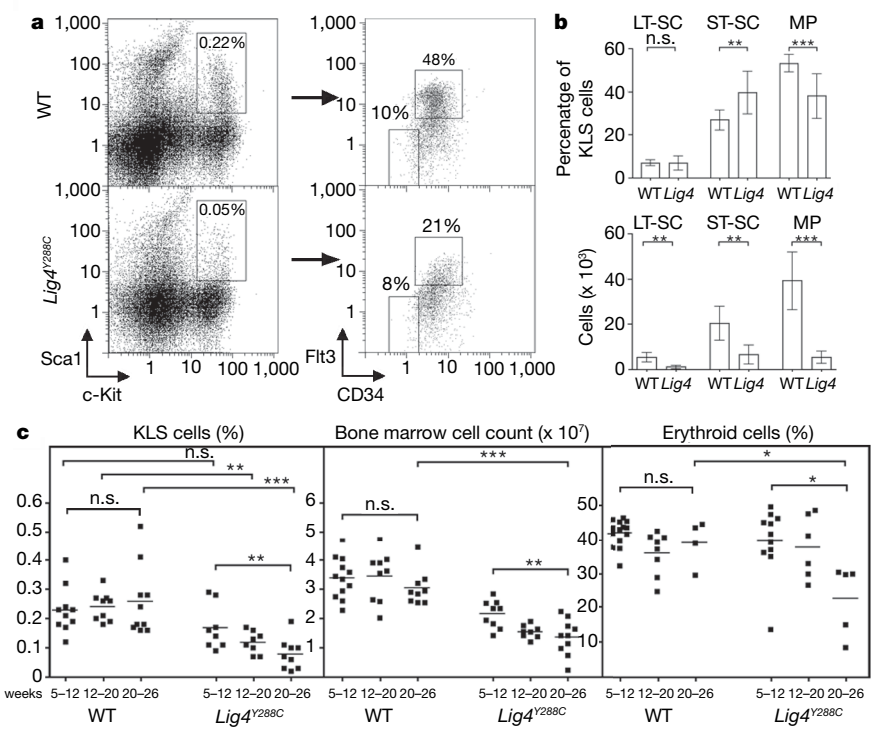

Figure 4 | *Lig4*^{Y288C} impairs the maintenance of adult haematopoietic stem cells. **a**, Flow cytometry of bone marrow cells from 20–26-week B6 homozygous *Lig4*^{Y288C} or wild-type (WT) animals gated on lineage-negative cells (left) and lineage$^-$ Sca1$^+$c-Kit$^+$ KLS cells (right). **b**, CD34$^-$Flt3$^-$ long-term haematopoietic stem cells (LT-SC), CD34$^+$Flt3$^-$ short-term stem cells (ST-SC) and CD34$^+$Flt3$^+$ multipotent progenitors (MP) as a percentage of KLS cells and in absolute number in 20–26-week WT and *Lig4*^{Y288C} (*Lig4*) bone marrow ($n = 9$; means and 95% confidence intervals are shown). **c**, The percentage of KLS cells (left), bone marrow cell count (middle) and percentage of TER119$^+$ erythroid precursor cells (right) in WT and *Lig4*^{Y288C} marrow at different ages. All bone marrow cell counts are for one tibia and femur and are not normalized for body size. n.s., not significant; asterisk, $P < 0.05$; two asterisks, $P < 0.01$; three asterisks, $P < 0.001$ (by analysis of variance (**c**) or *t*-test (**b**)).

frequency of affected cells may be explained by the effective clearance of dying cells in bone marrow or their reduced proliferation potential.

Conclusions

As in the blood system, the longevity of many tissues depends upon continuous regeneration from small pools of self-renewing stem cells. By taking advantage of a unique mouse strain with a hypomorphic *Lig4*^{Y288C} mutation and the highly specific role of LigIV in the repair of DNA double-strand breaks by NHEJ, we have shown that unrepaired DNA damage arising in stem cells under physiological conditions *in vivo* leads to adult stem cell exhaustion over time[2,34]. On the basis of our analysis of MEFs in culture and bone marrow cells *in vivo*, we propose that unrepaired double-strand breaks in KLS cells and their progenitors lead to decreased proliferative potential, increased turnover of the haematopoietic stem cell population, decreased self-renewal and hence age-dependent decline in multipotent cells within the KLS population, which becomes manifested as loss of bone marrow cellularity and erythropoiesis (Fig. 4c), features characteristic of normal ageing[32]. Similar proliferative exhaustion of stem cells has been reported for mice deficient in

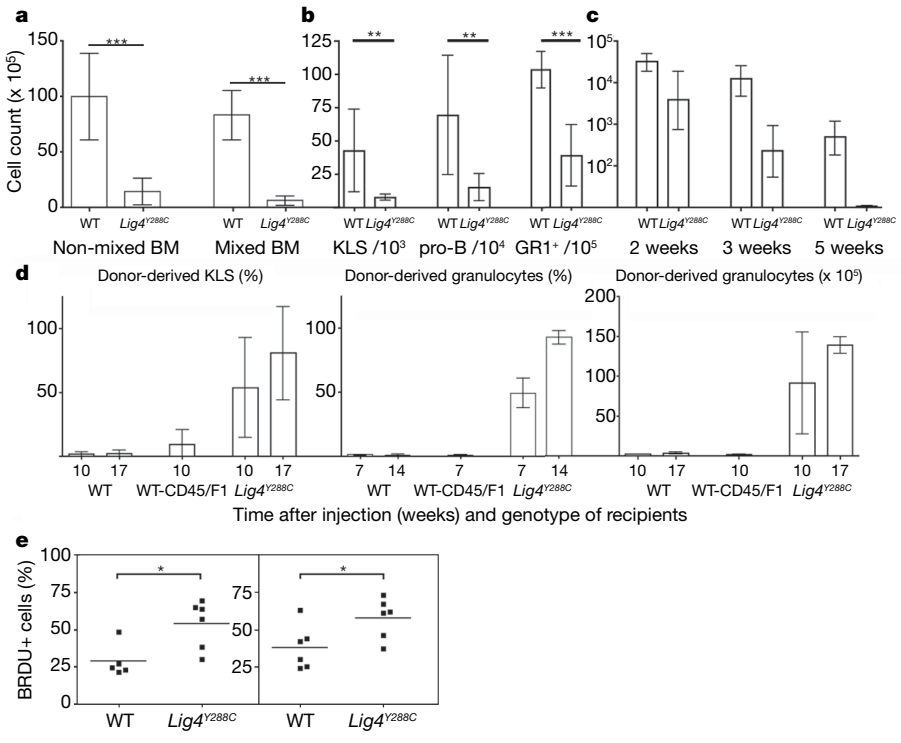

Figure 5 | *Lig4*^{Y288C} impairs the intrinsic function of adult haematopoietic stem cells. **a**, Donor-derived granulocyte (GR1$^+$) count in the bone marrow of irradiated recipients 8 weeks after reconstitution with 5×10^6 CD45 allotype-marked wild-type (WT) or *Lig4*^{Y288C} bone marrow cells (BM), either separately or mixed in 1:1 ratio, donor age 16–26 weeks, $n = 9$–12. **b**, Donor-derived KLS, pro-B (B220$^+$CD43$^+$), and granulocyte (GR1$^+$) cell numbers in the bone marrow of irradiated recipients 16 weeks after reconstitution with either 4×10^6 WT or 9×10^6 *Lig4*^{Y288C} marrow cells (controlled for different KLS cell number), donor age 5–8 weeks, $n = 3$–4. **c**, CAFC number in the bone marrow of 16–26-week WT and homozygous *Lig4*^{Y288C} mice. **d**, Haematopoietic stem cell engraftment into unconditioned *Lig4*^{Y288C} recipients. Results show the percentage of donor-derived KLS cells in the marrow (left) and granulocytes in the blood (middle), and the number of donor-derived granulocytes in the marrow of the recipients (right); $n = 3$–4. Means and 95% confidence intervals are shown. **e**, BrdU incorporation by long-term haematopoietic stem cells (LT-HSCs, left) and KLS cells (right) in age-matched WT or *Lig4*^{Y288C} 7–12-week-old mice over 40 h. All bone marrow cell counts are for one tibia and femur and are not normalized for body size. n.s., non-significant; asterisk, $P < 0.05$; two asterisks, $P < 0.01$; three asterisks, $P < 0.001$ (using *t*-test).

p21 and Gfi-1 (refs 35, 36). It is also possible that stem cells have low thresholds for damage checkpoint activation, exploiting apoptosis or checkpoint arrest to limit the potential harmful impact of genetic damage, which may contribute to their exhaustion during ageing[37,38]. The rate-limiting role for the repair of DNA double-strand breaks in the maintenance of adult stem cells *in vivo*, established here for blood stem cells, implies that inherited or environmental factors that increase oxidative DNA damage may be key determinants of tissue ageing and limiting factors for the efficient transplantation of adult stem cells.

METHODS SUMMARY

ENU mutagenesis and mapping was performed as described previously[26]. Primary unfixed cells were sorted by flow cytometry without prior depletion of lineage-positive cells. Primary MEFs were derived from wild-type and $Lig4^{Y288C}$ embryos, and double-strand break repair was analysed by γ-H2AX foci analysis. Gene Juice was used for transfection experiments. The TNT T7 Quick Coupled Transcription/Translation System (Promega) was used to generate LX complexes in reticulocyte lysates. Recombinant human XRCC4 and histidine-tagged wild-type and $LigIV^{Y288C}$ complexes were expressed in pFastBac vectors and purified from insect cells[39]. Complexes were assessed for function with the use of anti-XRCC4 immunoprecipitation, double-strand ligation and adenylation assays as described previously[19]. Immunofluorescence was used to assess γ-H2AX foci in confluent, non-dividing MEFs[14], and flow-sorted KLS cells were stained with anti-53BP1. Telomere length was measured by fluorescence *in situ* hybridization (FISH) with Flow-FISH[40], and the co-localization of γ-H2AX foci with telomeres was monitored by immuno-FISH. The CAFC assay[41] and single and mixed radiation chimaeras[42] were as described previously. In bone marrow transfers, 5×10^6 CD45.1-marked wild-type B6 bone marrow cells were intravenously injected into non-irradiated CD45.2-marked wild-type and CD45.2-marked $Lig4^{Y288C}$ B6 mice; and CD45.2-marked wild-type cells were injected into CD45.1 × CD45.2 F_1 wild-type recipients to control for immunological rejection[33]. Cell turnover was assessed in mice injected once and then fed with BrdU for 40 h (BrdU Flow Kit; BD Pharmingen). Statistical analysis was by analysis of variance or *t*-test with GraphPad Prism 4.00.

Full Methods and any associated references are available in the online version of the paper at www.nature.com/nature.

Received 5 February; accepted 24 April 2007.

1. Weissman, I. L. Stem cells: units of development, units of regeneration, and units in evolution. *Cell* **100,** 157–168 (2000).
2. Park, Y. & Gerson, S. L. DNA repair defects in stem cell function and aging. *Annu. Rev. Med.* **56,** 495–508 (2005).
3. Wang, Y., Schulte, B. A., LaRue, A. C., Ogawa, M. & Zhou, D. Total body irradiation selectively induces murine hematopoietic stem cell senescence. *Blood* **107,** 358–366 (2006).
4. Khanna, K. K. & Jackson, S. P. DNA double-strand breaks: signaling, repair and the cancer connection. *Nature Genet.* **27,** 247–254 (2001).
5. Karanjawala, Z. E., Murphy, N., Hinton, D. R., Hsieh, C. L. & Lieber, M. R. Oxygen metabolism causes chromosome breaks and is associated with the neuronal apoptosis observed in DNA double-strand break repair mutants. *Curr. Biol.* **12,** 397–402 (2002).
6. Weterings, E. & van Gent, D. C. The mechanism of non-homologous end-joining: a synopsis of synapsis. *DNA Repair (Amst.)* **3,** 1425–1435 (2004).
7. Lieber, M. R., Ma, Y., Pannicke, U. & Schwarz, K. Mechanism and regulation of human non-homologous DNA end-joining. *Nature Rev. Mol. Cell Biol.* **4,** 712–720 (2003).
8. Ito, K. *et al.* Regulation of oxidative stress by ATM is required for self-renewal of haematopoietic stem cells. *Nature* **431,** 997–1002 (2004).
9. Sedelnikova, O. A. *et al.* Senescing human cells and ageing mice accumulate DNA lesions with unrepairable double-strand breaks. *Nature Cell Biol.* **6,** 168–170 (2004).
10. Bender, C. F. *et al.* Cancer predisposition and hematopoietic failure in Rad50(S/S) mice. *Genes Dev.* **16,** 2237–2251 (2002).
11. Dumble, M. *et al.* The impact of altered p53 dosage on hematopoietic stem cell dynamics during aging. *Blood* **109,** 1736–1742 (2006).
12. Buck, D. *et al.* Cernunnos, a novel nonhomologous end-joining factor, is mutated in human immunodeficiency with microcephaly. *Cell* **124,** 287–299 (2006).
13. Ahnesorg, P., Smith, P. & Jackson, S. P. XLF interacts with the XRCC4–DNA ligase IV complex to promote DNA nonhomologous end-joining. *Cell* **124,** 301–313 (2006).
14. Riballo, E. *et al.* A pathway of double-strand break rejoining dependent upon ATM, Artemis, and proteins locating to γ-H2AX foci. *Mol. Cell* **16,** 715–724 (2004).
15. Hsu, H. L., Gilley, D., Blackburn, E. H. & Chen, D. J. Ku is associated with the telomere in mammals. *Proc. Natl Acad. Sci. USA* **96,** 12454–12458 (1999).
16. d'Adda di Fagagna, F. *et al.* Effects of DNA nonhomologous end-joining factors on telomere length and chromosomal stability in mammalian cells. *Curr. Biol.* **11,** 1192–1196 (2001).
17. Barnes, D. E., Stamp, G., Rosewell, I., Denzel, A. & Lindahl, T. Targeted disruption of the gene encoding DNA ligase IV leads to lethality in embryonic mice. *Curr. Biol.* **8,** 1395–1398 (1998).
18. Frank, K. M. *et al.* Late embryonic lethality and impaired V(D)J recombination in mice lacking DNA ligase IV. *Nature* **396,** 173–177 (1998).
19. O'Driscoll, M. *et al.* DNA ligase IV mutations identified in patients exhibiting developmental delay and immunodeficiency. *Mol. Cell* **8,** 1175–1185 (2001).
20. Ben-Omran, T. I., Cerosaletti, K., Concannon, P., Weitzman, S. & Nezarati, M. M. A patient with mutations in DNA Ligase IV: clinical features and overlap with Nijmegen breakage syndrome. *Am. J. Med. Genet. A.* **137,** 283–287 (2005).
21. van der Burg, M. *et al.* A new type of radiosensitive TBNK severe combined immunodeficiency caused by a LIG4 mutation. *J. Clin. Invest.* **116,** 137–145 (2006).
22. Enders, A. *et al.* A severe form of human combined immunodeficiency due to mutations in DNA ligase IV. *J. Immunol.* **176,** 5060–5068 (2006).
23. Toita, N. *et al.* Epstein–Barr virus-associated B-cell lymphoma in a patient with DNA ligase IV (LIG4) syndrome. *Am. J. Med. Genet. A* **143,** 742–745 (2007).
24. Gruhn, B. *et al.* Successful bone marrow transplantation in a patient with DNA ligase IV deficiency and bone marrow failure. *Orphanet J. Rare Dis.* **2,** 5 (2007).
25. Sekiguchi, J. M. & Ferguson, D. O. DNA double-strand break repair: a relentless hunt uncovers new prey. *Cell* **124,** 260–262 (2006).
26. Nelms, K. A. & Goodnow, C. C. Genome-wide ENU mutagenesis to reveal immune regulators. *Immunity* **15,** 409–418 (2001).
27. Quwailid, M. M. *et al.* A gene-driven ENU-based approach to generating an allelic series in any gene. *Mamm. Genome* **15,** 585–591 (2004).
28. Grawunder, U. *et al.* Activity of DNA ligase IV stimulated by complex formation with XRCC4 protein in mammalian cells. *Nature* **388,** 492–495 (1997).
29. Girard, P. M., Kysela, B., Harer, C. J., Doherty, A. J. & Jeggo, P. A. Analysis of DNA ligase IV mutations found in LIG4 syndrome patients: the impact of two linked polymorphisms. *Hum. Mol. Genet.* **13,** 2369–2376 (2004).
30. Okada, S. *et al. In vivo* and *in vitro* stem cell function of c-kit- and Sca-1-positive murine hematopoietic cells. *Blood* **80,** 3044–3050 (1992).
31. Morrison, S. J., Wandycz, A. M., Akashi, K., Globerson, A. & Weissman, I. L. The aging of hematopoietic stem cells. *Nature Med.* **2,** 1011–1016 (1996).
32. Rossi, D. J. *et al.* Cell intrinsic alterations underlie hematopoietic stem cell aging. *Proc. Natl Acad. Sci. USA* **102,** 9194–9199 (2005).
33. Bhattacharya, D., Rossi, D. J., Bryder, D. & Weissman, I. L. Purified hematopoietic stem cell engraftment of rare niches corrects severe lymphoid deficiencies without host conditioning. *J. Exp. Med.* **203,** 73–85 (2006).
34. Hasty, P. & Vijg, J. Accelerating aging by mouse reverse genetics: a rational approach to understanding longevity. *Aging Cell* **3,** 55–65 (2004).
35. Cheng, T. *et al.* Hematopoietic stem cell quiescence maintained by p21cip1/waf1. *Science* **287,** 1804–1808 (2000).
36. Hock, H. *et al.* Gfi-1 restricts proliferation and preserves functional integrity of haematopoietic stem cells. *Nature* **431,** 1002–1007 (2004).
37. Orelio, C. & Dzierzak, E. Bcl-2 expression and apoptosis in the regulation of hematopoietic stem cells. *Leuk. Lymphoma* **48,** 16–24 (2007).
38. Becker, K. A., Stein, J. L., Lian, J. B., van Wijnen, A. J. & Stein, G. S. Establishment of histone gene regulation and cell cycle checkpoint control in human embryonic stem cells. *J. Cell. Physiol.* **210,** 517–526 (2007).
39. Marchetti, C. *et al.* Identification of a novel motif in DNA ligases exemplified by DNA ligase IV. *DNA Repair (Amst.)* **5,** 788–798 (2006).
40. Cabuy, E., Newton, C., Roberts, T., Newbold, R. & Slijepcevic, P. Identification of subpopulations of cells with differing telomere lengths in mouse and human cell lines by flow FISH. *Cytometry A* **62,** 150–161 (2004).
41. Rodrigues, N. P. *et al.* Haploinsufficiency of GATA-2 perturbs adult hematopoietic stem-cell homeostasis. *Blood* **106,** 477–484 (2005).
42. Vinuesa, C. G. *et al.* A RING-type ubiquitin ligase family member required to repress follicular helper T cells and autoimmunity. *Nature* **435,** 452–458 (2005).

Supplementary Information is linked to the online version of the paper at www.nature.com/nature.

Acknowledgements We thank I. Weissman, D. Rossi, P. Papathanasiou, F. Alt, C. Yan, A. Gennery and A. Enders for comments and for exchanging unpublished findings. This work was supported by the Wellcome Trust, the Medical Research Council, the Human Frontiers Science Programme and EU grants. R.J.C. is a Wellcome Trust Senior Clinical Fellow.

Author Information Reprints and permissions information is available at www.nature.com/reprints. The authors declare no competing financial interests. Correspondence and requests for materials should be addressed to P.A.J. (p.a.jeggo@sussex.ac.uk) or R.J.C. (richard.cornall@ndm.ox.ac.uk).

METHODS

ENU mutagenesis. ENU mutagenesis was performed as described previously[26]. Experiments were approved by the Australian National University Animal Ethics and Experimentation Committee, and by the Oxford University Ethical Review Committee and UK Home Office Licence.

Complementation. Transformed *Lig4*^{Y288C} MEFs were transfected three times by using Gene Juice with Myc-tagged human *Lig4* cDNA cloned into a pCI-puro(myc) plasmid. Transfectants, identified by using the Myc tag, were scored for 53BP1 foci formation at the indicated times after exposure to 3 Gy of γ-radiation. 53BP1 rather than γ-H2AX foci were analysed because of the availability of secondary antibody, but control experiments have shown that the two analyses provide identical results. The transfection frequency was 10%. Results are the means and s.d. for three experiments.

Immunofluorescence for LigIV and XRCC4 expression. MEFs from the wild-type, *Lig4*^{Y288C} and *Lig4*-null mice (*Lig4*$^{-/-}$*p53*$^{-/-}$) were stained with anti-LigIV and anti-XRCC4 antibodies from Serotec.

Biochemical procedures. Preparation of whole cell extracts, anti-XRCC4 immunoprecipitation and adenylation of the endogenous LigIV were performed as described previously[19]. Because LX complexes expressed *in vivo* are pre-adenylated, immunoprecipitated complexes were pretreated with 5 mM disodium pyrophosphate (PP_i), as described previously, before the addition of labelled ATP to monitor adenylation activity[19]. Specific antibodies used for immunoprecipitation and the western blots were anti-XRCC4 (AHP387) and anti-DNA LigIV (AHP554) (Serotec).

The Promega TNT T7 Quick Coupled Transcription/Translation System was used for transcription and translation of LX complexes *in vitro*, as in Supplementary Fig. 1c. The vector pcDNA3 (Invitrogen) expressing wild-type human XRCC4 or human LigIV was used in these experiments and for site-directed mutagenesis.

pFastBac vectors expressing untagged human XRCC4 and histidine-tagged LigIV wild-type and Y288C mutant in insect cells were used to generate wild-type and Y288C LigIV–XRCC4 complexes.

Protein expression and purification were performed as described previously[39]. The concentration of the LigIV–XRCC4 complexes was determined by ultraviolet absorption measurements, with an extinction coefficient at 280 nm of 121,330 M^{-1} cm^{-1} estimated from the amino acid sequence (ProtParam, available at http://www.expasy.ch/). The adenylation and double-strand ligation assays with recombinant LigIV–XRCC4 complexes were as described previously[39]. For adenylation assays, wild-type and Y288C protein complexes were pretreated with 5 mM PP_i. For double-strand ligation assays, 20 ng of a 442-base-pair (bp) double-stranded DNA fragment with 4-bp overhangs at each end was produced from the pBluescript plasmid (Stratagene), 5′-end-labelled and incubated with LigIV–XRCC4 complexes without PP_i pretreatment and in the absence of ATP.

Cell culture and lifespan analysis. Primary MEFs derived from wild-type and *Lig4*^{Y288C} embryos were cultured in DMEM medium containing 15% heat-inactivated FCS. Population doublings (PDs) were determined by counting cell numbers after each passage. At later PDs, rapidly growing transformed cells were evident in some populations. Data shown for PDs are before such outgrowth. The results shown represent a single experiment but similar results were obtained in three independent experiments.

Foci analysis *in vitro*. Foci analysis was undertaken in non-dividing confluent cells as described previously[14]. Specific antibodies used were anti-phospho-H2AX (Ser 139) mouse monoclonal (Upstate Cell Signalling Solutions) and anti-ATM pS1981 (rabbit) (Rockland Immunochemicals). The γ-H2AX and p1981ATM foci counts were nearly identical in all experiments.

Examination of bone marrow cells for unrepaired double-strand breaks *in vivo*. Bone marrow cells were extracted from *rag1*$^{-/-}$*Lig4*^{Y288C} mice to establish whether double-strand break DNA damage accumulated in *Lig4*^{Y288C} cells independently of the activity of RAG (recombinase-activating gene) *in vivo*. Cells were carefully deposited on coverslips after cytospinning and were examined with anti-γ-H2AX (Ser 139) mouse monoclonal (Upstate Cell Signalling Solutions), polyclonal rabbit anti-53BP1 (Bethyl), anti-rabbit Cy3 and anti-mouse fluorescein isothiocyanate (FITC) (Dako) antibodies. Cells with overlapping foci for both markers were then scored. Previous analysis with MEFs exposed to ionizing radiation has shown that γ-H2AX and 53BP1 foci analysis yield identical results. This procedure decreased problems with background signal from each single antibody. Positive cells normally displayed only one or two foci per cell. Bone marrow cells were examined from four *rag1*$^{-/-}$*Lig4*^{Y288C} and four *rag1*$^{-/-}$*Lig4*^{WT} mice. The age of the mice ranged from 9 to 13 weeks, and mice were age- and sex-matched between the groups. Using this approach we found a mean of 0.3% cells with foci in total bone marrow from *rag1*$^{-/-}$*Lig4*^{WT} mice (individual percentages 0 out of 525, 0.26%, 0.29% and 0.8%), in contrast with 2.6% of cells in *rag1*$^{-/-}$*LigIV*^{Y288C} mice (individual percentages 0.7%, 2.1%, 2.6% and 5.6%).

For analysis of KLS cells, cold 10,000–50,000 unfixed stained KLS cells were sorted from whole bone marrow, without previous depletion, with a MoFlow Cytometer (Dako Cytomation) into a volume of 0.2 ml and were cytospun and stained with polyclonal rabbit anti-53BP1 and anti-rabbit FITC. Sorting yielded similar numbers of cells with foci to whole bone marrow (see the text). In this analysis only cells displaying 53BP1 foci were scored, because the use of fluorescent antibodies during FACS sorting excluded the use of multiple fluorochromes.

ROS detection. Analysis was undertaken on confluent cells grown in 3% O_2 using the Image-iT LIVE green ROS detection kit (Molecular Probes). Essentially, cells were labelled with or without 10 μM 2′,7′-dichlorodihydrofluorescein diacetate (H2DCFDA). After washing, the relevant cells were treated with 0.5 M *tert*-butyl hydroperoxide, a stable agent that induces oxidative damage providing a positive control. After further washing, cells were trypsin-treated, fixed and analysed by flow cytometry for measurement of H2DCFDA fluorescence.

Telomere analysis. Telomere length was measured by Flow-FISH as described previously[40]. Co-localization of γ-H2AX foci with telomeres was examined by a standard immuno-FISH procedure, staining γ-H2AX with monoclonal anti-phospho-H2AX antibody (Upstate), followed by the FISH protocol using Cy3-labelled telomeric probe. No chromosome aberrations, telomere/break fusions or loss of telomeric signals in individual chromosomes were observed by Q-FISH.

Flow cytometry. The following anti-mouse monoclonal antibodies were used: FITC antibodies against CD34 (RAM34), CD45.1 (A20), GR1 (RB6-8C5) (all from BD Pharmingen), B220, CD4, CD8, CD11b/MAC1 (all from Caltag), phycoerythrin (PE) anti-Sca1 (E13-161.7), allophycocyanin (APC) anti-c-Kit (2B8), biotin anti-TER119 (all from BD Pharmingen), biotin anti-Flt3 (A2F10, eBioscience), PE-Cy7 anti-c-Kit (2B8, Insight Biotech) and AlexaFluor-647 anti-CD34 (RAM34, Insight Biotech). Unconjugated rat anti-mouse lineage markers (BD Pharmingen), tricolour goat anti-rat IgG_1 (Caltag), streptavidin-tricolour (Caltag) and streptavidin-APC-Cy7 (BD Pharmingen) were also used. The data were collected with a FACSCanto (Becton Dickinson).

Bone marrow chimaeras. CD45 allotype-marked B6 mice were γ-irradiated with two 4.5-Gy doses 3 h apart, and injected intravenously with CD45.1-WT and CD45.2-*Lig4*^{Y288C} bone marrow cells, either separately or mixed in a 1:1 ratio. Either 5×10^6 cells were injected into each recipient (Fig. 5a) or more *Lig4*^{Y288C} cells were injected to control for the reduced proportion of KLS cells in the *Lig4*^{Y288C} donor bone marrow cells (Fig. 5b). The recipients were kept on 0.25 mg ml^{-1} amoxycillin.

Bone marrow transfers. CD45.1-WT B6 bone marrow cells (5×10^6) were intravenously injected into non-irradiated CD45.2-WT and CD45.2-*Lig4*^{Y288C} B6 mice; CD45.2-WT cells were injected into CD45.1 × CD45.2 F_1 wild-type recipients to control for immunological rejection[33].

BrdU incorporation. Mice were injected with 1.5–3.0 mg of BrdU in PBS (1 mg per 10 g body weight), and fed with BrdU at 1 mg ml^{-1} in drinking water, protected from light and supplemented with 1% glucose to prevent taste aversion, for 40 h. BrdU incorporation was assessed with a FITC BrdU Flow Kit (BD Pharmingen) in accordance with the manufacturer's protocol.

CAFC assay. The CAFC assay was performed as described previously[41].

Statistical analysis. Analysis of variance or *t*-test was performed with GraphPad Prism 4.00 (GraphPad Inc.).

LETTERS

The hottest planet

Joseph Harrington[1,2], Statia Luszcz[2,3], Sara Seager[4], Drake Deming[5] & L. Jeremy Richardson[6]

Of the over 200 known extrasolar planets, just 14 pass in front of and behind their parent stars as seen from Earth. This fortuitous geometry allows direct determination of many planetary properties[1]. Previous reports of planetary thermal emission[2–5] give fluxes that are roughly consistent with predictions based on thermal equilibrium with the planets' received radiation, assuming a Bond albedo of ~0.3. Here we report direct detection of thermal emission from the smallest known transiting planet, HD 149026b, that indicates a brightness temperature (an expression of flux) of 2,300 ± 200 K at 8 μm. The planet's predicted temperature for uniform, spherical, blackbody emission and zero albedo (unprecedented for planets) is 1,741 K. As models with non-zero albedo are cooler, this essentially eliminates uniform blackbody models, and may also require an albedo lower than any measured for a planet, very strong 8 μm emission, strong temporal variability, or a heat source other than stellar radiation. On the other hand, an instantaneous re-emission blackbody model, in which each patch of surface area instantly re-emits all received light, matches the data. This planet is known[6–9] to be enriched in heavy elements, which may give rise to novel atmospheric properties yet to be investigated.

The dimming of infrared light as a planet passes behind its star (secondary eclipse) yields the planet's intrinsic day-side emission, which can be expressed as a brightness temperature (see Fig. 1, and its legend for definition of several variables). We observed a secondary eclipse of HD 149026b on 24 August 2005 with the 8 μm channel of the Infrared Array Camera[10] on the Spitzer Space Telescope[11]. The instrument is very stable, but operates near its limits for this observation. We correct several instrumental effects with a model, detailed in the Supplementary Information, that achieves over 80% of the photon-limited signal-to-noise ratio. Figure 2 presents binned, raw photometry showing that the eclipse is evident even without this analysis model. Figure 3 shows the eclipse with two different binnings, after removing instrumental effects. The Supplementary Information also presents unbinned plots, the photometric data in machine-readable format, and the details of a method for calculating T_b without reference to the uncertain system distance. Table 1 gives the model fit results, including the unexpectedly large eclipse depth. Figure 4 shows that even an $F = 1$, $A = 0$, uniform, blackbody model is unlikely to explain that depth.

An $A = 0$, $F = 3/8$ (instantaneous re-emission), local, blackbody model matches the data well. Here, local thermal equilibrium with the incoming stellar radiation determines the temperature of each point on the planetary surface. This model has a substellar temperature of nearly 2,500 K and $T_{eq} = 2{,}200$ K. This scenario is plausible if the bulk of stellar energy is absorbed in an atmospheric region where the re-radiation timescale is much shorter than the timescale needed to advect heat around the planet[12]. A team (including us) recently observed[13] the latter condition on the non-transiting hot-Jupiter planet υ Andromedae b, although an albedo was not robustly determined.

If the planetary spectrum were that of a blackbody, the zero-albedo, instantaneous re-radiation T_{eq} would match the reported T_b. The spectrum could resemble a blackbody if most of the absorption occurred in a thick cloud of high-temperature condensates. Both the high metallicity of the parent star[6] ([Fe/H] = +0.36) and the enriched planetary composition[6–9] argue for a complex atmospheric chemistry. Condensing iron and forsterite are predicted for ~1,100 K exoplanets[14,15]. These materials are common in terrestrial rocks and, even as liquids, have plausibly low reflectivity. However, they are not expected to condense at 2,300 K, so this model is not attractive. Furthermore, most models of hot-Jupiter spectra depart significantly from a blackbody. For a variety of temperatures and atomic abundances, water vapour is the most spectroscopically active molecule expected in the 8 μm region, but it appears as an absorber that suppresses the spectrum there.

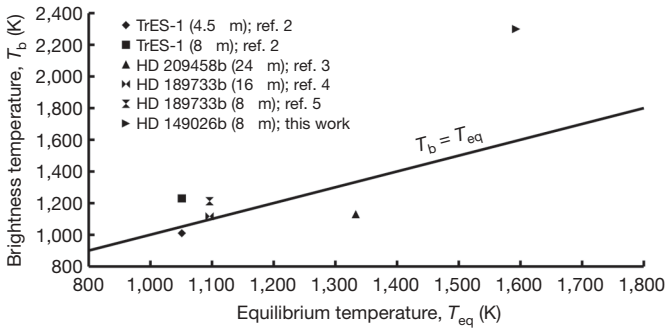

Figure 1 | Comparison of exoplanetary brightness T_b versus equilibrium temperatures T_{eq} for a Bond albedo (wavelength-independent reflectivity) A of 0.3 and uniform planetary emission. T_b is the temperature of a blackbody that would produce the same flux as was measured in a given filter. It is a statement of the measured flux (see Supplementary Information). Variations in T_b with wavelength are deviations from a blackbody spectrum, and yield insight into atmospheric properties. The effective temperature T_{eff} is that for which a blackbody would emit the same total flux as measured from the body. One can predict T_{eff} by assuming a value for A and balancing incoming stellar radiation with blackbody thermal emission at $T_{eq} = T_* \left(\frac{1-A}{4F}\right)^{1/4} \left(\frac{R_*}{a}\right)^{1/2}$, where T_* and R_* are the stellar T_{eff} and radius, respectively, a is the distance between the planet and the star, and F is equivalent to the fraction of the planet's surface that emits at T_{eq}. $F = 1$ for uniform planetary emission, $F = 1/2$ for uniform hemispheric emission (which is unphysical), and $F = 3/8$ for instantaneous re-emission of absorbed radiation without advection. In the latter case, each element of the surface acts as an isolated blackbody with its own temperature. Alternatively, if one assumes that $T_b = T_{eq}$, one can estimate A, to the extent that the planet's spectrum matches that of a blackbody. Objects named in the key (TrES-1, HD 149026b, and so on) are extrasolar planets.

[1]Department of Physics, University of Central Florida, Orlando, Florida 32816-2385, USA. [2]Center for Radiophysics and Space Research, Cornell University, Ithaca, New York 14853-6801, USA. [3]Department of Astronomy, University of California, Berkeley, California 94720-3411, USA. [4]Departments of Earth, Atmospheric, and Planetary Sciences and of Physics, Massachusetts Institute of Technology, Cambridge, Massachusetts 02139, USA. [5]Planetary Systems Laboratory, Code 693. [6]Exoplanet and Stellar Astrophysics Laboratory, Code 667, NASA's Goddard Space Flight Center, Greenbelt, Maryland 20771-0001, USA.

An alternative explanation for the high 8 μm T_b is thermal emission from an inversion layer (a region where temperature increases with altitude). Emission from H_2O could then create a high day-side T_b, while the planet's T_{eff} remained consistent with uniform redistribution of the incident stellar irradiation (≤1,741 K). Because one expects the stellar radiation to heat mainly the lower regions of the atmosphere, a very strong absorbing gas or solid species must act at altitude to create this inversion.

Fortney *et al.*[7] raised the possibility that TiO and VO gas molecules in an atmosphere enriched in heavy elements are the absorbers responsible for the inversion layer. This model predicts a contrast ratio for uniform emission of 0.00067, approaching within 1.4σ of our measurement, for solar levels of Ti, ten times the solar abundance of other heavy elements, and uniform planetary emission. Two other models of ref. 7 match our observation very well. However, the paper also notes that TiO should condense at a temperature minimum much deeper than the levels observed here, in a cold trap. The air above that level should be dry of TiO, just as Earth's stratosphere is dry due to trapping of water below the tropopause. The matching models both have abundant TiO at altitude, violating the cold trap, and it is not yet clear whether even the solar level of Ti is consistent with a cold trap. The TiO scenario could work, however, if the temperature is above the TiO condensation point at all depths, which may be plausible. A detailed investigation of TiO and VO is warranted, coupled to age-dependent luminosity models under high metallicity that may cause a hotter adiabat[16], and atmospheric circulation models that will clarify the temperature distribution in the lower atmosphere[17].

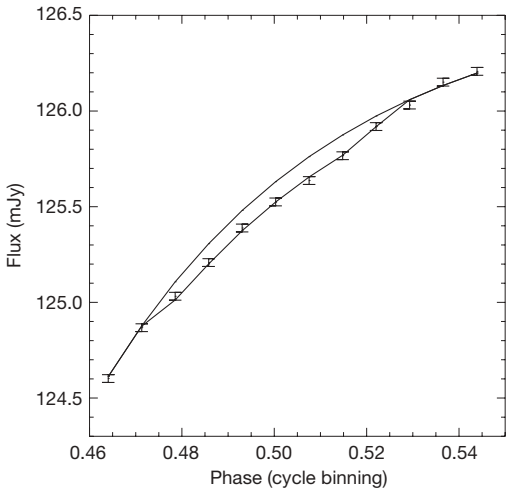

Figure 2 | Unprocessed photometric light curve for the 8 μm secondary eclipse of HD 149026b. Each point is the average of ~4,000 frames taken in exactly one cycle of nine telescope positions. This binning eliminates several instrumental effects from the plot, allowing the eclipse (lowest line and data points) to be distinguished from the fitted stellar model without an eclipse (top line). Phase refers to the orbit, where 0.5 is halfway between transits. The overall rise in the signal is a known instrumental effect[2,5] that we model by fitting an asymptotic function with three free parameters (top line, see Supplementary Information). It is removed in Fig. 3. Error bars and uncertainties throughout the paper are 1σ. The star is bright, but use of the 32 × 32-pixel subarray mode, a 0.4 s frame rate, and a nine-position, non-random dither pattern avoided saturating the detector. We cycled the telescope around the dither pattern 12 times and took 448 frames at each visit to a position. The six-hour sequence produced 48,145 usable images. Aperture photometry of each image produced a time series for the event. We account for sub-pixel motions of the stellar image by subdividing each pixel and including only the portion that falls inside the aperture or sky annulus, as appropriate. The Supplementary Information describes the photometry and analysis in detail, including the modelling and removal of several previously unidentified systematics. The modelling was necessary to obtain accurate timing, but the eclipse depth derived by an independent analysis (by us) without the model for new systematics agrees closely with that presented here. We used a different functional form for the overall signal rise in that analysis, as a consistency check.

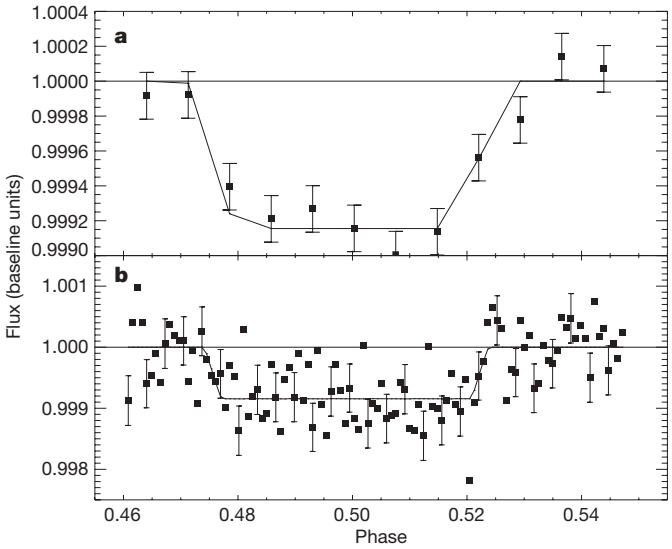

Figure 3 | Binned light curves, corrected for instrumental effects (see Supplementary Information). a, Same bins, horizontal axis, and lines as Fig. 2. **b**, One bin per telescope pointing, 108 in all, with only representative 1σ error bars for clarity. Unity on the vertical axis represents the system flux outside of eclipse. The eclipse model is a series of five line segments: two that are constant before and after the eclipse, one that is constant at the in-eclipse level, and two mirror-symmetric segments that connect the other three. The latter represent the planet's crossing of the stellar limb with sufficient accuracy for our purposes. The eclipse's mid-time, duration, and fractional depth are free parameters. The duration of stellar limb crossing was not well determined, so we fixed it at a nominal value. We fitted only to unbinned data. For plotting purposes, we evaluated the fitted eclipse model at the time of each data point, binned it identically to the data, and connected those points with line segments. The plotted line is thus a binned version of the model, not the model itself.

If the eclipse mid-time of a transiting planet is not exactly centred between transit times (orbital phase = 0.5), it indicates either a non-circular orbit, perturbations by other planets in the system[18], or (for small time offsets) an offset hotspot on the day side of the planet[19,20]. Our eclipse mid-time is heliocentric Julian date (HJD) 2,453,606.960 ± 0.001. We received an ephemeris for the planet from the team of ref. 21 that adds several unpublished, ground-based observations to those already published[6,22] to predict a substantially more precise mid-transit time of HJD 2,453,606.962 ± 0.001, including a 42 s correction for light-travel time across the orbit of HD 149026b. This prediction is consistent with our measurement at the 1σ level.

We emphasize that our single measurement is not enough to confirm any one atmospheric scenario. Alternative scenarios for the high T_b should be investigated, such as tidal heating[23] and spatio-temporal variability around a lower average flux[24]. A recent spectrum[25] of

Table 1 | Model parameters

Parameter	Value	1σ uncertainty		S/N
Planet-star contrast, f	0.00084	−0.00012	+0.00009	7.9
Eclipse centre, t_c	−0:02:58	−0:02:30	+0:01:40	1,994
Eclipse duration, t_d	3:13:12	−0:03:33	+0:04:08	50
Eclipse limb-crossing time, t_x	0:11:49.98	Fixed	Fixed	···
Rise-time offset (phase), t_0	0.251	−0.012	+0.006	27
Rise goal (μJy), l	126,862	−40	+56	2,621
Rise exponent (phase^{-1}), m	19.50	−1.2	+0.7	21

S/N is the signal (or systematic error parameter)-to-noise ratio, where N = half of the 1σ uncertainty range. The eclipse centre is the time relative to ephemeris phase 0.5, corrected for light-travel time (see text). Times are in h:mm:ss format. The eclipse duration is from half-light to half-light; add t_x for the duration from first to last contacts. See Supplementary Information for the variables; t_0, l and m are parameters for the rise in Fig. 2. Eclipse centre S/N is relative to the full orbit period of 2.876 days.

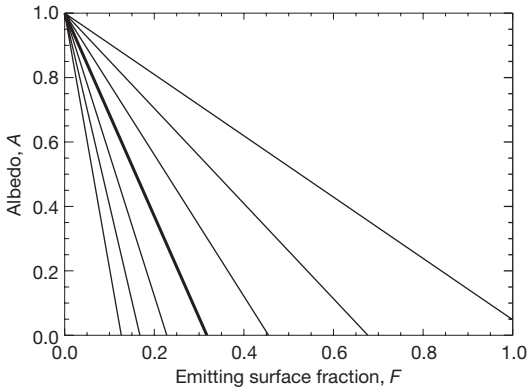

Figure 4 | Equilibrium temperature parameters. We refer to the assumptions described in Fig. 1. The lines show the relationship between A and F for a given T_{eq}. The bold line is our calculated T_b and the others are spaced at 1σ intervals. The line representing the data does not approach the lower-right corner, ruling out the often-assumed uniform blackbody emission at the 3σ level, even for 5% albedo.

HD 209458b tentatively shows a small emission peak in our bandpass, but the feature is too narrow and weak to explain HD 149026b's enhanced brightness on its own. Indeed, it was not identified in a spectrum[26] of HD 189733b. We thus call for further measurements of HD 149026b, at 8 μm to search for variability, and at other wavelengths to test the inversion interpretation by searching for departures from blackbody emission.

Received 28 January; accepted 17 April 2007.
Published online 9 May 2007.

1. Charbonneau, D., Brown, T. M., Burrows, A. & Laughlin, G. in *Protostars and Planets V* (eds Reipurth, B., Jewitt, D. & Keil, K.) 701–716 (Univ. Arizona Press, Tucson, Arizona, 2007).
2. Charbonneau, D. *et al.* Detection of thermal emission from an extrasolar planet. *Astrophys. J.* **626,** 523–529 (2005).
3. Deming, D., Seager, S., Richardson, L. J. & Harrington, J. Infrared radiation from an extrasolar planet. *Nature* **434,** 740–743 (2005).
4. Deming, D., Harrington, J., Seager, S. & Richardson, L. J. Strong infrared emission from the extrasolar planet HD 189733b. *Astrophys. J.* **644,** 560–564 (2006).
5. Knutson, H. A. *et al.* A map of the day-night contrast of the extrasolar planet HD 189733b. *Nature* **447**, 183–186 (2007).
6. Sato, B. *et al.* The N2K Consortium. II. A transiting hot Saturn around HD 149026 with a large dense core. *Astrophys. J.* **633,** 465–473 (2005).
7. Fortney, J. J., Saumon, D., Marley, M. S., Lodders, K. & Freedman, R. S. Atmosphere, interior, and evolution of the metal-rich transiting planet HD 149026b. *Astrophys. J.* **642,** 495–504 (2006).
8. Ikoma, M., Guillot, T., Genda, H., Tanigawa, T. & Ida, S. On the origin of HD 149026b. *Astrophys. J.* **650,** 1150–1159 (2006).
9. Broeg, C. & Wuchterl, G. The formation of HD 149026b. *Mon. Not. R. Astron. Soc.* **376,** L62–L66 (2007).
10. Fazio, G. G. *et al.* The Infrared Array Camera (IRAC) for the Spitzer Space Telescope. *Astrophys. J. Suppl.* **154,** 10–17 (2004).
11. Werner, M. W. *et al.* The Spitzer Space Telescope Mission. *Astrophys. J. Suppl.* **154,** 1–9 (2004).
12. Seager, S. *et al.* On the dayside thermal emission of hot Jupiters. *Astrophys. J.* **632,** 1122–1131 (2005).
13. Harrington, J. *et al.* The phase-dependent infrared brightness of the extrasolar planet υ Andromedae b. *Science* **314,** 623–626 (2006).
14. Cooper, C. S., Sudarsky, D., Milsom, J. A., Lunine, J. I. & Burrows, A. Modeling the formation of clouds in brown dwarf atmospheres. *Astrophys. J.* **586,** 1320–1337 (2003); erratum **595,** 573 (2003).
15. Fortney, J. J. The effect of condensates on the characterization of transiting planet atmospheres with transmission spectroscopy. *Mon. Not. R. Astron. Soc.* **364,** 649–653 (2005).
16. Burrows, A., Hubeny, I., Budaj, J. & Hubbard, W. B. Possible solutions to the radius anomalies of transiting giant planets. *Astrophys. J.* (in the press); preprint at ⟨http://arxiv.org/astro-ph/0612703⟩ (2007).
17. Cooper, C. S. & Showman, A. P. Dynamics and disequilibrium carbon chemistry in hot Jupiter atmospheres, with application to HD 209458b. *Astrophys. J.* **649,** 1048–1063 (2006).
18. Holman, M. J. & Murray, N. W. The use of transit timing to detect terrestrial-mass extrasolar planets. *Science* **307,** 1288–1291 (2005).
19. Williams, P. K. G., Charbonneau, D., Cooper, C. S., Showman, A. P. & Fortney, J. J. Resolving the surfaces of extrasolar planets with secondary eclipse light curves. *Astrophys. J.* **649,** 1020–1027 (2006).
20. Rauscher, E. *et al.* Toward eclipse mapping of hot Jupiters. *Astrophys. J.* (in the press); preprint at ⟨http://arxiv.org/astro-ph/0612412⟩ (2007).
21. Holman, M. J. *et al.* The Transit Light Curve Project. I. Four consecutive transits of the exoplanet XO-1b. *Astrophys. J.* **652,** 1715–1723 (2006).
22. Charbonneau, D. *et al.* Transit photometry of the core-dominated planet HD 149026b. *Astrophys. J.* **636,** 445–452 (2006).
23. Levrard, B. *et al.* Tidal dissipation within hot Jupiters: a new appraisal. *Astron. Astrophys.* **462,** L5–L8 (2007).
24. Rauscher, E., Menou, K., Cho, J. Y.-K., Seager, S. & Hansen, B. Hot Jupiter variability in eclipse depth. *Astrophys. J.* (in the press); preprint at ⟨http://arxiv.org/astro-ph/0612413⟩ (2007).
25. Richardson, L. J., Deming, D., Horning, K., Seager, S. & Harrington, J. A spectrum of an extrasolar planet. *Nature* **445,** 892–895 (2007).
26. Grillmair, C. J. *et al.* A Spitzer spectrum of the exoplanet HD 189733b. *Astrophys. J.* **658,** L115–L118 (2007).

Supplementary Information is linked to the online version of the paper at www.nature.com/nature.

Acknowledgements We thank Spitzer's Director for discretionary time; G. Squires, and the Spitzer staff for rapid proposal handling and scheduling; B. Hansen, C. Lisse, T. Loredo, and W. T. Reach for discussions; and A. Wolf, J. Winn, G. Henry, M. Holman, H. Knutson and D. Charbonneau for discussions and for sharing results before publication. W. Bowman assisted in preparing Fig. 1. We thank C. Markwardt, the Free Software Foundation, W. Landsman, other contributors to the Interactive Data Language Astronomy Library, and the open-source community for software. This work is based on observations made with the Spitzer Space Telescope, which is operated by the Jet Propulsion Laboratory, California Institute of Technology, under a contract with NASA. This material is based upon work supported by the US National Science Foundation and by the US National Aeronautics and Space Administration through an award issued by JPL/Caltech.

Author Information The original data are available from the Spitzer Space Telescope archive, program 254. Reprints and permissions information is available at www.nature.com/reprints. The authors declare no competing financial interests. Correspondence and requests for materials should be addressed to J.H. (jharring@physics.ucf.edu).

LETTERS

High-resolution, high-sensitivity NMR of nanolitre anisotropic samples by coil spinning

D. Sakellariou[1], G. Le Goff[2] & J.-F. Jacquinot[2]

Nuclear magnetic resonance (NMR) can probe the local structure and dynamic properties of liquids and solids, making it one of the most powerful and versatile analytical methods available today. However, its intrinsically low sensitivity precludes NMR analysis of very small samples—as frequently used when studying isotopically labelled biological molecules or advanced materials, or as preferred when conducting high-throughput screening of biological samples or 'lab-on-a-chip' studies. The sensitivity of NMR has been improved by using static micro-coils[1], alternative detection schemes[2,3] and pre-polarization approaches[4]. But these strategies cannot be easily used in NMR experiments involving the fast sample spinning essential for obtaining well-resolved spectra[5,6] from non-liquid samples. Here we demonstrate that inductive coupling allows wireless transmission of radio-frequency pulses and the reception of NMR signals under fast spinning of both detector coil and sample. This enables NMR measurements characterized by an optimal filling factor, very high radio-frequency field amplitudes and enhanced sensitivity that increases with decreasing sample volume. Signals obtained for nanolitre-sized samples of organic powders and biological tissue increase by almost one order of magnitude (or, equivalently, are acquired two orders of magnitude faster), compared to standard NMR measurements. Our approach also offers optimal sensitivity when studying samples that need to be confined inside multiple safety barriers, such as radioactive materials. In principle, the co-rotation of a micrometre-sized detector coil with the sample and the use of inductive coupling (techniques that are at the heart of our method) should enable highly sensitive NMR measurements on any mass-limited sample that requires fast mechanical rotation to obtain well-resolved spectra. The method is easy to implement on a commercial NMR set-up and exhibits improved performance with miniaturization, and we accordingly expect that it will facilitate the development of novel solid-state NMR methodologies and find wide use in high-throughput chemical and biomedical analysis.

According to the principle of reciprocity[7], the experimental parameters crucial for highly sensitive detection of the Faraday induction that gives rise to NMR signals are the ratio between the sample volume and the coil volume (the so-called filling factor), and the temperature and size of the sensor used. The introduction of micro-coils thus substantially improved the detection sensitivity of liquid-state NMR[1] of isotropic fluids, where brownian motion averages orientation-dependent (so-called anisotropic) interactions to yield narrow, chemically resolved spectra. Micro-coils owe much of their broad applicability to the fact that magnetic susceptibility line-broadening can be eliminated by either surrounding the coil with a susceptibility matching liquid, or using specially coated wires[8]. They have had a large effect on combined analytical methods (such as liquid chromatography (LC)-NMR), and even enabled micro-NMR and micro-magnetic resonance imaging (MRI) studies of single neurons[9,10].

Micro-coil NMR has recently also been used on static solid samples[11,12]. But in solids, the averaging of anisotropic interactions—essential if high-resolution spectra with narrow lines are to be obtained—can only be achieved by sample spinning[5,6] (so-called magic-angle spinning, MAS). So far, there is no obvious hardware design for a spinning micro-rotor[13] that would allow a micro-coil with a diameter of typically less than 1 mm to be placed around a sample spun many thousands of turns per second about an axis making the 'magic' angle $\theta = \theta_{MAS}$ of 54.7° with the external static magnetic field. The fact that MAS NMR requires a (static) sensor to be placed next to a rapidly rotating sample is also the reason why alternative detection schemes such as mechanical[3] or optical[2] detection have not yet been used for solid-state NMR: these schemes can only be used with static samples, so any improvement in detection sensitivity comes at the expense of poorer spectral resolution. Similarly, efforts to improve detector performance by lowering its temperature (cryo-cooling) seem very promising[14] but face a major engineering challenge when MAS is involved. Combining cryo-cooling of the detector and MAS will also result in a massive reduction in filling factor due to the need to keep the sample at room temperature. Finally, we note that all previous 'fixed-coil' approaches are optimal for a certain amount of sample filling the coil, and that their sensitivity decreases as smaller samples are used.

Here we present 'magic angle coil spinning' (MACS) as an alternative approach; this uses wireless inductive coupling between the static coil that is normally used for sample spin manipulation and signal reception, and a tuned micro-coil that is co-rotating with the sample container (usually referred to as the 'rotor'). Inductive coupling is a well-known mode of electromagnetic coupling[15] that requires no tethering of wires to the terminals of the coil. It is widely used in telemetry sensors[16], microelectromechanical systems (MEMS)[17], and MRI instrumentation[18] with either standard[19], cryogenically cooled[20] or implanted[21] radio-frequency (RF) coils. In our system, the existing (large) coil of a commercial probe is used to transmit power, and the probe's tuning elements are used to fine-tune the ensemble and achieve impedance matching. The ensemble of the probe coil and the micro-coil thus acts like a rotating transformer, and the rotating sample container becomes an active component in the NMR detection chain. When using static micro-coils, susceptibility effects have been a major source of line broadening, although approaches for eliminating them have been considered[8]. In our method, these effects are largely eliminated simply by placing the coil together with the tuning elements along the magic angle and spinning them. This is because broadening due to isotropic susceptibility effects transforms under rotation like a rank 2 tensor and its time independent part

[1]Laboratoire de Structure et Dynamique par Résonance Magnétique, Service de Chimie Moléculaire (Laboratoire Claude Fréjacques, CNRS URA 331) DSM/DRECAM/SCM, CEA Saclay, Gif-sur-Yvette 91191, France. [2]Service de Physique de l'Etat Condensé (CNRS URA 2464), DSM/DRECAM/SPEC, CEA Saclay, Gif-sur-Yvette 91191, France.

scales with the Legendre polynomial $P_2(\cos\theta)$, therefore most of it averages to zero by positioning and spinning at the magic angle[22].

A sketch of a typical configuration for the MACS apparatus is shown in Fig. 1. The micro-coil is wound around the sample, resulting in a filling factor close to unity. A long ceramic cylinder is tightly fitted inside a commercial rotor, in order to centre the sample-containing capillary that is placed together with a tuning chip capacitor along the axis of rotation. This guarantees constant electromagnetic coupling while spinning. With this set-up and for a wide range of coil geometries, the power originally dissipated in the primary coil is essentially entirely dissipated in the secondary circuit (that is, the micro-coil), as if it were wired up with tethered connections. This holds in the so-called 'over-coupling' regime[15]. The device thus produces high RF field amplitude B_1 per unit current without the introduction of additional noise, because the ensemble is matched to 50 Ω thereby leading to optimal sensitivity. This corresponds to an increase of the induced RF amplitude, for the same amplifier power, with respect to the coil of the MAS probe. This increase depends on the coils' volume ratio. By virtue of the reciprocity principle[7], an equal increase in signal-to-noise ratio (SNR) is obtained. The performance depends non-critically on the difference between the resonant frequency of the micro-coil and the Larmor frequency of the spins, and the enhancement is rather broadband (D.S. and J.-F.J., manuscript in preparation).

Optimized solid-state NMR of mass-limited samples is currently performed using small diameter coils and rotors, but can still suffer from low filling factors and artefact signals from the probe housing and the rotor. Rotating micro-coils can alleviate both drawbacks, as illustrated in Fig. 2. Figure 2a shows the ^{1}H spectrum recorded from a small, powdered sample of L-alanine using a 2.5 mm outer diameter rotor and a 2.5 mm cross-polarization MAS (CPMAS) probe. Subtraction eliminates the background signal due to stator proton signals and residual proton signals from the rotor cap, giving the spectrum in Fig. 2b. The MACS technique was then implemented using a commercial 7 mm CPMAS probe with a 7-mm-diameter rotor and a tuned micro-coil, and a powdered L-alanine sample of ~200 nl. Figure 2c shows the obtained proton spectrum after a π/2 excitation pulse, which can be easily identified as that of L-alanine. The enhancement in RF amplitude with respect to the 7 mm coil of the surrounding probe is of the order of 20, which compares well with the theoretical value expected from electromagnetic calculations. Further experiments to quantify the performance of MACS were conducted (see Supplementary Information for details), with Table 1 providing a summary of the results in terms of sensitivity. MACS offers a signal gain of ~8 even with respect to the 2.5 mm probe. By virtue of the reciprocity principle, the same improvement factor applies to the RF field amplitude: nutation frequencies of 0.5–1 MHz for protons were generated using 50–100 W of RF power.

In solid-state NMR experiments, the size of the anisotropic interactions is usually of the same order of magnitude or even larger than the RF field used to modulate them, and this often results in incomplete averaging. Experiments that use dipolar and quadrupolar decoupling, or broadband single and multiple quantum excitation, could benefit from large RF fields, as the manipulation of the hamiltonian could be treated more rigorously within the perturbation limits. The effect of the improvement in RF field amplitude offered by MACS has been investigated experimentally by exciting non-allowed multiple quantum transitions in inorganic materials (see Supplementary Information).

For biological tissue samples, even extremely low spinning frequency[23] high-resolution MAS (HRMAS) eliminates susceptibility broadenings and yields high-resolution NMR spectra that allow quantification of metabolites[24] in 'metabolomics' profiling studies. Spectra of bovine muscle tissue from a full 7 mm rotor (365 mg of sample) and from a 7 mm rotor having a MACS insert (~0.3 mg of sample), under moderate spinning conditions, are shown respectively in Fig. 3a and b. The resolution in the spectrum using MACS is sufficient (residual line width ~0.05 parts per million, p.p.m., of the static magnetic field) to detect quickly and identify resonances assigned to triglycerides, lactate and phosphocreatine[25]. Even though the presence of spinning sidebands (not visible within the proton chemical shift range of Fig. 3) implies the existence of some residual susceptibility effects, the sensitivity of the technique is demonstrated by the factor of ~22.5 in RF amplitude enhancement (and therefore in signal-to-noise ratio). We note here that the current tendency of

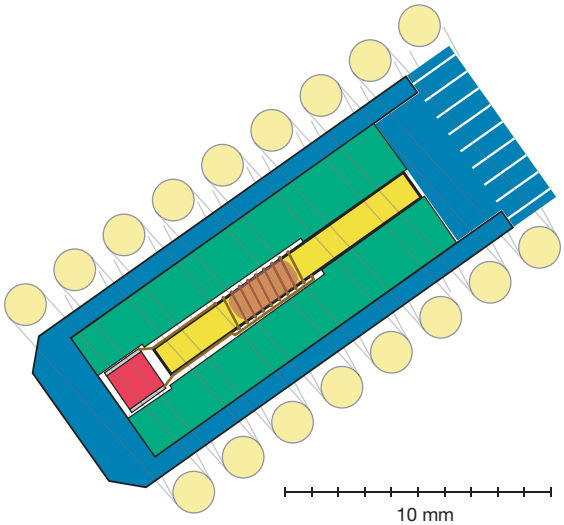

Figure 1 | Schematic diagram of the magic-angle coil spinning (MACS) insert. The sample in ordinary high-resolution solid-state NMR is placed inside a spinning sample holder (rotor in blue), which is pneumatically rotated at many thousands of revolutions per second and surrounded by the coil of the probe (light yellow). When the sample is too small to efficiently fill the rotor, the sensitivity is not optimal. In such cases a tuned micro-coil can be tightly wound around the sample, which is placed inside a glass capillary (dark yellow). A cylindrical ceramic insert (green) is used to keep the capillary and the tuning capacitor (red) centred while spinning. The scale in the figure is used only as an indication of the size of the rotor, as various size micro-coils and capillaries can be used (see Supplementary Information). Wireless coupling between the tuned circuit and the probe electronics generates a high RF field and enhances the detection sensitivity.

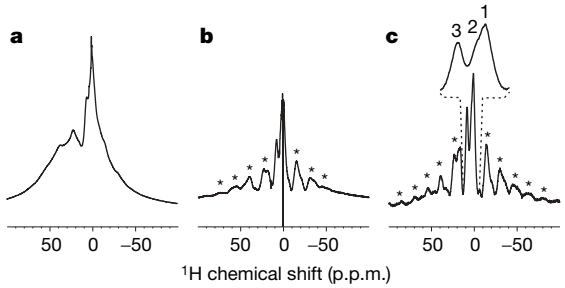

Figure 2 | Sensitivity comparison on ^{1}H (proton) MAS NMR spectra from small samples of powdered L-alanine. a, Spectrum acquired after a π/2 pulse (acquisition time ~12 h), using a standard 2.5 mm rotor. The sample (0.41 mg) was placed in the centre of the rotor. Most of this signal comes from the housing and rotor background, and can be eliminated. **b**, Spectrum after background subtraction (total acquisition time ~24 h), using the same set-up as in **a** (spinning sidebands are labelled with asterisks). The residual signal corresponds to the L-alanine signal plus some artefacts and has a signal-to-noise ratio (SNR) of 270. **c**, Spectrum obtained using the MACS technique on a 7 mm rotor, using 0.15 mg of sample (acquisition time ~8.5 min), after a π/2 pulse. The signal (SNR ≈ 110) comes only from the L-alanine sample and contains a centre band (shown expanded in the inset) and all spinning sidebands at multiples of the spinning frequency.

Table 1 | Sensitivity comparisons between conventional CPMAS probe sizes and MACS

	7 mm system	4 mm system	2.5 mm system	MACS (750 μm coil)
SNR per scan per sample mass (mg^{-1})	2.44	3.22	5.86	45.8
$B_1/\sqrt{P}$ ($mT\,W^{-1/2}$)	0.134	0.166	0.306	2.03
Relative MACS SNR enhancement	18.7	14.2	7.8	1.0

Data were acquired on small quantities of powdered L-alanine (see Supplementary Information). As expected, the smallest coil detector offers better signal-noise ratio (SNR) per sample mass and comes with a relative gain in RF amplitude. This confirms the reciprocity principle, as expressed in the second line of the table ($B_1/\sqrt{P}$, where B_1 is the RF magnetic field for a given transmitter power P, represents the probe efficiency, and is proportional to the SNR of a probe[7]). The last line shows the SNR enhancement the MACS approach offers in the case of ~200-nl-volume samples.

using very high magnetic fields to improve sensitivity is compatible with a reduction in sample size, but it comes at the expense of larger susceptibility effects because broadening increases with magnetic field; MACS eliminates simultaneously effects coming both from the intrinsic sample and coil susceptibilities.

In cases where the sample must be confined, such as when studying radioactive or biologically harmful materials, the filling factor is inherently low and cannot be enhanced simply by using static micro-coils[13]. For example, in the first—and to the best of our knowledge, only—MAS NMR study on radioactive samples[26], plutonium-containing ceramics were placed in triple barrier rotors to confine the emitted radiation and limit the risks in the case of rotor failure. The sample was positioned inside a ceramic container, which fitted inside a soft PTFE cylinder, with the ensemble then placed inside the rotor. This reduces the filling factor and hence the sensitivity of detection by a factor of roughly 4. To show that the MACS technique can retrieve this lost sensitivity, we used a rotating coil of 2.3 mm diameter (it was not really a micro-coil), fitted inside the innermost ceramic barrier, surrounded by the PTFE barrier and the 7 mm rotor. As a (dummy) sample, a cylinder made of Pyrex glass was used. Spectra with comparable signal-to-noise ratios were recorded in considerably shorter acquisition times and the RF field amplitude was largely enhanced (see Fig. 4). MACS could thus facilitate future studies of radioactive materials, for it requires less experimental time or much smaller quantities of samples and thus minimizes radiation activity, thereby rendering such studies more accessible.

Although MACS is still at an early stage of development, our results show it to be a promising new way for obtaining highly sensitive spectra from nano- to pico-litre volume samples[27], as miniaturization is advantageous for stable spinning and the amplification of RF field and sensitivity. Centrifugation effects commonly present in HRMAS of liquids and cell suspensions[28] are expected to be minimal in the MACS implementation because of the small capillary diameter. The high sensitivity offered by our method could potentially reduce the need for large biopsy samples, and HRMAS of a few cells should become possible. Furthermore, metabolomics studies could benefit from this new possibility of studying small frozen samples (temperature close to 0 °C), because freezing minimizes sample degradation, and the sample preparation does not require extraction and homogenization[24]. State-of-the art technologies in cryogenic MAS probe design could, in principle, be combined with MACS, as they offer the possibility to over-couple even smaller micro-coils and therefore further enhance the sensitivity of the technique. High amplitude RF fields of the order of MHz could change the landscape of modern solid-state NMR in areas such as dipolar decoupling, excitation in paramagnetic systems, and overtone spectroscopy, while using low RF power amplifiers[11]. Applications of MACS to high-pressure NMR and micro-imaging promise a significant advance over state-of-the-art technology, and provide a framework for new medical, industrial and chemical analysis. Further developments in miniaturization technology (coil and capacitor lithography[29,30]), together with variations in resonator geometry (RF shimming) and resonance mode (self-resonance), should eliminate any effects related to eddy currents, render the implementation more practical especially for smaller and faster spinning rotors, and further enhance the performance of MACS.

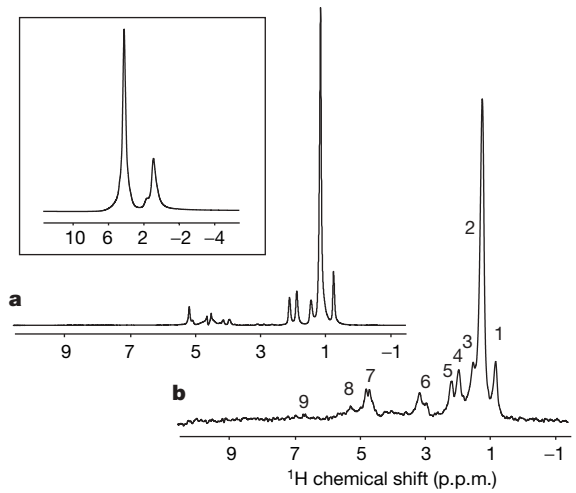

Figure 3 | Proton NMR spectra of bovine muscle tissue. a, The high-resolution spectrum from ~365 mg of bovine muscle tissue using a full 7 mm rotor spinning at 3,000 Hz was acquired in 33 s (8 scans). Pre-saturation of the water resonance (4.7 p.p.m.) was achieved using a 2 s irradiation before the π/2 hard pulse. **b**, High-resolution spectrum from ~0.3 mg of bovine muscle tissue using the MACS insert under the same experimental conditions. The susceptibility broadening is distributed in spinning sidebands outside the range of the proton chemical shifts and the line width is of the order of 0.05 p.p.m. for all resonances (no deuterium lock was used). This width is mainly attributed to temperature gradients (temperature difference less than 3–4 °C). Partial assignments can be made on the basis of the literature[25] (see Supplementary Information). In the absence of sample spinning, the susceptibility broadening hides most of the isotropic chemical shift information, as seen from the spectrum (inset) of the static sample used in **a**.

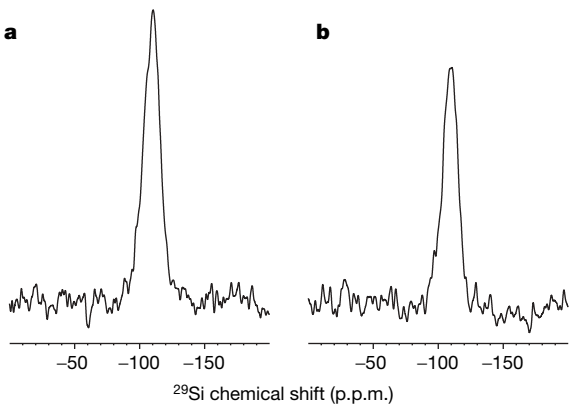

Figure 4 | ^{29}Si MAS NMR spectra of Pyrex. Sample spinning at the magic angle eliminates all chemical shift anisotropy, and reveals the distribution of the isotropic chemical shifts for distorted tetrahedral $Q^{(4)}$ sites. **a**, Spectrum acquired from a Pyrex glass sample confined inside a triple barrier rotor, simulating the conditions used in the acquisition of high-resolution MAS spectra from radioactive samples. The duration of the experiment was 1 day 21 hours, and the measured SNR was ~33. **b**, Spectrum obtained using the MACS technique, having an SNR of ~30 after 2.8 hours of acquisition under the same experimental conditions as in **a**.

METHODS SUMMARY

In most experiments involving rotating micro-coils, the samples were fitted inside a quartz capillary. The tuned micro-coils were made of ordinary coated copper thin wire (50–80 μm in diameter) manually wound around the capillary, and soldered to a chip capacitor. The resonant frequency and the quality factor of the tuned micro-coil were measured. Once the rotor was placed inside the MAS probe, depending on the coupling regime, one or two resonances might be visible on the wobbling curve[15]. Fine tuning to the exact value of the Larmor frequency and matching of the ensemble to 50 Ω was performed using the tuning and matching elements of the probe. A hollow aluminium nitride (Shapal-M) cylinder was used to centre the micro-coil-supporting capillary inside commercial rotors and allow smooth spinning. Shapal-M has one of the highest thermal conductivity coefficients, is very rigid and the geometry of the insert is optimized to evacuate almost entirely the heat generated by eddy currents of the rotating coil. The measurement and analysis of power dissipation is detailed in Methods.

Full Methods and any associated references are available in the online version of the paper at www.nature.com/nature.

Received 21 December 2006; accepted 27 April 2007.

1. Olson, D. L., Peck, T. L., Webb, A. G., Magin, R. L. & Sweedler, J. V. High-resolution microcoil ^{1}H-NMR for mass-limited, nanoliter-volume samples. *Science* **270,** 1967–1970 (1995).
2. Savukov, I. M., Lee, S.-K. & Romalis, M. V. Optical detection of liquid-state NMR. *Nature* **442,** 1021–1024 (2006).
3. Rugar, D. *et al.* Force detection of nuclear magnetic resonance. *Science* **264,** 1560–1563 (1994).
4. Ardenkjaer-Larsen, J. H. *et al.* Increase in signal-to-noise ratio of >10,000 times in liquid-state NMR. *Proc. Natl Acad. Sci. USA* **100,** 10158–10163 (2003).
5. Andrew, E. R., Bradbury, A. & Eades, R. G. Nuclear magnetic resonance spectra from a crystal rotated at high speed. *Nature* **182,** 1659 (1958).
6. Lowe, I. J. Free induction decays of rotating solids. *Phys. Rev. Lett.* **2,** 285–287 (1959).
7. Hoult, D. I. & Richards, R. E. The signal-to-noise ratio of the nuclear magnetic resonance experiment. *J. Magn. Reson.* **24,** 71–85 (1976).
8. Webb, A. G. Radiofrequency microcoils in magnetic resonance. *Prog. Nucl. Magn. Reson. Spectrosc.* **31,** 1–42 (1997).
9. Grant, S. C. *et al.* NMR spectroscopy of single neurons. *Magn. Reson. Med.* **44,** 19–22 (2000).
10. Grant, S. C., Buckley, D. L., Gibbs, S., Webb, A. G. & Blackband, S. J. MR microscopy of multicomponent diffusion in single neurons. *Magn. Reson. Med.* **45,** 1107–1112 (2001).
11. Yamauchi, K., Jannsen, J. W. G. & Kentgens, A. P. M. Implementing solenoid microcoils for wide-line solid-state NMR. *J. Magn. Reson.* **167,** 87–96 (2004).
12. van Bentum, P. J. M., Janssen, J. W. G. & Kentgens, A. P. M. Towards nuclear magnetic resonance μ-spectroscopy and μ-imaging. *Analyst* **129,** 793–803 (2004).
13. Janssen, H., Brinkmann, A., van Eck, E. R. H., van Bentum, J. M. & Kentgens, A. P. M. Microcoil high-resolution magic angle spinning NMR spectroscopy. *J. Am. Chem. Soc.* **128,** 8722–8723 (2006).
14. Brey, W. W. *et al.* Design, construction, and validation of a 1-mm triple-resonance high-temperature-superconducting probe for NMR. *J. Magn. Reson.* **179,** 290–293 (2006).
15. Terman, F. E. *Electronic and Radio Engineering* Ch. 3 (McGraw-Hill, New York, 1955).
16. Turner, J. D. The development of a thick-film non-contact shaft torque sensor for automotive applications. *J. Phys. E* **22,** 82–88 (1989).
17. Wu, J., Quinn, V. & Bernstein, G. H. Powering efficiency of inductive links with inlaid electroplated microcoils. *J. Micromech. Microeng.* **14,** 576 (2004).
18. Raad, A. & Darrasse, L. Optimization of NMR receiver bandwidth by inductive coupling. *Magn. Reson. Imag.* **10,** 55–65 (1992).
19. Hoult, D. I. & Tomanek, B. Use of mutually inductive coupling in probe design. *Concepts Magn. Reson. B* **15,** 262–285 (2002).
20. Ginefri, J. C., Darrasse, L. & Crozat, P. High-temperature superconducting surface coil for *in vivo* microimaging of the human skin. *Magn. Reson. Med.* **45,** 376–382 (2001).
21. Schnall, M. D., Barlow, C., Subramanian, V. H. & Leigh, J. S. J. Wireless implanted magnetic resonance probes for *in vivo* NMR. *J. Magn. Reson.* **68,** 161–167 (1986).
22. Barbara, T. Cylindrical demagnetization fields and microprobe design in high-resolution NMR. *J. Magn. Reson. A* **109,** 265–269 (1994).
23. Hu, J. Z., Rommereim, D. N. & Wind, R. A. High-resolution ^{1}H NMR spectroscopy in rat liver using magic angle turning at a 1 Hz spinning rate. *Magn. Reson. Med.* **47,** 829–836 (2002).
24. Cheng, L. L. *et al.* Quantitative neuropathology by high resolution magic angle spinning proton magnetic resonance spectroscopy. *Proc. Natl Acad. Sci. USA* **94,** 6408–6413 (1997).
25. Govindaraju, V., Young, K. & Maudsley, A. A. Proton NMR chemical shifts and coupling constants for brain metabolites. *NMR Biomed.* **13,** 129–153 (2000).
26. Farnan, I. *et al.* High-resolution solid-state nuclear magnetic resonance experiments on highly radioactive ceramics. *Rev. Sci. Instrum.* **75,** 5232–5236 (2004).
27. Minard, K. R. & Wind, R. A. Picoliter ^{1}H NMR spectroscopy. *J. Magn. Reson.* **154,** 336–343 (2002).
28. Chen, J.-H., Enloe, B. M., Xiao., Y., Cory, D. G. & Singer, S. Isotropic susceptibility shift under MAS: The origin of the split water resonances in ^{1}H MAS NMR spectra of cell suspensions. *Magn. Reson. Med.* **50,** 515–521 (2003).
29. Rogers, J. A., Jackman, R. J., Whitesides, G. M., Olson, D. L. & Sweedler, J. V. Using microcontact printing to fabricate microcoils on capillaries for high resolution proton nuclear magnetic resonance on nanoliter volumes. *Appl. Phys. Lett.* **70,** 2464–2466 (1997).
30. Malba, V. *et al.* Laser-lathe lithography — a novel method for manufacturing nuclear magnetic resonance microcoils. *Biomed. Microdevices* **5,** 21–27 (2003).

Supplementary Information is linked to the online version of the paper at www.nature.com/nature.

Acknowledgements We thank J. Virlet for discussions on inductive coupling, H. Desvaux for discussions and help with the manuscript, D. Hoult for discussions on inductive coupling and micro-coils, A. Trabesinger, C. A. Meriles, T. Charpentier and A. Llor for discussions, P. Berthault for help with the manuscript and F. Engelke for help with chip capacitors and hardware.

Author Contributions D.S. and J.-F.J. conceived the technique and carried out the NMR experiments. G.L.G. machined the ceramic and plastic rotor inserts. D.S. wrote the paper.

Author Information Reprints and permissions information is available at www.nature.com/reprints. The authors declare no competing financial interests. Correspondence and requests for materials should be addressed to D.S. (dimitrios.sakellariou@cea.fr).

METHODS

Rotating coils hardware. In most experiments involving rotating micro-coils, the microscopic samples were fitted inside a quartz capillary. The tuned micro-coils were made of ordinary coated copper thin wire (50–80 μm in diameter) manually wound around the capillary, soldered to a chip capacitor. A hollow Shapal-M cylinder, having an outer diameter (o.d.) of 5.5 mm, a length of 14 mm and an inner diameter (i.d.) of 1.1 mm, was used to centre the micro-coil-supporting capillary inside commercial 7 mm o.d. rotors. Shapal-M has a very high thermal conductivity coefficient ($>90\,W\,m^{-1}\,K^{-1}$), is very rigid, and the geometry of the insert is optimized to evacuate almost entirely the heat generated by eddy currents of the rotating coil. The take off, landing and stable spinning up to 7 kHz within 5 Hz were controlled using the automatic setting of the pneumatic MAS unit. For the confined-sample MACS experiments, we used a home-made triple barrier rotor system. The innermost container, made of Shapal-M, was 4.0 mm and 2.5 mm in o.d. and i.d., respectively. The second barrier was made of PTFE and had an o.d. of 5.6 mm and an i.d. of 4.0 mm. The zirconia rotor served as the third barrier, and the coil was directly wound on the cylindrical Pyrex sample.

Tuning protocol. Using approximate formulas for the inductance of the coil allowed us to estimate the capacitor values in order to tune the LC circuit close (within 1%) to the Larmor frequency of the spins. The resonant frequency and the quality factor of the tuned micro-coil were measured using a spectrum analyser and sniffer coils. Once the rotor was placed inside the MAS probe, depending on the coupling regime, one or two resonances might be visible on the wobbling curve[15]. Fine tuning of one of them to the exact value of the Larmor frequency and matching of the ensemble to 50 Ω was performed using the tuning and matching elements of the commercial probe.

Coupling regimes. In practical terms, the 'overcoupling' regime can be achieved when the volumes of the primary (large; V_1) and secondary (micro; V_2) coils satisfy: $V_2 > V_1/(Q_1Q_2)$, where Q_1 and Q_2 are their respective quality factors. In this case, and if all the RF power dissipation occurs in the detection coil, the field and the SNR enhancements are of the order of $\sqrt{[(V_1Q_2)/(V_2Q_1)]}$. The case of 'undercoupling' is not optimal for signal sensitivity, but it can also give significant enhancement (of the order of Q_2) with respect to classical detection using the primary coil (but not as large as $\sqrt{[(V_1Q_2)/(V_2Q_1)]}$).

Power dissipation. Heating effects due to eddy (or Foucault) currents in the coil have been observed and measured using a sample of lead nitrate. Stabilization cylinders made of KelF and Shapal-M were tested and their thermal properties compared. The measured values of the ^{207}Pb isotropic chemical shift indicate an increase in sample temperature of less than 30 °C when the powder sample is surrounded by a 900 μm o.d. copper micro-coil, a thermal conductivity paste, and a Shapal-M stabilization insert inside a rotor spinning at 7 kHz in a 11.7 T magnet (10 °C in temperature was recorded using a standard MAS rotor under the same spinning conditions, see Supplementary Information). The calculated power dissipation using a finite elements model (Flux3D, Cedrat Technologies) is ~100 mW. These effects increase with the strength of the static magnetic field and the spinning frequency. They also depend strongly on the wire diameter, and are expected to become negligible as the coil and wire sizes decrease. We are currently investigating better heat sinks for heat diffusion inside the rotor, and we are exploring alternatives to diminish eddy current effects (preliminary experiments using micro-coils made of so-called Litz wire proved to offer significant advantages).

LETTERS

Low Atlantic hurricane activity in the 1970s and 1980s compared to the past 270 years

Johan Nyberg[1], Björn A. Malmgren[2], Amos Winter[3], Mark R. Jury[4], K. Halimeda Kilbourne[5,6] & Terrence M. Quinn[5,7,8]

Hurricane activity in the North Atlantic Ocean has increased significantly since 1995 (refs 1, 2). This trend has been attributed to both anthropogenically induced climate change[3] and natural variability[1], but the primary cause remains uncertain. Changes in the frequency and intensity of hurricanes in the past can provide insights into the factors that influence hurricane activity, but reliable observations of hurricane activity in the North Atlantic only cover the past few decades[2]. Here we construct a record of the frequency of major Atlantic hurricanes over the past 270 years using proxy records of vertical wind shear and sea surface temperature (the main controls on the formation of major hurricanes in this region[1,3–5]) from corals and a marine sediment core. The record indicates that the average frequency of major hurricanes decreased gradually from the 1760s until the early 1990s, reaching anomalously low values during the 1970s and 1980s. Furthermore, the phase of enhanced hurricane activity since 1995 is not unusual compared to other periods of high hurricane activity in the record and thus appears to represent a recovery to normal hurricane activity, rather than a direct response to increasing sea surface temperature. Comparison of the record with a reconstruction of vertical wind shear indicates that variability in this parameter primarily controlled the frequency of major hurricanes in the Atlantic over the past 270 years, suggesting that changes in the magnitude of vertical wind shear will have a significant influence on future hurricane activity.

The years from 1995 to 2005 experienced an average of 4.1 major Atlantic hurricanes (category 3 to 5) per year, while the years 1971 to 1994 experienced an average of 1.5 major hurricanes per year[2]. A major hurricane is defined as a tropical cyclone with maximum sustained (1 minute) surface (measured 10 m above the surface) winds of $\geq 50\ m\ s^{-1}$. This increase in major hurricane frequency is thought to be caused by weaker vertical wind shear $|V_z|$ and warmer sea surface temperatures (SSTs) in the tropical and subtropical Atlantic[1,3], which some studies have attributed to a natural multidecadal variability in the thermohaline circulation[1], termed the Atlantic Multidecadal Oscillation (AMO)[6], and other studies to anthropogenic climate change[3]. Little information exists about the effects of the AMO variability on changes in tropical Atlantic climate and magnitudes of hurricane activity. Although hurricane intensity and destructiveness may increase with increasing global mean temperatures[3,7], the effect of climate warming on hurricane frequency is poorly known[8]. Furthermore, it is possible that hurricane activity responds to changes in other external forcings, such as solar activity[9] and aerosol loading[3]. The reliable observation record of hurricane activity over the North Atlantic exists only from 1944 (ref. 2) with continual satellite coverage from 1966 (ref. 10), providing a temporally limited perspective on these issues. The existing historical records of hurricane activity are based on archives documenting primarily US landfalls[11].

The Main Development Region (MDR)[1,5] is where 85% of all Atlantic major hurricanes and 60% of all non-major hurricanes (33 to 50 $m\ s^{-1}$) and tropical storms (18 to 32 $m\ s^{-1}$) are formed. The MDR is an area westward of Africa across the tropical Atlantic and Caribbean Sea at latitudes between 10° and 20° N (Figs 1 and 2). Here tropical cyclones are formed when easterly atmospheric waves propagate from Africa across the tropical North Atlantic[1,5]. Because the number of easterly waves are fairly constant from year to year[1,12], the dominant factors for major hurricane formation are the magnitude of $|V_z|$, and SSTs in the MDR during August to October, when almost all major hurricanes are formed[1,3–5,13]. Local vertical wind shear $|V_z| > \sim 8\ m\ s^{-1}$ (for example, upper winds opposed to lower easterly trade winds) is in general unfavourable for the formation of tropical cyclones owing to distortion of the vertical structure of the convective cloud cells[14]. The vertically tilted cloud cells are limited in their capacity to provide energy to the storm.

Local SSTs of ~27 °C or more and a warm mixed layer down to a depth of ~50 m are also considered necessary for major hurricane development[1,4]. Empirical studies indicate, however, that warmer local SSTs are not central in the formation of major hurricanes[1,4]. Regional Atlantic SSTs appear to be more important for the formation of major hurricanes through their interdependence with $|V_z|$ in the MDR[1,4], which may arise from interactions with the Pacific El Niño Southern Oscillation (ENSO)[15]. Warmer SSTs in the North Atlantic region coincide with reduced $|V_z|$ in the MDR and vice versa[1,4].

Comparisons between the hurricane index[2] and observed zonal winds show significant positive (westerly) correlation values from the surface up to 1.5 km (850 hPa) over latitudes ~10–20° N (Fig. 1), while significant negative (easterly) correlation values exist around 12 km (200 hPa) in these latitudes. Consequently, by using proxies of $|V_z|$ (trade wind strength) and SST anomalies in the MDR, robust longer-term estimations of major hurricane activity are possible.

To estimate $|V_z|$ we use four luminescence intensity records for the months August to October derived from coral cores[16] retrieved in the Caribbean off the southern Dominican Republic, south-western Puerto Rico and Mona Island together with one annual abundance record of the planktonic foraminifer *Globigerina bulloides* in a well-dated (^{14}C and ^{210}Pb) sediment core[17] from the Cariaco basin in the southern Caribbean Sea (Fig. 2a–d).

The significant relationships shown in Fig. 2a–d (see also Supplementary Information) are explained as follows: luminescence intensity in corals reflects the degree of terrestrial runoff, which is controlled by the amount of precipitation[16]. Decreased precipitation

[1]Geological Survey of Sweden, Box 670, SE-751 28 Uppsala, Sweden. [2]Department of Earth Sciences, Göteborg University, Box 460, SE-405 30 Göteborg, Sweden. [3]Department of Marine Sciences, University of Puerto Rico, PO Box 9013. [4]Department of Physics, University of Puerto Rico, PO Box 9016, PR 00681-9013, Mayagüez, Puerto Rico. [5]College of Marine Science, University of South Florida, 140, St Petersburg, Florida 33707, USA. [6]Physical Sicences Division R/PSD1, NOAA, Earth System Research Laboratory, 325 Broadway, Boulder, Colorado 80305, USA. [7]Department of Geological Sciences, Jackson School of Geosciences, University of Texas at Austin, 1 University Station C1100, Austin, Texas 78712, USA. [8]Institute for Geophysics, J. J. Pickle Research Campus, University of Texas at Austin, 10100 Burnet Road, Austin, Texas 78758, USA.

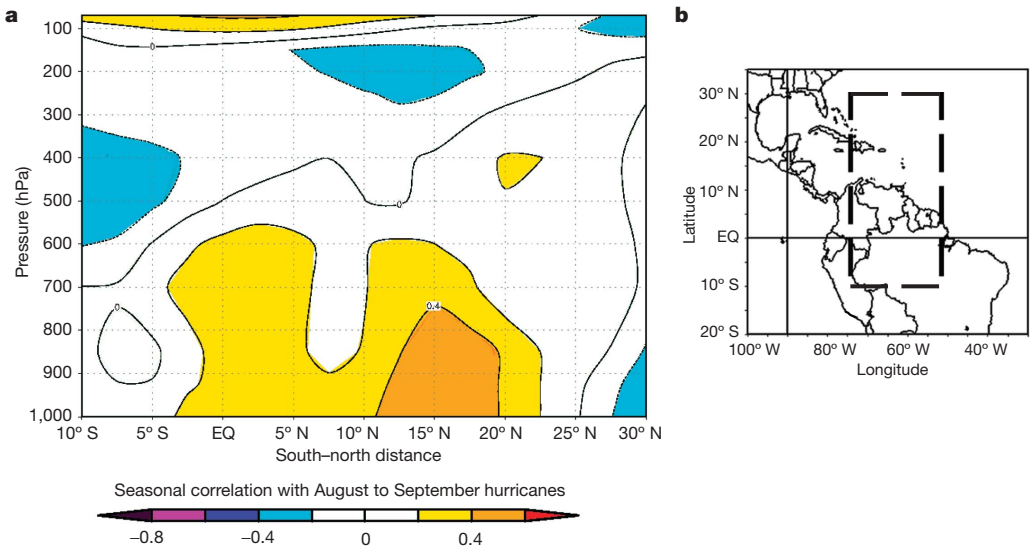

Figure 1 | Simultaneous correlation of zonal winds in August-September (1955–2004) with the unsmoothed Atlantic hurricane index[2]. NCEP/NCAR Reanalysis (285° E to 310° E). Positive (or negative) values on the colour scale refer to increased westerlies (or easterlies) in active hurricane years. Correlation values exceeding ±0.2 are significant above the 90% confidence level. The zonal winds are within the area marked by dashed lines in **b**.

in the northeastern Caribbean during the hurricane season is associated with increased trade-wind speed and high $|V_z|$ over the MDR[16,18,19] (Fig. 2). Increased trade-wind speed corresponds to higher sea-level pressures, enhanced sinking motion and drying and a more stable lower atmosphere, which results in lower precipitation and a more sheared environment in the tropical Atlantic during the hurricane season[18]. Higher abundance of *G. bulloides* reflects more nutrient supply caused by enhanced upwelling due to increased trade-wind strength, which is related to high $|V_z|$ over the MDR[17] (Fig. 2d, see also Supplementary Information). In addition, these wind-speed records are tightly linked to larger-scale SST anomalies in the North Atlantic region[16,17], which supports their robustness as a proxy of major hurricane activity. Figure 2a–d also displays an association between these four proxies and $|V_z|$ north of the MDR that is out of phase with $|V_z|$ within the MDR, supporting instrumental observations of an out-of-phase relationship between horizontal wind shear on either side of the main track of Atlantic hurricanes[5].

Back propagation artificial neural networks were used to estimate past $|V_z|$ and major hurricane activity. The networks were trained to

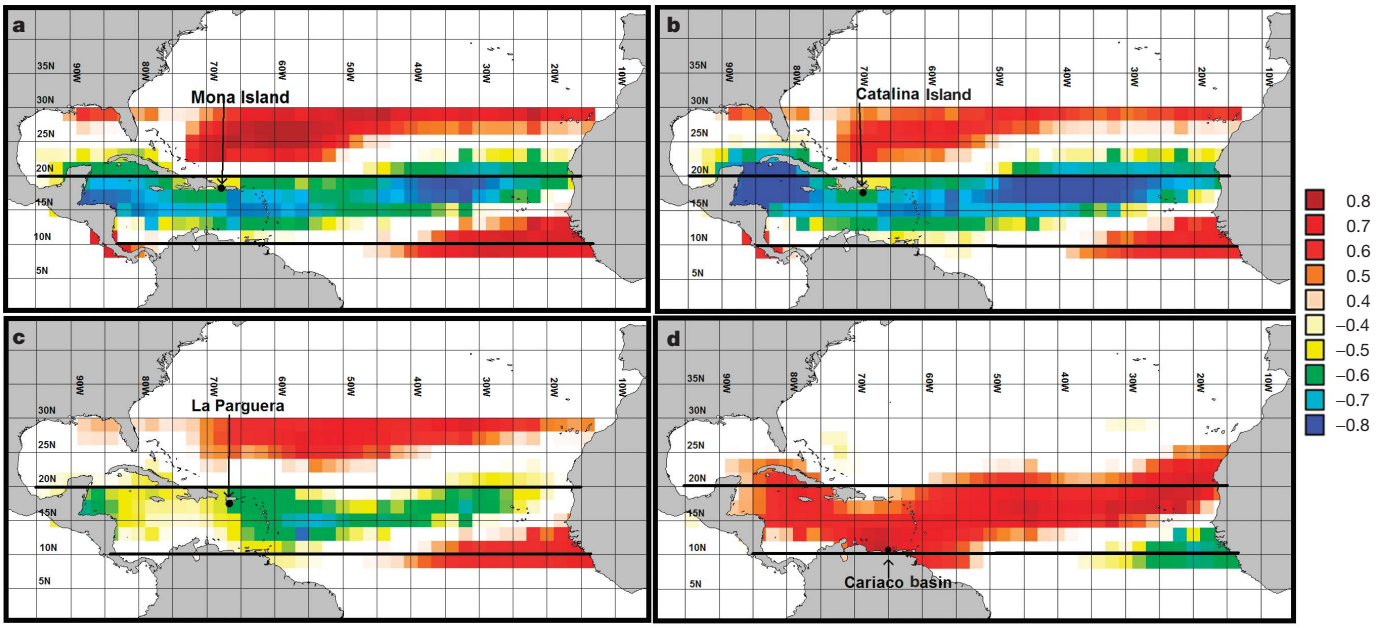

Figure 2 | Spatial correlations between instrumentally observed vertical windshear ($|V_z|$) in August–October and the proxies used. Luminescence intensity during August to October in the coral cores retrieved outside Mona Island, 1949–1992 (**a**), Catalina Island, 1949–1993 (**b**) and La Parguera, 1949–2000 (**c**). **d**, Annual abundance of the planktonic foraminifer *Globigerina bulloides* in the Cariaco basin, 1949–1990. The colour scale refers to all panels. Only statistically significant correlation values exceeding the 0.01 ($r_S < -0.4$ and $r_S > 0.4$) and 0.001 ($r_S < -0.5$ and $r_S > 0.5$) levels are shown and referred to in the colour scale. Solid lines in **a**–**d** give the north and south boundaries of the MDR.

learn the relationships between the combined input (independent) proxy records and each of the two output (dependent) instrumental records of $|V_z|$ and number of major hurricanes, respectively (Fig. 3). The SST anomaly record[20] was averaged between latitudes of 10 and 25° N and longitudes of 20 to 85° W, because the region where SST anomalies directly affect major hurricane activity is within and around the MDR[4,21]. Although instrumentally recorded $|V_z|$, luminescence intensity and *G. bulloides* show the strongest correlations with SST anomalies in the North Atlantic region between 50 and 60° N (refs 1, 16 and 17), these records also show statistical significant relationships with the instrumental SST anomaly record[20,22], averaged over the MDR, using five-year running averages (Fig. 3). This demonstrates the physical link between SST anomalies in the MDR and $|V_z|$.

Figure 3 shows that the switch from low to high abundance of *G. bulloides*, high to low luminescence intensity, and high to low SST anomalies is coincident with the shift towards high-$|V_z|$ conditions and decreased major hurricane activity in the period 1965–1971 (refs 1, 2). The shift back towards low $|V_z|$ conditions and increased major hurricane activity starts around 1987–1988, but is suppressed by the long-lasting (1990–1995) El Niño event[1] (Fig. 3). The record of *G. bulloides* (until 1990) reflects the shift around 1987–1988, while the luminescence-intensity records reflect both the El Niño event (1990–1995) and the evident shift towards increased major hurricane activity around 1995 (ref. 1 and Fig. 3).

The downward trend in the frequency of major hurricanes[23] from the 1940s to 1970s in the reliable observation record is matched by the

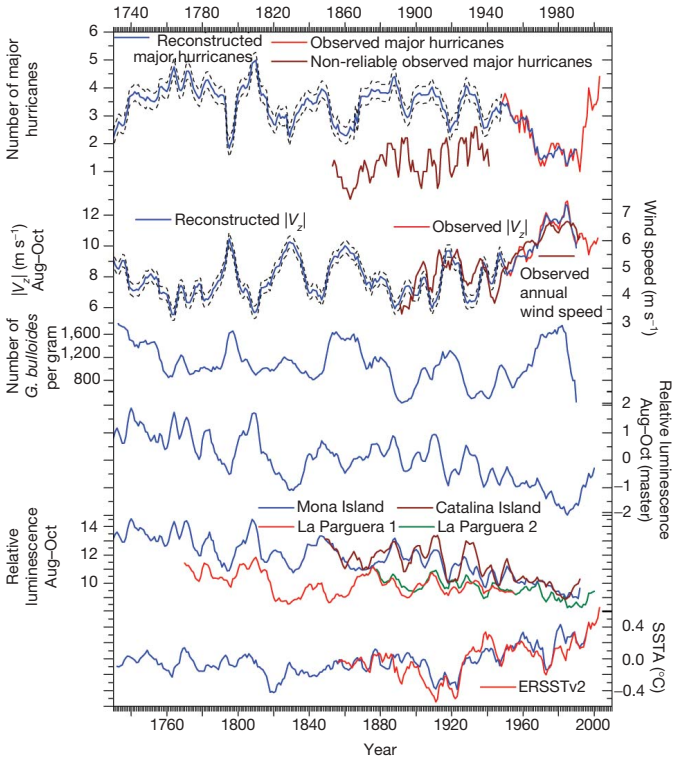

Figure 3 | The reconstructed major hurricane activity and $|V_z|$ series back to 1730. Also shown are the reliable observation records back to 1944 (ref. 2) and 1949 (ref. 19), respectively, the historical hurricane record back to 1851 (refs 10, 11), the ERSST v2 data[22] averaged over 10 to 26° N and 20 to 86° W during August–October back to 1854, zonal wind speed data centred at 11° N and 65° W (ref. 30) back to 1890 together with the SST anomalies[20], luminescence intensities, and abundance of *G. bulloides* upon which the reconstructions were based. The dashed lines indicate 95% confidence intervals for estimated numbers of hurricanes and $|V_z|$ values. All data are smoothed with a five-year running average. The 'master' luminescence curve is developed by averaging standardised luminescence intensity values during Aug–Oct in all of the coral cores for each year.

reconstruction (Fig. 3). The reconstruction also follows the variability during the 19th and 20th centuries of US East Coast hurricane landfalls[2,9,10,23,24], with a quiet period during the 1850s to the late 1860s, an active period from the 1870s to the 1890s, a quiescent period to 1926, and an active phase from 1926 to 1970. We note the reconstructed high activity around 1886, which is the most active hurricane season on record for the continental United States[11]. In addition, the reconstructed $|V_z|$ closely follows observed annual zonal wind speed data in the Caribbean back to 1890, and high reconstructed $|V_z|$ values back to 1851 coincide with low observed major hurricane activity[11] (Fig. 3). The exact numbers of observed major Atlantic hurricanes before 1944 are less accurate owing to the lack of observational networks[2,11], which probably explains the difference between the numbers of reconstructed and instrumentally observed major hurricanes (Fig. 3).

The reconstruction shows that there have been on average ~3–3.5 major hurricanes and a $|V_z|$ of ~8–9 m s^{-1} per year from 1730 to 2005. A gradual downward trend is evident from an average of ~4.1 (1755–1785) to ~1.5 major hurricanes during the late 1960s to early 1990s, which experienced strong $|V_z|$ and few major hurricanes compared to other periods since 1730. Only the periods ~1730–1736, 1793–1799, 1827–1830, 1852–1866 and 1915–1926 appear to have been marked by similarly low major hurricane activity and high $|V_z|$. Furthermore, the current active phase (1995–2005) is unexceptional compared to the other high-activity periods of ~1756–1774, 1780–1785, 1801–1812, 1840–1850, 1873–1890 and 1928–1933 (Fig. 3), and appears to represent a recovery to normal hurricane activity, despite the increase in SST.

Wavelet spectral analyses together with spectral analyses reveal the existence of significant ~8–11 and ~20–30-year cycles in the records (see Supplementary Information). Decadal signals in occurrences, formation areas, and landfalls of tropical storms and hurricanes have also been identified elsewhere and linked to the North Atlantic Oscillation[9,24,25].

To improve our understanding further, the derived records are compared with indices of the AMO[6,26] and total solar irradiance (TSI)[27] (Fig. 4). Reduced major hurricane activity coincides with a lower AMO index around 1820–1830, 1910–1920 and 1970–1990; enhanced activity coincides with a high index around 1750–1790, 1870–1900 and 1930–1960 (Fig. 4). Peaks and trends of higher major hurricane activity concur with lower TSI, and vice versa, several times since 1730 (Fig. 4). Results from a general circulation model show that circulation changes in the upper stratosphere, induced by interactions between solar irradiance and ozone levels, may penetrate

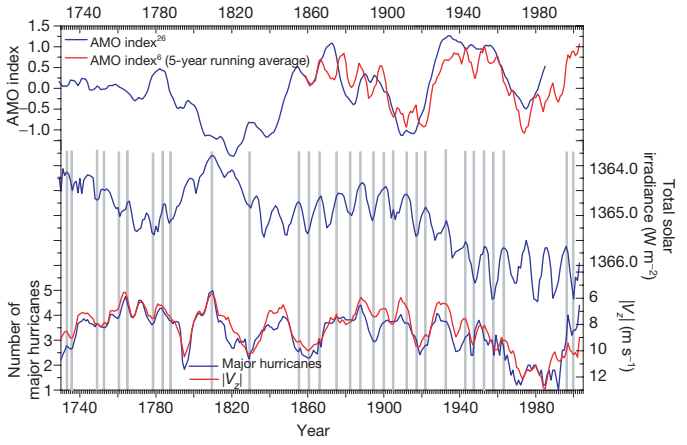

Figure 4 | The reconstructed major hurricane and $|V_z|$-series compared to total solar irradiance and AMO indices. The instrumental records of major hurricane activity and $|V_z|$ (five-year running averages) are shown from 1944 and 1949, respectively, to 2005. TSI and $|V_z|$ have increasing values downwards. Shaded lines mark concurrent peaks and lows in TSI, hurricane activity and/or $|V_z|$.

down to the troposphere, where surface winds and sea level pressures are affected[28]. In addition, the general circulation model shows a forced shift towards decreased sea level pressure in the subtropical Atlantic during reduced TSI, which would result in weaker easterly trade winds, weaker $|V_z|$ and higher major hurricane activity, and thus explains some of our observations.

Our results suggest that the frequency of major hurricanes since 1995 is not unusual, indicating that increases in SST during the past 270 years have been offset by increased $|V_z|$, which suppresses major hurricanes. A more rapid warming of the atmosphere relative to the ocean could have caused the anomalous calm period between the 1970s and 1990s. Air temperatures near the level of the trade-wind inversion (1.5 km) as well as 10 m air temperatures during the past 50 and 100 years, respectively, averaged over the Caribbean (see Supplementary Information), have risen faster than SSTs, indicating an enhanced stability of the lower atmosphere and a strengthening of the trade-wind inversion that reduces the influence of thermodynamic energy from a warmer ocean[29]. This physical mechanism leads to enhanced subsidence, trade-wind strength and $|V_z|$ in the MDR[29]. The reconstructed $|V_z|$ series may indicate that this trend has occurred over a longer period.

The future possibility of lower $|V_z|$ combined with increased SSTs in the MDR (Figs 3 and 4) may result in longer storm lifetimes and more moist enthalpy to power developing tropical cyclones, causing higher hurricane frequencies and greater storm intensities.

METHODS SUMMARY

The correlation coefficients are computed using the Spearman rank correlation (r_S) owing to the presumed lack of non-normality of the data series. The statistical significances are judged using a two-tailed significance test. The vertical wind shear V_z is calculated as the vector difference between the 200 and 850 mbar climatological winds[1] averaged for August–October from the NCEP/NCAR Reanalysis gridded ($2.5^\circ \times 2.5^\circ$ interval) monthly mean wind data set over the MDR region[19]. A single 'master' coral luminescence intensity curve was developed by averaging standardized luminescence intensity values in all of the four cores for each year.

The Trajan 6.0 Neural Network software was used for the autonomous learning of the relationships between the independent variables (master luminescence intensity, number of *G. bulloides* and SSTs) and dependent variables (number of instrumentally observed major hurricanes and vertical windshear). The data sets were split so that ~67% of the samples was used in the training set, ~20% in the selection set, and the remaining samples in the test set. Each of the reconstructed time series was derived from ensembles constituting ten independent networks. The prediction errors—the root-mean-square errors of predictions—were computed for each network as the square root of the sum of the squared differences between the observed and predicted values divided by the number of samples in the test sets using different training, selection and test cases. The 95% confidence intervals for the estimated values were then based on these ten different runs.

$|V_z|$ and major hurricane activity are associated primarily with the large-scale decadal SST fluctuations in the Atlantic[1,3]. Therefore, to emphasize lower-frequency variations, a five-year running average was used when training the networks. Significance tests account for the additional auto-correlation imposed by the filter.

Full Methods and any associated references are available in the online version of the paper at www.nature.com/nature.

Received 24 October 2006; accepted 1 May 2007.

1. Goldenberg, S. B., Landsea, C. W., Mestas-Nuñez, A. M. & Gray, W. M. The recent increase in Atlantic hurricane activity: causes and implications. *Science* **293,** 474–479 (2001).
2. Jarvinen, B. R., Neumann, C. J. & Davis, M. A. S. A tropical cyclone data tape for the North Atlantic basin, 1886–1983: Contents, limitations, and uses. *NOAA Tech. Memo. NWS NHC* Vol. 22, 1–21 (NOAA, Coral Gables, Florida, 1984).
3. Mann, M. E. & Emanuel, K. A. Atlantic hurricane trends linked to climate change. *Eos* **87,** 233–241 (2006).
4. Shapiro, L. J. & Goldenberg, S. B. Atlantic sea surface temperature and tropical cyclone formation. *J. Clim.* **11,** 578–590 (1998).
5. Goldenberg, S. B. & Shapiro, L. J. Physical mechanisms for the association of El Niño and West African rainfall with Atlantic major hurricane activity. *J. Clim.* **9,** 1169–1187 (1996).
6. Enfield, D. B., Mestas-Nuñez, A. M. & Trimble, P. J. The Atlantic multidecadal oscillation and its relation to rainfall and river flows in the continental U.S. *Geophys. Res. Lett.* **28,** 2077–2080 (2001).
7. Emanuel, K. Increasing destructiveness of tropical cyclones over the past 30 years. *Nature* **436,** 686–688 (2005).
8. Curry, J. A., Webster, P. J. & Holland, G. J. Mixing politics and science in testing the hypothesis that greenhouse warming is causing a global increase in hurricane intensity. *Bull. Am. Meteorol. Soc.* **87,** 1025–1038 (2006).
9. Elsner, J. B., Kara, A. B. & Owens, M. A. Fluctuations in North Atlantic hurricane frequency. *J. Clim.* **12,** 427–437 (1999).
10. Neumann, C. J., Jarvinen, B. R., McAdie, C. J. & Elms, J. D. *Tropical Cyclones of the North Atlantic Ocean, 1871–1998* 11–15 (National Climatic Data Center, Asheville, North Carolina, 1999).
11. Landsea, C. W. *et al.* in *Hurricanes and Typhoons: Past, Present and Future* (Murname, R. J. & Liu, K.-B.) 177–221 (Columbia Univ. Press, New York, 2004).
12. Avila, L. A., Pasch, R. J. & Jiing, J.-G. Atlantic tropical systems of 1996 and 1997: years of contrasts. *Mon. Weath. Rev.* **128,** 3695–3706 (2000).
13. Aiyyer, A. R. & Thorncroft, T. Climatology of vertical wind shear in the tropical Atlantic. *J. Clim.* **19,** 2969–2983 (2006).
14. DeMaria, M., Balk, J.-J. & Kaplan, J. Upper-level eddy angular momentum fluxes and tropical cyclone intensity change. *J. Atmos. Sci.* **50,** 1133–1147 (1993).
15. Dong, B., Sutton, R. T. & Scaife, A. A. Multidecadal modulation of El Niño–Southern Oscillation (ENSO) variance by Atlantic Ocean sea surface temperatures. *Geophys. Res. Lett.* **33,** L08705, doi:10.1029/2006GL025766 (2006).
16. Nyberg, J. Luminescence intensity in coral skeletons from Mona Island in the Caribbean Sea and its link to precipitation and wind speed. *Phil. Trans. R. Soc. Lond. A* **360,** 749–766 (2002).
17. Black, D. E. *et al.* Eight centuries of North Atlantic ocean atmosphere variability. *Science* **286,** 1709–1713 (1999).
18. Knaff, J. A. Implications of summertime sea level pressure anomalies in the tropical Atlantic region. *J. Clim.* **10,** 789–804 (1997).
19. Kalnay, E. *et al.* The NCEP/NCAR 40-year reanalysis. *Bull. Am. Meteorol. Soc.* **77,** 437–471 (1996).
20. Mann, M. E., Bradley, R. S. & Hughes, M. K. Global-scale temperature patterns and climate forcing over the past six centuries. *Nature* **392,** 779–787 (1998).
21. Vitart, F. & Anderson, J. L. Sensitivity of Atlantic tropical storm frequency to ENSO and interdecadal variability of SSTs in an ensemble of AGCM integrations. *J. Clim.* **14,** 533–545 (2001).
22. Smith, T. M. & Reynolds, R. W. Improved extended reconstruction of SST (1854–1997). *J. Clim.* **17,** 2466–2477 (2004).
23. Landsea, C. W., Nicholls, N., Gray, W. M. & Avila, L. A. Downward trends in the frequency of intense Atlantic hurricanes during the past five decades. *Geophys. Res. Lett.* **23,** 1697–1700 (1996).
24. Elsner, J. B., Jagger, T. & Kocher, B. Changes in the rates of North Atlantic major hurricane activity during the 20th century. *Geophys. Res. Lett.* **27,** 1743–1750 (2000).
25. Elsner, J. B. & Jagger, T. H. Prediction models for annual US hurricane counts. *J. Clim.* **19,** 2935–2952 (2006).
26. Gray, S. T., Graumlich, L. J., Betancourt, J. L. & Pederson, G. T. A tree-ring based reconstruction of the Atlantic Multidecadal Oscillation since 1567 AD. *Geophys. Res. Lett.* **31,** L12205, doi:10.1029/2004GL019932 (2004).
27. Lean, J. 2000. Evolution of the Sun's spectral irradiance since the Maunder Minimum. *Geophys. Res. Lett.* **27,** 2425–2428 (2000).
28. Shindell, D. T. *et al.* Solar forcing of regional climate during the Maunder Minimum. *Science* **294,** 2149–2152 (2001).
29. Held, I. M. & Soden, B. J. Robust responses of the hydrological cycle to global warming. *J. Clim.* **19,** 5686–5699 (2006).
30. Woodruff, S. D., Slutz, R. J., Jenne, R. L. & Steurer, P. M. A comprehensive ocean-atmosphere data set. *Bull. Am. Meteorol. Soc.* **68,** 1239–1250 (1987).

Supplementary Information is linked to the online version of the paper at www.nature.com/nature.

Acknowledgements This work is supported by grants from the Swedish Research Council (to J.N.).

Author Contributions J.N. derived the coral records, the vertical wind shear and hurricane reconstructions and wrote the paper, except for the Fig. 1 legend and parts of the penultimate paragraph, which were written by M.R.J. M.R.J., B.A.M., A.W. and K.H.K. assisted and commented on the manuscript. K.H.K. and T.M.Q. provided X-rayed slices from the coral core retrieved 2004 outside La Parguera.

Author Information Reprints and permissions information is available at www.nature.com/reprints. The authors declare no competing financial interests. Correspondence and requests for materials should be addressed to J.N. (johan.nyberg@sgu.se).

METHODS

Vertical windshear. The correlation coefficient (r_S) between the observed number of major hurricanes and $|V_z|$ averaged over the whole MDR during August to October is –0.76 ($P < 0.001$; time interval 1949–2003; five-year moving average). Our proxies respond to surface (mainly easterly) winds that are related to this zonal overturning Walker circulation. r_S between the instrumental observed annual wind speed[30] shown (Fig. 3) and instrumental observed vertical windshear averaged over MDR in August-October from 1949 to 1992 is 0.90. r_S between the instrumental observed annual windspeed and the estimated V_z derived from the neural network algorithm from 1890 to 1990 is 0.85.

Coral records. Luminescence and reflectivity were measured in ~4-mm-thick slices, dried, whitened and cleaned of organic material and adherent contaminants[16,31], and cut parallel to the growth axis in massive *Montastraea faveolata* skeletons. The core outside Catalina Island, southeastern Dominican Republic was drilled in March 1999 and spans back to 1847, and the core outside Mona Island was drilled in May 1998 and spans back to 1684 (ref. 16). The two cores outside La Parguera, southwestern Puerto Rico, were drilled in February 1998 and 2004, respectively. Four U/Th dates retrieved at the University of Minnesota, together with density-band counting, demonstrate that the first core represents ages ranging from 1768 to 1957. The second core spans back to 1870 on the basis of density-band counting.

The luminescence and reflectivity of the coral slices were measured in a plate reader attached to a Perkin-Elmer Model LS 50B luminescence spectrometer. The plate scan speed was set to 30 mm min^{-1} and the excitation and emission slit widths to 2.5 mm. The measurements were made every 0.1 mm along the growth axis through a lamp with a diameter of 1 mm. An excitation wavelength of 390 nm and an emission wavelength of 490 nm were chosen[16,31]. The relative luminescence was calculated according to ref. 31, in which measurements of luminescence and reflectivity of coral slices are corrected using measurements of background and calcium carbonate standards. For the background standard a black plate with roughened surface was used on which the coral slices were laid down during measurements. The calcium carbonate standard used was Suprapur $CaCO_3$ 99.95 (Merck, Darmstadt, Germany).

Luminescence and reflectance were measured for both the background and calcium carbonate standards at the start and end of each luminescence and reflectance run. Beginning and end measurements were required to be within 2% of each other. Luminescence and reflectivity were measured at the same points along 3 to 6 different columellas (growth axis) through the coral cores avoiding visible gaps and holes. Similar results were obtained and the averaging results from the luminescence profiles were used.

Coral chronology. The luminescence profiles were converted to time series by setting annual luminescence minima to occur in summer. This is the approximate time when high-density bands precipitate in *Montastraea faveolata* in this region[32]. August, September and October for each year was then determined by measuring the extension rate and assuming a linear relationship between time and extension rate for the given year. The average relative luminescence in the August–October interval is used. Thus, this data refers to a seasonally specific relationship between trade winds (for example, $|V_z|$) and rainfall.

The youngest 30–40 mm of growth in the coral cores were omitted owing to the risk of contamination from the upper 6–8-mm-thick, anomalously high luminescence tissue layer, which is possibly associated with oxidized organics. Cross-dating characteristic luminescent bands between the different cores was applied[33]. After correcting ages the annual luminescence intensity values were standardized in each core. The maximum value was assigned to be 3 and the minimum value –3.

Multiproxy calibrations and reconstructions. Back propagation artificial neural networks were used for the reconstructions, because the nonlinear mapping of the input variables to the output variable inherent in artificial neural networks was found to provide better predictions than conventional linear regression analysis (see Supplementary Information). The correlation coefficients (r_S) between the reconstructed and instrumentally recorded $|V_z|$ and number of major hurricanes are 0.97 ($P < 0.001$, 1949–1990) and 0.92 ($P < 0.001$, 1944–1990), respectively, and the root-mean-square errors of predictions are 0.21 m s^{-1} for $|V_z|$ and 0.21 for hurricanes, respectively.

Warm-season (April–September) SSTs used in the hurricane activity and vertical wind shear reconstructions were retrieved from $5 \times 5^\circ$ grids[20]. The raw warm-season instrumental data, which were used to calibrate temperature reconstructions in ref. 20, were also used here in the training of the networks and in the reconstructions back to 1902. A comparison between the SST data used and the ERSST v2 data[22] averaged over a slightly larger region (10 to 26° N and 20 to 86° W) during August–October back to 1856 yields an r_S of 0.77 ($P < 0.001$). r_S between ERSST v2, averaged over the region referred to above, and the instrumental $|V_z|$, averaged over the MDR, is –0.38 ($P < 0.01$; 1950–2003). r_S between ERSST v2 and number of *G. bulloides* is –0.43 ($P < 0.001$; 1900–1990). r_S between ERSST v2 and the master luminescence record is 0.28 ($P < 0.05$; 1950–2000).

No significant statistical relationships are found between the AMO index of ref. 26 and the major hurricane and $|V_z|$ records (1730–1985). The r_S between the AMO index of ref. 6 and the major hurricane record is 0.32 ($P < 0.001$; 1858–2003) and that between the AMO index of ref. 6 and $|V_z|$ is -0.22 ($P < 0.01$; 1858–2003). The r_S between TSI and the major hurricane record is –0.37 ($P < 0.001$; 1730–2003) and that between TSI and $|V_z|$ is 0.44 ($P < 0.001$; 1730–2003) using the instrumental major hurricane observations since 1944 and $|V_z|$ since 1949 (Fig. 4). Observational bias adjustments are taken into account by using 52 m s^{-1} as a threshold for major hurricanes during the time period 1944–1969.

31. Barnes, D. J., Taylor, R. B. & Lough, J. M. Measurement of luminescence in coral skeletons. *J. Exp. Mar. Biol. Ecol.* **295**, 91–106 (2003).
32. Watanabe, T. A., Winter, A., Oba, T., Anzai, R. & Ishioroshi, H. Evaluation of the fidelity of isotope records as an environmental proxy in the coral *Montastraea*. *Coral Reefs* **21**, 169–178 (2002).
33. Hendy, E. J., Gagan, M. K. & Lough, J. M. Chronological control of coral records using luminescent lines and evidence for non-stationary ENSO teleconnections in northeast Australia. *Holocene* **13**, 187–199 (2003).

LETTERS

Boron and oxygen isotope evidence for recycling of subducted components over the past 2.5 Gyr

Simon Turner[1], Sonia Tonarini[2], Ilya Bindeman[3]†, William P. Leeman[4] & Bruce F. Schaefer[5]

Evidence for the deep recycling of surficial materials through the Earth's mantle and their antiquity has long been sought to understand the role of subducting plates and plumes in mantle convection. Radiogenic isotope evidence for such recycling remains equivocal because the age and location of parent–daughter fractionation are not known. Conversely, while stable isotopes can provide irrefutable evidence for low-temperature fractionation, their range in most unaltered oceanic basalts is limited and the age of any variation is unconstrained. Here we show that $\delta^{18}O$ ratios in basalts from the Azores are often lower than in pristine mantle. This, combined with increased Nb/B ratios and a large range in $\delta^{11}B$ ratios, provides compelling evidence for the recycling of materials that had undergone fractionation near the Earth's surface. Moreover, $\delta^{11}B$ is negatively correlated with $^{187}Os/^{188}Os$ ratios, which extend to subchondritic values[1], constraining the age of the high Nb/B, ^{11}B-enriched endmember to be more than 2.5 billion years (Gyr) old. We infer this component to be melt- and fluid-depleted lithospheric mantle from a subducted oceanic plate, whereas other Azores basalts contain a contribution from ~3-Gyr-old melt-enriched basalt[2]. We conclude that both components are most probably derived from an Archaean oceanic plate that was subducted, arguably into the deep mantle, where it was stored until thermal buoyancy caused it to rise beneath the Azores islands ~3 Gyr later.

The dynamics of the Earth reflect its internal heat but the nature and timescales of mantle convection remain poorly constrained. Over the past decade tomography data have provided spectacular images of seismically fast material inferred to be cool zones of downwelling associated with subducting plates and suggest that these can extend beyond the 670 km discontinuity into the deep mantle, ponding at the core–mantle boundary[3]. Conversely, a significant component of return flow is associated with mantle plumes, many of which, including the Azores, appear to rise from the core–mantle boundary[4]. Thus, there has been much interest in developing independent evidence for entrainment of subducted material from the composition of ocean island basalts erupted above plumes. Radiogenic isotopes have long been used in this search because of their potential to constrain the timescales of recycling and many ocean island basalts have indeed been found to have signatures distinct from those of mid-ocean ridge basalts (MORB)[5] that sample the upper mantle. However, although such signals undoubtedly reflect the time-integrated effects of fractionated parent–daughter element ratios, the age and extent of this fractionation can rarely be deconvolved. Even if this is possible, the parent–daughter fractionation is not restricted to processes occurring near the Earth's surface and could instead reflect intra-mantle metasomatism[6,7]. In contrast, fractionation of isotopes of light elements such as O, B and Li results from low-temperature processes near the Earth's surface, and significant variations in the stable isotope ratios of MORB and ocean island basalts could provide unambiguous evidence for contributions from recycled material[8]. However, the range of O and B isotope ratios observed in MORB and ocean island basalts has generally been rather restricted and observed variations are often attributed to shallow-level assimilation of altered oceanic crust[8–14]. Furthermore, stable isotopes cannot be used to constrain the timescales of recycling.

Recent Os isotope analyses found that seven basalts from the Azores had subchondritic Os isotope ratios and here we supplement those data with new subchondritic Os data from a picrite from Faial which has 14% MgO, 0.117 p.p.b. Os and a $^{187}Os/^{188}Os$ ratio of 0.12559. These require a contribution from a component which must be at least 2.5 Gyr in age[1] and in Table 1 we report the first B and O isotope data from a subset of these well characterized samples[15,16].

Table 1 | $\delta^{11}B$ and $\delta^{18}O$ data for Azores basalts

Sample number	Island	MgO (%)	Nb (p.p.m.)	B (p.p.m.)	$\delta^{11}B$ (‰)	± 1 s.e.m.	Number of analyses, *n*	$\delta^{18}O$ (‰)	± 1 s.e.m.	*n*
S1	Sao Miguel	7.76	70.7	5.4	−6.0	0.5	1	4.88	0.058	3
S3	Sao Miguel	8.34	77.9	6.2	−6.8	0.1	2	Not analysed		
S10	Sao Miguel	8.33	68.8		5.0	0.5	2	5.10	0.007	2
S19	Sao Miguel	6.38	87.5	5.9	−7.4	0.2	1	5.28	0.028	2
SJ26	Sao Jorge	4.71	90.9	5.4	−3.3	0.1	2	5.14	0.047	3
SJ30	Sao Jorge	9.70	49.1	3.1	−4.7	0.3	1	4.94	0.057	2
T6	Terceira	8.70	40.8		Not analysed			4.87	0.070	3
T18	Terceira	7.94	41.5	3.4	−6.0	0.2	2	4.88	0.030	2
P5	Pico	9.63	37.6	2.4	−3.6	0.2	1	5.10	0.048	2
P25	Pico	8.24	43.1	3.8	−3.5	0.3	1	5.02	0.014	2
P29	Pico	8.16	52.4	3.7	−4.1	0.2	1	5.14	0.070	3
FCA-6	Faial	9.73	35.0	2.6	−3.3	0.5	2	5.02	0.014	2
FCA-24	Faial	13.99	30.2	5.9	−2.1	0.4	2	5.14	0.014	3
FCP-18	Faial	7.83	46.0	4.4	−7.6	0.5	2	5.09	0.057	2

[1]GEMOC, Department of Earth and Planetary Sciences, Macquarie University, Sydney, New South Wales 2109, Australia. [2]Istituto di Geoscienze e Georisorse, Via Moruzzi 1, 56147 Pisa, Italy. [3]Department of Geology and Geophysics, University of Wisconsin, 1215 West Dayton Street, Madison, Wisconsin 53706, USA. [4]National Science Foundation, 4201 Wilson Blvd, Arlington, Virginia 22230, USA. [5]School of Geosciences, Monash University, PO Box 28E, Clayton, Victoria 3800, Australia. †Present address: Department of Geological Sciences, 1272 University of Oregon, Eugene, Oregon 97403, USA.

The majority were measured in duplicate or triplicate. $^{18}O/^{16}O$ data were obtained by high-precision CO_2 laser fluorination and mass spectrometry[17] on separated olivine phenocrysts. Analyses were performed at the Universities of Wisconsin and Oregon using standards of garnet and mantle San Carlos olivine and similarly low $\delta^{18}O$ olivine values were obtained in both laboratories. The range of $\delta^{18}O$ values (5.14‰ to 4.87‰) exceeds analytical error and extends below the value (5.2 ± 0.2‰) value inferred for pristine mantle[9]. A comparable $\delta^{18}O$ range, extending down to 4.57, was also found in a recent study of olivine phenocrysts from Sao Miguel[18]. Similarly, MORB glass data[10] from 38–40° N along the mid-Atlantic ridge, across the centre of the Azores platform, range from 5.2‰ to 5.7‰ which is equivalent to 4.7‰ to 5.2‰ in olivine. Thus, $\delta^{18}O$ values below that of pristine mantle do appear to occur in the Azores[18] (Fig. 1). Such low $\delta^{18}O$ values are characteristic of the layer-3 gabbros and altered peridotites from the oceanic lithosphere ($\delta^{18}O = 3$–5) but are unlike altered oceanic crust ($\delta^{18}O = 5$–9) or pelagic sediments ($\delta^{18}O = 15$–25)[9]. Subcontinental lithospheric mantle is expected to have MORB-like $\delta^{18}O$ and so the presence of low $\delta^{18}O$ supports models of recycling of oceanic rather than subcontinental lithospheric mantle[1,19].

The $^{11}B/^{10}B$ isotope ratios and B concentrations were measured by thermal ionization mass spectrometry at Pisa using the di-caesium, meta-borate method[20] following alkali carbonate fusion and ion exchange separation[21]. Sample S10, which had visible evidence for alteration along cracks, yielded a $\delta^{11}B$ ratio of +5.02, providing strong evidence for seawater ($\delta^{11}B = +39$) contamination for this one sample. For the remaining samples, $\delta^{11}B$ data show a large range from −3.3 to −7.6‰. B concentrations vary from 2.4 to 6.2 p.p.m. and the samples with the lowest B concentrations have the highest B isotope ratios. Also, with the exception of one sample (FCP-18), B and O isotopic compositions are positively correlated, ranging from compositions within the normal range for oceanic basalts to low $\delta^{11}B$ and $\delta^{18}O$ (Fig. 2a). These relationships are in contrast to the effects of seawater contamination and thus the data are likely to reflect magmatic signatures. The source of MORB has $^{87}Sr/^{86}Sr \approx 0.7025$, an average $\delta^{11}B$ of −4.6‰ (refs 11–13) and Nb/B ≈ 3 (ref. 22), whereas the Azores samples have higher $^{87}Sr/^{86}Sr$ and Nb/B = 5–17 (Fig. 2b, c). These observations, in combination with the inverse relationship between B and $\delta^{11}B$ and the O isotope data, strongly suggest that the basalts sample a source that has been modified. The O and B isotope data implicate recycled material that had undergone fractionation at relatively low temperatures in the near-surface environment. Conversely, the absence of any strongly elevated $\delta^{11}B$ and $\delta^{18}O$ ratios, in conjunction with the observation that those samples with the highest $^{87}Sr/^{86}Sr$ also have the lowest $\delta^{18}O$ ratios, indicates that the magmas did not significantly interact with the local mid-Atlantic oceanic crust through which they ascended.

The nature of the recycled material is explored further on a plot of Nb/B versus $\delta^{11}B$ (Fig. 2b). Nb and B have very similar partitioning behaviour in mantle minerals and are unlikely to be fractionated significantly during melting or crystallization[22,23]. Instead, B is strongly fluid-mobile compared with Nb[22,24] and so Nb/B is mainly sensitive to fluid transfer and/or mixing processes, which will be linear on Fig. 2b. MORB and their source have a Nb/B ratio of 3–3.5 (refs 22, 25) whereas the Nb/B ratios in the Azores and many other ocean island basalts are all significantly higher than this (Fig. 2b), suggesting a source strongly depleted in B by fluid removal[22,24]. Fluids preferentially mobilize ^{11}B in the low-temperature environment[26] and so the source of the basalts must have had higher $\delta^{11}B$ than their measured values before fluid extraction of B. This suggests that their source originally had $\delta^{11}B > -2$, which is similar to that of oceanic lithosphere that has been altered by interaction with sea water. Subsequent fluid loss, such as that attending subduction, would raise the Nb/B ratios and lower $\delta^{11}B$; that is, in a manner consistent with the observed decrease in $\delta^{11}B$ downward

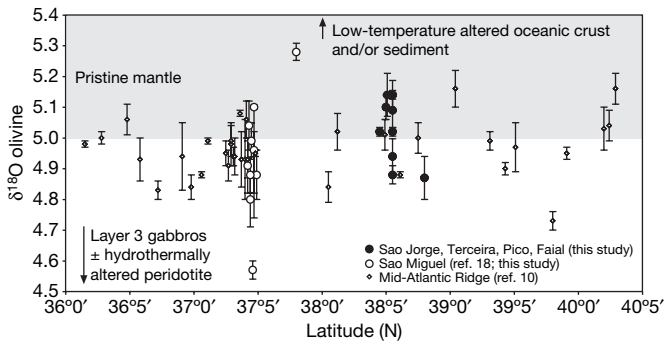

Figure 1 | Oxygen isotope variation across the Azores platform. Plot of $\delta^{18}O$ ($\pm 1\sigma$) versus latitude. Data from this study, and refs 10 and 18. Vectors indicate the sense of displacement during hydrothermal alteration[9].

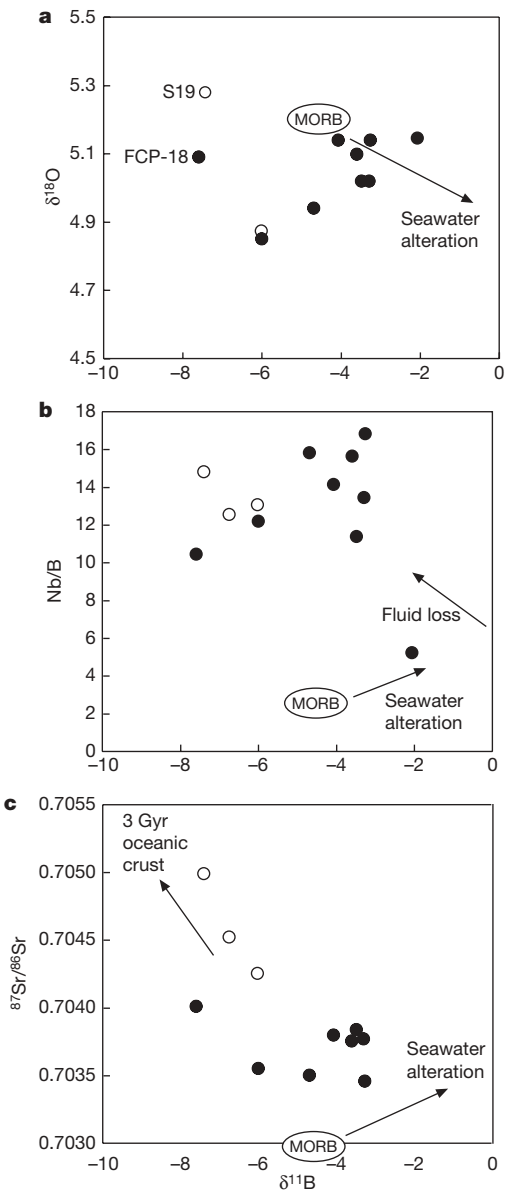

Figure 2 | Variation of B isotopes with other geochemical indices in the Azores. Plots of $\delta^{11}B$ versus $\delta^{18}O$ (**a**), Nb/B (**b**) and $^{87}Sr/^{86}Sr$ (**c**). Vectors indicate the effects of fluid loss[9]. Average MORB value was compiled from refs 11–13, 22, 25 and 30 and the subducted sediment value is taken from ref. 31. Sample numbers in **a** refer to Table 1. Open symbols identify data from Sao Miguel that have been argued to have increased $^{87}Sr/^{86}Sr$ owing to recycling of ~3 Ga oceanic basalts[2].

from altered oceanic crust into the underlying gabbros and peridotites in oceanic lithosphere[26] or decreasing $\delta^{11}B$ in volcanic rocks from cross-arc transects[27]. This could produce a component with $\delta^{11}B \approx -3$ and Nb/B ≈ 17 observed in our samples on Fig. 2b. Other Azores basalts, especially those from Sao Miguel, which trend towards lower $\delta^{11}B$ and Nb/B in Fig. 2b, could reflect involvement of recycled oceanic crust[2].

Although the B and O isotope data unambiguously seem to implicate the presence of recycled components in the Azores plume they do not by themselves constrain the age of these components. However, Fig. 3 shows that there are broad negative correlations of B concentration, Nb/B and $\delta^{11}B$ with $^{187}Os/^{188}Os$ and the observation that the high-Nb/B endmember extends to subchondritic Os isotope ratios uniquely constrains the age of this endmember to exceed 2.5 Gyr (ref. 1). Furthermore, the Sao Miguel rocks bearing evidence for involvement of recycled oceanic crust have high $^{187}Os/^{188}O$ and $^{87}Sr/^{86}Sr$ ratios and recent modelling of Hf–Nd isotope systematics suggests that this component is recycled, melt-enriched oceanic crust which could be as ancient as 3 Gyr (ref. 2). These combined observations provide compelling evidence for both the age and origin of material in a mantle plume.

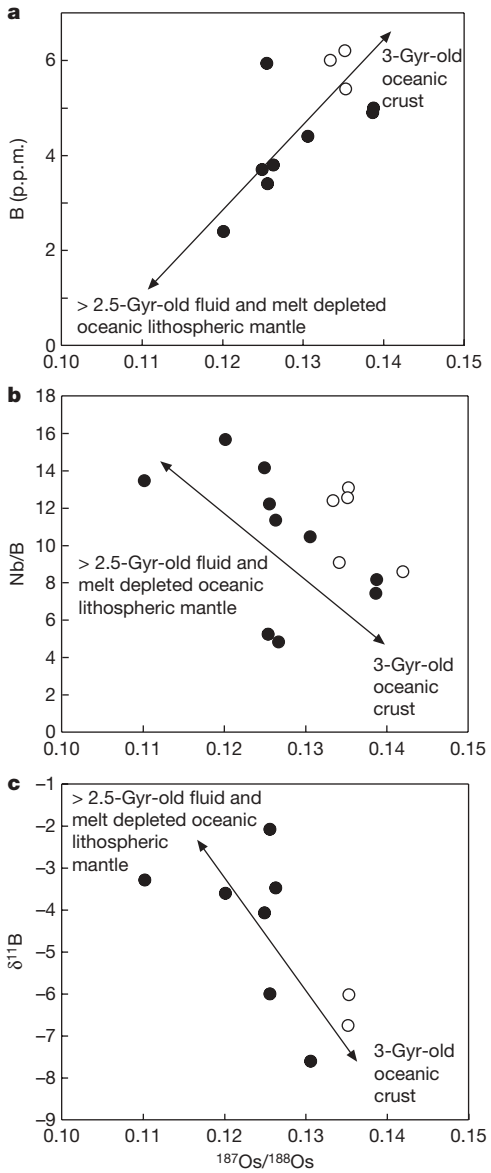

Figure 3 | Variation of Os isotopes with other geochemical indices in the Azores. Plots of $^{187}Os/^{188}Os$ versus B concentration (**a**), Nb/B (**b**) and $\delta^{11}B$ (**c**). Open symbols identify data from Sao Miguel.

Although the multi-stage, multi-component model precludes a unique quantitative treatment, the combined data may be interpreted in the following way. Large degree (≥20%) partial melting to produce Archaean oceanic crust also formed a refractory residual lithospheric mantle that was sufficiently depleted in Re to have a subchondritic Re/Os ratio. Hydrothermal or other surficial processes resulted in lowering of $\delta^{18}O$ and enrichment of B and $\delta^{11}B$ but, during later subduction, fluid loss from the lower gabbro and peridotite sections of the plate raised Nb/B ratios and lowered $\delta^{11}B$. Long-term storage of this material in the mantle resulted in the development of subchondritic Os isotopes while overlying, melt-enriched basalts developed their distinctive Hf-Nd isotope characteristics[2] and elevated $^{187}Os/^{188}O$. Later entrainment in a mantle plume brought these materials back to the shallow mantle, where decompression melting produced basaltic magmas that carry the integrated Os-O-B signal. Thus, the Azores basalts contain evidence for contributions from the two main components of an ancient oceanic plate and the broad symmetry and length scale observed in the isotope data[1] suggests that this component is intrinsic to the plume over 10–100 km. However, numerical fluid dynamic models suggest that subducted materials that remain in the mantle convection system will become highly attenuated and that the timescale for circulation through the mantle is likely to be of the order of 500 million years rather than many billions of years[28,29]. In contrast, recent seismic results suggest that some subducted plates may pile up at the core–mantle boundary[3], where they could remain stored for much longer periods of time. Seismic tomography suggests that the Azores plume is ascending from the core–mantle boundary[4] and so we suggest that this plume samples recycled material that was subducted to the core–mantle boundary and stored there since the Archaean era.

Received 6 February; accepted 30 April 2007.

1. Schaefer, B. F., Turner, S., Parkinson, I., Rogers, N. & Hawkesworth, C. Recycled Archaean oceanic mantle lithosphere in the Azores plume. *Nature* **420,** 324–327 (2002).
2. Elliott, T., Blichert-Toft, J., Heumann, A., Koetsier, G. & Forjaz, V. The origin of enriched mantle beneath Sao Miguel, Azores. *Geochim. Cosmochim. Acta* **71,** 219–240 (2007).
3. Hutko, A. R., Lay, T., Garnero, E. J. & Revenaugh, J. Seismic detection of folded, subducted lithosphere at the core–mantle boundary. *Nature* **441,** 333–336 (2006).
4. Montelli, R. *et al.* Finite-frequency tomography reveals a variety of plumes in the mantle. *Science* **303,** 338–343 (2004).
5. Hofmann, A. W. Mantle geochemistry: the message from oceanic volcanism. *Nature* **385,** 219–229 (1997).
6. DePaolo, D. J. & Wasserburg, G. J. Inferences about magma sources and mantle structure from variations in $^{143}Nd/^{144}Nd$. *Geophys. Res. Lett.* **3,** 743–746 (1976).
7. Sun, S. S. & McDonough, W. F. Chemical and isotopic systematics of oceanic basalts. *Geol. Soc. Spec. Publ.* **42,** 313–345 (1989).
8. Elliott, T., Thomas, A., Jeffcoate, A. & Niu, Y. Lithium isotope evidence for subduction-enriched mantle in the source of mid-ocean-ridge basalts. *Nature* **443,** 565–568 (2006).
9. Eiler, J. M. Oxygen isotope variations of basaltic lavas and upper mantle rocks. *Rev. Mineral. Geochem.* **43,** 319–364 (2001).
10. Cooper, K. M., Eiler, J. M., Asimow, P. D. & Langmuir, C. H. Oxygen isotope evidence for the origin of enriched mantle beneath the mid-Atlantic ridge. *Earth Planet. Sci. Lett.* **220,** 297–316 (2004).
11. Chaussidon, M. & Jambon, A. Boron content and isotopic composition of oceanic basalts: geochemical and cosmochemical implications. *Earth Planet. Sci. Lett.* **121,** 277–291 (1994).
12. Le Roux, P. J., Dixon, J. E., Shirey, S. B. & Hauri, E. H. Boron isotope compositions of South Atlantic MORB and mantle sources. *Geochim. Cosmochim. Acta* 69, abstr. A94 (2005).
13. Chaussidon, M. & Marty, B. Primitive boron isotope composition of the mantle. *Science* **269,** 383–386 (1995).
14. Roy-Barman, M., Wasserburg, G. J., Papanastassiou, D. A. & Chaussidon, M. Osmium isotopic compositions and Re-Os concentrations in sulfide globules from basaltic glasses. *Earth Planet. Sci. Lett.* **154,** 331–347 (1998).
15. Turner, S., Hawkesworth, C., Rogers, N. & King, P. U-Th isotope disequilibria and ocean island basalt generation in the Azores. *Chem. Geol.* **139,** 145–164 (1997).
16. Bourdon, B., Turner, S. P. & Ribe, N. M. Partial melting and upwelling rates beneath the Azores from a U-series isotope perspective. *Earth Planet. Sci. Lett.* **239,** 42–56 (2005).

17. Valley, J. W., Kitchen, N., Kohn, M. J., Niendorf, C. R. & Spicuzza, M. J. UWG-2, a garnet standard for oxygen isotope ratio: strategies for high precision and accuracy with laser heating. *Geochim. Cosmochim. Acta* **59,** 5223–5231 (1995).
18. Widom, E. & Farquhar, J. Oxygen isotope signatures in olivines from Sao Miguel (Azores) basalts: implications for crustal and mantle processes. *Chem. Geol.* **193,** 237–255 (2003).
19. Widom, E. Ancient mantle in a modern plume. *Nature* **420,** 281–282 (2002).
20. Leeman, W. P., Vocke, R. D., Beary, E. S. & Paulsen, P. J. Precise boron isotopic analysis of aqueous samples: ion exchange extraction and mass spectrometry. *Geochim. Cosmochim. Acta* **55,** 3901–3907 (1991).
21. Tonarini, S., Pennisi, M. & Leeman, W. P. Precise boron isotopic analysis of complex silicate (rock) samples using alkali carbonate fusion and ion exchange separation. *Chem. Geol.* **142,** 129–137 (1997).
22. Ryan, J. G., Leeman, W. P., Morris, J. D. & Langmuir, C. H. The boron systematics of intraplate lavlas: implications for crust and mantle evolution. *Geochim. Cosmochim. Acta* **60,** 415–422 (1996).
23. Brenan, J. M. *et al.* Behaviour of boron, beryllium and lithium during partial melting and crystallization: constraints from mineral-melt partitioning experiments. *Geochim. Cosmochim. Acta* **62,** 2129–2141 (1998).
24. Brenan, J. M., Ryerson, F. J. & Shaw, H. F. The role of aqueous fluids in the slab-to-mantle transfer of boron, beryllium, and lithium during subduction: experiments and models. *Geochim. Cosmochim. Acta* **62,** 3337–3347 (1998).
25. Salters, V. J. M. & Stracke, A. Composition of the depleted mantle. *Geochem. Geophys. Geosyst.* **5,** doi:10.1029/2003GC000597 (2004).
26. Ishikawa, T. & Nakamura, E. boron isotope geochemistry of the oceanic crust from DSDP/ODP hole 504B. *Geochim. Cosmochim. Acta* **56,** 1633–1639 (1992).
27. Leeman, W. P., Tonarini, S., Chan, L. H. & Borg, L. E. Boron and lithium isotopic variations in a hot subduction zone—the southern Washington Cascades. *Chem. Geol.* **212,** 101–124 (2004).
28. McKenzie, D. & O'Nions, R. K. The source regions of ocean island basalts. *J. Petrol.* **36,** 133–160 (1995).
29. Van Keken, P. E., Hauri, E. H. & Ballentine, C. J. Mantle mixing: the generation, preservation and destruction of chemical heterogeneity. *Annu. Rev. Earth Planet. Sci.* **30,** 493–525 (2002).
30. Chaussidon, M. & Jambon, A. Boron content and isotopic composition of oceanic basalts: geochemical and cosmochemical implications. *Earth Planet. Sci. Lett.* **121,** 277–291 (1994).
31. Nakano, T. & Nakamura, E. Boron isotope geochemistry of metasedimentary rocks and tourmalines in a subduction zone metamorphic suite. *Phys. Earth Planet. Inter.* **127,** 233–252 (2001).

Acknowledgements We are grateful to N. Rogers, K. Martyn and D. McKenzie, who originally supplied us with the samples analysed in this study, and also to T. Plank for the high-precision Nb concentration data. J. Valley provided access to his O isotope facility. We thank B. Bourdon, J. Gill, M. Reagan and A. Lini for discussions. A review by E. Hauri helped to improve the manuscript. S. Turner is funded by an ARC Federation Fellowship. This is GEMOC publication 466.

Author Information Reprints and permissions information is available at www.nature.com/reprints. The authors declare no competing financial interests. Correspondence and requests for materials should be addressed to S. Turner (sturner@els.mq.edu.au).

LETTERS

Pollinator shifts drive increasingly long nectar spurs in columbine flowers

Justen B. Whittall[1]† & Scott A. Hodges[1]

Directional evolutionary trends have long garnered interest because they suggest that evolution can be predictable. However, the identification of the trends themselves and the underlying processes that may produce them have often been controversial[1]. In 1862, in explaining the exceptionally long nectar spur of *Angraecum sesquipedale*, Darwin proposed that a coevolutionary 'race' had driven the directional increase in length of a plant's spur and its pollinator's tongue[2]. Thus he predicted the existence of an exceptionally long-tongued moth. Though the discovery of *Xanthopan morgani* ssp. *praedicta* in 1903 with a tongue length of 22 cm validated Darwin's prediction[3], his 'race' model for the evolution of long-spurred flowers remains contentious[4]. Spurs may also evolve to exceptional lengths by way of pollinator shifts as plants adapt to a series of unrelated pollinators, each with a greater tongue length[5]. Here, using a species-level phylogeny of the columbine genus, *Aquilegia*, we show a significant evolutionary trend for increasing spur length during directional shifts to pollinators with longer tongues. In addition, we find evidence for 'punctuated' change in spur length during speciation events[6], suggesting that *Aquilegia* nectar spurs rapidly evolve to fit adaptive peaks predefined by pollinator morphology. These findings show that evolution may proceed in predictable pathways without reversals and that change may be concentrated during speciation.

The contemporary evolutionary 'fit' of nectar spurs and pollinator tongue lengths has been repeatedly demonstrated[4,7,8], suggesting that these traits have evolved owing to their interaction. However, there remains a controversy surrounding the mechanism by which this relationship evolves[4,5]. Under a hypothesis first proposed by Darwin[2] and later elaborated by Wallace[9], nectar spurs and pollinator tongues are engaged in a one-to-one coevolutionary 'race'. They suggested that, within a population, the plants with the longest nectar spurs have a selective advantage because their reproductive organs optimally contact pollinators and thus they achieve the greatest reproduction, whereas pollinators with the longest tongues have a selective advantage because they obtain the largest food reward (Fig. 1a). Spur length and pollinator tongue length then coevolve by following gradually shifting adaptive peaks (Fig. 1b). Alternatively, the pollinator shift hypothesis posits that tongue lengths are relatively fixed and spurs evolve in a one-sided process to fit them[5] (Fig. 1c). The tongue length of a pollinator may have evolved before an association with a plant species owing to selection on body size or in response to the spur lengths of other plant species[2]. When a plant becomes newly associated with a pollinator owing to dispersal to a new environment or changes in pollinator abundance, spurs then evolve to fit the pollinator's tongue length (Fig. 1c). Shifts to pollinators with markedly shorter tongues are predicted to be less

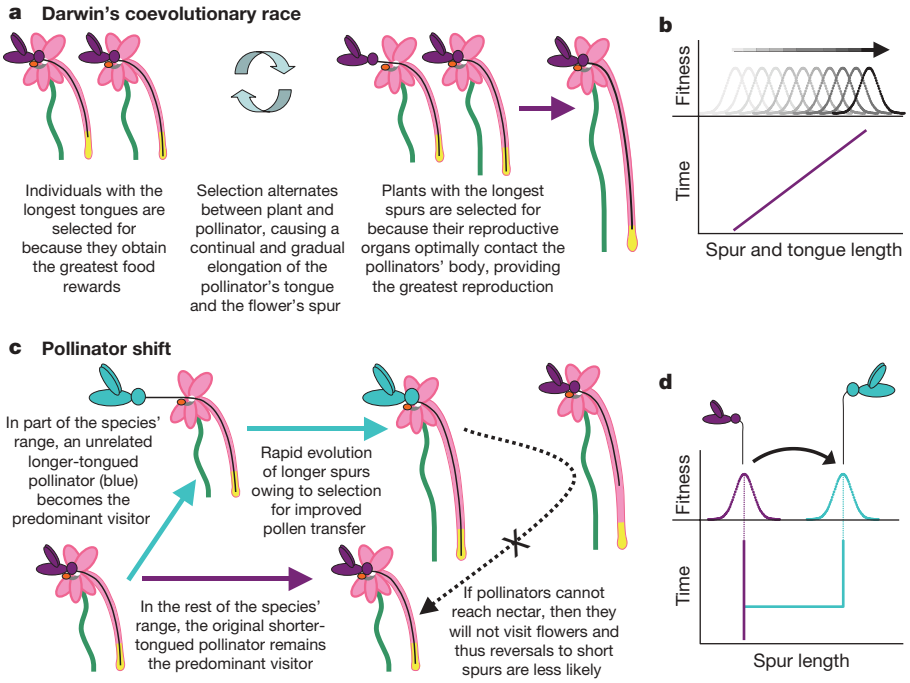

Figure 1 | Two contrasting hypotheses for the evolution of exceptionally long nectar spurs. Darwin's coevolutionary race model (**a**, **b**), which posits a gradual increase in both the pollinator's tongue and the plant's nectar spur, and the pollinator shift model (**c**, **d**), where spur length evolves owing to a switch to a new pollinator with a longer tongue. These models differ in whether adaptive peaks are constantly increasing (**b**), or whether they are relatively fixed optima based on pollinators' pre-existing tongue lengths (**d**). They also differ in whether spur-length evolution occurs gradually (**b**) or in a punctuated fashion (**d**).

[1]Department of Ecology, Evolution and Marine Biology, University of California, Santa Barbara, California 93106, USA. †Present address: Section of Evolution and Ecology, University of California, One Shields Avenue, Davis, California 95616, USA.

likely because pollinators avoid flowers when they cannot obtain a reward[10,11]. Thus, this model also predicts that nectar spurs will generally become longer through time as spurs evolve to match a series of relatively stable adaptive peaks defined by tongue lengths (Fig. 1d).

A major difference between the two hypotheses is whether change occurs gradually within a species' lineage during a coevolutionary race with the same pollinator, or rapidly during shifts to new pollinators (Fig. 1). As shifts to new pollinators generally result in reproductive isolation[12], the change in spur length would be concentrated at speciation. Therefore, comparative phylogenetic analyses of the pattern of spur-length evolution can test both the common prediction that spurs generally become longer through time and also whether one of the hypotheses better explains the overall pattern of spur-length evolution.

The columbine genus *Aquilegia* (Ranunculaceae) is the result of a recent and rapid radiation[13], thought to be due to a key evolutionary innovation, namely nectar spurs[14]. To determine how nectar spur length evolved in columbines, we used a comparative phylogenetic analysis of all 25 North American taxa, which have nectar spurs that vary in length over a 16-fold range (7.5–123 mm). To provide the phylogenetic framework for comparative tests, we used a genomic survey with amplified fragment length polymorphisms (AFLPs) for all taxa (Supplementary Table 1). Bayesian analysis[15] of 1,576 variable markers for 176 individuals results in a highly resolved and well supported phylogeny for the North American *Aquilegia* clade (Supplementary Fig. 1a). Eighty per cent of the 30 interspecific nodes are resolved with greater than 95% posterior probabilities. The phylogenetic results are robust to several alternative methods of phylogenetic reconstruction (Supplementary Fig. 1b–d). To map changes in pollination syndrome onto the phylogeny, we quantified multi-character pollination syndromes using principal components analysis (PCA) of ten floral traits, including nectar spur length. We found that the first two axes separate species into three distinct pollination syndromes (bumble-bee, hummingbird and hawkmoth) as described in ref. 16, and are consistent with direct pollinator observations for 11 of the taxa[17] (Fig. 2a; Supplementary Methods). These three syndromes have nearly non-overlapping distributions of spur lengths (Fig. 2b).

We used the phylogeny to determine the history of pollination syndrome evolution. Pollination syndromes are not all monophyletic (Shimodaira-Hasegawa test; $P < 0.00001$), indicating that multiple shifts have occurred. To identify the number of pollinator transitions, we mapped the three discrete pollination syndromes identified by PCA using local maximum-likelihood ancestral state reconstructions (Fig. 3a). This analysis indicates at least seven independent shifts between unrelated pollinators: two transitions from bumble-bee to hummingbird pollination and five shifts from hummingbird to hawkmoth pollination (Fig. 3a). To test for directionality in pollinator shifts, we developed a model describing the minimum number of transitions in pollination syndrome across the phylogeny[18]. Because transitions could be reversible, there are six possible transitions among the three syndromes. However, the maximum-likelihood solution resulted in only two significant transitions: bumble-bee to hummingbird, and hummingbird to hawkmoth (Fig. 3b; Supplementary Table 2). Therefore, there has been significant directionality in pollinator shifts and a lack of reversals in columbines.

Underlying the directionality of pollinator shifts are evolutionary transitions in spur length. To determine if spur length changes more when pollination syndromes shift, we used independent contrasts[19] and found that 73% of the total spur-length evolution occurs

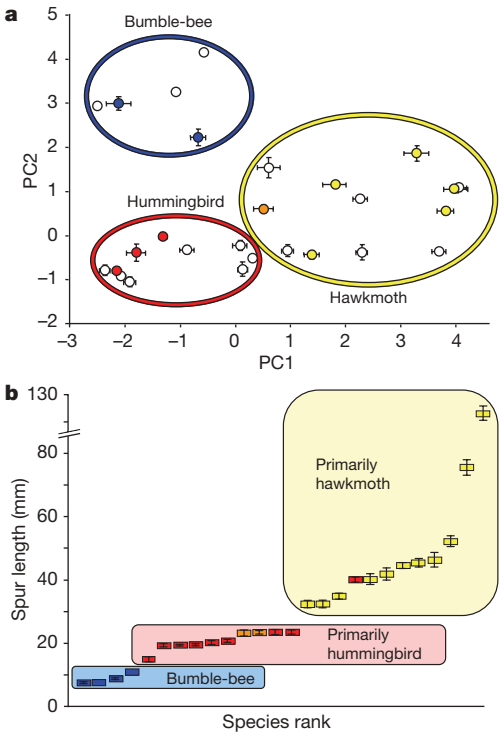

Figure 2 | Quantification of pollination syndromes and the distribution of spur lengths in *Aquilegia*. **a**, Principal components analysis of 10 floral traits clusters species according to pollination syndrome, as defined in ref. 16. Species with published records of pollinator visitation are indicated with coloured symbols (blue, bumble-bee; red, hummingbird; yellow, hawkmoth; orange, hummingbird and hawkmoth; see Supplementary Methods). The first principal components axis (PC1) and the second (PC2) are plotted. Error bars, ±1 s.e.m. **b**, The distribution of spur lengths among the North American *Aquilegia* ranked by size. Taxa in each syndrome are colour-coded as in **a**. Error bars, ±1 s.e.m.

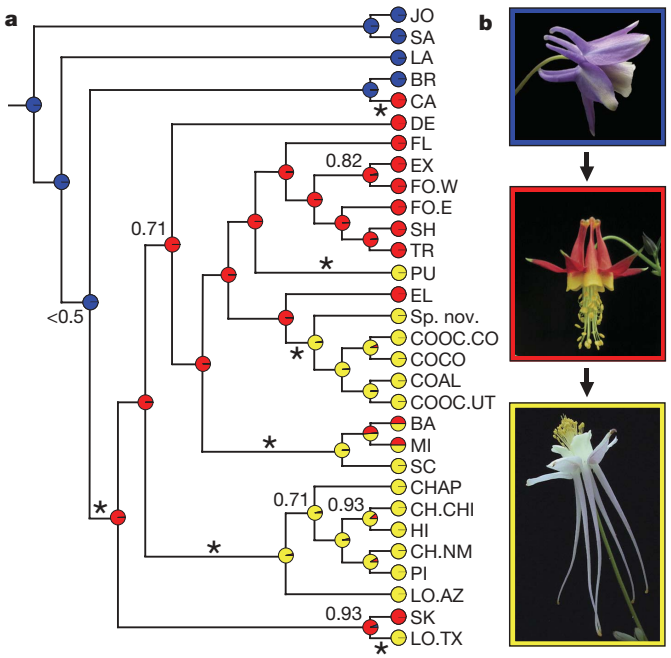

Figure 3 | Phylogenetic analysis of pollination syndrome evolution in *Aquilegia*. **a**, The majority-rule consensus bayesian cladogram with tips of the tree representing reciprocally monophyletic populations or species (see Supplementary Table 1). All interspecific nodes were supported by posterior probabilities >0.95 except where indicated. Species were assigned to pollination syndrome on the basis of Fig. 2a. The probability of each pollination syndrome occurring at ancestral nodes is indicated with pie charts at the nodes. Asterisks on the phylogeny indicate inferred shifts between pollination syndromes. **b**, Representative flowers of each pollination syndrome, with arrows indicating the only two significant transitions identified by the minimal model of evolution.

coincidently with pollinator shifts. This is significantly more than when pollinators do not change (Mann–Whitney, $z = 3.4$, one-tailed $P = 0.00016$). Though it is impossible to determine if spurs have lengthened or shortened when pollination syndromes remain constant, when syndromes shift they do so in ordered transitions (Fig. 3b) and thus we could infer the directionality of spur-length change. Twelve of the thirteen informative contrasts in pollination syndrome resulted in increases in spur length (sign test, one-tailed $P = 0.00171$). The only decrease in spur length occurred for the smallest pollination syndrome contrast (Fig. 4). Furthermore, larger pollination syndrome contrasts are correlated with greater spur-length evolution (regression analysis, $r^2 = 0.669$, $F = 56.58$, d.f. $= 28$, $P = 1.71 \times 10^{-8}$; Fig. 4). These finding are robust to the alternative pollination syndrome assignments for *Aquilegia micrantha* and *Aquilegia barnebyi* (Supplementary Methods) and several alternative branch length transformations (Supplementary Table 3).

The pollinator shift model also predicts that changes in pollination syndrome, and thus spur length, will occur in a 'punctuated' fashion[6], primarily during speciation events where at each node, one daughter lineage rapidly evolves to occupy a new adaptive peak and the other retains the ancestral condition (Fig. 1d). We tested for the existence of one or more stable evolutionary states in spur length by comparing models that incorporate 'adaptive peaks'[20] to a null model of brownian motion. We found significant preference for a model with three distinct optima (likelihood ratio 33.03, d.f. $= 6$, $P = 1.8 \times 10^{-6}$; Table 1), indicating that once a lineage has adapted to one pollination syndrome, spur length remains relatively stable until there is a transition to another pollination syndrome. We also explicitly tested whether spur length evolves gradually, in proportion to branch length, or in a punctuated fashion at speciation[6] (Fig. 1d), and found that the punctuated model was preferred (Supplementary Discussion; Supplementary Table 4).

Spur-length evolution within a pollination syndrome may often be due to Darwin's coevolutionary race hypothesis, though the pollinator shift model may also explain some of this variation. For example, pollinator shifts between distantly related hawkmoths may account for the substantial variation in spur length among hawkmoth-pollinated *Aquilegia* species (Fig. 2b). Hawkmoth pollinators with relatively short tongues, for example, *Hyles lineata* and *Eumorpha achemon* (38–46 mm)[21], belong to the Macroglossinae, whereas those with long tongues, for example, *Sphinx vashti* and *Manduca* spp. (54–137 mm)[21], belong to the Sphinginae. These subfamilies have been separated for at least 13.3 Myr (ref. 22), far longer than the age of the entire North American *Aquilegia* clade[23]. Thus, tongue-length differences among hawkmoths were probably established before their association with *Aquilegia*, perhaps owing to coevolutionary races with other plant species. Therefore, transitions within pollination syndromes may also be consistent with the one-sided pollinator shift model.

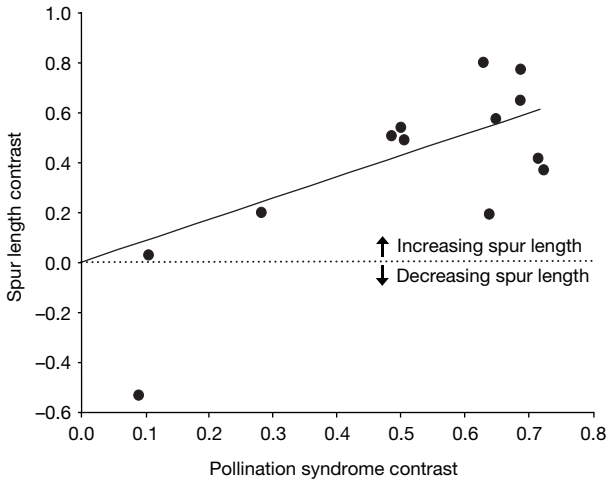

Figure 4 | Independent-contrasts regression analysis of pollination syndrome and spur-length evolution. Pollination syndromes were ordered so that contrasts reflected the minimum model's structured transitions (Fig. 3b). Transitions in pollination syndrome are significantly correlated with increasing spur lengths.

Table 1 | Alternative models of spur-length evolution

Evaluation method	BM model	Number of optima for adaptive models: One	Three
LnL	47.93	47.94	14.90*
AIC	51.93	55.94	26.90†
SIC	54.73	61.54	35.31†

Spur-length evolution was modelled using a non-adaptive, brownian motion (BM) model, as well as adaptive models constrained around one or three adaptive optima[20]. Alternative models were evaluated by log likelihood (LnL), Akaike information criterion (AIC) and Schwarz information criterion (SIC). As statistical criteria for model selection, AIC uses the LnL and the number of parameters whereas the SIC additionally incorporates the number of observations. In both methods, lower values are preferred.
* $P = 1.8 \times 10^{-6}$.
† Strongly preferred[20].

Our finding that spur length in *Aquilegia* evolves largely through directional transitions among pollination syndromes suggests that reaching some adaptive optima may require intermediate 'stepping stones'. Thus, the lack of an intermediate adaptive peak may prevent a species from shifting to an even more extreme morphology. For example, hummingbirds are absent from Eurasia, but hawkmoths do exist there[21]. Significantly, there is very little variation in spur length among Eurasian *Aquilegia* species (4.0–21.5 mm; mean ± s.e.m., 13.0 ± 0.59 mm) and no clear examples of the hawkmoth pollination syndrome. The length of the longest spurred Eurasian *Aquilegia* species (*Aquilegia alpina*, 21.5 mm) is more than 10 mm shorter than the shortest North American hawkmoth-pollinated species (*Aquilegia pubescens*, 32.4 mm). In the absence of hummingbirds or another appropriate pollinator with a comparable tongue length, Eurasian *Aquilegia* species may lack an adaptive 'stepping stone' necessary to reach the hawkmoth adaptive optimum.

Although Darwin's coevolutionary race may be responsible for spur-length evolution within species, our comparative phylogenetic evidence indicates that the majority of spur-length evolution in columbines fits the pollinator shift model. Because columbines have experienced a recent and rapid adaptive radiation[13], it is likely that pollinator tongue lengths were predominantly established before spur-length evolution, which has thus evolved primarily during repeated and directional shifts among pollination syndromes. Of particular note is the finding that shifts in pollination syndrome have occurred without reversals, resulting in the progressive lengthening of nectar spurs. Our results also indicate that large changes in spur length occur disproportionately at speciation events, resulting in 'punctuated' morphological changes.

METHODS SUMMARY

We sampled 155 individuals of all 25 North American *Aquilegia* taxa, and 21 individuals of 8 outgroup taxa, and genotyped them for AFLP markers. We conducted a bayesian phylogenetic analysis of the binary data under a restriction-site model in MRBAYES[15] and compared the resulting phylogeny with parsimony and distance-based phylogenetic analyses (Supplementary Methods). The majority rule consensus tree from the bayesian analysis was pruned to populations or species for subsequent comparative analyses.

For 10 floral traits, we measured 10–52 individuals representing 1 to 5 populations per species for 23 of the 25 taxa in an among-species principal components analysis (see Supplementary Table 5 for axis loadings). Trait data for the remaining two species were estimated from the literature (Supplementary Methods). We conducted local maximum-likelihood ancestral state reconstructions, and tested for directionality of pollination syndrome evolution using Bayes Multistate[18]. Adaptive models of spur-length evolution were compared using the likelihood ratio test, the Akaike information criterion (AIC) and the Schwarz information criterion (SIC) in OUCH![20], and the punctuated-speciational versus gradual models were compared using AIC values in CoMET[6].

Full Methods and any associated references are available in the online version of the paper at www.nature.com/nature.

Received 15 February; accepted 13 April 2007.

1. Gould, S. J. Cope's rule as psychological artefact. *Nature* **385,** 199–200 (1997).
2. Darwin, C. *The Various Contrivances by which Orchids are Fertilized by Insects* (John Murray, London, 1862).
3. Rothschild, L. W. & Jordon, K. A revision of the lepidopterous family Sphingidae. *Novit. Zool.* **9,** 1–972 (1903).
4. Nilsson, N. Deep flowers for long tongues. *Trends Ecol. Evol.* **13,** 259–260 (1998).
5. Wasserthal, L. T. The pollinators of the Malagasy star orchids *Angraecum sesquipedale, A. sororium* and *A. compactum* and the evolution of extremely long spurs by pollinator shift. *Bot. Acta* **110,** 343–359 (1997).
6. Lee, C., Blay, S., Mooers, A., Singh, A. & Oakley, T. H. CoMET: A Mesquite package for comparing models of continuous character evolution on phylogenies. *Evol. Bioinform. Online* **2**, 193–196 (2006); ⟨http://la-press.com/journals.php?pa=abstract&content_id=142⟩.
7. Fulton, M. & Hodges, S. A. Floral isolation between *Aquilegia formosa* and *Aquilegia pubescens*. *Proc. R. Soc. B* **266,** 2246–2252 (1999).
8. Johnson, S. D. & Steiner, K. E. Long-tongued fly pollination and evolution of floral spur length in the *Disa draconis* complex (Orchidaceae). *Evolution Int. J. Org. Evolution* **51,** 45–53 (1997).
9. Wallace, A. R. Creation by law. *Q. J. Sci.* **S140,** 471–486 (1867).
10. Grant, V. & Temeles, E. J. Foraging ability of rufous hummingbirds on hummingbird flowers and hawkmoth flowers. *Proc. Natl Acad. Sci. USA* **89,** 9400–9404 (1992).
11. Hodges, S. A. The influence of nectar production on hawkmoth behavior, self-pollination and seed production in *Mirabilis multiflora* (Nyctaginaceae). *Am. J. Bot.* **82,** 197–229 (1995).
12. Grant, V. Pollination systems as isolating mechanisms in angiosperms. *Evolution Int. J. Org. Evolution* **3,** 82–97 (1949).
13. Hodges, S. A. & Arnold, M. Columbines: A geographically widespread species flock. *Proc. Natl Acad. Sci. USA* **91,** 5129–5132 (1994).
14. Hodges, S. A. & Arnold, M. Spurring plant diversification: Are floral nectar spurs a key evolutionary innovation? *Proc. R. Soc. Lond. B* **262,** 343–348 (1995).
15. Huelsenbeck, J. P. & Ronquist, F. MRBAYES: Bayesian inference of phylogeny. *Bioinformatics* **17,** 754–755 (2001).
16. Grant, V. Isolation and hybridization between *Aquilegia formosa* and *A. pubescens*. *Aliso* **2,** 341–360 (1952).
17. Hodges, S. A., Fulton, M., Yang, J. Y. & Whittall, J. B. Verne Grant and evolutionary studies of *Aquilegia*. *New Phytol.* **161,** 113–120 (2004).
18. Pagel, M., Meade, A. & Barker, D. Bayesian estimation of ancestral character states on phylogenies. *Syst. Biol.* **53,** 673–684 (2004).
19. Felsenstein, J. Phylogenies and the comparative method. *Am. Nat.* **125,** 1–15 (1985).
20. Butler, M. A. & King, A. A. Phylogenetic comparative analysis: A modelling approach for adaptive evolution. *Am. Nat.* **164,** 683–695 (2004).
21. Miller, W. E. Diversity and evolution of tongue length in hawkmoths (Sphingidae). *J. Lepid. Soc* **5,** 9–31 (1997).
22. Hundsdoerfer, A. K., Kitching, I. J. & Wink, M. A molecular phylogeny of the hawkmoth genus *Hyles* (Lepidoptera: Sphingidae, Macroglossinae). *Mol. Phylogenet. Evol.* **35,** 442–458 (2005).
23. Kay, K., Whittall, J. B. & Hodges, S. A. A survey of nrITS substitution rates across angiosperms: An approximate molecular clock with life history effects. *BMC Evol. Biol.* **6,** 36 (2006).

Supplementary Information is linked to the online version of the paper at www.nature.com/nature.

Acknowledgements We thank D. Bush and B. Counterman for laboratory assistance; J. Yang, M. Fulton, S. Schaefer, Y. Kisel and J. Bean for greenhouse and field help; T. Oakley and B. O'Meara for technical assistance; C. Voelkel and C. Eckert for comments on earlier versions of this manuscript; and M. Hodges for help with the figures. Funding was provided by the Botanical Society of America, UCSB's Olivia Long Converse Fellowship, the National Science Foundation, UC Davis' Comparative Biology Postdoctoral Fellowship, and the Native Plant Societies of Wyoming, Colorado, and northern Nevada.

Author Contributions J.B.W. and S.A.H. designed the study and collected the samples; J.B.W. collected and analysed the phylogenetic and comparative data; J.B.W. and S.A.H. wrote the paper.

Author Information Reprints and permissions information is available at www.nature.com/reprints. The authors declare no competing financial interests. Correspondence and requests for materials should be addressed to J.B.W. (jbwhittall@ucdavis.edu) or S.A.H. (hodges@lifesci.ucsb.edu).

METHODS

Taxonomic sampling. One to three populations (2–5 individuals per population) of all 25 North American *Aquilegia* taxa were sampled (Supplementary Table 1). Outgroups consisted of seven Eurasian *Aquilegia* species and *Semiaquilegia adoxoides*.

AFLP methodology. DNA was extracted from fresh leaf material of wild collected plants or plants grown from wild collected seeds. The AFLP protocol followed a modified version of that in ref. 24, with a 5× digestion with *Eco*RI and *Mse*I and two fluorescently labelled E-primers in each selective amplification. Products from 20 selective amplifications were separated on a LiCor 4200 DNA sequencer and variable bands were manually scored with SAGA MX (LiCor).

Phylogenetic analyses. A bayesian analysis of the binary data incorporating differential rates of band gains and losses was conducted with the RESTRICTION model in MRBAYES v3.0 beta 4[15]. As only variable AFLP bands were scored, CODING was set to VARIABLE. Three runs of five million generations were sampled every 100 generations then combined after removing the burn-in (1.5 million generations per run). Posterior probabilities and branch lengths were calculated from the consensus of the posterior distribution of trees. To determine the robustness of the phylogenetic estimate, we conducted a series of additional phylogenetic analyses under distance and parsimony optimality criteria (see Supplementary Methods). For comparative analyses, the bayesian phylogeny was pruned to populations or species using the average branch-length to the clade's descendants and outgroups were removed. The rooted phylogeny was then converted to an ultrametric tree using the NPRS algorithm in r8s (ref. 25) with a smoothing factor of -0.00001. The single unresolved node in the bayesian consensus phylogeny ($PP < 0.5$) was grafted in both alternative arrangements with a minimum branch length (1×10^{-6}) for comparative analyses that require a strictly bifurcating phylogeny[26].

Quantification of floral traits. Ten floral traits were quantified for all species (see Supplementary Methods). PCA among species was then used to validate previously assigned pollination syndromes[16,17] and to help assign syndromes to the few remaining species (see Supplementary Methods). Trait loadings on the first two principal components axes are presented in Supplementary Table 5. *Aquilegia micrantha* and *A. barnebyi* were considered polymorphic for hummingbird and hawkmoth pollination syndrome or, when polymorphic coding was not an option, separate comparative analyses were conducted with these species coded as alternative character states.

Spur lengths. Spur lengths were log-transformed (Kolmogorov–Smirnov test for normality, $P > 0.15$) for comparative analyses.

Pollination syndrome evolution. Local maximum-likelihood ancestral state reconstructions for the three discrete pollination syndromes were conducted in Bayes Multistate[18]. This program was then used to estimate a minimum model of pollination syndrome evolution (Supplementary Table 2). We first tested for irreversible transitions by restricting the smallest rates to equal zero. Likelihood ratios >2 were used to determine if rates were significantly different from zero. To determine if any of the remaining transition rates were significantly different from one another, we compared a two-rate model with a one-rate model. We used a likelihood ratio test to determine statistical significance following a χ^2 distribution with one degree of freedom based on the difference in the number of free parameters between the two models.

Calculation of independent contrasts. We tested for correlated evolution of pollination syndrome and spur length using independent contrasts[19] as implemented in the PDAP module[27] of Mesquite[28]. Pollination syndromes were coded as discrete states as assigned (Fig. 2a) and ordered on the basis of the minimum model of pollination syndrome evolution (Fig. 3b). Combining continuous and discrete characters does not violate the statistical assumptions of independent contrasts[29]. Independent contrasts analysis can be sensitive to branch-length assignments, so we used a branch-length diagnostic[29] and several alternative branch-length transformations (Supplementary Table 3). All contrasts, including non-informative pollinator contrasts, were included in the regression analysis providing a conservative estimate of correlated evolution between pollination syndrome and nectar spur length[29].

Tempo and mode of spur-length evolution. We tested a series of alternative evolutionary models to determine the tempo and mode of spur-length evolution. First, we examined the fit of several adaptive models in OUCH![20] to compare the maximum likelihood of the brownian motion model with successively more complex adaptive models that incorporate an Orenstein-Uhlenbeck elasticity parameter modelling adaptive optima. We compared adaptive models with one versus three optima as described in ref. 20. The fit of the data to the models was estimated using a likelihood ratio test, the Akaike information criterion and the Schwarz information criterion.

We examined the importance of topology and alternative branch-length scaling using CoMET[6] implemented in Mesquite[28]. We compared results from a gradual model of evolution (termed pure-phylogenetic distance[6]) to a punctuated, speciational model (termed punctuated average equal[6]). Alternative models were evaluated using the Akaike information criterion. The maximum likelihood solution assigns which descendent lineage evolves and which remains constant.

24. Vos, P. *et al.* AFLP: A new technique for DNA fingerprinting. *Nucleic Acids Res.* **23**, 4407–4414 (1995).
25. Sanderson, M. J. r8s: inferring absolute rates of molecular evolution and divergence times in the absence of a molecular clock. *Bioinformatics* **19**, 301–302 (2003).
26. Pagel, M. The maximum likelihood approach to reconstructing ancestral character states of discrete characters on phylogenies. *Syst. Biol.* **48**, 612–622 (1999).
27. Midford, P., Garland Jr., T. & Maddison, W. P. PDAP package of Mesquite. Version 1.07 (2005); ⟨http://mesquiteproject.org/pdap_mesquite/index.html⟩.
28. Maddison, W. P. & Maddison, D. R. Mesquite: A modular system for evolutionary analysis. Version 1.05 (2004); ⟨http://mesquiteproject.org/mesquite/mesquite.html⟩.
29. Garland, T., Harvey, P. H. & Ives, A. R. Procedures for the analysis of comparative data using phylogenetically independent contrasts. *Syst. Biol.* **41**, 18–32 (1992).

LETTERS

West Nile virus emergence and large-scale declines of North American bird populations

Shannon L. LaDeau[1], A. Marm Kilpatrick[2] & Peter P. Marra[1]

Emerging infectious diseases present a formidable challenge to the conservation of native species in the twenty-first century[1]. Diseases caused by introduced pathogens have had large impacts on species abundances[2], including the American chestnut[3], Hawaiian bird species[4] and many amphibians[5]. Changes in host population sizes can lead to marked shifts in community composition and ecosystem functioning[3,4,6]. However, identifying the impacts of an introduced disease and distinguishing it from other forces that influence population dynamics (for example, climate[7]) is challenging and requires abundance data that extend before and after the introduction[2,5]. Here we use 26 yr of Breeding Bird Survey (BBS)[8] data to determine the impact of West Nile virus (WNV) on 20 potential avian hosts across North America. We demonstrate significant changes in population trajectories for seven species from four families that concur with a priori predictions and the spatio-temporal intensity of pathogen transmission. The American crow population declined by up to 45% since WNV arrival, and only two of the seven species with documented impact recovered to pre-WNV levels by 2005. Our findings demonstrate the potential impacts of an invasive species on a diverse faunal assemblage across broad geographical scales, and underscore the complexity of subsequent community response.

Seven years after the emergence of WNV in New York City in 1999, the population-level impacts of this disease on wild birds remain largely unknown[9,10]. Tens of thousands of dead individuals from wild, zoo and pet populations have tested positive for WNV across North America[11], and challenge experiments have demonstrated interspecific variability in mortality rates under laboratory conditions[12]. Early field studies documented mortality in some species[13,14] and evidence of spatially heterogeneous fluctuations[9,15,16], but overall population patterns were inconclusive. Our study tests the hypothesis that WNV has caused significant population declines in a broad taxonomic range of avian hosts across North America. We explicitly considered variability in host susceptibility, spatio-temporal heterogeneity in pathogen transmission, and impacts on populations.

To test this hypothesis, we developed a set of independent predictions of WNV impact for 20 species of birds from 11 families on the basis of published laboratory infection experiments, mosquito feeding studies and seroprevalence surveys (Table 1 and Supplementary Table 1). Target species span a range of expected impacts, from crows with high mortality to gray catbirds and mourning doves, which seem to tolerate infection without significant morbidity[12,17]. Additionally, we chose five species (Baltimore oriole, chipping sparrow, eastern bluebird, eastern towhee and white-breasted nuthatch) that have not been the focus of previous work to assess potential disease impacts on a broader community. We then used a bayesian hierarchical regression fit to 26 yr of survey data to test these species-specific predictions across the large geographical scale represented by WNV emergence in North America.

Table 1 | Predicted and observed impact of WNV, climate influence and 10- and 26-yr minimum abundances

Species	Predicted impact	Observed impact	Change in DIC with climate (%)	Minimum abundance	
				10-yr	26-yr
American crow (*Corvus brachyrhynchos*)	High	Yes	4.6	2004*	2004*
Blue jay (*Cyanocitta cristata*)	High	Yes	−14.5‡	2004*	2004*
Fish crow (*Corvus ossifragus*)	High	No	0.01	2005*	2005*
Tufted titmouse (*Baeolophus bicolor*)	High	Yes	−1.1‡	2004*	1980
American robin (*Turdus migratorius*)	Moderate	Yes	5.7	2005*	1981
House wren (*Troglodytes aedon*)	Moderate	Yes	0.1	2003*	2003*
Chickadee† (*Poecile* spp.)	Moderate	Yes	−23.8‡	1996	1985
Common grackle (*Quiscalus quiscula*)	Moderate	No	0	2003*	2003*
Northern cardinal (*Cardinalis cardinalis*)	Moderate	No	2.1	1997	1980
Song sparrow (*Melospiza melodia*)	Moderate	No	−5.4‡	2004*	2004*
Downy woodpecker (*Picoides pubescens*)	Low	No	−1.0‡	2003*	1984
Gray catbird (*Dumetella carolinensis*)	Low	No	−1.2‡	1997	1986
Mourning dove (*Zenaida macroura*)	Low	No	−1.8‡	1997	1980
Northern mockingbird (*Mimus polyglottos*)	Low	No	0.4	1997	1997
Wood thrush (*Hylocichla mustelina*)	Low	No	0.1	2003*	2003*
Eastern bluebird (*Sialia sialis*)	Unknown	Yes	0.4	2003*	1980
Baltimore oriole (*Icterus galbula*)	Unknown	No	4.4	2004*	2004*
Chipping sparrow (*Spizella passerina*)	Unknown	No	4.3	1997	1980
Eastern towhee (*Pipilo erythrophthalmus*)	Unknown	No	−1.2‡	2004*	1991
White-breasted nuthatch (*Sitta carolinensis*)	Unknown	No	0.2	1996	1984

See Supplementary Table 1 for full details of predicted impact data. Impact of WNV is measured as abundance below 95% CIs after WNV arrival. Data are for 20 North American bird species.
* The indicated years follow peak human WNV epidemics in the United States (2002–03).
† Black-capped (*Poecile atricapilla*) and Carolina chickadee (*Poecile carolinensis*) numbers were combined, as species-specific data are unreliable in areas of range overlap.
‡ Negative values for deviance information criterion (DIC) indicate improved model fit with inclusion of climate for these species.

[1]Smithsonian Migratory Bird Center, National Zoological Park, Washington DC 20008, USA. [2]Consortium for Conservation Medicine, New York, New York 10001, USA.

Thirteen of the twenty species studied reached 10-yr population lows after the large-scale human WNV epidemics that occurred in much of the United States in 2002–03 (ref. 11) ($P = 0.002$, assuming probability of 10-yr low after 2002 = 0.30), and eight recorded their lowest abundance over the 26 yr studied ($P = 0.001$, assuming probability of 26-yr low after 2002 = 0.12) (Table 1 and Fig. 1). However, to determine whether WNV was involved in these declines, changes in abundance must be evaluated in the context of long-term trends, climate and habitat availability. We included climate variability (El Niño/Southern Oscillation) in final population models for eight species for which model fit was significantly improved (Table 1 and Supplementary Information). We did not include a land-use component in the population model and thus, are unable to rule out a potentially confounding role of changes in land cover during this study (but see below).

Observed abundances after WNV emergence were significantly lower than expected given two decades of population variability for seven species across multiple geographical regions (Figs 2 and 3). Six of these species were independently predicted to suffer high or moderate impacts, and the seventh was previously unstudied (Table 1). These seven species included two members of the family Corvidae (American crow and blue jay), two from Turdidae (American robin and eastern bluebird), two from Paridae (chickadees and tufted titmouse) and one from Troglodytidae (house wren). Population deviations (average difference between modelled and observed abundances) were highly correlated with categorical predicted impacts for the 15 species with prior information (Supplementary Information; $r = -0.67$, $n = 15$, $P = 0.007$). All seven of these species are peridomestic, with known suburban association[8,18]. Thus, the declines observed for these species are opposite from expectations given continued suburbanization after 1999[19], but are consistent with impacts owing to WNV.

Observed impacts included steep and sometimes progressive multi-year declines in regional populations of American crows (Fig. 2), American robins, chickadees and eastern bluebirds, which were all increasing before WNV arrival (Fig. 1). Other species, including blue jays, tufted titmice and house wrens showed strong 1- or 2-yr declines after intense WNV epidemics, but little or no impacts at other times. Regionally, we found significant deviations from expected abundances for all seven species in the eastern United States (Figs 2 and 3). In other areas where WNV has been present for fewer years, the intensity of impact varied among species (Supplementary Fig. 1). Common grackle populations in Maryland declined significantly after WNV emergence in that state, although in other regions this species remained at expected abundances (Supplementary Fig. 2).

The intensity of declines after pathogen emergence was most marked in American crows (Fig. 2). By 2005, crow abundances had declined regionally by up to 45% from 1998 levels, although they had increased steadily for two decades. American crow declines were positively correlated with the intensity of human WNV epidemics within each region ($r = -0.56$, $n = 21$, $P = 0.0003$), despite variability in human behaviour and feeding of mosquitoes on humans compared with birds[11,17,20]. Similar correlations between human infections and impacts on other avian species were strongest for house wrens and eastern bluebirds ($P < 0.002$), marginally significant for tufted titmice, American robins and chickadees ($0.05 < P < 0.10$), and non-significant for blue jays ($P = 0.34$; Supplementary Table 2) and the 13 species without detectable WNV impact (P-values > 0.1).

Similarly, the intensity of WNV impacts on these six affected species was not always consistent across species or regions (Fig. 3). American robin, eastern bluebird and tufted titmouse populations remained below expected abundance across their entire ranges in 2005. Deviations in chickadee populations were significantly reduced in the east but not at their western range limits. Neither house

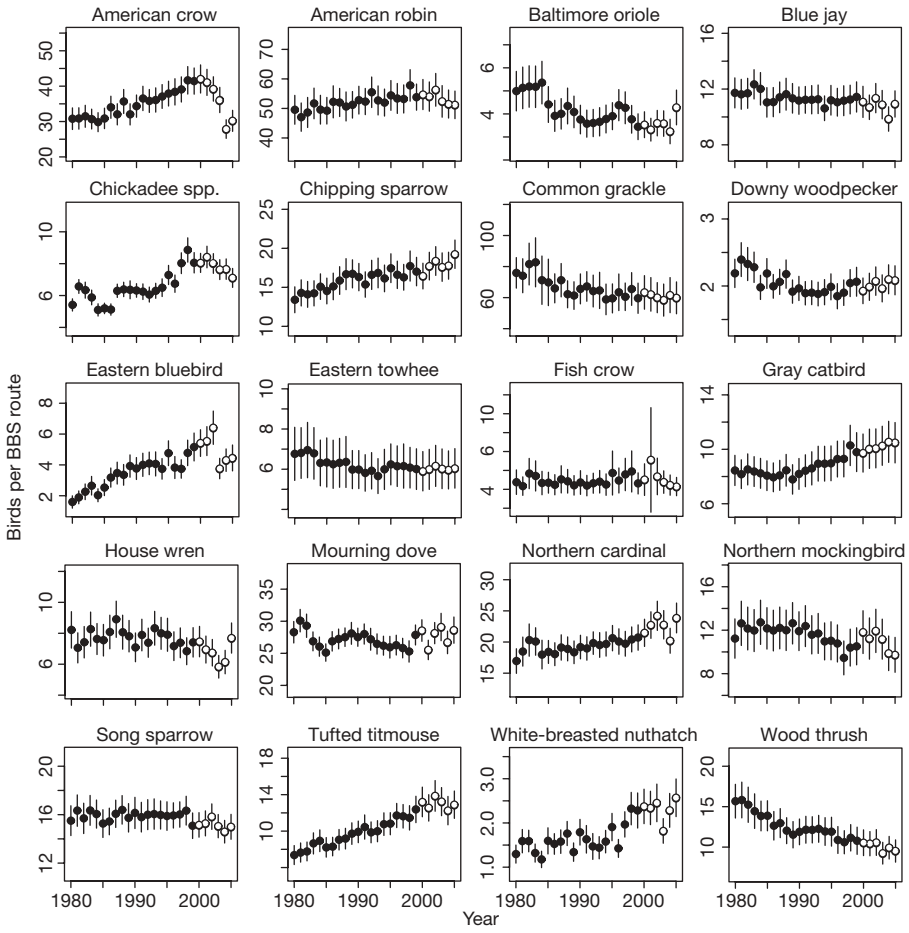

Figure 1 | Time series of mean abundance per BBS route adjusted for missing observations and observer variance. Error bars show 2 standard errors. Open circles denote years after WNV was first detected in North America. Population growth rates between 1980 and 1998 that were significantly different from 0: American crow (95% CI for linear trends (0.014, 0.020)), American robin (0.06, 0.010), Black-capped and Carolina chickadees (0.003, 0.012), chipping sparrow (0.118, 0.175), eastern bluebird (0.046, 0.060), northern cardinal (0.006, 0.011), tufted titmouse (0.026, 0.033), white-breasted nuthatch (0.014, 0.028), Baltimore oriole (−0.0.016, −0.006), common grackle (−0.022, −0.014) and wood thrush (−0.023, −0.017).

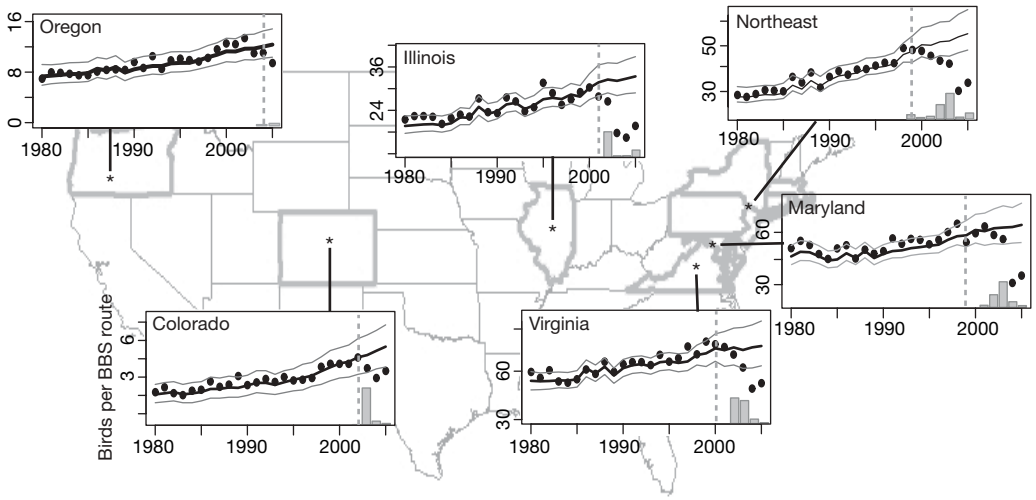

Figure 2 | Declining American crow populations. Observed abundances (circles) versus mean posterior estimates (solid line, with 95% CIs) by region across North America are shown. Values on the *y* axis are the average number of birds observed per BBS route adjusted for observer differences and missing data. Shaded histograms show numbers of reported annual human infections[11] per region (maximum cases per year in northeast, 370; Maryland, 73; Virginia, 29; Illinois, 884; Colorado, 2,947; and Oregon, 7). Vertical dotted lines denote the initial detection of WNV in birds, mosquitoes or humans[11].

wren nor blue jay populations showed significant declines in Virginia, whereas abundances were up to 22% and 26% below that expected in other regions before recovering in 2005 (Supplementary Information).

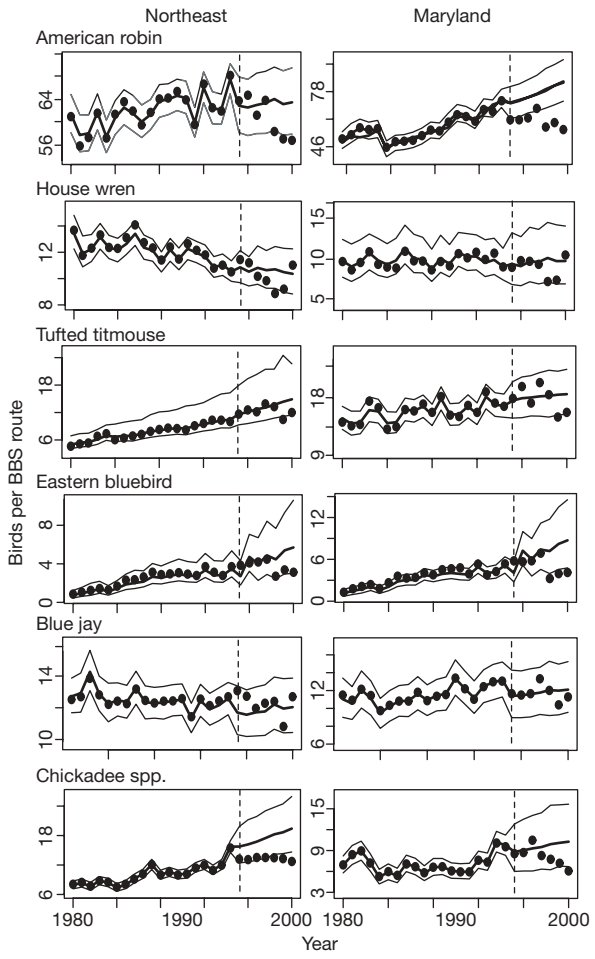

Figure 3 | Population declines and WNV epidemics in the northeastern United States and Maryland. Observed abundances (circles; birds observed per BBS route) versus mean posterior estimated population abundances (solid line, with 95% CIs) for six impacted species are shown. The vertical dotted lines denote the initial detection of WNV in birds, mosquitoes or humans[11]. The complete version of this figure presents observed and expected abundances for each species in each geographical region where it is present (Supplementary Fig. 1).

Assessing the impacts of an invasive pathogen on host populations across a continent requires difficult assumptions regarding exposure rates, and analyses that are correlational in nature. We approached these challenges by using two decades of local population surveys and climate data to predict species abundance distributions in all years after WNV was first identified. We further strengthened our conclusions by comparing our results to the species-specific impacts predicted from a collection of previous studies (Table 1 and Supplementary Table 1) and to the spatial and temporal pattern in human epidemics (Fig. 2 and Supplementary Table 2). We detected significant declines for six species predicted to have high or moderate WNV impacts, and did not detect declines in the five species with predicted low impact. Additionally, we identified sudden and significant declines in eastern bluebird populations, highlighting the possibility that species that have not been studied with respect to WNV may also be affected by this disease. The fact that we did not detect declines in the eight other species, which appeared to persist at the same abundance or even show increased abundance in the presence of WNV (Baltimore oriole, chipping sparrow, eastern towhee, northern cardinal, white-breasted nuthatch), suggests that the impacts of WNV were relatively low or that detection of population declines may have been masked by regional variability in population fluctuations or long term declines (common grackle, fish crow, song sparrow).

After significantly low abundances, both blue jays and house wrens returned to expected population levels in 2005. The resiliency of species and the lasting impact of WNV will ultimately depend on the species-specific interactions between susceptibility, exposure and intrinsic population growth rates. The rank of observed impacts in corvids is consistent with susceptibility to experimental WNV infection studies, which suggest that American crows suffer the greatest mortality (100%), followed by blue jays (75%) and then fish crows (53%)[12]. Such interspecific differences in pathogen effects on populations have been observed in other disease systems[7,21] and can result in important changes in community composition.

The spatial heterogeneity in disease impact apparent for some species may reflect underlying regional differences in the intensity of viral transmission. Several key factors in WNV transmission are known to vary across the continental United States, including the dominant enzootic vectors[22], the relationships between vector abundance and land use[23], and differences in the composition of host communities that can, in turn, influence mosquito feeding preferences[20]. The role of these and other factors in determining WNV transmission and exposure among hosts is an important topic for future research.

Changes in population abundance such as those documented in this study may themselves alter WNV transmission dynamics[20,24]. Mortality is likely to facilitate WNV amplification because the

infectiousness of hosts (magnitude of viraemia and length of viral shedding) is greater in individuals that die relative to those that survive[12], and hosts that die from infections are not present as immune or dead-end hosts. Mortality also increases the vector to host ratio, which increases the reproductive ratio of the pathogen, R_0. Decreases in host abundance may have other impacts on WNV transmission. For example, decreases in the abundance of American robins, which appear to be an important WNV amplification host in several regions of the USA[17,25], have been linked to higher incidences of mosquitoes feeding on humans and intensified human WNV epidemics[20].

The impacts of invasive pathogens compound existing stressors and create formidable challenges for protecting native wildlife[1,26]. West Nile virus will continue to affect avian communities in the foreseeable future, and substantial ecosystem effects may become evident with time. Finally, we believe that the findings presented here are probably conservative estimates of population-level impacts because the hardest hit avian sub-populations may reside outside the BBS survey areas, which are limited to secondary roads and generally exclude urban centres where the predominant *Culex* mosquito vectors in the eastern United States are most common. Nonetheless, the population changes that we have documented have already led to marked changes in the composition of avian communities across North America.

METHODS SUMMARY

We selected 20 common North American bird species that were regularly present along survey routes in the northeastern United States where WNV first emerged. We further chose species with available background information regarding susceptibility to WNV infection (Supplementary Information), and selected the species pool to cover the range of expected mortality. Finally, we randomly selected five species from the group that satisfied our general survey criteria but had not been previously studied with regard to WNV. This produced a total of 20 species, which was chosen as the number that we could efficiently model and evaluate.

We used 26 yr of North American BBS[8] data (1980–2005) for each of the species selected. We included data from an average of 38 routes (range 15–88) and 1,900 distinct census points per region (selected to represent WNV dispersal westward from its east coast introduction) so that the patterns we detected would represent regional population changes, rather than local-scale stochasticity[9,15,16]. We used a hierarchical bayesian regression model[27] fit to data collected before the emergence of WNV to estimate probability distributions for expected abundance in all subsequent years to 2005. Posterior distributions for expected abundance explicitly incorporated trends before WNV emergence and regional climate variability (Supplementary Information), as well as stochasticity associated with location and observation error. We considered a species to have been significantly affected when observed abundances fell outside 95% credible intervals (95% CIs) from the posterior abundance distributions. We validated our results by comparing the species-specific deviations from expected population abundances with predicted WNV impacts based on a collection of previous exposure and mortality studies. Finally, we evaluated the agreement between the timing of our estimated WNV impacts with known WNV presence in a region (first documented and human epidemics).

Full Methods and any associated references are available in the online version of the paper at www.nature.com/nature.

Received 8 November 2006; accepted 11 April 2007.
Published online 16 May 2007.

1. Daszak, P., Cunningham, A. A. & Hyatt, A. D. Emerging infectious diseases of wildlife—threats to biodiversity and human health. *Science* **287,** 443–449 (2000).
2. Hochachka, W. M. & Dhondt, A. A. Density-dependent decline of host abundance resulting from a new infectious disease. *Proc. Natl Acad. Sci. USA* **97,** 5303–5306 (2000).
3. Paillet, F. L. Chestnut: history and ecology of a transformed species. *J. Biogeogr.* **29,** 1517–1530 (2002).
4. Van Riper, C. III, Van Riper, S. G., Goff, M. L. & Laird, M. The epizootiology and ecological significance of malaria in Hawaiian (USA) land birds. *Ecol. Monogr.* **56,** 327–344 (1986).
5. Lips, K. R. *et al.* Emerging infectious disease and the loss of biodiversity in a Neotropical amphibian community. *Proc. Natl Acad. Sci. USA* **103,** 3165–3170 (2006).
6. Hooper, D. U. *et al.* Effects of biodiversity on ecosystem functioning: A consensus of current knowledge. *Ecol. Monogr.* **75,** 3–35 (2005).
7. Daszak, P. *et al.* Amphibian population declines at savannah river site are linked to climate, not chytridiomycosis. *Ecology* **86,** 3232–3237 (2005).
8. Sauer, J. R., Hines, J. E. & Fallon, J. The North American Breeding Bird Survey, Results and Analysis 1966–2005. Version 6.2. 2006 ⟨http://www.mbr-pwrc.usgs.gov/bbs/bbs.html⟩ (2005).
9. Caffrey, C. & Peterson, C. C. Christmas bird count data suggest West Nile virus may not be a conservation issue in Northeastern United States. *Am. Birds* **57,** 14–21 (2003).
10. Marra, P. P. *et al.* West Nile virus and wildlife. *Bioscience* **54,** 393–402 (2004).
11. Center for Disease Control and Prevention. West Nile virus: Statistics, surveillance, and control ⟨http://www.cdc.gov/ncidod/dvbid/westnile/surv&control.htm⟩ (2006).
12. Komar, N. *et al.* Experimental infection of North American birds with the New York 1999 strain of West Nile virus. *Emerg. Infect. Dis.* **9,** 311–322 (2003).
13. Caffrey, C., Smith, S. C. R. & Weston, T. J. West Nile virus devastates an American crow population. *Condor* **107,** 128–132 (2005).
14. Naugle, D. E. *et al.* West Nile virus: pending crisis for greater sage-grouse. *Ecol. Lett.* **7,** 704–713 (2004).
15. Bonter, D. & Hochachka, W. M. Combined data of project FeederWatch and the Christmas bird count indicate declines of chickadees and corvids: possible impacts of West Nile virus. *Am. Birds* **57,** 22–25 (2003).
16. Hochachka, W. M., Dhondt, A. A., McGowan, K. J. & Kramer, L. D. Impact of West Nile virus on American crows in the northeastern United States, and its relevance to existing monitoring programs. *Ecohealth* **1,** 60–68 (2004).
17. Kilpatrick, A. M., Daszak, P., Jones, M. J., Marra, P. P. & Kramer, L. D. Host heterogeneity dominates West Nile virus transmission. *Proc. R. Soc. B* **273,** 2327–2333 (2006).
18. Marzluff, J. M., Bowman, R. & Donnelly, R. E. (eds) *Avian Conservation and Ecology in an Urbanizing World* (Kluwer, New York, New York, 2001).
19. Acevedo, W., Taylor, J. L., Hester, D. J., Mladinich, C. S. & Glavac, S. (eds) *Rates, Trends, Causes, and Consequences of Urban Land-Use Change in the United States* (US Geological Survey, Denver, Colorado, 2006).
20. Kilpatrick, A. M., Kramer, L. D., Jones, M. J., Marra, P. P. & Daszak, P. West Nile virus epidemics in North America are driven by shifts in mosquito feeding behavior. *PLoS Biol.* **4,** e82 (2006).
21. Atkinson, C. T., Lease, J. K., Drake, B. M. & Shema, N. P. Pathogenicity, serological responses, and diagnosis of experimental and natural malarial infections in native Hawaiian thrushes. *Condor* **103,** 209–218 (2001).
22. Turell, M. J., Sardelis, M. R., O'Guinn, M. L. & Dohm, D. J. in *Japanese Encephalitis and West Nile Viruses* Vol. 267 Current Topics in Microbiology and Immunology (eds Mackenzie, J., Barrett, A. & Deubel, V.) 241–252 (Springer, Berlin, 2002).
23. Spielman, A. & D'Antonio, M. Mosquito: a natural history of our most persistent and deadly foe (Hyperion, New York, 2001).
24. Reisen, W. K. *et al.* Role of corvids in epidemiology of West Nile virus in southern California. *J. Med. Entomol.* **43,** 356–367 (2006).
25. Molaei, G., Andreadis, T., Armstrong, P., Anderson, J. & Vossbrinck, C. Host feeding patterns of *Culex* mosquitoes and West Nile virus transmission, northeastern United States. *Emerg. Infect. Dis.* **12,** 468–474 (2006).
26. Chapin, F. S. III *et al.* Consequences of changing biodiversity. *Nature* **405,** 234–242 (2000).
27. Clark, J. S. Uncertainty and variability in demography and population growth: A hierarchical approach. *Ecology* **84,** 1370–1381 (2003).

Supplementary Information is linked to the online version of the paper at www.nature.com/nature.

Acknowledgements This study is based on work supported by the Smithsonian Institution, The National Science Foundation under a grant awarded to S.L.L., a NIAID contract, and the joint NSF-NIH Ecology of Infectious Disease program (A.M.K., P.P.M). We thank C. Robbins and the United State Geological Survey for creating and maintaining the BBS monitoring programme. We also thank all BBS data support and volunteers, as well as C. Calder, J. S. Clark, W. A. Link, J. R. Sauer, C. Studds and W. Thogmartin for comments.

Author Information Reprints and permissions information is available at www.nature.com/reprints. The authors declare no competing financial interests. Correspondence and requests for materials should be addressed to S.L.L. (ladeaus@si.edu).

METHODS

Data selection. We used data from 228 North American Breeding Bird Survey (BBS)[8] routes across ten states (Massachusetts, Connecticut, New Jersey, New York, Pennsylvania, Maryland, Virginia, Illinois, Colorado, Oregon) that represent WNV dispersal westward from the 1999 east coast introduction. We included routes that had at least 80% coverage from 1980 to 2005, and a maximum of two missing observations in years after WNV emergence. We selected 20 widespread and common North American bird species according to six criteria: (1) native to North America; (2) distribution includes New England/Mid-Atlantic states where WNV has been present the longest; (3) were regularly detected on BBS routes and in sufficient numbers along secondary roads, given habitat expectation and data; (4) breeding and vocalization season overlap with timing of BBS collection; (5) species for which some background information on susceptibility to WNV infection was available (Supplementary Table 1); and (6) chose species pool to cover the range of expected WNV impact. Finally, we randomly selected five additional species from the group that satisfied criteria 1–4 but that had not been studied in WNV infection experiments. This produced a total of 20 species, which was chosen as the number that we could efficiently model and evaluate.

Model. Our modelling goal was to propagate stochasticity and trend associated with two decades of avian population data before WNV arrival to construct probability distributions for expected abundance in years after WNV emergence.

We fit an overdispersed, Poisson regression model for counts at each route-by-year node where stochastic relationships among routes and observers were normally distributed random variables with mean zero and unknown variance[28]. For a given species, individual counts, c_{jt}, were conditionally Poisson

$$c_{jt} \approx \text{Pois}\,(\lambda_{jt}) \qquad j = 1,\ldots, m;\ t = t,\ldots,T \tag{1}$$

where subscripts j and t refer to route and year, respectively.

The expected value λ_{jt} for a given annual count was

$$\log\,(\lambda_{jt}) = \beta_k\,(t - t^{\star}) + \kappa_k + \Phi_j + \Omega_{jt} + \varepsilon_{jt} \tag{2}$$

where β_k is the linear trend centred at mean year $t^{\star}$ over all routes in region k, Φ and Ω are random effects for variation among routes and observers respectively, and ε_{jt} are normally distributed error terms with mean zero. We evaluated each species' model individually for inclusion of region-specific inter-annual climate covariates κ (El Niño/Southern Oscillation (ENSO) index and North Atlantic Oscillation (NAO) evaluated in Supplementary Information) for reduced deviance information criterion[29] (DIC) values over a model with no inter-annual climate covariate. Model predictive ability was improved by including an annual ENSO effect for blue jay, chickadee, downy woodpecker, eastern towhee, gray catbird, mourning dove, song sparrow and tufted titmouse populations. Delineation of geographical regions (k) was also identified by DIC model comparison and fell generally along separation by state (except in the northeast where Pennsylvania, New York, New Jersey, Massachusetts and Connecticut were aggregated). We used standard vague priors on all unknown parameters. Hyperprior distributions for precision parameters were given inverse gamma distributions with mean 1 and variance 1,000. Models were fit by Gibbs sampler using the WinBUGS program[29]. All models were run for 50,000 iterations following a 10,000 to 15,000 iteration 'burn-in'. Convergence was assessed through visual inspection and Gelman–Rubin diagnostics[29] on multiple Markov chains.

Of the total 5,928 route-by-year nodes, 576 were missing in the raw data. These missing data were scattered throughout the 228 routes but occurred disproportionately in the early part of the time series (most often between 1980 and 1987). We fit the model to BBS data and used the Gibbs sampler to adjust for differences among observers (skill and effort levels) and to estimate probability distributions for abundance in years and routes with missing observations. We fit the model to the 26-yr data set to create a replicate and complete time series for each route. We used a cross-validation procedure[30] that randomly removed 30% of the data and evaluated the model's ability to estimate these missing nodes. Correlation coefficients comparing observed and estimated nodes (given model presented) ranged between 0.68 and 0.98 among fits for individual species.

Predicted abundance estimates. We fit the model described above to data collected before WNV emergence only, and then estimated expected abundances at each route location in all subsequent years (that is, from 1999 for east coast, 2001 for Illinois, 2002 for Colorado and 2004 for Oregon[11]). We directly compared the posterior probability distributions of expected abundances in post-WNV years with the true observations. We assigned significance to years where observed abundances fell outside 95% posterior credible intervals (95% CIs). If WNV emergence did not cause detectable mortality rates then we would expect no significant deviation between observed abundance and posterior predicted abundance estimates (Supplementary Fig. 2).

28. Link, W. A. & Sauer, J. R. A hierarchical analysis of population change with application to Cerulean Warblers. *Ecology* **83**, 2832–2840 (2002).
29. Spiegelhalter, D. J., Best, N. G., Carlin, B. P. & van der Linde, A. d. Bayesian measures of model complexity and fit (with discussion). *J. Roy. Stat. Soc. B.* **64**, 583–640 (2002).
30. Gelfand, A. E. in *Markov Chain Monte Carlo in Practice* (eds Gilks, W. R., Spiegelhalter, D. J. & Richardson, S.) 145–158 (Chapman and Hall, London, 2006).

LETTERS

The medaka draft genome and insights into vertebrate genome evolution

Masahiro Kasahara[1]*, Kiyoshi Naruse[2]*, Shin Sasaki[1]*, Yoichiro Nakatani[1]*, Wei Qu[1], Budrul Ahsan[1], Tomoyuki Yamada[1], Yukinobu Nagayasu[1], Koichiro Doi[1], Yasuhiro Kasai[1], Tomoko Jindo[2], Daisuke Kobayashi[2], Atsuko Shimada[2], Atsushi Toyoda[3], Yoko Kuroki[3], Asao Fujiyama[3,4], Takashi Sasaki[5], Atsushi Shimizu[5], Shuichi Asakawa[5], Nobuyoshi Shimizu[5], Shin-ichi Hashimoto[6], Jun Yang[6], Yongjun Lee[6], Kouji Matsushima[6], Sumio Sugano[7], Mitsuru Sakaizumi[8], Takanori Narita[2,9], Kazuko Ohishi[9], Shinobu Haga[9], Fumiko Ohta[9], Hisayo Nomoto[9], Keiko Nogata[9], Tomomi Morishita[9], Tomoko Endo[9], Tadasu Shin-I[9], Hiroyuki Takeda[2], Shinichi Morishita[1] & Yuji Kohara[9]

Teleosts comprise more than half of all vertebrate species and have adapted to a variety of marine and freshwater habitats[1]. Their genome evolution and diversification are important subjects for the understanding of vertebrate evolution. Although draft genome sequences of two pufferfishes have been published[2,3], analysis of more fish genomes is desirable. Here we report a high-quality draft genome sequence of a small egg-laying freshwater teleost, medaka (*Oryzias latipes*). Medaka is native to East Asia and an excellent model system for a wide range of biology, including ecotoxicology, carcinogenesis, sex determination[4–6] and developmental genetics[7]. In the assembled medaka genome (700 megabases), which is less than half of the zebrafish genome, we predicted 20,141 genes, including ~2,900 new genes, using 5′-end serial analysis of gene expression tag information. We found single nucleotide polymorphisms (SNPs) at an average rate of 3.42% between the two inbred strains derived from two regional populations; this is the highest SNP rate seen in any vertebrate species. Analyses based on the dense SNP information show a strict genetic separation of 4 million years (Myr) between the two populations, and suggest that differential selective pressures acted on specific gene categories. Four-way comparisons with the human, pufferfish (*Tetraodon*), zebrafish and medaka genomes revealed that eight major interchromosomal rearrangements took place in a remarkably short period of ~50 Myr after the whole-genome duplication event in the teleost ancestor and afterwards, intriguingly, the medaka genome preserved its ancestral karyotype for more than 300 Myr.

We applied the whole-genome shotgun approach to an inbred strain, Hd-rR (ref. 8), derived from the southern Japanese population, as the main target. A total of 13.8 million reads amounting to approximately 10.6-fold genome coverage were obtained from the shotgun plasmid, fosmid and bacterial artificial chromosome (BAC) libraries. A newly developed RAMEN assembler was used to process the shotgun reads to generate contigs and scaffolds. The N50 values (50% of nucleotides in an assembly are in scaffolds—or contigs—longer than or equal to the N50 value) are ~1.41 megabases (Mb) for scaffolds and ~9.8 kilobases (Kb) for contigs. The total length of the contigs reached 700.4 Mb, which, from now on, we refer to as the medaka genome size.

To construct ultracontigs, the scaffolds were integrated with the medaka genetic map by using SNP markers. For this purpose, we further obtained about 2.8-fold coverage of shotgun reads from another inbred strain HNI (refs 9, 10), which is derived from the northern Japanese population. The reads were assembled by RAMEN to scaffolds covering 648 Mb. Aligning the HNI contigs with the Hd-rR genome using BLASTZ[11], we identified 16.4 million SNPs as well as 1.40 million insertions and 1.45 million deletions in non-repetitive regions (Supplementary Table 2). We selected 2,401 SNPs and genetically mapped them onto medaka chromosomes using a backcross panel between the two strains. Where possible, at least one SNP marker was selected in each Hd-rR scaffold of greater than 60 Kb. As a result, the N50 ultracontig size became ~5.1 Mb (excluding gaps), and 89.7% of the assembled nucleotides were anchored to the chromosomes. Aligning the Hd-rR assembly with reference BACs totalling 2.3 Mb showed that the overall nucleotide level accuracy was 99.96% when 100 base pairs of contig ends were excluded (Supplementary Table 4). Details of genome assembly and analysis of basic features such as CpG islands and repeat elements are described in Supplementary Information.

We first focus on polymorphisms between the two inbred strains, Hd-rR and HNI. The genome-wide SNP rate is 3.42%, which is, to our knowledge, the highest SNP rate seen in any vertebrate species. The SNP rate is not constant among chromosomes (Kruskal–Wallis test, $P < 10^{-5}$) (Fig. 1a), like the divergence between chimpanzee and human[12]. This variation can not be accounted for by the difference in gene density alone, because the SNP rates in exons and introns are correlated in most regions across chromosomes (Fig. 1a). The substitution rate in CpG dinucleotides and the frequency of repetitive sequences might cause the variation because these factors loosely correlate with local nucleotide divergence rates ($R^2 = 0.378$ and 0.455, respectively, as illustrated in Supplementary Fig. 5b and 5c).

In human–chimpanzee analysis, the sex chromosomes exhibit the highest (Y) and lowest (X) mutation rates[12]. Medaka also has an XX–XY sex-determining system[4], but the differentiation of its sex chromosomes seems primitive; chromosome 1 (Chr 1; 33.7 Mb) serves as the X chromosome, whereas a duplicate Chr 1 with a 250-kb Y-specific

[1]Department of Computational Biology, Graduate School of Frontier Sciences, The University of Tokyo, Kashiwa 277-0882, Japan. [2]Department of Biological Sciences, Graduate School of Science, The University of Tokyo, Tokyo 113-0033, Japan. [3]RIKEN Genomic Sciences Center, Yokohama 230-0045, Japan. [4]National Institute of Informatics, Tokyo 101-8430, Japan. [5]Department of Molecular Biology, Keio University School of Medicine, Tokyo 160-8582, Japan. [6]Department of Molecular Preventive Medicine, School of Medicine, The University of Tokyo, Tokyo 113-0033, Japan. [7]Department of Medical Genome Sciences, Graduate School of Frontier Sciences, The University of Tokyo, Tokyo 108-8639, Japan. [8]Department of Environmental Science, Faculty of Science, Niigata University, Niigata 950-2181, Japan. [9]Center for Genetic Resource Information, National Institute of Genetics, Mishima 411-8540, Japan.
*These authors contributed equally to this work.

region that contains the male-determining gene, *DMY* (also known as *dmrt1b*)[6], serves as the Y chromosome. The Y-specific region is thought to have jumped to Chr 1 about 10 Myr ago, before the separation of the medaka lineage[13]. Thus, although we sequenced male genomes, it is difficult to distinguish whether the sequence reads of Chr 1 are derived from the X- or Y-chromosome. Indeed, the overall divergence rate in the medaka sex chromosome (Chr 1) does not differ much from autosomes (Fig. 1a). In the Hd-rR draft genome, the assembly of the Y-specific region is incomplete presumably owing to repetitive elements; instead, we detected polymorphisms in the reads from the region spanning at least 3.5 Mb around the Y-specific region, whereas the other region is highly homozygous. These polymorphisms in the inbred strain demonstrate the local suppression of crossing-over near the male-determining region, which has long been known in medaka genetic recombination tests[14]. It seems that the male-determining region causes restriction of recombination but its effect is limited to 10% of the length of Chr 1. The medaka Y chromosome might be at an early stage of sex differentiation.

The two medaka inbred strains Hd-rR and HNI are estimated to have diverged about 4 Myr ago[15]. Recent study using the mitochondrial cytochrome *b* gene has elucidated the detailed phylogenetic relations among four genetically different wild populations

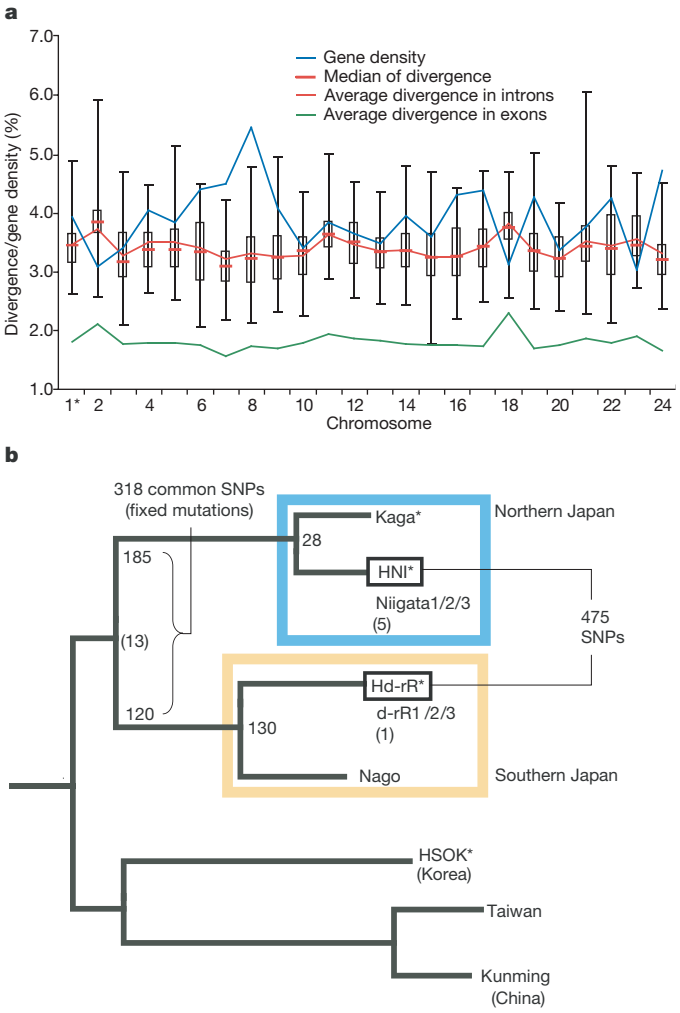

Figure 1 | Genetic variation between two medaka strains. a, Sequence diversity in 200 Kb segments of chromosomes. Box edges, the quartiles; vertical bars, the range; 1*, sex chromosome. **b**, Phylogenetic analysis of the SNPs identified between Hd-rR and HNI during regional diversification. From the parental populations of HNI and Hd-rR, six individuals named Niigata 1/2/3 and d-rR 1/2/3 were analysed to find 5 and 1 additional SNPs, respectively. * indicates an inbred strain.

(Northern Japanese, Southern Japanese, East Korean and Chinese–West Korean)[15] (Fig. 1b). Despite the indubitable accumulation of genetic variation, they all can mate and produce healthy and fertile offspring. The massive SNP resources and living stock of medaka regional strains enabled us to perform a genome-wide SNP analysis for the history of wild populations during regional diversification. We analysed genetic variation in 47 PCR-amplified regions (approximately 24.9 Kb in total) as shown in Fig. 1b. Nago and Kaga strains were chosen because they are most distantly related to Hd-rR and HNI within each population, respectively[15]. We focused on 475 SNP sites identified between Hd-rR and HNI. The comparative analysis first revealed that 130 (27%) and 28 (5.8%) of 475 SNP sites were polymorphic in the southern and northern populations, respectively, and one mutation happened to be shared by both populations (Fig. 1b). The remaining 318 (475−(130+28−1)) Hd-rR/HNI SNPs were thus preserved or fixed between the southern and northern populations (common SNPs in Fig. 1b). In comparison with the consensus sequence of the outgroup, Korea–Taiwan–China medaka (a regional medaka species with genetic variations compared with the Japanese medaka) strains, 120 and 185 mutation events were assigned to the southern and northern lineages, respectively, whereas 13 events were unclear. Overall, the total number of mutations introduced over 4 Myr is 250 (120+130) for Hd-rR and 213 (185+28) for HNI, indicating that almost the same level of mutations accumulated in the history of the two strains (chi-squared test, $\chi^2 = 3.11$, d.f. = 1, $P < 0.05$). On the other hand, the lower levels of polymorphism in the northern lineage support their rapid and recent expansion from a small size population (that is, a bottleneck effect), which has been suggested in a study with mitochondrial DNA[15]. More importantly, the high ratio of common SNPs (>65%) as well as few shared polymorphic sites indicates a strict genetic separation between the two populations for 4 Myr without major species differentiation (or speciation). Further analysis will shed light on the genetic variations and speciation in vertebrates.

To generate the medaka gene catalogue, we obtained over one million 5′-end serial analysis of gene expression (5′SAGE) tags[16], which correspond to the transcription start sites. The tags were grouped and, on the basis of transcription start site information, we predicted 20,141 non-redundant gene structures by a newly developed algorithm that uses Genscan. These predicted genes are really transcribed, however, the predicted exons may not be entirely accurate as an unavoidable consequence of the *ab initio* method. Thus, we compared the predicted gene structures with 85 known full-length complementary DNA sequences. They matched by BLASTP at 83/85 (97.6%) (expected value (*E*-value) $< 10^{-10}$) or at 72/85 (84.7%) (*E*-value $< 10^{-50}$). Furthermore, 407 (58.6%) out of 694 exons in the 85 cDNA sequences were perfectly predicted by our algorithm in which Genscan was used with the default setting for vertebrates. Full details are in Supplementary Information.

To characterize the 20,141 predicted medaka genes, we used TBLASTX[17] to compare them with the genes of six other vertebrates—human, *Tetraodon nigroviridis*, zebrafish, *Takifugu rubripes*, chicken and mouse—in the RefSeq database, and also with the gene clusters of aves, amphibia, ray-finned fish and ascidiacea in the UniGene database. We found that 3,727 have no homologues even with loose criterion (*E*-value $< 10^{-4}$) in a TBLASTX search (Fig. 2a). Then, we examined whether these novel gene candidates have any unique protein domains according to a PROSITE scan (http://ca.expasy.org/prosite/). With a stringent search criteria, by which unique domains of more than 20 amino acids were detected for 35.1% of non-novel predicted genes, only 30/3,727 (0.8%) of the new gene candidates were recognized as having known domains, suggesting that most of them are structurally unique. Interestingly, 64.4% of these candidates have CpG islands on their upstream regions and the ratio is higher than the average (50.5%) of all the predicted genes.

Among the 3,727 new gene candidates, 2,078 had no similarity even to medaka expressed sequence tags. Because 1,443 of 2,078 had open reading frames shorter than 100 amino acids, many of them might be non-coding; therefore we tried to validate the new gene candidates by testing the expression of the predicted transcripts by PCR with reverse transcription (RT–PCR). As a result, we estimated the number of 'true novel genes' to be 1,287 out of 2,078 (see Supplementary Information for details). Taking into account the remaining 1,649 expressed-sequence-tag-supported ones, at least 2,936 medaka-specific novel genes are estimated in the draft genome. This large number of new genes will provide a valuable genetic resource for medaka biology.

Of the 20,141 predicted medaka genes, we further analysed 11,617 (57.7%) that had human orthologues. Four-thousand three-hundred and forty-two (21.6%) genes constituted medaka–human reciprocally best 1:1 orthologue pairs such that TBLASTX *E*-values are less than 10^{-4} and the ratios of reciprocally aligned portions shared by two orthologues are at least 30%. Of these orthologue pairs, 2,292 were assigned the gene ontology (GO) 'biological process' annotations of their corresponding human genes (Fig. 2b). Orthologues involved in carbohydrate metabolism, alcohol metabolism and catabolism were found to be more conserved than genes implicated in the immune response, transcription, reproduction, apoptosis and stress response. Furthermore, 925 of the 1,395 human disease genes in the Online Mendelian Inheritance in Man (OMIM) database have strong orthologues among the medaka genes, such as *A2M* (alpha-2-macroglobulin) and *PSEN1* (presenilin 1), which is implicated in Alzheimer's disease, and *TP53* (tumour suppressor protein p53) and *DLEC1* (deleted in lung cancer-1; also known as *CLEC4C*) which are both involved in carcinogenesis.

To gain insight into gene evolution and species differentiation, we examined rapidly and slowly evolving gene categories between the two medaka inbred strains Hd-rR and HNI. The average K_A/K_S ratio of 8,889 qualified medaka predicted genes between the two strains is 0.413—significantly higher than that for the human–chimpanzee lineage (0.23 for K_A/K_S)[12], which has experienced major speciation for 5 Myr. We used the median K_A/K_S ratio of each GO-based functional category of medaka genes, and plotted it against that of human–chimpanzee (Fig. 2c). We focus here on the specific categories referred to by previous analyses among mammalian species, which included immunity, host defence, reproduction and olfaction as rapidly evolving categories, and intracellular signalling, neurogenesis

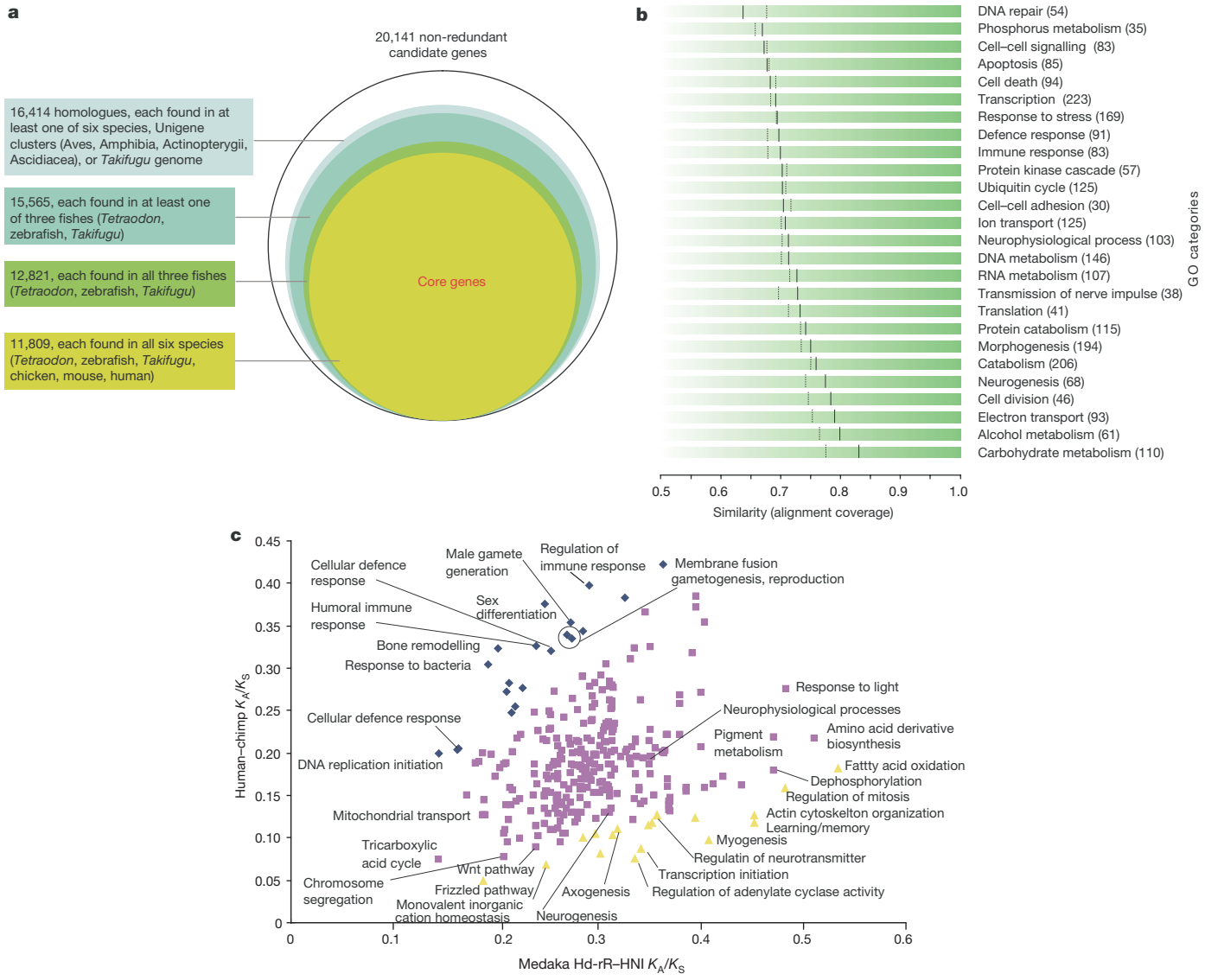

Figure 2 | Medaka genes. **a**, Breakdown of medaka gene homologues in other species. **b**, Similarity of medaka–human 1:1 orthologous pairs is arranged by GO category. Number of orthologues is in parentheses. Bars show median (thick) and mean (dashed) similarity of orthologues. **c**, Dots represent pairs of medians of K_A/K_S ratios in the medaka strains and the human–chimpanzee lineage for GO categories with ≥10 genes. Rapidly and slowly evolving GO categories in medaka relative to the hominid lineage are coloured yellow and blue, respectively.

and neurophysiology as slowly evolving ones[12]. The rapidly evolving categories are thought to be involved in adaptation to environment and sexual separation, both of which are essential processes during and/or after speciation. Intriguingly, these rapidly evolving categories are not evident in the medaka lineage, whereas mammalian slowly evolving neural-related categories exhibit relaxed constraint. Thus the reduced rate of evolution in the reproduction- and sex-related categories might explain why the two medaka strains can mate and produce fertile offspring even after a long period of geographical and genetic separation. One example is the ubiquitin specific protease 9Y (*USP9Y*) gene for male gametogenesis on hominid Y chromosome ($K_A/K_S = 1.0$) or on medaka LG21 autosome ($K_A/K_S = 0.27$). In general, the extent of phenotypic variation between organisms is not strictly related to the degree of sequence variation, and this is also the case for species differentiation of medaka. Our comparative analysis thus suggests that differential selective pressures act on specific categories in a lineage-specific manner, and this may contribute to a pattern of evolution, for example, adaptation with or without speciation.

Whole-genome duplication (WGD) and subsequent asymmetric changes in duplicated genes are thought to have an important role in genome evolution[18]. Recently, several studies have examined WGD in the teleost lineage[3,19–23] and have reconstructed ancestral karyotypes using the available genomic data[3,19,20]. Although these previous studies attempted to estimate the number of proto-chromosomes before the WGD event, interchromosomal genome rearrangements during evolution, and the correspondence between the proto-chromosomes and present chromosomes, there have been no clear answers concerning the timing of major interchromosomal rearrangements. Thus, we have conducted large-scale four-way comparisons of the medaka, human, zebrafish and *Tetraodon* genomes (see Supplementary Information for full details of scenario construction).

Here we summarize our scenario of genome evolution from the ancestral karyotype to the three teleost genomes. Figure 3 illustrates one example of how we inferred the ancestral chromosomes, and Fig. 4 depicts our scenario. The date we adopt for the WGD and lineage divergence is based on molecular clock estimates[24,25]. The key events we propose are as follows.

- In a relatively short period of ~50 Myr after the WGD event (336–404 Myr ago), the MTZ-ancestor (the last common ancestor of medaka, *Tetraodon*, and zebrafish) had 24 chromosomes and had undergone 8 major interchromosomal rearrangements (2 fissions, 4 fusions and 2 translocations).
- In contrast, since zebrafish diverged about 314–332 Myr ago, the medaka genome has preserved its ancestral genomic structure without undergoing major interchromosomal rearrangements for more than 300 Myr. The *Tetraodon* genome underwent fusion events on three occasions after separating from the medaka lineage about 184–198 Myr ago.

The zebrafish genome seems to have experienced many interchromosomal rearrangements during evolution by extensive translocations, but the precise scenario remains to be solved because of a relatively small number of zebrafish genome markers that we used in the present study. Nevertheless, these zebrafish genome markers were useful in revealing the eight major interchromosomal rearrangements

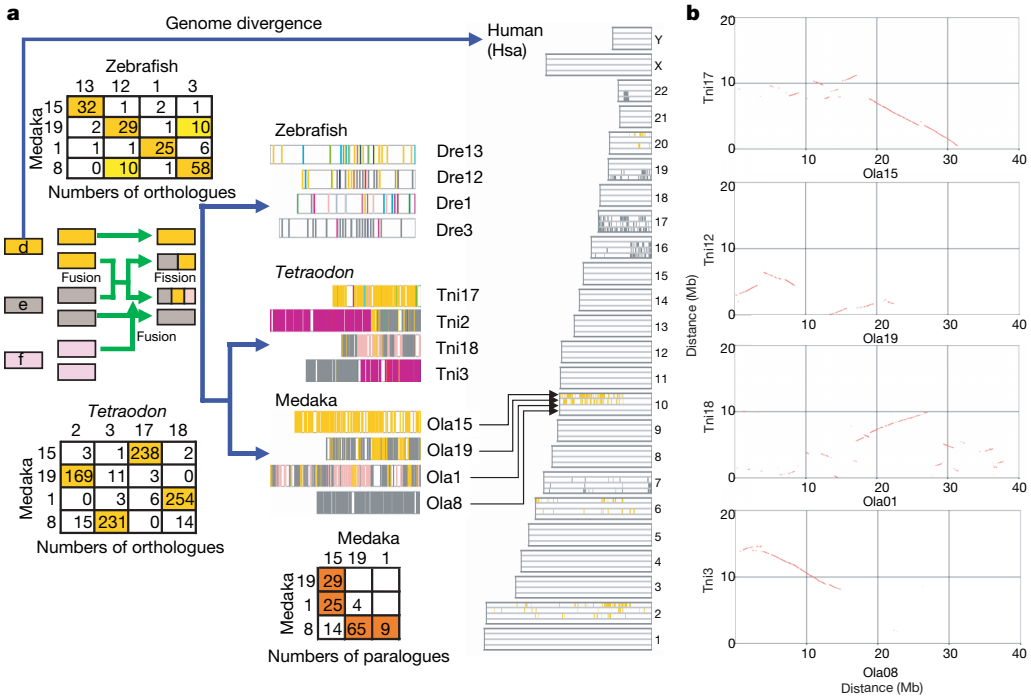

Figure 3 | Reconstruction of proto-chromosomes. **a**, Doubly conserved synteny (DCS) blocks[3,30] between one human and two medaka chromosomes were searched to identify duplicated medaka chromosomes. Human–medaka orthologues are plotted by orange or grey bars in the rows of human chromosomes (Hsa), corresponding to counterpart medaka chromosomes; in this case, four rows corresponding to Ola15, Ola19, Ola1, and Ola8. The series of co-occurrences of orthologues (orange plots) in the rows of Ola15 and Ola19 in Hsa10 shows a DCS block, and similarly more DCS blocks are found in other chromosomes. Medaka chromosomes that share a DCS block are thought to share a proto-chromosome. Ola8 and Ola15 share no DCS blocks, implying that they were from distinct proto-chromosomes. On the basis of this logic, we deduced that parts of Ola15, Ola19 and Ola1 are derived from a proto-chromosome (d, orange), whereas parts of Ola19, Ola1 and Ola8 are from another proto-chromosome (e, grey). Purple, traces of teleost proto-chromosome c (see Fig. 4 and Supplementary Fig. 13). Next, to analyse chromosome fission events, we acknowledge that two chromosomes generated by a fission event are unlikely to have common paralogues derived from the WGD in teleost. The table (centre, bottom) shows the number of paralogues between medaka chromosomes. The fairly small number between Ola1 and Ola19 imply that they were the results of chromosome fission. Finally, the correspondence among chromosomes of the three fishes was determined using the orthologue information in the tables (left, top and bottom). See Supplementary Fig. 13 for information on the other proto-chromosomes. **b**, The dot plots exhibit focal synteny blocks between medaka and *Tetraodon* chromosomes, which presents more accurate synteny than does the table of orthologue numbers. Ola, *Oryzias latipes* chromosome; Dre, *Danio rerio* chromosome; Tni, *Tetraodon nigroviridis* chromosome; and Hsa, *Homo sapiens* chromosome.

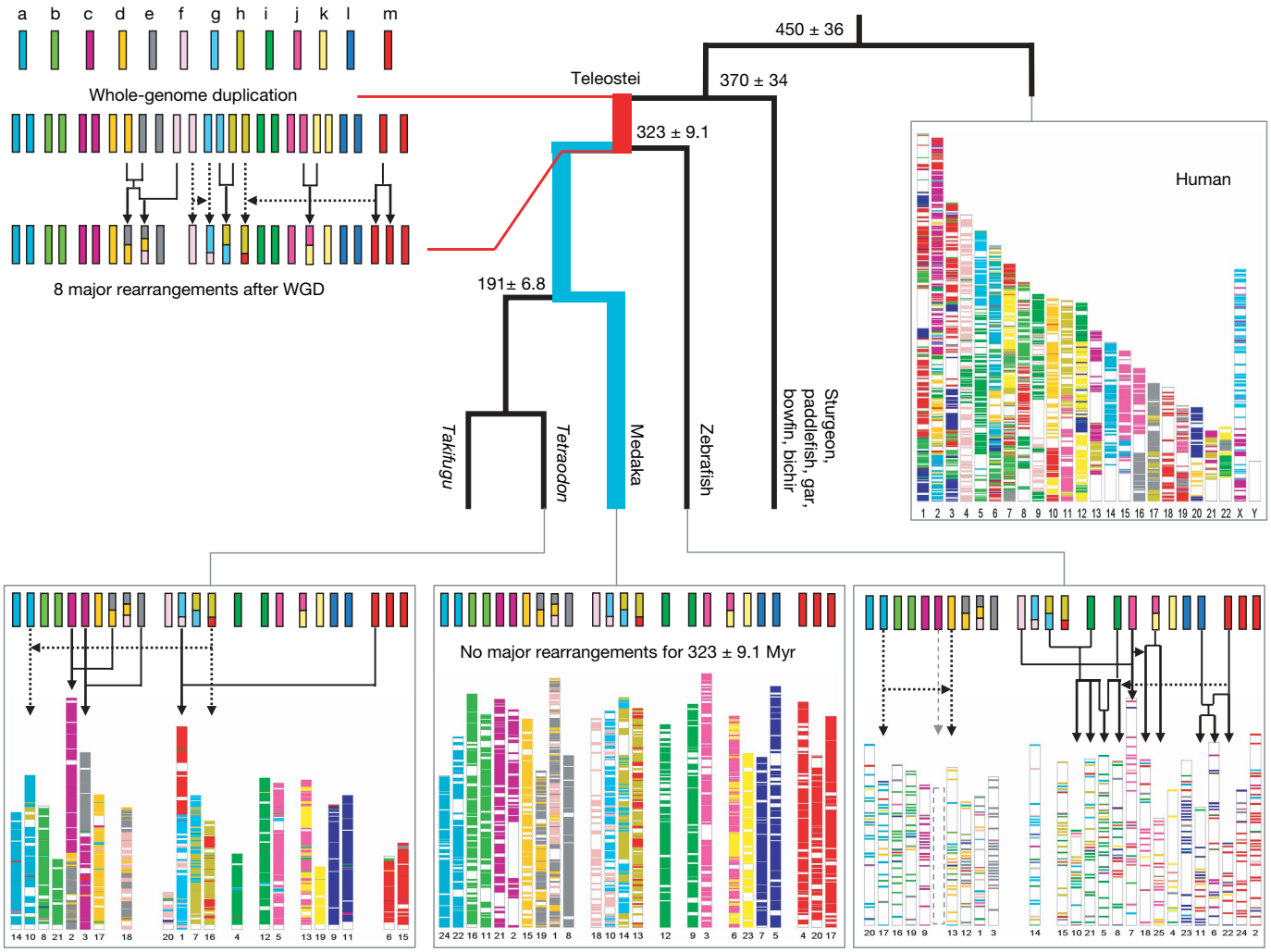

Figure 4 | Teleost genome evolution. The figure depicts a model for the distribution of ancestral chromosome segments in the human, zebrafish, medaka and *Tetraodon* genomes. Thirteen reconstructed ancestral chromosomes are represented by the coloured bars, and the genomic regions originating in the ancestral chromosomes (a–m) have the same colour coding. Major rearrangements are represented by arrows and lineage-specific small-scale translocations by dotted arrows. A dashed box in the zebrafish genome indicates that most parts of the corresponding ancestral chromosome were lost by extensive rearrangements. Individual ancestral chromosomes are labelled a–m, which corresponds to the evolutionary scenarios in Supplementary Information.

before the divergence of the three fishes. Because more than half of all the teleost species examined have either 24 or 25 chromosomes, it has been speculated that the teleost ancestor also had 24 or 25 chromosomes[19]. This is consistent with our current findings that the reconstructed MTZ-ancestor, which is the common ancestor of most teleosts[1,26,27], had 24 chromosomes. Our scenario is the most likely one, but there is an alternative: that Ola10, 13, and 14 are derived from one ancestral chromosome instead of two; and one of the duplicated ancestral chromosomes became Ola14, whereas the other underwent a fission event, yielding Ola10 and Ola13 (12 ancestral chromosome model). The alternative scenario seems unlikely because it assumes that the fission occurred in the same position in human and fish chromosomes derived from the common ancestor (Supplementary Fig. 15).

The high-quality medaka draft genome will provide a key resource for developmental genetics and serve as an important reference for various ray-finned fishes that have yet to be sequenced. Cichlids and stickleback, which are newly emerging model systems for understanding the genetic basis of vertebrate speciation, are evolutionarily closer to medaka than zebrafish. The same is true for many commercially important fish species, which include tuna, flounder, sea bream and fugu as well[28]. Indeed, the medaka and *Tetraodon* genomes have long synteny blocks in the genome (Supplementary Fig. 12). Furthermore, there are many close relatives of medaka that are indigenous from East to Southeast Asia[29], many of which are now maintained in laboratories. Together with the medaka draft genome, low-coverage shotgun genome sequences of these fish species will shed further light on the mechanisms underlying speciation and diversity, which have yet to be fully addressed at the genome-sequence level.

METHODS

Full details of methods are described in Supplementary Information. The medaka strain Hd-rR was provided by Y. Ishikawa. Other strains (HNI, d-rR, Kaga, Nago, HSOK, Taiwan and Kunming) were from our (H.T. and M.S.) laboratory stocks, except for Niigata from H. Mitani. These strains are available from the National BioResource Project (http://shigen.lab.nig.ac.jp/medaka/). Sperm DNA of Hd-rR was provided by M. Matsuda and used for whole-genome shotgun. Genomic DNA was also prepared from male adult bodies. Messenger RNA for 5′SAGE analysis was obtained from 0–7-day-old embryos and adult body tissue. Whole-genome shotgun assembly was made with the RAMEN assembler (to be published elsewhere) and using adaptations to various problems, including PCR slippage. Ultracontigs were produced by anchoring scaffolds to the chromosomes by using genetic markers, including a large number of SNP markers. The descriptions of sequence assembly refer to the latest assembly version 1.0, whereas other analyses were based on version 0.9. The two assemblies have almost the same contigs and scaffolds, but the former assembly has longer ultracontigs because more genetic markers were integrated. The

medaka gene catalogue was generated by our transcription-start-site-based gene prediction algorithm. The point of this algorithm is to enable us to predict the first exon and 5′ UTR, which were difficult to predict solely by a conventional gene prediction tool like Genscan. A formula was developed to define CpG islands for medaka. Novel repeats that occupied 9.2% of the medaka genome were found by our *de novo* repeat detection algorithm. The synonymous (K_S) and the non-synonymous (K_A) substitution rates of individual genes were calculated using the PAML package. The method for reconstruction of the ancestral karyotype is described briefly in the legend of Fig. 3. The method used orthologous chromosome correspondence among the three teleost genomes, paralogous chromosome correspondence between the medaka and *Tetraodon* genomes, and doubly conserved synteny blocks between the medaka and human genomes.

Received 10 November 2006; accepted 11 April 2007.

1. Nelson, J. S. *Fishes of the World* (John Wiley & Sons, New York, 1994).
2. Aparicio, S. *et al.* Whole-genome shotgun assembly and analysis of the genome of *Fugu rubripes*. *Science* **297,** 1301–1310 (2002).
3. Jaillon, O. *et al.* Genome duplication in the teleost fish *Tetraodon nigroviridis* reveals the early vertebrate proto-karyotype. *Nature* **431,** 946–957 (2004).
4. Aida, T. On the inheritance of color in a fresh-water fish, *Aplocheilus latipes* Temminck and Schlegel, with special reference to sex-linked inheritance. *Genetics* **6,** 554–573 (1921).
5. Yamamoto, T. Artificially induced sex-reversal in genotypic males of the Medaka (*Oryzias latipes*). *J. Exp. Zool.* **123,** 571–594 (1953).
6. Matsuda, M. *et al. DMY* is a Y-specific DM-domain gene required for male development in the medaka fish. *Nature* **417,** 559–563 (2002).
7. Furutani-Seiki, M. & Wittbrodt, J. Medaka and zebrafish, an evolutionary twin study. *Mech. Dev.* **121,** 629–637 (2004).
8. Hyodo-Taguchi, Y. Inbred strains of the medaka, *Oryzias latipes*. *Fish Biol. J. Medaka* **8,** 11–14 (1990).
9. Wittbrodt, J., Shima, A. & Schartl, M. Medaka—a model organism from the Far East. *Nature Rev. Genet.* **3,** 53–64 (2002).
10. Naruse, K., Hori, H., Shimizu, N., Kohara, Y. & Takeda, H. Medaka genomics: a bridge between mutant phenotype and gene function. *Mech. Dev.* **121,** 619–628 (2004).
11. Schwartz, S. *et al.* Human–mouse alignments with BLASTZ. *Genome Res.* **13,** 103–107 (2003).
12. Chimpanzee Sequencing and Analysis Consortium. Initial sequence of the chimpanzee genome and comparison with the human genome. *Nature* **437,** 69–87 (2005).
13. Zhang, J. Evolution of *DMY*, a newly emergent male sex-determination gene of medaka fish. *Genetics* **166,** 1887–1895 (2004).
14. Kondo, M., Nagao, E., Mitani, H. & Shima, A. Differences in recombination frequencies during female and male meioses of the sex chromosomes of the medaka, *Oryzias latipes*. *Genet. Res.* **78,** 23–30 (2001).
15. Takehana, Y., Nagai, N., Matsuda, M., Tsuchiya, K. & Sakaizumi, M. Geographic variation and diversity of the cytochrome *b* gene in Japanese wild populations of medaka, *Oryzias latipes*. *Zoolog. Sci.* **20,** 1279–1291 (2003).
16. Hashimoto, S. *et al.* 5′-end SAGE for the analysis of transcriptional start sites. *Nature Biotechnol.* **22,** 1146–1149 (2004).
17. Altschul, S. F. *et al.* Gapped BLAST and PSI-BLAST: a new generation of protein database search programs. *Nucleic Acids Res.* **25,** 3389–3402 (1997).
18. Ohno, S. *Evolution by Gene Duplication* (Springer, New York, 1970).
19. Naruse, K. *et al.* A medaka gene map: the trace of ancestral vertebrate proto-chromosomes revealed by comparative gene mapping. *Genome Res.* **14,** 820–828 (2004).
20. Woods, I. G. *et al.* The zebrafish gene map defines ancestral vertebrate chromosomes. *Genome Res.* **15,** 1307–1314 (2005).
21. Taylor, J. S., Braasch, I., Frickey, T., Meyer, A. & Van de Peer, Y. Genome duplication, a trait shared by 22,000 species of ray-finned fish. *Genome Res.* **13,** 382–390 (2003).
22. Christoffels, A. *et al.* Fugu genome analysis provides evidence for a whole-genome duplication early during the evolution of ray-finned fishes. *Mol. Biol. Evol.* **21,** 1146–1151 (2004).
23. Vandepoele, K., De Vos, W., Taylor, J. S., Meyer, A. & Van de Peer, Y. Major events in the genome evolution of vertebrates: paranome age and size differ considerably between ray-finned fishes and land vertebrates. *Proc. Natl Acad. Sci. USA* **101,** 1638–1643 (2004).
24. Crow, K. D., Stadler, P. F., Lynch, V. J., Amemiya, C. & Wagner, G. P. The "fish-specific" hox cluster duplication is coincident with the origin of teleosts. *Mol. Biol. Evol.* **23,** 121–136 (2006).
25. Yamanoue, Y., Miya, M., Inoue, J. G., Matsuura, K. & Nishida, M. The mitochondrial genome of spotted green pufferfish *Tetraodon nigroviridis* (Teleostei: Tetraodontiformes) and divergence time estimation among model organisms in fishes. *Genes Genet. Syst.* **81,** 29–39 (2006).
26. Hedges, S. B. & Kumar, S. Genomics. Vertebrate genomes compared. *Science* **297,** 1283–1285 (2002).
27. Miya, M. *et al.* Major patterns of higher teleostean phylogenies: a new perspective based on 100 complete mitochondrial DNA sequences. *Mol. Phylogenet. Evol.* **26,** 121–138 (2003).
28. Inoue, J. G., Miya, M., Tsukamoto, K. & Nishida, M. Basal actinopterygian relationships: a mitogenomic perspective on the phylogeny of the "ancient fish". *Mol. Phylogenet. Evol.* **26,** 110–120 (2003).
29. Takehana, Y., Naruse, K. & Sakaizumi, M. Molecular phylogeny of the medaka fishes genus *Oryzias* (Beloniformes: Adrianichthyidae) based on nuclear and mitochondrial DNA sequences. *Mol. Phylogenet. Evol.* **36,** 417–428 (2005).
30. Kellis, M., Birren, B. W. & Lander, E. S. Proof and evolutionary analysis of ancient genome duplication in the yeast *Saccharomyces cerevisiae*. *Nature* **428,** 617–624 (2004).

Supplementary Information is linked to the online version of the paper at www.nature.com/nature.

Acknowledgements This work was supported by a Grant-in-Aid for Scientific Research on Priority Areas "Genome" from the Ministry of Education, Culture, Sports, Science and Technology of Japan (MEXT), and the Japan Science and Technology Corporation (JST). We thank the Human Genome Center, University of Tokyo for computational time, and the National BioResource Project of MEXT for medaka strain supply and other support. We thank T. Koh for his assistance in genome assembly, A. Mori, T. Shishiki and T. Furudate for their assistance in genome browser development, Y. Ishikawa, H. Mitani and M. Matsuda for medaka resources, M. Shinya and T. Kimura for the Hd-rR/HNI F_2 panel, N. Shibata for *O. curvinotus*, and A. Hase, N. Hasegawa, S. Iiyama, N. Ishihara, K. Kawaguchi, Y. Minakuchi, S. Miura, J. Miyamoto, H. Miyauchi, M. Mizukoshi, Y. Mochizuki, Y. Sugiyama, H. Takizawa-Hayashi, M. Tamiya, T. Tandoh and E. Yokoyama for their technical assistance.

Author Contributions Project planning and supervision by Y. Kohara, S.M. and H.T.; whole-genome shotgun assembly and primer design for SNP markers by M.K. and S. Sasaki.; Analysis of SNPs and genomic alternations around the transcription start sites by S. Sasaki.; reconstruction of the teleost genome evolution by Y. Nakatani; homologue, orthologue and paralogue analysis by W.Q.; Evolutionary rate analysis of protein coding genes by S. Sasaki and W.Q.; gene prediction using 5′SAGE tags by B.A.; elucidation of novel repetitive elements by T.Y.; validation of primer specificity and efficiency by M.K., W.Q., B.A. and T.Y.; medaka genome browser development by Y. Nagayasu, Y. Kasai and K.D.; supervision of bioinformatics analysis by S.M.; whole-genome shotgun sequencing and data management by K.O., S. Haga, F.O., H.N., K. Nogata, T.M., T.E., T. Shin-I and Y. Kohara; construction of fosmid and 7.5 Kb plasmid libraries by K. Naruse, T.N. and H.T.; BAC library construction and end sequencing by A.T., Y. Kuroki, A.F., T. Sasaki, A. Shimizu, S.A. and N.S.; high-density SNP map construction by K. Naruse, T.J., A. Shimada and H.T.; genetic mapping using the panel of Kumming and Hd-rR by M.S.; 5′SAGE library construction by S-i.H., J.Y., Y.L., S. Sugano and K.M.; identification of non-coding genes and microRNA (miRNA) candidates by B.A.; expression analysis of medaka novel genes and miRNA by D.K. and H.T.; and paper writing by S.M. jointly with H.T., Y. Kohara, M.K., S. Sasaki, Y. Nakatani, W.Q., B.A., K. Naruse and T.Y.

Author Information The *Oryzias latipes* whole-genome shotgun project data have been deposited at DDBJ/EMBL/GenBank under the project accessions BAAF03000000 (Hd-rR, version 0.9), BAAF04000000 (Hd-rR, version 1.0), BAAE01000000 (HNI), and ACAAA0000001–ACAAA0356693 (5′SAGE tags). The assembly and annotations are also available from UT Genome Browser (http://medaka.utgenome.org/), NIG (http://dolphin.lab.nig.ac.jp/medaka/) and Ensembl (http://www.ensembl.org/). Reprints and permissions information is available at www.nature.com/reprints. The authors declare no competing financial interests. Correspondence and requests for materials should be addressed to Y.Kohara (ykohara@lab.nig.ac.jp), S.M. (moris@cb.k.u-tokyo.ac.jp) and H.T. (htakeda@biol.s.u-tokyo.ac.jp).

LETTERS

Dscam2 mediates axonal tiling in the *Drosophila* visual system

S. Sean Millard[1], John J. Flanagan[1], Kartik S. Pappu[1], Wei Wu[1] & S. Lawrence Zipursky[1]

Sensory processing centres in both the vertebrate and the invertebrate brain are often organized into reiterated columns, thus facilitating an internal topographic representation of the external world. Cells within each column are arranged in a stereotyped fashion and form precise patterns of synaptic connections within discrete layers. These connections are largely confined to a single column, thereby preserving the spatial information from the periphery. Other neurons integrate this information by connecting to multiple columns. Restricting axons to columns is conceptually similar to tiling. Axons and dendrites of neighbouring neurons of the same class use tiling to form complete, yet non-overlapping, receptive fields[1–3]. It is thought that, at the molecular level, cell-surface proteins mediate tiling through contact-dependent repulsive interactions[1,2,4,5], but proteins serving this function have not yet been identified. Here we show that the immunoglobulin superfamily member Dscam2 restricts the connections formed by L1 lamina neurons to columns in the *Drosophila* visual system. Our data support a model in which Dscam2 homophilic interactions mediate repulsion between neurites of L1 cells in neighbouring columns. We propose that Dscam2 is a tiling receptor for L1 neurons.

The *Drosophila* visual system is a modular structure[6,7]. The retina contains 750 simple eyes, each containing eight photoreceptor neurons or R cells (R1–R8). R cells project into the brain, where they make connections within two neuropils, the lamina and medulla. R1–R6 neurons target to the lamina, where they form synapses with lamina neurons (L1–L5). R7, R8 and L1–L5 form connections in single columns within layers in the medulla, and each column contains one axon of each of these cell types. As a consequence of this wiring pattern, each column processes motion (lamina neurons) and colour (R7 and R8) from a single point in space[6]. Although some progress has been made in understanding how neurons select different layers within each of the 750 columns[6], the molecular mechanisms that restrict synaptic connections to a single column are not known.

Dscam2 belongs to a conserved family of cell-surface proteins expressed in the nervous systems of many different organisms[8–10]. Down syndrome cell adhesion molecule (DSCAM) was originally identified as an open reading frame in a region of human chromosome 21 critical for Down's syndrome[11]. There are four *Dscam* genes in the fly genome (*Dscam*, and *Dscam2–4*). They encode type I transmembrane proteins that share about 30% sequence identity and have a common extracellular domain comprising ten immunoglobulin and six fibronectin type III repeats (Fig. 1a). These proteins have divergent cytoplasmic tails. The genomic organization of each fly *Dscam* family member differs considerably. *Dscam* encodes four cassettes of alternative exons that can potentially generate 38,016 different proteins through mutually exclusive alternative splicing[12]. Dscam has a function in forming neural circuits throughout the fly

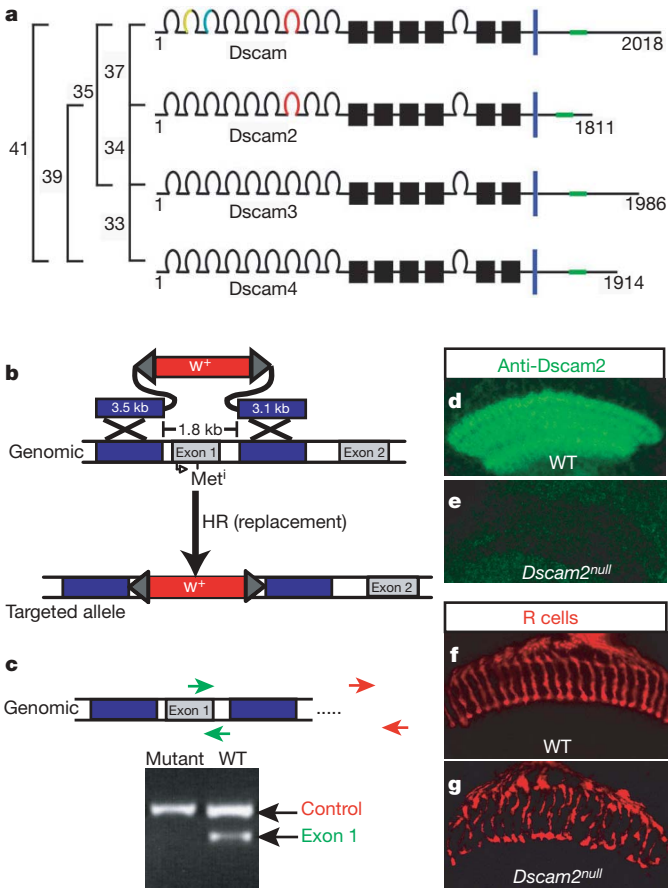

Figure 1 | Dscam2 is required for visual system development. a, *Drosophila* Dscam family members. The percentage identity between the extracellular domains is shown at the left, and the number of amino acid residues in the protein at the right. Dscam isoforms differ within three immunoglobulin domains (coloured horseshoes). Dscam2 has two isoforms differing at immunoglobulin domain 7 (red horseshoe). Immunoglobulin domains, horseshoes; FN domains, black boxes; transmembrane domains, blue bars. **b**, Homologous recombination (HR) scheme to knock out *Dscam2* (see Methods). kb, kilobases; w+ indicates the *white* gene which is used as a marker to detect recombinants. **c**, Molecular verification of the targeting event by polymerase chain reaction. WT, wild type. **d**, **e**, *Dscam2* mutants are protein-null. The images show wild-type (**d**) and *Dscam2* mutant (**e**) pupal brains stained with a Dscam2 antibody 40 h after puparium formation (APF). **f**, **g**, R7 and R8 projections in the medulla stained with monoclonal antibody 24B10 (red) are disorganized in adult *Dscam2* mutant brains. The projections of other neuronal classes were also disrupted (see Supplementary Fig. 1).

[1]Howard Hughes Medical Institute, Department of Biological Chemistry, David Geffen School of Medicine, University of California, Los Angeles, Los Angeles, California 90095, USA.

brain[12–17]. Dscam isoforms bind homophilically[18], and *in vivo* studies indicate that these interactions promote repulsion[18–21]. *Dscam2–4* do not show extensive isoform diversity, and in this way these family members are more similar to mammalian DSCAMs. Dscam2 has two alternative immunoglobulin 7 domains that share about 50% sequence identity and are referred to as Dscam2A and Dscam2B. Given the structural similarities between Dscam and Dscam2 and the prominent expression of Dscam2 on neurites in the developing brain (see Fig. 1d), we proposed that interactions between Dscam2 proteins are required for patterning neuronal connections.

To assess the function of Dscam2, we generated protein-null mutations in the gene by homologous recombination[22] (Fig. 1b–e; see Methods). The *Dscam2* mutants were viable but had marked defects in R-cell projections into the medulla (Fig. 1f, g). Using a panel of cell-type specific markers in the medulla (Supplementary Fig. 1), we observed widespread defects in axonal and dendritic organization. As wiring defects in one class of neurons may indirectly affect other classes, it was not possible to accurately assess the function of Dscam2 in homozygous mutant animals.

To identify a specific cell type that requires Dscam2, we removed it from subsets of neurons by using genetic mosaic techniques. We targeted four cell types (R7, R8, L1 and L2) that connect to specific layers within each medulla column (Fig. 2a). To assess whether Dscam2 was required in R7 and R8, genetically mosaic animals were generated in which mutant R7 and R8 cells projected into an otherwise wild-type brain. R7 ($n = 87$) and R8 neurons ($n = 336$; see Methods) lacking Dscam2 formed patterns of projections that were indistinguishable from their wild-type counterparts (Fig. 2b, c).

We extended our analysis to a subset of lamina neurons, L1 and L2. L1 axons arborize in two medulla layers, m1 and m5. In contrast, L2 axons form a single terminal arborization at the m2 layer. To assess whether Dscam2 is required in L1 and L2 neurons, we generated single mutant cells in an otherwise wild-type background, using the MARCM technique[23]. To do this, we expressed FLP recombinase under the control of a *Dachshund* (*Dac*) enhancer[24] (see Methods) to induce recombination selectively in lamina precursor cells just before their final cell division (Fig. 2d). In wild-type controls, fewer than ten lamina neurons were labelled per optic lobe. Of these, 90% were L1

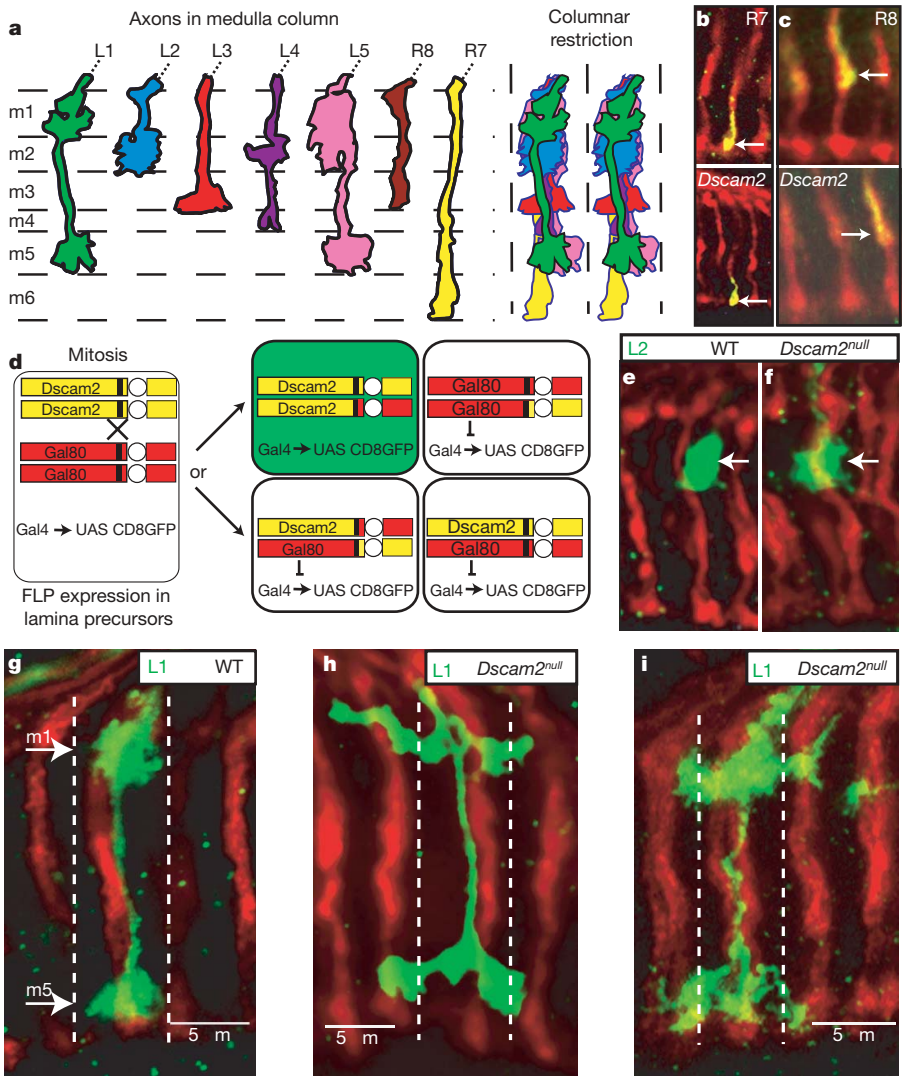

Figure 2 | Dscam2 restricts L1 arbors to columns. **a**, Schematic of lamina neuron and R-cell projections in the medulla. Each cell targets to a specific layer (m1–m6, left) and is restricted to a single column (right). **b**, **c**, R7 and R8 do not require *Dscam2*. The terminals of mutant R7 (**b**) and mutant R8 (**c**) (yellow, bottom) in adult brains are indistinguishable from wild-type R7 and R8 (yellow, top). All R7 and R8 axons (red) are stained with monoclonal antibody 24B10 in this figure. **d**, MARCM scheme. A lamina-specific enhancer was used to drive FLP in lamina precursor cells. Homozygous mutant cells lacking the Gal80 repressor were labelled with actin-Gal4 and UAS-CD8GFP (green). **e**, **f**, L2 cells do not require *Dscam2*. Wild-type (**e**) and mutant (**f**) L2 terminals (green) were indistinguishable. **g–i**, L1 cells require *Dscam2* for columnar restriction. Wild-type L1 axons (**g**) arborized in the m1 and m5 layers of the medulla and were restricted to a single column (dashed lines). Mutant L1 cells (**h**, **i**) targeted to the correct layers, but their arbors were not restricted to a single column. Animals were analysed at about 70% APF in **e–i**.

neurons and 10% were L2. Wild-type L1 (Fig. 2g; $n = 165$) and L2 (Fig. 2e; $n = 28$) cells arborized in the correct layers and were restricted to a single column. Other lamina neurons were not labelled by this procedure (see Methods).

Dscam2 mutant L1 neurons arborized in the correct layers. These arbors, however, were no longer restricted to a single column (67%; $n = 228$) and often extended over several columnar units (Fig. 2h, i). These neurons formed terminal structures within the appropriate layers in adjacent columns. Phenotypes were observed in m1, in m5 or in both of these layers. In some cases (less than 10%) L1 axons bifurcated between m1 and m5 and each branch targeted to the appropriate layer in adjacent columns (see Supplementary Fig. 2). In marked contrast to mutant L1 neurons, the terminal arbors of mutant L2 neurons were indistinguishable from the wild type (Fig. 2e, f; $n = 97$). In summary, *Dscam2* is required within L1 neurons to restrict arbors to a single column. Conversely, R7, R8 and L2 axons are restricted to a single column by Dscam2-independent mechanisms.

How might Dscam2 restrict L1 processes to a single column? Columnar restriction in the medulla is reminiscent of dendritic tiling[25]. Here dendrites of neighbouring cells of the same class do not overlap. Although the molecular mechanisms underlying tiling are not known, it has been proposed that they involve homotypic repulsion between cells of the same type[4]. If Dscam2 restricts L1 processes in this manner then we would predict, first, that Dscam2 would exhibit homophilic binding; second, that L1 processes expressing Dscam2 would contact each other during development and then retract to a single column; and third, that wild-type L1 axonal processes would extend into adjacent columns in which L1 neurons were *Dscam2* mutant.

To assess whether Dscam2 exhibits homophilic binding, we used cell aggregation assays and pull-down experiments as described previously for Dscam[18,19]. Two S2 cell populations expressing different Dscam2 isoforms (Dscam2A and Dscam2B) segregated into isoform-specific clusters (Fig. 3a, b). Similar results were obtained from mixing experiments between Dscam2 and either Dscam or Dscam3 (data not shown). Confirming this binding specificity, Dscam2 ectodomains fused to human Fc bound only to the full-length Dscam2 proteins with the identical ectodomain (Fig. 3c, d). In summary, Dscam2 interacts with itself in an isoform-specific manner and does not bind to other Dscam family members.

To assess whether L1 processes contact each other during development and whether Dscam2 is expressed in these layers, we examined wild-type L1 arborization patterns and Dscam2 antibody staining during pupal development. Using MARCM to label L1 cells, we observed growth cone expansions and immature interstitial branches at 30 h after puparium formation (APF) (Fig. 3e). About 10 h later, m1 and m5 arbors were exuberant, not restricted to columns, and neurites from neighbouring labelled cells contacted each other (Fig. 3f). During subsequent development these processes retracted and were restricted to a single column by 70 h APF (Fig. 3g). Dscam2 was expressed within these layers throughout this time course. Expression peaked at 40 h APF and was markedly reduced by 70 h APF, by which time L1 arbors were restricted to a single column (Fig. 3h–j). It is not possible to determine which cells within these two layers account for the Dscam2 immunoreactivity; however, the results of our genetic studies make it likely that minimally, L1 processes are Dscam2 positive. Dscam2 is also found in other layers, but at only low levels or not at all in R7 and R8 growth cones (Fig. 3j).

If L1 axons are restricted to a single column by Dscam2 homophilic interactions, then wild-type L1 arbors should display a phenotype when they contact mutant axons lacking Dscam2. To address this, we used reverse MARCM[26]. As with MARCM, both wild-type and mutant lamina neurons are generated, but in reverse MARCM only the wild-type cells are labelled (Fig. 4a). As the frequency of generating labelled cells is low, the likelihood that a labelled wild-type L1 axon and a mutant lamina axon will be present in the same or an adjacent column is correspondingly low. In control experiments, labelled wild-type cells were restricted to columns in a wild-type genetic background (Fig. 4b; $n = 444$). In contrast, of 466 wild-type

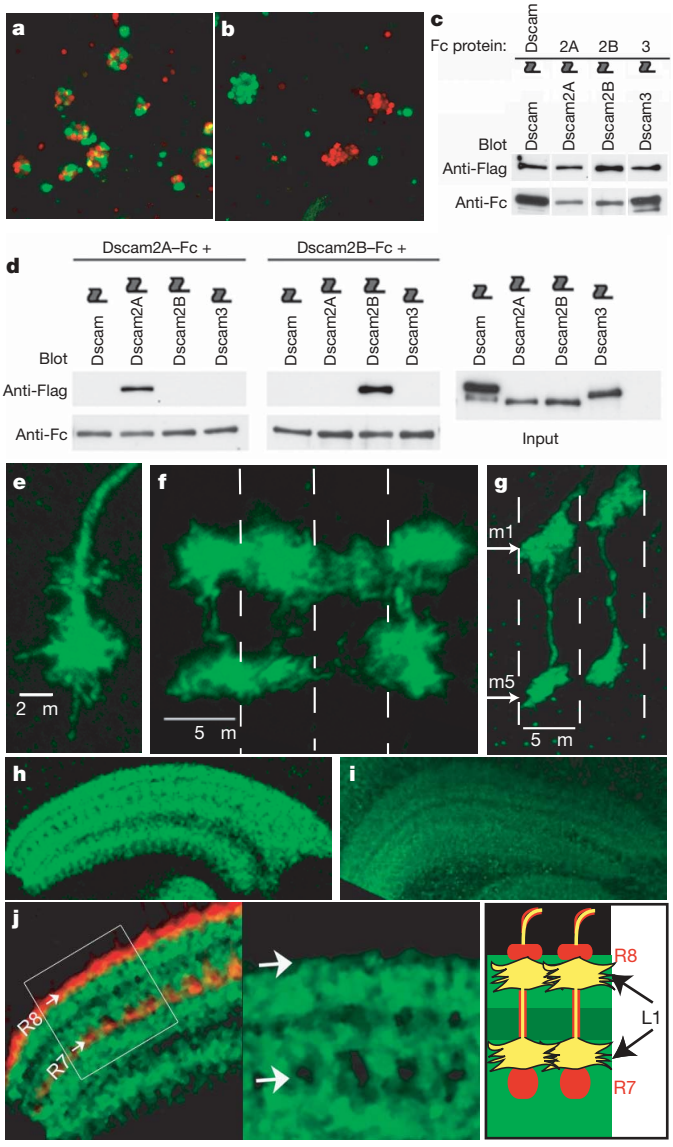

Figure 3 | Dscam2 binds homophilically and its expression is correlated with L1 arbor retraction during development. **a**, **b**, Cell aggregation assay (see Methods). **a**, Control. Cells expressing Dscam2A (marked by co-expression of red fluorescent protein) mixed with cells expressing Dscam2A (marked by co-expression of green fluorescent protein). **b**, Cells expressing Dscam2A (red) and Dscam2B (green) segregate from one another, showing that homophilic interactions are isoform-specific. **c**, **d**, Pull-down assay. Dscam, Dscam2A, Dscam2B and Dscam3 ectodomain–Fc fusion proteins bound their cognate Flag-tagged full-length protein in extracts of transfected S2 cells (**c**; see Methods). **d**, Dscam2A or Dscam2B ectodomain–Fc fusion proteins bind to themselves but not other Dscam proteins. Right, inputs. The flag symbols in **c** and **d** indicate the Flag epitope. **e**–**g**, Wild-type L1 arbor development. At 30 h APF (**e**), wild-type L1 cells consist of a terminal growth cone and nascent m1 arbors. At about 40 h APF (**f**), L1 arbors in adjacent columns contact each other. The third column from the left does not contain a labelled L1 cell and this permits the detection of invading neurites from columns 2 and 4. At about 70 h APF (**g**), L1 processes are restricted to a single column. **h**, **i**, Dscam2 protein expression in the medulla during pupal development. Dscam2 expression peaks during the retraction phase of L1 development (40 h APF; **h**), and is then downregulated (70 h APF; **i**). **j**, Dscam2 distribution (green) is non-uniform at 40 h APF. Left, image also stained with monoclonal antibody 24B10 (red). Middle, ×2.5 magnification of the boxed region. Right, at this stage, L1 arbors reside immediately above R7 and immediately below R8 in layers with strong Dscam2 staining.

L1 neurons examined using reverse MARCM, we observed 15 neurons extending processes into adjacent columns (Fig. 4c–e). Thus, Dscam2 homophilic interactions are required for restricting L1 arbors to columns.

As both L1 and L2 mutant neurons are generated by *Dac-FLP* induced MARCM (see above), Dscam2 could restrict L1 arbors either through repulsive interactions between L1 axons in adjacent columns or through adhesive interactions between L1 and L2 axons in the same column. Interactions with L2 axons are unlikely for two reasons: first, although L2 axons extend through the m1 layer, and thus could mediate interactions with L1 processes in this layer, they do not extend to the m5 layer, and second, the reverse MARCM phenotype is exclusively asymmetric, suggesting that the mutant axon resides in an adjacent column (Fig. 4f, and Supplementary Fig. 2). In MARCM experiments, 61% of the mutant arbors extended in both directions, but under reverse MARCM conditions none of the phenotypes were bidirectional. These data argue that Dscam2 mediates axonal tiling between L1 processes in neighbouring columns (Fig. 4f, g).

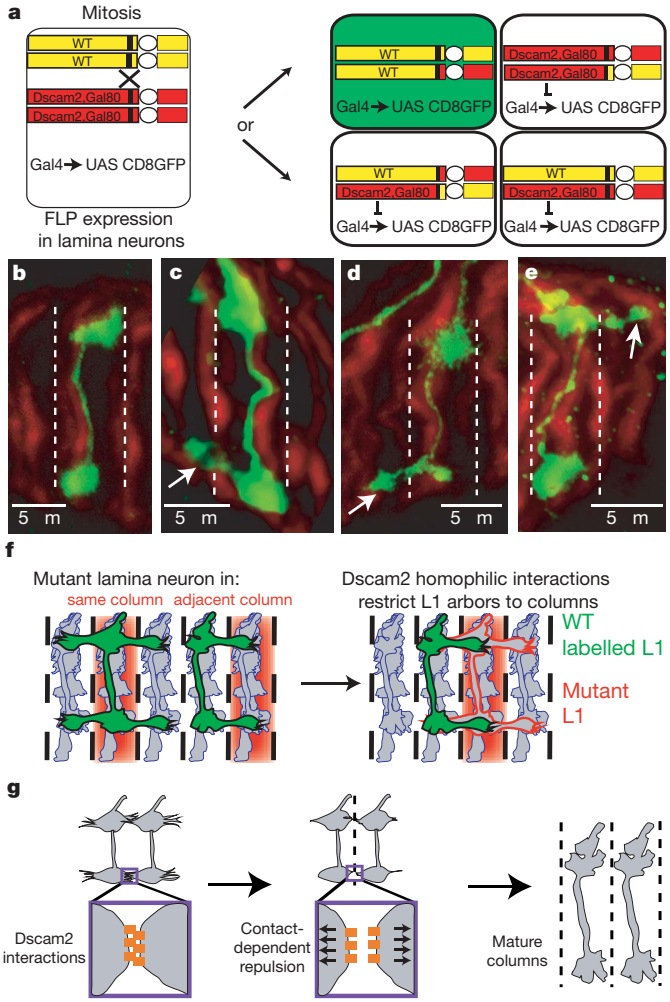

Figure 4 | Dscam2 homophilic interactions are required for axonal tiling. **a**, Reverse MARCM scheme. The *Dscam2* mutation is on the Gal80-containing chromosome so that the wild-type, but not mutant, cells are labelled. **b**, A wild-type L1 neuron (green) in a wild-type background generated by MARCM (control). **c–e**, Non-autonomous tiling phenotypes in wild-type cells using the reverse MARCM technique. Note the unidirectional nature of the phenotype. R cells (red) are labelled with monoclonal antibody 24B10. **f**, Left, Possible outcomes of reverse MARCM. Non-autonomous phenotypes could arise from interactions with a *Dscam2* mutant cell in the same or an adjacent column. A requirement in the same column would generate a bidirectional phenotype, whereas a requirement in an adjacent column would generate a unidirectional phenotype. Right, Observed result and interpretation. The reverse MARCM phenotype is exclusively unidirectional (see also Supplementary Fig. 2), indicating that Dscam2 homophilic interactions mediate repulsion. We propose this is due to a mutant 'unlabelled' L1 neuron (red) in the adjacent column. **g**, Model for columnar restriction of L1 arbors. Neurites from L1 cells in adjacent columns interact through Dscam2 homophilic contacts. This generates a repulsive signal resulting in the retraction of neurites to their column of origin. It is important to note that if Dscam2 expression is not restricted to L1 neurons in the layer, then isoform-specific or co-receptor-specific mechanisms may restrict Dscam2 activity to L1 neurons within these layers.

Columnar restriction is a common organizing principle used by many sensory systems that relay spatial information from the periphery to processing centres in the brain. As a result of the reiterative nature of these circuits, multiple targets are available in close proximity to each other within the same layer. Local repulsion between axonal processes of identical neurons in adjacent columns, which make connections with these targets, provides a developmental strategy for preserving the spatial information in each circuit. Here we show that Dscam2 is a homophilic tiling receptor for L1 neurons. Axonal tiling ensures that synaptic connections are made exclusively with targets in a single column.

The functions of Dscam and Dscam2 have intriguing similarities and differences. Although both promote homophilic repulsion between neurites, they do so in different cellular contexts. As each neuron expresses a unique set of Dscam isoforms, neurites from the same cell selectively recognize and repel each other[17–21,27,28]. This process, called 'self avoidance', facilitates the uniform coverage of synaptic fields in the nervous system[14,19–21]. By contrast, Dscam2 mediates repulsive interactions between neurites of the same cell type. This process, called tiling, limits connections to a local area. Tiling and self avoidance therefore act in concert to pattern dendritic and axonal fields in the nervous system.

METHODS SUMMARY

MARCM and reverse MARCM experiments. To generate *Dscam2* mutant lamina neurons, we used a *Dac-FLP* source on chromosome II and labelled the mutant cells with *actin-Gal4, UAS-CD8GFP*. Only L1 and L2 lamina neurons were labelled using this scheme. Using a different *Dac-FLP* source and other Gal4 sources, and performing mitotic recombination on a different chromosome arm, clones in all lamina neurons can be generated with this system (A. Nern and S.L.Z., unpublished observations). Thus, it remains formally possible that our MARCM experiments generated some unlabelled mutant lamina neurons. For reverse MARCM, two copies of *Dac-FLP* were used to increase the frequency of mitotic recombination (see fly stocks in Methods). Again, L1 and L2 cells were preferentially labelled. Wild-type MARCM clones generated with two copies of *Dac-FLP* were used as controls for the reverse MARCM experiments. Control and experimental samples were coded, mixed together, and scored blindly to avoid any bias. All other experimental procedures are described in Methods.

Full Methods and any associated references are available in the online version of the paper at www.nature.com/nature.

Received 20 January; accepted 17 April 2007.

1. Blackshaw, S. E., Nicholls, J. G. & Parnas, I. Expanded receptive fields of cutaneous mechanoreceptor cells after single neurone deletion in leech central nervous system. *J. Physiol. (Lond.)* **326**, 261–268 (1982).
2. Grueber, W. B., Ye, B., Moore, A. W., Jan, L. Y. & Jan, Y. N. Dendrites of distinct classes of *Drosophila* sensory neurons show different capacities for homotypic repulsion. *Curr. Biol.* **13**, 618–626 (2003).
3. Sagasti, A., Guido, M. R., Raible, D. W. & Schier, A. F. Repulsive interactions shape the morphologies and functional arrangement of zebrafish peripheral sensory arbors. *Curr. Biol.* **15**, 804–814 (2005).
4. Jan, Y. N. & Jan, L. Y. The control of dendrite development. *Neuron* **40**, 229–242 (2003).
5. Kramer, A. P. & Stent, G. S. Developmental arborization of sensory neurons in the leech *Haementeria ghilianii*. II. Experimentally induced variations in the branching pattern. *J. Neurosci.* **5**, 768–775 (1985).
6. Clandinin, T. R. & Zipursky, S. L. Making connections in the fly visual system. *Neuron* **35**, 827–841 (2002).
7. Meinertzhagen, I. A. & Hanson Thomas, E. *The Development of Drosophila melanogaster* (Cold Spring Harbor Laboratory Press, New York, 1993).
8. Barlow, G. M., Lyons, G. E., Richardson, J. A., Sarnat, H. B. & Korenberg, J. R. DSCAM: an endogenous promoter drives expression in the developing CNS and neural crest. *Biochem. Biophys. Res. Commun.* **299**, 1–6 (2002).

9. Fusaoka, E., Inoue, T., Mineta, K., Agata, K. & Takeuchi, K. Structure and function of primitive immunoglobulin superfamily neural cell adhesion molecules: a lesson from studies on planarian. *Genes Cells* **11,** 541–555 (2006).
10. Graveley, B. R. *et al.* The organization and evolution of the dipteran and hymenopteran Down syndrome cell adhesion molecule (Dscam) genes. *RNA* **10,** 1499–1506 (2004).
11. Yamakawa, K. *et al.* DSCAM: a novel member of the immunoglobulin superfamily maps in a Down syndrome region and is involved in the development of the nervous system. *Hum. Mol. Genet.* **7,** 227–237 (1998).
12. Schmucker, D. *et al. Drosophila* Dscam is an axon guidance receptor exhibiting extraordinary molecular diversity. *Cell* **101,** 671–684 (2000).
13. Chen, B. E. *et al.* The molecular diversity of Dscam is functionally required for neuronal wiring specificity in *Drosophila*. *Cell* **125,** 607–620 (2006).
14. Hummel, T. *et al.* Axonal targeting of olfactory receptor neurons in *Drosophila* is controlled by Dscam. *Neuron* **37,** 221–231 (2003).
15. Wang, J., Zugates, C. T., Liang, I. H., Lee, C. H. & Lee, T. *Drosophila* Dscam is required for divergent segregation of sister branches and suppresses ectopic bifurcation of axons. *Neuron* **33,** 559–571 (2002).
16. Zhu, H. *et al.* Dendritic patterning by Dscam and synaptic partner matching in the *Drosophila* antennal lobe. *Nature Neurosci.* **9,** 349–355 (2006).
17. Zipursky, S. L., Wojtowicz, W. M. & Hattori, D. Got diversity? Wiring the fly brain with Dscam. *Trends Biochem. Sci.* **31,** 581–588 (2006).
18. Wojtowicz, W. M., Flanagan, J. J., Millard, S. S., Zipursky, S. L. & Clemens, J. C. Alternative splicing of *Drosophila* Dscam generates axon guidance receptors that exhibit isoform-specific homophilic binding. *Cell* **118,** 619–633 (2004).
19. Matthews, B. J. *et al.* Dendrite self-avoidance is controlled by Dscam. *Cell* **129,** 593–604 (2007).
20. Hughes, M. E. *et al.* Homophilic Dscam interactions control complex dendrite morphology. *Neuron* **54,** 417–427 (2007).
21. Soba, P. *et al. Drosophila* sensory neurons require Dscam for dendritic self-avoidance and proper dendritic field organization. *Neuron* **54,** 403–416 (2007).
22. Gong, W. J. & Golic, K. G. Ends-out, or replacement, gene targeting in *Drosophila*. *Proc. Natl Acad. Sci. USA* **100,** 2556–2561 (2003).
23. Lee, T. & Luo, L. Mosaic analysis with a repressible cell marker for studies of gene function in neuronal morphogenesis. *Neuron* **22,** 451–461 (1999).
24. Pappu, K. S. *et al.* Dual regulation and redundant function of two eye-specific enhancers of the *Drosophila* retinal determination gene dachshund. *Development* **132,** 2895–2905 (2005).
25. Grueber, W. B., Jan, L. Y. & Jan, Y. N. Tiling of the *Drosophila* epidermis by multidendritic sensory neurons. *Development* **129,** 2867–2878 (2002).
26. Lee, T., Winter, C., Marticke, S. S., Lee, A. & Luo, L. Essential roles of *Drosophila* RhoA in the regulation of neuroblast proliferation and dendritic but not axonal morphogenesis. *Neuron* **25,** 307–316 (2000).
27. Zhan, X. L. *et al.* Analysis of Dscam diversity in regulating axon guidance in *Drosophila* mushroom bodies. *Neuron* **43,** 673–686 (2004).
28. Neves, G., Zucker, J., Daly, M. & Chess, A. Stochastic yet biased expression of multiple Dscam splice variants by individual cells. *Nature Genet.* **36,** 240–246 (2004).
29. Lee, C. H., Herman, T., Clandinin, T. R., Lee, R. & Zipursky, S. L. N-cadherin regulates target specificity in the *Drosophila* visual system. *Neuron* **30,** 437–450 (2001).
30. Lee, T. & Luo, L. Mosaic analysis with a repressible cell marker (MARCM) for *Drosophila* neural development. *Trends Neurosci.* **24,** 251–254 (2001).

Supplementary Information is linked to the online version of the paper at www.nature.com/nature.

Acknowledgements We thank E. DeRobertis, U. Banerjee, W. Grueber, I. Meinertzhagen, A. Sagasti and members of the Zipursky laboratory for comments on the manuscript; J. Clemens for identifying and characterizing the *Dscam* paralogues; D. Gunning for cloning *Dscam3* and *Dscam4*; G. Marden for providing unpublished reagents that allowed us to generate the *Dac-FLP* construct; and Y. Zhu and R. Imondi for identifying the two medulla neuron Gal4 lines used in this study. S.L.Z. is an investigator of the Howard Hughes Medical Institute. This work was also supported by the NIH (S.L.Z). S.S.M. was supported by a Cellular Neurobiology training grant from the NIH.

Author Information Reprints and permissions information is available at www.nature.com/reprints. The Dscam2–4 sequences can be found in the NCBI database under accession numbers AE014296, AE003718 and AE003556, respectively. The authors declare no competing financial interests.
Correspondence and requests for materials should be addressed to S.L.Z. (lzipursky@mednet.ucla.edu).

METHODS

Fly stocks. The following stocks were used for ends-out homologous recombination (see below for a description of the method): 'HR stock', *w*; *P*[*70-ISce-1*],*4P*[*70-FLP*], *ScO*/*CyO* and 'Tester stock', *w*; *70-FLP* (constitutive); *TM2*/*TM6b*. The *Dscam2* mutant alleles generated by homologous recombination were designated as *Dscam2*$^{null-1}$, *Dscam2*$^{null-2}$ *and Dscam2* $^{null-3}$ and were maintained over TM6b. Markers for C3 and T1 neurons were *568-Gal4* and *10-50-Gal4*, respectively. R7 MARCM was performed largely as previously described[29]. The stocks used were *GMRFLP*; *Dscam2*^{null}, *FRT79*/*CyO*:*TM6b* and *PanR7-Gal4*, *UAS N-synaptobrevin GFP*/*CyO*; *Gal80, FRT79*/*TM6b.* The stocks used for R8 mosaics were *ey3.5FLP*; *RpS17*, *arm-lacZ*, *FRT80B*/TM6b and *w*; *Rh6-lacZ*/*CyO*; *Dscam2*$^{null-3}$, FRT80B/TM6b. For lamina neuron-specific MARCM the stocks were w; *Dac-FLP*/*CyO Kr-GFP*; *Dscam2*^{null}, *FRT79*/*TM6b*, and w; *actin-Gal4, UAS-CD8GFP*; *Gal80*, *FRT79*/*TM6b* (gift from A. Nose). The stocks used for reverse MARCM were *Dac-FLP*; *Dac-FLP*; *FRT79*/*CyO*:*TM6b* and *w*; *actin-Gal4*, *UAS CD8GFP*; *Gal80*, *Dscam2*$^{null-1}$, *FRT79*/*TM6b.*

Homologous recombination. Ends-out homologous recombination was performed essentially as described[22]. In brief, an 'ends-out' targeting construct, pW37 *Dscam2*, was generated that contained the *white* gene, immediately flanked upstream and downstream by insulator sequences from pPelican vector, followed by 3.5-kb and 3.1-kb homologous arms lying upstream and downstream from exon1 of *Dscam2*, respectively. Four independent donor lines harbouring the targeting transgene were crossed to the HR stock described above. Progeny from this cross were heat-shocked for 1 h at 38 °C at 0–48 h of development. About 600 mosaic females from each donor line were crossed to the tester stock (above) and non-mosaic progeny were then backcrossed to the tester stock. Stocks were established from flies that lacked eye colour mosaicism and were analysed by PCR. Three of the 40 lines established from 'red-eyed' flies contained targeted insertions.

Molecular verification of Dscam2 targeting. DNA was extracted from homozygous viable candidate lines, and genomic PCR was performed. Primers annealing outside the *Dscam2* locus were used in combination with primers annealing within the deleted region in the same reaction (Fig. 1c). The lack of band from the deleted exon1 region indicated the presence of the targeted allele.

Construction of a lamina neuron-specific FLP source. A 325-bp subfragment of 3EE^{390} (ref. 24) was used to build a lamina-specific FLP transgene. A *Not*I–*Bam*HI fragment containing the entire FLP coding region and a simian virus 40 (SV40)-poly(A) tail from the UAS-FLP vector (gift from J. Duffy) was cloned into the *Not*I–*Bam*HI-digested pCasper-4. The 325-bp enhancer fragment was then added as an *Eco*RI fragment upstream of the FLP-SV40-PolyA sequence. Finally, an hsp70 minimal promoter was inserted as a *Kpn*I–*Not*I adaptor fragment between the lamina enhancer and the FLP coding region to generate the dac-lamina-FLP vector. This vector was injected, in accordance with standard protocols, to generate several independent transgenic fly lines.

Histology. Immunohistochemistry was performed as described[30]. The rabbit polyclonal antibody raised against the Dscam2 cytoplasmic domain was used at a 1:2,000 dilution for immunohistochemistry.

Cell aggregation. To generate plasmids containing both a *Dscam* cDNA and a fluorescent marker, pIZGM was created by removing the OpIE2 promoter from pIZT (Invitrogen) and replacing it with the metallothionine inducible promoter, MtnA, from pRMHA3. pIZRM was created by replacing GFP in pIZGM with a PCR product containing RFP. *Dscam* and *Dscam3* were excised from pBluescript, filled in to create blunt ends, and cloned into pIZGM or pIZRM. *Dscam2* was excised from pOTB7, filled in to create blunt ends, and cloned into pIZGM or pIZRM. Aggregation assays were performed as described[19].

Pull-down assays. Dscam2A, Dscam2B, and Dscam3 full-length were modified with two tandemly arrayed Flag or haemagglutinin tags. These were introduced into each construct by cloning annealed oligonucleotides containing the epitope in frame with the cytoplasmic domains of each Dscam family member. Dscam2A–Fc and Dscam2B–Fc were generated as described previously for Dscam–Fc proteins[18]. These fusion proteins comprised the N-terminal nine immunoglobulin domains and a single FNIII repeat from Dscam2 followed by human FcH. Pull-down assays were performed as described[18].

LETTERS

Deficiencies in DNA damage repair limit the function of haematopoietic stem cells with age

Derrick J. Rossi[1]*, David Bryder[1]*†, Jun Seita[1], Andre Nussenzweig[2], Jan Hoeijmakers[3] & Irving L. Weissman[1]

A diminished capacity to maintain tissue homeostasis is a central physiological characteristic of ageing. As stem cells regulate tissue homeostasis, depletion of stem cell reserves and/or diminished stem cell function have been postulated to contribute to ageing[1]. It has further been suggested that accumulated DNA damage could be a principal mechanism underlying age-dependent stem cell decline[2]. We have tested these hypotheses by examining haematopoietic stem cell reserves and function with age in mice deficient in several genomic maintenance pathways including nucleotide excision repair[3,4], telomere maintenance[5,6] and non-homologous end-joining[7,8]. Here we show that although deficiencies in these pathways did not deplete stem cell reserves with age, stem cell functional capacity was severely affected under conditions of stress, leading to loss of reconstitution and proliferative potential, diminished self-renewal, increased apoptosis and, ultimately, functional exhaustion. Moreover, we provide evidence that endogenous DNA damage accumulates with age in wild-type stem cells. These data are consistent with DNA damage accrual being a physiological mechanism of stem cell ageing that may contribute to the diminished capacity of aged tissues to return to homeostasis after exposure to acute stress or injury.

In the murine haematopoietic system, long-term multilineage differentiation and self-renewal are mediated by long-term reconstituting haematopoietic stem cells (LT-HSCs), which can be isolated from the bone marrow of young and old mice by their unique cell surface phenotype (lineage$^-$c-Kit$^+$Sca-1$^+$flk2$^-$CD34$^-$)[9,10] (Supplementary Fig. 1). To evaluate the effect of deficiencies in nucleotide excision repair (NER), non-homologous end-joining (NHEJ) and telomere maintenance on stem cell reserves during ageing, we quantified the frequency and absolute numbers of LT-HSCs in the bone marrow of young and old XPD^{TTD} (refs 3, 4), $Ku80^{-/-}$ (refs 7, 8), and late-generation $mTR^{-/-}$ (refs 5, 6) mice and controls. These analyses revealed that, regardless of age, neither stem cell frequency (Fig. 1a–d) nor absolute numbers (Supplementary Fig. 2) were appreciably reduced in any of the mutants examined. Indeed, rather than being diminished, the frequency of LT-HSCs in the bone marrow of the mutants increased significantly with age (Fig. 1e–g), which is consistent with the expansion of LT-HSC reserves in BL6 strains of mice ageing naturally (Fig. 1h)[9–11]. Moreover, the degree to which the stem cell pool expanded in each of the mutant strains was closely correlated with age-matched controls (Supplementary Fig. 3). We next evaluated the impact of genomic maintenance and ageing on downstream multipotent progenitor (MPP) and oligopotent progenitor populations (Supplementary Fig. 1)[12]. These analyses revealed that whereas short-term (ST)-HSC reserves were not significantly affected in any of the mutants assayed (Supplementary Fig. 4), downstream MPP^{flk2+}, common myeloid progenitor (CMP) and common lymphoid progenitor (CLP) progenitor populations were frequently diminished in the mutants, although this was not strictly correlated with age (Fig. 1i–k). Taken together, these results indicate that deficiencies in NER, telomere maintenance or NHEJ do not significantly affect the establishment, maintenance or expansion of LT-HSC reserves with age. This suggests that LT-HSCs may be cytoprotected against the accumulation of different types of DNA lesion with ageing, perhaps as a consequence of their largely quiescent state[13]. In contrast, downstream progenitors, which cycle more rapidly[14], were more adversely affected in these mutants, indicating that these populations might be more susceptible to DNA damage responses such as growth arrest or apoptosis, which are characteristically activated in cycling cells at the G1/S and G2/M checkpoints[15].

Although we and others have assayed HSC activity in young telomerase-deficient mice[16,17], the consequence of advancing age and accumulated damage resulting from telomere attrition on LT-HSC function has not been evaluated. We therefore purified LT-HSCs from old (60-week) late-generation (G_3) $mTR^{-/-}$ mutants and controls, and competitively transplanted 50 stem cells against 2×10^5 competitor bone marrow cells with the use of the CD45 congenic system[9]. We reasoned that this strategy would maximize the genomic damage associated with critically short telomeres in LT-HSCs as increased genomic instability[6], and signal-free telomere ends[18] have been shown to accompany the ageing of haematopoietic cells in late-generation $mTR^{-/-}$ mice (Supplementary Fig. 5). Analysis of transplant recipients revealed that short-term reconstitution was modestly reduced in the G_3 $mTR^{-/-}$ LT-HSC-transplanted recipients, yet by 20 weeks after transplantation it had dropped off precipitously (Fig. 2a), with B-cell, T-cell and myeloid lineages all being significantly affected (Fig. 2b). Granulocyte chimaerism was monitored throughout the course of the experiment as a measure of ongoing stem cell function because granulocytes are short-lived and require continued stem cell activity to be generated[19]. These analyses indicated a progressive loss of stem cell function that approached exhaustion by 20 weeks after transplantation (Fig. 2c). Consistent with this, stem cells from primary G_3 $mTR^{-/-}$ transplanted recipients were incapable of serially transplanting secondary recipients, indicating that they had become functionally exhausted (Fig. 2d). Transplantation experiments performed in parallel with LT-HSCs from younger (36-week) G_3 $mTR^{-/-}$ mice revealed that although stem cells from these donors were compromised in comparison with controls (Fig. 2e), the magnitude of the functional decline was not as marked as when stem cells from older G_3 $mTR^{-/-}$ mice were assayed (Fig. 2c).

To test whether diminished self-renewal might underlie the functional exhaustion of aged G_3 $mTR^{-/-}$ LT-HSCs, we assayed the

[1]Department of Pathology, and Institute for Stem Cell Biology and Regenerative Medicine, Stanford University School of Medicine, Stanford, California 94305, USA. [2]Experimental Immunology Branch and Laboratory for Receptor Biology, National Cancer Institute, National Institutes of Health, Bethesda, Maryland 20892, USA. [3]MGC-CBG Department of Cell Biology and Genetics, Erasmus Medical Center, PO Box 1738, 3000DR, Rotterdam, The Netherlands. †Present address: Lund University, Institute for Experimental Medical Science, BMC I13, 22184, Lund, Sweden.
*These authors contributed equally to this work.

capacity of these cells to self-renew in primary transplant recipients[9]. These experiments showed that LT-HSCs from aged G_3 $mTR^{-/-}$ donors were 16-fold less capable than controls of giving rise to phenocopies of themselves (Fig. 2f). We next assayed the intrinsic proliferative capacity of telomerase-deficient stem cells by quantifying the total progeny-cell output of cultured KLSflk2$^-$ cells (LT-HSCs and ST-HSCs combined) from young (19-week), and old (51-week) G_3 mutants and controls. This showed that there was a significant decline in the proliferative capacity of the $mTR^{-/-}$ cells, which was exacerbated with advanced age (Fig. 2g) and underwritten by an increased apoptotic response (Fig. 2h). Cumulatively, these results indicate that telomere attrition limits stem cell function in an age-dependent manner by intrinsically diminishing self-renewal and proliferative capacity, and rendering LT-HSCs susceptible to apoptosis under conditions of stress.

To assay the effect of NER on LT-HSC functional capacity, we competitively transplanted 50 LT-HSCs from 26-week-old XPD^{TTD} and $XPD^{+/+}$ mice. Stem cells from the XPD^{TTD} mice showed a significant diminution in multilineage reconstitution potential (Fig. 3a, b) and a progressive loss of stem activity that approached exhaustion by 16 weeks after transplantation (Fig. 3c). The observation that XPD^{TTD} LT-HSCs were incapable of stably reconstituting secondary hosts during serial transplantation confirmed that stem cell activity had become exhausted (Fig. 3d). Transplantation experiments performed in parallel with stem cells from younger (12-week) XPD^{TTD} and control mice revealed that although stem cells from younger XPD^{TTD} mice were functionally compromised in comparison with controls (Fig. 3e), they performed significantly better than stem cells from older XPD^{TTD} mice (Fig. 3c).

To determine whether diminished self-renewal capacity contributed to the functional decline of XPD^{TTD} stem cells, we assayed the capacity of LT-HSCs to self-renew in primary transplant recipients, which showed that XPD^{TTD} LT-HSCs had a 5.2-fold reduced capacity for self-renewal than controls (Fig. 3f). We next tested the intrinsic proliferative capacity of KLSflk2$^-$ cells from young (16-week) and old (73-week) XPD^{TTD} mutants and controls and found that whereas the cells from young mutants were marginally affected, stem cells from old XPD^{TTD} mice showed significantly reduced proliferative capacity (Fig. 3g), which was associated with increased apoptosis (Fig. 3h). Taken together, these results identify a significant role for xeroderma pigmentosum complementation group D (XPD)-mediated NER in maintaining the functional capacity of LT-HSCs

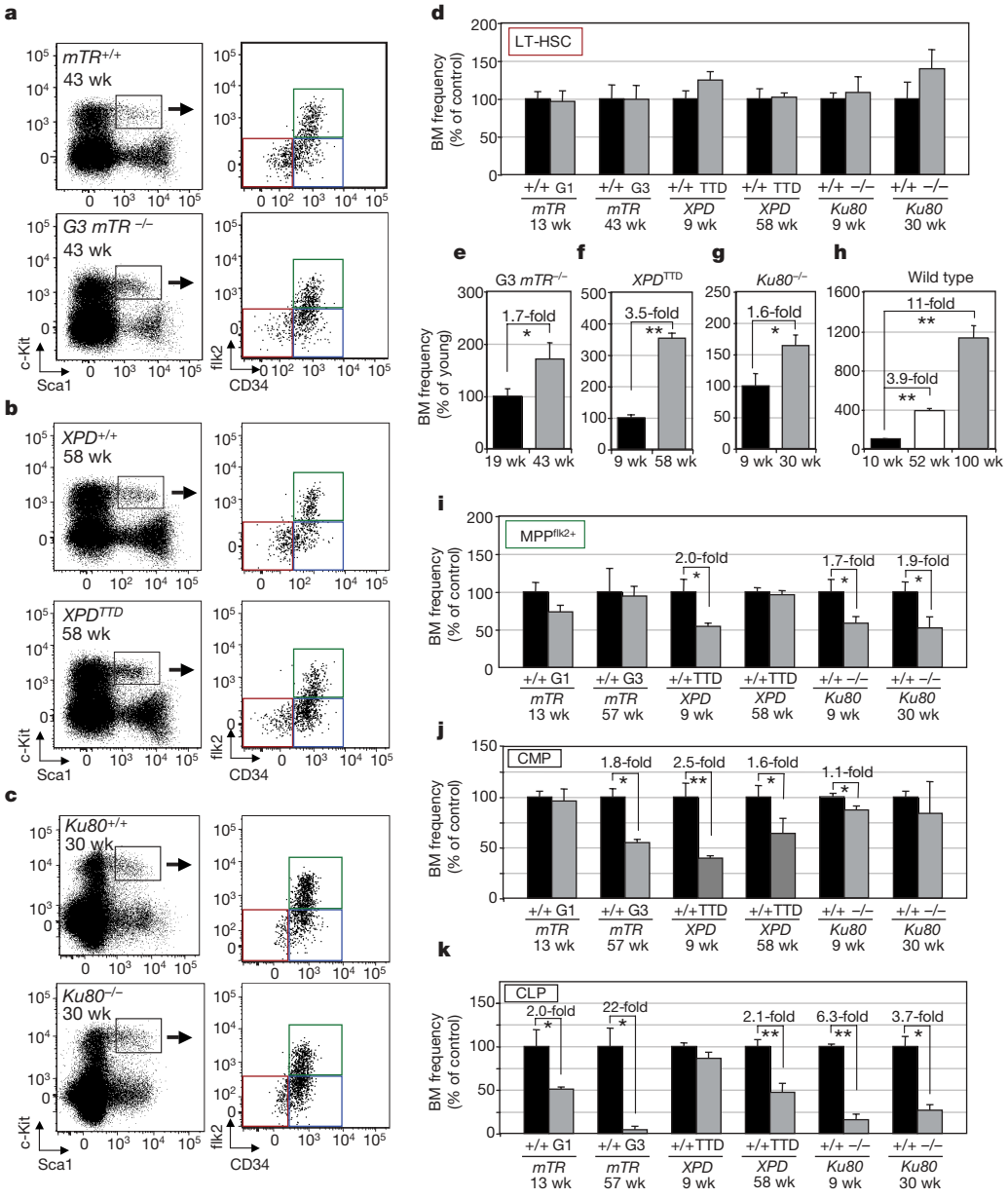

Figure 1 | Stem and progenitor reserves with age in genomic maintenance-deficient mice. **a–c**, Representative FACS profiles pre-gated on live, lineage$^-$ cells showing LT-HSCs, ST-HSCs and MPP^{flk2+} (red, blue and green gates, respectively) in aged G_3 $mTR^{-/-}$ (**a**), XPD^{TTD} (**b**) and $Ku80^{-/-}$ (**c**) mice and controls. **d**, Frequency of LT-HSCs in bone marrow. **e–h**, Expansion of LT-HSCs with age in G_3 $mTR^{-/-}$ (**e**), XPD^{TTD} (**f**), $Ku80^{-/-}$ (**g**) and wild-type (**h**) mice. **i–k**, Frequency of MPP^{flk2+} (**i**), CMP (**j**) and CLP (**k**) cells in bone marrow. Ages are indicated in weeks (wk). Cohorts ranging from $n = 8$ to $n = 13$ mice were used. Significant differences (Student's t-test) are indicated as follows: asterisk, $P < 0.05$; two asterisks, $P < 0.005$. Error bars denote s.e.m.

with age by preserving reconstitution ability, self-renewal potential and proliferative capacity, and by preventing programmed cell death under conditions of stress.

We next assayed the importance of NHEJ on stem cell function by competitive transplantation of LT-HSCs from Ku80-deficient mice and controls. As expected, *Ku80*$^{-/-}$ LT-HSCs were unable to generate mature B and T cells as a result of an inability to undergo V(D)J recombination[7]. Ku80-deficient stem cells were also sharply impaired in their ability to reconstitute myeloid lineages, indicating severely diminished stem cell activity (Fig. 4a, b). Consistent with this was our observation that *Ku80*$^{-/-}$ LT-HSCs were 26-fold less capable of giving rise to phenocopies of themselves than controls in primary transplant recipients, indicative of an attenuated self-renewal capacity (Fig. 4c). Moreover, cultured KLSflk2^{-} cells from *Ku80*$^{-/-}$ mutants had a reduced capacity to proliferate, which was greatly exacerbated with age (Fig. 4d) and was associated with increased apoptosis (Fig. 4e). Cumulatively, these results identify a role for Ku80 and NHEJ in maintaining LT-HSC function by conserving reconstitution potential, self-renewal capacity, proliferative capacity and stem cell viability under conditions of stress.

Our data showing an age-dependent diminution of stem cell function in three different genomic maintenance-deficient settings suggested that accumulated genomic damage might be an important physiological mechanism contributing to stem cell decline with age. To test whether DNA damage accumulation accompanied normal stem cell ageing, we immunostained LT-HSCs from young (10-week) and old (122-week) mice for phosphorylation of histone H2AX (γ-H2AX) as an indicator of DNA damage[20], and quantified the number of γ-H2AX foci in individual stem cells. This analysis revealed that whereas LT-HSCs from young mice were largely devoid of γ-H2AX foci, the vast majority (82%) of the stem cells from old mice stained positively for γ-H2AX, with more than 70% of the cells showing multiple foci (Fig. 4g, h). Similarly, ST-HSCs and MPP^{flk2+} isolated from old mice contained significantly more γ-H2AX foci than their young counterparts (Fig. 4i, j), although the percentage of γ-H2AX-positive old cells decreased as the cells progressed from LT-HSCs through the

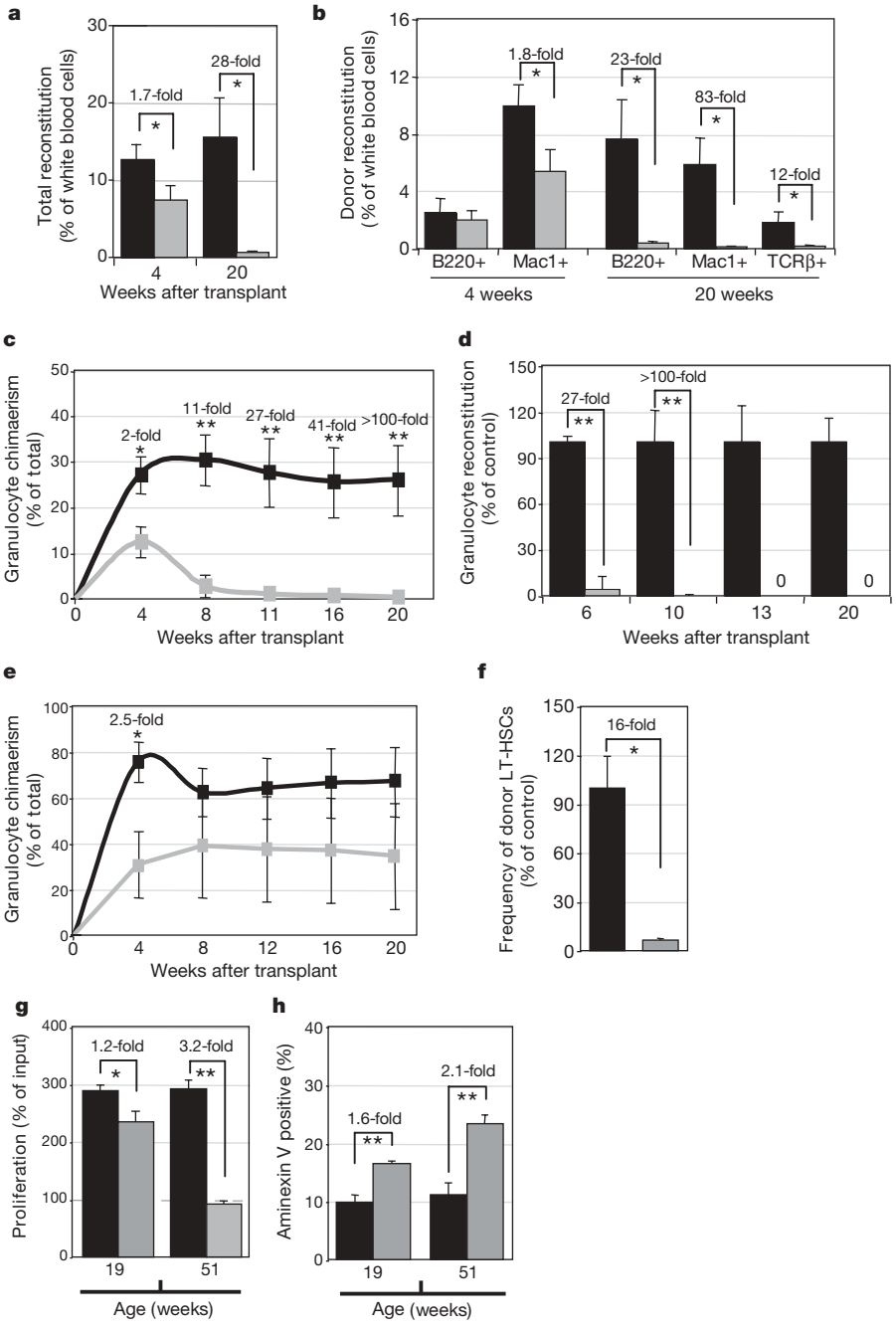

Figure 2 | Telomerase-deficiency limits LT-HSC function with age. a–c, Competitive transplantation of LT-HSCs from 60-week *mTR*$^{+/+}$ (black) or G$_3$ *mTR*$^{-/-}$ (grey) donors ($n = 9$ and $n = 10$ recipients, respectively) showing total reconstitution (**a**), contribution to B cells (B220^{+}), myeloid cells (Mac1^{+}) and T cells (TCR-β^{+}) (**b**), and granulocyte chimaerism (**c**). **d**, Secondary transplantation of *mTR*$^{+/+}$ (black bars) or G$_3$ *mTR*$^{-/-}$ (grey bars) stem cells ($n = 6$ and $n = 5$ recipients, respectively). **e**, Competitive transplantation of LT-HSCs from 36-week *mTR*$^{+/+}$ (black line) or G$_3$ *mTR*$^{-/-}$ (grey line) donors ($n = 6$ and 5 recipients respectively). **f**, Donor LT-HSC frequency from recipients described in **a**. (**g**) Proliferative potential of *mTR*$^{+/+}$, and G$_3$ *mTR*$^{-/-}$ KLSflk2^{-} cells. (**h**) Annexin V positive cells in the experiment described in **g**. Significant differences (Student's *t*-test) are indicated as follows: asterisk, $P < 0.05$; two asterisks, $P < 0.005$. Error bars denote s.e.m.

more committed progenitors (65% in old ST-HSCs; 25% in old MPP^{flk2+}). By the CLP^{flk2+} and CMP stages of differentiation, significant differences in γ-H2AX staining between young and old mice were no longer observed (data not shown). Taken together, these data indicate that DNA damage accumulates in stem cells with age, and suggests that proliferating progenitor cells are either repaired more readily or are eliminated on accumulating damage.

Although studies with purified HSCs have provided great detail about how ageing alters the functional capacity of HSCs[9–11,21], much less is known about the mechanisms driving these changes. Because HSCs are long-lived, age-dependent functional decline could be postulated to result from the accumulation of macromolecular damage in general[22], or DNA damage in particular[2]. In support of this, stem cells from mice with mutations in *Brca2* (ref. 23) or *Msh2* (ref. 24) have reduced repopulating abilities, whereas *Ercc1*-deficient mice have multilineage cytopenias indicating possible stem or progenitor cell dysfunction[25]. Evidence that DNA damage response has a significant bearing on the function of HSCs during ageing was provided in studies demonstrating that reactive oxygen species limit the functional capacity of HSCs from ataxia-telangiectasia mutated (ATM)-deficient mice[26] in a p38-MAPK-dependent manner[27], and in studies on mice bearing a mutated *Rad50* allele, which undergo haematopoietic failure in an ATM-Chk2-dependent fashion[28,29]. The present demonstration that genetic deficiencies in telomere maintenance, NER and NHEJ intrinsically diminish LT-HSC function in an age-dependent manner under conditions of stress indicates that DNA damage accrual may underlie the reduced capacity of stem cells to mediate a return to homeostasis after exposure to injury or stress. Our findings also have implications for stem cell involvement in oncogenesis because they establish that relatively quiescent stem cells can persist in the face of age-dependent DNA damage accrual, and in such a way might serve as a reservoir for the multiple mutagenic events underlying oncogenic transformation.

METHODS SUMMARY

Purification and transplantation of cells. LT-HSCs ($lineage^{-}c\text{-}Kit^{+}Sca1^{+}flk2^{-}CD34^{-}$) were purified and transplanted as described[9]. In brief, bone marrow cells were enriched for c-Kit, stained with fluorescence-conjugated antibodies against Sca1, c-Kit, CD34, flk2 and lineage (CD3, CD4, CD8, Mac-1, B220, Gr-1 and Ter119) and purified by fluorescence-activated cell sorting (FACS). Fifty test cells (CD45.2) were transplanted against 2×10^5 bone marrow competitor cells (CD45.1) into lethally irradiated recipients (CD45.1). Peripheral blood was analysed with simultaneous detection of CD45.1, CD45.2, T-cell antigen receptor (TCR)-β, B220, Mac1 and Ter119.

Proliferation and annexin V analysis. Equivalent cell numbers were sorted and cultured for 3.5–4.5 days in RPMI medium containing 10% fetal calf serum, 10 ng ml^{-1} stem cell factor, thrombopoietin, interleukin (IL)-3, IL-6, IL-11 and Flt3 ligand at 37 °C, 2.5% O_2 and 5% CO_2. Cells were then stained with annexin V and propidium iodide, and analysed by FACS.

γ-H2AX immunostaining. γ-H2AX was revealed by using the SCIPhos (single-cell imaging of phosphorylation) assay[30]. In brief, cells were sorted into droplets of PBS on poly(L-lysine)-coated slides, then fixed, permeabilized and stained with phospho-specific (Ser 139) histone H2AX antibody (Biolegend). After being washed, the cells were stained with a secondary Alexa Fluor 488-conjugated antibody and 4,6-diamidino-2-phenylindole. Quantification of γ-H2AX foci was performed by fluorescence microscopy and analysed statistically with the Mann–Whitney *U*-test.

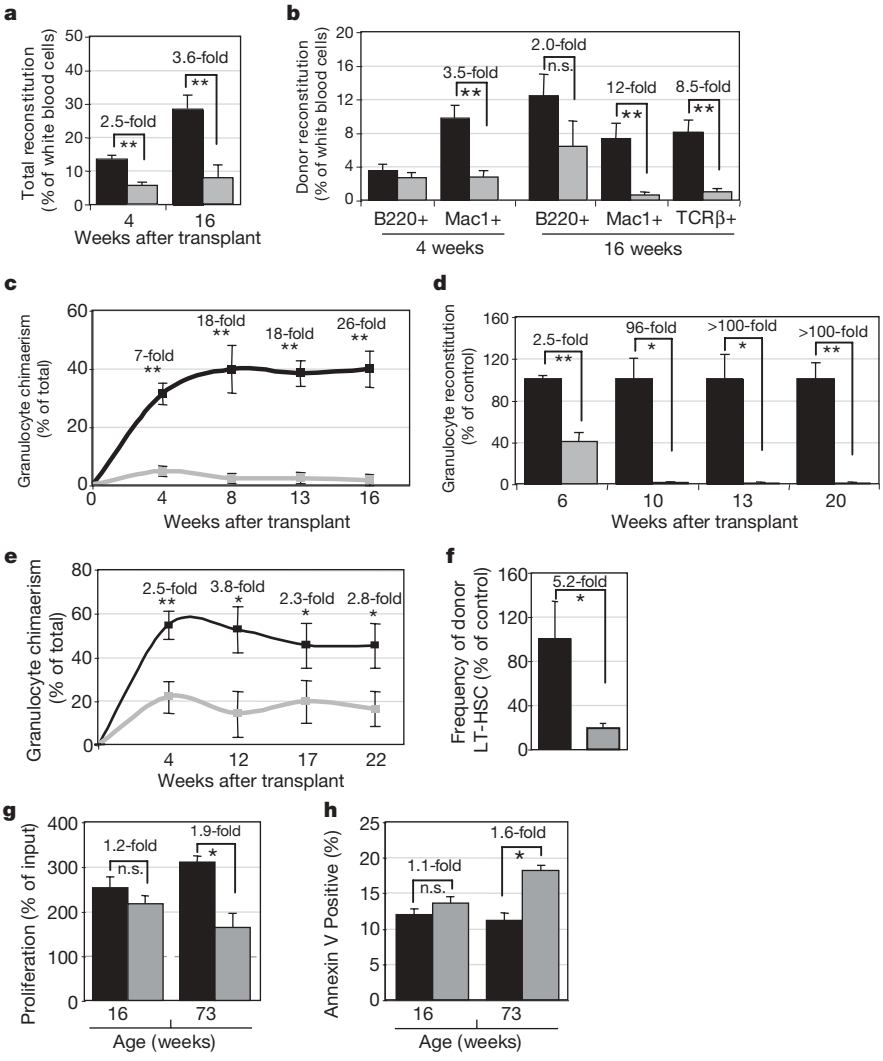

Figure 3 | NER deficiency limits LT-HSC function with age. a–c, Competitive transplantation of LT-HSCs from 26-week $XPD^{+/+}$ (black) or XPD^{TTD} (grey) donors ($n = 9$ recipients for each) showing total reconstitution (**a**), lineage contribution to B cells ($B220^{+}$), myeloid cells ($Mac1^{+}$) and T cells ($TCR\text{-}\beta^{+}$) (**b**), and granulocyte chimaerism (**c**). **d**, Secondary transplantation of LT-HSCs from $XPD^{+/+}$ (black bars) or XPD^{TTD} (grey bars) donors ($n = 5$ recipients for each). **e**, Competitive transplantation of LT-HSCs from 12-week $XPD^{+/+}$ (black line) or XPD^{TTD} (grey line) donors ($n = 8$ and $n = 9$ recipients, respectively). **f**, Donor LT-HSC frequency from recipients described in **a**. **g**, Proliferative potential of $XPD^{+/+}$ (black bars) and XPD^{TTD} (grey bars) $KLSflk2^{-}$ cells. **h**, Annexin V-positive cells in the experiment described in **g**. Significant differences (Student's *t*-test) are indicated as follows: asterisk, $P < 0.05$; two asterisks, $P < 0.005$; n.s., not significant. Error bars denote s.e.m.

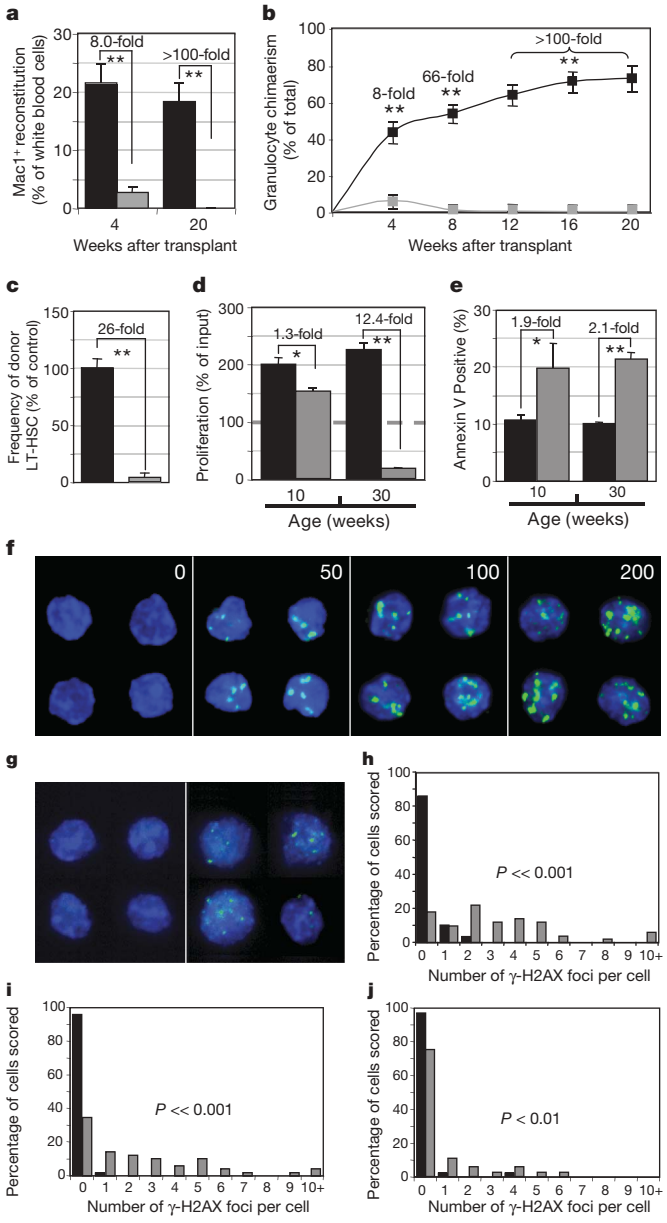

Figure 4 | NHEJ deficiency and endogenous damage accumulation in stem cells with age. a–c, Competitive transplantation of LT-HSCs from 16-week *Ku80*$^{+/+}$ (black) or *Ku80*$^{-/-}$ (grey) donors ($n = 9$ and $n = 7$ recipients, respectively) showing myeloid (Mac1^{+}) reconstitution (**a**) and granulocyte chimaerism (**b**). **c**, Donor LT-HSC frequency from the recipients described in **a**. **d**, Proliferative potential of *Ku80*$^{+/+}$ (black bars) or *Ku80*$^{-/-}$ (grey bars) KLSflk2^{-} cells. **e**, Annexin V-positive cells in the experiment described in **d**. Significant differences (Student's *t*-test) are indicated as follows: asterisk, $P < 0.05$; two asterisks, $P < 0.005$. Error bars denote s.e.m. **f**, Immunostaining of γ-H2AX in c-Kit^{+}Sca1^{+}lin^{-} cells showing irradiation dose (in rads) dependence. **g**, LT-HSCs from 10-week-old (left) and 122-week-old (right) mice immunostained for γ-H2AX. **h–j**, γ-H2AX distribution in LT-HSCs (**h**), ST-HSCs (**i**) and MPP^{flk2+} (**j**). Black bars, 10-week-old mice; grey bars, 122-week-old mice.

Full Methods and any associated references are available in the online version of the paper at www.nature.com/nature.

Received 23 January; accepted 18 April 2007.

1. Schlessinger, D. & Van Zant, G. Does functional depletion of stem cells drive aging? *Mech. Ageing Dev.* **122,** 1537–1553 (2001).
2. Park, Y. & Gerson, S. L. DNA repair defects in stem cell function and aging. *Annu. Rev. Med.* **56,** 495–508 (2005).
3. de Boer, J. *et al.* A mouse model for the basal transcription/DNA repair syndrome trichothiodystrophy. *Mol. Cell* **1,** 981–990 (1998).
4. de Boer, J. *et al.* Premature aging in mice deficient in DNA repair and transcription. *Science* **296,** 1276–1279 (2002).
5. Blasco, M. A. *et al.* Telomere shortening and tumor formation by mouse cells lacking telomerase RNA. *Cell* **91,** 25–34 (1997).
6. Rudolph, K. L. *et al.* Longevity, stress response, and cancer in aging telomerase-deficient mice. *Cell* **96,** 701–712 (1999).
7. Nussenzweig, A. *et al.* Requirement for Ku80 in growth and immunoglobulin V(D)J recombination. *Nature* **382,** 551–555 (1996).
8. Nussenzweig, A., Sokol, K., Burgman, P., Li, L. & Li, G. C. Hypersensitivity of Ku80-deficient cell lines and mice to DNA damage: the effects of ionizing radiation on growth, survival, and development. *Proc. Natl Acad. Sci. USA* **94,** 13588–13593 (1997).
9. Rossi, D. J. *et al.* Cell intrinsic alterations underlie hematopoietic stem cell aging. *Proc. Natl Acad. Sci. USA* **102,** 9194–9199 (2005).
10. Sudo, K., Ema, H., Morita, Y. & Nakauchi, H. Age-associated characteristics of murine hematopoietic stem cells. *J. Exp. Med.* **192,** 1273–1280 (2000).
11. Morrison, S. J., Wandycz, A. M., Akashi, K., Globerson, A. & Weissman, I. L. The aging of hematopoietic stem cells. *Nature Med.* **2,** 1011–1016 (1996).
12. Bryder, D., Rossi, D. J. & Weissman, I. L. Hematopoietic stem cells: the paradigmatic tissue-specific stem cell. *Am. J. Pathol.* **169,** 338–346 (2006).
13. Yamazaki, S. *et al.* Cytokine signals modulated via lipid rafts mimic niche signals and induce hibernation in hematopoietic stem cells. *EMBO J.* **25,** 3515–3523 (2006).
14. Passegue, E., Wagers, A. J., Giuriato, S., Anderson, W. C. & Weissman, I. L. Global analysis of proliferation and cell cycle gene expression in the regulation of hematopoietic stem and progenitor cell fates. *J. Exp. Med.* **202,** 1599–1611 (2005).
15. Ishikawa, K., Ishii, H. & Saito, T. DNA damage-dependent cell cycle checkpoints and genomic stability. *DNA Cell Biol.* **25,** 406–411 (2006).
16. Allsopp, R. C., Morin, G. B., DePinho, R., Harley, C. B. & Weissman, I. L. Telomerase is required to slow telomere shortening and extend replicative lifespan of HSCs during serial transplantation. *Blood* **102,** 517–520 (2003).
17. Samper, E. *et al.* Long-term repopulating ability of telomerase-deficient murine hematopoietic stem cells. *Blood* **99,** 2767–2775 (2002).
18. Choudhury, A. R. *et al.* Cdkn1a deletion improves stem cell function and lifespan of mice with dysfunctional telomeres without accelerating cancer formation. *Nature Genet.* **39,** 99–105 (2007).
19. Domen, J., Cheshier, S. H. & Weissman, I. L. The role of apoptosis in the regulation of hematopoietic stem cells: Overexpression of Bcl-2 increases both their number and repopulation potential. *J. Exp. Med.* **191,** 253–264 (2000).
20. Rogakou, E. P., Pilch, D. R., Orr, A. H., Ivanova, V. S. & Bonner, W. M. DNA double-stranded breaks induce histone H2AX phosphorylation on serine 139. *J. Biol. Chem.* **273,** 5858–5868 (1998).
21. Kim, M., Moon, H. B. & Spangrude, G. J. Major age-related changes of mouse hematopoietic stem/progenitor cells. *Ann. NY Acad. Sci.* **996,** 195–208 (2003).
22. Kirkwood, T. B. Understanding the odd science of aging. *Cell* **120,** 437–447 (2005).
23. Navarro, S. *et al.* Hematopoietic dysfunction in a mouse model for Fanconi anemia group D1. *Mol. Ther.* **14,** 525–535 (2006).
24. Reese, J. S., Liu, L. & Gerson, S. L. Repopulating defect of mismatch repair-deficient hematopoietic stem cells. *Blood* **102,** 1626–1633 (2003).
25. Prasher, J. M. *et al.* Reduced hematopoietic reserves in DNA interstrand crosslink repair-deficient Ercc1−/− mice. *EMBO J.* **24,** 861–871 (2005).
26. Ito, K. *et al.* Regulation of oxidative stress by ATM is required for self-renewal of haematopoietic stem cells. *Nature* **431,** 997–1002 (2004).
27. Ito, K. *et al.* Reactive oxygen species act through p38 MAPK to limit the lifespan of hematopoietic stem cells. *Nature Med.* **12,** 446–451 (2006).
28. Bender, C. F. *et al.* Cancer predisposition and hematopoietic failure in Rad50$^{S/S}$ mice. *Genes Dev.* **16,** 2237–2251 (2002).
29. Morales, M. *et al.* The Rad50S allele promotes ATM-dependent DNA damage responses and suppresses ATM deficiency: implications for the Mre11 complex as a DNA damage sensor. *Genes Dev.* **19,** 3043–3054 (2005).
30. Seita, J. *et al.* Lnk negatively regulates self-renewal of hematopoietic stem cells by modifying thrombopoietin-mediated signal transduction. *Proc. Natl Acad. Sci. USA* **104,** 2349–2354 (2007).

Supplementary Information is linked to the online version of the paper at www.nature.com/nature.

Acknowledgements We thank D. Bhattacharya for critical reading of the manuscript. A.N. was supported by NCI's Center for Cancer Research. D.J.R. was supported by the Damon Runyon Cancer Foundation and the California Institute of Regenerative Medicine. D.B. was supported by a Swedish Medical Research Council scholarship (STINT) and a Cancerfonden grant.

Author Information Reprints and permissions information is available at www.nature.com/reprints. The authors declare no competing financial interests. Correspondence and requests for materials should be addressed to D.J.R. (drossi@stanford.edu).

METHODS

Mice. Strains of mice used included XPD^{TTD} mice, which model the human segmental progeroid syndrome trichothiodystrophy (TTD) and have a mutation of the XPD helicase with pleiotropic functional deficits including a partial defect in NER[31,32], $KU80^{-/-}$ mice, which are defective in NHEJ and in double-strand break repair as a result of ablation of KU80 (refs 33–35), and $mTR^{-/-}$ mice, which are defective in telomere maintenance as a result of the targeted disruption of the telomerase RNA component[36,37]. Because mice have long telomeres, the telomerase $mTR^{-/-}$ mutants were backcrossed for several generations to allow telomeres to shorten enough to become debilitating (late generation). When initially reported, $mTR^{-/-}$ mice on a mixed background needed to be backcrossed for four to six generations for telomere dysfunction to be manifested[36,37,38]. However, because mTR is haploinsufficient for telomere maintenance[39], and the BL6 strain to which we backcrossed the mutation have shorter telomeres than other inbred strains[40], the $mTR^{-/-}$ mice could only be interbred through two (G_2) to three generations (G_3) before becoming sterile and showing overt signs of telomere dysfunction such as cachexia and reduced life span (Supplementary Fig. 5) due to critically short telomeres and increased chromosome instability[41]. In all experiments, age-matched wild-type littermate controls were used when possible. For the late-generation telomerase mutants whose breeding scheme did not produce wild-type littermate controls, age-matched controls of the same genetic background were used. All mice were on a C57BL/6 background and were maintained at the Stanford University Laboratory Animal Facility.

Absolute numbers of LT-HSCs. Absolute numbers were calculated from the bone marrow cellularity of the four hindlimb bones, the bone marrow frequency of LT-HSCs and the weight of each mouse, to control for differences in animal size.

Secondary transplantation. Serial transplantation was performed in several ways. Primary recipients were transplanted either competitively with 50 LT-HSCs as described above, or non-competitively with about 5×10^5 bone marrow cells obtained from test or control mice. In the latter case, flow cytometry staining for LT-HSCs was first performed to ensure that the frequency of LT-HSCs in bone marrow from test and control mice was comparable so that we would be transplanting stem cell equivalents. Variations in frequency in bone marrow were adjusted for before transplantation. For secondary transplants, if primary recipients were competitively transplanted we sorted donor-derived (test or control) LT-HSCs from the bone marrow and competitively transplanted 25 or 100 of these cells into the secondary host as described above. If primary recipients had been transplanted non-competitively, 10^6 bone marrow cells were transplanted into lethally irradiated secondary recipients. Peripheral blood analysis of secondary recipients was performed as described above.

Self-renewal determination. Self-renewal was determined as described previously[42]. In brief, primary lethally irradiated recipients (CD45.1) were transplanted non-competitively with stem cell equivalents of test or control bone marrow. Stem cell equivalents were determined by staining donor bone marrow for LT-HSCs to determine frequency before transplantation. At 5–7 months after transplantation, primary recipients were sacrificed and the frequency of donor-derived (CD45.2) LT-HSCs in bone marrow was determined by using an eight-colour flow cytometric protocol with simultaneous detection of CD45.1, CD45.2, lineage, c-Kit, Sca1, CD34 and flk2, along with discrimination of dead cells (propidium iodide). In each experiment three to five recipients transplanted with test or control cells were assayed.

31. de Boer, J. *et al.* A mouse model for the basal transcription/DNA repair syndrome trichothiodystrophy. *Mol. Cell* **1,** 981–990 (1998).
32. de Boer, J. *et al.* Premature ageing in mice deficient in DNA repair and transcription. *Science* **296,** 1276–1279 (2002).
33. Nussenzweig, A. *et al.* Requirement for Ku80 in growth and immunoglobulin V(D)J recombination. *Nature* **382,** 551–555 (1996).
34. Nussenzweig, A., Sokol, K., Burgman, P., Li, L. & Li, G. C. Hypersensitivity of Ku80-deficient cell lines and mice to DNA damage: the effects of ionizing radiation on growth, survival, and development. *Proc. Natl Acad. Sci. USA* **94,** 13588–13593 (1997).
35. Difilippantonio, M. J. *et al.* DNA repair protein Ku80 suppresses chromosomal aberrations and malignant transformation. *Nature* **404,** 510–514 (2000).
36. Rudolph, K. L. *et al.* Longevity, stress response, and cancer in aging telomerase-deficient mice. *Cell* **96,** 701–712 (1999).
37. Blasco, M. A. *et al.* Telomere shortening and tumour formation by mouse cells lacking telomerase RNA. *Cell* **91,** 25–34 (1997).
38. Lee, H. W. *et al.* Essential role of mouse telomerase in highly proliferative organs. *Nature* **392,** 569–574 (1998).
39. Hathcock, K. S. *et al.* Haploinsufficiency of mTR results in defects in telomere elongation. *Proc. Natl Acad. Sci. USA* **99,** 3591–3596 (2002).
40. Allsopp, R. C., Cheshier, S. & Weissman, I. L. Telomere shortening accompanies increased cell cycle activity during serial transplantation of hematopoietic stem cells. *J. Exp. Med.* **193,** 917–924 (2001).
41. Herrera, E. *et al.* Disease states associated with telomerase deficiency appear earlier in mice with short telomeres. *EMBO J.* **18,** 2950–2960 (1999).
42. Rossi, D. J. *et al.* Cell intrinsic alterations underlie haematopoietic stem cell ageing. *Proc. Natl Acad. Sci. USA* rr. **102,** 9194–9199 (2005).

Vol 447|7 June 2007|doi:10.1038/nature05842

LETTERS

The ATM repair pathway inhibits RNA polymerase I transcription in response to chromosome breaks

Michael Kruhlak[1], Elizabeth E. Crouch[2]*, Marika Orlov[2]*, Carolina Montaño[2]*, Stanislaw A. Gorski[3], André Nussenzweig[1], Tom Misteli[3], Robert D. Phair[4] & Rafael Casellas[2]

DNA lesions interfere with DNA and RNA polymerase activity. Cyclobutane pyrimidine dimers and photoproducts generated by ultraviolet irradiation cause stalling of RNA polymerase II, activation of transcription-coupled repair enzymes, and inhibition of RNA synthesis[1,2]. During the S phase of the cell cycle, collision of replication forks with damaged DNA blocks ongoing DNA replication while also triggering a biochemical signal that suppresses the firing of distant origins of replication[3,4]. Whether the transcription machinery is affected by the presence of DNA double-strand breaks remains a long-standing question. Here we monitor RNA polymerase I (Pol I) activity in mouse cells exposed to genotoxic stress and show that induction of DNA breaks leads to a transient repression in Pol I transcription. Surprisingly, we find Pol I inhibition is not itself the direct result of DNA damage but is mediated by ATM kinase activity and the repair factor proteins NBS1 (also known as NLRP2) and MDC1. Using live-cell imaging, laser micro-irradiation, and photobleaching technology we demonstrate that DNA lesions interfere with Pol I initiation complex assembly and lead to a premature displacement of elongating holoenzymes from ribosomal DNA. Our data reveal a novel ATM/NBS1/MDC1-dependent pathway that shuts down ribosomal gene transcription in response to chromosome breaks.

To study the effects of DNA double-strand breaks (DSBs) on RNA synthesis we monitored transcription of ribosomal genes in cells exposed to genotoxic stress. The large copy number and tandem array distribution of ribosomal transcription units provide an ideal system to measure the kinetics of transcription in real time[5]. We exposed mouse embryonic fibroblasts (MEFs) to increasing doses of ionizing radiation and ongoing ribosomal RNA synthesis was assessed by fluorouridine (FUrd) incorporation in *in situ* run-on assays (Supplementary Fig. 1). In non-irradiated MEFs, we observed high FUrd incorporation at nucleolar sites (Fig. 1a). In contrast, we found that exposure to γ-irradiation led to a pronounced decrease in nuclear FUrd incorporation in a dose-dependent manner. Fibroblasts exposed to 2.5 Gy of irradiation showed a 30% reduction, whereas exposure to 10 Gy of irradiation reduced FUrd by nearly 60% (Fig. 1a), indicating that induction of DNA DSBs results in Pol I transcriptional arrest. Consistent with these results, irradiated cells showed segregation of upstream binding factor 1 (UBF1; also known as UBTF) into fibrillar caps, a characteristic feature of transcriptionally inactive cells[6] (Supplementary Fig. 2). To investigate the dynamics of Pol I inhibition, we exposed primary MEFs to γ-irradiation or 20 μM etoposide and assessed transcription at twenty-minute intervals following treatment. Both irradiation and etoposide treatment led to a transient inhibition of rRNA synthesis. Following a ~60% decrease at 20 min, FUrd incorporation 60 min post-DNA damage was indistinguishable from that of untreated cells (Fig. 1b and Supplementary Fig. 3), indicating Pol I transcription is restored approximately within an hour of genotoxic stress. We conclude that DNA breaks elicit a transient block in Pol I rRNA synthesis.

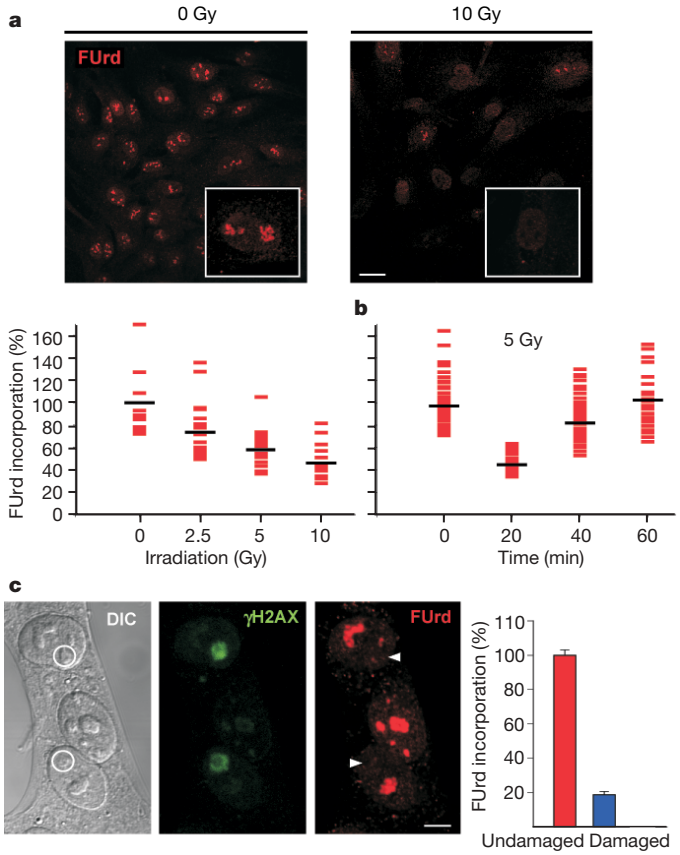

Figure 1 | DNA DSBs inhibit Pol I transcription. a, Primary MEFs were untreated (left) or exposed to 10 Gy of irradiation (right) and ongoing rRNA synthesis was monitored by FUrd run-on assays. Lower graph represents percentage of FUrd incorporation in fibroblasts exposed to different doses of irradiation. The mean (represented by cross lines) of anti-FUrd antibody fluorescence in non-irradiated (0 Gy) cells was set to 100%; scale bar, 15 μm. **b**, FUrd incorporation in wild-type MEFs assessed at 20, 40 and 60 min post irradiation (5 Gy). **c**, MEF nucleoli were exposed to localized laser micro-irradiation (white circles; differential interference contrast image). γH2AX (green) and FUrd incorporation (red) were assessed by immunocytochemistry (scale bar, 2 μm). Bar graph quantifies FUrd incorporation in undamaged and damaged nucleoli. Values represent mean ± s.d. ($n = 20$).

[1]Experimental Immunology, NCI, [2]Genomic Integrity and Immunity, NIAMS, [3]Biology of Genomes, NCI, National Institutes of Health, Bethesda, Maryland 20892, USA. [4]Integrative Bioinformatics, Los Altos, California 94024, USA.
*These authors contributed equally to this work.

Induction of DNA damage in the S phase of the cell cycle inhibits DNA polymerases at a distance from damaged sites[4], whereas transcription-coupled repair blocks RNA polymerase activity only at ultraviolet radiation (UV)-damaged genes[7]. To investigate whether Pol I transcription is globally or locally inhibited by DNA damage, we introduced localized DNA DSBs using laser micro-irradiation in Hoechst-sensitized cells[8]. To ensure a moderate DSB density, micro-irradiation was calibrated to introduce approximately a single lesion per megabase (Mb) of DNA[8], or one DSB for every 23 ribosomal transcription units. We found that although Pol I transcription was blocked in micro-irradiated nucleoli, transcriptional activity continued undisrupted in neighbouring nucleoli (Fig. 1c). We conclude that Pol I transcription is only inhibited in proximity to DNA DSBs.

Previous studies have shown that the DNA-dependent protein kinase (DNA-PK; also known as PRKDC) and Ku (also known as XRCC5) protein heterodimer interferes with Pol I activity near DSBs *in vitro*[9]. To investigate whether DNA-PK inhibits rRNA synthesis *in vivo* we irradiated *Ku80*$^{-/-}$ MEFs and assessed Pol I transcription by FUrd run-on assays. As in wild-type cells, FUrd incorporation was abolished in irradiated *Ku80*$^{-/-}$ fibroblasts (Fig. 2a), demonstrating that Ku is dispensable for nucleolar transcriptional arrest. Likewise, the JNK2 (also known as MAPK9) signalling pathway, shown to inhibit rRNA synthesis in response to cellular stress[10], was dispensable (Supplementary Fig. 4). In addition, proteosome activity, which degrades stalled polymerases during transcription-coupled repair[11], was not required to shut down rRNA synthesis following induction of DNA breaks (Supplementary Fig. 4). To investigate whether other DNA repair pathways were involved in blocking Pol I activity we screened several DNA repair deficient MEFs. Surprisingly, we found that *Atm*$^{-/-}$ fibroblasts are unable to block Pol I post γ-irradiation (Fig. 2a). Similarly, *Atm*-null cells cultured in the presence of etoposide or exposed to localized micro-irradiation failed to downregulate Pol I transcription (Supplementary Fig. 5), and no changes were seen in UBF1 localization in irradiation-treated *Atm*$^{-/-}$ MEFs (Supplementary Fig. 5). Altogether, these data argue that Pol I transcription is not blocked by DNA damage itself, but by the action of DNA repair enzymes.

ATM kinase activity is essential for cellular signalling in response to DNA breaks[12,13]. We found that pre-treatment of wild-type MEFs with the specific ATM kinase inhibitor KU55933 leads to radioresistant rRNA synthesis (Fig. 2b), indicating ATM phosphorylation is required for Pol I inhibition. To assess directly the role of DNA repair substrates involved in the ATM pathway, we screened MEFs that are deficient for various repair factors. We found that Pol I transcription is efficiently blocked in irradiated cells lacking 53BP1 (also known as TRP53BP1), BRCA1 or histone H2AX (also known as H2AFX) (Fig. 2c). Compared to wild-type fibroblasts, however, resumption of rRNA synthesis was significantly delayed in DNA-repair-compromised cells (Fig. 2c), suggesting that restoration of transcription in damaged nucleoli is dependent on successful repair of DNA lesions. In support of this idea, resumption of rRNA synthesis in irradiated wild-type cells (Fig. 1b) correlates with the disappearance of phosphorylated H2AX (γH2AX) foci[14] (Supplementary Fig. 6).

Analogous to *Atm*$^{-/-}$, *Mdc1*-null fibroblasts and to a lesser extent MEFs expressing a hypomorphic mutation in *Nbs1* (*Nbs1*$^{657\Delta5}$; ref. 15) showed radioresistant rRNA synthesis (Fig. 2c). The incomplete penetrance of the *Nbs1* allele in this assay is probably due to the residual capacity of NBS1$^{657\Delta5}$ to activate ATM and trigger a sub-optimal DNA damage response[15]. These results demonstrate that ATM kinase activity, MDC1 and NBS1 are required for blocking Pol I transcription in response to DNA breaks, whereas Ku, BRCA1, 53BP1 and histone H2AX are dispensable.

Using Pol I–green fluorescent protein (GFP) fusion proteins and photobleaching techniques[5] (Supplementary Fig. 7) we next investigated the dynamics of Pol I nucleolar entry, initiation complex assembly at the promoter and holoenzyme elongation in the presence or absence of micro-irradiation. We first monitored rRNA transcription with GFP-labelled RPA194, one of two Pol I catalytic subunits that directly interacts with DNA[16]. In agreement with published observations[5], RPA194–GFP recovery in undamaged nucleoli was biphasic with a rapid recovery phase followed by a slow component ~50 s after photobleaching (Fig. 3b, control curve). The fast recovery phase represents predominantly Pol I subunits and auxiliary factors that rapidly and continuously exchange between the nucleoplasm and the nucleolus[17], whereas the slower phase largely represents assembly of initiation complexes at the promoter, and elongating holoenzymes[5] (Fig. 3a). In marked contrast, the initial RPA194–GFP recovery phase in micro-irradiated nucleoli reached its maximum ~40 s post-bleaching and was followed by a time-dependent decline in fluorescence (Fig. 3b). This declining phase became less pronounced as the time between DNA damage and photobleaching was increased and eventually it was transformed to a near plateau when photobleaching was performed 300 s post damage (Fig. 3c). Analogous kinetics were observed for the transcriptional initiation factor-IA (TIF-IA; also known as RRN3) and the polymerase-associated factor 53 (PAF53; also known as POLR1E) (Supplementary Fig. 8). These changes in

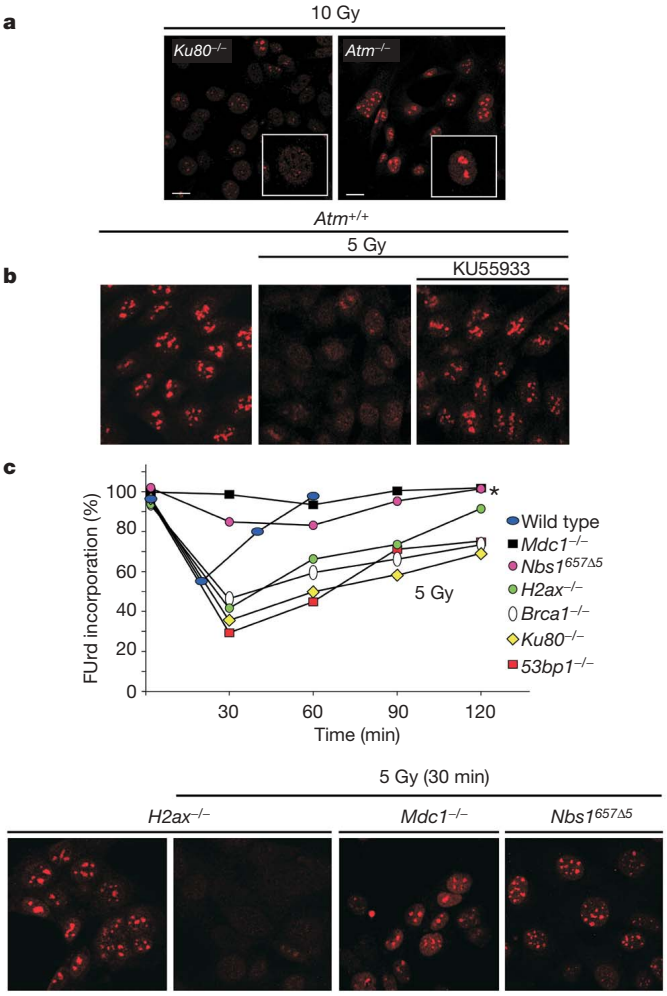

Figure 2 | *Atm*$^{-/-}$, *Nbs1*$^{657\Delta5}$ and *Mdc1*$^{-/-}$ fibroblasts show radioresistant rRNA synthesis. **a**, *Ku80*$^{-/-}$ and *Atm*$^{-/-}$ primary MEFs were exposed to 10 Gy of irradiation and ongoing rRNA transcription was monitored by FUrd incorporation (scale bar, 15 μm). **b**, *Atm*$^{+/+}$ MEFs were untreated (0 Gy) or irradiated (5 Gy) in the presence or absence of the ATM kinase inhibitor KU55933, and Pol I activity was assessed by FUrd nuclear run-ons. **c**, Upper panel, wild type or MEFs deficient in MDC1, H2AX, BRCA1, Ku80, 53BP1 or expressing the human NBS1 mutant protein (*Nbs1*$^{657\Delta5}$) were irradiated with 5 Gy, and FUrd was assessed over time. Values represent the mean ± s.d. ($n = 200$; $^*P < 0.0001$; versus 53BP1); for comparative purposes the mean value of each cell line at time 0 was set to 100%. Lower panel, *H2ax*$^{-/-}$, *Mdc1*$^{-/-}$ and *Nbs1*$^{657\Delta5}$ were untreated or irradiated (5 Gy) and Pol I activity was determined by FUrd incorporation 30 min post DNA damage.

Pol I kinetics were not influenced by the presence of Hoechst dye because similar results were obtained in nucleoli damaged by multi-photon micro-irradiation[18] in the absence of a sensitizing dye (Supplementary Fig. 9). In addition, experiments in *Atm*-null cells showed little change in RPA194–GFP recovery in damaged or undamaged nucleoli (Fig. 3e). In the presence of ATM, 300 s recovery curves were in all cases analogous to those observed in transcriptionally inactive mitotic cells (Fig. 3d, metaphase curve), demonstrating that Pol I transcriptional arrest is complete within 5 min of DNA DSB induction.

To elucidate the mechanistic details of rDNA transcriptional arrest we analysed our fluorescence recovery after photobleaching (FRAP) data on the basis of a previous model of Pol I kinetics[5]. Using standard principles of physical chemistry, four possible mechanistic theories were tested: (1) inhibition of Pol I entry to damaged nucleoli; (2) inhibition of initiation complex assembly at rDNA promoters; (3) block of Pol I elongation; and (4) premature displacement of elongating holoenzymes from rDNA. We found that each theory was able to explain some features of our Pol I experimental results, but no single mechanism could simultaneously fit all FRAP curves (Supplementary Fig. 10 and Supplementary Information). However, a model that evaluated both inhibition of initiation complex assembly and a progressive displacement of elongating holoenzymes from rDNA accounted for all FRAP data simultaneously (Fig. 4a and Supplementary Information).

In the assembly/displacement model the time required to halt transcription of 90% of rDNA genes within the damaged area was 93 s, implying that some ribosomal transcription units are not immediately affected by DNA breaks within the damaged area. Consistent with this idea, the elongation rate of active holoenzymes before completion of transcriptional arrest (before 300 s post micro-irradiation) was analogous to that measured in unirradiated nucleoli (104 nucleotides per second; Supplementary Information and refs 5, 19). These kinetics could be explained if rDNA genes distant from DNA breaks are repressed at a later time point than those found in close proximity to a lesion. Continual transcription in the first few minutes following micro-irradiation would thus allow unbleached Pol I–GFP molecules to enter the elongating pool of rDNA genes not yet inhibited by DNA damage (Fig. 4b). In this scenario the fluorescence decline observed in 20 s-post-damage FRAP curves represents the eventual loss of these unbleached holoenzymes as they either terminate transcription or are prematurely displaced from rDNA. To empirically validate this idea,

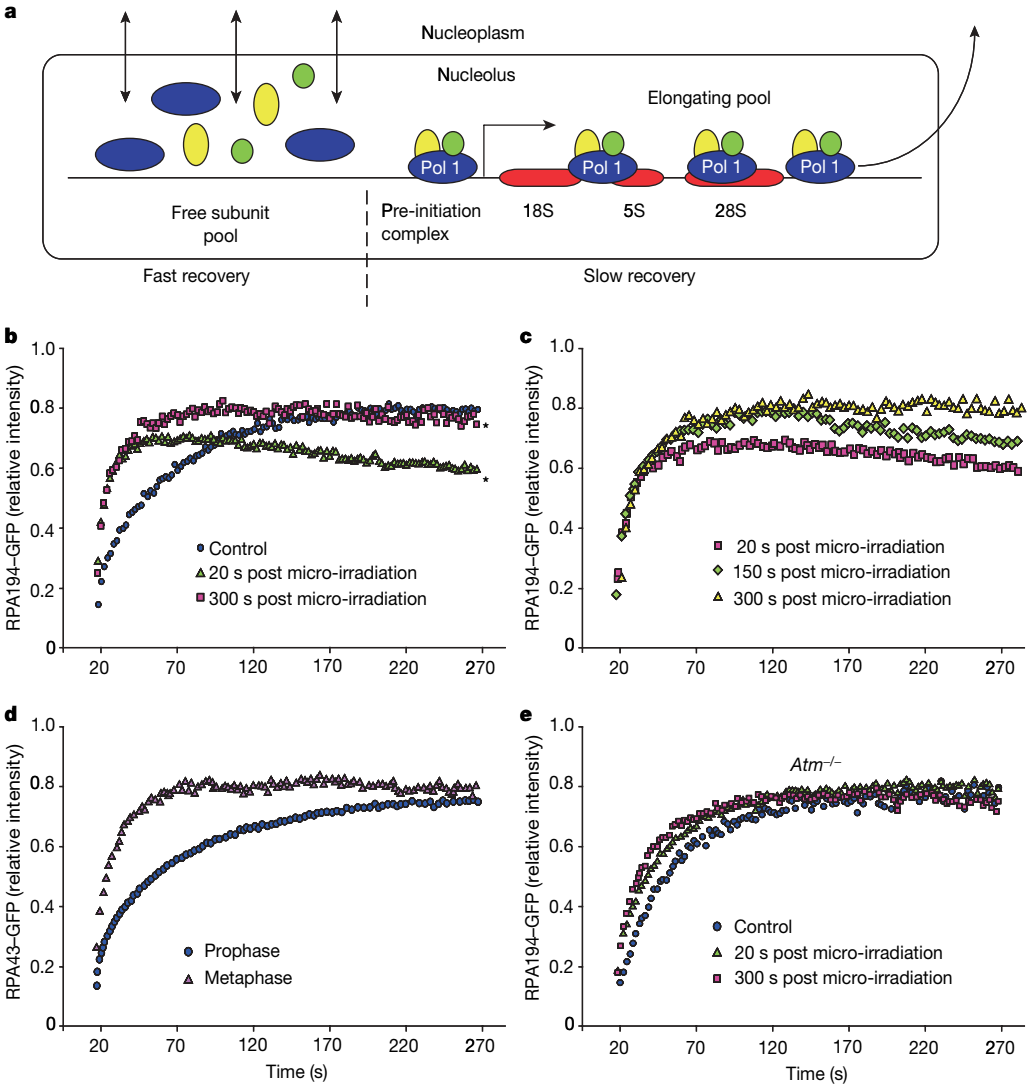

Figure 3 | Pol I dynamics at damaged nucleoli. a, Schematic representation of the major Pol I fractions in transcriptionally active nucleoli. Their approximate recovery during FRAP analysis is stated: free subunit pool, fast recovery; pre-initiation complex and elongating pools, slow recovery. **b**, **c**, FRAP analysis of GFP–RPA194 or RPA43–GFP in control and micro-irradiated nucleoli of CMT3 monkey kidney cells. Photobleaching was performed either 20 s, 150 s, or 300 s post damage. **d**, FRAP analysis of undamaged nucleoli from CMT3 cells in prophase or metaphase expressing RPA43–GFP. **e**, FRAP and damage-FRAP analysis of $Atm^{-/-}$ MEFs expressing RPA194–GFP. Values in all panels represent mean ± s.d. (n = 10–20 cells per condition; $^{*}P < 0.002$).

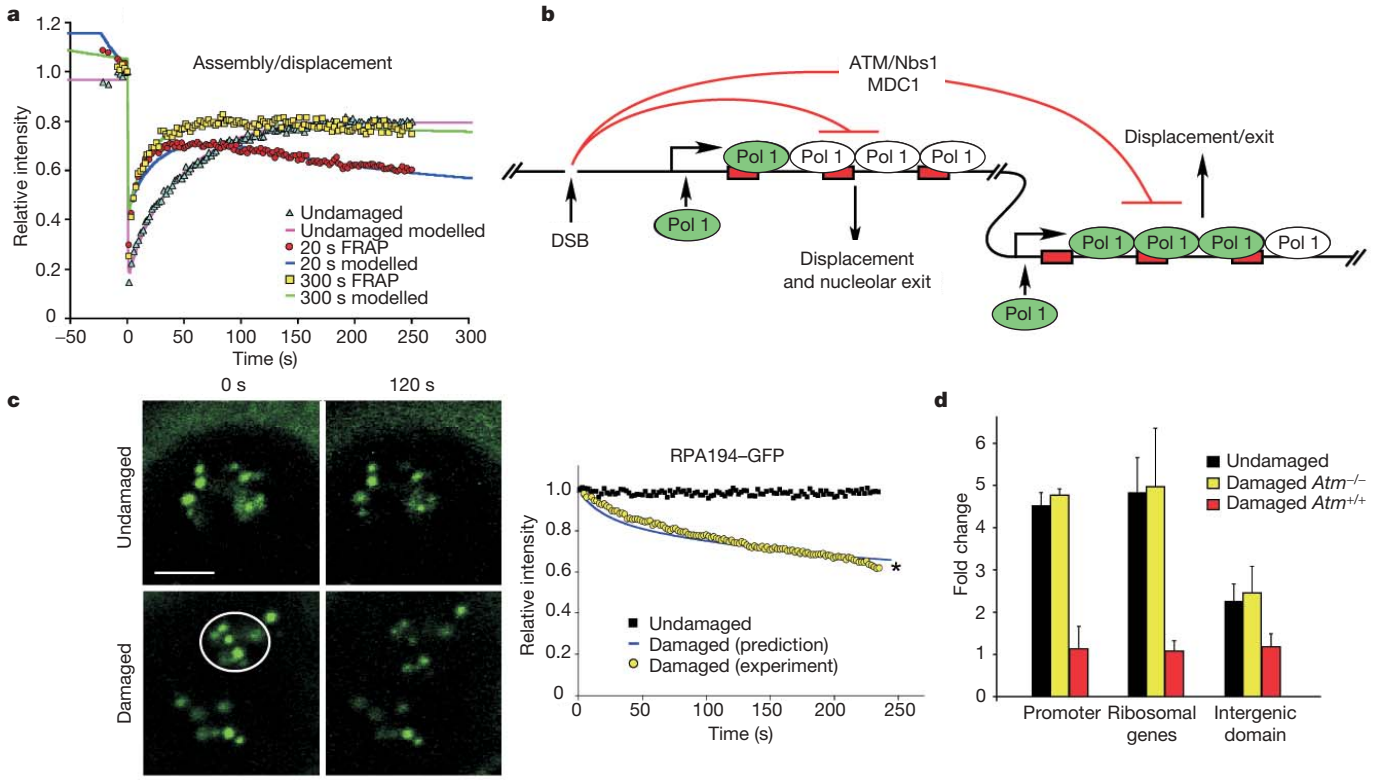

Figure 4 | Displacement of Pol I from rDNA in response to DNA breaks. **a**, RPA194–GFP FRAP results (Fig. 3b) are accounted for by a kinetic model postulating simultaneous inhibition of initiation complex assembly and displacement of elongating holoenzymes from damaged rDNA. **b**, The assembly/displacement model proposes that immediately following micro-irradiation and photobleaching, recruited, unbleached Pol I–GFP (represented by green ovals) enters the elongating pool of rRNA transcription units (RTUs) distant from lesion sites. Eventually these holoenzymes are dislodged from rDNA by an ATM/NBS1/MDC1-dependent mechanism. **c**, RPA194–GFP fluorescence monitored for 250 s (right panel) in undamaged and damaged nucleoli (left panel; scale bar, 2 μm). Blue line in graph represents the loss of Pol I as predicted by the assembly/displacement model; values represent the mean ± s.d. ($n = 15$; $^*P < 0.0001$). **d**, Interaction of RPA194 with ribosomal gene promoters, ribosomal genes, and intergenic domains in $Atm^{+/+}$ or $Atm^{-/-}$ fibroblasts as determined by chromatin immunoprecipitation and quantitative PCR. Cells were either untreated (undamaged) or exposed to 10 Gy of γ-radiation (damaged). Values represent the mean ± s.d. ($n = 4$).

we micro-irradiated nucleoli from CMT3 cells expressing RPA194–GFP and recorded fluorescence loss by time-lapse microscopy (Fig. 4c, left panel). As predicted by our mathematical modelling, introduction of DNA DSBs led to a progressive loss of RPA194-GFP, so that at 250 s post-damage around 40% of RPA194-GFP molecules were excluded from micro-irradiated nucleoli compared to non-damaged sites (Fig. 4c, right panel). Importantly, chromatin immunoprecipitation analysis showed a marked reduction in the interaction of Pol I with promoter and transcription areas in irradiated $Atm^{+/+}$ cells whereas no changes were found in *Atm*-null fibroblasts (Fig. 4d).

Our studies indicate that activation of ATM, NBS1 and MDC1 following DNA damage interferes with Pol I initiation complex assembly and leads to a progressive displacement of elongating holoenzymes from rDNA. A priori, transcriptional arrest around DNA breaks might ensure efficient DNA end-processing by preventing transcription across DNA lesions. However, mounting evidence also indicates that Pol I regulation has a critical role in monitoring cellular stress[20]. Conditions that inhibit Pol I transcription, such as UV irradiation, result in nucleolar structural changes and release of ribosomal proteins that suppress the MDM2 protein, leading to the accumulation of p53 (also known as TRP53) and apoptosis[21]. In response to DNA DSBs, the ATM kinase phosphorylates a multitude of key substrates, including p53 (ref. 22). It will be important to determine whether the ATM pathway also regulates p53 by inhibition of Pol I rRNA synthesis.

METHODS

The Methods section describes the following: (1) how DNA DSBs were introduced in living cells using DNA micro-irradiation as well as γ-irradiation (a step-by-step description on how DNA DSB density was calculated is also provided); (2) confocal microscopy conditions and FRAP analysis; (3) cell culture conditions; and (4) chromatin immunoprecipitation assays. Pol I kinetic modelling and statistical analysis are given as Supplementary Information.

Full Methods and any associated references are available in the online version of the paper at www.nature.com/nature.

Received 24 November 2006; accepted 13 April 2007.

1. Mayne, L. V. & Lehmann, A. R. Failure of RNA synthesis to recover after UV irradiation: an early defect in cells from individuals with Cockayne's syndrome and xeroderma pigmentosum. *Cancer Res.* **42**, 1473–1478 (1982).
2. Hanawalt, P. C. Subpathways of nucleotide excision repair and their regulation. *Oncogene* **21**, 8949–8956 (2002).
3. Nyberg, K. A., Michelson, R. J., Putnam, C. W. & Weinert, T. A. Toward maintaining the genome: DNA damage and replication checkpoints. *Annu. Rev. Genet.* **36**, 617–656 (2002).
4. Bartek, J., Lukas, C. & Lukas, J. Checking on DNA damage in S phase. *Nature Rev. Mol. Cell Biol.* **5**, 792–804 (2004).
5. Dundr, M. *et al.* A kinetic framework for a mammalian RNA polymerase *in vivo*. *Science* **298**, 1623–1626 (2002).
6. Shav-Tal, Y. *et al.* Dynamic sorting of nuclear components into distinct nucleolar caps during transcriptional inhibition. *Mol. Biol. Cell* **16**, 2395–2413 (2005).
7. Mone, M. J. *et al.* Local UV-induced DNA damage in cell nuclei results in local transcription inhibition. *EMBO Rep.* **2**, 1013–1017 (2001).
8. Kruhlak, M. J. *et al.* Changes in chromatin structure and mobility in living cells at sites of DNA double-strand breaks. *J. Cell Biol.* **172**, 823–834 (2006).
9. Michaelidis, T. M. & Grummt, I. Mechanism of inhibition of RNA polymerase I transcription by DNA-dependent protein kinase. *Biol. Chem.* **383**, 1683–1690 (2002).
10. Mayer, C. & Grummt, I. Cellular stress and nucleolar function. *Cell Cycle* **4**, 1036–1038 (2005).

11. Kleiman, F. E. *et al.* BRCA1/BARD1 inhibition of mRNA 3′ processing involves targeted degradation of RNA polymerase II. *Genes Dev.* **19,** 1227–1237 (2005).
12. Kastan, M. B. & Lim, D. S. The many substrates and functions of ATM. *Nature Rev. Mol. Cell Biol.* **1,** 179–186 (2000).
13. Shiloh, Y. ATM and related protein kinases: safeguarding genome integrity. *Nature Rev. Cancer* **3,** 155–168 (2003).
14. Rogakou, E. P., Boon, C., Redon, C. & Bonner, W. M. Megabase chromatin domains involved in DNA double-strand breaks *in vivo*. *J. Cell Biol.* **146,** 905–916 (1999).
15. Difilippantonio, S. *et al.* Role of Nbs1 in the activation of the Atm kinase revealed in humanized mouse models. *Nature Cell Biol.* **7,** 675–685 (2005).
16. Seither, P., Coy, J. F., Pouska, A. & Grummt, I. Molecular cloning and characterization of the cDNA encoding the largest subunit of mouse RNA polymerase I. *Mol. Gen. Genet.* **255,** 180–186 (1997).
17. Chen, D. & Huang, S. Nucleolar components involved in ribosome biogenesis cycle between the nucleolus and nucleoplasm in interphase cells. *J. Cell Biol.* **153,** 169–176 (2001).
18. Mari, P. O. *et al.* Dynamic assembly of end-joining complexes requires interaction between Ku70/80 and XRCC4. *Proc. Natl Acad. Sci. USA* **103,** 18597–18602 (2006).
19. Stefanovsky, V., Langlois, F., Gagnon-Kugler, T., Rothblum, L. I. & Moss, T. Growth factor signaling regulates elongation of RNA polymerase I transcription in mammals via UBF Phosphorylation and r-chromatin remodeling. *Mol. Cell* **21,** 629–639 (2006).
20. Olson, M. O. Sensing cellular stress: another new function for the nucleolus? *Sci. STKE* **2004,** pe10 (2004).
21. Mayer, C., Bierhoff, H. & Grummt, I. The nucleolus as a stress sensor: JNK2 inactivates the transcription factor TIF-IA and down-regulates rRNA synthesis. *Genes Dev.* **19,** 933–941 (2005).
22. Banin, S. *et al.* Enhanced phosphorylation of p53 by ATM in response to DNA damage. *Science* **281,** 1674–1677 (1998).

Supplementary Information is linked to the online version of the paper at www.nature.com/nature.

Acknowledgements We thank Y. Shiloh for reagents and comments. We are grateful to Z. Lou, J. Chen and C. Deng for cell lines, J. Ionita, K. Zaal and S. Twitty for technical assistance, and I. Grummt for antibodies and protocols. We also thank S. Wincovitch for access to the multi-photon microscope. This research was supported (in part) by the Intramural Research Program of the National Institute of Arthritis and Musculoskeletal and Skin Diseases and the Center for Cancer Research of the National Cancer Institute, National Institutes of Health.

Author Contributions M.K. and R.C. planned the project and did experimental work, data analysis, and wrote the manuscript. E.E.C., M.O., C.M. and R.D.P. did experimental work, data analysis, and provided assistance in writing the manuscript. S.A.G. shared unpublished data and provided advice during experimental design. A.N. and T.M. provided advice and expertise and proof-read the manuscript.

Author Information Reprints and permissions information is available at www.nature.com/reprints. The authors declare no competing financial interests. Correspondence and requests for materials should be addressed to R.C. (casellar@mail.nih.gov).

METHODS

DSB density at nuclear and nucleolar focused domains. DNA DSBs were introduced into cell nuclei using a UV laser on a Zeiss LSM 510 *META* confocal microscope. Nucleolar or nuclear areas of 15.2 μm^3 were consistently exposed to laser micro-irradiation at 0.86 nJ per pixel using 50% laser output. Given a nuclear volume of 500 μm^3 and 6×10^9 base pairs (bp) of DNA in non-replicated nuclei, we calculated a density of 1.2×10^7 bp of DNA per nuclear μm^3. Thus, approximately 1.7×10^8 bp of DNA were exposed to micro-irradiation in 15.2 μm^3. In γ-irradiated cells, one Gy results in 35 DSBs approximately. From the calculated equivalence of UV laser micro-irradiation to Gy of γ-irradiation, the DNA at damaged sites was exposed to 5.25 Gy of irradiation, inducing ~185 DSBs. These conditions correspond to a density of 1 DSB for every 940 kb of DNA, or 23 ribosomal transcription units.

To introduce DNA breaks by laser micro-irradiation using near-infrared multi-photon microscopy, we used a Zeiss LSM510 NLO microscope (Carl Zeiss) equipped with a 63× (numerical aperture 1.4) Plan-Apochromat objective lens to focus 800 nm laser light from a Ti:sapphire femtosecond pulsed laser (Coherent) mode-locked at wavelength 800 nm (116 MHz, 12 mW output at the sample). Laser exposure was restricted to 17.6 μm^2 regions with a total exposure time of 60 ms. Subsequent FRAP time series were performed as mentioned above, except a consistent 6.2 μm^2 circular area was used for photobleaching the GFP. Images were collected with 0.14 μm *x*–*y* pixel sampling.

Microscopy equipment and settings. Samples were imaged using a 40× C-Apochromat (numerical aperture 1.2) water immersion lens coupled to a Zeiss LSM510 META confocal microscope (Carl Zeiss MicroImaging) and the multi-time macro (version z) accompanying the Zeiss LSM software. To introduce DNA DSBs by UV laser micro-irradiation, we used configurations specific for exposing living transfected cells to a 364 nm laser (Coherent Enterprise II) at intensities equivalent to approximately 0.86 nJ per pixel. As the first block in the multi-time macro, we performed one pre-micro-irradiation scan. We then micro-irradiated a restricted region of interest with the 364 nm laser approximately 4 μm^2 in size to cover a single or partial fibrillar center, and finished with a post-micro-irradiation scan. Within the second block of the multi-time macro, fluorescence recovery after photobleaching experiments were performed using FRAP specific configurations. The photobleaching was restricted to a consistent 3.14 μm^2 area within the UV laser exposed region of interest within the nucleolus. GFP was excited and photobleached using the 488 nm line of Argon multi-line laser (Lasos). Excitation intensity was set at 2% of the laser intensity used to ablate GFP fluorescence in the photobleaching step. Five pre-bleach images were collected; after bleaching, cells were monitored at 2 s intervals for 250 s. To measure the fluorescence recovery, the mean fluorescence intensities of both a region within the bleached area and in the total nuclear area were recorded. Background fluorescence was measured from control non-transfected cells. The relative intensity was normalized by first subtracting mean background fluorescence from the total nuclear area fluorescence and the signal in the region of interest. Then, the fluorescence in the region of interest was divided by the nuclear area fluorescence to obtain a relative fluorescence ratio. These values were normalized to one by dividing by the mean of the fluorescence intensity ratios in the five pre-bleach scans. All images were acquired using Zeiss LSM version 3.2 (at 8 bit depth). The scaling was 0.22 μm × 0.22 μm and the stack size of 1,024 × 1,024, 230.3 μm × 230.3 μm. The pixel time was 1.60 μs. Unfixed live cells were maintained at 37 °C in phenol-red-free DMEM during imaging. The filter used was LP 560 and the objective lens a 40× C-Apochromat (numerical aperture 1.2). TIFF images were further processed using Canvas software. The brightness was adjusted to 65 and the contrast to 40 in all files, with the exception of images shown in Fig. 4c, for which both the brightness and contrast were adjusted to 25.

Cell culture. CMT3, *Ku80*$^{-/-}$ MEFs, *ATR* hypomorphic human cells (Seckel) and *Atm*$^{-/-}$ MEFs were grown in DMEM (American Tissue Culture Collection) supplemented with 10% FCS (ATCC), 1% penicillin and streptomycin at 37 °C in 5% CO_2. Cells were transfected by electroporation using an ECM 830 electroporator with 5 μg RPA194–GFP, PAF53–GFP or RPA43–GFP constructs and 15 μg of sheared salmon sperm DNA. Fluorouridine incorporation was performed by incubating transfected cells with 2 mM FUrd (Sigma) DMEM media for 15 min at 37 °C and 5% CO_2. Cells were then fixed with 2% paraformaldehyde for 15 min at room temperature, washed twice with PBS, and stored in PBS at 4 °C until data acquisition. To introduce DNA DSBs by laser micro-irradiation, cells were incubated with Hoechst 33342 dye (0.8 μl ml^{-1}, Molecular Probes) for 20 min, the media was replaced with new media containing 2 mM FUrd, and cells were incubated for 10 min at 37°C and 5% CO_2. Cells were then damaged at specified nucleoli using the 364 nm laser, and returned to the incubator for a further 10 min, and finally fixed in 2% PFA. Cells exposed to 10 Gy of γ-irradiation were incubated under normal growth conditions for 30 min, media was then replaced with DMEM containing 2 mM FUrd for 15 min at 37 °C and 5% CO_2, and finally fixed in 2% PFA. FUrd was visualized by incubating cells with monoclonal anti-BrdU (Sigma) for 1 h, washing twice with PBS, and then staining for 30 min with Goat-anti-mouse coupled to Alexa 546 (Molecular Probes). Damaged cells were visualized using anti-phospho-Histone H2AFX-FITC (Upstate).

Chromatin immunoprecipitation. 293T or *Atm*$^{-/-}$ fibroblasts were transfected with Flag tagged RPA194. Cells (4×10^7) were exposed to γ-irradiation (5 or 10 Gy), incubated for 15 min at 37 °C, and crosslinked by formaldehyde (0.25%) for 10 min. Cells were then washed with PBS and resuspended in 1 ml of high magnesium buffer (10 mM HEPES, pH 7.5, 0.88 M sucrose, 12 mM $MgCl_2$, and 1 mM dithiothreitol, plus protease inhibitors). Nucleoli were then released by sonicating on ice (8 bursts of 10 s at 12% amplitude) using a Branson digital sonifier. The release of nucleoli was monitored microscopically. Nucleoli were resuspended in 1.0 ml of low magnesium buffer (10 mM HEPES, pH 7.5, 0.88 M sucrose, 1 mM $MgCl_2$ and 1 mM dithiothreitol, plus protease inhibitors), resonicated (10 s at 12% amplitude), and resuspended in 0.2 ml of 20/2TE (20 mM Tris, pH 8.0, 2 mM EDTA), after which a 1/10 volume of 20% SDS was added. Samples were incubated at 37 °C for 15 min and sonicated (7 bursts of 10 s each at 12% amplitude) following addition of 0.8 ml of 20/2TE. The resulting sheared nucleolar chromatin was then diluted tenfold in 0.01% SDS, 1.1% Triton X-100, 1.2 mM EDTA, 16.7 mM Tris-HCl, pH 8.1, 167 mM NaCl, and protease inhibitors. From this suspension 100 μl were saved as input DNA. To reduce non-specific background, samples were nutated for 30 min with 400 μl of 50% slurry of Protein G agarose beads pre-equilibrated with bovine serum albumin and salmon sperm DNA. Samples were then pelleted and incubated overnight with 25 μl of monoclonal anti-Flag antibody (F1804, Sigma). A 50% slurry of Protein G agarose beads (150 μl) was added to the mixture and nutated for 1 h at 4°C. Immunoprecipitated DNA was recovered following Upstate protocol. DNA concentration was measured using Picogreen (Molecular Probes) and FLUOstar Optima fluorescence software. Samples were resuspended to 0.015 ng ml^{-1}, and 1 μl of DNA was used as a template for quantitative PCR.

LETTERS

Control of DNA methylation and heterochromatic silencing by histone H2B deubiquitination

Vaniyambadi V. Sridhar[1]*, Avnish Kapoor[1]*, Kangling Zhang[2], Jianjun Zhu[3], Tao Zhou[3], Paul M. Hasegawa[3], Ray A. Bressan[3] & Jian-Kang Zhu[1]

Epigenetic regulation involves reversible changes in DNA methylation and/or histone modification patterns[1–7]. Short interfering RNAs (siRNAs) can direct DNA methylation and heterochromatic histone modifications, causing sequence-specific transcriptional gene silencing[1,4,8,9]. In animals and yeast, histone H2B is known to be monoubiquitinated, and this regulates the methylation of histone H3 (refs 10, 11). However, the relationship between histone ubiquitination and DNA methylation has not been investigated. Here we show that mutations in an *Arabidopsis* deubiquitination enzyme, SUP32/UBP26, decrease the dimethylation on lysine 9 of H3, suppress siRNA-directed methylation of DNA and release heterochromatic silencing of transgenes as well as transposons. We found that *Arabidopsis* histone H2B is monoubiquitinated at lysine 143 and that the levels of ubiquitinated H2B and trimethyl H3 at lysine 4 increase in *sup32* mutant plants. SUP32/UBP26 can deubiquitinate H2B, and chromatin immunoprecipitation assays suggest an association between H2B ubiquitination and release of silencing. These data suggest that H2B deubiquitination by SUP32/UBP26 is required for heterochromatic histone H3 methylation and DNA methylation.

We have previously established a transcriptional gene silencing (TGS) system in which a low level of siRNAs does not result in TGS in the wild type as a result of the active DNA demethylation activity of ROS1 (refs 12, 13). In *ros1-1* mutant plants, however, the siRNAs cause promoter DNA hypermethylation at the *RD29A-LUC* (firefly luciferase reporter driven by the stress-responsive *RD29A*

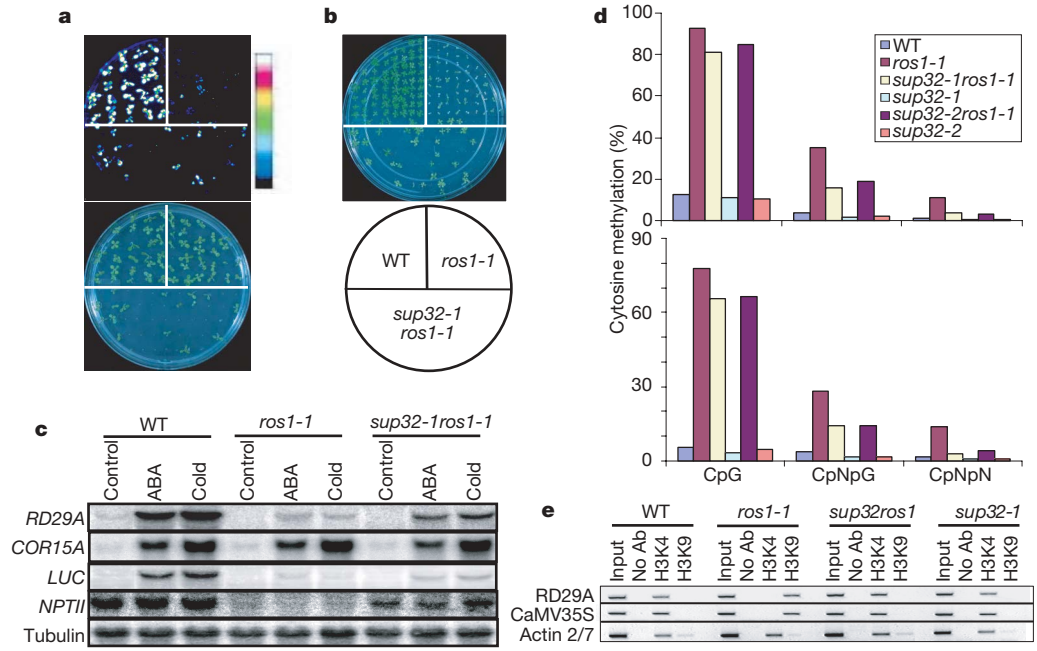

Figure 1 | Effect of *sup32* mutations on transcriptional gene silencing, DNA methylation and histone H3 methylation. **a**, *sup32-1* suppresses *RD29A-LUC* transgene silencing in *ros1-1*. Shown are luciferase images of plants treated with cold stress. The colour scale at the right shows the luminescence intensity from dark blue (lowest) to white (highest). WT, wild type. **b**, *sup32-1* suppresses the kanamycin sensitivity of *ros1-1*. Seeds were planted on MS medium supplemented with kanamycin (35 mg l^{-1}) and grown for 2 weeks. **c**, Northern analysis of transcript levels of the endogenous *RD29A* gene and the *LUC* and *NPTII* transgenes. *COR15A* was used as a control for stress treatment, and *TUBULIN* was a control for equal loading. ABA, abscisic acid. **d**, Cytosine methylation present at endogenous (top) and transgene (bottom) *RD29A* promoters as determined by bisulphite sequencing. N represents A, T or C. Detailed methylation data can be found in Supplementary Fig. S2a, b. **e**, ChIP analysis using antibodies against dimethyl H3K4 and dimethyl H3K9 at *RD29A* and *CaMV 35S* promoters in the wild type (WT), *ros1-1*, *sup32-1ros1-1* and *sup32-1*. *ACTIN* was used as a control. 'No Ab' corresponds to chromatin treated without antibody.

[1]Center for Plant Cell Biology and Department of Botany and Plant Sciences, [2]Mass Spectrometry Facility, Department of Chemistry, University of California Riverside, California 92521, USA. [3]Department of Horticulture and Landscape Architecture, Purdue University, West Lafayette, Indiana 47907, USA.
*These authors contributed equally to this work.

promoter) transgene as well as the endogenous *RD29A* gene. The *35S-NPTII* (neomycin phosphotransferase II driven by the *CaMV 35S* promoter) transgene is also silenced in *ros1-1* because of heterochromatic spreading from the adjacent *RD29A-LUC* locus[14]. We performed a screen and found *sup32-1* as a suppressor of the *ros1-1* mutant. In *sup32-1ros1-1* mutant plants, silencing of the *RD29A-LUC* and *35S-NPTII* transgenes as well as the endogenous *RD29A* was partly released (Fig. 1a–c, and Supplementary Fig. S1a, b).

RNA blot analysis showed that the level of siRNAs generated from the transgene *RD29A* promoter was not affected by the *sup32-1* mutation (Supplementary Fig. S1c, d). This result suggests that *SUP32* is not important for siRNA biogenesis but is required for the activity of siRNAs to trigger TGS. Bisulphite sequencing revealed that the release of TGS at both the *RD29A–LUC* and endogenous *RD29A* loci was accompanied by a substantial decrease in promoter DNA methylation in CpNpG and CpNpN sequence contexts (Fig. 1d, and Supplementary Fig. S2). CpG methylation at the two loci was affected only slightly by the *sup32-1* mutation. An allelic mutant, *sup32-2*, obtained from the Salk T-DNA (*Agrobacterium*-transferred DNA) collection showed similar phenotypes in releasing TGS in the *ros1-1* background (Supplementary Fig. S3a) and decreasing DNA methylation (Fig. 1d, and Supplementary Fig. S2). In *Arabidopsis*, dimethylated H3K4 (lysine 4 of histone H3) and H3K9 are marks of active and silent chromatins, respectively[15]. We examined the status of histone H3 methylation at the *RD29A* and *35S* promoters by chromatin immunoprecipitation (ChIP) assays. As shown in Fig. 1e, these promoters in the wild type were associated with abundant H3K4 dimethylation, whereas in *ros1-1* they were preferentially associated with H3K9 dimethylation. In contrast, dimethylated H3K4 was enriched in *sup32-1ros1-1* compared with dimethylated H3K9 at both the *RD29A* and *35S* promoters. In the *sup32-1* single mutant, the promoters were also preferentially associated with dimethylated H3K4. These results show that the *SUP32* gene is required for H3K9 dimethylation, CpNpG and CpNpN methylation and TGS. The lack of difference in histone and DNA methylation at the transgenes between the wild type and the *sup32-1* single mutant suggests that *SUP32* is important for silent but not already active loci.

Transposons are prominent endogenous targets of TGS and are associated with high levels of DNA methylation and H3K9 dimethylation[15]. The expression of transposon *AtMULE1* and retrotransposons *AtLINE1-4*, *AtGP1* and *AtSN1* was enhanced by the *sup32* mutation in the *ros1-1* or wild-type background (Fig. 2a, and Supplementary Fig. S3b). Interestingly, *AtGP1* expression was more in *sup32-1* than in *sup32-1ros1-1* (Fig. 2a), supporting the notion that ROS1 has a negative role in the TGS of this transposon[16]. For all of the transposons, CpG methylation levels were comparable in the wild type and in *ros1-1*, *sup32-1ros1-1* and *sup32-1*, but there were substantial decreases in the levels of CpNpG and CpNpN methylation in *sup32-1ros1-1* and *sup32-1* (Fig. 2b, c, and Supplementary Fig. S4a-d). As shown in Fig. 2d, in both the wild type and *ros1-1*, dimethylated H3K9 was enriched in these loci compared with dimethylated H3K4. In contrast, dimethylated H3K4 was enriched relative to dimethylated H3K9 in *sup32-1ros1-1* and *sup32-1*, which is consistent with the increased expression of these loci in these mutant plants. Taken together, the results suggest that the *sup32-1* mutation releases TGS of the transposons and this involves decreases in non-CpG DNA methylation and H3K9 dimethylation.

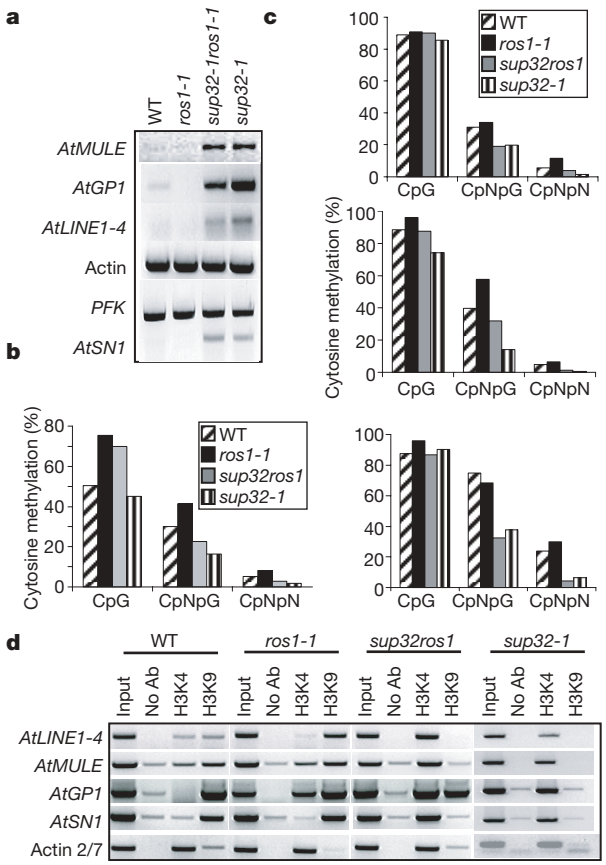

Figure 2 | Effect of *sup32* mutation on the expression, and DNA and histone methylation patterns, of transposons. a, Expression analysis of the transposons by RT–PCR. *PFK* and *ACTIN* were used as internal controls. **b**, **c**, Bisulphite sequencing results showing percentage methylation. **b**, *AtLINE1-4*; **c**, *AtMULE* (top), *AtGP1* (middle) and *AtSN1* (bottom). Detailed methylation data can be found in Supplementary Fig. S4a–d. **d**, ChIP analysis using antibodies against dimethyl H3K4 and dimethyl H3K9 at transposon loci. *ACTIN* was used as a control. 'No Ab' corresponds to chromatin treated without antibody.

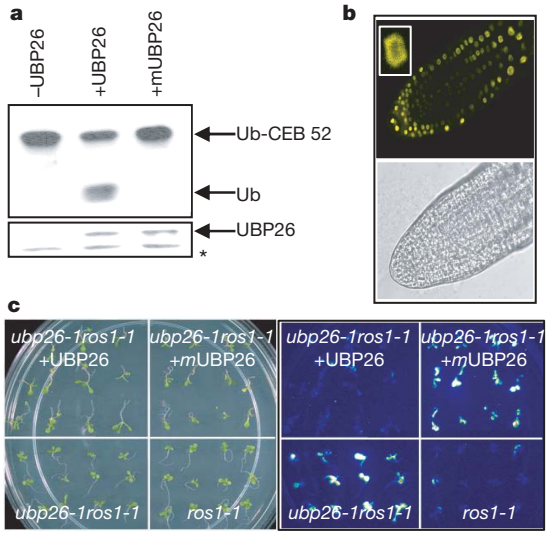

Figure 3 | *SUP32* encodes a nuclear ubiquitin protease. a, UBP activity of SUP32/UBP26 *in vivo* in *E. coli*. The substrate UB-CEP 52 was co-expressed with XPress tag (−UBP26), XPress-tagged UBP26 (+UBP26) or XPress-tagged UBP26C115S (+mUBP26). Upper panel, immunoblot probed with anti-ubiquitin antibody; lower panel, *E. coli* extracts probed with Xpress antibody showing expression of recombinant UBP26 and UBP26C115S. The antibody also cross-reacted with a smaller non-specific band (marked by an asterisk), which served as a loading control. **b**, UBP26–YFP fusion protein is localized in the nucleus. The picture shows YFP signal in the nuclei of root cells of *Arabidopsis* plants transformed with *CaMV 35S* promoter-driven UBP26–YFP. The inset is a close-up of one of the nuclei. **c**, Rescue of *ubp26-1ros1-1* mutant phenotype by expressing *CaMV 35S* promoter-driven *UBP26* (+UBP26), but not by expressing *UBP26(115)S* mutant (+mUBP26) cDNAs. Luciferase imaging was performed after 48 h of cold treatment.

Thermal asymmetric interlaced polymerase chain reaction (TAIL-PCR) was performed to clone the *SUP32* gene. A single insertion was found in the third intron of AT3G49600/*UBP26*, which encodes a protein of 1,067 amino acids and shows similarity to ubiquitin-specific proteases (UBPs)[17]. The *sup32-2* allele has an insertion in the seventh exon (Supplementary Fig. S5a). UBPs are thiol proteases that specifically cleave ubiquitin carboxy-terminal glycine from covalently attached proteins[17]. To test the UBP activity of SUP32/UBP26, we co-expressed XPress-tagged UBP26 together with the substrate UB-Cep52 in *Escherichia coli*[18]. As shown in Fig. 3a, ubiquitin monomer was detected in extracts from bacterial cells expressing UBP26 but not in those expressing XPress tag alone. A mutant version of UBP26 in which an active-site Cys 115 was changed to serine did not show the UBP activity, although the mutant protein was expressed at a similar level to the wild-type protein (Fig. 3a). A fusion protein of UBP26 and yellow fluorescent protein (YFP) was found to be localized in the nucleus in transgenic plants (Fig. 3b). Promoter-GUS (β-D-glucuronidase) experiments together with reverse transcriptase (RT)–PCR analysis indicated a ubiquitous expression pattern of *UBP26* in plants (Supplementary Fig. S5b, c). To confirm that AT3G49600 is the *SUP32/UBP26* gene, we expressed AT3G49600 complementary DNA under the *CaMV 35S* promoter in *ubp26-1ros1-1*. Luciferase imaging of the transformants indicated that the mutant was complemented (Fig. 3c). When the UBP26C(115)S mutant cDNA was expressed, luciferase imaging indicated that it failed to complement the *ubp26-1ros1-1* mutant (Fig. 3c). These results show that UBP26 is a nuclear UBP and its deubiquitination activity is required for TGS.

Recently, studies in animals and yeasts have found that ubiquitination of histone H2B and H2A is involved in transcriptional regulation[10]. It is not known whether any *Arabidopsis* histone is ubiquitinated. We isolated total histones from *Arabidopsis* seedlings and used mass spectrometry to examine modifications in H2A and H2B. We did not detect any ubiquitinated H2A but found that H2B is monoubiquitinated at Lys 143 in the C terminus (AVTKFTSS) (Fig. 4a). The amino-acid sequences surrounding the H2B ubiquitination sites are highly conserved between yeast, human and *Arabidopsis* (Supplementary Fig. S6).

We examined the relative levels of ubiquitinated H2B (ubH2B) in the wild type, *ros1-1*, *sup32-1ros1-1* and *sup32-1* mutant plants. Anti-H2B antibodies detected not only an approximately 19-kDa protein corresponding to unubiquitinated H2B, but also an approximately 27-kDa band corresponding to monoubiquitinated H2B (ubH2B) in *Arabidopsis* total histone preparations (Fig. 4b, top panel). Indeed, this approximately 27-kDa band was also recognized by anti-ubiquitin antibodies (Fig. 4b, middle panel). The levels of ubH2B were higher in *sup32-1ros1-1* and *sup32-1* than in *ros1-1* or the wild type (Fig. 4b). Consistent with the western blot results, mass spectrometry analysis also indicated higher levels of ubH2B in *sup32-1* and *sup32-1ros1-1* mutant plants (data not shown). To determine whether UBP26 can deubiquitinate ubH2B, we expressed UBP26 in a yeast strain that expresses Flag-tagged H2B and carries deletions in the yeast UBP8 and UBP10 (ref. 19). As shown in Fig. 4c, the level of yeast ubH2B is decreased in the presence of UBP26 but not mutant UBP26 (in which the active-site Cys 115 was changed to serine) compared with that in the vector control. We also investigated whether UBP26 can deubiquitinate *Arabidopsis* ubH2B *in vitro*. As shown in Fig. 4d (top and middle panels), the level of ubH2B in a sample of purified *Arabidopsis* histones is decreased by incubation with UBP26 but not with the buffer control or the inactive UBP26 mutant, as revealed by probing with an anti-H2B antibody. Probing of these same samples with an anti-ubiquitin antibody showed the appearance of free ubiquitin accompanying the disappearance of ubH2B, in the sample treated with UBP26 but not with the buffer control or mutant UBP26 (Fig. 4d, bottom panel). Together, these data show that UBP26 can deubiquitinate ubH2B, and a loss-of-function mutation in UBP26 causes an elevated level of ubH2B in plants.

In a further examination of the consequence of increased mono-ubiquitination of H2B in *ubp26-1* (that is, *sup32-1*), steady-state levels of histone H3 methylation were determined by using specific antibodies. As shown in Fig. 4e, *ubp26-1* had higher levels of tri-methylated H3K4, and also a slight increase in dimethylated H3K4, compared with wild-type plants. In contrast, no increase was found for dimethylated H3K9 in the mutant.

In the absence of antibodies specific for ubiquitinated H2B, we performed chromatin double immunoprecipitation (ChDIP) assays to test for an association between H2B ubiquitination and release of TGS. Chromatin was first immunoprecipitated with an anti-ubiquitin

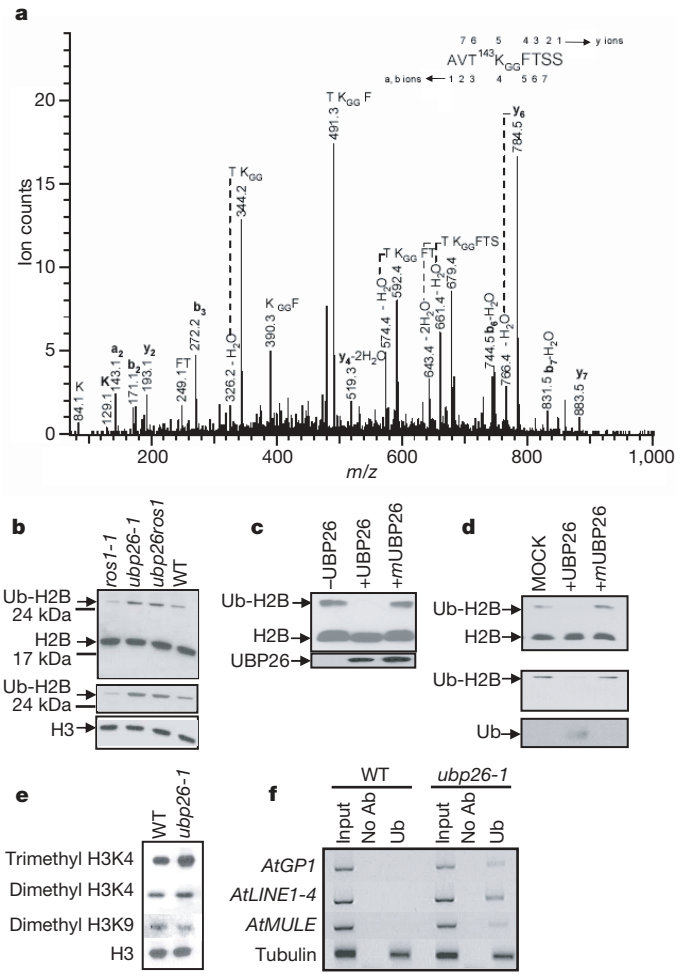

Figure 4 | Analysis of H2B ubiquitination and its association with gene activation. **a**, Identification of H2B ubiquitination site by mass spectrometry. Detailed information is included in Methods. **b**, Western analysis of purified *Arabidopsis* histones with anti-H2B antibody (top panel), anti-ubiquitin antibody (middle panel) and anti-H3 antibody (bottom panel). **c**, Effect of UBP26 expression on histone H2B ubiquitination *in vivo* in yeast. Ubiquitination levels of Flag–H2B were assayed in yeast whole-cell lysates by using anti-Flag antibody (15% SDS–PAGE). The expression level of Flag–UBP26 was also determined in the lysates with the use of anti-Flag antibody (8% SDS–PAGE). **d**, Deubiquitination activity of UBP26 on *Arabidopsis* ubiquitinated H2B *in vitro*. Purified histones were incubated with buffer control (mock), UBP26 (+UBP26) or UBP26C115S mutant protein (+mUBP26). Deubiquitination was assessed by immunoblotting with anti-H2B antibody (top panel) or anti-ubiquitin antibody (middle and bottom panels). **e**, Western blot analysis of histone H3 methylation levels in *Arabidopsis*. **f**, ChDIP analysis by immunoprecipitating chromatin first with anti-ubiquitin antibodies and then with anti-H2B antibodies. The eluted DNA was subjected to PCR for *AtGP1*, *AtLINE1-4* and *AtMULE1*. *Tubulin* was used as an internal control. 'No Ab' and Ub correspond to chromatin first treated without and with anti-ubiquitin antibodies, respectively.

antibody and eluted from the precipitate with ubiquitin. The supernatant was immunoprecipitated with an anti-H2B antibody, and the resulting DNA was eluted and subjected to PCR for transposon loci affected by the *ubp26* mutation. As shown in Fig. 4f, we found an enrichment of *AtGP1*, *AtMULE1* and *AtLINE1-4* in the double-immunoprecipitated chromatin from *ubp26-1* plants, in which these transposons are transcriptionally active. In contrast, there was no enrichment in wild-type plants, in which the same transposons are inactive (Fig. 4f). These data show an association between H2B ubiquitination and release of TGS.

Our data show that histone H2B is monoubiquitinated in plants, and that the nuclear ubiquitin protease, UBP26, has a critical function in non-CpG DNA methylation and TGS. The results implicate UBP26 in the deubiquitination of H2B in *Arabidopsis* and suggest that this deubiquitination is required for H3K9 dimethylation, which has been shown to direct CpNpG and CpNpN methylation[20,21]. In yeast and animals, H2B ubiquitination is known to be required for methylation of H3K4 (ref. 11) and H3K79 (ref. 22), leading to active transcription. Given the bulky size of ubiquitin (relative to acetyl, methyl or phosphoryl groups) and the role of ubiquitinated H2B in keeping chromatin in an open state[10], H2B deubiquitination is likely to be an early and crucial event in heterochromatin formation. UBP26-mediated deubiquitination may be an upstream event in the siRNA-directed TGS pathway. Alternatively, H2B deubiquitination might not depend on siRNAs but the deubiquitination might be required to make the chromatin competent for siRNA-directed DNA methylation and TGS. In any event, the accumulation of active chromatin marks such as ubH2B and trimethylated H3K4 as well as the release of TGS in the *ubp26* mutant suggest that UBP26 has an important function in controlling DNA methylation and heterochromatin formation by initiating the removal of active histone modification marks.

METHODS SUMMARY

The *sup32-1* mutant was isolated by screening a T-DNA mutagenized *ros1-1* population. The suppressor mutant was characterized by analysing the expression level using northern blots and RT–PCR, DNA methylation using bisulphite sequencing and histone modification patterns by using ChIP, at various transgenic and endogenous loci. Histone 2B ubiquitination was determined by mass spectrometry and western blot analysis.

Full Methods and any associated references are available in the online version of the paper at www.nature.com/nature.

Received 23 February; accepted 24 April 2007.

1. Matzke, M. A. & Birchler, J. A. RNAi-mediated pathways in the nucleus. *Nature Rev. Genet.* **6,** 24–35 (2005).
2. He, Y. & Amasino, R. M. Role of chromatin modification in flowering-time control. *Trends Plant Sci.* **10,** 30–35 (2005).
3. Bastow, R. *et al.* Vernalization requires epigenetic silencing of *FLC* by histone methylation. *Nature* **427,** 164–167 (2004).
4. Baulcombe, D. RNA silencing in plants. *Nature* **431,** 356–363 (2004).
5. Richards, E. J. & Elgin, S. C. Epigenetic codes for heterochromatin formation and silencing: rounding up the usual suspects. *Cell* **108,** 489–500 (2002).
6. Tariq, M. & Paszkowski, J. DNA and histone methylation in plants. *Trends Genet.* **20,** 244–251 (2004).
7. Martienssen, R. A. & Colot, V. DNA methylation and epigenetic inheritance in plants and filamentous fungi. *Science* **293,** 1070–1074 (2001).
8. Chan, S. W., Henderson, I. R. & Jacobsen, S. E. Gardening the genome: DNA methylation in *Arabidopsis thaliana*. *Nature Rev. Genet.* **6,** 351–360 (2005).
9. Grewal, S. I. & Moazed, D. Heterochromatin and epigenetic control of gene expression. *Science* **301,** 798–802 (2003).
10. Zhang, Y. Transcriptional regulation by histone ubiquitination and deubiquitination. *Genes Dev.* **17,** 2733–2740 (2003).
11. Sun, Z. W. & Allis, C. D. Ubiquitination of histone H2B regulates H3 methylation and gene silencing in yeast. *Nature* **418,** 104–108 (2002).
12. Agius, F., Kapoor, A. & Zhu, J. K. Role of the *Arabidopsis* DNA glycosylase/lyase ROS1 in active DNA demethylation. *Proc. Natl Acad. Sci. USA* **103,** 11796–11801 (2006).
13. Gong, Z. *et al.* ROS1, a repressor of transcriptional gene silencing in *Arabidopsis*, encodes a DNA glycosylase/lyase. *Cell* **111,** 803–814 (2002).
14. Kapoor, A. *et al.* Mutations in a conserved replication protein suppress transcriptional gene silencing in a DNA-methylation-independent manner in *Arabidopsis*. *Curr. Biol.* **15,** 1912–1918 (2005).
15. Gendrel, A. V., Lippman, Z., Yordan, C., Colot, V. & Martienssen, R. A. Dependence of heterochromatic histone H3 methylation patterns on the *Arabidopsis* gene *DDM1*. *Science* **297,** 1871–1873 (2002).
16. Zhu, J., Kapoor, A., Sridhar, V. V., Agius, F. & Zhu, J. K. The DNA glycosylase/lyase ROS1 functions in pruning DNA methylation patterns in *Arabidopsis*. *Curr. Biol.* **17,** 54–59 (2007).
17. Yan, N., Doelling, J. H., Falbel, T. G., Durski, A. M. & Vierstra, R. D. The ubiquitin-specific protease family from *Arabidopsis*. AtUBP1 and 2 are required for the resistance to the amino acid analog canavanine. *Plant Physiol.* **124,** 1828–1843 (2000).
18. Rao-Naik, C., Chandler, J. S., McArdle, B. & Callis, J. Ubiquitin-specific proteases from *Arabidopsis* thaliana: cloning of *AtUBP5* and analysis of substrate specificity of AtUBP3, AtUBP4, and AtUBP5 using *Escherichia coli in vivo* and *in vitro* assays. *Arch. Biochem. Biophys.* **379,** 198–208 (2000).
19. Gardner, R. G., Nelson, Z. W. & Gottschling, D. E. Ubp10/Dot4p regulates the persistence of ubiquitinated histone H2B: distinct roles in telomeric silencing and general chromatin. *Mol. Cell. Biol.* **25,** 6123–6139 (2005).
20. Jackson, J. P., Lindroth, A. M., Cao, X. & Jacobsen, S. E. Control of CpNpG DNA methylation by the KRYPTONITE histone H3 methyltransferase. *Nature* **416,** 556–560 (2002).
21. Tamaru, H. & Selker, E. U. A histone H3 methyltransferase controls DNA methylation in *Neurospora crassa*. *Nature* **414,** 277–283 (2001).
22. Ng, H. H., Xu, R. M., Zhang, Y. & Struhl, K. Ubiquitination of histone H2B by Rad6 is required for efficient Dot1-mediated methylation of histone H3 lysine 79. *J. Biol. Chem.* **277,** 34655–34657 (2002).

Supplementary Information is linked to the online version of the paper at www.nature.com/nature.

Acknowledgements We thank R. Martienssen and Z. Lippman for providing primer information for transposon analysis; Y. Zhang for advice on ChDIP and deubiquitination assays and critical reading of the manuscript; M. Osley and D. Gottschling for providing yeast strains; and T. Jenuwin for the gift of antibody against dimethyl H3K9. This work was supported by a US National Institutes of Health grant to J.-K.Z.

Author Information Reprints and permissions information is available at www.nature.com/reprints. The authors declare no competing financial interests. Correspondence and requests for materials should be addressed to J.-K.Z. (jian-kang.zhu@ucr.edu).

METHODS

Plant growth, mutant screening, and cloning. The wild-type plants are in the C24 background and carry the homozygous *RD29A-LUC* transgene[23]. A T-DNA population in the *Arabidopsis thaliana* mutant *ros1-1* background was obtained after floral transformation of inflorescences with *Agrobacterium* GV3101 carrying the binary vector pSUPERTAG[14]. Plants were grown in a controlled room at 22 °C with 16 h of light and 8 h of darkness. Seedlings to be used for luciferase (LUC) imaging were planted on Murashige and Skoog (MS) medium and were stratified for 2–4 days at 4 °C. About 200 T_2 seedlings from each 50-line pool were screened after cold (0 °C, 2 days) or treatment with 100 μM abscisic acid for 3 h), and *RD29A-LUC* expression was analysed as described[24]. Image acquisition (5 min) with use of a charge-coupled device system and processing were performed as described[23,24]. Mutants were also evaluated after being sown on MS medium supplemented with kanamycin.

The genomic sequence flanking the T-DNA insertion was determined by using the thermal asymmetric interlaced PCR procedure[25] with primers corresponding to nested regions internal to the left border and degenerate primers.

The *sup32-1* mutant was backcrossed to *ros1-1* to eliminate extraneous mutations and to confirm that the mutation was recessive. An additional allele (*sup32-2*) was also obtained from the ABRC *Arabidopsis* stock centre (SALK_024392.40.25.X).

DNA and RNA analysis. DNA methylation assays and RNA blot analysis were as described[14]; 15–20 clones were analysed in the bisulphite sequencing experiments to determine the methylation status of a locus in each genotype. For RT–PCR analysis of transposons, total RNA was extracted from 15-day-old seedlings with Trizol (Invitrogen) and treated with DNaseI and further purified with RNAeasy columns (Qiagen). For *AtSN1* expression analysis, total RNA was extracted from inflorescences; 100 ng of RNA was used as input in RT–PCR reactions with a one-step RT–PCR kit (Qiagen). PCR conditions and primer sequences were as described previously[14].

Chromatin immunoprecipitation. ChIP assays were performed on 20-day-old seedlings as described previously[15]. Chromatin samples were immunoprecipitated with antibodies against H3 dimethyl Lys 4 or ubiquitin (Upstate), or with antibody against H3 dimethyl Lys 9 (gift from T. Jenuwein). The PCR conditions and the primer sequences were as described previously[14]. For ChDIP, the chromatin samples were immunoprecipitated with anti-ubiquitin antibody (Upstate) and then eluted with ubiquitin (1 μg μl^{-1}); 90% of the eluted sample was immunoprecipitated with anti-H2B antibody (Upstate), and DNA was eluted and detected as in standard ChIP assays.

UBP activity assay. Ub-CEP 52 (p8185) was co-expressed with UBP26 and mutant UBP26 in *E. coli*. Exponential-phase cultures were induced for 15 min with 0.3 mM isopropyl β-D-thiogalactoside, and equal numbers of cells, determined by A_{600}, were suspended in Laemmli sample buffer and run on a 15% SDS–PAGE gel. Substrate and ubiquitin were detected with an anti-ubiquitin immunoblot[18]. For UBP activity tests in yeast, Flag–UBP26 and Flag–UBP26 mutant were separately cloned into the vector pYES3 (Invitrogen), transformed into yeast strain UCC6393 and detected with anti-Flag antibody as described previously[19]. The *in vitro* deubiquitination assay was performed with purified histones from *Arabidopsis* as described[26].

***Arabidopsis* histone isolation and analysis.** Histone preparation from *Arabidopsis* was performed as described previously[27]; 10 μg of purified histone was separated on 15% acrylamide gel and blotted to Hybond enhanced chemiluminescence (ECL) membrane (Amersham). The membrane was probed with antibodies against H2B, ubiquitin, trimethyl H3K4, dimethyl H3K4 or dimethyl H3K9 (Upstate) and detected with the enhanced ECL system (Amersham). The membrane was stripped in accordance with the manufacturer's protocol before being reprobed with other antibodies (Upstate). For *in vitro* deubiquitination assays, *Arabidopsis* nuclei were extracted in an isolation buffer (0.25 M sucrose, 25 mM HEPES pH 7.5, 3 mM $CaCl_2$, 10 mM NaCl, 1 mM phenylmethylsulphonyl fluoride (PMSF), 1 mM dithiothreitol (DTT), 0.25% Nonidet P40, leupeptin and pepstatin A). The nuclei were pelleted by centrifugation at 1,300*g* for 10 min. The nuclei were washed twice with the isolation buffer. Histones were extracted from the nuclei with 0.2 M HCl and the supernatant was precipitated with acetone. The isolated histones were renatured by dialysis against multiple changes of dialysis buffer (25 mM HEPES pH 7.5, 0.1 mM EDTA, 12.5 mM $MgCl_2$, 50 mM KCl, 1 mM PMSF, leupeptin, 1 mM DTT and 10% glycerol).

Transgenic plant analysis. A cDNA clone containing the full-length *UBP26* open reading frame was amplified by RT–PCR from *Arabidopsis* inflorescence and cloned in a Gateway recombination vector in pDONR207 (Invitrogen) after PCR with the primers pDON-UBPFP and pDON-UBPRP1 (to make a clone with a stop codon) and pDON-UBPFP and pDON-UBPRP2 (to make a clone without a stop codon). We refer to these clones as pDONRUBP1 and pDONRUBP2, respectively, and they were used for cloning UBP26 in destination vectors after recombination. Primer information is available from the authors on request. For complementation analysis, we also made an active site mutant, carrying a single amino-acid substitution at Cys 115 by using primers 5′-GTTGGCATAAGAAGTAGCACCCAAATTAGTCAG-3′ and 5′- GGTGCTAC-TTCTTATGCCAACAGTATACTTCAG-3′. These clones were then introduced into the binary vector pMDC32 (obtained from M. D. Curtis[28]), which has a dual *35S* promoter for constitutive expression of the gene after recombination.

For protein localization, we made a UBP26–YFP translational fusion with the use of a pEG101 binary vector obtained from C. Pikaard and performed a recombination reaction to make pEG101UBP26. For construction of *UBP26* promoter-*GUS* transcriptional fusion, a 2-kilobase region upstream of the start codon was amplified with primers pDON-UBPProF and pDON-UBPProR from the BAC clone T9C5. This PCR product was cloned in pDONR207 and subsequently in the binary vector pMDC164 (obtained from M. D. Curtis[28]) after recombination, to make pMDC164UBPPro.

All binary vectors for plant transformation were transferred to *Agrobacterium tumefaciens* GV3101 (pMP90) by electroporation. After selection with appropriate antibiotics, *Agrobacterium* was grown overnight at 28 °C in Luria–Bertani medium and then used for floral dip transformation. The wild-type cDNA overexpression and the mutant cDNA overexpression constructs were transformed in the *sup32-1ros1-1* background. The YFP fusion construct was transformed in the wild-type (C24 containing *RD29A-LUC* transgene) background, and the *UBP26* promoter-*GUS* fusion was transformed in the *Columbia* wild type.

Transgenic lines were selected for the transgene by sowing seeds on MS medium supplemented with hygromycin at a concentration of 30 mg l^{-1} (for pMDC32UBP and pMDC164UBPPro) or with glufosinate ammonium (for pEG101UBP).

Mass spectrometry. Liquid chromatography–mass spectrometry (LC–MS) and liquid chromatography–tandem mass spectrometry (LC–MS/MS) experiments were performed on a hybrid quadrupole-time of flight (Q-TOF) mass spectrometer (Waters), which was coupled with an Agilent HP1100 capillary HPLC running at a flow rate of 5 μl min^{-1} on a Zorbax SB-C_{18} (150 mm × 0.5 mm, 5 μm bore) column with a gradient from 2% mobile phase B (mobile A was 0.1% formic acid in water and mobile phase B was 0.1% formic acid in acetonitrile) to 65% mobile phase B in 60 min. For LC–MS/MS experiments, the Q-TOF mass spectrometer was run in a survey mode as described previously. The raw data were converted into peak-list (PKL) files that were processed by MASCOT (http://www.matrixscience.com) for searching proteins and protein post-translational modification sites. *De novo* sequencing, with the aid of Prospector-Product software (http://prospector.ucsf.edu), was also performed for the confirmation of modification sites reported by MASCOT and for finding modification sites that MASCOT might fail to determine. For LC–MS experiments, the Q-TOF mass spectrometer was run in a single-positive electrospray ionization mode.

Identification of H2B ubiquitination site. On the basis of our knowledge that ubiquitination occurs at Lys 123 of human H2B on the C-terminal peptide $AVT^{123}KYTSS$ or at Lys 120 of yeast on the C-terminal peptide $AVT^{120}KYSSS$, we reasoned that Lys 143 of plant H2B on the C-terminal peptide $AVT^{143}KFTSS$ might be ubiquitinated. Trypsin cuts after the C-terminal arginine and thus removes all except two glycine residues attached to the previously ubiquitinated lysine residue, resulting in an increment of 114 Da to the peptide mass, which can be used by mass spectrometry for diagnosis of the ubiquitination site. We therefore analysed the MS/MS spectrum of the precursor ion manually at *m/z* 477.7, which was doubly charged and was 57 mass units heavier than the H2B C-terminal peptide AVTKFTSS. Observed amino-terminal fragmentation ions, namely 'a' and 'b' ions (a_2, b_2, b_3, b_6 and b_7 or their water-loss ions), and the C-terminal ions, namely 'y' ions (y_2, y_4, y_6 and y_7 and their water-loss ions), matched well the peptide sequence $AVT_{GG}KFTSS$ with a GG chain attached to the lysine amino acid. A GG chain was observed linking with the lysine amino acid by the fact that a 114-Da mass increase was added to b_6, b_7, y_6 and y_7 ions, which cover the fragments including the lysine amino acid and a series of internal fragmentation ions and their water-loss ions (cleavage from both N-terminal and C-terminal directions) corresponding to TK_{GG}, $K_{GG}F$, $TK_{GG}F$ and $TK_{GG}FT$. All of these had a 114-Da mass increase from their counterparts in which the lysine amino acid was not modified. H2B ubiquitination at Lys 143 was therefore unambiguously determined by MS.

Relative quantification of H2B ubiquitination was performed by LC–MS analysis of the Arg_C and V8 dual-enzyme digestion of H2B protein. The percentage ubiquitination was calculated as the relative peak intensity between the ion at *m/z* 620.8, corresponding to the dual-enzyme-cleaved ubiquitinated peptide $GTKAVT_{GG}KFTSS$, and the ion at *m/z* 563.8, corresponding to the unmodified peptide GTKAVTKFTSS.

23. Ishitani, M., Xiong, L., Stevenson, B. & Zhu, J. K. Genetic analysis of osmotic and cold stress signal transduction in *Arabidopsis*: interactions and convergence of

abscisic acid-dependent and abscisic acid-independent pathways. *Plant Cell* **9,** 1935–1949 (1997).
24. Chinnusamy, V., Stevenson, B., Lee, B. H. & Zhu, J. K. Screening for gene regulation mutants by bioluminescence imaging. *Sci. STKE* **2002,** PL10 (2002).
25. Liu, Y. G., Mitsukawa, N., Oosumi, T. & Whittier, R. F. Efficient isolation and mapping of *Arabidopsis* thaliana T-DNA insert junctions by thermal asymmetric interlaced PCR. *Plant J.* **8,** 457–463 (1995).
26. Henry, K. W. *et al.* Transcriptional activation via sequential histone H2B ubiquitylation and deubiquitylation, mediated by SAGA-associated Ubp8. *Genes Dev.* **17,** 2648–2663 (2003).
27. Waterborg, J. H., Winicov, I. & Harrington, R. E. Histone variants and acetylated species from the alfalfa plant *Medicago sativa*. *Arch. Biochem. Biophys.* **256,** 167–178 (1987).
28. Curtis, M. D. & Grossniklaus, U. A gateway cloning vector set for high-throughput functional analysis of genes *in planta*. *Plant Physiol.* **133,** 462–469 (2003).

The generation game

Proteomics is hungry for well-validated antibodies. Nathan Blow looks at the options and sees how researchers are redefining the way to generate an antibody.

The products of more than 22,700 genes make up the human proteome. But researchers hoping to unpick the mysteries of the proteome are restricted by the fact that antibodies against only a small percentage of these proteins are available. Although commercial production of antibodies is well established, the market has so far been driven by the popularity of particular antibody targets. More than 1,000 antibodies against the tumour suppressor p53 are available, for example, but the less sought-after targets frequently have none.

With the rise of proteomics, the need for antibodies has become global and is no longer limited to a small number of targets central to most hypothesis-driven research projects. "One of the hurdles in proteomics is a lack of high-quality, well characterized affinity reagents," says Henry Rodriguez, director of the clinical proteomic technologies initiative for cancer at the US National Cancer Institute (NCI) in Bethesda, Maryland.

Not only do researchers need access to more antibodies, they also need to know how these antibodies have been characterized to determine whether they will work in the assay they are using. "Large numbers of antibodies are already available, but an investigator has to navigate through a complex system to find out which target antibodies are going to be appropriate for his or her particular assays," says Adam Clark, who works on the NCI's proteomic technologies initiative.

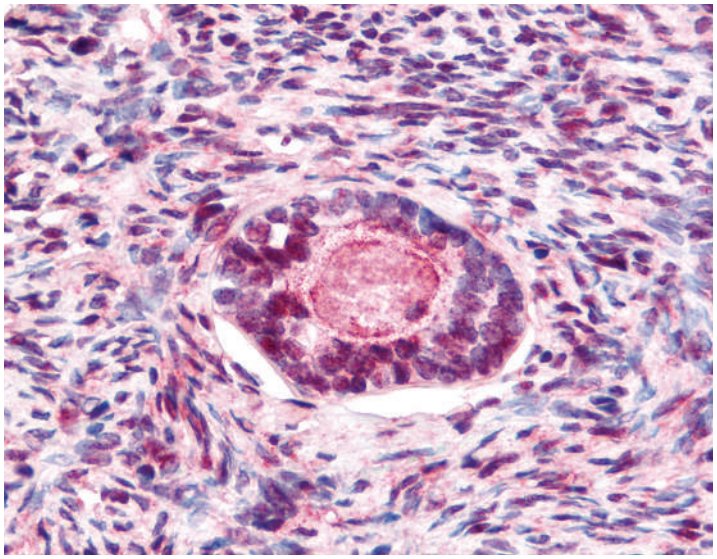

Image of ovarian tissue stained using a commercial antibody.

ROCKLAND IMMUNOCHEMICALS

Standard issue

At present, there is no universal validation: an antibody that works wonders for a Western blot may perform poorly in immunohistochemistry. This growing need for faster antibody production and stronger validation data is leading many groups to explore high-throughput methodologies for creating and validating affinity reagents.

A group led by Mathias Uhlén at the Royal Institute of Technology in Stockholm, Sweden, is spearheading an initiative to assemble the Human Protein Atlas (www.proteinatlas.org). The project aims to explore the entire human proteome using antibodies. Uhlén's group is producing polyclonal antibodies directed against each human protein, and then characterizing the antibodies using Western blots, protein microarrays and immunohistochemistry.

The project generates around ten new polyclonal antibodies and more than 10,000 immunohistochemistry images every day — an achievement that relies heavily on high-throughput methodology. Although most steps in the process are amenable to automation, some, such as annotating tissue immunohistochemistry images, are proving to be a significant challenge. Indeed, analysing these images still involves ten pathologists who have to annotate them manually. "All the annotation is Internet based. The pathologists view and evaluate 600 tissue images per antibody via a web-based tool on their personal computers, and the results are stored in our database," says Uhlén.

Mathias Uhlén is using antibodies to unravel the human proteome.

AFFIBODY

In addition to producing and testing their own antibodies, Uhlén and his team will put antibodies from commercial sources through their standardized quality-control pipeline. Uhlén says he was surprised that only about 35% of commercial antibodies seemed to work — although he notes that this could be a result of the way his group analyses them. "We decided to use a very standardized way of validating antibodies: if they don't work, we don't try other ways of doing it," he says. The success rate may be low, but such a standardized quality-control process offers researchers a rare level of confidence in the antibodies that pass the test.

Currently, the atlas consists of more than 1,500 antibodies, half of which have been provided by commercial sources. In October 2007, a new release will be made available bringing the total number of antibodies to slightly less than 3,000. Confocal microscopy images of tissues stained with the antibodies will also be released in October to complement immunohistochemistry images. "We are committed to showing the public all the primary validation of the antibodies," says Uhlén. Although polyclonal antibodies are not renewable, a limited number of aliquots of each antibody generated by the atlas will be made available through Atlas Antibodies of Stockholm.

Other initiatives are focusing on monoclonal, rather than polyclonal, antibodies against proteins on a large scale. In 2002, for example, the Wellcome Trust Sanger Institute near Cambridge, UK, launched the Atlas of Gene Expression. Although a change in focus at the institute means that this is closing down, the atlas was set up to generate high-quality monoclonal antibodies that were well characterized for a variety of assays. Much as for the Human Protein Atlas, a well-standardized characterization was key. "Historically, the validation of antibodies has been ad hoc with different people generating antibodies that have been assessed in different ways," says project leader John McCafferty.

The project involved four key groups. One generated the proteins of interest and did quality control. This team used the Gateway cloning system made by Invitrogen of Carlsbad, California, to move a variety of open reading frames between different expression vectors and so improve yields for troublesome proteins. A second group used phage display for high-throughput screening of a single-chain antibody library generated at the Sanger Institute and containing more than 10^{10} phage

clones. The other two groups were dedicated to immunohistochemistry and the informatics infrastructure necessary to deal with the large volume of data.

To deal with image acquisition issues, the institute collaborated with Applied Imaging of San Jose, California, to develop an automated high-throughput image-analysis system suitable for tissue microarray applications. So far, the Sanger project has generated more than 4,000 monoclonal antibodies to 290 antigens, which are available to buy from Geneservice in Cambridge, UK.

Although the project is being discontinued, McCafferty says that much has been learned about the bottlenecks of high-throughput generation of antibodies and how these can be overcome. "Surprisingly, the generation of the antibodies was not the major issue," he says. "The bottlenecks were generating good quality protein product to do selection, and how to deal with the large amounts of image data a project such as this produces."

Finding affinity

Even as the Sanger project comes to a close, other initiatives are beginning to gather steam — although these have been hampered somewhat by a lack of funding. "There seems to be a reluctance from the funding agencies to put money into large-scale antibody initiatives," says Andrew Bradbury of the biosciences division at Los Alamos National Laboratory in New Mexico. The NCI's five-year, $104-million clinical proteomic technologies initiative

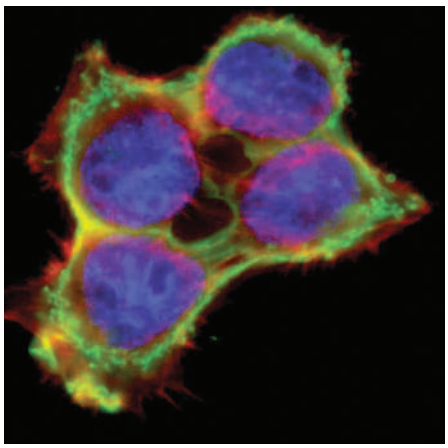

MILLIPORE

Cells stained with the 4G10 anti-phosphotyrosine antibody from Millipore.

that is now getting off the ground may be the start of a change.

In 2005, the NCI held a workshop to discuss affinity capture. It found that the scientific community wanted renewable resources that were well characterized for performance data, says Clark. The meeting also revealed that the community was concerned by the lack of characterization data for most available antibodies.

Following this lead, the NCI proteomics reagent core, one of the centres in the clinical proteomic technology initiative, is embarking on the production of affinity reagents. To focus its efforts, it has identified a list of protein targets: all cancer-related proteins for which no commercial antibodies are yet available. The core will develop monoclonal antibodies that will be characterized by Western blots, enzyme-linked immunosorbent assay (ELISA), immunohistochemistry and immunoprecipitation followed by mass spectrometry. "All the raw data on how the antibodies perform on a variety of assays will be provided and an investigator will be able to acquire these antibodies through a website organized by the NCI," says Clark.

In Europe, another group of investigators plans to generate affinity reagents against the human proteome. The group, called ProteomeBinders, consists of 26 European Union and two US institutional partners. "The goal or the hope is to get funding from the European Union to put a project together next year or the year after," says Bradbury, one the US participants.

Although the antibody remains the affinity reagent of choice, the exploration of alternative binders by large groups, such as ProteomeBinders, shows how far these non-traditional reagents have come in a relatively short time.

Gold standard

A quick glance through the catalogues from commercial vendors and researchers reveals thousands of antibodies not only to proteins, but also to specific protein changes such as post-translational modifications. Still other companies offer to produce antibodies to an investigator's antigen of interest.

Monoclonal antibodies produced by animal immunization remain the 'gold standard' of

ANTIBODIES IN THE FAST LANE

In making recombinant antibodies, the resulting antibody is only as good as the combinatorial library and the screening assay. The trick is to find the molecule of highest affinity and specificity for the target among a library of millions of clones. Traditionally, recombinant antibody libraries have been phage-based and the screening relied on enzyme-linked immunosorbent assay (ELISA), not a high-throughput method. Changes in both phage display and screening methods are now moving recombinant antibody production into a high-throughput world.

Flow cytometry has become the assay of choice for rapid screening of clones from recombinant antibody libraries. "We looked at different ways of screening. Flow cytometry was the only one that seemed to meet our throughput requirements," says Andrew Bradbury of Los Alamos National Laboratory in New Mexico. Bradbury's group has developed a flow-cytometry assay to screen its single-chain antibody-fragment phage libraries using a mixture of beads coated with specific and non-specific antigens. The method rapidly identifies antibodies that have good affinity for the protein of interest while discarding those that show low specificity.

Phage-display screening methods are also used to identify antibodies that target post-translational modifications (PTMs) such as phosphorylation or acetylation. As PTMs have a role in many processes — from gene regulation to apoptosis — they are of growing interest for the biological community. Companies have responded by developing antibodies targeting proteins in a specific state of modifications. "Antibodies to PTMs are gaining in importance with customers," says Kumar Bala, director of antibody technologies for Millipore in the company's lab in Temecula, California.

But obtaining antibodies directed against PTMs is not a trivial task. Rockland Immunochemicals of Gilbertsville, Pennsylvania, has put in a lot of effort to develop antibodies for looking at phosphorylated and non-phosphorylated forms of various proteins in a sequence independent context, says Daniel O'Shannessy, the company's vice-president of corporate development.

LANL

Andrew Bradbury develops recombinant single-chain antibodies.

Antibodies that recognize PTMs independently of the protein site on which the modification occurs are useful — particularly for enriching, for example, all phosphorylated proteins from a cell. But such antibodies are hard to make by animal immunization as the PTM itself is not immunogenic. So scientists are turning to recombinant molecules and *in vitro* screening such as phage display to isolate 'pan-PTM' affinity reagents.

Although making steps in the right direction, many more antibodies and further improvements in affinity reagent technology will be needed to understand and characterize the full range of PTMs found in nature. Still, Bala argues that the "best tools for purifying, identifying, differentiating and characterizing PTMs are antibodies". N.B.

affinity reagents. They are relatively renewable, can usually be made with high specificity and affinity for their target and can be used in common biochemical assays such as Western blotting, ELISA and immunochemistry. But the traditional monoclonal antibody has its drawbacks. Its production can be challenging, time-consuming and costly. So there is a lot of interest in identifying novel affinity reagents that would be less expensive and quicker to produce. "The future is with alternative binders," says Bradbury, who works with single-chain antibodies (see 'Antibodies in the fast lane', page 743).

Optimistic expression

The structural characteristics of antibodies make it difficult to produce recombinant versions in bacteria and restricts their use in some high-throughput screening methods. But George Georgiou and his colleagues at the University of Texas at Austin have come up with a method to produce and screen full-length immunoglobulin G (IgG) antibodies expressed in *Escherichia coli* (Y. Mazor *et al. Nature Biotechnol.* **25,** 563–565; 2007).

The technology produces full-length antibodies that are initially tethered to the inner membrane of the bacterium. When the bacteria are treated with EDTA and lysozyme, the resulting spheroplasts with exposed antibodies can be selected in a high-throughput manner by using fluorescently labelled antigens and flow cytometry.

"We can isolate several bacterial clones expressing full-length IgG antibodies that can bind to the antigen with the requisite affinity," says Georgiou. "The advantage of the technology is that the expression of the antibodies is directly in bacteria and we can use the bacteria to produce the antibody without going through the steps of reformatting the antibody and then expressing in a mammalian system." But the antibodies are not glycosylated, which limits some of the therapeutic applications.

The more traditional way to screen and obtain IgG antibodies rapidly is the generation of recombinant antibody fragments. Single-chain variable (scFv) antibody fragments are created by the fusion of the variable regions of the heavy and light chains of immunoglobulins using a short peptide linker. This allows scFv fragments to be expressed from a single open reading frame and screened by phage display or other high-throughput approaches.

AFFIBODY

The structure of an affibody affinity reagent.

Although larger than scFv fragments and still composed of two independent polypeptide chains, Fab antibody fragments are also being used and are usually favoured for their high stability and compatibility with existing antibody-based assays. The Fab antibody region is the antigen-binding region of the immunoglobulin. Fab fragments consist of one constant and one variable domain from each of the heavy and light chains.

Both scFv- and Fab-based technologies are developing rapidly, with several companies now supplying either scFv or Fab libraries and screening systems to consumers. One such company is BioInvent of Lund, Sweden, which provides the n-CoDeR human-antibody library based on both the scFv and Fab formats. Other companies, including Cambridge Antibody Technology in Cambridge, UK, and MorphoSys in Martinsried, Germany, have developed human-derived phage-display libraries using either the scFv or Fab format to identify binding regions for development of therapeutic monoclonal antibodies.

Although rapidly generated and effective for many *in vitro* applications, scFv and Fab fragments are less effective for therapeutic applications because they have short half-lives. "Single-chain fragments can't really be used in animals because they are cleared very rapidly — the half-life of a single chain Sv is about 10 minutes, whereas full-length antibodies can persist for several days," says Georgiou.

Breaking with tradition

Described for the first time in 1997 by Uhlén and his colleagues, affibodies were among the first non-immunoglobulin-based affinity reagents. These small molecules are based on a bacterial receptor (*Staphylococcus aureus* protein A), and use combinatorial protein engineering to introduce random mutations in the affinity region. Affibody of Bromma in Sweden, which was co-founded by Uhlén, currently produces affibody-based reagents for basic research laboratories and commercial partners.

ACCURI CYTOMETERS

Flow cytometry is the assay of choice for screening recombinant-antibody libraries.

Another non-immunoglobulin-based affinity reagent that is becoming more widely used is the aptamer. Made of DNA, RNA or modified nucleic acids and typically 15–40 bases in length, aptamers have a stable tertiary structure that permits protein binding through van der Waals forces, hydrogen bonding and electrostatic interactions. Early studies showed that aptamers can be highly specific for target proteins, with the ability to distinguish between related members of a protein family (S. D. Seiwart *et al. Chem. Biol.* **7,** 833–843; 2000).

Unlike the scFv and Fab fragments, both aptamers and affibodies are useful for *in vivo* applications because they have longer half-lives. In addition, both function well in the reducing environment of the cell cytosol, which is a problem for larger monoclonal antibodies. Currently, Affibody is testing an HER2-binding affibody as an alternative to herceptin for treatment of HER-2-positive breast cancer with a clinical proof-of-principle microdosing study to occur this year.

Archemix in Cambridge, Massachusetts, has three aptamer-based therapeutics in phase I clinical trials. Two aptamers target coagulation processes and the third targets nucleolin, a protein that is involved in the development of some cancers.

Overall, there is much optimism regarding the future of alternative affinity reagents. But several problems have to be overcome before they are adopted more widely by the scientific community. One of the most pressing issues is the inability to produce these reagents at a truly high-throughput scale. Overcoming this obstacle would make these alternative binders not only cheaper to produce than traditional antibodies, but would also require significantly less time. "I would love to see a major technology breakthrough where someone shows that you can actually produce these in a high-throughput manner, but so far I don't think anyone has been able to do that," says Uhlén. ■

Nathan Blow is the technology editor for *Nature* and *Nature Methods*.

clones. The other two groups were dedicated to immunohistochemistry and the informatics infrastructure necessary to deal with the large volume of data.

To deal with image acquisition issues, the institute collaborated with Applied Imaging of San Jose, California, to develop an automated high-throughput image-analysis system suitable for tissue microarray applications. So far, the Sanger project has generated more than 4,000 monoclonal antibodies to 290 antigens, which are available to buy from Geneservice in Cambridge, UK.

Although the project is being discontinued, McCafferty says that much has been learned about the bottlenecks of high-throughput generation of antibodies and how these can be overcome. "Surprisingly, the generation of the antibodies was not the major issue," he says. "The bottlenecks were generating good quality protein product to do selection, and how to deal with the large amounts of image data a project such as this produces."

Finding affinity

Even as the Sanger project comes to a close, other initiatives are beginning to gather steam — although these have been hampered somewhat by a lack of funding. "There seems to be a reluctance from the funding agencies to put money into large-scale antibody initiatives," says Andrew Bradbury of the biosciences division at Los Alamos National Laboratory in New Mexico. The NCI's five-year, $104-million clinical proteomic technologies initiative

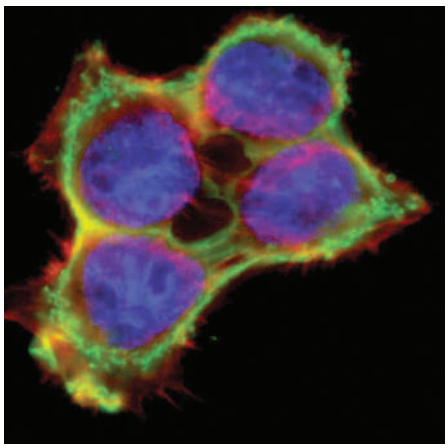

MILLIPORE

Cells stained with the 4G10 anti-phosphotyrosine antibody from Millipore.

that is now getting off the ground may be the start of a change.

In 2005, the NCI held a workshop to discuss affinity capture. It found that the scientific community wanted renewable resources that were well characterized for performance data, says Clark. The meeting also revealed that the community was concerned by the lack of characterization data for most available antibodies.

Following this lead, the NCI proteomics reagent core, one of the centres in the clinical proteomic technology initiative, is embarking on the production of affinity reagents. To focus its efforts, it has identified a list of protein targets: all cancer-related proteins for which no commercial antibodies are yet available. The core will develop monoclonal antibodies that will be characterized by Western blots, enzyme-linked immunosorbent assay (ELISA), immunohistochemistry and immunoprecipitation followed by mass spectrometry. "All the raw data on how the antibodies perform on a variety of assays will be provided and an investigator will be able to acquire these antibodies through a website organized by the NCI," says Clark.

In Europe, another group of investigators plans to generate affinity reagents against the human proteome. The group, called ProteomeBinders, consists of 26 European Union and two US institutional partners. "The goal or the hope is to get funding from the European Union to put a project together next year or the year after," says Bradbury, one the US participants.

Although the antibody remains the affinity reagent of choice, the exploration of alternative binders by large groups, such as ProteomeBinders, shows how far these non-traditional reagents have come in a relatively short time.

Gold standard

A quick glance through the catalogues from commercial vendors and researchers reveals thousands of antibodies not only to proteins, but also to specific protein changes such as post-translational modifications. Still other companies offer to produce antibodies to an investigator's antigen of interest.

Monoclonal antibodies produced by animal immunization remain the 'gold standard' of

ANTIBODIES IN THE FAST LANE

In making recombinant antibodies, the resulting antibody is only as good as the combinatorial library and the screening assay. The trick is to find the molecule of highest affinity and specificity for the target among a library of millions of clones. Traditionally, recombinant antibody libraries have been phage-based and the screening relied on enzyme-linked immunosorbent assay (ELISA), not a high-throughput method. Changes in both phage display and screening methods are now moving recombinant antibody production into a high-throughput world.

Flow cytometry has become the assay of choice for rapid screening of clones from recombinant antibody libraries. "We looked at different ways of screening. Flow cytometry was the only one that seemed to meet our throughput requirements," says Andrew Bradbury of Los Alamos National Laboratory in New Mexico. Bradbury's group has developed a flow-cytometry assay to screen its single-chain antibody-fragment phage libraries using a mixture of beads coated with specific and non-specific antigens. The method rapidly identifies antibodies that have good affinity for the protein of interest while discarding those that show low specificity.

Phage-display screening methods are also used to identify antibodies that target post-translational modifications (PTMs) such as phosphorylation or acetylation. As PTMs have a role in many processes — from gene regulation to apoptosis — they are of growing interest for the biological community. Companies have responded by developing antibodies targeting proteins in a specific state of modifications. "Antibodies to PTMs are gaining in importance with customers," says Kumar Bala, director of antibody technologies for Millipore in the company's lab in Temecula, California.

But obtaining antibodies directed against PTMs is not a trivial task. Rockland Immunochemicals of Gilbertsville, Pennsylvania, has put in a lot of effort to develop antibodies for looking at phosphorylated and non-phosphorylated forms of various proteins in a sequence independent context, says Daniel O'Shannessy, the company's vice-president of corporate development.

LANL

Andrew Bradbury develops recombinant single-chain antibodies.

Antibodies that recognize PTMs independently of the protein site on which the modification occurs are useful — particularly for enriching, for example, all phosphorylated proteins from a cell. But such antibodies are hard to make by animal immunization as the PTM itself is not immunogenic. So scientists are turning to recombinant molecules and *in vitro* screening such as phage display to isolate 'pan-PTM' affinity reagents.

Although making steps in the right direction, many more antibodies and further improvements in affinity reagent technology will be needed to understand and characterize the full range of PTMs found in nature. Still, Bala argues that the "best tools for purifying, identifying, differentiating and characterizing PTMs are antibodies". N.B.

Antibody manufacturers, suppliers and services

COMPANY	PRODUCTS/ACTIVITY	LOCATION	URL	
21st Century Biochemicals	Custom monoclonal and polyclonal antibodies	Marlboro, Massachusetts	www.21stcenturybio.com	
Abcam	Antibodies	Cambridge, UK	www.abcam.com	
Abnova	Catalogue monoclonal antibodies	Taipei City, Taiwan	www.abnova.com.tw	
Affinity Labeling Technologies	Nucleotide-based photoaffinity reagents for antibody labelling	Lexington, Kentucky	www.altcorp.com	
AnaSpec	Catalogue and custom monoclonal and polyclonal antibodies	San Jose, California	www.anaspec.com	
Antibodies Incorporated	Custom and secondary monoclonal and polyclonal antibodies and reagents	Davis, California	www.antibodiesinc.com	
Atlas Antibodies	Antibodies and affinity reagents	Stockholm, Sweden	www.atlasantibodies.com	●
Aves Labs	Polyclonal chicken antibody services	Tigard, California	www.aveslab.com	
BD Biosciences	Catalogue and custom antibodies	San Diego, California	www.bdbiosciences.com	
Beckman Coulter	Catalogue monoclonal and polyclonal antibodies	Fullerton, California	www.beckmancoulter.com	
BioGenes	Custom monoclonal and polyclonal antibody production	Berlin, Germany	www.biogenes.de	●
BioLegend	Catalogue antibodies	San Diego, California	www.biolegend.com	
Biomeda	ELISA kits, monoclonal and polyclonal antibodies	Foster City, California	biomeda.com	
Biotrend	Catalogue antibodies, custom antibody services	Cologne, Germany	www.biotrend.com	
Boston Biochem	Antibodies targeting ubiquitin proteosome pathway	Cambridge, Massachusetts	www.bostonbiochem.com	
Cambridge Research Biochemicals	Custom peptide synthesis, polyclonal antibody production	Billingham, UK	www.crbdiscovery.com	
Cayman Chemical	Catalogue antibodies	Ann Arbor, Michigan	www.caymanchem.com	
Cell Signaling Technology	Antibodies for cell signalling through pathways such as MAP kinase, AKT and PKC	Danvers, Massachusetts	www.cellsignal.com	
Cytomyx	Antibodies for kinases and ion channels	Cambridge, UK	www.cytomyx.com	
Delta Biolabs	Catalogue antibodies to wide range of cell-signalling proteins	Campbell, California	www.deltabiolabs.com	
Diaclone	Catalogue monoclonal antibodies; ELISA and Elispot	Stamford, Connecticut	www.diaclone.com	
Dragonfly Sciences	Custom monoclonal and polyclonal antibody production	Wellesley, Massachusetts	www.dragonflysciences.com	
eBioscience	Catalogue cytokine antibodies	San Diego, California	www.ebioscience.com	
ECM Biosciences	Antibodies to post-translational modifications in proteins and peptides	Versailles, Kentucky	www.ecmbiosciences.com	
EMD Biosciences	Catalogue antibodies	San Diego, California	www.emdbiosciences.com	
Fusion Antibodies	Custom monoclonal or polyclonal antibodies, scFv production	Belfast, UK	www.fusionantibodies.com	
Geneservice	Antibodies	Cambridge, UK	www.geneservice.co.uk	
Genovac	Custom antibody services	Freiburg, Germany	www.genovac.com	
GenScript	Antibody purification resins, custom peptide synthesis	Piscataway, New Jersey	www.genscript.com	
Harlan	Custom antibody services, peptide synthesis	Indianapolis, Indiana	www.harlan.com	
Invitrogen	Antibodies, fluorescently tagged antibodies	Carlsbad, California	www.invitrogen.com	
Lake Placid Biologicals	Antibodies for studying chromatin	Lake Placid, New York	www.lpbio.com	
Lonza Biologics	Contract manufacturing of therapeutic antibodies	Portsmouth, New Hampshire	www.lonzabiologics.com	●
Mabtech	Catalogue antibodies suitable for cytokine detection in ELISpot, ELISA and intracellular staining	Nacka Strand, Sweden	www.mabtech.com	
Millipore	Catalogue antibodies	Billerica, Massachusetts	www.millipore.com	●
Molecular Diagnostic Services	Custom monoclonal or polyclonal antibody production	San Diego, California	www.mds-usa.com	
MorphoSys	Phage-based antibody library screening services, therapeutic antibody discovery	Martinsried, Germany	www.morphosys.com	
New England Biolabs	Antibodies	Ipswich, Massachusetts	www.neb.com	●
Novus Biologicals	Custom and catalogue antibodies	Littleton, Colorado	www.novus-biologicals.com	
Open Biosystems	Custom antibody services	Huntsville, Alabama	www.openbiosystems.com	
OriGene	Catalogue antibodies	Rockville, Maryland	www.origene.com	●
PeproTech	Anticytokine antibodies	Rocky Hill, New Jersey	www.peprotech.com	
ProSci	Catalogue antibodies, custom monoclonal and polyclonal antibodies	Poway, California	www.prosci-inc.com	
QED Bioscience	Custom monoclonal and polyclonal antibody production, genetic immunization,cell-culture services	San Diego, California	www.qedbio.com	
Rockland Immunochemicals	Catalogue antibodies; primary, secondary and fluorescently tagged antibodies	Gilbertsville, Pennsylvania	www.rockland-inc.com	●
Sigma-Aldrich	Catalogue monoclonal and polyclonal antibodies; chemicals and reagents	St Louis, Missouri	www.sigmaaldrich.com	●
Spring Valley Laboratories	Custom monoclonal and polyclonal antibody production	Woodbine, Maryland	www.svlab.com	
Zyomyx	Human cytokine profiling system	Hayward, California	www.zyomyx.com	

Antibody-based drug discovery and development

Abbott	Monoclonal-antibody-based drug discovery and development	Abbott Park, Illinois	www.abbott.com	
AbD Serotec (MorphoSys)	Phage-display libraries, antibody drug development	Martinsried, Germany	www.ab-direct.com	●
Ablynx	Nanobodies development, drug discovery based on nanobodies	Ghent, Belgium	www.ablynx.com	

COMPANY	PRODUCTS/ACTIVITY	LOCATION	URL	
Affibody	Development of Affibodies as alternative binders, Affibody-based drug discovery	Bromma, Sweden	www.affibody.com	
Affimed Therapeutics	Phage-display human antibody libraries	Heidelberg, Germany	www.affimed.com	
Amgen	Monoclonal-antibody-based therapeutics, Enbrel	Thousand Oaks, California	www.amgen.com	
Archemix	Aptamer-based drug discovery and development	Cambridge, Massachusetts	www.archemix.com	
BioInvent	Developed n-CoDeR phage libraries, drug discovery and development	Lund, Sweden	www.bioinvent.com	
Biotecnol	Monoclonal-antibody-based therapeutics focused on cancer	Baltimore, Maryland	www.biotecnol.com	
Cambridge Antibody Technology	Monoclonal-antibody therapeutics	Cambridge, UK	www.cambridgeantibody.com	
Centocor	Monoclonal-antibody-based therapeutics targeting immune-mediated inflammatory disorders	Malvern, Pennsylvania	www.centocor.com	
Dyax	Phage-display Fab libraries, drug discovery	Cambridge, Massachusetts	www.dyax.com	
Ortho Biotech	Antibody-based drug discovery, Orthoclone OTK3 monoclonal antibody	Bridgewater, New Jersey	www.orthobiotech.com	
PDL BioPharma	Antibody-based drug discovery	Mountain View, California	www.pdl.com	
Regeneron	Development of hybrid antibody molecules as therapeutics	Tarrytown, New York	www.regeneron.com	
XOMA	Antibody-based therapeutics, Raptiva monoclonal-antibody therapy	Berkeley, California	www.xoma.com	
Immunoassay and immuohistochemistry				
Accuri Cytometers	Flow cytometry instrumentation	Ann Arbor, Michigan	www.accuricytometers.com	
Active Motif	ELISA kits for transcription-factor assays, antibodies	Carlsbad, California	www.activemotif.com	
Alpha Diagnostic	Custom peptides and polyclonal antibodies, kits for ELISA	San Antonio, Texas	www.4adi.com	
Applied Imaging	Developed Ariol high-throughput immunohistochemistry system	San Jose, California	www.aicorp.com	
Amersham Biosciences	Reagents for immunochemistry assays	Uppsala, Sweden	www.amersham.com	
Assay Designs	Immunoassays (ELISA), antibodies	Ann Arbor, Michigan	www.assaydesigns.com	
Beecher Instruments	Tissue microarray instruments and reagents	Sun Prairie, Wisconsin	www.beecherinstruments.com	
Bender MedSystems	Flow cytometry systems, ELISA systems and reagents	Vienna, Austria	www.bendermedsystems.com	
Bio-Rad	Bio-Plex multiplex antibody assays	Hercules, California	www.bio-rad.com	●
Dako	Flow cytometry kits and reagents, antibodies	Carpinteria, California	www.dakousa.com	
Diagnostic Biosystems	Monoclonal and polyclonal antibodies, kits and stains for immunohistochemistry	Pleasanton, California	www.dbiosys.com	
GenBio	Assays for antibodies characteristic of Lyme disease	San Diego, California	www.genbio.com	
Panomics	Luminex- and ELISA-based assays	Redwood City, California	www.panomics.com	
Perkin Elmer Life Sciences	Automated immunoassays	Waltham, Massachusetts	las.perkinelmer.com	
Pierce Biotechnology	Antibody production and purification, immunoassays	Rockford, Illinois	www.piercenet.com	●
R&D Systems	Immunoassay kits and reagents, antibodies, ELISA, flow-cytometry kits	Minneapolis, Minnesota	www.rndsystems.com	●
Thermo Fisher Scientific	Antibodies and immunoassay reagents	Waltham, Massachusetts	www.thermofisher.com	●
Vision Biosystems	Automated immunohistochemistry systems and reagents	Mount Waverely, Australia	www.vision-bio.com	
General				
BioFX Laboratories	Secondary antibodies, immunohistochemistry reagents and substrates	Owings Mills, Maryland	www.biofx.com	
Cambio	Molecular biology reagents, specialized biochemicals	Cambridge, UK	www.cambio.co.uk	
Carl Zeiss	Imaging systems	Jena, Germany	www.zeiss.com	
Integra Biosciences	Cell cultivation systems	Chur, Switzerland	www.integra-biosciences.com	
MP Biomedicals	Reagents and chemicals for research	Aurora, Ohio	www.mpbio.com	
New Brunswick Scientific	Cell cultivation instruments	Edison, New Jersey	www.nbsc.com	
Nikon Instruments	Imaging systems	Melville, New York	www.nikoninstruments.com	
Peptide Specialty Laboratories	Custom peptide synthesis	Heidelberg, Germany	www.peptid.de	
USB	Chemicals and reagents for molecular biology	Cleveland, Ohio	www.usbweb.com	

● see advertisement

naturejobs

JOBS OF THE WEEK

By the time you've read this, I will have effectively traded *Nature* for nature — my wife and I will be about 50 miles into our 1,000-mile hike on the Appalachian trail from West Virginia to Maine (http://1000milesummer.blogspot.com). So before I lace my boots and hoist my backpack, here's some final thoughts I've gained from this editorial adventure.

Career paths aren't linear. To follow these paths, planning and formal training help, but it's perhaps more important to build skills that will help you match your interests with opportunities. The boundaries between industry, academia and government are blurring. To negotiate them, consider what skills you have and how they can be transferred from sector to sector. Don't want to choose one sector over another? You don't have to. You can work in each simultaneously. Aren't comfortable going from sector to sector or from on to off the bench? It's OK. You can get as much or as little formal training as you like before you make your next move. Some people prefer to get additional degrees whereas others opt for more informal education.

It's important to think globally. New hotbeds of scientific research — from Singapore to St Louis — are springing up worldwide, and researchers are collaborating in increasingly large groups. Scientists are also more mobile than they used to be, moving from one continent to another to follow the right opportunity, the right project or to pursue the best chance for funding and research freedom.

In any case, I advocate working outside your comfort zone. It's frightening but exhilarating to move into unfamiliar areas. Perhaps that's why I've decided to make the move, quite literally, on to a different path. Where will this walk lead? I suspect that it will take me to a place where I will divide my time into thirds: teaching, journalism and creative projects. Just as I don't expect to find our hike easy and comfortable, I don't anticipate that my career change will be without challenge. Anyway, before I slip into my sleeping bag and make an invocation for a bear-free evening, I'd like to thank all *Naturejobs* readers for your support and feedback. I wish everyone a successful career adventure. Happy trails!

Paul Smaglik, *Naturejobs* editor

CONTACTS
Editor: Paul Smaglik
Assistant Editor: Gene Russo

European Head Office, London
The Macmillan Building,
4 Crinan Street,
London N1 9XW, UK
Tel: +44 (0) 20 7843 4961
Fax: +44 (0) 20 7843 4996
e-mail: naturejobs@nature.com

European Sales Manager:
Andy Douglas (4975)
e-mail: a.douglas@nature.com
Business Development Manager:
Amelie Pequignot (4974)
e-mail: a.pequignot@nature.com
***Nature*events:**
Claudia Paulsen Young
(+44 (0) 20 7014 4015)
e-mail: c.paulsenyoung@nature.com

France/Switzerland/Belgium:
Muriel Lestringuez (4994)
Southwest UK/RoW:
Nils Moeller (4953)
Scandinavia/Spain/Portugal/Italy:
Evelina Rubio-Hakansson (4973)
Northeast UK/Ireland:
Matthew Ward (+44 (0) 20 7014 4059)
North Germany/The Netherlands:
Reya Silao (4970)
South Germany/Austria:
Hildi Rowland (+44 (0) 20 7014 4084)

Advertising Production Manager:
Stephen Russell
To send materials use London
address above.
Tel: +44 (0) 20 7843 4816
Fax: +44 (0) 20 7843 4996
e-mail: naturejobs@nature.com
***Naturejobs* web development:**
Tom Hancock

***Naturejobs* online production:**
Jasmine Myer
US Head Office, New York
75 Varick Street, 9th Floor,
New York, NY 10013-1917
Tel: +1 800 989 7718
Fax: +1 800 989 7103
e-mail: naturejobs@natureny.com

US Sales Manager: Peter Bless

Japan Head Office, Tokyo
Chiyoda Building,
2-37 Ichigayatamachi,
Shinjuku-ku,
Tokyo 162-0843
Tel: +81 3 3267 8751
Fax: +81 3 3267 8746

Asia-Pacific Sales Manager:
Ayako Watanabe
e-mail: a.watanabe@natureasia.com

The hard cell

Ethical quandaries aside, stem-cell science is attracting researchers worldwide. **Ricki Lewis** reports.

Despite disagreements about the ethics of embryonic stem-cell science, research in the field is thriving globally. At least 500 companies and collaborations have sprung up, 100 of them in the past year alone, according to industry watchers. And although therapies are still largely at the preclinical and safety-testing stages, coaxing these cells to recapitulate development *in vitro* is already unveiling the beginnings of pathogenesis, revealing new drug targets. Basic and translational research positions are proliferating, drawing on a pool of applicants with diverse biomedical backgrounds.

"Stem-cell research has brought us to the threshold of an entire new era in biomedicine," says Sally Temple, a professor in the centre for neuropharmacology and neuroscience at Albany Medical College in New York. The cells are the centrepiece of regenerative medicine, either alone or combined with semi-synthetic scaffolds in tissue engineering. And job opportunities are likely to expand if opposition to using cells from human embryos dissipates. It's a distinct possibility, as ageing populations seek treatments for degenerative diseases, private funding is on the rise and public support grows.

In short, stem-cell science is already exploding, with discoveries of more niches for the cells and innovative approaches to using them in illness and injury. "It's rare that an advance in science could have such an impact on society," says John Gearhart, director of the stem-cell programme at Johns Hopkins Medicine in Baltimore, Maryland. Runaway expectations are a risk, though. "It is having a big effect even before much has been demonstrated, and that is part of the problem."

So far, a bigger problem has been the moral objections and political wavering. Australia last year eased restrictions, whereas Germany is going the other way. Research in the United States has had an uphill struggle — currently, only the few lines available before a 2001 ban on new ones can be used in federally funded work — although some states such as California and Wisconsin are strong backers. However, most moral objections are to the use of embryos, and human embryonic stem cells are only part of the story.

M. STOJKOVIC/SPL

T. STANLEY

Stem-cell supporters: Susan Solomon (top) and John McCulloch.

"They are a small niche of the stem-cell therapy world," says Darin Weber, a senior consultant with Biologics Consulting Group in Alexandria, Virginia. Non-human animals continue to be valuable sources of stem cells for research, he says. Also, the human body harbours many variations on the theme. Adult stem cells can also be used, as can those from the placenta and umbilical cord. Some companies use interesting semantic twists to cover themselves: EndGenitor Technologies of Indianapolis touts its work with "adult tissues that are free from any ethical controversy".

Finding your niche

With so many companies springing up, niches are being defined and providing a variety of career choices. A common focus is bone-marrow-derived stem cells, because they both readily generate progeny of several distinct cell types and have been studied for half a century. Some companies offer intriguing spins on the bone-marrow theme. Cellerant Therapeutics of San Carlos, California, for example, is developing myeloid progenitor cells to restore bone marrow damaged in combat or from radiation.

Other companies are coaxing stem cells from adipose tissue to yield cartilage, neurons, bone or muscle tissue; fashioning stem cells from teeth into personalized dental implants; and even growing replacement heart tissue, skin and bladders. Vet-Stem of Poway, California, treats horses with tendons and ligaments nurtured from adipose-tissue stem cells, and Vet Biotechnology of North Adelaide, Australia, is freezing cord blood cells from valued foals.

Yet another tier of companies provides consumables such as reagents, culture media and instrumentation such as cell sorters and cryogenic apparatus.

A solid background for a researcher includes a doctorate in molecular, cell or developmental biology, as well as skills to work with specific cell or tissue types acquired in at least two years of postdoc or industrial research. Degrees in pharmacology, immunology and

C. SPICOLUK/MARS DISCOVERY DISTRICT

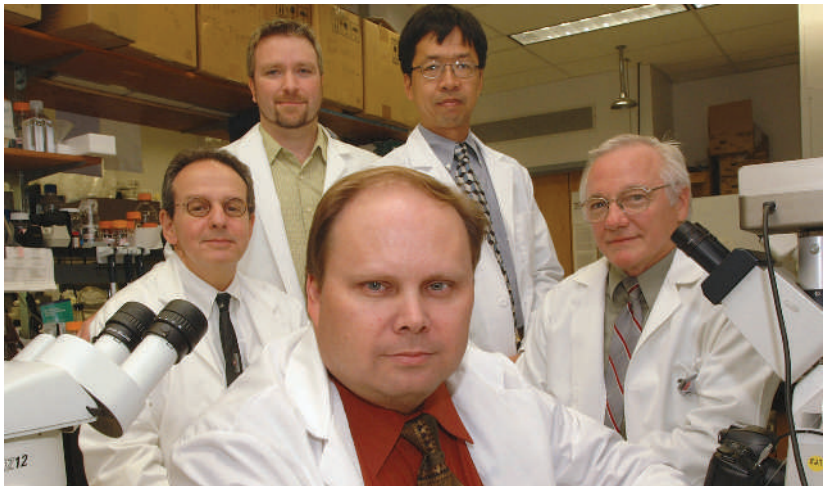

Cell mates: Dennis Steindler (left), Bryon Petersen (front) and their colleagues.

neuroscience are useful. Some companies hire at the bachelor's and master's level: the North East England Stem Cell Institute in Newcastle is one of several facilities to offer a master's degree in stem-cell research.

Positions may call for broad skills. For example, a post at PrimeCell Therapeutics in Irvine, California, needs expertise in gene-expression analysis and monitoring, establishing and expanding cell cultures and working with tissue scaffolding. Some positions seek experience with specific cell lineages. At Centocor, part of the Johnson & Johnson Stem Cell Internal Venture in Radnor, Pennsylvania, a retinal cell biologist will isolate and culture progenitor cells from the retina, establish degenerative-disease cell lines and develop assays for disease markers. Odontis, in London, seeks expertise in craniofacial development, and several companies seek skills in isolating pancreatic islet cells.

As therapies edge closer to the clinic, other skills will be needed. Egg retrieval for nuclear-transfer experiments requires lab and clinical experience, according to Alison Murdoch, head of reproductive medicine at Newcastle University, UK. Investigators need the clinical skills to counsel patients, give medication and collect eggs. But they also need to understand psychological and social aspects of fertility treatment. "Experience in a clinical embryology laboratory is an advantage," she says.

Companies and collaborations

Stem-cell science is gestating quietly in small biotech companies and academic–clinical alliances. "The drug industry is watching the beginning of clinical trials and starting to posture themselves," says Bryon Petersen, associate professor in the pathology, stem-cell biology and regenerative-medicine programme at the University of Florida in Gainesville. "They're still on the sidelines, but there is no turning back."

The drug industry is waiting for research elsewhere to pass the phase I hurdle, where projects stop if they don't show efficacy or they entered clinical trials too soon, says Weber. But, he adds, drug companies will need expertise in molecular and cell-culture techniques and the ability to translate basic research into a product.

The downside of stem-cell science at a biotech firm is the directed focus. Most small companies are venture-capital funded, so there is pressure not to do experiments that may show only an incremental change. "A small biotech company is looking for bigger leaps in progress," says Weber. Academic scientists, says Petersen, don't have to worry about a backer who wants a $100-million return on a $40-million donation in four years. "I have the luxury of following the science — and you can never predict where that will take you," he says.

Collaborations are catalysing networking and resource-sharing. The London Regenerative Medicine Network, for example, has 2,500-plus members and holds monthly meetings with speakers; sponsors include GlaxoSmithKline and Thomson Pharma. In Canada, a translational development company, Aggregate Therapeutics in Ontario, represents 37 leading principal investigators, pooling discoveries rather than working through individual technology transfer offices, says John McCulloch, adviser to the MaRS Venture Group in Toronto. The EuroStemCell Consortium provides cell lines and facilitates skills and knowledge-sharing. An investigator with an idea for an experiment but working in a country with restrictive policies, such as Germany or Italy, may be able to visit a lab with more freedom, such as in Norway or Britain.

World of opportunity

Meanwhile, Singapore continues to recruit top scientists as part of government and private efforts to boost biomedical research. Big names such as Neal Copeland and Nancy Jenkins — formerly of the US National Institutes of Health (NIH) — as well as early-career scientists are among those enjoying its ample funding and minimal research restrictions. The Australian Stem Cell Centre in Clayton, Victoria, a collaboration of academia and biotechs, is recruiting under new executive director Joseph Sambrook, a veteran of Cold Spring Harbor Laboratory in New York.

In the United States, private and state support tops up federal funding, which totalled roughly $40 million in 2006. It isn't the NIH budget that is so restrictive, researchers say, but the need for meticulous separation of work using non-approved cells from any other experiments, down to each pipette: investigators must delineate 'NIH-free' zones. This policy led to the birth of the private New York Stem Cell Foundation (NYSCF) in 2005, which funds human embryonic stem-cell research and provides limited lab space in the US northeast. "We started the foundation because we felt that it would be some time before the various funding, policy and controversies are solved, and in the meanwhile, scientists' work was ready to be done," says co-founder Susan Solomon. In 2006 the foundation opened the first 'safe haven' lab at an undisclosed location. It is unofficially called the 'underground railroad', after the Civil War slaves' escape route. The lab has developed patient-derived embryonic stem-cell lines for diabetes and Parkinson's disease. In addition to grants and annual meetings, the NYSCF sponsors three-year postdocs.

The foundations of the field are still being laid, many say. "We will be first learning how to manipulate stem cells and get a better understanding of the limits and possibilities, both in the United States and globally," says Gil Sambrano, scientific review officer for the California Institute for Regenerative Medicine. But the pace is accelerating. "Progress in our understanding of the basic biology of stem cells has been tremendous in the past decade," says Dennis Steindler, executive director of the McKnight Brain Institute at the University of Florida. "We are certain to see these findings translate to treatments in the not-too-distant future." ■

Ricki Lewis is a freelance science writer in Schenectady, New York.

Web links

California Institute for Regenerative Medicine
www.cirm.ca.gov
Stem Cell Network, Canada
www.stemcellnetwork.ca
EuroStemCell
www.eurostemcell.org
International Society for Stem Cell Research
www.isscr.org
London Regenerative Medicine Network
www.regenmednetwork.com
National Institutes of Health, Stem Cell Information
stemcells.nih.gov/research/registry
New York Stem Cell Foundation
www.nyscf.org
Stem Cell Research Foundation
www.stemcellresearchfoundation.org

The inside track from academia and industry

Great expectations

You may have got the job, but making sure it's the right fit is important for both employer and employee.

Joann Boughman

Landing a good job is a challenge, and the process can be daunting. Choosing a position and negotiating the details may not be easy, especially in an academic setting, but the first steps will set the tone for your future work relationships.

If you have made it through the initial selection and interview stages, then you have already made yourself known, and your skills, training and experience have been recognized by those involved in the selection process. It is incumbent on you to find the best possible arrangement.

You should research the institution and specific unit in which you will be working. Know exactly what they are looking for, going beyond the advertisement. Determine how your skills and experience fit their needs, but do not err by overselling your abilities. It is always best to be honest, but if there are new skills that you must master, show an eagerness to learn.

Understanding the relationships and the 'cast of characters' at the job site is very important. Learn enough about the administrative structure to know which people have the authority to make decisions, including financial decisions. Although the principal investigator or laboratory director may be hiring, be aware that the division chief, programme director or department chair may have the ultimate authority for salary, space, or equipment and supply needs.

Do enough background research to understand how the unit you may be joining fits into the larger context of the department, school, university or company. For example, is the unit a part of an entity that depends on extramural grant funds, or is there clear institutional support as well? If the position of interest would be funded only through grants, you should be aware of the potential consequences and timeframe in the event that funding is not renewed.

Expectations

Theirs It is important that you know what is expected of you in the new position. Will you be performing only research? Is teaching involved? If so, what is the time commitment and what types of student will you be responsible for? Are you expected to supply any of your salary in the form of grants and, if yes, how soon? Are there duties outside the lab setting or designated teaching load? What are the routine and style of the unit (work hours and environment, sharing of equipment or space, teamwork on any or all projects)?

These questions are important not only for the day-to-day work routine, but also with respect to the amount of support and interaction that you can count on in times of stress or need. The style of the research workplace has an impact, and not only on how the lab or team operates. It also provides insight into communication processes, distribution of responsibilities, credit for grants, presentations, manuscripts and other professional opportunities.

> "You must be willing to ask for what you want — and you must be ready to settle for what you need...but no less."

Yours You should know the components of the salary and benefits package that is being offered. Questions are essential, and if the prospective employer is not responsive, you should ask yourself why. Determine whether their expectations mesh with yours. What degree of independence is available, and how much independence is expected? Will you have sufficient mentoring as well as supervision? What is the evaluation process, and what type of feedback on performance will you receive? What personnel will you have access to (laboratory, central or core facilities, and administrative support)? Will there be opportunities to pursue activities of importance in your long-term goals (teaching, mentoring or participation in university activities)?

The process

Just as in any professional setting, competing for a position in science can be an arduous and sometimes uncomfortable process. You must present yourself professionally and competently. Be assertive although not aggressive, with a pleasant but persistent tone.

Prioritize your own needs and expectations. Know your limits and what you are willing to compromise on. During the process, figure out what fits and what does not meet your needs. Remember that each position is a step in a life-long career process. Although you may not know your future goals in detail, you should constantly be re-evaluating both your short- and long-term goals.

During any interview and negotiation process, you must be willing to ask for what you want. At the same time, you must be ready to settle for what you need…but no less. There are multiple paths to any career goal. Use your creativity and observational skills to their best advantage, not only in your scientific research, but also in the processes that allow you the opportunity to perform your life's work. ■

Joann Boughman is the executive vice-president of the American Society of Human Genetics in Bethesda, Maryland.